STUDIES OF THE ROLE OF LIGANDS IN DETERMINING THE STRUCTURES OF POLYNUCLEAR METAL COMPOUNDS

(Volume 1)

A Thesis submitted to the Council for
National Academic Awards in partial
fulfilment of the requirements for
the Degree of Doctor of Philosophy

by
Trushar Adatia

The Polytechnic of North London August 1988.

DECLARATION

Whilst registered as a candidate for this degree, the author has not been registered as a candidate for any other award.

T. Adatia.

DEDICATED TO MY PARENTS

Wisdom consists of one thing -
to know what steers all through
all.

Heraclitus

ACKNOWLEDGEMENTS

My thanks go to Dr. M. McPartlin, my Supervisor and Director of Studies, for her enthusiastic guidance and advice during the research programme.

I would also like to thank G. Conole, A. Bashall and H. Powell for creating a friendly atmosphere to work in.

A special thanks to T.N. Watts for supporting and encouraging me throughout.

The award of an S.E.R.C Research Studentship for the duration of my studies is gratefully acknowledged.

ABBREVIATIONS

Me	Methyl, CH_3
Et	Ethyl, C_2H_5
Pr	Propyl, C_3H_7
Pr^i	iso-propyl, $C(H)(CH_3)_2$
Bu^t	Tertiary butyl, $C(CH_3)_3$
Ph	Phenyl, C_6H_5
Cp	C_5H_5, in an η^5-bonding mode, unless otherwise stated.
Tol	Tolyl, $C_6H_4CH_3$
Cy	Cyclohexyl, C_6H_{11}
Hal	Halogen
dppm	$P(C_6H_5)_2$-CH_2-$P(C_6H_5)_2$
dppe	$P(C_6H_5)_2$-$(CH_2)_2$-$P(C_6H_5)_2$
dppp	$P(C_6H_5)_2$-$(CH_2)_3$-$P(C_6H_5)_2$
dppb	$P(C_6H_5)_2$-$(CH_2)_4$-$P(C_6H_5)_2$
dppol	$P(C_6H_5)_2$-$CH{=}CH$-$P(C_6H_5)_2$
PPN	$N(PPh_3)_2$
i.r.	Infrared
n.m.r.	Nuclear magnetic resonance
TM	Transition metal
L	Ligand
M	Metal
AO	Atomic Orbital
MO	Molecular Orbital
C.E.	Cohesive Energy
P.E.	Potential Energy
E.A.N	Effective Atomic Number

STUDIES OF THE ROLE OF LIGANDS IN DETERMINING THE STRUCTURES OF POLYNUCLEAR METAL COMPOUNDS

T. Adatia

ABSTRACT

Full X-ray structure analyses of sixteen metal cluster compounds of nuclearity 3 to 11 have been carried out to investigate to what extent the attached surface ligands govern the structure in the solid state and how this relates to the chemistry of the cluster in solution.

The structure of the tetranuclear cluster $[AgRu_3(CO)_9(C_2Bu^t)(PPh_3)]$ has completed a series of related clusters $[MRu_3(CO)_9(C_2Bu^t)(PPh_3)]$ [M = Cu, Ag or Au]. This is only the second example of a complete series of Group IB cluster analogues and confirms earlier evidence that the bonds from gold are different in character to those from silver and copper.

The structures of the copper clusters $[Cu_2Ru_4(\mu_3\text{-}H)_2(CO)_{12}\{P(C_6H_{11})_3\}_2]$ and $[Cu_2Ru_4(\mu_3\text{-}H)_2(CO)_{12}\{P(CHMe_2)_3\}_2]$ compared to the reported structure $[Cu_2Ru_4(\mu_3\text{-}H)_2(CO)_{12}(PPh_3)_2]$ indicate that the 'bulk' of the organophosphine groups is a major factor in determining the type of metal geometry adopted by this type of compound in the solid state.

Comparison of the structural results obtained for the hexanuclear clusters $[M_2Ru_4(CO)_{13}(PPh_3)_2]$ [M = Cu or Ag] to those reported for the hydrido analogues $[M_2Ru_4(\mu_3\text{-}H)_2(CO)_{12}(PPh_3)_2]$ have shown that small changes in the surface ligand set can have marked effects on the metal geometry in the solid state, providing further evidence that the energy differences between the various structural types are small for heteronuclear clusters containing Group IB metal atoms.

The X-ray structure analyses of $[Au_2Ru_4(\mu\text{-}H)(\mu_3\text{-}H)(CO)_{12}\{\mu\text{-}Ph_2PCH{=}CHPPh_2\}]$ and $[Au_3Ru_4(\mu\text{-}H)(CO)_{12}\{\mu\text{-}Ph_2PCH_2PPh_2\}(PPh_3)]$ have enabled the correlation of earlier structural data of related hexanuclear and heptanuclear mixed-metal clusters to account for the marked differences between the structures of gold-ruthenium clusters with monodentate organophosphines, compared to those with bidentate phosphine ligands.

The X-ray structures of the isomers $[Os_3H_2(CCHOEt)(CO)_9]$ and $[Os_3H_2(HCCOEt)(CO)_9]$ provide a rare example of cluster isomers differing only in the nature of the organo ligands.

The structures of the high nuclearity hydrido clusters $[Os_6H_2(CO)_{17}\text{-}P(OMe)_3]$, $[Os_7H_2(CO)_{22}]$, and $[Os_7H_2(CO)_{19}\{MeC{=}CMe\}]$ have shown novel metal frameworks, supporting previous observations that when hydrido ligands are present, osmium cluster geometries can often be unpredictable in the solid state.

The structural characterisation of the large hydrido cluster monoanions $[H_5Os_{10}(CO)_{24}]^-$ and $[HOs_{11}C(CO)_{27}]^-$ have provided evidence for the presence of interstitial hydrido ligands. Comparison of these results to those reported for related compounds supports the view that in some cases, interstitial ligands become important in preventing surface ligand overcrowding.

CONTENTS

Introduction.

During the past twenty years the growth in the study of transition metal cluster chemistry has been truly remarkable, representing a major achievement in modern inorganic chemistry.[1] Cluster compounds may be defined as having metal units within one molecule bonded to at least two or more other metal atoms. These molecular species have a protective sheath of ligands bonded to the peripheral metal atoms which makes the clusters inert towards decomposition to the bulk metal. The growth in the field of transition cluster chemistry may be attributed to the successful collaboration between synthetic groups and crystallographers, since in most cases X-ray analysis is a vital tool for complete structural characterisation of new polynuclear cluster compounds. Fourier transform n.m.r. and i.r. spectroscopic techniques have also been useful in studying the dynamic behaviour and aspects of structural rearrangements for many of these cluster species in solution.[2-4] The use of clusters as molecular models also provide a way of studying some fundamental questions concerning the evolution of properties from molecular to bulk states;[5-7] in addition these systems demonstrate how bonding requirements change as larger aggregates are formed by condensation via vertex, edge and face sharing processes.[8] For high nuclearity clusters, the bonding must begin to approach that observed for the bulk metal and therefore provides an opportunity for studying the development of metallic properties.[9]

Mechanisms associated with heterogenous catalysis on metal surfaces has also initiated research into these polynuclear systems, since common geometrical faces {eg. M_3 (triangular), M_4 (square planar), or M_4 (butterfly)} adopted are similar to units present on bulk metal surface. Study of various modes of reaction with simple molecules on such cluster faces therefore provide some insight into catalytic processes on bulk metal.[10] Metal clusters have shown to be effective catalysts in their own right initiating a variety of reactions, such as isomerization and oligomerization of hydrocarbons.[11] For example, it has been well established that the tetranuclear compound $[Ru_4(\mu\text{-}H)_4(CO)_{12}]$ catalyses the isomerisation of pent-1-ene.[12] However, recent studies have shown that the heteronuclear clusters $[AuRu_4(\mu_3\text{-}H)(\mu\text{-}H)_2(CO)_{12}(PPh_3)]$ and $[Au_2Ru_4(\mu_3\text{-}H)(\mu\text{-}H)(CO)_{12}(PPh_3)_2]$ act more effectively in catalysing the isomerisation process.[13] The cluster species $[M_2Ru_6C(CO)_{16}(NCR)_2]$ [M = Cu, Ag, or Au; R = alkyl or aryl] have been shown to act as effective catalysts in the preparation of methanol from CO + H_2, and from the same starting reagents, the higher nuclearity cluster $[Au_2Rh_{12}(CO)_{30}]$ has been reported to effectively catalyse the formation of ethylene glycol, glycerol and 1,2 propylene glycol.[14] The expanding structural interest in such species involves uncovering the range of possible polyhedral metal core geometries adopted in the solid state and the unusual bonding modes of the attached ligands. The most widely studied clusters are polynuclear carbonyls, in which the transition metal unit is surrounded by closely packed carbonyl surface ligands which are strong π-acceptors.[15] For these carbonyl compounds the polyhedral shape adopted by the metal core atoms determines the total number of valence electrons required. However, it has been shown that a range of alternative metal core geometries are theoretically possible for the same electron count, and it appears that other ligands present in addition to carbonyls are important in determining which polyhedron is adopted in a particular case.[16-18] A wide variety of bonding modes have been established for the single atom donors H and C, and in certain cases they have been shown to stabilize unexpected solid state geometries for a particular electron count.[19-21]

Another class of surface ligands currently attracting a great deal of interest are organophosphines. The number of known transition metal compounds containing tertiary phosphine compounds is immense and includes monodentate, bidentate, tridentate and higher chelating phosphines.[22-28] It is well established that altering the substituents on tertiary phosphines produces substantial changes in the chemical and physical properties of their mononuclear transition metal complexes.[29-34]

In the present work structural studies of several heteronuclear clusters containing Group IB metal phosphine fragments, $M(PR_3)$, [M = Cu, Ag, or Au], have been carried out to investigate the existence of similar effects in polynuclear systems. The factors influencing the siting of hydrido ligands interstitially as opposed to on the surface have also been examined in several large osmium hydrido clusters.

References.

1. Transition metal clusters, Eds. B.F.G. Johnson, Wiley, New York, 1981, p. 5.

2. S. Martinengo, B.T. Heaton, R.J. Goodfellow, and P. Chini, J. Chem. Soc., Chem. Commun., 1977, 39.

3. J.W. Diesveld, E.M. Menger, H.T. Edzes, and W.S. Veeman, J. Am. Chem. Soc., 1980, 102, 7935.

4. N.J. Clayden, C.M. Dobson, K.P. Hall, D.M.P. Mingos, and D.J. Smith, J. Chem. Soc., Dalton Trans., 1985, 1811.

5. J.W. Lauher, J. Am. Chem. Soc., 1978, 100, 5305.

6. J.W. Lauher, J. Am. Chem. Soc., 1979, 101, 2604.

7. D.M.P. Mingos, Chem. Soc. Rev., 1986, 15, 31.

8. D.M.P. Mingos, J. Chem. Soc., Chem. Commun., 1983, 706.

9. R.E. Benfield, P.P. Edwards, W.J.H. Nelson, M.D. Vargas, D.C. Johnson, and M.J. Sienko, Nature (London), 1985, 314, 231.

10. E.L. Muetterties, T.N. Rhodin, E. Brand, C.F. Bruker, and W.R. Pretzer, Chem. Soc. Rev., 1979, 79, 91.

11. E.L. Muetterties and M.J. Krause, Angew. Chem., Int. Ed. Engl., 1983, 22, 135.

12. P. Frediani, U. Matteoli, M. Bianchi, F. Piacenti, G. Menchi, J. Organomet. Chem., 1978, 150, 273.

13. J. Evans and G. Jingxing, J. Chem. Soc., Chem. Commun., 1985, 39.

14. P. Braunstein and J. Rose, Gold Bull, 1985, 18, 17.

15. R. Colton and M.J. McCormick, Coord. Chem. Rev., 1980, 31, 1.

16. M. McPartlin, Polyhedron, 1984, 3, 1279.

17. M. McPartlin and D.M.P. Mingos, Polyhedron, 1984, 3, 1321.

18. S.M. Owen, Polyhedron, 1988, 7, 253.

19. E.L. Muetterties, M. Tachikawa, Prog. Inorg. Chem., 1981, 28, 203.

20. R.G. Teller, R. Bau, Struct. Bonding, (Berlin), 1981, 44, 1.

21. J. Lewis and B.F.G. Johnson, Pure and Appl. Chem., 1982, 54, 97.

22. A.R. Sanger, J. Chem. Soc., Chem. Commun., 1975, 893.

23. R.J. Puddephatt, Chem. Soc. Rev., 1983, 99.

24. J.A. Clucas, D.F. Foster, M.M. Harding, and A.K. Smith, J. Chem. Soc., 1984, 949.

25. A.J. Deeming, S. Donovan-Mtunzi, and S.E. Kabir, J. Organomet. Chem., 1984, 276, 276

26. N. Lugan, J.J. Bonnet, and J.A. Ibers, J. Am. Chem. Soc., 1985, 107, 4484.

27. M.I. Bruce, G.N. Pain, C. Hughes, J.M. Patrick, B.W. Skelton, and A.H. White J. Organomet. Chem., 1986, 307, 343.

28. A.J. Deeming, S. Donovan-Mtunzi, and S.E. Kabir, J. Organomet. Chem., 1987, 333, 253.

29. C.A. Tolman, J. Am. Chem. Soc., 1970, 92, 2953.

30. C.A. Tolman, J. Am. Chem. Soc., 1970, 92, 2956.

31. A. Pidcock, Transition Metal Complexes of Phosphorus, Arsenic and Antimony Ligands, C.A. McAuliffe, Ed., Wiley, New York, 1973.

32. R.W. Taft, Steric Effects in Organic Chemistry, M.S. Newman, Ed., Wiley, New York, 1972.

33. A.D.U. Hardy and G.A. Sim, J. Chem. Soc., Dalton Trans., 1972, 1900.

34. C.A. Tolman, Chem. Rev., 1977, 77, 313.

CHAPTER 1

Monodentate organophosphines: The structural chemistry of their mixed-metal cluster compounds containing Group IB metal atoms, Cu, Ag and Au.

Section 1.1. Introduction.

Development of the bonding relationships between the hydrido ligand and the isolobal counterpart, $Au(PR_3)$ [R = alkyl or aryl].

The term isolobal relationship, was first introduced by Hoffmann in 1976 and further developed in his Nobel lecture in 1982.[1] From extended Hückel molecular orbital calculations on a variety of transition metal-ligand fragments, ML_n, a connection was established between the frontier orbitals in these units to those displayed by simple hydrocarbon radicals, CH_3, CH_2, and CH. For example, the d^7-fragments, $[Mn(CO)_5]$ and $[MnH_5]^{5-}$, were observed to have above the three lone pairs in the t_{2g} set, a single electron in a hybrid orbital pointing away from the metal atom. This was found to be similar to the single electron in the sp^3 hybrid orbital of the methyl radical, {Figure 1.1(a)}. Although the two fragments, CH_3 and d^7-ML_5 were not iso-structural nor iso-electronic, they both possessed a frontier orbital which looked approximately the same. Importantly, the resemblance between the two fragments was also apparent in their ability to dimerize and start radical chains, CH_3 to C_2H_6 and $Mn(CO)_5$ to $Mn_2(CO)_{10}$. Hoffmann proposed that two fragments should be called isolobal, if the number of symmetry properties, approximate energy, and the shape of the frontier orbital, together with the number of electrons in them are similar.

The structural relationship between hydrido-metal compounds and their $Au(PPh_3)$ derivatives was first reported by Lauher and Wald in 1981.[2] They observed that the structure of the gold cobalt complex, $[AuCo(CO)_4(PPh_3)]$ reported[3] by Blundell and Powell in 1971 was similar to the structure of the tetra-carbonyl cobalt hydrido compound $[HCo(CO)_4]$, studied by gas-phase electron diffraction

analysis by McNeill and Scholer in 1976.[4] In both structures the cobalt atom was described as five co-ordinate with a carbonyl group and an Au(PPh$_3$) unit or H ligand, forming the apices of a trigonal bi-pyramid in the respective solid state structures, with the remaining three CO groups bent towards the gold atom in [AuCo(CO)$_4$(PPh$_3$)] and the hydrogen atom in [HCo(CO)$_4$], {Figure 1.1(b)}. Lauher and Wald also pointed out[2] that similar bonding modes between the Au(PPh$_3$) group and the H atom were also present in other transition metal complexes reported previously,
[Fe(CO)$_4$(L)$_2$] [L = H[4] or Au(PPh$_3$)[5]] and
[Os$_3$(CO)$_{10}$(μ-X)(μ-L)] [X = Cl or Br;L = H[6,7] or Au(PPh$_3$)[8]].

The workers also reported the synthesis and X-ray structural analysis of the tetra-metallic cluster [AuFeCo$_3$(CO)$_{12}$(PPh$_3$)], which adopted a trigonal bi-pyramidal metal core, with the Au(PPh$_3$) group at one apical position.[2] This was the first example of a gold atom triply bridging three transition metal atoms, Figure 1.1(c). The μ_3-bonding mode of the Au(PPh$_3$) group in this complex was found to be analogous to that adopted by the hydrido ligand in the tri-methyl phosphine derivative,[9,10] [HFeCo$_3$(CO)$_9${P(OMe)$_3$}$_3$] determined by Kaesz in 1978 and confirmed in a neutron study[11] by Koetzle and Bau in the same year {Figure 1.1(c)}. From these observations Lauher and Wald suggested that the structural relationship between H-ligand and Au(PPh$_3$) groups could be used to provide direct evidence for hydrido-ligand location in complexes where both analogues were available, since X-ray diffraction studies could not always directly locate the 1 electron hydrogen atom.[2] These structural similarities were first thought of as being rather surprising, since the gold-phosphine group and the hydrogen atom would have little in common from either overall electronic or steric view point. However, the workers proposed that since the gold atom was larger in size there would be minimal steric hinderance due to the formation of longer Au-M bonds, keeping the $Au(PPh_3)$ unit further away from the transition metal.

In 1982 two related tetra-osmium structures $[AuOs_4(\mu\text{-}H)(CO)_{13}(PEt_3)]$ and $[AuOs_4(\mu\text{-}H)_3(CO)_{12}(PEt_3)]$ reported by Raithby and co-workers,[12] further displayed the isolobal relationship. The structure of the mono-hydride was found to be similar to the di-hydrido ruthenium cluster $[Ru_4(\mu\text{-}H)_2(CO)_{13}]$,[13] and the tri-hydride closely resembled the structure of the tetra-hydrido osmium cluster $[Os_4(\mu\text{-}H)_4(CO)_{12}]$.[14] The co-ordination of the $AuPEt_3$ groups in both AuH and AuH_3 clusters was described as linear with one lobe of an sp orbital pointing at the midpoint of the bond, Os(1)-Os(2), giving near linear angles, $Et_3P\text{-}Au\text{-}M$ of 177.9° for the AuH derivative and 177.7° for the AuH_3 cluster [M = midpoint of the bond Os(1)-Os(2)]. The gold atom in both structures was therefore envisaged to donate one electron to the bridged Os-Os bond to form a delocalized 3c-2e Os-Au-Os interaction, {Figures 1.1(d) and 1.1(e), respectively}.[12] From the few examples described so far, it was becoming evident that in many cases, when both analogues were available for comparison, the bonding modes of the H-ligand and the $Au(PR_3)$ group were similar in their respective solid state structures. However, the growing interest in the synthesis of gold derivatives to compare structural features to their isolobal hydrido cluster compounds required understanding of the bonding capabilities of the $Au(PR_3)$ fragment.

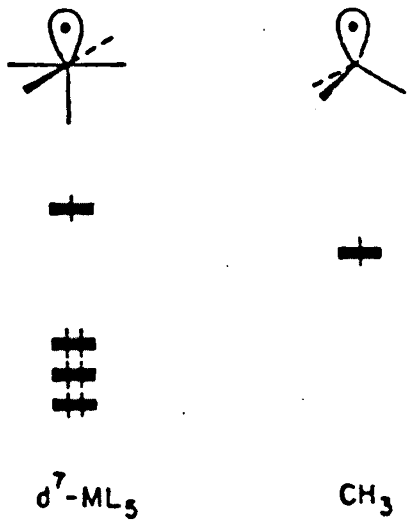

Figure 1.1(a).[1]

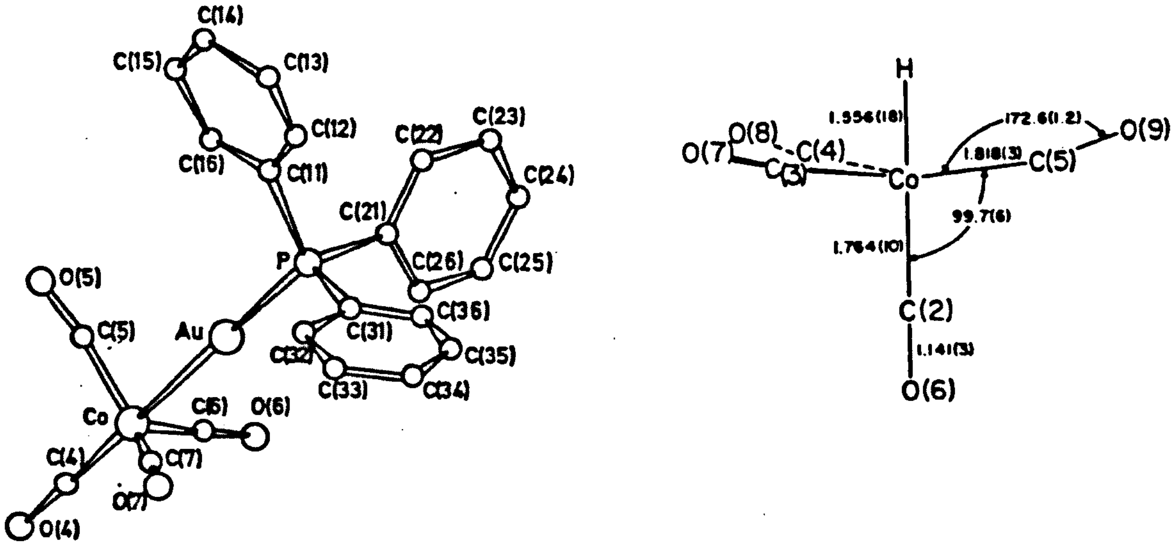

Figure 1.1(b).

Molecular structures of

$[AuCo(CO)_4(PPh_3)]$[3] and $[HCo(CO)_4]$.[4]

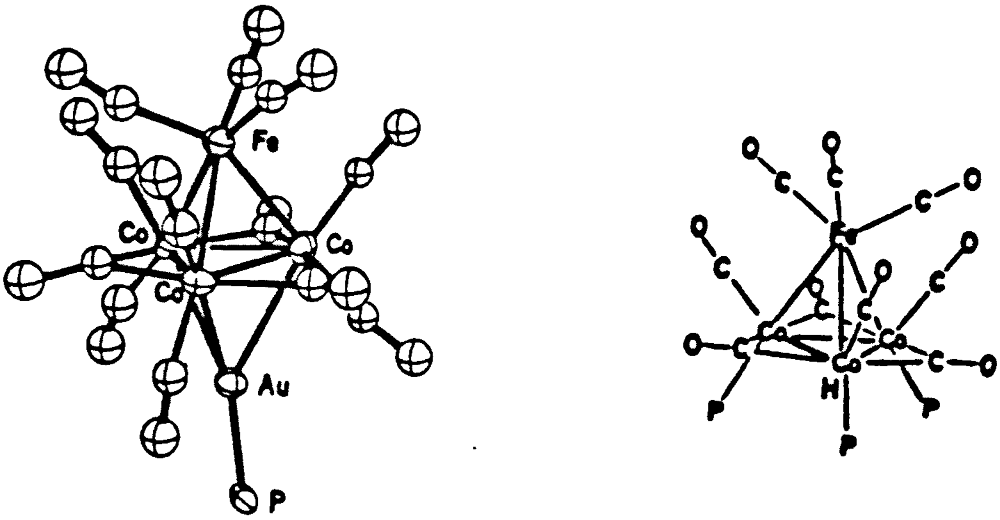

Figure 1.1(c).

Molecular structures of

$[AuFeCo_3(CO)_{12}(PPh_3)]^2$ and $[HFeCo_3(CO)_9\{P(OMe)_3\}_3]$.^{9,10}

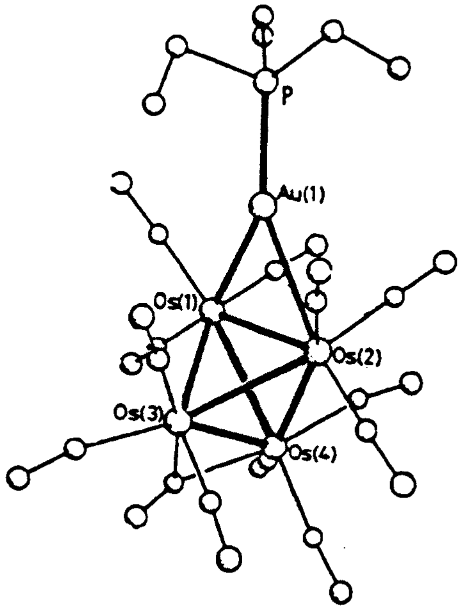

Figure 1.1(d).[12]

$[AuOs_4(\mu\text{-}H)(CO)_{13}(PEt_3)]$

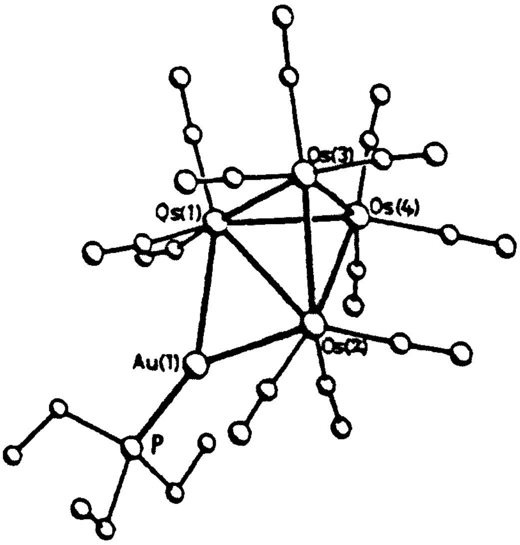

Figure 1.1(e).[12]

$[AuOs_4(\mu\text{-}H)_3(CO)_{12}(PEt_3)]$

Section 1.1.1. Theoretical studies on the bonding capabilities of the Au(PR_3) group, [R = alkyl or aryl].

In the period 1965-1976 there were several reports of results obtained from molecular orbital calculations on homonuclear cluster compounds of gold.[15-22] For instance, Mingos in 1976 carried out extended Hückel calculations[23] on both the uncomplexed $[Au_6]^{2+}$ cluster and the triphenyl phosphine derivative $[Au_6(PPh_3)_6]^{2+}$. The results showed that the 5d orbitals of the gold combined to form a narrow band of 30 molecular orbitals of lowest energies, {Figure 1.1.1(a)}. The energy spread of these orbitals was small, resulting from the contraction of the d atomic orbitals due to inefficient screening effects, a characteristic feature of elements with increasing atomic number in the transition series. Six molecular orbitals with predominantly 6s character were found to lie at higher energy, with further 18 orbitals of predominantly 6p character occupying the highest energy levels.

In the uncomplexed hexanuclear cation $[Au_6]^{2+}$, the 64 valence electrons were therefore distributed, 60 in the 5d band of 30 molecular orbitals and the remaining two pairs occupying the two lower 6s orbitals, A_{1g} and T_{1u}. It was pointed out that the trans-6s-6s overlap intergrals generating the T_{1u} molecular orbitals, were insignificant and were essentially non-bonding in character. Therefore, it was evident that in the cluster species $[Au_6]^{2+}$, the bonding interactions between adjacent gold atoms were weak due to the presence of only a single electron pair in the bonding molecular orbital, A_{1g}. Importantly, Mingos observed that gold-gold bonding was encouraged by the co-ordination of triphenyl phosphine ligands to the vertices of the cluster, arising from the effective overlap of the lone-pair orbitals of the ligand with the metal 6s, 6p, and 5d orbitals, {Figure 1.1.1(a)}.[23] The additional electron pairs introduced by the phosphine ligands were found to occupy the low lying A_{1g}, E_g, and T_{1u} orbitals enhancing strong metal-metal and metal-phosphorus bonds, primarily supported by the effective $s\text{-}d_{z^2}$ hybridisation of the metal orbitals. Thus, the molecular orbital calculations for the cationic species $[Au_6]^{2+}$ illustrated that the overlap of gold 6s orbitals made a dominant contribution to the bonding, and co-ordination of 2e-donor ligands promoted more favourable hybridisation of the metal orbitals resulting in stronger radial metal-metal bonds.

A direct analogy between the bonding modes of the hydrido ligand and $Au(PR_3)$ fragments in mixed-metal clusters was provided by Evans and Mingos in 1982.[24] Using extended Hückel molecular orbital calculations, they analysed the stoichiometries and geometries of gold and platinum tertiary phosphine cluster compounds of the type $M_n(PR_3)_n^{x+}$ (n = 3-6). Their results showed that the bonding characteristics of the $Au(PH_3)$ group was determined primarily by the hybrid orbital h(s-z) [a_1 symmetry] and the higher lying degenerate pair of p_x and p_y [e symmetry] orbitals. The calculations revealed that the p_x and p_y orbitals were higher in energy than the hybrid (s-z) orbital, {Figure 1.1.1(b)}, and as a result could not accept back donation of electron density, playing a secondary role in bonding. The $Au(PH_3)$ group was therefore found to utilise its hybrid(s-z) orbital of a_1 symmetry in bridging a M-M bond in a three-centre two electron bonding interaction. Alternatively, the a_1 and e symmetry frontier orbitals in a μ_3-capping mode were found to be destabilised by interaction with the triangular three-metal atom face and as a result were not available for skeletal bonding. Thus, the $Au(PH_3)$ group was proposed to be isolobal with H, CH_3, and $Mn(CO)_5$, each having a single frontier orbital participating in bonding.

To support this bonding scheme Mingos and Hall[25] further highlighted the similarity in bonding modes of the H-ligand and the $Au(PPh_3)$ fragment with the previously reported crystal structures of the tri-osmium gold cluster compound $[AuOs_3(\mu\text{-}H)(CO)_{10}(PPh_3)]$,[26] and the hydrido analogue $[Os_3(\mu\text{-}H)_2(CO)_{10}]$.[27] The solid state structure of the gold derivative described a triangular array of three osmium atoms, with the $Au(PPh_3)$ and the hydrido ligand doubly bridging one edge of the Os_3 triangle {Figure 1.1.1(c)}. Similarly, the two hydrogen atoms in the di-hydrido analogue, doubly bridged the same edge of the osmium triangle, {Figure 1.1.1(c)}.

The existence of this isolobal relationship in both structures was further reflected in the Os-Os bond lengths, with the doubly bridged bond in both structures being very similar, but markedly shorter than the mean of the two unbridged bonds.

	$[AuOs_3(\mu\text{-}H)(CO)_{10}(PPh_3)]$[26]	$[Os_3(\mu\text{-}H)_2(CO)_{10}]$[27]
Os-Os bridged	2.683(1)	2.699(1) Å
Os-Os unbridged	2.815(1)	2.834(1) Å [mean]

This was found to be consistent with earlier observations reported by Churchill, proposing that when an Os-Os vector was spanned by a single bridging hydrogen atom, elongation of the vector relative to a normal Os-Os single bond was observed. However, when a μ_2-H ligand was accompanied by another μ_2-ligand about the same metal-metal vector, the resulting distance was found to be shorter than, or equivalent to a non-bridged M-M bond.[6,7,28]

The structural relationship between the $Au(PPh_3)$ and the hydrogen atom was also pointed out by Braunstein and co-workers in 1984, between the novel gold-nickel osmium cluster $[AuNiOs_3(\mu\text{-}H)_2(CO)_9(PPh_3)(\eta\text{-}C_5H_5)]$[29] and the previously reported hydrido compound $[NiOs_3(\mu\text{-}H)_3(CO)_9(\eta\text{-}C_5H_5)]$.[30] The $Au(PPh_3)$ group was found to bridge one edge of the $NiOs_3$ tetrahedron in a similar manner to the three equivalent hydrogen atoms in the related hydrido cluster.

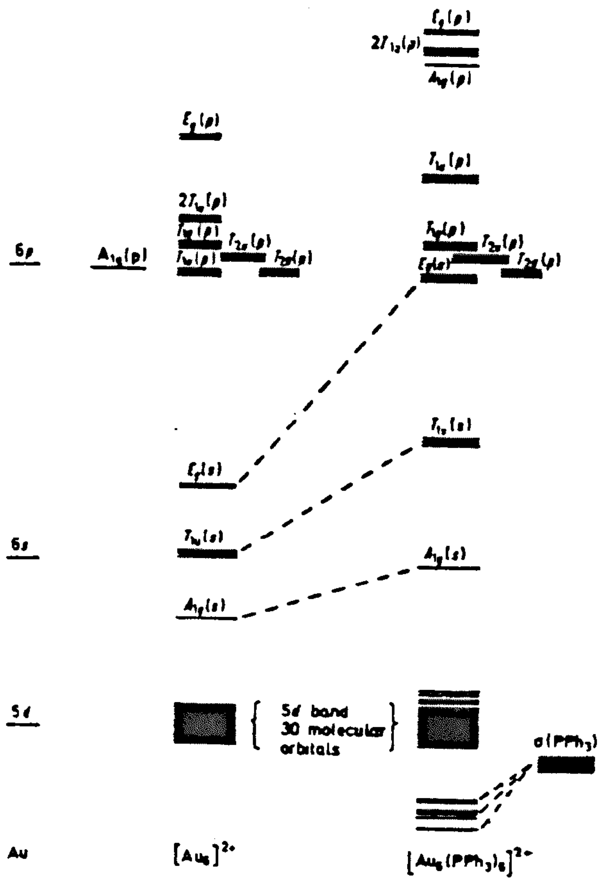

Figure 1.1.1(a). M.O correlation diagram calculated for $[Au_6]^{2+}$ and $[Au_6(PPh_3)_6]^{2+}$.[23]

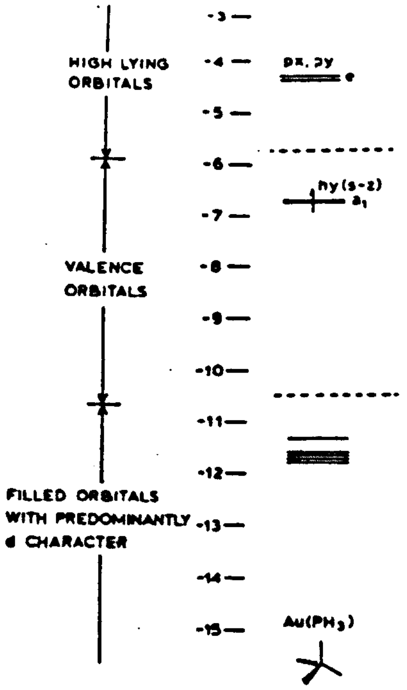

Figure 1.1.1(b). The relative energies of the frontier orbitals in $Au(PH_3)$.[24]

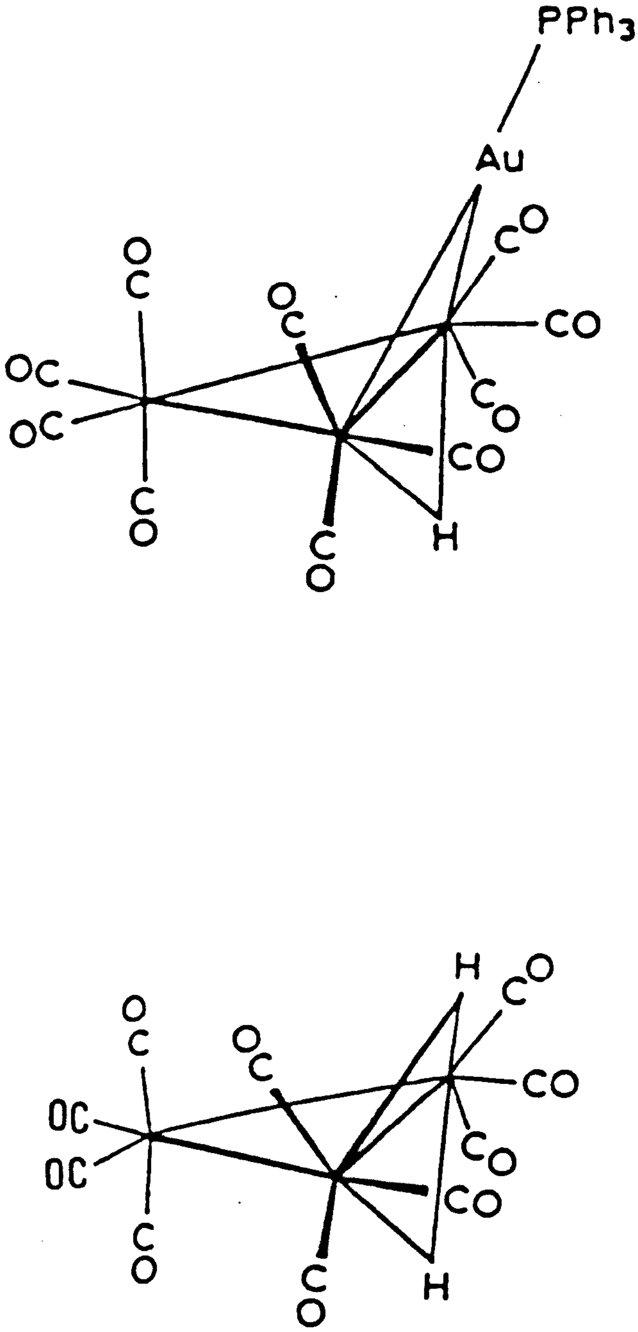

Figure 1.1.1(c). Molecular structures of $[AuOs_3(\mu\text{-}H)(CO)_{10}(PPh_3)]$[26] and $[Os_3(\mu\text{-}H)_2(CO)_{10}]$.[27]

Section 1.1.2. Development of the isolobal relationships for the related Group IB metal phosphine groups, $Cu(PR_3)$ and $Ag(PR_3)$ [R = alkyl or aryl].

In 1984 Stone reviewed the importance of the isolobal connection relating the frontier orbitals of organic groups with those of metal-ligand fragments in preparative work, leading to new compounds in the field of organometallic chemistry.[31] In the review he discussed how the established isolobal analogy between the $Au(PPh_3)$ group with H or CH_3, provided a useful basis in devising synthesis of compounds containing a single Au atom. For example, the di-chromium anion $[Cr_2(\mu\text{-}H)(CO)_{10}]^-$ was considered to be a combination of two fragments, $[CrH(CO)_5]^-$ and $[Cr(CO)_5]$, the former behaving as an electron pair donor and the latter an electron pair acceptor, being isolobal to CH_3^+. Due to the existing isolobal relationship between CH_3^+ and $Au(PPh_3)$,[24] it was proposed that the neutral complex $[AuCr(\mu\text{-}H)(CO)_5(PPh_3)]$ could exist under favourable conditions. The compound was infact obtained from the reaction between $[N(PPh_3)_2][CrH(CO)_5]$ and $[AuCl(PPh_3)]$ in tetrahydrofuran.[32] The following compounds were also synthesised by similar routes:[31]

$[AuMo(\mu\text{-}H)(CO)_5(PPh_3)]$
$[AuW(\mu\text{-}H)(CO)_5(PPh_3)]$
$[AgCr(\mu\text{-}H)(CO)_5(PMe_3)]$
$[AgW(\mu\text{-}H)(CO)_5(PMe_3)]$

illustrating the isolobal relationships,

$Cr(CO)_5 \longrightarrow M(CO)_6$ [M = Mo or W] and
$Au(PPh_3) \longrightarrow Ag(PMe_3)$.

Stone also pointed out that since it was known[1] that $Ni(\eta^5\text{-}C_5H_5)$ [ML_3, d^9] fragment was isolobal with CH, the relationship between

$Cu(\eta^5-C_5H_5)$ $[ML_3, d^{10}]$ to CH_2 would also hold. Thus, it was becoming evident that besides the known isolobal connection between $Au(PR_3)$ and the hydrido ligand, the related Group IB metal fragments, CuL and AgL were also exhibiting isolobal relationships. The important connection to be made was whether the groups $Cu(PR_3)$ and $Ag(PR_3)$ were infact isolobal to $Au(PR_3)$ and the hydrogen atom, having one frontier molecular orbital suitable to participate in cluster bonding.

During the period 1981 to 1984 few examples of mixed-metal cluster containing the fragments $Cu(PR_3)$ and $Ag(PR_3)$ were reported, and in comparison to the $Au(PR_3)$ unit, very little experimental evidence concerning the bonding capabilities of the $M(PR_3)$ [M = Cu or Ag] groups was available. However, Evans and Mingos had earlier pointed out that extended Hückel molecular orbital calculations on the $Cu(PH_3)$ fragment showed an isolobal connection with the unit $M(CO)_3$ [M = Co or Mn], since their frontier orbital energies were found to be approximately the same, {Figure 1.1.2(a)}.[24] In contrast to the $Au(PH_3)$ group {Figure 1.1.1(b)}, the $Cu(PH_3)$ group had available three frontier orbitals for bonding, the p_x, p_y and hybrid h(s-z). It was therefore suggested that the $Cu(PR_3)$ unit preferred to cap triangular faces of metal polyhedra since in the edge-bridging mode, one component of the e set of its frontier orbitals was not effectively used in bonding.[24] Thus, in a capping situation the frontier molecular orbitals for $Cu(PR_3)$ groups were likely to involve the two π-type orbitals and the hybrid h(s-z) orbital, whereas for $Au(PR_3)$, only the latter would be important in bonding.

A direct comparison between the bonding modes of a single copper and gold metal phosphine group bonded to different transition metal atoms was provided with the X-ray structures of the high nuclearity carbido cluster anions, $[MOs_{10}C(CO)_{24}(L)]^-$ [M = Cu, L = NCMe; M =

Au, L = PPh_3].[33] The solid state structure of the gold derivative established a μ_2-edge-bridging site for the $Au(PPh_3)$ group, whereas for the copper analogue, the Cu(NCMe) unit capped an Os_3 triangular face, {Figures 1.1.2(b) and 1.1.2(c), respectively}. Detailed analogies of the $Ag(PR_3)$ unit and its isolobal counterparts had not been discussed extensively, but it was thought that the bonding scheme of the group resembled that of the $Cu(PR_3)$ fragment, with the orbitals of e symmetry lying at an intermediate energy between those in $Au(PR_3)$ and $Cu(PR_3)$ fragments.[24] The first comparative study of the structural similarities and differences in the bonding modes of all three Group IB metal phosphines was reported by Stone and Salter from the spectroscopic studies of the cluster series, $[MRu_4(H)_3(CO)_{12}(PPh_3)]$ [M = Cu, Ag or Au].[34] The i.r. and n.m.r. data for both the copper and silver analogues were very similar, proposing a μ_3-capping site for the hetero-metal atoms in their respective solid state structures, {Figure 1.1.2(d)}. In contrast, the spectroscopic results for the gold derivative were consistent with the $Au(PPh_3)$ unit bridging one edge of the ruthenium tetrahedron, {Figure 1.1.2(e)}.

In more recent years there have been numerous reports of mixed-metal cluster compounds with one or more $M(PR_3)$ units [M = Cu, Ag, or Au;R = alkyl or aryl] bonded to other different transition metals, forming a part of the overall mixed-metal polyhedron. Greater emphasis has been placed in the chemistry of cluster compounds containing $Au(PR_3)$ fragments and analogous compounds with $M(PR_3)$ [M = Cu or Ag] groups still receiving much less attention. Although research groups have concentrated in obtaining synthetic routes for the preparation of series of related heteronuclear clusters containing one or more of these $M(PR_3)$ units, more recent theoretical studies into their bonding capabilities still remain relatively rare.

In 1986 Braunstein and co-workers reported the synthesis and X-ray structural studies for the pentanuclear mixed-metal clusters $[MRuCo_3(CO)_{12}(PPh_3)]$ [M = Cu or Au].[35] The metal frameworks of the two related compounds were described in terms of a trigonal bi-pyramidal arrangement of the five metal atoms with the Ru and M (Cu or Au) atoms capping opposite faces of the Co_3 triangle, {Figure 1.1.2(f)}. The workers also carried out extended Hückel calculations based on the fragments $Au(PH_3)^+$ and $Cu(PH_3)^+$ interacting with $[Co_3(CO)_9]^{3-}$. They concluded that the bonding patterns of the two fragments, $Au(PH_3)^+$ and $Cu(PH_3)^+$ were similar but more importantly, they did not find any interaction of importance between the symmetry related orbitals of $[Co_3(CO)_9]^{3-}$ and the p_x and p_y (e symmetry) low lying empty orbitals of the $Cu(PH_3)^+$ group. Therefore, they concluded that the energies of the degenerate pair of orbitals, p_x and p_y in the unit, $Cu(PH_3)^+$, were not significantly lower than those in $Au(PH_3)^+$, indicating that both fragments should exhibit similar bonding properties. These results were supported by experimental observations, which revealed that by taking the different covalent radii of Cu and Au into account, the ranges of Cu-Co and Au-Co distances for the face capping units in $[MCo_3Ru(CO)_{12}(PPh_3)]$ [M = Cu or Ag] were not significantly different. These results were somewhat contradictory to the earlier conclusions reached by Evans and Mingos (vide supra).[24]

Either way, the isolation and characterisation of a number of stable mixed-metal cluster compounds containing either a single $Cu(PR_3)$ or an $Ag(PR_3)$ fragment has established both edge-bridging and face-capping bonding modes for the Group IB metal atoms, (section

1.1.4). In a number of cases, these hetero-metal atoms have been found to occupy the same bonding site as that of the hydrido ligand in the related hydrido-metal cluster, a structural feature well recognised for mixed-metal cluster compounds with a single $Au(PR_3)$ group. Thus, in contrast to the theoretical conclusions relating the differences and similarities in the bonding capabilities for the Group IB metal phosphines,[24,35] the growing experimental evidence supports, that the energy differences between face-capping and edge-bridging bonding modes adopted by the $M(PR_3)$ fragments [M = Cu, Ag, or Au] can be very small and interconversion from one form to another is therefore probable, (section 1.1.8).

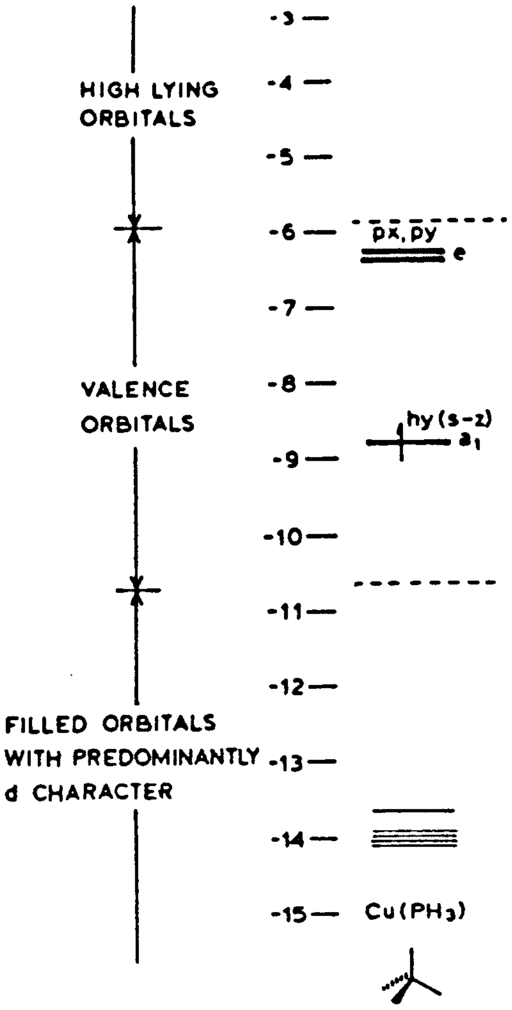

Figure 1.1.2(a). The relative energies of the frontier orbitals in $Cu(PH_3)$.[24]

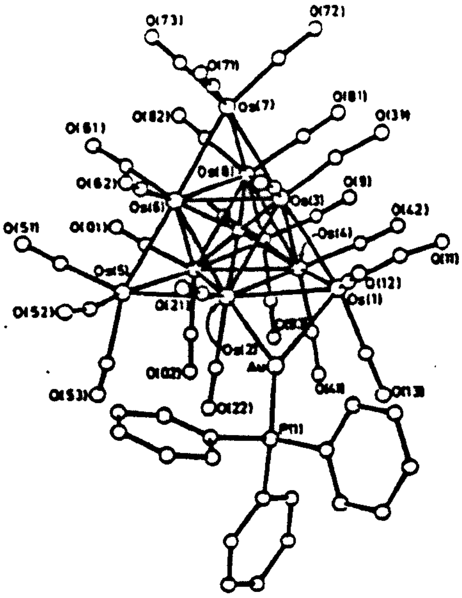

Figure 1.1.2(b).[33]

$[AuOs_{10}C(CO)_{24}(PPh_3)]^-$

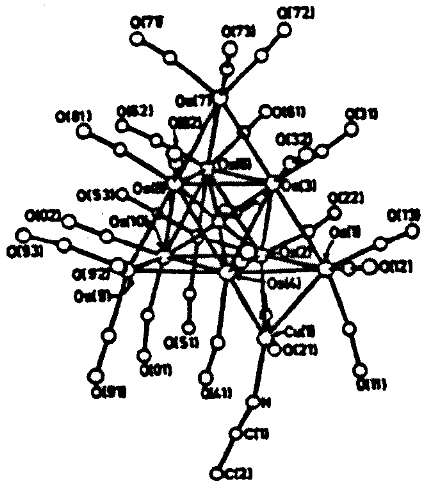

Figure 1.1.2(c).[33]

$[CuOs_{10}C(CO)_{24}(NCMe)]^-$.

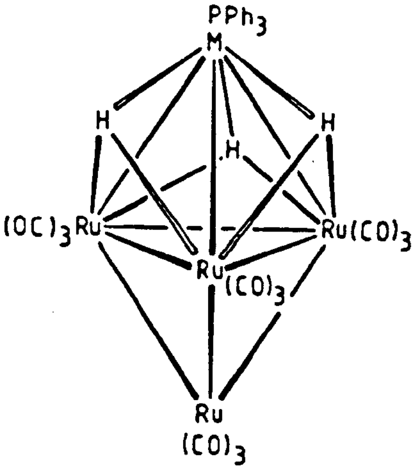

Figure 1.1.2(d)

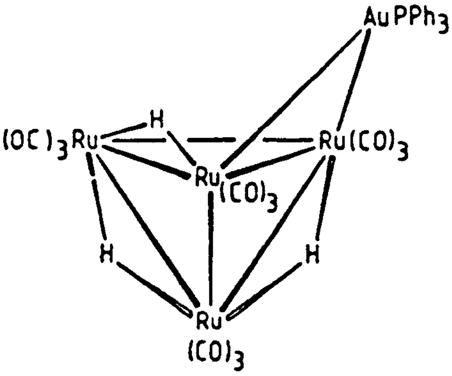

Figure 1.1.2(e)

Proposed structures[34] for

$[MRu_4H_3(CO)_{12}(PPh_3)]$ and $[AuRu_4H_3(CO)_{12}(PPh_3)]$.

[M = Cu or Ag]

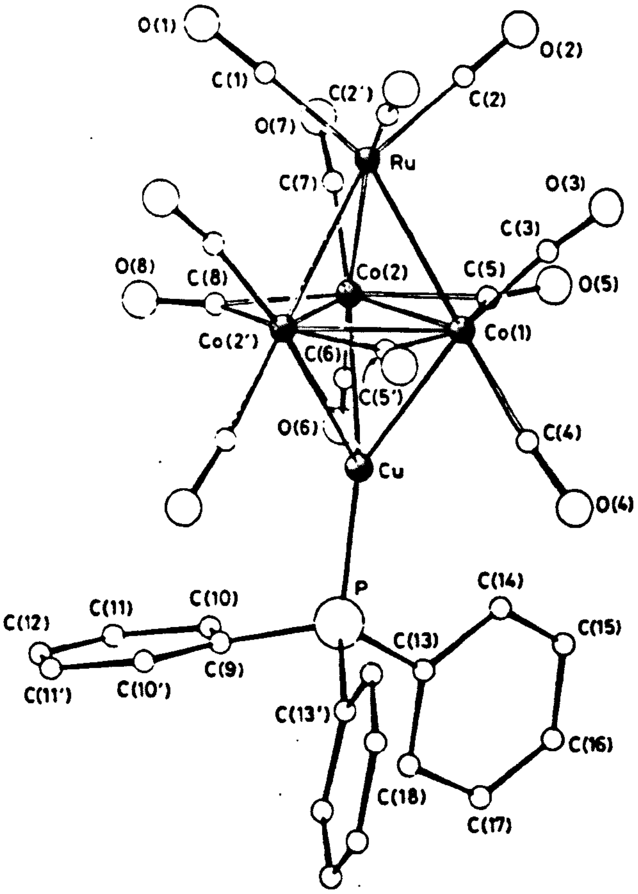

Figure 1.1.2(f). Molecular structure of $[CuRuCo_3(CO)_{12}(PPh_3)]$.[35]

A

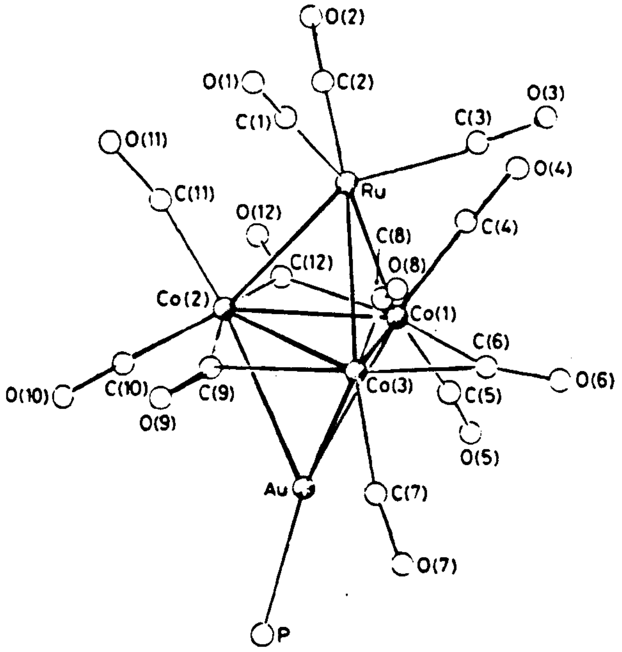

Figure 1.1.2(f). Molecular structure of [AuRuCo$_3$(CO)$_{12}$(PPh$_3$)].[35]

B

Section 1.1.3 Limitations of the isolobal relationship between the $Au(PR_3)$ group and the hydrido ligand.

Although a direct isolobal connection between the hydrido ligand and the $Au(PR_3)$ group was evident in many structures containing a single gold atom, it was recognised that this relationship could not cover all cases. For example, the gold triphenyl phosphine group in $[AuFe_3(\mu_3\text{-HC=NBu}^t)(CO)_9(PPh_3)]$[36] was found to bridge a different edge of a trigonal planar Fe_3 unit to that bridged by the hydrogen atom in $[Fe_3(\mu\text{-H})(\mu_3\text{-MeC=NH})(CO)_9]$,[37] {Figure 1.1.3(a)}. The cluster dianion $[Re_7C(\mu_3\text{-H})(CO)_{21}]^{2-}$ was found to exist as two isomers in solution,[38] and although the predominant isomer had the hydrido ligand capping the same Re_3 face as the $Au(PPh_3)$ group in the gold analogue $[AuRe_7C(CO)_{21}(PPh_3)]^{2-}$, the minor isomer had the hydrido ligand capping a different Re_3 face.

Importantly, the breakdown of the isolobal relationship became more apparent with structural evidence supporting interstitial sites for hydrido ligands in high nuclearity cluster compounds. For example, from both the ^1H n.m.r. and X-ray data for the carbido(hydrido)decaosmium cluster $[HOs_{10}C(CO)_{24}]^-$, McPartlin and co-workers concluded that the H-atom in this cluster was occupying an interstitial site in one of the four tetrahedral caps (section 3.1).[39] In contrast, for the related gold-osmium cluster $[AuOs_{10}C(CO)_{24}(PPh_3)]^-$, X-ray diffraction study established that the $Au(PPh_3)$ unit bridged an outer edge of a capping tetrahedron.[33] The structural characterisation of the above clusters illustrated that in certain cases it was impossible to maintain the isolobal relationship, simply due to the steric and electronic differences between the two. Further difficulties in relating the isolobal connection between metal clusters containing Au(PR_3) units and their hydrido counterparts, became noticeable in heteronuclear clusters containing more than one Au(PR_3) unit incorporated into the metal polyhedron (section 1.1.5). From theoretical studies of bonding in homonuclear cluster compounds of gold, Mingos[23] reported that when more than one gold atom was present in a cluster there was a pronounced tendency towards formation of gold-gold bonds, which was evident for example, in the centred icosahedral gold cluster $[Au_{13}(PMe_2Ph)_{10}Cl_2][PF_6]_3$.[40]

The presence of a gold-gold bond in a mixed-metal cluster was first reported by Raithby and co-workers with the X-ray analysis of the di-gold osmium cluster $[Au_2Os_4(H)_2(CO)_{12}(PPh_3)_2]$.[41] The four osmium atoms defined a distorted tetrahedron, with one edge doubly bridged by the two Au(PPh_3) groups, resulting in a direct Au-Au bond, {Figure 1.1.3(b)}. In contrast, the solid state structure of the isolobally related hydrido analogue,[14] $[Os_4(\mu\text{-}H)_4(CO)_{12}]$ described a tetrahedron of osmium atoms, with the four hydrogen atoms bridging four of the six longer Os-Os bonds respectively. Therefore, unlike the situation for compounds containing a single Au(PR_3) unit, cases of gold-phosphine fragments occupying similar positions to those of the isolobal hydrido ligand in related hydrido-metal clusters were found to be exceptions rather than the normal rule for clusters containing more than one gold atom. However, in some cases the structural relationship was still found to hold. For example, in the di-gold tri-osmium cluster, $[Au_2Os_3(CO)_{10}(PPh_3)_2]$ the two Au(PPh_3) groups were found to bridge the same edge of the Os_3 triangle forming a 'butterfly' arrangement analogous to the bonding of the two hydrido ligands in the di-hydrido cluster $[Os_3(\mu\text{-}H)_2(CO)_{10}]$, {Figure 1.1.3(c)}.[42] However, the fact that the hydrido ligand could not be involved in similar bonding interactions to those which were found to occur between adjacent $Au(PR_3)$ groups meant that when more than one $Au(PR_3)$ fragments were directly bonded in heteronuclear metal clusters, the stereochemical and bonding analogy with H was not necessarily observed.

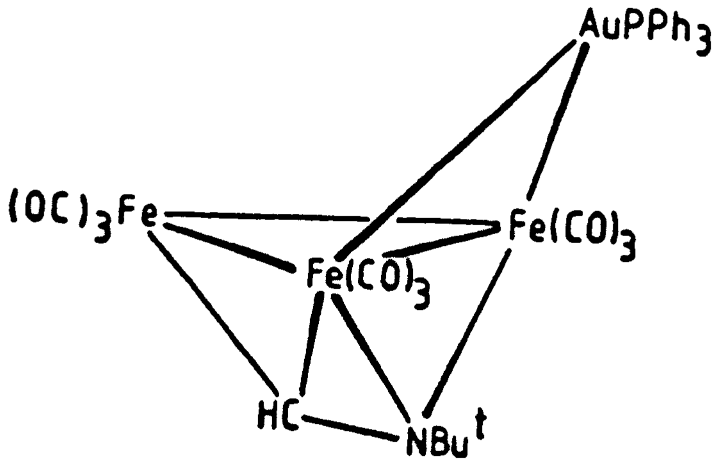

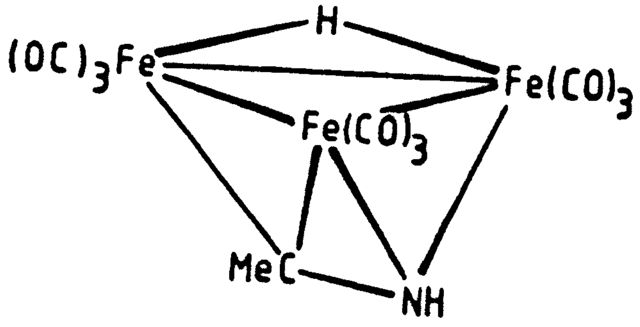

Figure 1.1.3(a). The structures of $[AuFe_3(\mu_3\text{-}HC{=}NBu^t)(CO)_9(PPh_3)]$[36] and $[Fe(\mu\text{-}H)(\mu_3\text{-}MeC{=}NH)(CO)_9]$.[37]

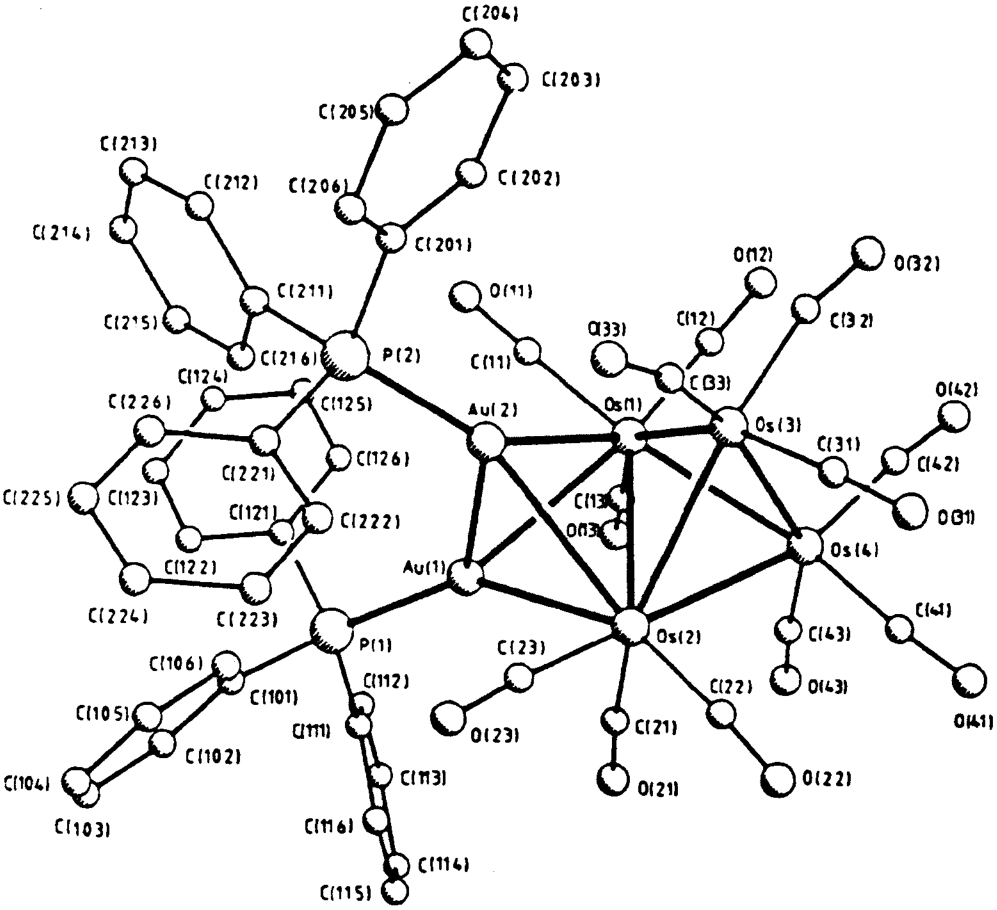

Figure 1.1.3(b). Molecular structure of $[Au_2Os_4(H)_2(CO)_{12}(PPh_3)_2]$.[41]

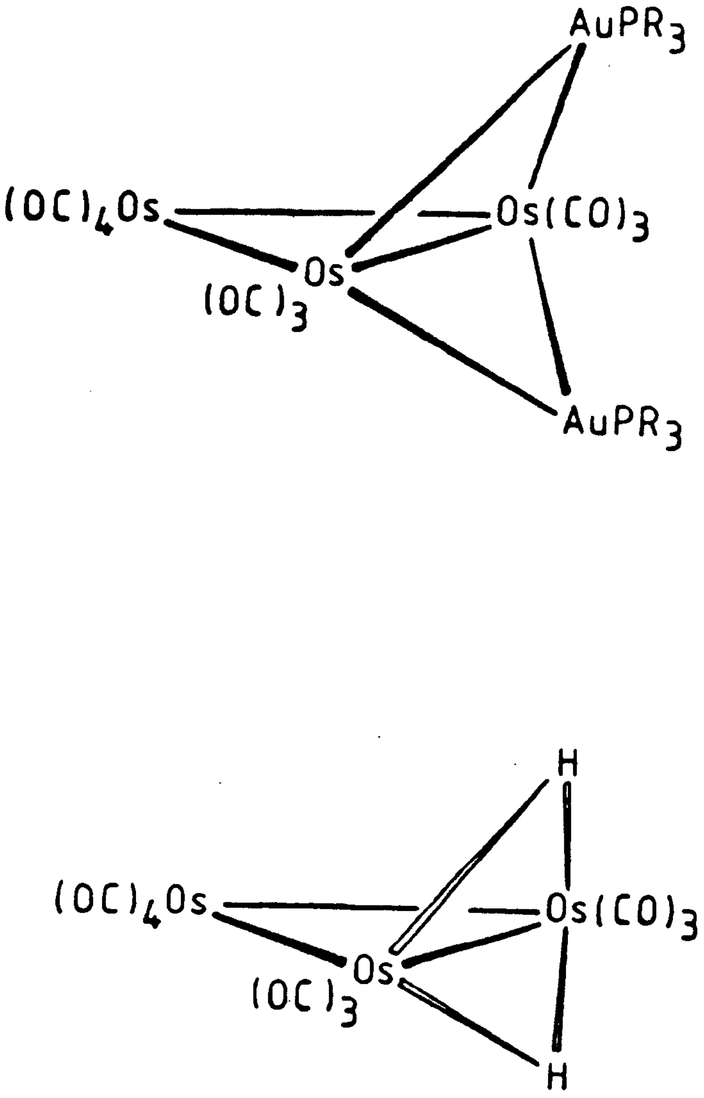

Figure 1.1.3(c). The structures of the clusters $[Au_2Os_3(CO)_{10}(PR_3)_2]$ [R = Ph or Et] and $[Os_3(\mu\text{-}H)_2(CO)_{10}]$, showing the isolobal relationship between the edge-bridging $Au(PR_3)$ units and the hydrido ligands.[42]

Section 1.1.4. The bonding modes of the Group IB metal organophosphines, M(PR_3) [M = Cu, Ag, or Au; R = alkyl or aryl] in mixed-metal clusters.

Only in the last three years have investigations of the chemistry of heteronuclear clusters containing copper and silver monodentate organophosphines bonded directly to transition metals started to develop. In contrast analogous compounds containing Au(PR_3) groups have been structurally characterised and studied far more extensively. Mixed-metal clusters with one M(PR_3) unit forming a part of the metal polyhedron can be divided into structural frameworks with the Group IB metal phosphines adopting either, an edge-bridging (-μ_2) site,

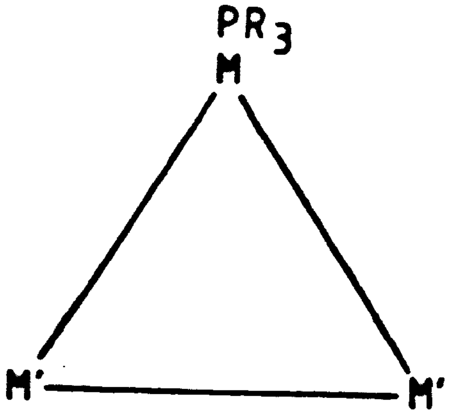

or a face capping (-μ_3) bonding mode.

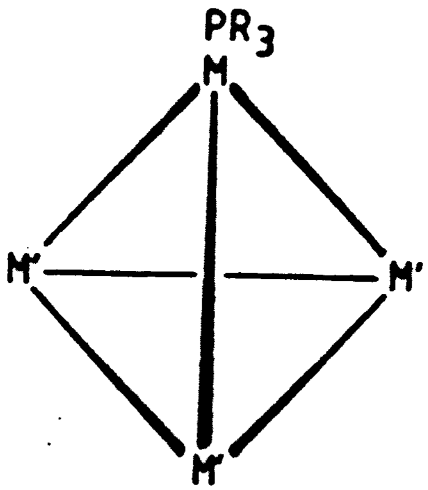

(a) Mixed-metal clusters containing one Cu(PR_3) group.

One of the early examples of a mixed-metal cluster with an edge-bridging Cu(PR_3) group was reported by Raithby and co-workers with the X-ray structural analysis of the tetranuclear cluster $[CuOs_3(\mu\text{-}H)_3(CO)_{10}(PPh_3)]$.[43] The three Os atoms were found to lie at the vertices of an isosceles triangle, with the longer edge bridged by the Cu(PPh_3) unit forming a 'butterfly' arrangement, {Figure 1.1.4(a)}. Further examples of reported X-ray structures of mixed-metal clusters describing a μ_2-bonding mode for the Cu(PR_3) unit include,

$[CuFe_3(\mu\text{-}CMe)(CO)_{10}(PPh_3)]$[44]
$[CuW_2(\mu_3\text{-}CC_6H_4Me\text{-}4)(CO)_4(PPh_3)(\eta\text{-}C_5H_5)]$[45]
$[CuRu_3(CO)_9(C_2Bu^t)(PPh_3)]$[46]
$[CuRu_3(\mu_3\text{-}PhPCH_2PPh_2)(CO)_9(PPh_3)]$[47]

The X-ray structure analysis of the pentanuclear cluster $[N(PPh_3)_2][CuFe_4(CO)_{13}(PPh_3)]$ described one of the early examples of a mixed-metal cluster with a face-capping Cu(PPh_3) group.[48,49] The four Fe atoms formed a tetrahedron with the copper atom capping a triangular Fe_3 face, {Figure 1.1.4(b)}. Further examples of reported crystal structures of heteronuclear clusters with a μ_3-Cu(PR_3) group include,

$[PMePh_3][CuOs_{11}C(CO)_{27}(NCMe)]$[50]
$[CuRu_4(\mu_3\text{-}H)_3(CO)_{12}(PMePh_2)]$[46]
$[CuCo_3Ru(CO)_{12}(PPh_3)]$[35]
$[CuOs_4\{\mu_3\text{-}N(CO)Me\}(CO)_{12}(PPh_3)]$[51]
$[PMePh_3][CuOs_{10}C(CO)_{24}(NCMe)]$[33]

(b) Mixed-metal clusters containing one $Ag(PR_3)$ group.

Although several mixed-metal clusters containing a single $Ag(PPh_3)$ unit have been synthesised, isolated and studied by i.r. and n.m.r. spectroscopic methods, reports of crystal structures remain minimal. Table 1.1.4(a) lists examples of structures of heteronuclear clusters studied by i.r. and n.m.r. techniques which infer edge-bridging bonding modes for the $Ag(PR_3)$ unit, and those in which a μ_3-$Ag(PR_3)$ group have been proposed are listed in Table 1.1.4(b).

Table 1.1.4(a).

$[AgMn_2(\mu\text{-}PPh_2)(CO)_8(PEt_3)]^{52}$

$[AgRu_3(\mu\text{-}H)(\mu_3\text{-}PPh)(CO)_9(PEt_3)]^{53}$

$[AgOs_3(\mu\text{-}CH{=}CHPh)(CO)_9(PPh_3)]^{54}$

$[AgFe_3(\mu\text{-}COMe)(CO)_{10}(PPh_3)]^{46}$

$[AgRu_3(CO)_9(C_2Bu^t)(NCMe)]^{46}$

$[AgRu_3(\mu_3\text{-}PhPCH_2PPh_2)(CO)_9(PPh_3)]^{47*}$

$[AgOs_6P(CO)_{18}(PPh_3)]^{55}$

$[AgM_2\{\mu\text{-}(EtO)_2POP(OEt)_2\}_n(\mu\text{-}Br)(CO)_{8-2n}(PPh_3)][M = Mn \text{ or } Re;\ n = 1 \text{ or } 2]^{56}$

$[AgRu_3(\mu\text{-}H)(\mu_3\text{-}S)(CO)_8L(PPh_3)][L = CO \text{ or } PPh_3]^{46}$

$[AgPt_2(\mu_3\text{-}S)(CO)(PPh_3)_4][PF_6]^{57}$

* crystal structure reported.

Table 1.1.4(b).

$[NMe_3(CH_2Ph)][AgRh_6C(CO)_{15}(PEt_3)]^{58}$

$[NEt_4]_2[AgRe_7C(CO)_{21}(PPh_3)]^{59}$

$[AgRu_4(\mu_3\text{-}H)_3(CO)_{12}(PPh_3)]^{34}$

$[AgPt_3(\mu_3\text{-}CO)_3(PPh_3)_5][ClO_4]^{60*}$

* crystal structure reported.

(c) Mixed-metal clusters containing one $Au(PR_3)$ group.

One of the early examples of a mixed-metal cluster containing an edge-bridging $Au(PR_3)$ unit was reported by Nyholm and co-workers, with the preliminary X-ray analysis of the gold osmium cluster $[AuOs_3(\mu\text{-}X)(CO)_{10}(PPh_3)]$ [X = Cl or Br].[8] The framework of the complexes described an Os_3 triangle with the halogen and the gold atom doubly bridging one Os-Os vector, {Figure 1.1.4(c)}. Table 1.1.4(c) lists further examples of X-ray structures of heteronuclear cluster compounds with an edge-bridging $Au(PR_3)$ unit.

Table 1.1.4(c).

$[AuOs_3(\mu\text{-}SCN)(CO)_{10}(PPh_3)]$[26]

$[AuOs_3(\mu\text{-}H)(CO)_{10}(PPh_3)]$[26,54,61]

$[AuOs_4(\mu\text{-}H)_3(CO)_{12}(PEt_3)]$[12]

$[AuOs_4(\mu\text{-}H)(CO)_{13}(PEt_3)]$[12]

$[AuFe_4C(\mu\text{-}H)(CO)_{12}(PPh_3)]$[62]

$[AuFe_3(\mu_3\text{-}HC{=}NBu^t)(CO)_9(PPh_3)]$[63]

$[AuRu_3(\mu\text{-}H)(\mu_3\text{-}S)(CO)_9(PPh_3)]$[64-66]

$[AuRu_3(\mu\text{-}COMe)(CO)_{10}(PPh_3)]$[67]

$[AuRu_3(\mu\text{-}H)_2(\mu_3\text{-}COMe)(CO)_9(PPh_3)]$[67,68]

$[AuRu_4(\mu_3\text{-}H)(\mu\text{-}H)_2(CO)_{12}(PPh_3)]$[69,70]

$[AuRu_5C(CO)_{13}(\mu\text{-}I)(PPh_3)]$[71]

$[AuRu_5C(CO)_{14}(\mu\text{-}Br)(PPh_3)]$[71]

$[AuRu_5C(CO)_{15}Cl(PPh_3)]$[72]

$[AuOs_3(CO)_8(2\text{-}NHC_5H_4N)(PPh_3)_2]$[73]

$[AuPtW(\mu_3\text{-}CC_6H_4Me\text{-}4)(CO)_2(PMe_3)_3(\eta\text{-}C_5H_5)][PF_6]$[74]

$[AuMn_2(\mu\text{-}PPh_2)(CO)_8(PMe_2Ph)]$[52]

$[AuCoFeRu(\mu_3\text{-}X)(CO)_9(PPh_3)]$[X = S or PMe][75]

$[AuRu_3(\mu\text{-}H)(\mu_3\text{-}PPh)(CO)_9(PMe_2Ph)]$[53]

$[AuRu_4C(\mu-H)(CO)_{12}(PPh_3)]$[76]
$[AuRu_4C(\mu-I)(CO)_{12}(PEt_3)]$[76]
$[AuRu_5C(CO)_{13}(PPh_3)(n-C_5H_5)]$[77]
$[AuRu_5C(CO)_{14}(\mu-n-MeCO)(PPh_3)]$[71,77]
$[AuFe_2(\mu-C_{11}H_{19}S)(CO)_6(PPh_3)]$[78]
$[AuFe_4(COMe)(CO)_{12}(PEt_3)]$[48,49]
$[AuRu_3(CO)_9(C_2Bu^t)(PPh_3)]$[79]
$[AuRu_3(\mu_3-SBu^t)(CO)_9(PPh_3)]$[65]
$[AuRu_5C(CO)_{13}(NO)(PEt_3)]$[80]
$[AuOs_3(\mu-CH{=}CHR)(CO)_{10}(PPh_3)][R = C_6F_5$ or $Ph]$[54]
$[AuRh_2(\mu-CO)(\mu-Ph_2PCH_2PPh_2)(PPh_3)(\eta-C_5H_5)_2][BF_4]$[81]
$[AuCoFe_2(\mu_3-COMe)(u_3-CO)(CO)_6(PPh_3)(\eta-C_5H_5)]$[82]
$[AuRu_3(\mu_3-PhPCH_2PPh_2)(CO)_9(PPh_3)]$[47]
$[AuRu_3(\mu-Cl)(CO)_{10}(PPh_3)]$[83]
$[AuOs_3(CO)_{10}(C_2Ph)(PMe_2Ph)]$[84]
$[AuOs_6P(CO)_{18}(PPh_3)]$[55]
$[PMePh_3][AuOs_{10}C(CO)_{24}(PPh_3)]$[33]
$[AuMn_2\{\mu-(EtO)_2POP(OEt)_2\}(\mu-Br)(CO)_6(PPh_3)]$[56]
$[AuRe_2(\mu-H)_3H_4(PPh_3)_5]$[85]
$[AuFeRu_3(\mu_4-N)(CO)_{12}(PPh_3)]$[86]
$[AuCo_2Fe(\mu_3-CPh)(CO)_9(PPh_3)]$[87]
$[AuPt_2(\mu_3-S)(CO)(PPh_3)_4][PF_6]$[57]

The first crystal structure of a heteronuclear cluster with an Au(PR$_3$) group adopting a μ_3-bonding site was reported for the tetranuclear complex, [AuFeCo$_3$(CO)$_{12}$(PPh$_3$)].[2] The structure was found to consist of a trigonal bi-pyramidal metal core, with the gold atom at one apical position, capping a triangular Co$_3$ face, {Figure 1.1(c)}. Table 1.1.4(d) presents numerous examples of reported X-ray structures of mixed-metal clusters, with one Au(PR$_3$) group adopting a face-capping position.

Table 1.1.4(d).

$[AuRu_6C(CO)_{15}(NO)(PPh_3)]$[88]

$[AuIr_3H_6(NO)_3(Ph_2P(CH_2)_2PPh_2)_3][BF_4]$[89]

$[AuCoRu_3(\mu\text{-}CO)_3(CO)_{10}(PPh_3)]$[90]

$[AuPt_3(\mu\text{-}CO)_3\{P\text{-}(cyclo\text{-}C_6H_{11})_3\}_4][PF_6]$[91]

$[AuRu_5C(CO)_{13}(NO)(PEt_3)]$[80]

$[AuCo_{3-x}Rh_xRu(CO)_{12}(PPh_3)][x = 1\text{-}3]$[92]

$[PPh_4][AuRe_3(\mu\text{-}H)_3(CO)_9(PPh_3)]$[36]

$[AsPh_4]_2[AuRe_7C(CO)_{21}(PPh_3)]$[38]

$[AuCo_3Ru(CO)_{12}(PPh_3)]$[35]

$[AuOs_4\{\mu_3\text{-}N(CO)Me\}(CO)_{12}(PPh_3)]$[51]

$[AuPt_3(\mu\text{-}CO)_2(\mu\text{-}SO_2)\{P(cyclo\text{-}C_6H_{11})_3\}_4][PF_6]$[91]

$[AuPt_3(\mu\text{-}SO_2)_2(\mu\text{-}Cl)\{P(cyclo\text{-}C_6H_{11})_3\}_3\{P(C_6H_4F\text{-}4)_3\}]$[91]

$[AuPt_3(\mu\text{-}CO)_3(PPh_3)_5][NO_3]$[93]

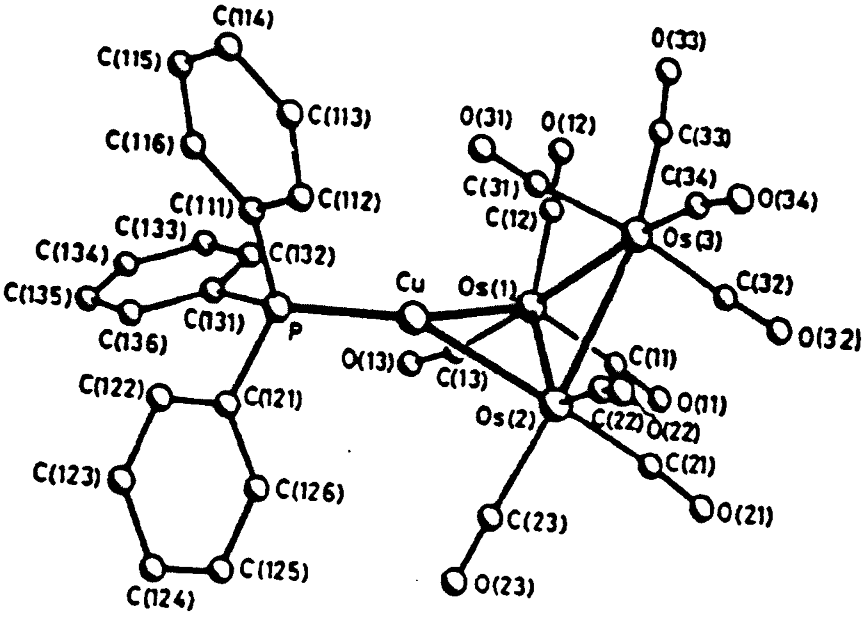

Figure 1.1.4(a). Molecular structure of [CuOs$_3$(μ-H)$_3$(CO)$_{10}$(PPh$_3$)].[4

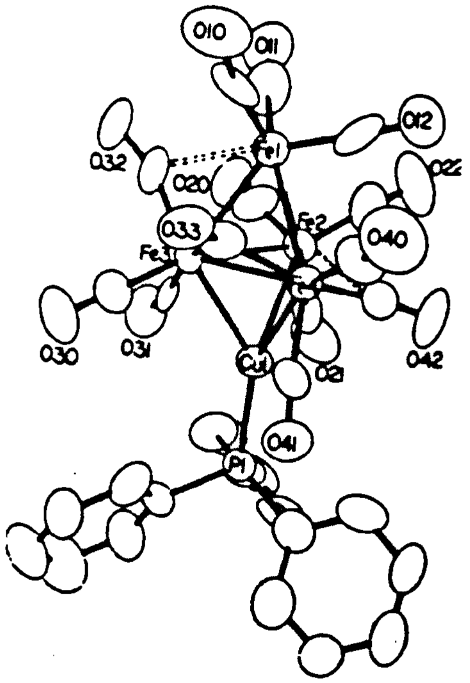

Figure 1.1.4(b). Molecular structure of [CuFe$_4$(CO)$_{13}$(PPh$_3$)]$^-$.[48,49]

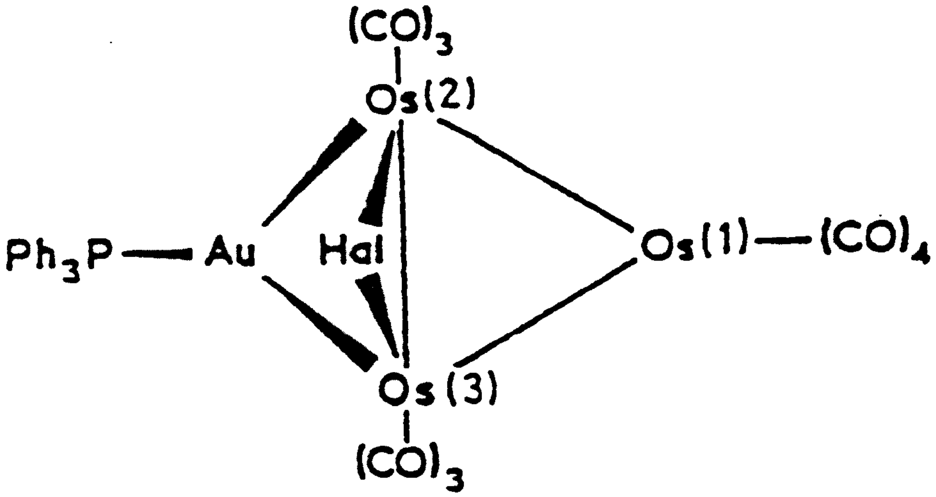

Figure 1.1.4(c). Structure of the tetranuclear cluster $[AuOs_3(\mu\text{-Hal})(CO)_{10}(PPh_3)]$ [Hal = Cl or Br].[8]

Section 1.1.5. Mixed-metal clusters containing two M(PR_3) units [M = Cu, Ag or Au; R = alkyl or aryl].

Heteronuclear clusters having two M(PR_3) units forming a part of a mixed-metal polyhedron can be suitably classified into four structural types:

(1) Heteronuclear clusters in which M(PR_3) groups are edge-bridging with no contact between the Group IB metal atoms.

There are only two known examples of copper and silver containing mixed-metal clusters belonging to this structural group which have been characterised by i.r. studies,

$[Cu_2Mn_2\{\mu-(EtO)_2POP(OEt)_2\}(CO)_6(PPh_3)_2]$[94] and

$[Ag_2Mn_2\{\mu-(EtO)_2POP(OEt)_2\}(CO)_6(PPh_3)_2]$.[94]

In contrast several heteronuclear clusters containing two Au(PR_3) groups have been characterised by X-ray diffraction studies. One of the early examples of a reported crystal structure with two Au(PR_3) groups adopting edge-bridging positions in the solid state, with no contact between the gold atoms, was established for $[Au_2Os_3(CO)_{10}(PEt_3)_2]$.[42] The molecule was found to exhibit C_2 symmetry with a 2-fold axis passing through Os(1) and bisecting the Os(2)-Os(2') bond {Figure 1.1.5(a)}. The two Au(PEt_3) groups doubly bridged the same edge of the Os_3 triangle, with no direct Au-Au interaction. Further examples of reported crystal structures of mixed-metal clusters, having two Au(PR_3) groups edge-bridging with no contact between the gold atoms include,

$[Au_2Os_5C(CO)_{14}(PPh_3)_2]$[95]
$[Au_2Ru_4C(CO)_{12}(PMe_2Ph)_2]$[76]
$[Au_2Ru_6C(CO)_{16}(PMePh_2)_2]$[96]
$[Au_2Ru_5WC(CO)_{17}(PEt_3)_2]$[96]
$[Au_2Re_4H_6(PMe_2Ph)_4(PPh_3)_2]$.[97]

(2) Mixed-metal clusters in which two $M(PR_3)$ units adopt edge-bridging positions with a direct bond between the Group IB metal atoms.

For this structural type, only cluster compounds with two $Au(PR_3)$ groups have been isolated in the solid state and analysed by X-ray diffraction methods. The X-ray structure of the pentanuclear gold-ruthenium cluster $[Au_2Ru_3(\mu\text{-}H)(\mu_3\text{-}COMe)(CO)_9(PPh_3)_2]$ described an asymmetric square pyramidal metal core, with the two $Au(PPh_3)$ groups, effectively bridging two adjacent edges of an Ru_3 triangle, with a resulting Au-Au bond of 3.176(1) Å {Figure 1.1.5(b)}.[64,67,68] Other related clusters exhibiting similar arrangements of two $Au(PR_3)$ units include, $[Au_2Os_3(CO)_{10}(PPh_3)_2]$[42] and $[Au_2Os_4(CO)_{13}(PEt_3)_2]$.[98]

(3) Heteronuclear cluster compounds containing two face-capping $M(PR_3)$ units with no close contact between the two Group IB metal atoms.

Although for this structural type, several heteronuclear clusters have been studied by spectroscopic techniques, reports of single crystal X-ray analyses are limited:

(3a) Copper clusters,

$[Cu_2Rh_6(CO)_{15}(NCMe)_2]$[99]

$[Cu_2Ru_6(CO)_{18}(C_6H_5Me)_2]$[100]

$[Cu_2Ru_4(\mu\text{-}CO)_3(CO)_{10}(PPh_3)_2]$.[101]

(3b) Silver clusters,

$[Ag_2Ru_4(\mu\text{-}CO)_3(CO)_{10}(PPh_3)_2]$.[101]

The crystal structures of the related analogues $[M_2Ru_4(\mu\text{-}CO)_3(CO)_{10}(PPh_3)_2]$ [M = Cu or Ag] reported by McPartlin and

Adatia established a tetrahedron of ruthenium atoms, with two opposite triangular faces capped by the $M(PPh_3)$ units, resulting in no contact between the Group IB metal atoms, {Figure 1.1.5(c)}.[101]

(c) Gold clusters.

The reaction of the bi-capped octahedral dianion $[Os_8(CO)_{22}]^{2-}$ with $AuPPh_3Cl$ was reported to give $[Au_2Os_8(CO)_{22}(PPh_3)_2]$, and subsequent X-ray analysis carried out by Raithby, established that the anionic metal geometry had changed with the resulting Os_8Au_2 framework consisting of two octahedra sharing one edge, but with the equatorial Au-Au bond missing, {Figure 1.1.5(d)}.[102] The only other reported crystal structures with two $Au(PR_3)$ units adopting capping positions with no contact between the gold atoms has been for $[Au_2Os_4(CO)_{12}(PMePh_2)_2]$[98] and the gold-platinum cluster $[Au_2Pt_3(\mu\text{-}SO_2)_2(\mu\text{-}Cl)\{P(cyclo\text{-}C_6H_{11})_3\}_3\{P(C_6H_4F\text{-}4)_3\}_2][PF_6]$.[103]

(4) Mixed-metal clusters containing two face capping $M(PR_3)$ units with the hetero-metal atoms in close contact.

This metal framework seems to be common in cluster compounds having two $Au(PR_3)$ groups. However, several compounds containing $Cu(PR_3)$ and $Ag(PR_3)$ units have been studied using i.r. and n.m.r. spectroscopic techniques:

(4a) Copper clusters,

$[Cu_2Ru_4(\mu_3\text{-}H)_2(CO)_{12}(PPh_3)_2]$[104*]

$[Cu_2Ru_3(\mu_3\text{-}S)(CO)_9(PPh_3)_2]$[105]

$[CuAgRu_4(\mu_3\text{-}H)_2(CO)_{12}(PPh_3)_2]$[106]

$[CuAuRu_4(\mu_3\text{-}H)_2(CO)_{12}(PPh_3)_2]$.[106]

(4b) Silver clusters,

$[Ag_2Ru_4(\mu_3\text{-}H)_2(CO)_{12}(PPh_3)_2]$[104*]

$[Ag_2Ru_4(\mu_3\text{-}S)(CO)_9(PPh_3)_2]$.[105]

* crystal structure reported

(4c) Gold clusters, (examples of reported X-ray structures)

$[Au_2Os_3S_2(CO)_{10}(PPh_3)_2]$[8]

$[Au_2Os_4(\mu\text{-}H)_2(CO)_{12}(PPh_3)_2]$[41]

$[Au_2Fe_3(\mu_3\text{-}S)(CO)_9(PPh_3)_2]$[107]

$[Au_2Ru_3(\mu_3\text{-}S)(CO)_9(PPh_3)_2]$[64-66]

$[Au_2Ru_3(\mu_3\text{-}S)(CO)_8(PPh_3)_2]$[64]

$[Au_2Ru_4(\mu_3\text{-}H)(\mu\text{-}H)(CO)_{12}(PPh_3)_2]$[104]

$[Au_2Co_2Ru_2(\mu\text{-}CO)_2(CO)_{10}(PPh_3)_2]$[107]

$[Au_2CoRu_3(\mu\text{-}H)(CO)_{12}(PPh_3)_2]$[90]

$[Au_2Ru_5WC(CO)_{17}(PEt_3)_2]$[96]

$[Au_2Ru_3(\mu_3\text{-}C{=}CHBu^t)(CO)_9(PPh_3)_2]$[108]

$[Au_2Ir_4(CO)_9(PEt_3)_2(\mu\text{-}PhPPPh)Ir_4(CO)_{11}]$[109]

The solid state structures of the mixed-metal cluster series $[M_2Ru_4(H)_2(CO)_{12}(PPh_3)_2]$ [M = Cu, Ag or Au], reported by Orpen and co-workers established similar capped trigonal bi-pyramidal metal cores.[104] The four ruthenium atoms formed a tetrahedron, with one $M(PPh_3)$ unit capping an Ru_3 face, with the second $M(PPh_3)$ group capping an adjacent MRu_2 face, resulting in a direct bond between the Group IB metal atoms, {Figure 1.1.5(e)}.

There have been few examples of heteronuclear cluster compounds containing two $Au(PR_3)$ units which do not belong to the structural classes (1)-(4) described above. For example, the X-ray structure of the di-gold hexanuclear cluster $[Au_2Fe_4(BH)(CO)_{12}(PPh_3)_2]$ reported by Housecroft and co-workers, established a Fe_4 'butterfly' with the boron atom interacting with all four Fe atoms.[110] One $Au(PPh_3)$ unit was found to cap an Fe_2B face and the other an AuFeB face, resulting in a direct bond between the two gold atoms, {Figure 1.1.5(f)}. The X-ray structure of the hexanuclear cluster $[Au_2Fe_4C(CO)_{12}(PEt_3)_2]$ reported by Raithby and co-workers, described an Au_2Fe_4 octahedron with an interstitial carbido atom with the two gold atoms in close contact.[62] The solid state structure of the heptanuclear cluster $[Au_2Fe_5C(\mu\text{-}CO)_3(CO)_{11}(PEt_3)_2]$ established a square pyramid of the five Fe atoms encapsulating the carbido atom.[111] One of the two $Au(PEt_3)$ groups adopted a μ_2-bridging site, whereas the other adopted a μ_4-bonding mode with no interaction between the two gold atoms, {Figure 1.1.5(g)}.

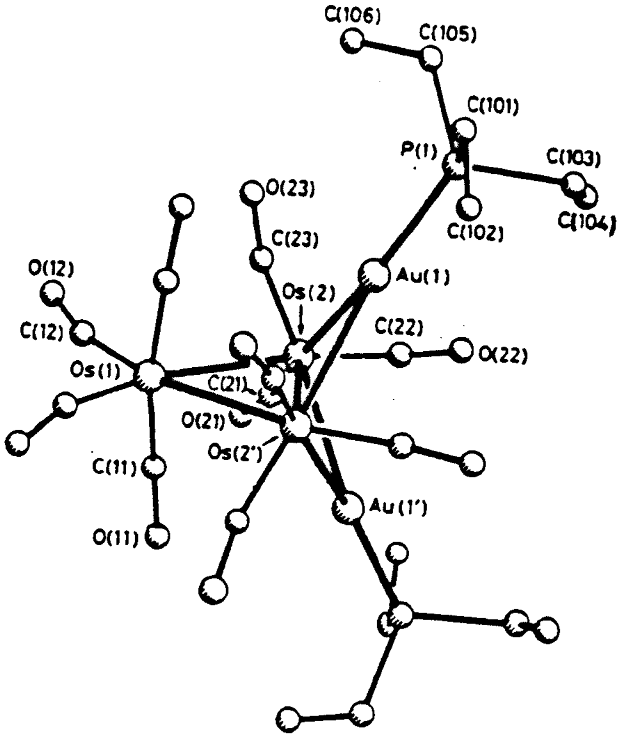

Figure 1.1.5(a). Molecular structure of $[Au_2Os_3(CO)_{10}(PEt_3)_2]$.[42]

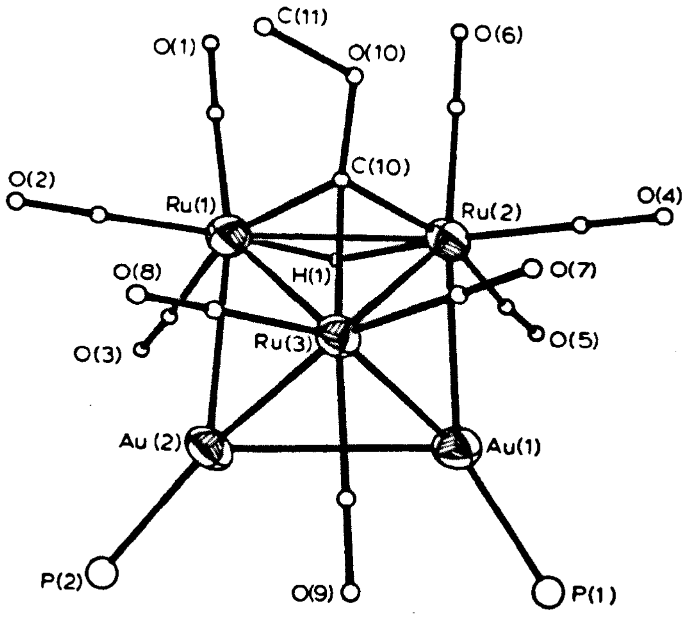

Figure 1.1.5(b). Molecular structure of $[Au_2Ru_3(\mu\text{-}H)(\mu_3\text{-}COMe)(CO)_9(PPh_3)_2]$.[64,67,68]

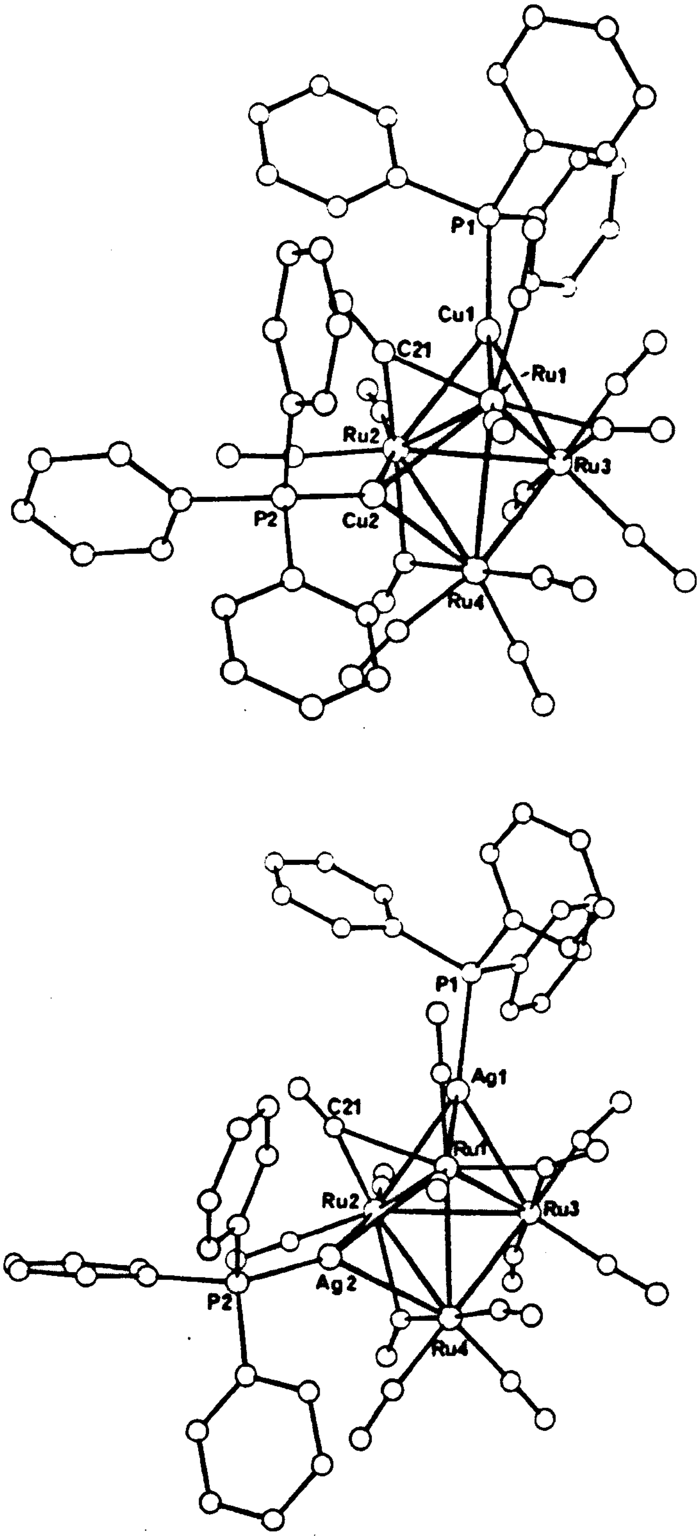

Figure 1.1.5(c). Molecular structures of $[M_2Ru_4(\mu\text{-CO})_3(CO)_{10}(PPh_3)_2]$ [M = Cu or Ag].[101]

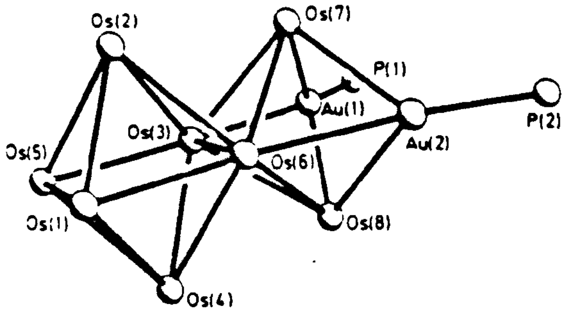

Figure 1.1.5(d). Metal core structure of $[Au_2Os_8(CO)_{22}(PPh_3)_2]$.[102]

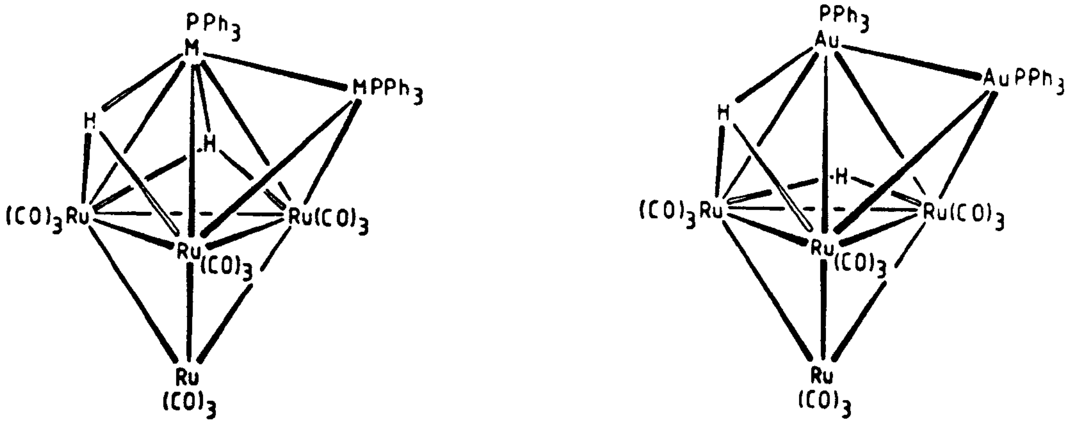

Figure 1.1.5(e). Molecular structure of $[M_2Ru_4(\mu_3\text{-}H)_2(CO)_{12}(PPh_3)_2]$ [M = Cu or Ag] and $[Au_2Ru_4(\mu\text{-}H)(\mu_3\text{-}H)(CO)_{12}(PPh_3)_2]$.[104]

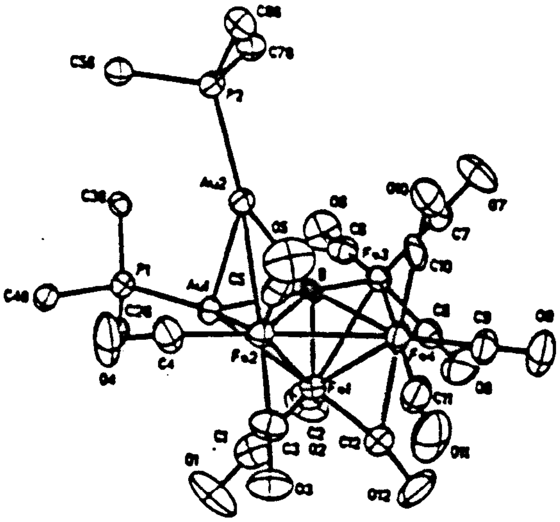

Figure 1.1.5(f). Molecular structure for the hexanuclear cluster $[Au_2Fe_4(BH)(CO)_{12}(PPh_3)_2]$.[110]

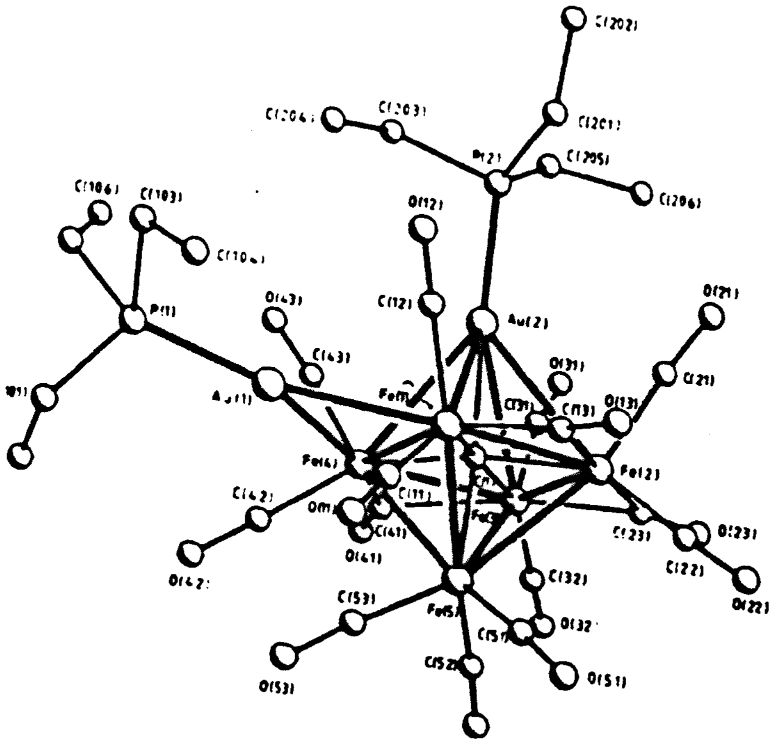

Figure 1.1.5(g). Molecular structure of $[Au_2Fe_5C(\mu\text{-}CO)_3(CO)_{11}(PEt_3)_2]$.[111]

Section 1.1.6. Mixed-metal clusters containing three $M(PR_3)$ groups.

Heteronuclear clusters having three monodentate $M(PR_3)$ groups incorporated into a mixed-metal polyhedron have been found to be restricted to compounds having three $Au(PR_3)$ units, apart from the tri-copper pentanuclear cluster $[Cu_3Ir_2H_6(NCMe)_3(PMe_2Ph)_6][PF_6]$ which adopts a trigonal bi-pyramidal Cu_3Ir_2 metal core with three equatorial Cu(NCMe) groups.[112] The tri-gold clusters can be classified into three different structural types:

(1) Three face-capping $Au(PR_3)$ groups with the gold atoms in contact, examples of reported crystal structures include,

$[Au_3Ru_3(\mu\text{-}COMe)(CO)_9(PPh_3)_3]$[67] {Figure 1.1.6(a)}

$[Au_3Ru_4(\mu_3\text{-}H)(CO)_{12}(PPh_3)_3]$[68,69,113]

$[Au_3Ru_3(\mu_3\text{-}C_{12}H_{15})(CO)_8(PPh_3)_3]$[66,114]

$[Au_3CoRu_3(CO)_{12}(PPh_3)_3]$.[90]

(2) Mixed-metal clusters containing a tetrahedral Au_3M unit [M = transition metal], examples of X-ray structures include,

$[Au_3V(CO)_5(PPh_3)_3]$[115] {Figure 1.1.6(b)}

$[Au_3RhH(CO)(PPh_3)_5][PF_6]$[116,117(a)]

$[Au_3ReH_2(PMe_2Ph)_3(PPh_3)_3]$[118]

$[Au_3ReH_3(PMe_2Ph)_3(PPh_3)_3][BF_4]$.[118]

(3) Mixed-metal clusters containing a planar or nearly planar Au_3M unit [M = transition metal], examples include,

$[Au_3ReH(PMe_2Ph)_3(PPh_3)_3]$[118] {Figure 1.1.6(c)}

$[Au_3Mn(CO)_4(PPh_3)_3]$[119]

$[Au_3Ir(NO)_3(PPh_3)_5][PF_6]$.[89]

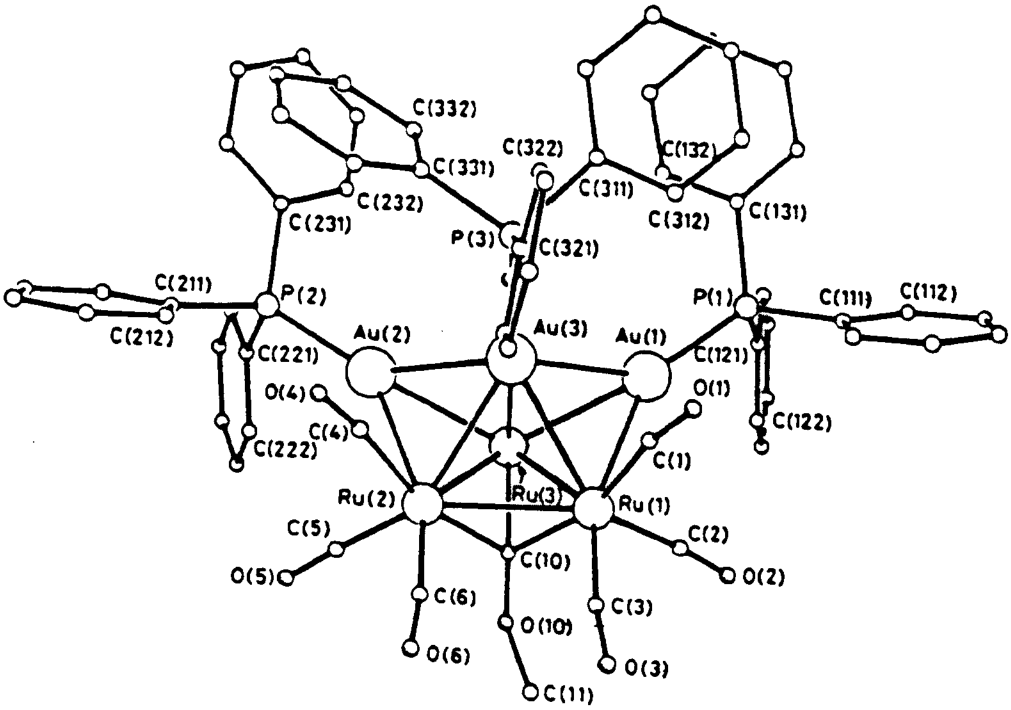

Figure 1.1.6(a). Molecular structure of $[Au_3Ru_3(\mu\text{-}COMe)(CO)_9(PPh_3)_3]$.[67]

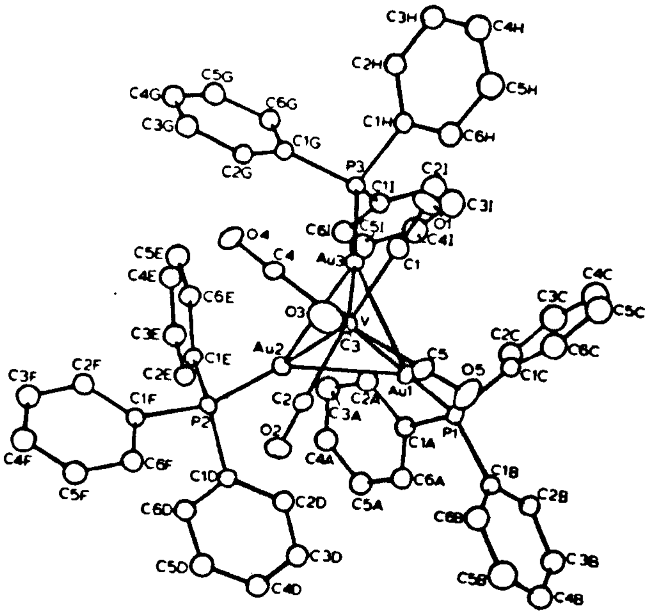

Figure 1.1.6(b). Molecular structure of $[Au_3V(CO)_5(PPh_3)_3]$.[115]

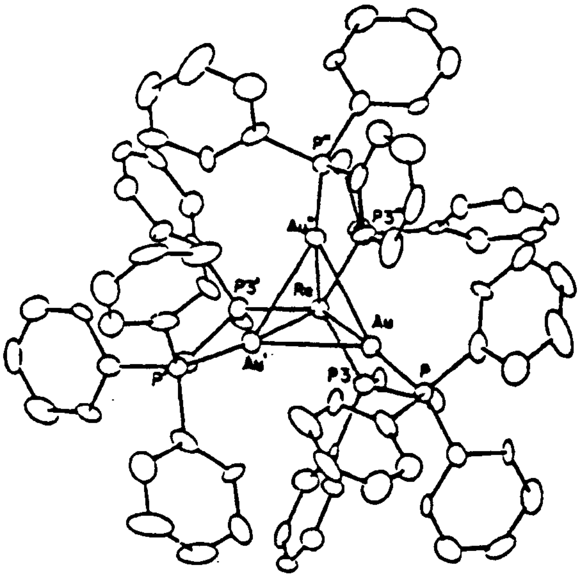

Figure 1.1.6(c). Molecular structure of [$Au_3ReH(PMe_2Ph)_3(PPh_3)_3$].[118]

Section 1.1.7. Mixed-metal clusters with more than three $M(PR_3)$ units [M = Cu, Ag, or Au; R = alkyl or aryl].

Heteronuclear clusters containing more than three $M(PR_3)$ fragments remain relatively rare adopting a wide variety of metal frameworks in the solid state.

(a) Clusters having four $M(PR_3)$ groups:

For example, the solid state structure of the tetra-gold cluster $[Au_4ReH_4\{P(C_6H_4Me\text{-}4)_3\}_2(PPh_3)_4][BPh_4]$ established an Au_3Re tetrahedron with the fourth $Au(PPh_3)$ group bridging one Au-Re edge, {Figure 1.1.7(a)}.[117(b)] The X-ray structure of the mixed-metal cluster $[Au_4Ir\ H_2(PPh_3)_6][BF_4]$ displayed an Au_4Ir trigonal bi-pyramid with the Ir atom occupying an equatorial site.[120]

(b) Clusters having five $M(PR_3)$ groups:

For example, the X-ray structure of the hexanuclear cluster $[Au_5ReH_4(PPh_3)_7][PF_6]_2$ described two Au_3Re tetrahedra, sharing a common Au-Re edge, {Figure 1.1.7(b)}.[116]

(c) Clusters containing six $M(PR_3)$ groups.

The solid state structure of the silver mixed-metal cluster $[Ag_6Fe_3(\mu_3\text{-}(Ph_2P)_3CH)(CO)_{12}]$ established an Ag_6 octahedron with $Fe(CO)_4$ units capping three Ag_3 faces, {Figure 1.1.7(c)}.[121] The gold-cobalt structure, $[Au_6Co_2(CO)_8(PPh_3)_4]$ displayed an Au_6 edge-sharing bi-tetrahedron with two Au atoms linked by $Co(CO)_4$ units.[122]

(d) Clusters containing more than six $M(PR_3)$ groups:

The crystal structure of the high nuclearity silver-gold cluster $[Ag_{12}Au_{13}Cl_6(PPh_3)_{12}]^{m+}$ illustrated the great versatility in the bonding modes of the $M(PR_3)$ units. The structure consisted of three interpenetrating icosahedral units sharing common pentagonal faces, with interstitial Au atoms encapsulated within, {Figure 1.1.7(d)}.123,124

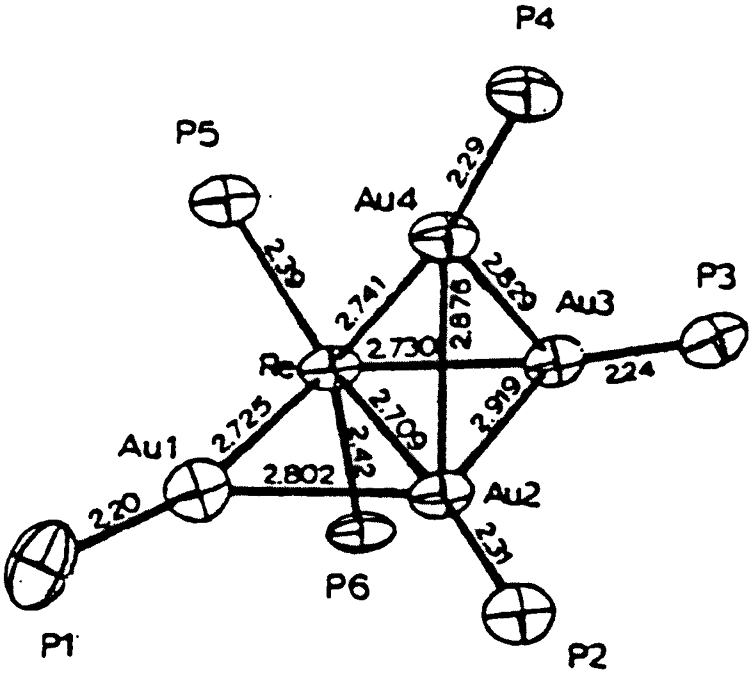

Figure 1.1.7(a). Metal core geometry for $[Au_4ReH_4\{P(C_6H_4Me-4)_3\}_2(PPh_3)_4][BPH_4]$.[117(b)]

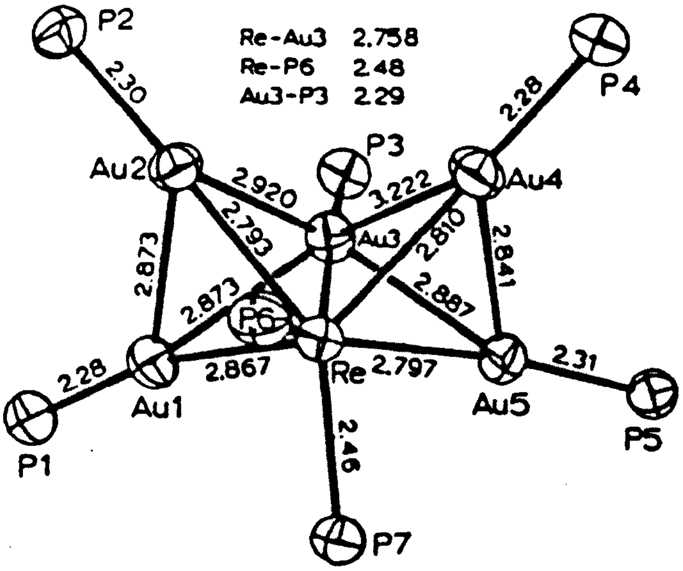

Figure 1.1.7(b). Metal core geometry for $[Au_5ReH_4(PPh_3)_7][PF_6]_2$.[116]

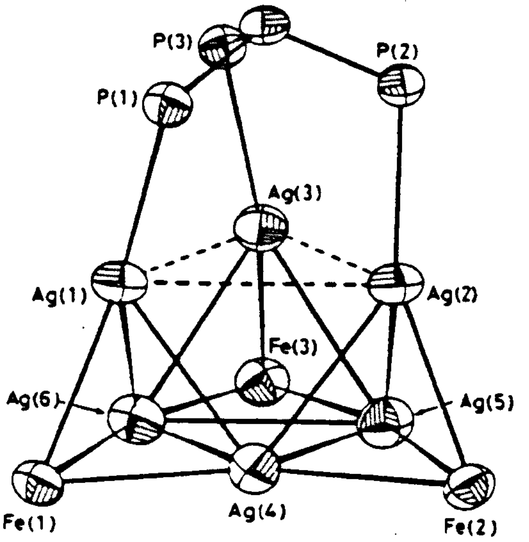

Figure 1.1.7(c). Molecular structure of $[Ag_6Fe_3(\mu_3\text{-}(Ph_2P)_3CH)(CO)_{12}]$.[121]

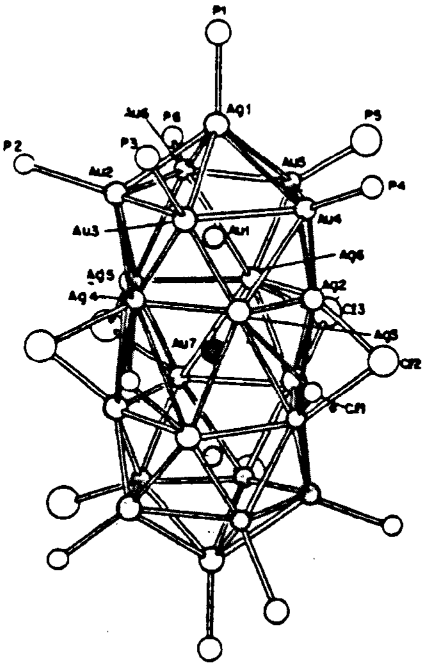

Figure 1.1.7(d). Molecular structure of $[Ag_{12}Au_{13}Cl_6(PPh_3)_{12}]$.[123,124]

Section 1.1.8. Differences in energy between edge-bridging and face capping bonding modes in heteronuclear cluster compounds with $M(PR_3)$ groups [M = Cu, Ag, or Au; R = alkyl or aryl].

In the last three years the growing interest in the chemistry of mixed-metal clusters containing Group IB metal phosphines has allowed the development of experimental evidence to support that the energy differences between face-capping ($-\mu_3$) and edge-bridging ($-\mu_2$) bonding modes adopted by $M(PR_3)$ units can be very small. A single crystal X-ray diffraction study of the hexanuclear cluster $[AuRu_5C(CO)_{13}(NO)(PEt_3)]$ reported by McPartlin and co-workers in 1985, revealed two independent molecules with different metal core geometries.[80] Both molecules adopted a basic Ru_5 square pyramid, with the $Au(PEt_3)$ group in one molecule capping a triangular Ru_3 face, whereas in the other it bridged a Ru-Ru edge, {Figure 1.1.8(a)}. Horwitz and co-workers in the same year reported[48,49] the existence of two isomeric forms of the cluster anions, $[MFe_4(CO)_{13}L]^-$ [M = Cu, L = PPh_3 or $CNC_6H_3Me_2$-2,6; M = Au, L = PPh_3 or PEt_3] in solutions. Isomer (1) was proposed to adopt a tetrahedron of iron atoms with one triangular face capped by the ML unit, {Figure 1.1.8(b)}. Isomer (2) was thought to adopt a metal framework consisting of an Fe_4 'butterfly' with the ML fragments edge-bridging the 'hinge' of the 'butterfly', {Figure 1.1.8(b)}. Interestingly, the solid state structures of the two copper-iron clusters exhibited metal cores postulated for isomer (1), and the two analogous gold-iron clusters adopted structures proposed for isomer (2).[48,49]

The presence of skeletal isomers has also been reported for several heteronuclear clusters containing two $M(PR_3)$ groups. For example, Lewis and co-workers reported the isolation of two isomeric forms of the hexanuclear cluster [$Au_2Os_4(\mu\text{-}H)_2(CO)_{12}(PR_3)_2$] [R = Ph or Et].[41] X-ray diffraction study for the major isomer estabished a metal core consisting of two tetrahedra sharing one Os-Os edge, {Figure 1.1.3(b)}. Unfortunately the structure of the minor isomer, as yet, is unknown. Recently, Sutherland and co-workers reported the presence of two structurally different isomers for the gold-rhenium cluster [$Au_2Re_2H_6(PMe_2Ph)_4(PPh_3)_2$].[97] The major isomer (1) was characterised by i.r. and n.m.r. studies, proposing a metal core with one Au(PPh_3) unit bridging a Re-Re bond and one edge of the trigonal planar $AuRe_2$ unit so formed, further bridged by the second Au(PPh_3) group, resulting in a direct Au-Au bond, {Figure 1.1.8(c)}. The minor isomer (2) was analysed by X-ray diffraction methods to exhibit the two Au(PPh_3) groups doubly bridging the Re-Re bond giving rise to a 'butterfly' arrangement, with no contact between the gold atoms.[97] McPartlin and Adatia also observed that the the formal replacement of two hydrido ligands in the related clusters [$M_2Ru_4(\mu_3\text{-}H)_2(CO)_{12}(PPh_3)_2$] by a -CO ligand in [$M_2Ru_4(\mu\text{-}CO)_3(CO)_{10}(PPh_3)_2$] [M = Cu or Ag] caused a marked difference in the bonding arrangement of the Group IB metal atoms on the Ru_4 tetrahedra.[101] The solid state structures of the hydrido clusters described capped trigonal bi-pyramidal metal cores with the two hetero-atoms in contact {section 1.1.5, Figure 1.1.5(e)}. In contrast, the non-hydrido analogues displayed trigonal bi-pyramidal metal skeletons with the two M(PPh_3) units capping opposite faces of the ruthenium tetrahedra, resulting in no contact between the Group IB metal atoms, {section 1.1.5, Figure 1.1.5(c)}. Similar variation in coinage metal arrangement was also observed for two Cu_2Ru_6 clusters, when an interstitial carbido atom was replaced by two -CO groups. In the carbido cluster [$Cu_2Ru_6C(CO)_{16}(NCMe)_2$],[125] the Cu atoms were in bonding distance to each other, whereas in $[Cu_2Ru_6(CO)_{18}(C_6H_5Me)_2]$,[100] the two $Cu(C_6H_5Me)$ units capped opposite faces of a Ru_6 octahedron.

These examples have illustrated that small changes in the attached ligands can cause remarkable effects on the overall geometry adopted by the Group IB heteronuclear clusters, and provide suitable evidence to support that the energy differences between various structural types are small in many of these cluster compounds.

atoms were in bonding distance to each other, whereas in $[Cu_2Ru_6(CO)_{18}(C_6H_5Me)_2]$,[100] the two $Cu(C_6H_5Me)$ units capped opposite faces of a Ru_6 octahedron.

These examples have illustrated that small changes in the attached ligands can cause remarkable effects on the overall geometry adopted by the Group IB heteronuclear clusters, and provide suitable evidence to support that the energy differences between various structural types are small in many of these cluster compounds.

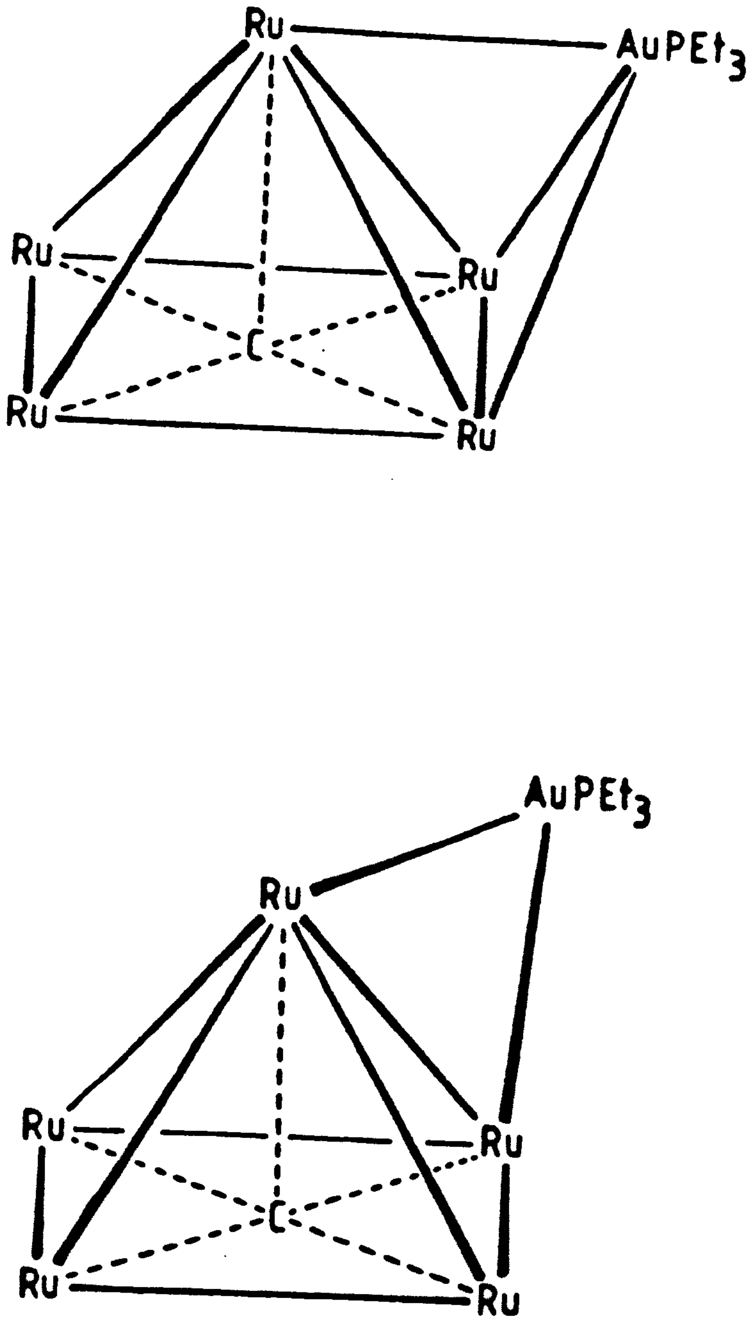

Figure 1.1.8(a). Structures of the skeletal isomers of the cluster $[AuRu_5C(CO)_{13}(NO)(PEt_3)]$, with CO and NO ligands omitted for clarity.[80]

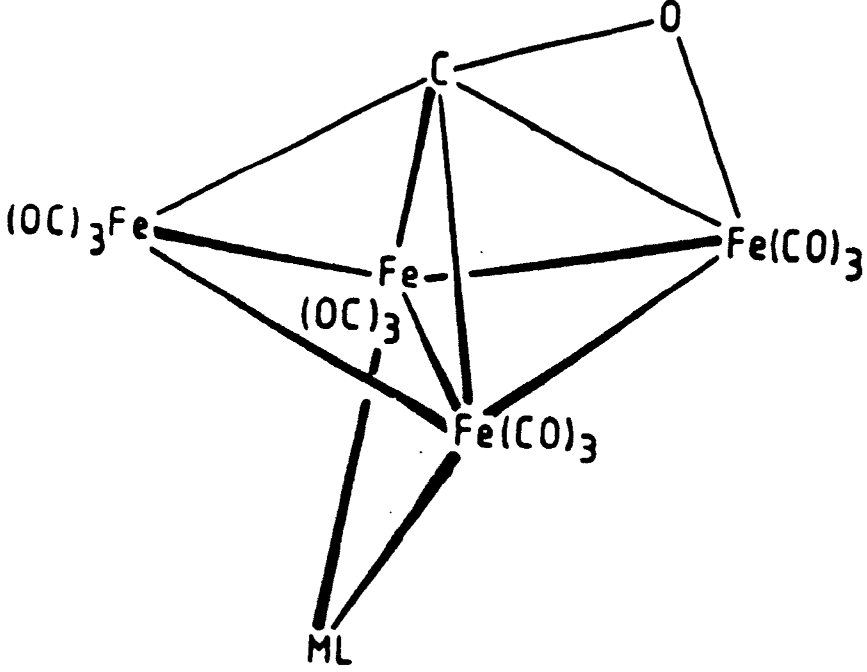

1

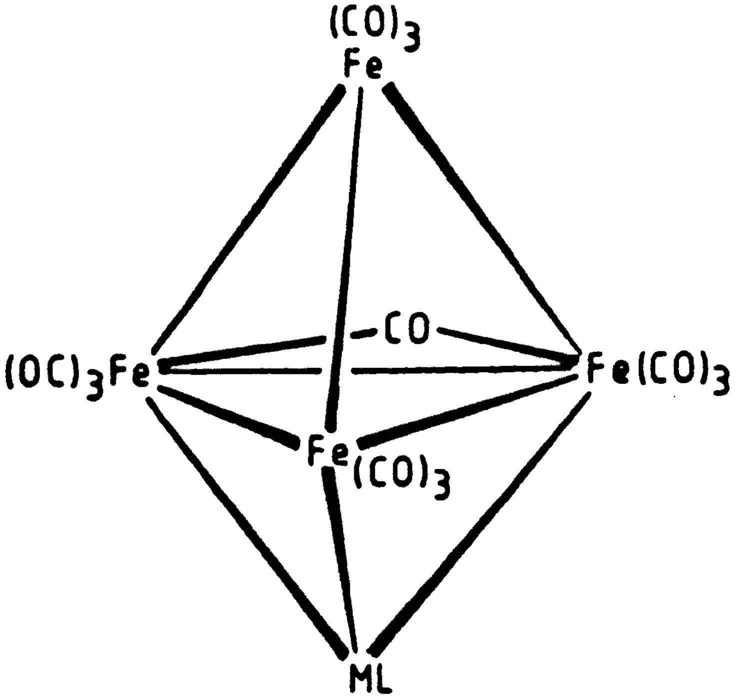

2

Figure 1.1.8(b). Structures of the two skeletal isomers of the cluster anions, $[MFe_4(CO)_{13}L]^-$ [M = Cu or Au; L = PPh_3].[48,49]

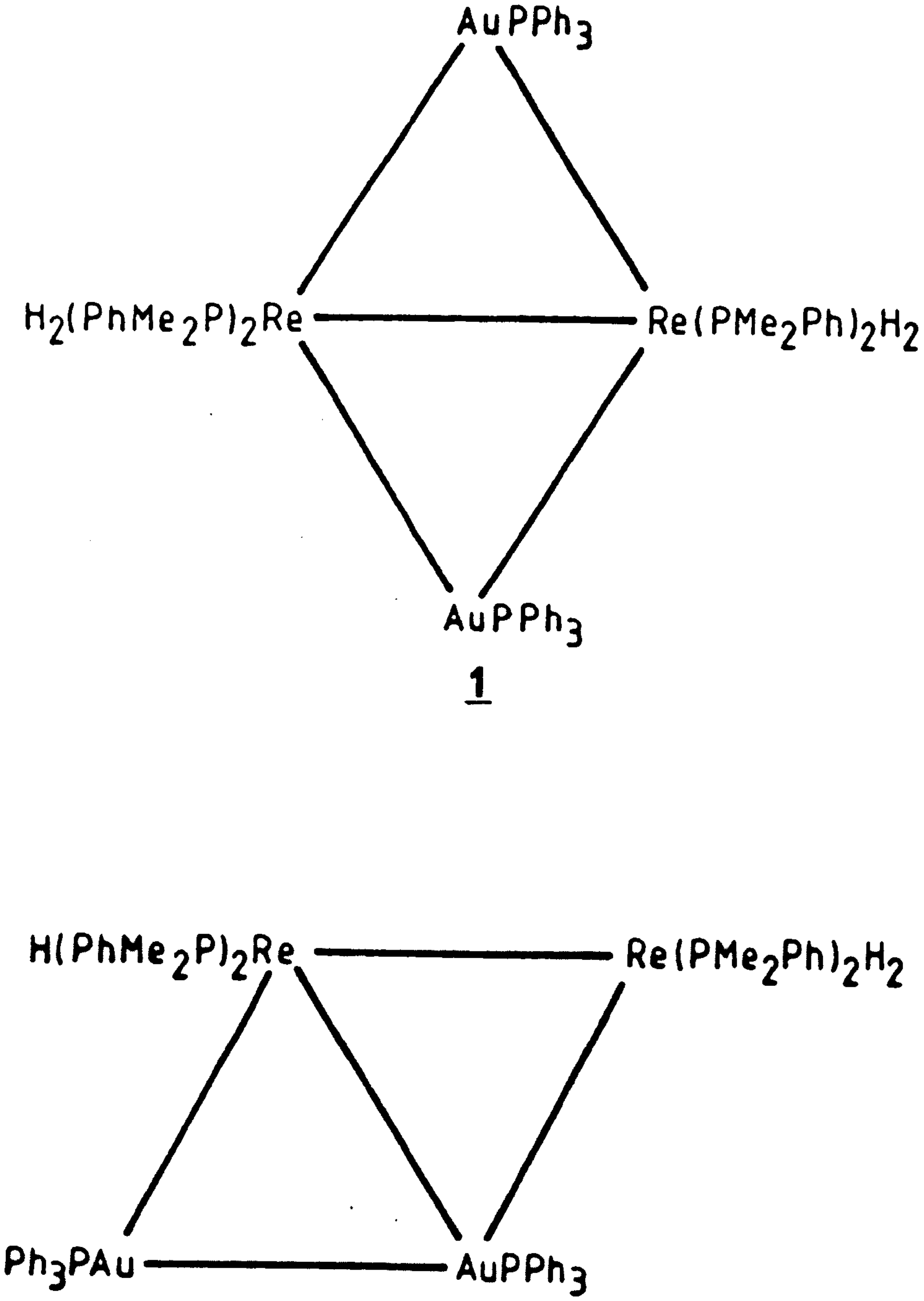

<u>1</u>

<u>2</u>

Figure 1.1.8(c). Structures of the skeletal isomers of the cluster $[Au_2Re_2H_6(PMe_2Ph)_4(PPh_3)_2]$, with the three and two hydrido ligands which bridge the Re-Re vectors of isomers 1 and 2 respectively, omitted for clarity.[97]

Section 1.1.9 Fluxionality in the solutions of heteronuclear clusters containing more than one $M(PR_3)$ group [M = Cu, Ag or Au;R = alkyl or aryl].

Studies on homonuclear and heteronuclear gold phosphine clusters using $^{31}P-\{^1H\}$ n.m.r spectroscopic technique have revealed interesting factors associated with their fluxional behaviour in solution. For the majority of homonuclear phosphine gold cluster compounds, interpretation of $^{31}P-\{^1H\}$ n.m.r. spectra have been found to be much simpler relative to their complex structures characterised in the solid state. The early reports of X-ray structures of the enneanuclear cluster $[Au_9(PAr_3)_8]^{3+}$ [Ar = $p-C_6H_4CH_3$][22] and the undecanuclear compound $[Au_{11}(SCN)_3(PAr_3)_7]$ [Ar = Ph or $p-C_6H_4Cl$],[20] were found to adopt solid state structures with the phosphine ligands in different chemical environments. However, $^{31}P-\{^1H\}$ n.m.r solution spectra revealed a single resonance even at temperatures of -90°C. In 1981 Mingos and co-workers also observed that the $^{31}P-\{^1H\}$ n.m.r. spectra of the centred icosahedral gold cluster $[Au_{13}(PMePh_2)_{10}Cl_2][(PF_6)_3]$ taken at -60°C, showed only one peak.[40]

This was consistent with the established solid state structure having the two chlorine atoms at para-positions, Figure 1.1.9(a). Upon warming the solution to room temperature, additional resonances were found to be present, indicating that at higher temperatures the structure with the two Cl atoms at para-positions converted into alternative metal frameworks by a low energy pathway, with the two Cl atoms occupying either meta- or ortho- positions, {Figures 1.1.9(b) and 1.1.9(c), respectively}. In 1984 Beurskens and co-workers also observed that further addition of free PPh_3 to $[Au_{11}(SCN)_3(PAr_3)_7]$ showed no exchange between the free and co-ordinated phosphines.[126]

To account for these observations, they suggested a rapid intramolecular process with respect to the n.m.r time scale. The stereochemical non-rigidity in gold cluster compounds allowing the breaking and making of gold-gold bonds in the rearrangement process to alternative metal frameworks in solutions, was highlighted by the crystallisation of two modifications of the enneanuclear gold cluster $[Au_9\{P(C_6H_4OMe)_3\}_8][NO_3]_3$.[127] Single crystal X-ray analyses on these modifications revealed the presence of two very different skeletal geometries. Isomer (1) was based on a centred chair conformation, {Figure 1.1.9(d)} and isomer (2) on a centred crown conformation, {Figure 1.1.9(d)}. However, in solutions, n.m.r. and electronic spectral data indicated the presence of one metal framework. This was found to be consistent with earlier n.m.r. studies carried out by Vollenbroek and co-workers for the related cluster, $[Au_9(PPh_3)_8]^{3+}$, which indicated that the compound was stereochemically non-rigid in solution.[128] Differences in solid state geometries within related cluster compounds was also reported with the hexanuclear cluster $[Au_6(Ptol_3)_6][BPh_4]_2$ adopting an octahedral structure whereas the closely related complex $[Au_6(PPh_3)_6][NO_3]_2$ had a structure based on two tetrahedra sharing a common edge.[129]

The fluxionality of phosphine ligands has also been observed for many heteronuclear clusters containing more than one $M(PR_3)$ monodentate unit [M = Cu, Ag, Au; R = alkyl or aryl] forming a part of the overall metal skeleton. In 1983, Stone and co-workers first reported the synthesis and X-ray structure characterisation of the Au_2Ru_3 clusters, $[Au_2Ru_3(\mu\text{-}H)(\mu_3\text{-}COMe)(CO)_9(PPh_3)_2]$ and $[Au_2Ru_3(\mu_3\text{-}S)(CO)_9(PPh_3)_2]$.[64] They observed that the $^{31}P\{^1H\}$ n.m.r. spectra of both clusters showed only one resonance for the two phosphorus nucleii at -90°C. This was not consistent with the solid state structures of the two compounds established from X-ray diffraction studies, which revealed non-equivalent environments for the two P atoms, {Figure 1.1.9(e)}. Detailed analysis of these spectra showed the retention of ^{31}P-^{1}H and ^{31}P-^{31}P coupling, indicating that the PPh_3 dissociation was not responsible for the single resonance observed at -90°C. It was concluded that the most feasible explanation of these results was a rearrangement of the metal core in solution, through which the two phosphorus atom nucleii appeared equivalent on the n.m.r. time scale. The workers postulated a Berry pseudo rotation mechanism, involving a square pyramidal intermediate, to account for the intramolecular rearrangement of the metal cores in the above di-gold clusters, {Figure 1.1.9(f)}.[64]

Subsequently the Berry pseudo rotation mechanism was also put forward to account for metal core rearrangements in solutions of several heptanuclear clusters, for example, $[Au_3Ru_4(\mu_3\text{-}H)(CO)_{12}(PPh_3)_3]$[68,69,113] and $[Au_3CoRu_3(CO)_{12}(PPh_3)_3]$[90] whose low temperature ^{31}P-$\{^{1}H\}$ n.m.r. spectra indicted equivalent environments for the phosphorus atoms, whereas the solid state structures clearly established non-equivalent sites. Similar results of ^{31}P-$\{^{1}H\}$ n.m.r. studies in which a spectrum taken at ambient temperatures was found not to correspond to the solid state structure of the heteronuclear cluster, is now a common feature in the chemistry of a variety of mixed-metal cluster compounds having more than one Group IB metal phosphine units bonded to different transition metal atoms. For example, in the series of analogous clusters $[M_2Ru_4(H)_2(CO)_{12}(PPh_3)_2]$ and [M = Cu, Ag, or Au],[104] a broadened singlet was observed in the ^{31}P-$\{^{1}H\}$ n.m.r spectrum of the Cu_2Ru_4 cluster at ambient temperature, whereas at -90°C, two singlets were visible. The low temperature $^{31}P-\{^1H\}$ n.m.r. spectrum was consistent with the solid state structure having two non-equivalent phosphorus environments, {Figure 1.1.5(e)}. Similar results were obtained for the analogous Au_2Ru_4 cluster, with a single resonance in the $^{31}P-\{^1H\}$ n.m.r. spectrum at ambient temperatures. However, well resolved peaks could not be obtained at -90°C, although the signal was found to broaden. In any case, the singlet observed at room temperature was not consistent with the solid state geometry, in which the two P atoms were occupying non-equivalent sites, {Figure 1.1.5(e)}. For both the Cu_2Ru_4 and Au_2Ru_4 cluster compounds, the ^1H n.m.r hydrido ligand signal was found to retain $^{31}P-\{^1H\}$ coupling throughout the temperature range from -90°C to room temperature. Salter and co-workers therefore concluded that the fluxional process which averaged the phosphorus enivronments was intramolecular.[104] Since examples of intramolecular exchange of phosphine ligands between metal atoms had not been previously reported, they postulated that the actual metal frameworks of the related clusters $[Cu_2Ru_4(\mu_3\text{-}H)_2(CO)_{12}(PPh_3)_2]$ and $[Au_2Ru_4(\mu\text{-}H)(\mu_3\text{-}H)(CO)_{12}(PPh_3)_2]$ were in motion, undergoing a Berry pseudo rotation mechanism proposed earlier {Figure 1.1.9(f)}, through which the two phosphorus atoms appeared equivalent on the n.m.r. time scale.

For the related silver-ruthenium cluster $[Ag_2Ru_4(\mu_3\text{-}H)_2(CO)_{12}(PPh_3)_2]$, the interpretation of the n.m.r spectra was complicated by the presence of a second fluxional process. Two very broad peaks were obtained in the $^{31}P-\{^1H\}$ n.m.r. spectrum at ambient temperatures and the ^1H n.m.r. spectrum showed a broad triplet with no $^{31}P-\{^1H\}$ coupling. However, at -50°C, $^{31}P-\{^1H\}$ coupling was observed. At -90°C the ^1H and $^{31}P-\{^1H\}$ n.m.r spectra were found to be consistent with the solid state structure, in which the two phosphorus atoms were again in non-equivalent sites, {Figure 1.1.5(e)}. To investigate the idea of phosphine ligand exchange, the workers observed that on addition of one equivalent of free PPh_3 to the $CDCl_3$ and $CDCl_2$ solutions of the Ag_2Ru_4 cluster, the $^{31}P-\{^1H\}$ n.m.r spectrum showed only one broad peak at room temperature.[104] This detection of one signal for an averaged PPh_3 environment indicated that the PPh_3 groups bonded to the silver atoms were exchanging with the free ligand in solution. From these results, they concluded that the silver-ruthenium cluster was undergoing a fluxional process involving intermolecular exchange of PPh_3 groups between clusters in addition to the intramolecular metal core rearrangement proposed for the copper-ruthenium and gold-ruthenium analogues.

An alternative rearrangement process of the metal skeletons of these cluster compounds in solutions was recently proposed by Johnson, which involved a pathway where the energy associated in the 'breaking' of attractive forces holding the M-M bonds was kept to a minimum.[130] The attractive forces were correlated in terms of the cohesive energy (C.E.) within a metal polyhedron, (for transition metal atoms the C.E is proportional to the square root of the connectivity Z). The connectivity of a metal atom in a polyhedron was defined, as the number of surrounding metal atoms which were in bonding distance. For example, within an M_4 tetrahedron, each metal is linked to three other atoms giving a connectivity of 3 {total C.E. = 6.93}. For a trigonal bipyramidal metal core, two metals have a connectivity of 3, and the remaining three a connectivity of 4, {total C.E. = 9.46}. Within the Berry pseudo rotation mechanism, {Figure 1.1.9(f)}, the intermediate in the rearrangement process was postulated to involve a square pyramid, with four basal atoms exhibiting a connectivity of 3, and the apical atom having a connectivity of 4, {total C.E. = 8.93}. Thus a difference in C.E. of 0.53 was found to result when the trigonal bi-pyramidal metal skeleton 'opened out' to the square pyramid in the rearrangement process.

The alternative pathway[130] involved the rearrangement of one trigonal bi-pyramidal framework to another chemically equivalent metal core, through an edge-bridged tetrahedral intermediate, {Figure 1.1.9(g)}, having two metal atoms with a connectivity of 4, two a connectivity of 3 and one with a connectivity of 2 {total C.E. = 8.87}. The overall process was viewed to involve a,

$$\text{Cap} \rightleftharpoons \text{Edge-bridge} \rightleftharpoons \text{Cap} \quad \text{interconversion.}$$

A difference in C.E. of 0.59 resulted for this rearrangement process, being slightly higher in value to that calculated for the Berry pseudo rotation mechanism, {vide supra}, but both rearrangement pathways keeping the breaking of M-M bonds to a minimum.

This cap $\rightleftharpoons$ edge-bridge $\rightleftharpoons$ cap interconversion pathway describing molecular rearrangement of heteronuclear clusters in solutions was also recently proposed by Lewis and co-workers to account for the presence of two isomers in solutions of the deca-osmium cluster series $[MOs_{10}C(CO)_{24}(PR_3)]^-$ [M = Cu, Ag, or Au; R = alkyl or aryl].[131] For all three related cluster compounds both the $^{31}P-\{^1H\}$ and ^1H n.m.r. spectra taken over the temperature range 250-280 K, exhibited signals which were consistent with the existence of two distinct isomeric structures in solutions. Importantly, the observed ratio in which the two isomers were present varied noteably.[131] To account for these spectroscopic results, Lewis and co-workers concluded that the two isomeric forms of the monoanion cluster compounds, $[CuOs_{10}C(CO)_{24}(PMe_2Ph)]^-$, $[AgOs_{10}C(CO)_{24}(PPh_3)]^-$, and $[AuOs_{10}C(CO)_{24}(PMe_2Ph)]^-$ were undergoing rapid interconversion via an intramolecular rearrangement of their respective metal skeletons in solutions. One possible mechanism which was put forward by the workers involved the cap$\rightleftharpoons$edge$\rightleftharpoons$cap intercoversion process, {Figure 1.1.9(h)}. The X-ray structure of the gold-osmium cluster $[AuOs_{10}C(CO)_{24}(PPh_3)]^-$ reported previously, had established that the Group IB metal phosphine bridged the outer edge of a capping tetrahedron.[33] The i.r. spectra of the copper, silver and gold analogues described above, were found to be very similar,[131] indicating that perhaps all three analogues adopted similar metal frameworks with the $M(PR_3)$ group in a μ_2-edge-bridging position, thus supporting the proposed mechanism for the intramolecular rearrangement of their respective metal cores. Lewis and co-workers also proposed that in the solutions of di-gold decaosmium cluster $[Au_2Os_{10}C(CO)_{24}(PPh_3)_2]$, the n.m.r. data was consistent with the presence of two isomers interconverting through a similar edge$\rightleftharpoons$cap$\rightleftharpoons$edge pathway, Figure 1.1.9(i).[131]

The X-ray studies of the cluster compounds,
$[AgRu_3(CO)_9(C_2Bu^t)(PPh_3)]$,
$[Cu_2Ru_4(\mu_3\text{-}H)_2(CO)_{12}\{P\text{-}(C_6H_{11})_3\}_2]$,
$[Cu_2Ru_4(\mu_3\text{-}H)_2(CO)_{12}\{P\text{-}(CHMe_2)_3\}_2]$,
$[Cu_2Ru_4(\mu\text{-}CO)_3(CO)_{10}(PPh_3)_2]$ and
$[Ag_2Ru_4(\mu\text{-}CO)_3(CO)_{10}(PPh_3)_2]$
presented in the following sections, have further stimulated the interest in the chemistry of heteronuclear clusters having Group IB metal phosphine groups forming a part of the mixed-metal polyhedron.

Comparison of the structural results obtained from their respective X-ray studies, to those previously reported for analogous clusters, have established interesting trends in M-Ru and M-P (M = Cu, Ag or Au) bond distances, together with novel solid state geometries, governed primarily by the 'type' of organophosphine ligand bonded to the hetero-metal atoms.

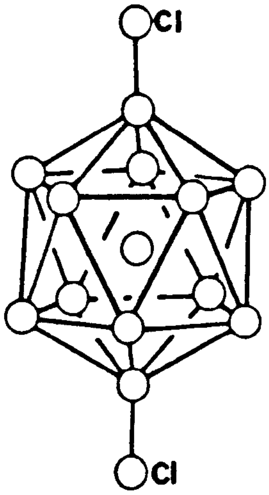

Figure 1.1.9(a).

Para-isomer of $[Au_{13}(PMePh_2)_{10}Cl_2][(PF_6)_3]$.[40]

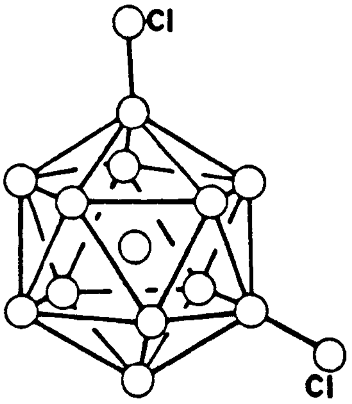

Figure 1.1.9(b).

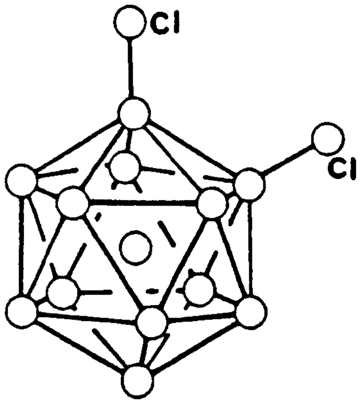

Figure 1.1.9(c).

meta- and ortho-isomers for $[Au_{13}(PMePh_2)_{10}Cl_2][(PF_6)_3]$.[40]

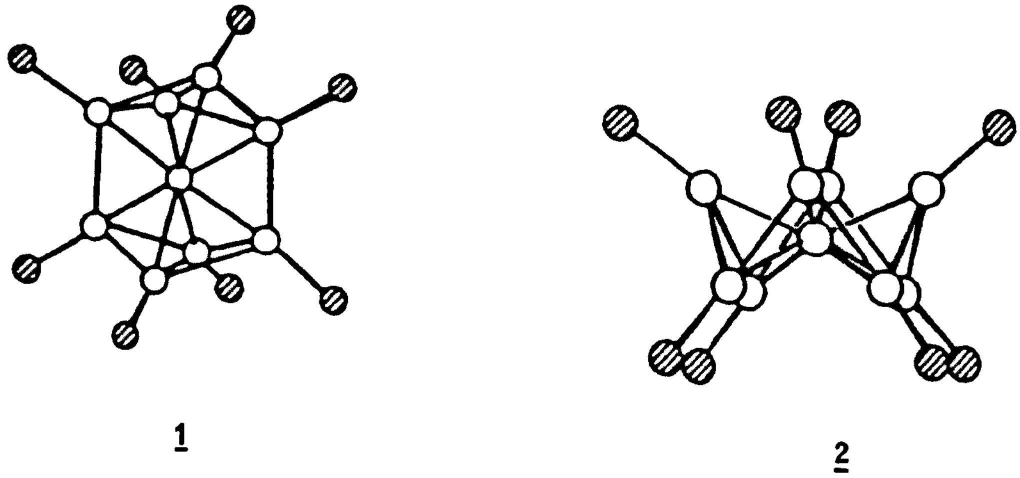

Figure 1.1.9(d). Chair (1) and crown (2) conformations for $[Au_9\{P(C_6H_4OMe)_3\}_8][NO_3]_3$.[127]

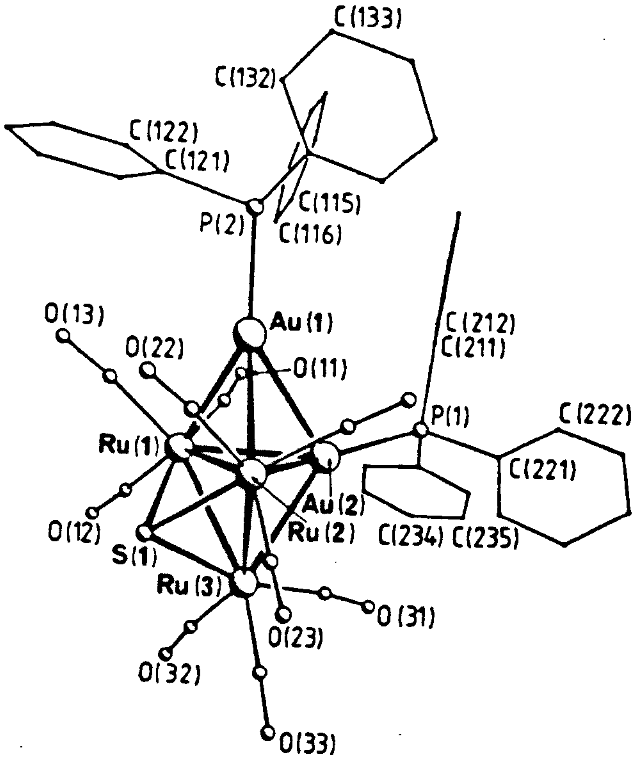

Figure 1.1.9(e). Molecular structure of $[Au_2Ru_3(\mu_3\text{-}S)(CO)_9(PPh_3)_2]$.[64]

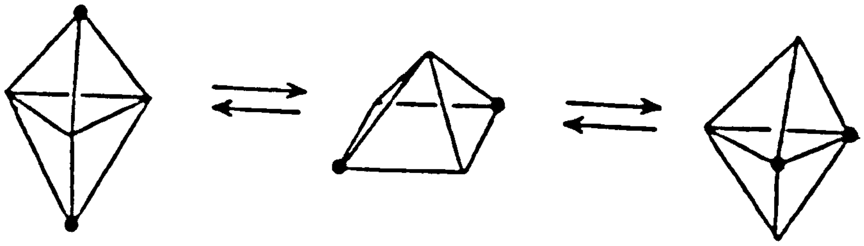

Figure 1.1.9(f). The Berry pseudo rotation mechanism, involving a square pyramidal intermediate.[64,130]

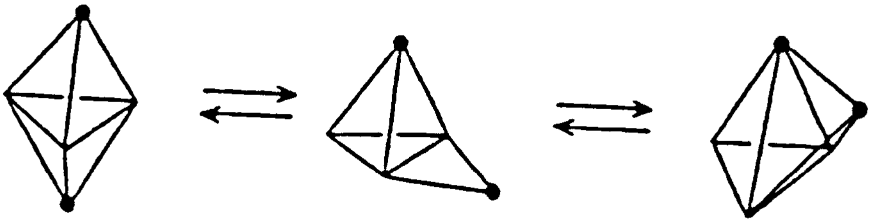

Figure 1.1.9(g). An alternative rearrangement pathway, involving an edge-bridged tetrahedron.[130]

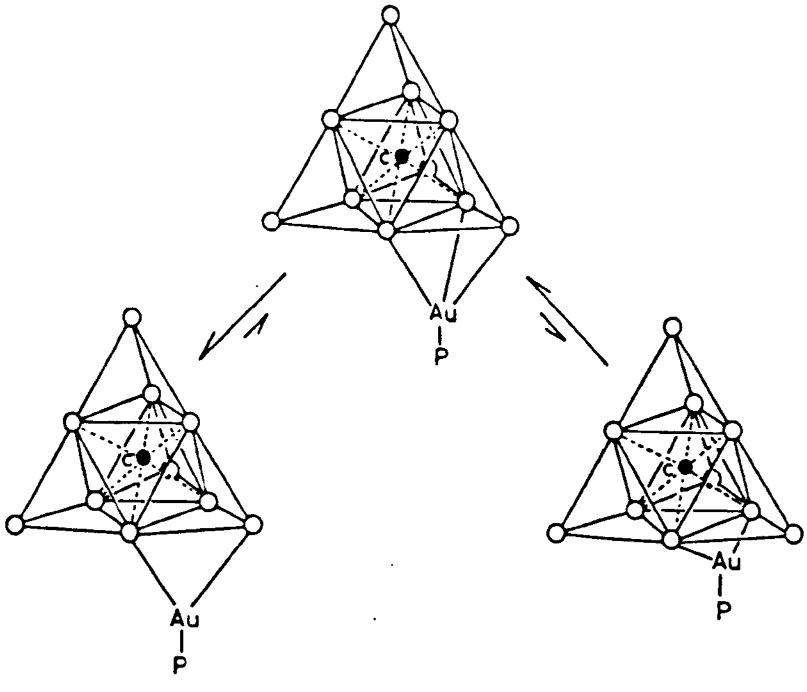

Figure 1.1.9(h). Proposed mechanism of interconversion of isomers of $[AuOs_{10}C(CO)_{24}(PPh_3)]^-$ in solution.[131]

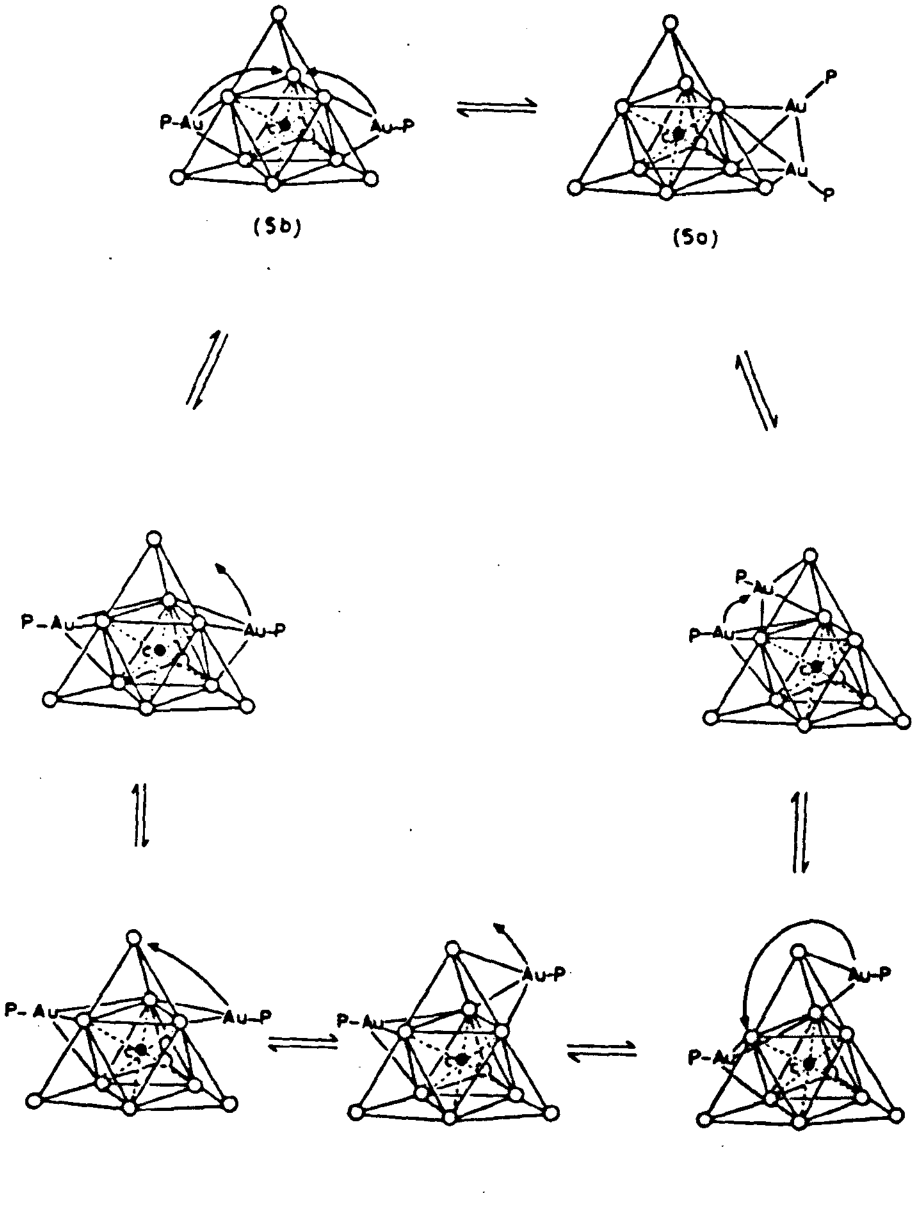

Figure 1.1.9(i). Proposed structures of the isomeric forms of [$Os_{10}C(CO)_{24}(AuPMe_2Ph)_2$], and a possible mechanism for their interconversion in solution.[131]

Section 1.2. X-ray structural analysis of the silver-ruthenium cluster [$AgRu_3(CO)_9(C_2Bu^t)(PPh_3)$] (1).

Crystal data, methods of data collection, structure solution and refinement are presented in section 4.2.

Tables of fractional co-ordinates, anisotropic temperature factors, bond lengths, bond angles, intermolecular and intramolecular distances for (1) are given in the appendix, (Vol.2).

The X-ray analysis of the silver-ruthenium cluster $[AgRu_3(CO)_9(C_2Bu^t)(PPh_3)]$ (1) was of interest in completing a series of related Group IB metal cluster compounds and allowing comparison of the structural data to that previously reported for the copper and gold analogues, $[MRu_3(CO)_9(C_2Bu^t)(PPh_3)]$ [M = Cu(2)[46] and Au(3)[79]]. The first comparative study of the effect of the nature of all three Group IB metals on the structures of a series of related cluster compounds $[MRu_3(\mu_3\text{-}PhPCH_2PPh_2)(CO)_9(PPh_3)]$ [M = Cu, Ag, or Au] was recently reported by Bruce, White and co-workers, showing an interesting trend in the M-Ru and M-P bond lengths between the solid state structures of the respective mixed-metal compound.[47]

1.2.1. Structural description of $[AgRu_3(CO)_9(C_2Bu^t)(PPh_3)]$ (1).

The X-ray diffraction study of the tetranuclear cluster compound $[AgRu_3(CO)_9(C_2Bu^t)(PPh_3)]$ (1), {Figure 1.2.1}, established a 'butterfly' arrangement of the four metal atoms, with the silver atom occupying a 'wing-tip' site. The t-butylacetylide ligand was found to lie on the convex side of the 'butterfly' metal core, interacting with all three ruthenium atoms via one σ-bond to the 'wing-tip' ruthenium atom, Ru(2) and two π-bonds to the ruthenium atoms which formed the 'hinge' of the 'butterfly', Ru(1) and Ru(3). Each ruthenium atom carried three essentially linear terminal carbonyl groups, {Ru-C-O 173-178°}, with the triphenyl phosphine group co-ordinated to the silver atom.

1.2.2. Results and Discussion.

X-ray structure analysis showed that the tetranuclear silver cluster $[AgRu_3(CO)_9(C_2Bu^t)(PPh_3)]$ (1) adopted a similar 'butterfly' metal core structure to those previously established for the

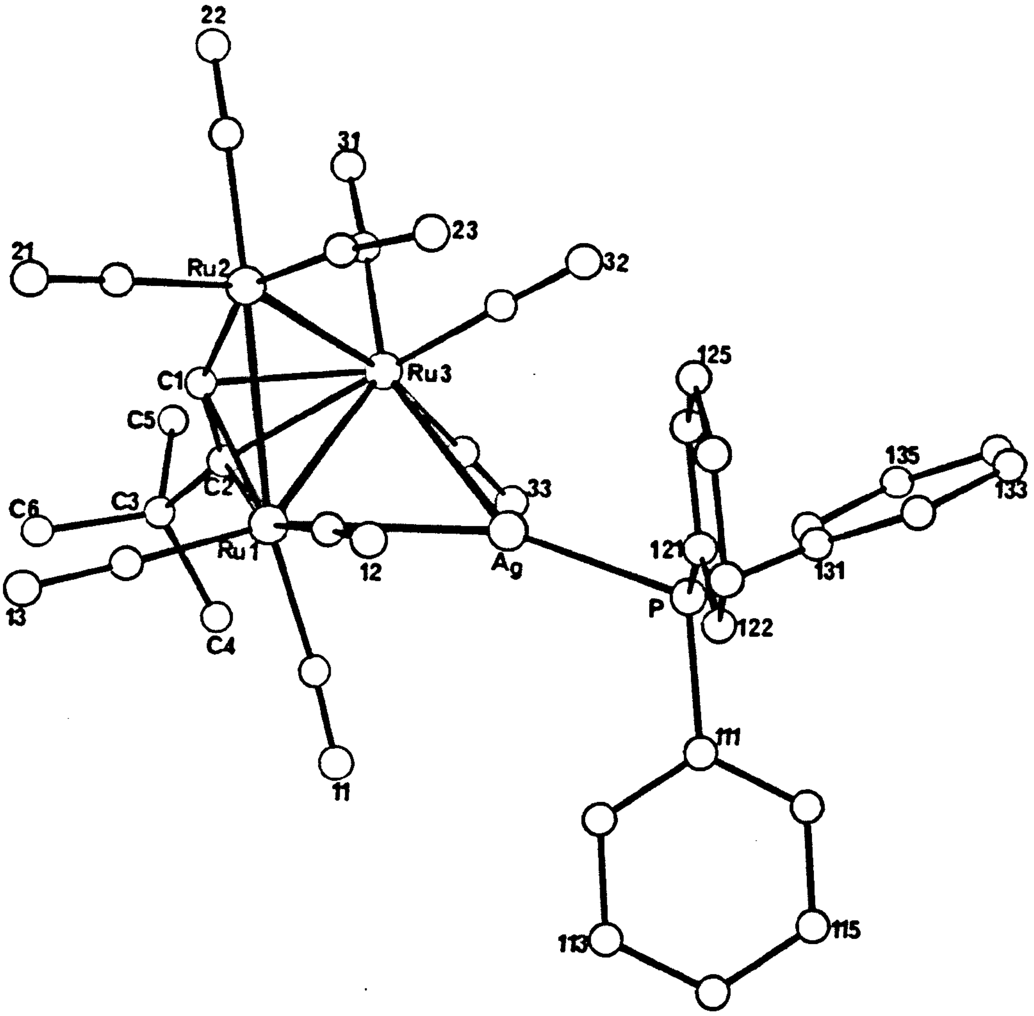

Figure 1.2.1. The molecular structure of the tetranuclear cluster $[AgRu_3(CO)_9(C_2Bu^t)(PPh_3)]$ (1). The carbonyl C atoms have the same numbering as the O atoms to which they are attached.

analogous copper and gold compounds $[MRu_3(CO)_9(C_2Bu^t)(PPh_3)]$ [M = Cu(2)[46] and Au(3)[79]; Figure 1.2.2], with the hetero-metal atom in a 'wing-tip' site. The mixed-metal clusters (1)-(3) were all formally envisaged to be derived from the tri-hydrido compound $[Ru_3(\mu\text{-}H)(CO)_9(C_2Bu^t)]$ (4)[132] by replacement of the μ-H ligand by a bridging $M(PPh_3)$ fragment. Table 1.2.2 lists selected bond lengths for (1), and those reported for the related structures (2), (3), (4), and the parent monoanion $[Ru_3(CO)_9(C_2Bu^t)]^-$ (5).[133]

The study of the silver complex (1) established that as in all the complexes included in Table 1.2.2, the t-butylacetylide ligand was found to lie on the convex side of the 'butterfly' metal core, interacting with all three ruthenium atoms via one σ-bond to the 'wing-tip' atom, Ru(2) (Ru(2)-C(1) 2.02(3) Å) and two π-bonds, one to each of the atoms forming the 'hinge' of the 'butterfly' (Ru(1)-C(1) 2.20(3), Ru(1)-C(2) 2.27(3), Ru(3)-C(1) 2.23(3), and Ru(3)-C(2) 2.25(3) Å). These bond lengths in (1) were found not to differ significantly from those reported for the related compounds (2), and (3)-(5), (Table 1.2.2). The dihedral angle between the 'wings' of the butterfly [Ru(1)-Ru(2)-Ru(3) and Ru(1)-Ru(3)-Ag] in (1) was calculated to be 120.6°, intermediate in value between that of 115.7° in (2) and 129.3° in (3). In the silver compound $[AgRu_3(CO)_9(C_2Bu^t)(PPh_3)]$ (1), the lengths of the chemically equivalent bonds Ru(1)-Ru(2) and Ru(2)-Ru(3) [2.814(3) and 2.799(3) Å respectively] were significantly different. There was no obvious reason for this, but, interestingly a slight asymmetry also occured in the related structures,

compound	vector	distance/ Å
$[CuRu_3(CO)_9(C_2Bu^t)(PPh_3)]$ (2)[46]	Ru(1)-Ru(2)	2.819(1)
	Ru(2)-Ru(3)	2.808(1)

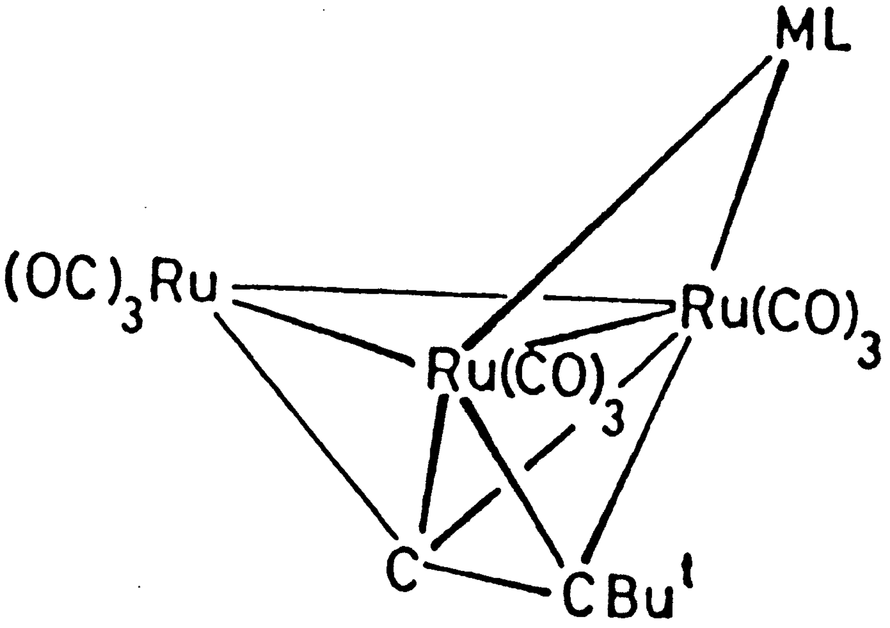

Figure 1.2.2. Metal core structure for the clusters $[MRu_3(CO)_9(C_2Bu^t)(PPh_3)]$ [M = Cu (2)^{46} and Au (3)^{79}].

$[AuRu_3(CO)_9(C_2Bu^t)(PPh_3)]$ (3)[79]	Ru(1)-Ru(2)	2.800(1)
	Ru(2)-Ru(3)	2.786(2)
$[Ru_3(CO)_9(C_2Bu^t)]^-$ (5)[133]	Ru(1)-Ru(2)	2.800(3)
	Ru(2)-Ru(3)	2.790(3)

The chemically unique Ru(1)-Ru(3) bond of length 2.655(3) Å reported for the 'parent' monoanion (5) was very much shorter than the mean of the other two Ru-Ru bonds {2.795(2) Å}.

In complex (1), the silver-bridged Ru(1)-Ru(3) bond {2.805(2) Å} was markedly elongated compared to that in (5), and was found to be very close to the mean lengths of the other two unbridged Ru-Ru bonds {2.807(3) Å}. This observation was very similar to that reported for the analogous monohydrido species $[Ru_3(\mu\text{-}H)(CO)_9(C_2Bu^t)]$ (4), where the hydrido-bridged Ru(1)-Ru(3) bond length {2.792(3) Å} was also longer than the equivalent distance in the monoanion (5), but similar to the remaining Ru-Ru lengths {mean 2.797(3) Å}.[132] In contrast to the silver complex (1), the bridged bond Ru(1)-Ru(3) in the copper complex (2) was markedly shorter (0.052 Å)[46] and that in the gold complex (3) was longer (0.027 Å)[79] than the mean of the other two Ru-Ru bonds. Thus, the length of the 'hinge' bond, bridged by $M(PPh_3)$, increased with increasing atomic number of the Group IB metal in the order Cu <Ag <Au.

The X-ray analysis of (1) revealed that all 9 carbonyl ligands exhibited expected linearity {Ru-C-O 173-178(3)°}. However, an extremely short contact between one of the carbonyl ligands and the silver atom was observed (Ag...C(32) 2.69(2) Å). This was very similar to a contact present in the di-silver hexanuclear clusters $[Ag_2Ru_4(CO)_{13}(PPh_3)_2]$ (Ag(1)...C(32) 2.694(3) Å),[101] and $[Ag_2Ru_4(\mu\text{-}H)_2(CO)_{12}(Ph_2PCH_2PPh_2)]$ (Ag(1)...C(18) 2.68(3) Å).[134] This type of Group IB metal to carbonyl interaction was also a structural feature in the gold and copper analogues of (1), $[MRu_3(CO)_9(C_2Bu^t)(PPh_3)]$ [M = Cu(1)[46] and Au(3)[79]], with the same carbonyl ligand making a short contact with the hetero-metal atom [Cu...C 2.47(3) in (2) and Au...C 2.69(1) Å in (3)]. These short M...C contacts were thought to be attributed to interaction either, attractive[33,45] or repulsive[125] between the Group IB metals and the carbonyl ligands, or resulting from steric effects in the solid.[35]

The most interesting feature in the study of the silver-ruthenium complex (1) was the variation in M-Ru and M-P bond lengths in comparison to those previously established for the related copper-ruthenium (2) and gold-ruthenium (3) analogues. It was observed that the mean Ag-Ru length of 2.787(3) Å in the silver complex $[AgRu_3(CO)_9(C_2Bu^t)(PPh_3)]$ (1), was not only very much longer than the mean Cu-Ru distance of 2.603(1) Å in the copper cluster $[CuRu_3(CO)_9(C_2Bu^t)(PPh_3)]$ (2),[46] but also considerably longer than the mean Au-Ru distance of 2.760(1) Å in the structure of the gold analogue $[AuRu_3(CO)_9(C_2Bu^t)(PPh_3)]$ (3).[79] This structural trend was also reflected in the M-P bond lengths, with the Ag-P bond [2.405(9) Å in (1)] being considerably longer than both the Cu-P and Au-P distances [2.217(2) in (2) and 2.276(3) Å in (3), respectively]. The presence of anomalously longer M-Ag bond lengths was also previously observed in the anionic complexes $[M\{Os_3H(CO)_{10}\}_2]^-$ [M = Ag or Au].[135,136] In both solid state structures, the Group IB metal atom was found to 'link' two triangular $Os_3H(CO)_{10}$ units, bridging one Os-Os bond of each fragment giving the hetero-metal atom square planar co-ordination. Importantly, the mean of the four Ag-Os bonds in the silver complex {2.864(1) Å} was found to be 0.057 Å longer than the mean of the four Au-Os distances in the related gold derivative, {mean Au-Os 2.807(1) Å}.

1.2.3 Conclusions.

The structural study of the tetranuclear cluster (1) described a μ_2-bonding mode for the Ag(PPh$_3$) group analogous to that previously established for the Group IB metal phosphine fragments, Cu(PPh$_3$) and Au(PPh$_3$) in the related copper (2) and gold (3) compounds. The comparative study of the structural features in the cluster series [MRu$_3$(CO)$_9$(C$_2$Bu^t)(PPh$_3$)] [M = Cu (2), Ag (1), Au (3)] established that the M-Ru and M-P distances increased in the order, Ag-Ru;Ag-P > Au-Ru;Au-P > Cu-Ru;Cu-P. These results were found to closely parallel those observed by Bruce, White and co-workers for the cluster series [MRu$_3$(μ_3-PhPCH$_2$PPh$_2$(CO)$_9$(PPh$_3$)].[47] The mean M-Ru distances were significantly longer for M = Ag than for M = Cu or Au [2.781(1), 2.615(1) and 2.764(1) Å, respectively]. Furthermore the Ag-P {2.422(3) Å} distance in this series was found to be very long not only compared to the Cu-P {2.228(2) Å} but also to the Au-P bond length {2.2972(2) Å}. To account for the anomalously longer Ag-Ru bond distance, the workers proposed[47] that in the edge-bridging bonding mode both Cu(PPh$_3$) and Ag(PPh$_3$) groups utilised the hybrid (s-z) and one of the degenerate p_x and p_y orbitals, (section 1.1.2). Whereas, in the analogous gold complex, the Au(PPh$_3$) unit had available only the low lying hybrid (s-z) orbital for bonding (section 1.1.1), resulting in a closer approach and better overlap with the appropriate orbitals of the Ru$_3$ triangle. These observed trends in M-Ru and M-P bond lengths indicated that these structural features could be a general characteristic of mixed-metal clusters containing an edge-bridging M(PR$_3$) (R = alkyl or aryl) unit.

Table 1.2.2.

Bond distances (Å)	(1)	(2)[46*]	(3)[79*]	(4)[132*]	(5)[133*]
Ru(1)-Ru(2)	2.814(3)	2.819(1)	2.800(1)	2.799(3)	2.800(3)
Ru(1)-Ru(3)	2.805(2)	2.762(1)	2.820(1)	2.792(3)	2.655(3)
Ru(2)-Ru(3)	2.799(3)	2.808(1)	2.786(2)	2.795(3)	2.790(3)
Ru(1)-M	2.788(3)	2.603(1)	2.763(1)	-	-
Ru(3)-M	2.785(3)	2.603(1)	2.757(1)	-	-
M -P(1)	2.405(9)	2.217(2)	2.276(3)	-	-
Ru(1)-C(1)	2.20(3)	2.203(6)	2.22(1)	2.214(3)	2.18(2)
Ru(2)-C(1)	2.02(3)	1.945(7)	1.95(2)	1.947(3)	1.95(2)
Ru(3)-C(1)	2.23(3)	2.211(7)	2.19(1)	2.207(3)	2.16(2)
Ru(1)-C(2)	2.27(3)	2.260(7)	2.21(1)	2.271(3)	2.24(2)
Ru(3)-C(2)	2.25(3)	2.259(6)	2.27(1)	2.268(3)	2.24(2)

* re-numbered for comparison.

Section 1.3. X-ray structural studies of the copper-ruthenium clusters, $[Cu_2Ru_4(\mu_3-H)_2(CO)_{12}(L)_2]$ [L = P-$\{C_6H_{11}\}_3$ (1) and P-$\{CHMe_2\}_3$ (2)].

Crystal data, methods of data collection, structure solution and refinement for both (1) and (2) are presented in section 4.3.

Tables of fractional atomic co-ordinates, anisotropic temperature factors, bond lengths, bond angles, intermolecular and intramolecular distances for both (1) and (2) are given in the appendix, (Vol.2).

1.3.1 Introduction.

It has been well recognised that changing substituents on phosphorus ligands can cause marked changes in behaviour of the free ligand and their transition metal complexes.[137-139] Both steric and electronic effects induced by co-ordinated organophosphine groups together with crystal packing forces, attribute to the overall metal frameworks adopted in the solid state.[140,141] The steric hinderance associated with the increase in size of the phosphine ligand is quantitatively measured by the phosphine ligand cone angle, Θ, introduced by Tolman in 1977.[142] Organophosphines with large cone angles have shown to congest the P atom and decrease the binding ability of the ligand to transition metals, having important effects on both the spectroscopic and chemical properties of their complexes. Increasing the size of the organic substituent co-ordinated to the phosphorus atoms has shown to have for example, the following effects,

(a) increase in bond lengths of M-P and other ligands,

(b) increase in the basicity of the lone pair on the P atom,

(c) favour bonding of other ligands, which are in competition for co-ordination sites and

(d) favour structural isomers in preventing surface ligand crowding.

The X-ray studies of the hexanuclear mixed-metal clusters $[Cu_2Ru_4(\mu_3\text{-}H)_2(CO)_{12}(P\text{-}\{C_6H_{11}\}_3)_2]$ (1) and $[Cu_2Ru_4(\mu_3\text{-}H)_2(CO)_{12}\{P\text{-}(CHMe_2)_3\}_2]$ (2) completed a series of compounds in which the 'bulk' size of the organophosphine group attached to the Group IB copper atoms had been varied. The X-ray structure of the related cluster $[Cu_2Ru_4(\mu_3\text{-}H)_2(CO)_{12}(PPh_3)_2]$ (3) was recently reported by Orpen and co-workers,[104] and the interesting feature of comparison in these structures was the effect on the solid state metal core geometries, with the variation of the 'bulkiness' of the phosphine ligand. The i.r. and n.m.r. spectroscopic data of $[Cu_2Ru_4(\mu_3\text{-}H)_2(CO)_{12}(P\text{-}\{C_6H_{11}\}_3)_2]$ (1) were found to be significantly different to those reported for the PPh_3 analogue (3).[143] This indicated that (1) probably adopted a different metal core structure in the solid state to the capped trigonal bi-pyramidal geometry established for (3).

The $^{31}P\text{-}\{^1H\}$ n.m.r. spectrum at -100°C for the solutions of the hexanuclear cluster (1) showed two broadened singlets, indicating that the two phosphorus atoms were in different environments. In contrast, the $^{31}P\text{-}\{^1H\}$ n.m.r. spectra of the solutions of the analogous copper-ruthenium cluster $[Cu_2Ru_4(\mu_3\text{-}H)_2(CO)_{12}(P\{CHMe_2\}_3)_2]$ (2) showed three singlets at -90°C, (relative intensities 1:0.6:1), with a corresponding sharp doublet in the ^1H n.m.r spectrum at -90°C, which broadened to give a singlet at -100°C.[143] These results were consistent with the presence of two distinct skeletal isomers in solution. The two singlets of equal intensity were found to closely resemble the low temperature n.m.r. data reported for the PPh_3 analogue (3).[104] Therefore, isomer (2A) was thought to adopt a similar capped trigonal bi-pyramidal metal core to that reported for (3). The presence of a second isomer (2B) in the solutions of (2) was deduced from the remaining signals in both the $^{31}P\text{-}\{^1H\}$ n.m.r. and the ^1H n.m.r spectra. Interestingly, the remaining singlet in the $^{31}P\text{-}\{^1H\}$ n.m.r. spectrum at -90°C (intensity 0.6) for isomer (2B) indicated that the two P atoms were in identical environments, which was in contrast to the corresponding signals observed in the spectrum of the PCy_3 analogue (1). This suggested that isomer (2B) adopted a different metal core geometry not only to that proposed for isomer (2A) but also to to metal skeleton of (1). Another feature to arise from the n.m.r. analysis of the solutions of (2) was that with the raise in temperature, the three singlets observed in the $^{31}P-\{^{1}H\}$ n.m.r. spectrum at -90°C all coalesced, together with the two hydrido signals in the ^{1}H n.m.r spectrum. At room temperature the $^{31}P-\{^{1}H\}$ spectrum gave a broadend singlet, whereas the ^{1}H n.m.r spectrum showed a high field triplet. These observations were consistent with isomers (2A) and (2B) interconverting in solution at room temperature.[143]

1.3.2 Structural description of $[Cu_2Ru_4(\mu_3-H)_2(CO)_{12}(P-\{C_6H_{11}\}_3)_2]$ (1).

The X-ray analysis of the mixed-metal cluster (1) established a novel edge-bridged capped tetrahedral geometry, Figure 1.3.2. The four ruthenium atoms, Ru(1), Ru(2), Ru(3), and Ru(4) formed a tetrahedron with the edge, Ru(1)-Ru(3) bridged by one $Cu(PCy_3)$ unit and the adjacent triangular face, Ru(2)-Ru(3)-Ru(4) capped by the second $Cu(PCy_3)$ group, resulting in no contact between the two copper atoms. Each ruthenium atom was found to carry three essentially linear carbonyl groups, {Ru-C-O range 160-178(4)°}. Although the two hydrido ligands were not located from the X-ray analysis, their positions were deduced from potential energy minimisation calculations,[144] which gave suitable minima in P.E. for one hydride to cap the face Cu(2)-Ru(2)-Ru(4) and the second to cap the face Cu(2)-Ru(3)-Ru(4).

1.3.3 Structural description of isomer $[Cu_2Ru_4(\mu_3-H)_2(CO)_{12}\{P-(CHMe_2)_3\}_2]$ (2A).

The X-ray analysis of isomer (2A) described a capped trigonal

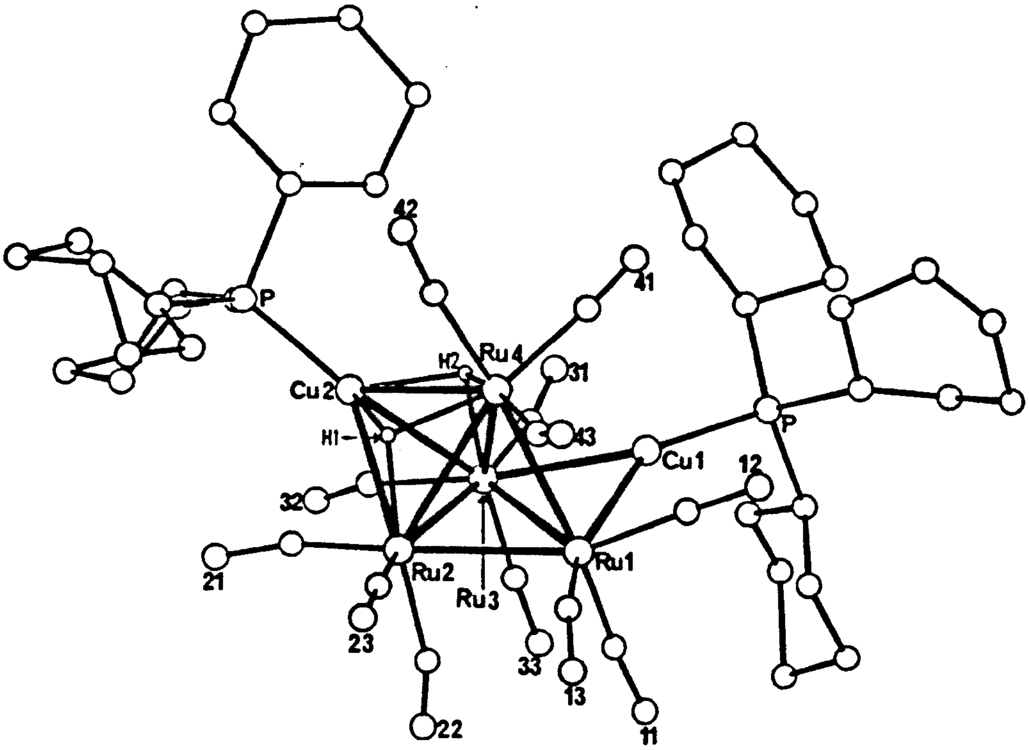

Figure 1.3.2. The molecular structure of the copper-ruthenium cluster $[Cu_2Ru_4(\mu_3\text{-}H)_2(CO)_{12}\{P(C_6H_{11})_3\}_2]$ (1). The carbonyl C atoms have the same numbering as the O atoms to which they are attached.

bi-pyramidal metal core geometry, Figure 1.3.3. The four ruthenium atoms, Ru(1), Ru(2), Ru(3) and Ru(4) formed a tetrahedron, whose triangular face Ru(2)-Ru(3)-Ru(4) was capped by Cu(2), with Cu(1) capping the adjacent face Cu(2)-Ru(3)-Ru(4), resulting in a direct bond between the two copper atoms. Each ruthenium atom carried three essentially linear carbonyl groups {Ru-C-O range 160-176(3)°}, with the two organophosphine groups, $P\text{-}(CHMe_2)_3$, co-ordinated to the two copper atoms. Due to the crystallographic problems of pseudo symmetry and resulting disorder in the overall structure of (2A), (section 4.3.5), the positions of the two hydrido ligands were difficult to determine, although potential energy minimisation calculations[144] gave reasonable minima in P.E. for one hydride to cap the face Cu(2)-Ru(2)-Ru(4) and the second to cap the triangular face Cu(2)-Ru(2)-Ru(3). Unfortunately, the only well established structural feature which was derived from the X-ray study of (2A) was the metal core in the solid state.

1.3.4 Proposed solid state structure for isomer (2B).

Only one type of crystal was obtained from the solutions of (2), and therefore isomer (2B) as yet, was not observed in the solid state. However, the n.m.r. data for (2B)[143] (section 1.3.1) was consistent with the two P atoms occupying identical environments and giving rise to the observed singlet of intensity 0.6 in the $^{31}P\text{-}\{^1H\}$ n.m.r spectrum at -90°C. It was therefore proposed that (2B) adopted a structure where the two copper atoms capped two triangular faces of the ruthenium tetrahedron which were symmetry related, giving the two phosphorus ligands identical environments, but with no contact between the two copper atoms. Thus, the proposed structure was thought to define an edge-sharing bi-capped tetrahedron, {Figure 1.3.4}.

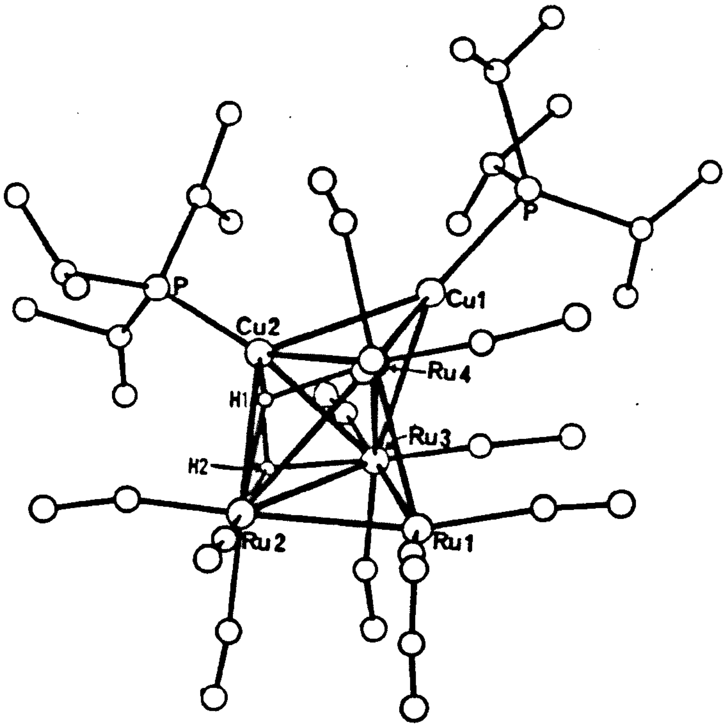

Figure 1.3.3. The molecular structure of the hexanuclear cluster $[Cu_2Ru_4(\mu_3\text{-}H)_2(CO)_{12}\{P(CHMe_2)_3\}_2]$ (2A).

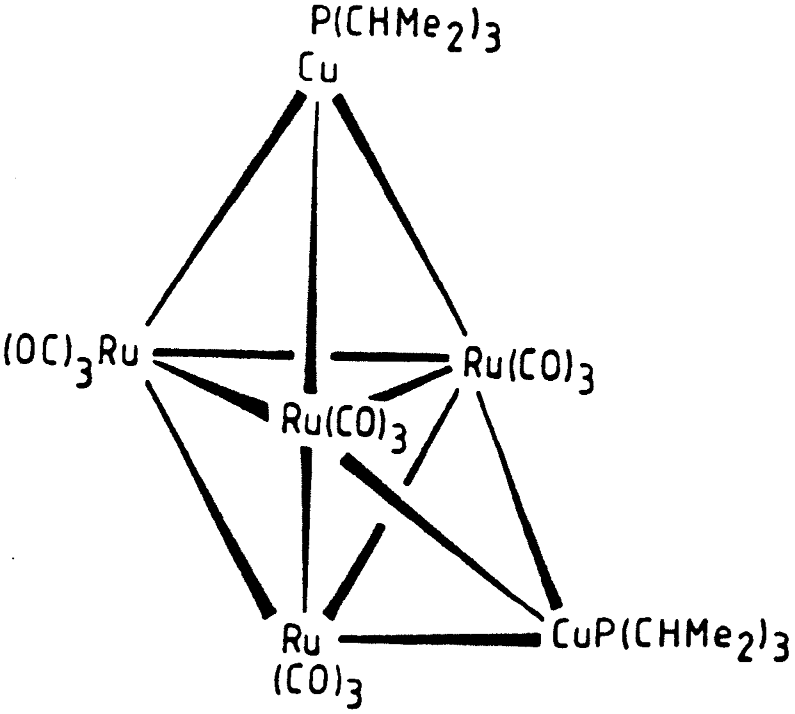

Figure 1.3.4. Proposed solid state structure for a second isomer in solution of $[Cu_2Ru_4(\mu_3\text{-}H)_2(CO)_{12}\{P(CHMe_2)_3\}_2]$.

1.3.5 Discussion and results.

The comparison of the structural data obtained from the X-ray structural studies of the related hexanuclear mixed-metal clusters $[Cu_2Ru_4(\mu_3\text{-}H)_2(CO)_{12}(P\text{-}\{C_6H_{11}\}_3)_2]$ (1), $[Cu_2Ru_4(\mu_3\text{-}H)_2(CO)_{12}\{P\text{-}(CHMe_2)_3\}_2]$ (2A) and $[Cu_2Ru_4(\mu_3\text{-}H)_2(CO)_{12}(PPh_3)_2]$ (3)[104] established an interesting variation in their respective solid state geometries governed by the nature of the attached organophosphine ligands. The presence of the 'bulky' tri-cyclohexyl phosphine groups in (1) described an overall metal framework with one of the two copper atoms edge-bridging and the second copper atom capping the adjacent face of the ruthenium tetrahedron, resulting in no contact between the two hetero-metal atoms, {Figure 1.3.2}. In contrast, with the presence of the less bulky phosphine group in isomer (2A), the six metal atoms defined a capped trigonal bi-pyramidal geometry, with the two copper atoms forming a direct linkage, {Figure 1.3.3}. Although the solid state structure of isomer (2B) was not characterised by an X-ray diffraction study, the n.m.r. evidence (section 1.3.1) proposed a structure with the two copper atoms capping two symmetry related triangular faces of the ruthenium tetrahedron with no contact between the two metal atoms, {Figure 1.3.4}. The X-ray structure of the previously reported PPh_3 analogue $[Cu_2Ru_4(\mu_3\text{-}H)_2(CO)_{12}(PPh_3)_2]$ (3) established a capped trigonal bi-pyramidal metal core, similar to that adopted by isomer (2A), with the two copper atoms in contact {Figure 1.3.5}.[104] Table 1.3.5 lists the M-M bond lengths for the related copper-ruthenium cluster compounds, (1), (2A) and those reported for (3).

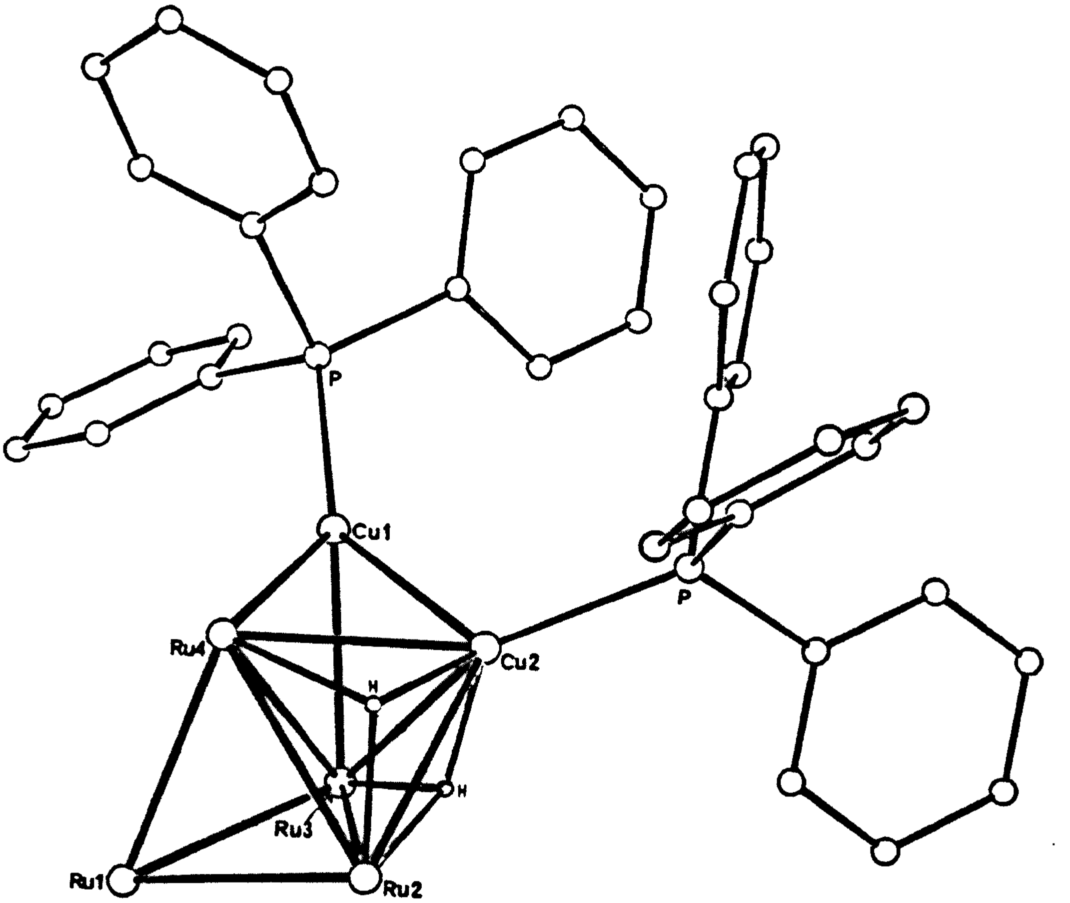

Figure 1.3.5. Molecular structure of $[Cu_2Ru_4(\mu_3\text{-}H)_2(CO)_{12}(PPh_3)_2]$ (3).[104] Carbonyl ligands have been omitted for clarity.

The observed Cu-Cu bond length in the copper-ruthenium isomer $[Cu_2Ru_4(\mu_3\text{-}H)_2(CO)_{12}\{P(CHMe_2)_3\}_2]$ (2A) {3.008(6) Å} was markedly longer than the analogous bond in the structures of the PPh_3 analogue $[Cu_2Ru_4(\mu_3\text{-}H)_2(CO)_{12}(PPh_3)_2]$ (3) {2.699(2) Å} and the octanuclear copper-ruthenium cluster $[Cu_2Ru_6C(CO)_{16}(NCMe)_2]$ {2.692(1) Å}.125 The mean Cu-Ru bond in $[Cu_2Ru_4(\mu_3\text{-}H)_2(CO)_{12}\{P\text{-}(C_6H_{11})_3\}_2]$ (1) {2.643(3) Å} was significantly shorter than the corresponding mean bonds in isomer (2A) {2.792(8) Å} and (3) {2.706(2) Å}. In both structurally related cluster compounds, (2A) and (3), the three Cu-Ru bonds associated with the capping copper atom, Cu(2), displayed marked asymmetry, with one bond markedly longer than the other two, {Table 1.3.5}. The mean of these three bonds in (2A) {2.751(10) Å} was found to be significantly shorter than the mean of the two Cu-Ru bonds from Cu(1) {2.854 Å}. In contrast in the PPh_3 analogue (3) the mean of the three Cu-Ru bonds from Cu(2) {2.718(2) Å} was noteably longer than the mean of the two bonds from Cu(1) {2.689(2) Å}. In the cyclohexyl derivative (1) the three Cu-Ru bonds related to the capping copper atom, Cu(2), also showed marked asymmetry with one bond being significantly longer than the other two. The mean of these three bonds, {2.657(3) Å} was found to be 0.035 Å longer than mean of the two Cu-Ru bonds bridged by Cu(1), {mean 2.622(3) Å}.

The range of Ru-Ru bonds in (1) {2.792(2)-2.960(2) Å} was similar to the corresponding range observed in (3) {2.790(2)-2.966(2) Å}, but both range of distances were markedly shorter in comparison to those observed in isomer (2A) {2.699(7)-3.253(4) Å}. In both the capped trigonal bi-pyramidal metal core structures of (2A) and (3), the Ru-Ru bonds also exhibited asymmetry, with the mean of the three bonds, Ru(2)-Ru(3), Ru(2)-Ru(4), and Ru(3)-Ru(4) capped by Cu(2) {3.121(5) Å in (2A) and 2.945(2) Å in (3)} being significantly longer than the remaining three Ru-Ru bonds of the tetrahedron, {Table 1.3.5}. Similar asymmetry of the ruthenium bonds was also observed in the solid state structure of the cyclohexyl derivative (1), with the mean of the three bonds capped by Cu(2) {2.909(2) Å} being markedly longer not only to the bond, Ru(1)-Ru(3) bridged by Cu(1) {2.885(2) Å} but also to the two remaining Ru-Ru bonds of the tetrahedron, {Table 1.3.5}. In all three related cluster compounds, (1), (2A) and (3), the two hydrido ligands were not located directly from their respective X-ray studies, although suitable positions were obtained from potential energy calculations,[144] for the ligands to cap two triangular $CuRu_2$ faces, {Figures 1.3.2, 1.3.3 and 1.3.5, respectively}. Interestingly, in each structure the two Ru-Ru bonds of the two triangular $CuRu_2$ faces capped by the hydrido ligand showed marked lengthening relative to the remaining Ru-Ru bonds and the two Cu-Ru bonds associated with each face exhibited marked asymmetry:

$[Cu_2Ru_4(\mu_3\text{-}H)_2(CO)_{12}\{P(C_6H_{11})_3\}_2]$ (1)

face Cu(2)-Ru(2)-Ru(4);		Cu(2)-Ru(3)-Ru(4)	
capped by H(1)		capped by H(2)	
Cu(2)-Ru(2)	2.771(3);	Cu(2)-Ru(3)	2.634(3) Å
Cu(2)-Ru(4)	2.565(3);	Cu(2)-Ru(4)	2.565(3) Å
Ru(2)-Ru(4)	2.946(2);	Ru(3)-Ru(4)	2.960(2) Å

$[Cu_2Ru_4(\mu_3\text{-}H)_2(CO)_{12}\{P(CHMe_2)_3\}_2]$ (2A)

face Cu(2)-Ru(2)-Ru(4);		Cu(2)-Ru(2)-Ru(3)	
capped by H(1)		capped by H(2)	
Cu(2)-Ru(2)	3.050(5);	Cu(2)-Ru(2)	3.050(5) Å
Cu(2)-Ru(4)	2.586(10);	Cu(2)-Ru(3)	2.617(5) Å
Ru(2)-Ru(4)	3.204(4);	Ru(2)-Ru(3)	3.253(4) Å

[Cu$_2$Ru$_4$(μ_3-H)$_2$(CO)$_{12}$(PPh$_3$)$_2$] (3)[104]

face Cu(2)-Ru(2)-Ru(4);		Cu(2)-Ru(2)-Ru(3)	
capped by H(1)		capped by H(2)	
Cu(2)-Ru(2)	2.809(2);	Cu(2)-Ru(2)	2.809(2) Å
Cu(2)-Ru(4)	2.674(2);	Cu(2)-Ru(3)	2.671(2) Å
Ru(2)-Ru(4)	2.947(2);	Ru(2)-Ru(3)	2.966(2) Å

The two Cu-P distances in (1) showed slight variation, with the bond, Cu(2)-P(2) {2.333(9) Å} being 0.070 Å longer than the related Cu(1)-P(1) bond {2.263(9) Å}. Similar lengthening of one of the two Cu-P bonds was also observed in the structure of the PPh$_3$ analogue (3).[107] However, the mean Cu-P bonds in both structures, {2.298(9) Å in (1) and 2.234(3) Å in (3)} were found to lie in the range previously reported for related mixed-metal cluster compounds, {2.217-2.235(4) Å}.[44-52] Unfortunately, due to the disorder of the organophosphine groups in the structure of isomer (2A), the Cu-P distances could not be compared to those established in (1) and (3). The X-ray analysis of the mixed-metal cluster [Cu$_2$Ru$_4$(μ_3-H)$_2$(CO)$_{12}${P(C$_6$H$_{11}$)$_3$}$_2$] (1) showed that each ruthenium atom was bonded to three essentially linear carbonyl groups {Ru-C-O 160-178(4)°}. A short contact between one of the carbonyl ligands and Cu(2) was observed (Cu(2)...C(32) 2.43(5) Å) with a corresponding contact of 2.45(5) Å made by C(12) to Cu(1). In the related Cu$_2$Ru$_4$ cluster (2A), a short contact of 2.53(3) Å was found to occur between C(31) and Cu(1) and with a longer contact of 2.82(3) Å between C(42) and Cu(2).

1.3.6 Conclusions.

Within the series of heteronuclear clusters, $[Cu_2Ru_4(\mu_3\text{-}H)_2(CO)_{12}(PR_3)_2]$ [R=C_6H_{11}(Cy) (1), R = $CHMe_2$ (2A), R = Ph (3)], the respective solid state structures showed the presence of three distinct types of Cu_2Ru_4 metal frameworks related to the variation in the steric requirements of the different bulky organophosphine groups. The capped trigonal bi-pyramidal metal skeletons with a direct Cu-Cu bond was found to be the preferred geometry of the smaller PPh_3 ligand in (3) (cone angle 145°)[142] and was the only form observed in the solid state. With the slightly larger phosphine ligand $P\{(CHMe)_2\}_3$ (cone angle 160°),[142] a Cu_2Ru_4 metal core with a Cu-Cu bond was still formed as characterised for isomer (2A), although the marked lengthening of the Cu-Cu bond {3.008(6) Å} reflected upon a weaker copper-copper interaction, resulting from the steric congestion of the larger organophosphine ligand. Unfortunately, due to the problems of pseudo symmetry and overall disorder of the molecule, the certainty of the Cu-Cu bond length in the solid state structure of isomer (2A) was questionable.

However, the presence of a structurally different isomer (2B) in the solutions of (2), {section 1.3.1}, with two separate capping Cu atoms, could have easily resulted from the breaking of the weak Cu-Cu bond in isomer (2A), allowing the μ_2-copper atom to cap the symmetry related triangular face, Ru(1)-Ru(3)-Ru(4), {Figure 1.3.6} and creating identical chemical environments for the two phosphorus atoms. In contrast, in the solid state structure of (1) the greater steric demands of the tri-cyclohexyl phosphine ligand (cone angle 170.0°)[142] was established with the Cu-Cu bond no longer being observed and with one of the copper atoms forced to adopt a less sterically demanding edge-bridging position, whilst the other copper atom capped the opposite face of the Ru_4 tetrahedron. Similar rearrangements of metal cores containing $CuPR_3$ units were also recently observed upon the replacement of the two hydrido ligands in $[Cu_2Ru_4(u_3\text{-}H)_2(CO)_{12}(PPh_3)_2]$ (3)[104] by a 2e donor carbonyl group in $[Cu_2Ru_4(CO)_{13}(PPh_3)_2]$ (4).[101] The X-ray structure of (4) established a different capped trigonal bi-pyramidal geometry to that adopted by the hydrido analogue (3), with the two copper atoms capping opposite faces of the ruthenium tetrahedron, resulting in no contact of the two hetero-atoms, a metal framework analogous to that proposed for isomer (2B). This difference in the arrangement of the copper atoms was also previously reported when the interstitial carbon atom in $[Cu_2Ru_6C(CO)_{16}(NCMe)_2]$[125] was replaced by two carbonyl groups in $[Cu_2Ru_6(CO)_{18}(C_6H_5Me)_2]$.[100] In the former structure, the two copper atoms doubly capped adjacent faces of the octahedron resulting in a direct Cu-Cu bond, whereas in the latter compound the two $Cu(C_6H_5Me)$ units capped opposite faces of the Ru_6 octahedron, with no contact between the copper atoms. It has been discussed in section 1.1.8, that there is now a considerable amount of experimental evidence to support that the energy differences of various structural frameworks can be very small for many of these heteronuclear cluster compounds, and interconversion from one form to another is therefore most probable.

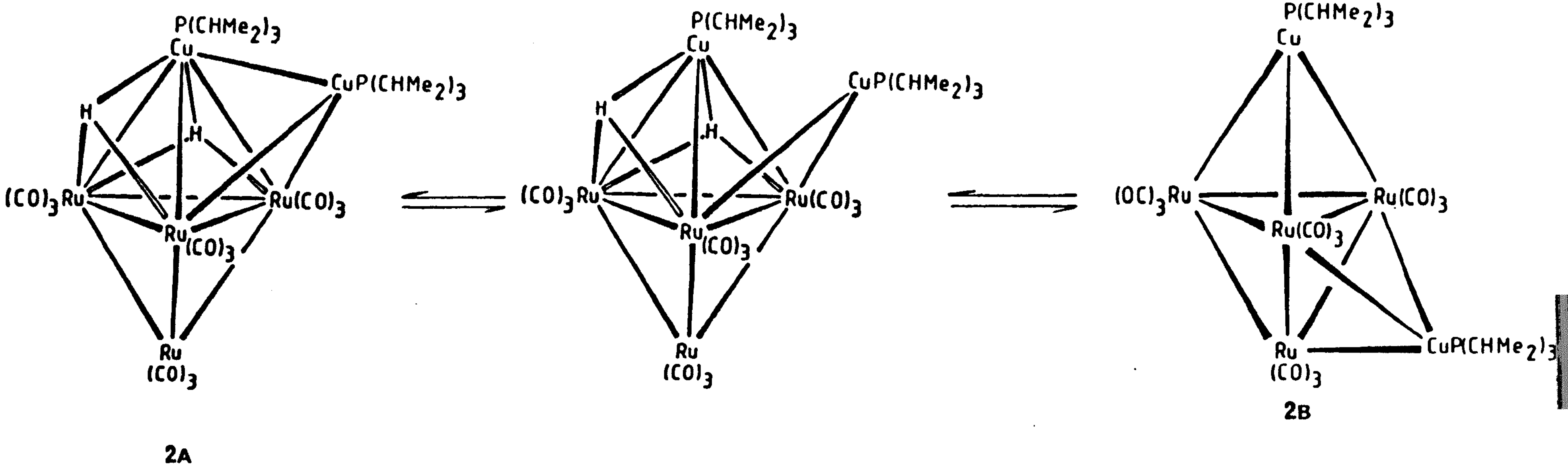

Figure 1.3.6. Proposed rearrangement of the two skeletal isomers in solution of $[Cu_2Ru_4(\mu_3\text{-}H)_2(CO)_{12}\{P(CHMe_2)_3\}_2]$ (2).

Table 1.3.5.

bond		distance/ Å	
	(1)	(2A)	(3)[104*]
Cu(1)-Cu(2)	-	3.008(6)	2.699(2)
Cu(1)-Ru(1)	2.619(3)	-	-
Cu(1)-Ru(3)	2.625(3)	2.798(8)	2.679(2)
Cu(1)-Ru(4)	(3.22)	2.910(9)	2.699(2)
Cu(2)-Ru(2)	2.771(3)	3.050(5)	2.809(2)
Cu(2)-Ru(3)	2.634(3)	2.617(10)	2.671(2)
Cu(2)-Ru(4)	2.565(3)	2.586(10)	2.674(2)
Ru(1)-Ru(2)	2.792(2)	2.835(4)	2.790(2)
Ru(1)-Ru(3)	2.885(2)	2.699(7)	2.795(2)
Ru(1)-Ru(4)	2.807(2)	2.743(8)	2.800(2)
Ru(2)-Ru(3)	2.822(2)	3.253(4)	2.966(2)
Ru(2)-Ru(4)	2.946(2)	3.204(4)	2.947(2)
Ru(3)-Ru(4)	2.960(2)	2.906(5)	2.923(2)

*re-numbered for comparison.

Section 1.4. X-ray analysis on the mixed-metal clusters $[M_2Ru_4(\mu\text{-}CO)_3(CO)_{10}(PPh_3)_2]$ [M = Cu (1) or Ag (2)].

Crystal data, methods of data collection, structure solution and refinement for both (1) and (2) are presented in section 4.4.

Tables of fractional atomic co-ordinates, anisotropic temperature factors, bond lengths, bond angles, intramolecular and intermolecular distances for both (1) and (2) are given in the appendix, (Vol.2).

The X-ray diffraction studies of the copper and silver hexanuclear clusters $[M_2Ru_4(\mu\text{-}CO)_3(CO)_{10}(PPh_3)_2]$ [M = Cu (1) and Ag (2)] were of structural interest in comparing relative differences in their solid state geometries, to those adopted by the previously reported hydrido clusters $[M_2Ru_4(\mu_3\text{-}H)_2(CO)_{12}(PPh_3)_2]$ [M = Cu (3) and Ag (4)].[104] The ^1H and $^{31}P\text{-}\{^1H\}$ n.m.r. spectral data for both (3) and (4) were consistent with fluxional behaviour of their respective metal cores in solutions, with marked differences between the spectra at ambient temperatures and -90°C, (section 1.1.9). In contrast, in the study of the related non-hydrido clusters (1) and (2) their respective $^{31}P\text{-}(^1H\}$ n.m.r. spectra showed no variation throughout the temperature range 25°C to -90°C, exhibiting only one singlet.[101] These results indicated that perhaps the replacement of two hydrido ligands in (3) and (4) by a carbonyl group in (1) and (2), may have resulted in a different arrangement of the Group IB metal atoms on the ruthenium tetrahedron in the solid state.

1.4.1. Structural description of $[M_2Ru_4(\mu\text{-}CO)_3(CO)_{10}(PPh_3)_2]$ [M = Cu (1) and Ag (2).

X-ray structural studies of (1) and (2) established that both cluster compounds adopted similar capped trigonal bi-pyramidal metal cores, {Figures 1.4.1(a) and 1.4.1(b), respectively}. In both structures the four ruthenium atoms defined a tetrahedron, with the face Ru(1)-Ru(2)-Ru(3) capped by one $M(PPh_3)$ unit, with the second $M(PPh_3)$ group capping the face Ru(1)-Ru(2)-Ru(4), resulting in no contact between the Group IB metal atoms. In both (1) and (2), the ruthenium atoms, Ru(1) and Ru(2) carried two terminal carbonyl groups, whereas Ru(3) and Ru(4) were bonded to three terminal -CO ligands. The remaining three carbonyl groups, {CO(13), CO(21), and

CO(24)}, in both structures bridged the bonds, Ru(1)-Ru(3), Ru(1)-Ru(2), and Ru(2)-Ru(4), respectively.

1.4.2. Discussion and results.

X-ray analyses of the related clusters $[M_2Ru_4(\mu\text{-}CO)_3(CO)_{10}(PPh_3)_2]$ [M = Cu (1) and Ag (2)] described capped trigonal bi-pyramidal metal frameworks, with the two Group IB metal phosphines in both structures capping two triangular faces of the ruthenium tetrahedron, with no direct bonding interactions between the two hetero-metal atoms. The arrangement of the two $M(PPh_3)$ groups in both (1) and (2), {Figures 1.4.1(a) and 1.4.1(b), respectively} was in marked contrast to the bonding sites adopted by the Group IB metal phosphine groups in the previously reported hydrido clusters, $[M_2Ru_4(\mu_3\text{-}H)_2(CO)_{12}(PPh_3)_2]$ [M = Cu (3) and Ag (4), Figure 1.4.2].^{104} The bonding of the copper and silver metal phosphines in both (3) and (4) was envisaged to involve, firstly the capping of one $M(PPh_3)$ unit onto a triangular Ru_3 face of the ruthenium tetrahedron, followed by the second $M(PPh_3)$ group capping the 'newly' formed MRu_2 face, resulting in a direct bond between the hetero-metal atoms. Interestingly, the replacement of two hydrido ligands in (3) and (4) by a 2e-donor carbonyl group in the structures of (1) and (2) resulted in a marked difference in the bonding arrangement of the Group IB metal phosphines in the solid state. Table 1.4.2 lists M-M bond lengths for clusters $[M_2Ru_4(\mu\text{-}CO)_3(CO)_{10}(PPh_3)_2]$ [M = Cu (1) and Ag (2)] and those reported for the related hydrido structures $[M_2Ru_4(\mu_3\text{-}H)_2(CO)_{12}(PPh_3)_2]$ [M = Cu (3) and Ag (4)].

The overall range of Cu-Ru distances in the hexanuclear cluster $[Cu_2Ru_4(\mu\text{-}CO)_3(CO)_{10}(PPh_3)_2]$ (1) {2.608-2.848(2) Å} was found to be

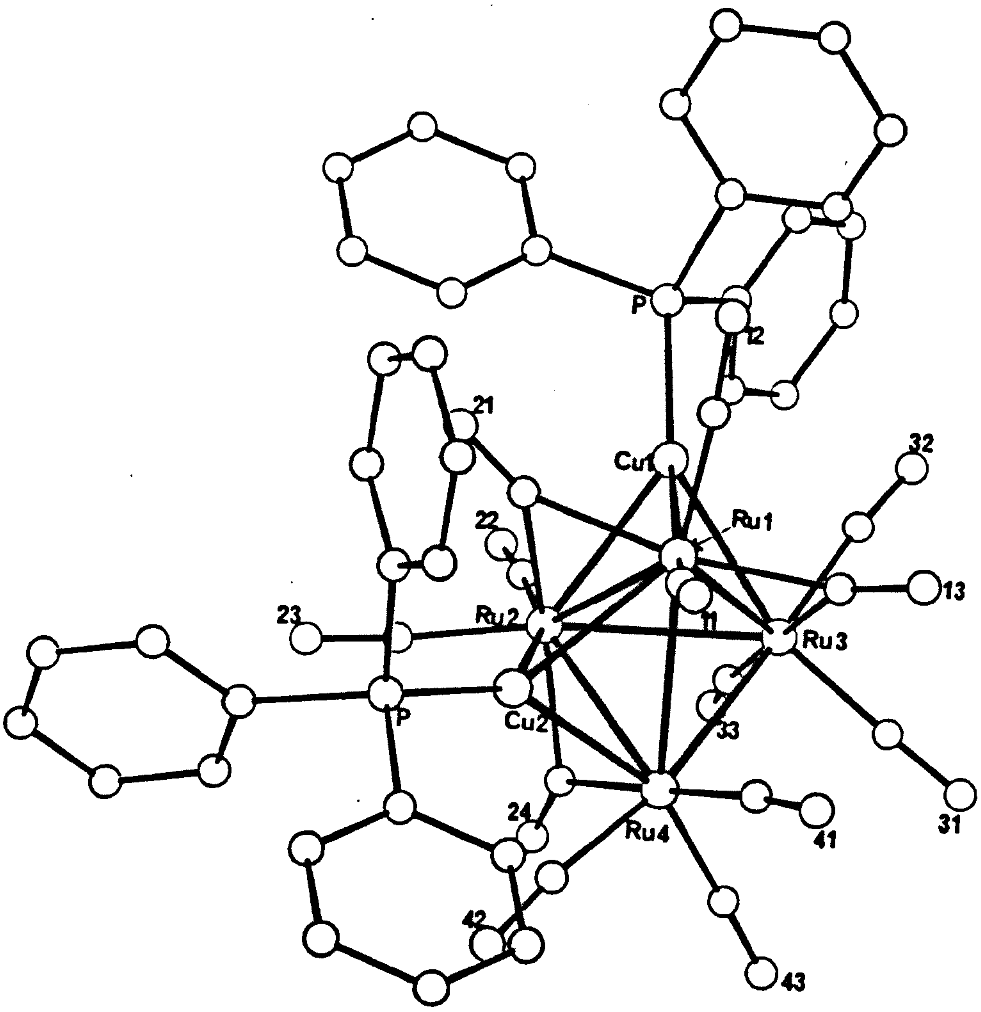

Figure 1.4.1(a). The molecular structure of the copper-ruthenium cluster $[Cu_2Ru_4(\mu\text{-}CO)_3(CO)_{10}(PPh_3)_2]$ (1). The carbonyl C atoms have the same numbering as the O atoms to which they are attached.

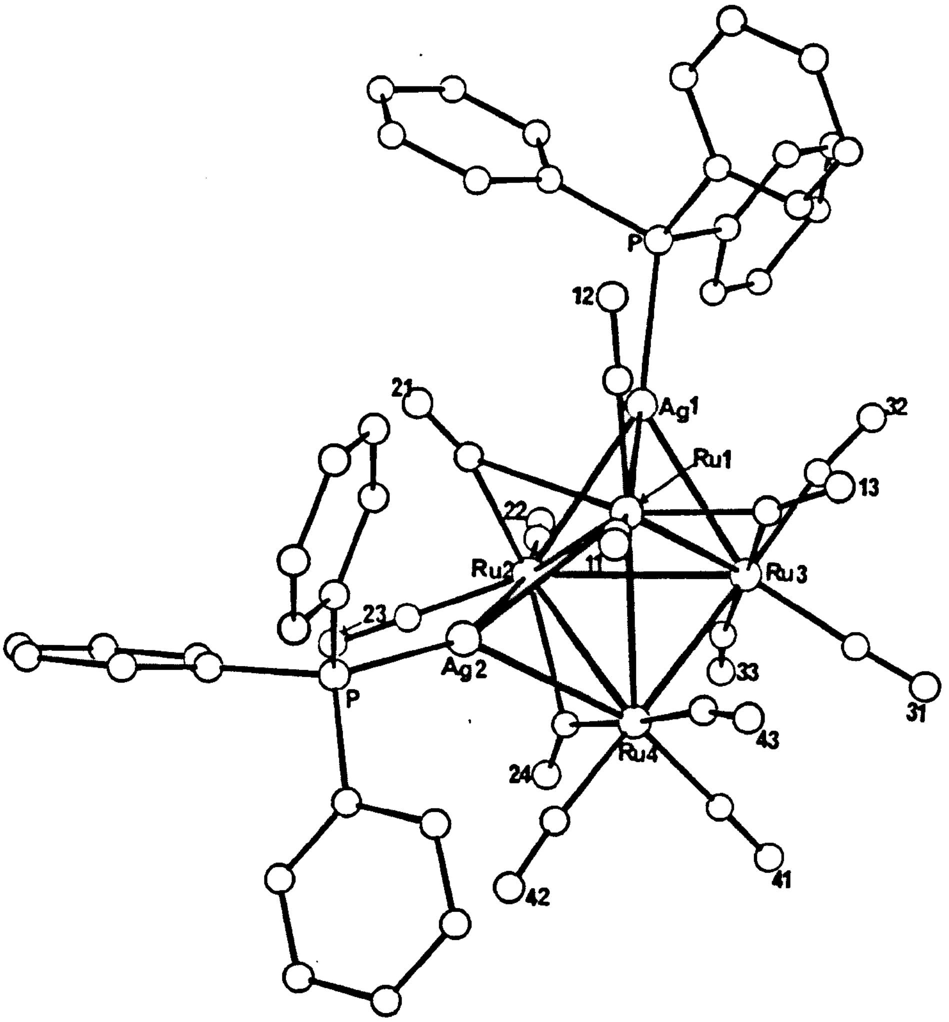

Figure 1.4.1(b). The molecular structure of the silver-ruthenium cluster $[Ag_2Ru_4(\mu\text{-}CO)_3(CO)_{10}(PPh_3)_2]$ (2). The carbonyl C atoms have the same numbering as the O atoms to which they are attached.

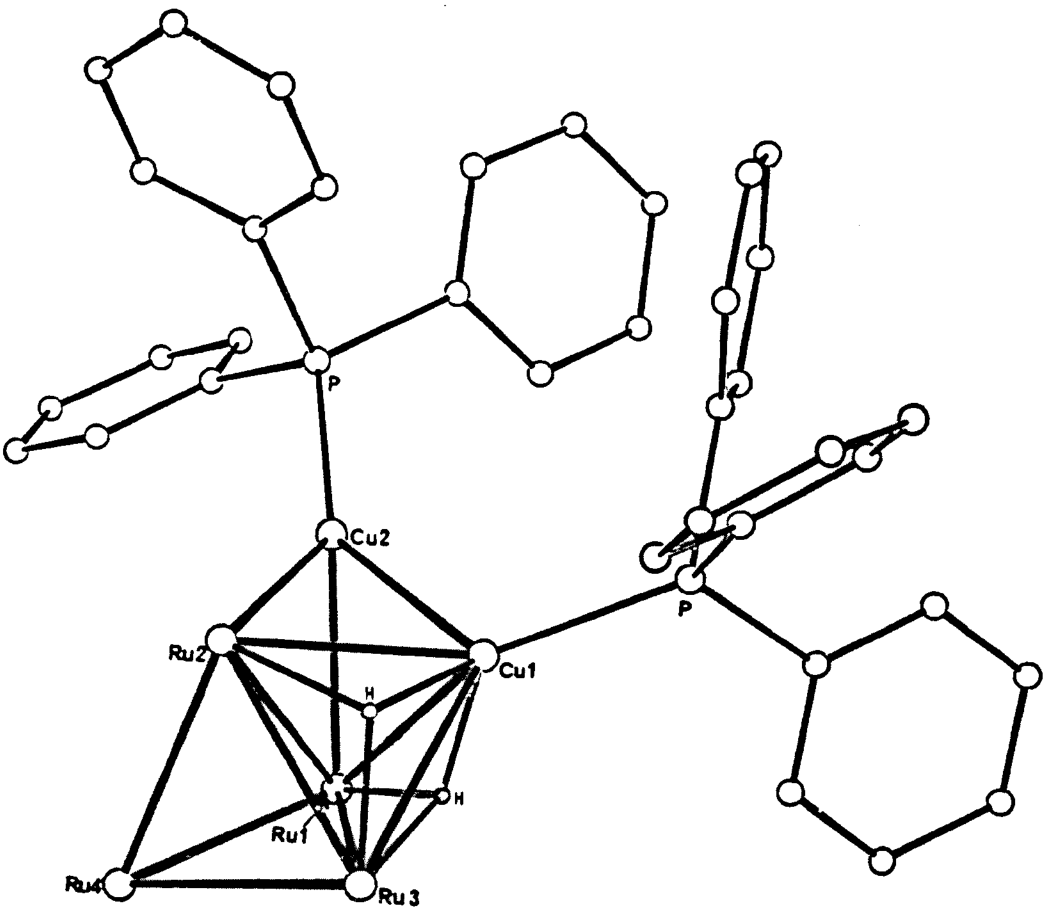

Figure 1.4.2. Molecular structures of the hydrido clusters $[M_2Ru_4(\mu_3\text{-}H)_2(CO)_{12}(PPh_3)_2]$ [M = Cu (3) and Ag (4)].[104] The carbonyl ligands have been omitted for clarity.

similar to that reported for the hydrido cluster $[Cu_2Ru_4(\mu_3-H)_2(CO)_{12}(PPh_3)_2]$ (3) {2.669-2.809(2) Å}. The mean Cu-Ru bond length in both (1) {2.702(2) Å} and (3) {2.706(2) Å} was significantly shorter than the corresponding mean bond in the structure of the pentanuclear cluster $[CuRu_4(\mu_3-H)_3(CO)_{12}\{PMePh_2\}]$ {mean Cu-Ru 2.738(1) Å}.[46] However, this mean bond in both (1) and (3) was markedly longer to that observed in the structures of the hexa-ruthenium cluster $[Cu_2Ru_6(CO)_{18}(C_6H_5Me)_2]$ {mean Cu-Ru 2.650(9) Å}[100] and the tetranuclear complex $[CuRu_3(CO)_9(C_2Bu^t)(PPh_3)]$ {mean Cu-Ru 2.603(1) Å}.[46] The two $Cu(PR_3)$ groups in (1) were found to cap the respective Ru_3 faces asymmetrically, with one Cu-Ru distance in each cap being significantly longer than the other two. The tetrahedral cap from Cu(1) was observed to have slightly enlarged than the symmetry related cap from Cu(2), with the mean of the six tetrahedral M-M bonds defining cap 1 {2.770(2) Å} being 0.011 Å longer than the corresponding mean for cap 2 {2.739(2) Å}:

Cap 1		Cap 2	
vector	distance/ Å		
Cu(1)-Ru(1)	2.806(2);	Cu(2)-Ru(1)	2.662(2)
Cu(1)-Ru(2)	2.656(2);	Cu(2)-Ru(2)	2.848(2)
Cu(1)-Ru(3)	2.633(2);	Cu(2)-Ru(4)	2.608(2)

The mean Ag-Ru bond in the hexanuclear cluster $[Ag_2Ru_4(\mu-CO)_3(CO)_{10}(PPh_3)_2\}]$ (2) {2.876(1) Å} was noteably shorter than the corresponding mean bond observed in the structure of the related hydrido cluster $[Ag_2Ru_4(\mu_3-H)_2(CO)_{12}(PPh_3)_2]$ (4) {2.894(1) Å}},[104] but longer than the mean of the two Ag-Ru bonds reported for the silver-copper cluster $[AgCuRu_4(\mu_3-H)_2(CO)_{12}(PPh_3)_2$ {2.822(1) Å}.[106]

The two Ag(PPh$_3$) groups in (2) were also found to adopt asymmetric capping positions, although the differnce between the longer and two shorter Ag-Ru separations from Ag(2) was not as significant as that from Ag(1). However, the mean of the six M-M bonds defining the tetrahedral cap from Ag(1) {2.895(1) Å} was found to be only 0.003 Å longer than the corresponding mean bond from Ag(2) {2.892(1) Å}.

Cap 1		Cap 2	
vector	distance/ Å		
Ag(1)-Ru(1)	2.977(1);	Ag(2)-Ru(1)	2.838(1)
Ag(1)-Ru(2)	2.861(1);	Ag(2)-Ru(2)	2.905(1)
Ag(1)-Ru(3)	2.806(1);	Ag(2)-Ru(4)	2.872(1)

In the copper-ruthenium cluster (1), the Ru-Ru distances associated with the two capping Cu(PPh$_3$) groups also exhibited marked asymmetry, with one bond in each cap being markedly longer than the other two, although the difference in the mean of the three Ru-Ru distances capped by each copper atom was very small:

vector	distance/ Å		
Ru(1)-Ru(2)	2.771(2);	Ru(1)-Ru(2)	2.771(2)
Ru(1)-Ru(3)	2.797(2);	Ru(1)-Ru(4)	2.981(2)
Ru(2)-Ru(3)	2.958(2);	Ru(2)-Ru(4)	2.793(2)
mean	2.842(2)		2.848(2)

Similar asymmetry was also observed in the Ru-Ru bond lengths capped by the two Ag(PPh$_3$) groups in (2), with the mean of the three Ru-Ru bonds capped by Ag(1) being 0.021 Å longer than the corresponding mean bond associated with Ag(2):

vector	distance/ Å		
Ru(1)-Ru(2)	2.797(1);	Ru(1)-Ru(2)	2.797(1)
Ru(1)-Ru(3)	2.853(1);	Ru(1)-Ru(4)	2.997(1)
Ru(2)-Ru(3)	3.074(1);	Ru(2)-Ru(4)	2.866(1)
mean	2.908(1)		2.887(1)

In the hexanuclear cluster $[Cu_2Ru_4(\mu\text{-}CO)_3(CO)_{10}(PPh_3)_2]$ (1) the bonds Ru(1)-Ru(4) {2.981(2) Å} and Ru(2)-Ru(3) {2.958(2) Å} were markedly longer not only to the mean of the three ruthenium bonds, Ru(1)-Ru(2), Ru(1)-Ru(3) and Ru(2)-Ru(4) bridged by carbonyl groups, {mean 2.787(2) Å}, but significantly longer to the unbridged bond, Ru(3)-Ru(4) {2.842(2) Å}. Similarly, in the related Ag_2Ru_4 cluster $[Ag_2Ru_4(\mu\text{-}CO)_3(CO)_{10}(PPh_3)_2]$ (2), the analogous bonds, Ru(1)-Ru(4) {2.997(1) Å} and Ru(2)-Ru(3) {3.074(1) Å}, were noteably longer than the mean of the three Ru-Ru bonds bridged by carbonyl groups {2.839(1) Å}, and the unbridged bond, Ru(3)-Ru(4) {2.849(1) Å}. All six Ru-Ru bonds in the silver-ruthenim cluster (2) were found to be longer than the related bonds in the copper-ruthenium cluster (1), {Table 1.4.2}. Importantly, the mean Ru-Ru distance in (1) {2.857(2) Å} was observed to be 0.013 Å shorter than the corresponding mean bond in the hydrido analogue $[Cu_2Ru_4(\mu_3\text{-}H)_2(CO)_{12}(PPh_3)]$ (3) {mean bond 2.870 Å}. As expected the hydride bridged bond, Ru(1)-Ru(3) in (3) was markedly longer than the corresponding bond in the non-hydrido cluster compound (1), however, the second H-bridged bond, Ru(2)-Ru(3) in (3) was slightly shorter than the analogous bond in (1), {Table 1.4.2}. The mean Ru-Ru bond in the non-hydrido silver complex (2) {2.906(1) Å} was found to be 0.023 Å longer than mean bond in the hydrido silver derivative $[Ag_2Ru_4(\mu_3\text{-}H)_2(CO)_{12}(PPh_3)_2]$ (4) {mean bond 2.883(1) Å}. The hydride bridged bonds in (4) also showed asymmetry, with the bond Ru(1)-Ru(3) being longer than the bond in (2), whereas the second bridged bond, Ru(2)-Ru(3) was noteably shorter than the corresponding bond length in (2), {Table 1.4.2}.

In the di-copper complex $[Cu_2Ru_4(\mu\text{-}CO)_3(CO)_{10}(PPh_3)_2]$ (1), the ten terminal CO groups showed expected linearity, {Ru-C-O 165-177(3)^o}, and the three bridging carbonyls exhibited symmetrical bonding:

Bond	Distance/ Å	Angle/^{o}	
Ru(1)-C(13)	2.065(4)	O(13)-C(13)-Ru(1)	136(2)
Ru(3)-C(13)	2.105(4)	O(13)-C(13)-Ru(3)	139(2)
Ru(1)-C(21)	2.126(5)	O(21)-C(21)-Ru(1)	142(2)
Ru(2)-C(21)	2.230(3)	O(21)-C(21)-Ru(2)	139(2)
Ru(2)-C(24)	2.031(4)	O(24)-C(24)-Ru(2)	136(1)
Ru(4)-C(24)	2.145(4)	O(24)-C(24)-Ru(4)	140(1)

In the analogous silver complex $[Ag_2Ru_4(\mu\text{-}CO)_3(CO)_{10}(PPh_3)_2]$ (2), the ten terminal carbonyls also exhibited similar linearity {Ru-C-O 162-175(3)^o}, however, of the three bridging carbonyl groups, CO(21) was found to show marked asymmetric bonding to Ru(1) and Ru(2), with this Ru-Ru bond being shortest in the structure, {Table 1.4.2}.

Bond	Distance/ Å	Angle/^{o}	
Ru(1)-C(13)	1.953(3)	O(13)-C(13)-Ru(1)	142(1)
Ru(3)-C(13)	2.193(3)	O(13)-C(13)-Ru(3)	132(1)
Ru(1)-C(21)	2.589(3)	O(21)-C(21)-Ru(1)	129(1)

Ru(2)-C(21)	1.967(4)	O(21)-C(21)-Ru(2)	156(1)
Ru(2)-C(24)	2.196(3)	O(24)-C(24)-Ru(2)	132.9(9)
Ru(4)-C(24)	2.044(3)	O(24)-C(24)-Ru(4)	142(1)

Three short contacts between the copper atoms and the carbonyl groups in compound (1) were observed, (Cu(1)...C(32) 2.59(3);Cu(1)...C(22) 2.63(3);Cu(2)...C(11) 2.66(3);Cu(2)...(C42) 2.45(3) Å). Whereas in the silver cluster (2), only one significantly short contact occurred, (Ag(1)...C(32) 2.69(4) Å). Similar short Group IB metal to carbon contacts were also a structural feature in the reported tetranuclear cluster $[CuRu_3(CO)_9(C_2Bu^t)(PPh_3)]$, (short Cu-C contact 2.552(7) and 2.4967(7) Å)[46] and $[AgRu_3(CO)_9(C_2Bu^t)(PPh_3)]$ (short Ag-C contact 2.69(2) Å). The mean Cu-P bond in (1) {2.234(6) A} was found to closely resemble the corresponding mean observed in the structure of the hydrido analogue (3) {2.234(4) Å},[104] but both mean lengths were markedly longer than the Cu-P bond length reported for the clusters $[CuRu_4(\mu_3\text{-}H)_3(CO)_{12}(PMePh_2)]$ {Cu-P 2.197(2) Å}, and $[CuRu_3(CO)_9(C_2Bu^t)(PPh_3)]$ {Cu-P 2.217(2) Å}.[46] The mean Ag-P bond length in (2) {2.418(3) Å} was noteably longer than the analogous mean bond in the hydrido cluster (4) {2.402(3) Å}[104] and the Ag-P bond length reported for the hexanuclear mixed-metal cluster $[AgCuRu_4(\mu_3\text{-}H)_2(CO)_{12}(PPh_3)_2]$ {2.400(2) Å}.[106]

Interestingly, on comparison of the Cu-P and Ag-P bond distances in clusters (1)-(4) to the Au-P bonds in the related gold-ruthenium cluster,[104] $[Au_2Ru_4(\mu_3\text{-}H)(\mu_2\text{-}H)(CO)_{12}(PPh_3)_2]$, a significant trend in the M-P bonds was observed:

compound	mean M-P/ Å
$[Cu_2Ru_4(\mu\text{-}CO)_3(CO)_{10}(PPh_3)]$ (1)	2.234(6)
$[Ag_2Ru_4(\mu\text{-}CO)_3(CO)_{10}(PPh_3)_2]$ (2)	2.418(3)
$[Cu_2Ru_4(\mu_3\text{-}H)_2(CO)_{12}(PPh_3)_2]$ (3)	2.234(3)
$[Ag_2Ru_4(\mu_3\text{-}H)_2(CO)_{12}(PPh_3)_2]$ (4)	2.402(2)
$[Au_2Ru_4(\mu_2\text{-}H)(\mu_3\text{-}H)(CO)_{12}(PPh_3)_2]$	2.284(4)

The mean Ag-P bond lengths in clusters (2) and (4) were markedly longer not only to the mean Cu-P distance in the related clusters (1) and (3), but markedly longer than the mean Au-P bond in the structure of the gold-ruthenium hydrido cluster $[Au_2Ru_4(\mu_2\text{-}H)_2(CO)_{12}(PPh_3)_2]$, a trend not anticipated with respect to the increasing atomic number of the Group IB metal atoms, Au > Ag > Cu.

1.4.3 Conclusions.

The following conclusions were drawn from the X-ray analysis of the hexa-ruthenium clusters $[M_2Ru_4(\mu\text{-}CO)_3(CO)_{10}(PPh_3)_2]$ [M = Cu (1) and Ag (2)]. The capped trigonal bipyramidal skeletal geometeries adopted by (1) and (2) were in marked contrast to the metal frameworks previously established for the related hydrido clusters $[M_2Ru_4(\mu_3\text{-}H)_2(CO)_{12}(PPh_3)_2]$ [Cu (3) and Ag (4)]. In both structures, one triangular face of the Ru_4 tetrahedron was capped by one $M(PPh_3)$ group and the resulting MRu_2 face further capped by the second $M(PPh_3)$ unit leading to the formation of Cu-Cu and Ag-Ag bonds, respectively.[104] The replacement of two hydrido ligands in (3) and (4) by a -CO group in (1) and (2) resulted in a major change in the positions adopted by the Group IB metal atoms on the ruthenium tetrahedra. The two copper and silver metal phosphines in their respective structures capped triangular Ru_3 faces, with no contact between the two hetero-metal atoms. As observed in the structures of compounds (1)-(4), relatively small changes in the attached ligands can have marked effects on the solid state geometries adopted by Group IB mixed-metal clusters. These results together with those presented in sections 1.1.8 and 1.3.6 provided further evidence to support that the energy differences between the various metal frameworks can be very small for many mixed-metal clusters containing Group IB metal phosphine groups, and the likelihood of interconversion from one form to another is therefore probable.

Table 1.4.2.

M(1) = Cu in (1) and (3); Ag in (2) and (4)

M(2) = Cu in (1) and (3); Ag in (2) and (4)

Bond	Distance/ Å			
	(1)	(2)	(3)[104*]	(4)[104*]
M(1)-M(2)	-	-	2.669(2)	2.857(1)
M(1)-Ru(1)	2.806(2)	2.977(1)	2.671(2)	2.880(1)
M(1)-Ru(2)	2.656(2)	2.861(1)	2.674(2)	2.913(1)
M(1)-Ru(3)	2.633(2)	2.806(1)	2.809(2)	2.980(1)
M(2)-Ru(1)	2.662(2)	2.838(1)	2.679(2)	2.855(1)
M(2)-Ru(2)	2.848(2)	2.905(1)	2.699(2)	2.842(1)
M(2)-Ru(4)	2.608(2)	2.872(1)	-	-
Ru(1)-Ru(2)	2.771(2)	2.797(1)	2.923(2)	2.961(1)
Ru(1)-Ru(3)	2.797(2)	2.853(1)	2.966(2)	2.967(1)
Ru(1)-Ru(4)	2.981(2)	2.997(1)	2.795(2)	2.806(1)
Ru(2)-Ru(3)	2.958(2)	3.074(1)	2.947(2)	2.979(1)
Ru(2)-Ru(4)	2.793(2)	2.866(1)	2.800(2)	2.799(1)
Ru(3)-Ru(4)	2.842(2)	2.849(1)	2.790(2)	2.785(1)
mean M-P	2.234(6)	2.418(3)	2.234(3)	2.402(3)

* re-numbered for comparison.

Section 1.5. References.

1. M. Elian, M.M.L. Chen, D.M.P. Mingos, R.Hoffmann, Inorg. Chem., 1976, 15, 1148; R. Hoffmann, Angew. Chem., Int. Ed. Eng., 1982, 21, 711.

2. J.W. Lauher and K. Wald, J. Am. Chem. Soc., 1981, 103, 7648.

3. T.L. Blundell, H.M. Powell, J. Chem. Soc.(A), 1971, 1685.

4. E.A. McNeill and F.R. Scholer, J. Am. Chem. Soc., 1977, 99, 6243.

5. F.E. Simon, J.W. Lauher, J. Am. Chem. Soc., 1982, 102, 7448.

6. M.R. Churchill, R.A. Lashewycz, Inorg. Chem., 1979, 18, 1926.

7. M.R. Churchill, R.A. Lashewycz, Inorg. Chem., 1979, 18, 3261.

8. C.W. Bradford, W. van Bronswijk, R.J.H. Clark, and R.S. Nyholm, J. Chem. Soc.(A), 1970, 2889.

9. B.T. Huie, C.B. Knobler, and H.D. Kaesz, J. Chem. Soc., Chem. Commun., 1975, 684.

10. B.T. Huie, C.B. Knobler, and H.D. Kaesz, J. Am. Chem. Soc., 1978, 100, 3059.

11. R.G. Teller, R.D. Wilson, R.K. McMullan, T.F. Koetzle, and R. Bau, J. Am. Chem. Soc., 1978, 100, 3071.

12. B.F.G. Johnson, D.A. Kaner, J. Lewis, P.R. Raithby, and M.J. Taylor, J. Chem. Soc., Chem. Commun., 1982, 314.

13. D.B.W. Yawney and R.J. Doedens, Inorg. Chem., 1972, 11, 838.

14. B.F.G. Johnson, J. Lewis, P.R. Raithby, and C. Zuccaro, Acta Cryst., 1981, B37, 1728.

15. L. Malatesta, L. Naldini, G. Simonetta, and F. Cariati, J. Chem. Soc., Chem. Commun., 1965, 212.

16. L. Malatesta, L. Naldini, G. Simonetta, and F. Cariati, Co-ordination Chem. Rev., 1966, 1, 255.

17. L. Malatesta, L. Naldini, G. Simonetta, and F. Cariati, Inorg. Chim. Acta, 1967, 1, 24, 315.

18. F. Cariati and L. Naldini, Inorg. Chim. Acta, 1971, 5, 172.

19. M. McPartlin, R. Mason, and L. Malatesta, J. Chem. Soc., Chem. Commun., 1969, 334.

20. V.G. Albano, P.L. Bellon, M. Manaserro, and M. Sansoni, J. Chem. Soc., Chem. Commun., 1970, 1210.

21. P.L. Bellon, M. Manaserro, and M. Sansoni, J. Chem. Soc., Dalton Trans., 1972, 1481.

22. P.L. Bellon, F. Cariati, M. Manaserro, L. Naldini, and M. Sansoni, J. Chem. Soc., Chem. Commun., 1971, 1423.

23. D.M.P. Mingos, J. Chem. Soc., Dalton Trans., 1976, 1163.

24. D.G. Evans and D.M.P. Mingos, J. Organomet. Chem., 1982, 232, 171.

25. K.P. Hall and D.M.P. Mingos, Prog. Inorg. Chem., 1984, 32, 237.

26. B.F.G. Johnson, D.A. Kaner, J. Lewis, and P.R. Raithby, J. Organomet. Chem., 1981, 215, C33.

27. M.R. Churchill, F.J. Hollander, J.P. Hutchinson, Inorg. Chem., 1977, 16, 2697.

28. M.R. Churchill, R.A. Lashewycz, and F.J. Rotella, Inorg. Chem., 1977, 16, 265.

29. P. Braunstein, J. Rosé, A.M. Manotti-Lanfredi, A. Tiripicchio, and E. Sappa, J. Chem. Soc., Dalton Trans., 1984, 1843.

30. S.G. Shore, W.L. Hsu, C.R. Weisenberger, M.L. Caste, M.R. Churchill, and C. Bueno, Organometallics, 1982, 1, 1405.

31. F.G.A. Stone, Angew. Chem., Int. Ed. Engl., 1984, 23, 89.

32. M. Green, A.G. Orpen, I.D. Salter, F.G.A. Stone, J. Chem. Soc., Chem. Commun., 1982, 813.

33. B.F.G. Johnson, J. Lewis, W.J.H. Nelson, M.D. Vargas, D. Braga, and M. McPartlin, J. Organomet. Chem., 1983, 246, C69; B.F.G. Johnson, J. Lewis, W.J.H. Nelson, M.D. Vargas, D. Braga, K. Henrick, M. McPartlin, J. Chem. Soc., Dalton Trans., 1986, 975.

34. I.D. Salter and F.G.A. Stone, J. Organomet. Chem., 1984, 260, C71.

35. P. Braunstein, J. Rosé, A. Dedieu, A. Dusausoy, J.P. Mangeot, A. Tiripicchio, and M. Tiripicchio-Camellini, J. Chem. Soc., Dalton Trans., 1986, 225.

36. T. Beringhelli, G. Ciani, G. D'Alfonso, V. De Maldé, and M. Freni, J. Chem. Soc., Chem. Commun., 1986, 735.

37. B.F.G. Johnson, J. Lewis, A.G. Orpen, P.R. Raithby, and G. Süss, J. Organomet. Chem., 1979, 173, 187.

38. T.J. Henly, J.R. Shapley, and A.L. Rheingold, J. Organomet. Chem., 1986, 310, 55.

39. P.F. Jackson, B.F.G. Johnson, J. Lewis, M. McPartlin, and W.J.H. Nelson, J. Chem. Soc., Chem. Commun., 1982, 49.

40. C.E. Briant, B.R.C. Theobald, J.W. White, L.K. Bell, and D.M.P. Mingos, J. Chem. Soc., Chem. Commun., 1981, 201.

41. B.F.G. Johnson, D.A. Kaner, J. Lewis, P.R. Raithby, and M.J. Taylor, Polyhedron, 1982, 1, 105.

42. K. Burgess, B.F.G. Johnson, D.A. Kaner, J. Lewis, P.R. Raithby, and S.N.A.B. Syed-Mustaffa, J. Chem. Soc., Chem. Commun., 1983, 455.

43. B.F.G. Johnson, J. Lewis, P.R. Raithby, S.N.A.B. Syed-Mustaffa, M.J. Taylor, K.H. Whitmire, and W. Clegg, J. Chem. Soc., Dalton Trans., 1984, 2111.

44. S. Attali, F. Dahan, and R. Mathieu, J. Chem. Soc., Dalton Trans., 1985, 2521.

45. M. Müller-Glieman, S.V. Hoskins, A.G. Orpen, A.L. Ratermann, and F.G.A. Stone, Polyhedron, 1986, 5, 791.

46. R.A. Brice, S.C. Pearse, I.D. Salter, and K. Henrick, J. Chem. Soc., Dalton Trans., 1986, 2181.

47. M.I. Bruce, M.L. Williams, J.M. Patrick, B.W. Skelton, and A.H. White, J. Chem. Soc., Dalton Trans., 1986, 2557.

48. C.P. Horwitz and D.F. Shriver, J. Am. Chem. Soc., 1985, 107, 8147.

49. C.P. Horwitz, E.M. Holt, C.P. Brock, and D.F. Shriver, J. Am. Chem. Soc., 1985, 107, 8136.

50. D. Braga, K. Henrick, B.F.G. Johnson, J. Lewis, M. McPartlin, W.J.H. Nelson, A. Sironi, and M.D. Vargas, J. Chem. Soc., Chem. Commun., 1983, 1131.

51. J. Puga, R.A. Sanchez-Delgado, J. Ascanio, and D. Braga, J. Chem. Soc., Chem. Commun., 1986, 1631.

52. J.A. Iggo, M.J. Mays, P.R. Raithby, K. Henrick, J. Chem. Soc., Dalton Trans., 1984, 633.

53. M.J. Mays, P.R. Raithby, P.L. Taylor, and K. Henrick, J. Chem. Soc., Dalton Trans., 1984, 959.

54. M.I. Bruce, E. Horn, J.G. Matisons, and M.R. Snow, J. Organomet. Chem., 1985, 286, 271.

55. S.B. Colbran, C.M. Hay, B.F.G. Johnson, F.J. Lahoz, J. Lewis, and P.R. Raithby, J. Chem. Soc., Chem. Commun., 1986, 1766.

56. V. Riera, M.A. Ruiz, A. Tiripicchio, and M. Tiripicchio-Camellini, J. Chem. Soc., Dalton Trans., 1987, 1551.

57. M.F. Hallam, M.A. Luke, D.M.P. Mingos, and I.D. Williams, J. Organomet. Chem., 1987, 325, 271.

58. B.T. Heaton, L. Strona, S. Martinengo, D. Strumolo, V.G. Albano, and D. Braga, J. Chem. Soc., Dalton Trans., 1983, 2175.

59. T. Beringhelli, G. D'Alfonso, M. Freni, G. Ciani, and A. Sironi, J. Organomet. Chem., 1985, 295, C7.

60. S. Bhaduri, K. Sharma, P.G. Jones, and C. Freire Erdbrügger, J. Organomet. Chem., 1987, 326, C46.

61. L.J. Farrugia, J.A.K. Howard, P. Mitrprachachon, J.L. Spencer, F.G.A. Stone, and P. Woodward, J. Chem. Soc., Chem. Commun., 1978, 260.

62. B.F.G. Johnson, D.A. Kaner, J. Lewis, P.R. Raithby, and M.J. Rosales, J. Organomet. Chem., 1982, 231, C59.

63. M.I. Bruce, and B.K. Nicholson, J. Organomet. Chem., 1983, 250, 627.

64. L.J. Farrugia, M.J. Freeman, M. Green, A.G. Orpen, F.G.A. Stone, and I.D. Salter, J. Organomet. Chem., 1983, 249, 273.

65. M.I. Bruce, O. bin Shawkataly, and B.K. Nicholson, J. Organomet. Chem., 1985, 286, 427.

66. T. Blumenthal, M.I. Bruce, O. bin Shawkataly, B.N. Green, and I. Lewis, J. Organomet. Chem., 1984, 269, C10.

67. L.W. Bateman, M. Green, K.A. Mead, R.M. Mills, I.D. Salter, F.G.A. Stone, and P. Woodward, J. Chem. Soc., Dalton Trans., 1983, 2599.

68. L.S. Moore, R.V. Parish, S.S.D. Brown, and I.D. Salter, J. Chem. Soc., Dalton Trans., 1987, 2333.

69. M.I. Bruce and B.K. Nicholson, J. Organomet. Chem., 1983, 252, 243.

70. J. Evans, A.G. Street, and M. Webster, Organometallics, 1987, 6, 794.

71. A.G. Cowie, B.F.G. Johnson, J. Lewis, J.N. Nicholls, P.R. Raithby, and M.J. Rosales, J. Chem. Soc., Dalton Trans., 1983, 2311.

72. B.F.G. Johnson, J. Lewis, J.N. Nicholls, and K. Whitmire, J. Chem. Soc., Dalton Trans., 1983, 787.

73. K. Burgess, B.F.G. Johnson, J. Lewis, and P.R. Raithby, J. Chem. Soc., Dalton Trans., 1983, 1661.

74. G.A. Carriedo, J.A.K. Howard, F.G.A. Stone, and M.J. Went, J. Chem. Soc., Dalton Trans., 1984, 2545.

75. K. Fischer, M. Müller, and H. Vahrenkamp, Angew. Chem., Int. Ed. Engl., 1984, 23, 140.

76. A.G. Cowie, B.F.G. Johnson, J. Lewis, and P.R. Raithby, J. Chem. Soc., Chem. Commun., 1984, 1710.

77. A.G. Cowie, B.F.G. Johnson, J. Lewis, J.N. Nicholls, P.R. Raithby, and A.G. Swanson, J. Chem. Soc., Chem. Commun., 1984, 637.

78. H. Umland, U. Behrens, J. Organomet. Chem., 1985, 287, 109.

79. P. Braunstein, G. Predieri, A. Tiripicchio, and E. Sappa, Inorg. Chim. Acta. 1982, 63, 113.

80. K. Henrick, B.F.G. Johnson, J. Lewis, J. Mace, M. McPartlin, and J. Morris, J. Chem. Soc., Chem. Commun., 1985, 1617.

81. S.L. Schiavo, G. Bruno, F. Nicholo, P. Piraino, F. Faraone, Organometallics, 1985, 4, 2091.

82. A.A. Aitchison and L.J. Farrugia, Organometallics, 1986, 5, 1103.

83. G. Lavigne, F. Papageorgiou, and J.J. Bonnet, Inorg. Chem., 1984, 23, 609.

84. A.J. Deeming, S. Donovan-Mtunzi, and K. Hardcastle, J. Chem. Soc., Dalton Trans., 1986, 543.

85. G.A. Moehring, P.E. Fanwick, and R.W. Walton, Inorg. Chem., 1987, 26, 1861.

86. M.L. Blohm, and W.L. Gladfelter, Inorg. Chem., 1987, 26, 459.

87. M. Ahlgren, T.T. Pakkanen, and I. Tahvanainen, J. Organomet. Chem., 1987, 323, 91.

88. B.F.G. Johnson, J. Lewis, W.J.H. Nelson, J. Puga, P.R. Raithby, D. Braga, M. McPartlin, and W. Clegg, J. Organomet.Chem., 1983, 243, C13.

89. A.L. Casalnuovo, L.H. Pignolet, J.W.A. van der Velden, J.J. Bour, and J.J. Steggerda, J. Am. Chem. Soc., 1983, 105, 5957.

90. M.I. Bruce and B.K. Nicholson, Organometallics, 1984, 3, 101.

91. D.M.P. Mingos and R.W.M. Wardle, J. Chem. Soc., Dalton Trans., 1986, 73.

92. J. Pursianen, M. Ahlgren, and T.A. Pakkanen, J. Organomet. Chem., 1985, 297, 391.

93. J.J. Bour, R.P.F. Kanters, P.P.J. Schlebos, W. Bos, W.P. Bosman, H. Behm, P.T. Beur, and J.J. Steggerda, J. Organomet. Chem., 1987, 329, 405.

94. V. Riera, M.A. Ruiz, A. Tiripicchio, and M. Tiripicchio-Camellini, J. Chem. Soc., Chem. Commun., 1985, 1505.

95. B.F.G. Johnson, J. Lewis, W.J.H. Nelson, J.N. Nicholls, J. Puga, P.R. Raithby, W.J. Rosales, M. Schroder, and M.D. Vargas, J. Chem. Soc., Dalton Trans., 1983, 2447.

96. S.R. Bunkhall, H.D. Holden, B.F.G. Johnson, J. Lewis, G.N. Pain, P.R. Raithby, and M.J. Taylor, J. Chem. Soc., Chem. Commun., 1984, 25.

97. B.R. Sutherland, D.M. Ho, J.C. Huffman, and K.G. Caulton, Angew. Chem., Int. Ed. Engl., 1987, 26, 135.

98. C.M. Hay, B.F.G. Johnson, J. Lewis, R.C.S. McQueen, P.R. Raithby, R.M. Sorrell, and M.J. Taylor, Organometallics, 1985, 4, 202.

99. V.G. Albano, D. Braga, S. Martinengo, P. Chini, M. Sansoni, and D. Strumolo, J. Chem. Soc., Dalton Trans., 1980, 52.

100. G.B. Ansell, M.A. Modrick, and J.S. Bradley, Acta Cryst., 1984, C40, 365.

101. S.S.D. Brown, I.D. Salter, T. Adatia, and, M. McPartlin, J. Organomet.Chem., 1987, 332, C6.

102. B.F.G. Johnson, J. Lewis, W.J.H. Nelson, P.R. Raithby, and M.D. Vargas, J. Chem. Soc., Chem. Commun., 1983, 608.

103. D.M.P. Mingos, P. Oster, and D.J. Sherman, J. Organomet. Chem., 1987, 320, 257.

104. M.J. Freeman, A.G. Orpen, and I.D. Salter, J. Chem. Soc., Dalton Trans., 1987, 379.

105. S.S.D. Brown, S. Hudson, I.D. Salter, and M. McPartlin, J. Chem. Soc., Dalton Trans., 1987, 1967.

106. M.J. Freeman, A.G. Orpen, and I.D. Salter, J. Chem. Soc., Dalton Trans., 1987, 1001.

107. E. Roland, K. Fischer, and H. Vahrenkamp, Angew. Chem., Int. Ed. Engl., 1983, 22, 326.

108. M.I. Bruce, O. bin Shawkataly, and B.K. Nicholson, J. Organomet. Chem., 1985, 280, 289.

109. J.N. Nicholls, P.R. Raithby, and M.D. Vargas, J. Chem. Soc., Chem. Commun., 1986, 1617.

110. C.E. Housecroft and A.L. Rheingold, Organometallics, 1987, 6, 1332.

111. B.F.G. Johnson, D.A. Kaner, J. Lewis, and M.J. Rosales, J. Organomet. Chem., 1982, 238, C73.

112. L.F. Rhodes, J.C. Huffman, and K.G. Caulton, J. Am. Chem. Soc., 1985, 107, 1759.

113. J.A.K. Howard, I.D. Salter, and F.G.A. Stone, Polyhedron, 1984, 3, 567.

114. M.I. Bruce, O. bin Shawkataly, and B.K. Nicholson, J. Organomet. Chem., 1984, 275, 223.

115. J. Ellis, J. Am. Chem. Soc., 1981, 103, 6106.

116. P.D. Boyle, B.J. Johnson, A. Buehler, and L.H. Pignolet, Inorg. Chem., 1986, 25, 5.

117. (a) P.D. Boyle, B.J. Johnson, B.D. Alexander, J.A. Casalnuovo, P.R. Gannon, S.M. Johnson, E.A. Larka, A.M. Mueting, and L.H. Pignolet, Inorg. Chem., 1987, 26, 1346;(b) P.D. Boyle, B.J. Johnson, J.A. Casalnuovo, S.M. Johnson, A.M. Mueting, and L.H. Pignolet, Inorg. Chem., 1987, 26, 2547.

118. B.R. Sutherland, K. Floting, W.E. Steib, D.M. Ho, J.C. Huffman, and K.G. Caulton, J. Am. Chem. Soc., 1987, 109, 3489.

119. J.E. Ellis and R.A. Faltynek, J. Am. Chem. Soc., 1977, 99, 1801.

120. A.L. Casalnuovo, J.A. Casalnuovo, P.V. Nilsson, and L.H. Pignolet, Inorg. Chem., 1985, 24, 2554.

121. C.E. Briant, R.G. Smith, and D.M.P. Mingos, J. Chem. Soc., Chem. Commun., 1984, 586.

122. J.W.A. van der Velden, J.J. Bour, B.F. Otterloo, W.P. Bosman, and J.H. Noordik, J. Chem. Soc., Chem. Commun., 1981, 583.

123. B.K. Teo, and K. Keating, J. Am. Chem. Soc., 1984, 106, 2224.

124. B.K. Teo, K. Keating, and Y-H Kao, J. Am. Chem. Soc., 1987, 109, 3494.

125. J.S. Bradley, R.L. Pruett, E. Hill, G.B. Ansell, M.E. Leonowicz, and M.A. Modrick, Organometallics, 1982, 1, 748.

126. J.W.A. van der Velden, P.T. Beurskens, J.J. Bour, W.P. Bosman, J.H. Noordik, K.M. Kolenbrander, and J.A.K.M. Buskes, Inorg. Chem., 1984, 23, 497.

127. C.E. Briant, K.P. Hall, and D.M.P. Mingos, J. Chem. Soc., Chem. Commun., 1984, 290.

128. F.A. Vollenbroek, J.P. van der Berg, J.W.A. van der Velden, and J.J. Bour, Inorg. Chem., 1980, 19, 2685.

129. C.E. Briant, K.P. Hall, D.M.P. Mingos, J. Organomet. Chem., 1982, 299, C5.

130. B.F.G. Johnson, J. Chem. Soc., Chem. Commun., 1986, 27.

131. S.R. Drake, B.F.G. Johnson, J.Lewis, J. Organomet. Chem., 1988, 340, C31.

132. M. Catti, G. Gervasio, and S.A. Mason, J. Chem. Soc., Dalton Trans., 1977, 2260.

133. C. Braner-Thorsen, K.I. Hardcastle, E. Rosenberg, J. Siegel, A.M. Manotti-Lanfredi, A. Tiripicchio, and M. Tiripicchio-Camellini, Inorg. Chem., 1981, 20, 4306.

134. P.A. Bates, S.S.D. Brown, A.J. Dent, M. Hursthouse, G.F.M. Kitchen, A.G. Orpen, I.D. Salter, and V. Sik, J. Chem. Soc., Chem. Commun., 1986, 600.

135. M. Fajardo, M.P. Gomez-Sal, H.D. Holden, B.F.G. Johnson, J. Lewis, R.C.S. McQueen, and P.R. Raithby, J. Organomet. Chem., 1984, 267, C25.

136. B.F.G. Johnson, D.A. Kaner, J. Lewis, and P.R. Raithby, J. Chem. Soc., Chem. Commun., 1981, 751.

137. C.A. Tolman, J. Am. Chem. Soc., 1970, 92, 2953.

138. C.A. Tolman, J. Am. Chem. Soc., 1970, 92, 2956

139. A. Pidcock, Transition Metal Complexes of Phosphorus, Arsenic and Antimony Ligands, C.A. McAuliffe, Ed., Wiley New York, 1973.

140. R.W. Taft, Steric Effects in Organic Chemistry, M.S. Newman, Ed., Wiley, New York, 1972.

141. A.D.U. Hardy and G.A. Sim, J. Chem. Soc., Dalton Trans., 1972, 1900.

142. C.A. Tolman, Chem. Rev., 1977, 77, 313.

143. T. Adatia, M. McPartlin, P. McCarthy, M. Rizza, I.D. Salter, J. Chem. Soc., Chem. Commun., in press.

144. A.G. Orpen, J. Chem. Soc., Dalton Trans., 1980, 2509.

CHAPTER 2

Bidentate organophosphines: The structural studies of their mixed-metal clusters containing Group IB metal atoms Cu, Ag, or Au.

Section 2.1. Introduction.

The ability of tertiary phosphine ligands to bind to transition metal atoms in co-ordination chemistry has been well established. The interesting feature in the synthesis of these organophosphine groups arises with the great ease in the variation of their steric and electronic properties, simply by changing the substituents on the phosphorus atom.[1-6] The ligands have found to bond strongly to many transition metals in low oxidation state and are commonly used to stabilize organometallic and hydride derivatives of the elements in isolated compounds or as intermediates in homogenous or heterogenous catalysis.[7-14] The chemistry of binuclear metal complexes, for example, $[RhCl(CO)\{Ph_2P(CH_2)_nPPh_2\}]$ [n = 1 (dppm), 2 (dppe), 3 (dppp), and 4 (dppb)] has described the ability of these bidentate ligands to chelate in such compounds in the formation of four membered rings.[3-6] The cyclic rings formed with the di-phosphine group, dppm, can often be strained leading to a greater flexibility of the group to act as either a monodentate or bidentate co-ordinating ligand. More recent interest in these complexes has been stimulated by the structural feature of the bridging phosphine to 'link' two metal centres, for example in the dimer $[RhCl(CO)\{dppm\}]_2$, preventing dissociation of the dimeric molecule to a monomer and promoting reactions involving formation and cleavage of M-M bonds.[15-17]

The use of bridging phosphine groups has been extended to polynuclear metal cluster systems to prevent cluster degradation under severe conditions. Subsequent isolation and characterisation of these compounds has displayed a variety of bonding modes adopted by the phosphine bridges. Importantly, correlation of the structural data for related mixed-metal cluster compounds has shown, that in some cases the steric strains imposed by the bidentate organophosphine ligands have been sufficent, to have marked effects on the overall metal core geometries adopted in the solid state.

Survey of bonding modes adopted by bidentate organophosphine ligands in related homonuclear ruthenium clusters of nuclearity 3 to 6.

The reaction between bis(diphenylphosphino)methane (dppm) and the trinuclear cluster $[Ru_3(CO)_{12}]$ was first reported by Cotton and Hanson in 1977, together with the fluxional properties of the resulting complex $[Ru_3(CO)_{10}\{\mu\text{-}Ph_2PCH_2PPh_2\}]$.[18] From ^{13}C n.m.r. spectral data, two possible co-ordination sites for the dppm ligand were proposed, firstly with the phosphine group chelated in an equatorial plane to a single ruthenium atom, and secondly, bridging two ruthenium atoms with the phosphorus atoms in the equatorial plane. The complete structural analysis of the trinuclear complex, $[Ru_3(CO)_{10}\{\mu\text{-}Ph_2PCH_2PPh_2\}]$ was not reported until 1984 by Lavigne and co-workers.[19] The geometry was established with one edge of the ruthenium metal triangle bridged by the dppm ligand, {Figure 2.1(a)}. The workers also observed that among the three ruthenium bonds, Ru(1)-Ru(2) supported by the bridging dppm ligand {2.834(1) Å} was significantly shorter than the two unbridged bonds {2.841(1) and 2.860(1) Å, respectively}, in contrast to that previously observed in the tri-ruthenium complex, $[Ru_3(CO)_{10}\{Me_2AsC{=}C(AsMe_2)CF_2.CF_2\}]$,[20] where the two unbridged bonds were significantly shorter than the bridged Ru-Ru bond. They proposed that the observed variations in the M-M bond distances could have been attributed to the strain of the chelated ring. The intracyclic M-M-P angles in the dppm complex were found to be smaller in comparison to the M-M-As angles in the ditertiary arsine compound, {Figure 2.1(b)}.

Similar shortening of Ru-Ru bonds bridged by bidentate di-phosphine ligands was also previously observed in the related cluster compound $[Ru_3(CO)_8\{\mu\text{-}Ph_2PCH_2PPh_2\}_2]$.[21] The two edges of the ruthenium atom triangle supported by the organophosphine ligands, {Ru(1)-Ru(2) 2.826(2);Ru(1)-Ru(3) 2.833(2) Å} were significantly shorter than the unbridged bond, Ru(2)-Ru(3) {2.858(2) Å}, {Figure 2.1(c)}. In contrast, the X-ray structure of the dppe analogue $[Ru_3(CO)_{10}\{\mu\text{-}Ph_2P(CH_2)_2PPh_2\}]$ established that lengthening of the organic side chain of the bidentate ligand resulted in no significant variation of the three Ru-Ru bond distances, with the Ru-Ru bond bridged by the di-phosphine ligand {2.856(1) Å} being slightly longer than the two unbridged bonds, {2.855(1) and 2.847(1) Å, respectively}.[22]

The co-ordination of a bridging organophosphine ligand to a tetranuclear ruthenium metal core was reported by Bruce and co-workers in 1986, with the X-ray analysis of the tetra-hydrido cluster $[Ru_4(\mu\text{-}H)_4(CO)_{10}\{\mu\text{-}Ph_2PCH_2PPh_2\}]$, {Figure 2.1.(d)}.[23] The geometry was described as a distorted tetrahedral Ru_4 metal core with the dppm ligand 'spanning' the hydride bridged Ru(1)-Ru(2) vector. This bond distance of 2.987(1) Å was found to be markedly longer than the mean of the remaining five Ru-Ru bonds, {2.881(1) Å}. They also observed that the dppm ligand adopted a μ_3-bonding mode in the solid state structure of the tetra-ruthenium hydrido cluster $[Ru_4(\mu\text{-}H)_3(\mu\text{-}CO)_2(CO)_8\{\mu_3\text{-}PhPCH_2PPh_2\}]$, with one of the phosphorus atoms of the bridge acting as a 3e donor, {Figure 2.1(e)}.[23] Interestingly, with the longer organic backbone in the related dppe derivative $[Ru_4(\mu\text{-}H)_4(CO)_{10}\{Ph_2PCH_2CH_2PPh_2\}]$, the di-phosphine ligand was found to chelate to one ruthenium atom of the tetrahedron {Figure 2.1(f)}.[24] However, in the presence of trimethylamine oxide, Churchill and co-workers observed that the substitution of two carbonyl groups in $[Ru_4(\mu\text{-}H)_4(CO)_{12}]$ by the bridging dppe ligand occurred rapidly to yield a second isomer for the cluster compound $[Ru_4(\mu\text{-}H)_4(CO)_{10}\{\mu\text{-}Ph_2PCH_2CH_2PPh_2\}]$, whose X-ray structural analysis revealed a μ_2-bridging mode of the phosphine ligand, {Figure 2.1(g)}.[25] The available flexibility for bridging phosphine ligands with increasing organic side chains was well illustrated in the solid state structure of the penta-ruthenium carbido cluster, $[Ru_5C(CO)_{13}\{\mu\text{-}Ph_2P(CH_2)_4PPh_2\}]$.[26] The dppb ligand was found to 'strapp' across the square face of the ruthenium square pyramid, {Figure 2.1(h)}. In contrast, the bidentate ligand with a shorter organic backbone in the di-hydrido cluster $[Ru_5(\mu\text{-}H)_2C(CO)_{12}\{Ph_2PCH_2CH_2PPh_2\}]$ was found to chelate to one of the basal ruthenium atoms of the square pyramid, with one phosphorus atom occupying an axial and the other an equatorial site, {Figure 2.1(i)}.[27]

The co-ordination of a bidentate organophosphine group in a hexanuclear ruthenium cluster was recently reported by Gracey and co-workers with the X-ray analysis of the ruthenium carbido cluster compound $[Ru_6C(CO)_{15}\{\mu\text{-}Ph_2PCH_2PPh_2\}]$.[28] Low temperature ^{31}P n.m.r. data revealed that the two phosphorus atoms were in non-equivalent sites, which was consistent with the X-ray structure in which the dppm ligand was found to bridge one Ru-Ru edge of the octahedral cage, thus forming a five membered Ru-Ru-P-C-P ring, {Figure 2.1(j)}. The Ru-Ru bond length bridged by the dppm ligand {2.986(1) Å} was observed to be significantly longer not only to the remaining 11 Ru-Ru bonds of the Ru_6 octahedron, {2.898(1) Å}, but also to the mean of the 12 Ru-Ru bonds in the parent cluster $[Ru_6C(CO)_{17}]$ {mean 2.903(6) Å}.[29]

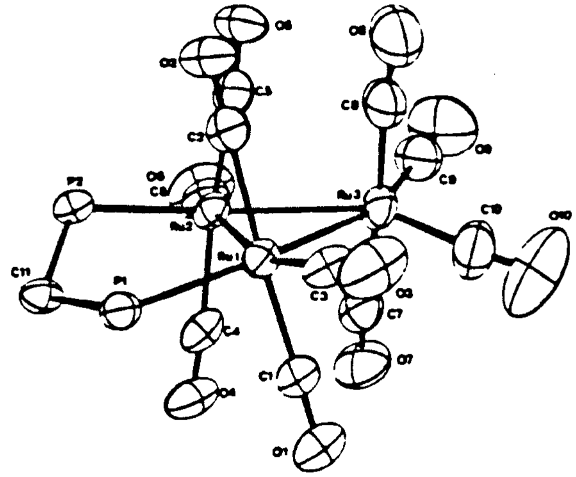

Figure 2.1(a). Molecular structure of $[Ru_3(CO)_{10}\{\mu\text{-dppm}\}]$.[19]

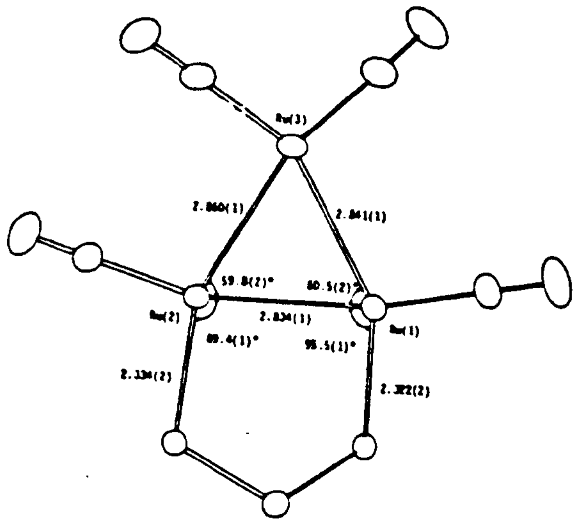

Figure 2.1(b). Intracyclic M-M-P angles in the trinuclear complex, $[Ru_3(CO)_{10}\{\mu\text{-dppm}\}]$.[19]

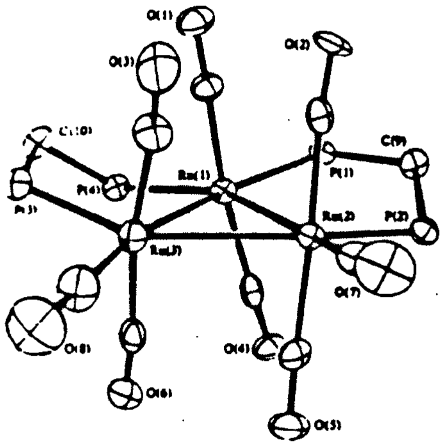

Figure 2.1(c). Molecular structure of $[Ru_3(CO)_8\{\mu\text{-dppm}\}_2]$.[21]

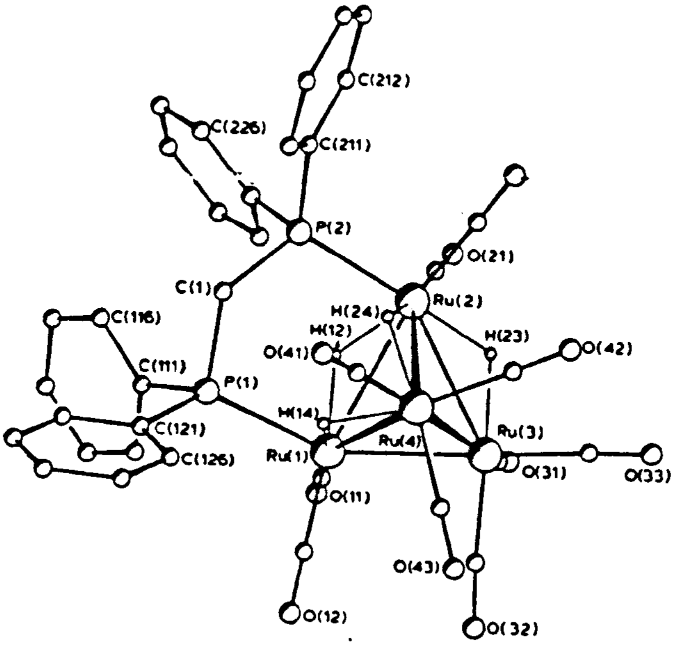

Figure 2.1(d). Molecular structure of the tetranuclear complex, $[\mathrm{Ru}_4(\mu\text{-H})_4(\mathrm{CO})_{10}\{\mu\text{-dppm}\}]$.[23]

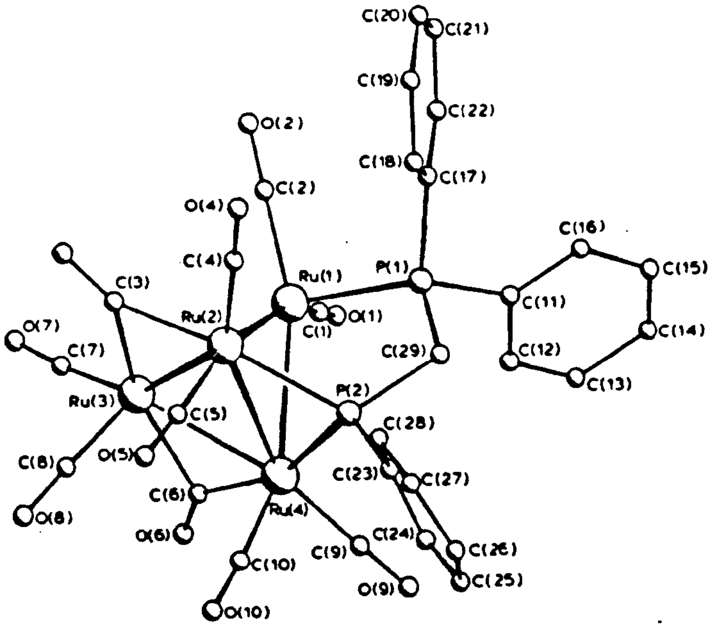

Figure 2.1(e). Molecular structure of $[\mathrm{Ru}_4(\mu\text{-H})_3(\mu\text{-CO})_2(\mathrm{CO})_8\{\mu_3\text{-PhPCH}_2\mathrm{PPh}_2\}]$.[23]

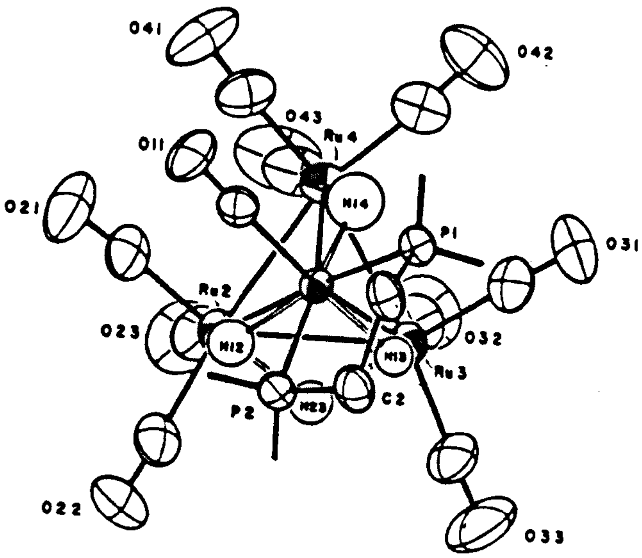

Figure 2.1(f)[24]

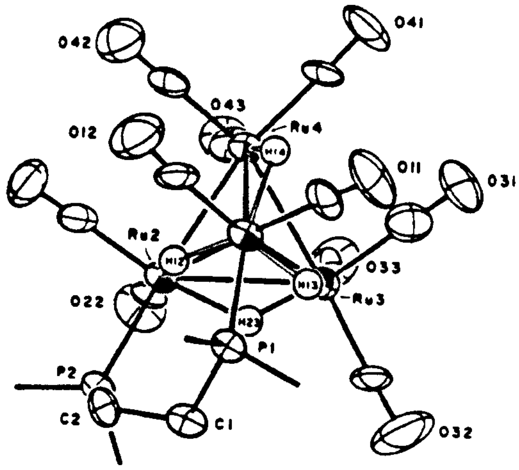

Figure 2.1(g)[25]

Isomeric structures of the tetranuclear cluster $[Ru_4(\mu\text{-}H)_4(CO)_{10}\{dppe\}]$.

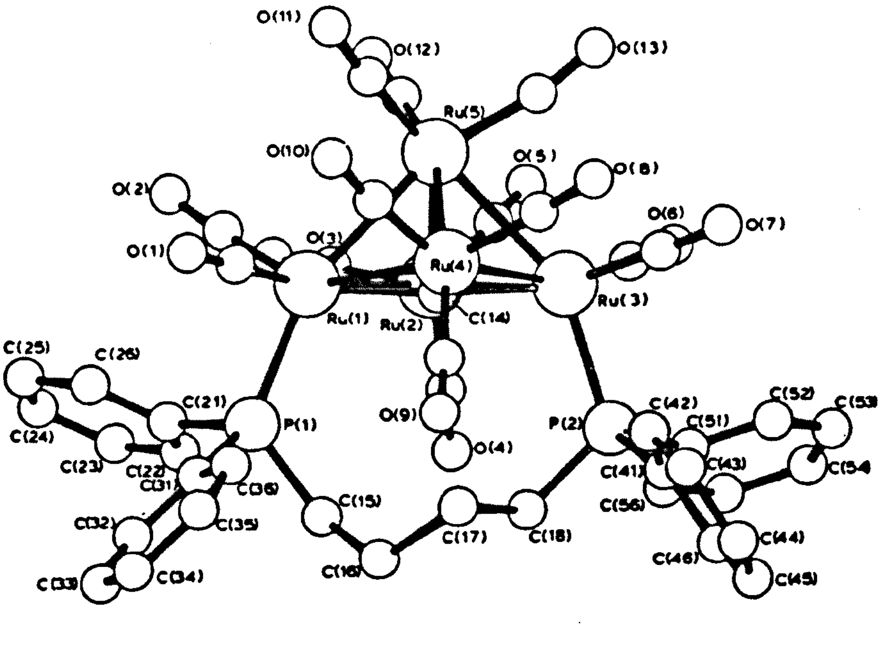

Figure 2.1(h). Molecular structure of the penta-ruthenium cluster $[Ru_5C(CO)_{13}\{\mu\text{-}dppb\}]$.[26]

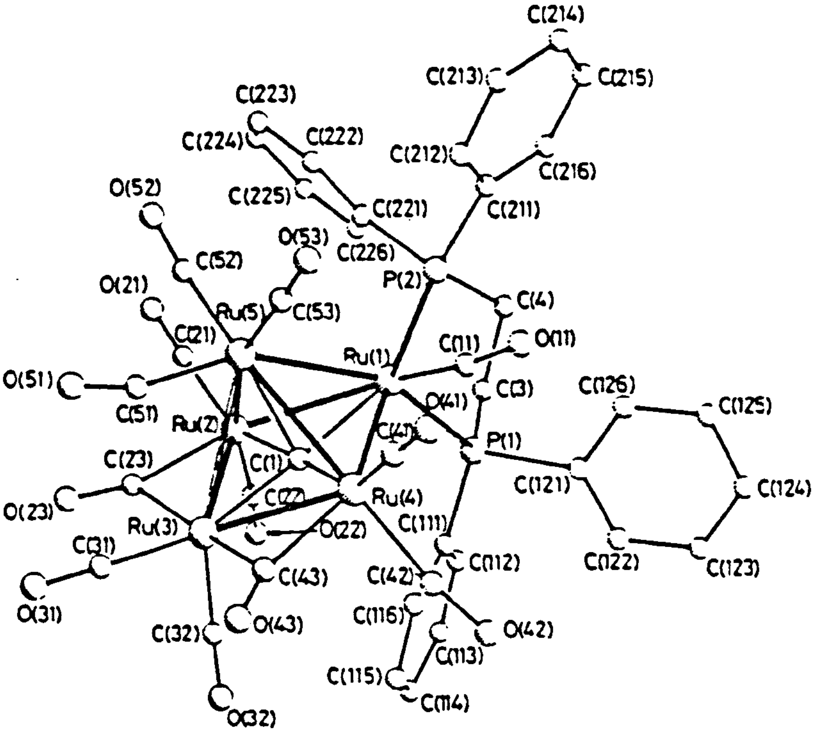

Figure 2.1(i). Molecular structure of $[Ru_5(\mu\text{-}H)_2C(CO)_{12}\{dppe\}]$.[27]

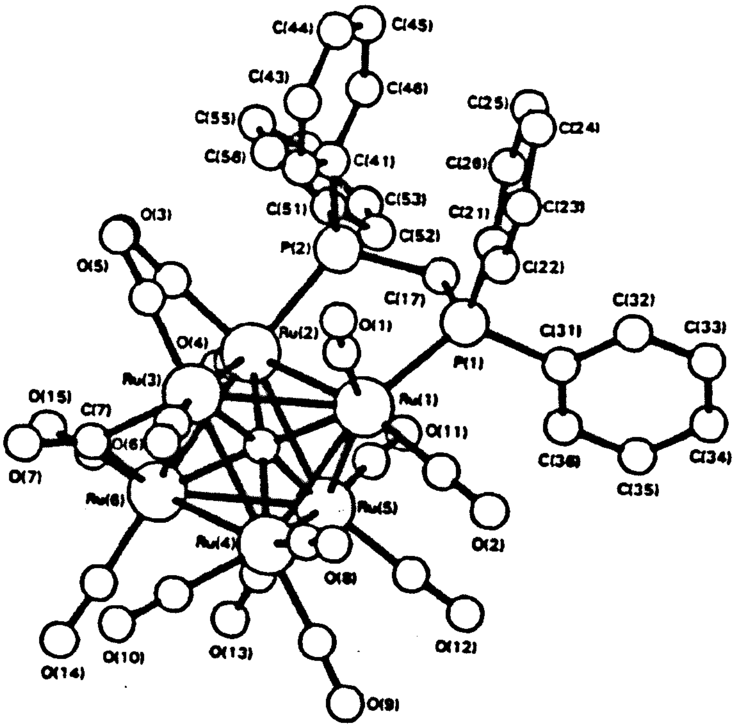

Figure 2.1(j). Molecular structure of the hexa-ruthenium cluster $[Ru_6C(CO)_{15}\{\mu\text{-}dppm\}]$.[28]

Section 2.1.1. Survey of bonding modes adopted by bidentate organophosphine ligands in homonuclear osmium clusters of nuclearity 3 to 5.

The first synthesis of a tri-osmium cluster containing a bridging di-phosphine ligand, $[Os_3(CO)_{10}\{Ph_2PCH_2PPh_2\}]$ and its conversion to the unsaturated species $[Os_3H(CO)_8\{Ph_2PCH_2PPh(C_6H_4)\}]$ was reported by Clucas and co-workers[30] in 1984. ^{31}P n.m.r studies were consistent with the bidentate ligand bridging one of the three Os-Os bonds in both structures. The X-ray structural analysis of the related di-hydrido cluster $[Os_3(H)_2(CO)_8\{\mu\text{-}Ph_2PCH_2PPh_2\}]$ was subsequently reported and showed that the two hydrides and the di-phosphine ligand triply bridged the same Os-Os bond of the Os_3 triangle, {Figure 2.1.1(a)}.[31] The length of this bond, {2.681(1) Å}, was found to be shorter than the other two unbridged bonds {2.820(1) and 2.812(1) Å respectively}. Similar variations in Os-Os bond lengths were also reported by Raithby and co-workers for the tri-osmium cluster compounds $[Os_3H(CO)_9\{\mu\text{-}Me_2PCHPMe_2\}]$ and $[Os_3H(OH)(CO)_8\{\mu\text{-}Ph_2PCH_2PPh_2\}]$.[32] In the non-hydroxy derivative, the Os-Os bond supported by the phosphine and hydrido ligand {3.104(1) Å} was markedly longer than the remaining two unbridged bonds, {2.832(1) and 2.839(1) Å, respectively}. However, in the dppm complex the opposite asymmetry was observed, with the bridged Os-Os distance {2.774(1) Å} being shorter than the other two bond lengths {2.826(1) and 2.856(1) Å, respectively}.

A recent review by Deeming and co-workers reported the synthesis and spectroscopic characterisation of a series of tri-osmium cluster compounds with di-phosphine ligands of varying lengths of organic side chain, $[Os_3(CO)_{10}\{Ph_2P(CH_2)_nPPh_2\}]$ [n = 1 (dppm), 2 (dppe), 3 (dppp), and 4 (dppb)].[33] The X-ray structures[34] of the dppe derivative [$Os_3(CO)_{10}\{\mu-Ph_2PCH_2CH_2PPh_2\}$] and the monoprotonated analogue [$Os_3(\mu-H)(CO)_{10}\{\mu-Ph_2PCH_2CH_2PPh_2\}$][$PF_6$] were reported by the workers, establishing that in the non-hydrido dppe structure, {Figure 2.1.1(b)}, the di-phosphine ligand bridged one edge of the Os_3 triangle, with a bond length of 2.891(1) Å being significantly longer than the remaining two Os-Os bond distances, {2.878(1) and 2.871(1) Å, respectively}. The related di-hydrido complex was found to crystallise as two independent molecules in the asymmetric unit, with the organophosphine group and the hydrogen atom in each molecule, doubly bridging one Os-Os bond of the triangle, {Figure 2.1.1(c)}. The bridged bond length in both molecules {3.058(1) Å molecule (A) and 3.060(1) Å molecule (B)} were markedly longer than the two unbridged bonds, {2.896(1) and 2.893(1) Å in molecule (A); 2.890(1) and 2.895(1) Å in molecule (B)}.

Importantly, in the non-hydrido dppe compound the axial OC-Os-CO directions were found not to be perpendicular to the Os_3 plane, but were 'screwed' with respect to each other, whereas this distortion was not observed in the hydrido dppe derivative.[34] The close similarity of the i.r. and n.m.r. data of the structurally characterised dppe cluster [$Os_3(CO)_{10}\{\mu-Ph_2PCH_2CH_2PPh_2\}$] and the analogous dppm, dppp and dppb complexes, indicated that all four compounds were isostructural, displaying similar bonding modes for the bridging organophosphine ligands.[33] The workers also reported the spectroscopic studies of the cluster series [$Os_3(CO)_{11}L$] [L = dppm, dppe, dppp, and dppb], whose individual $^{31}P-\{^1H\}$ n.m.r. spectra were consistent with one phosphorus atom co-ordinated and the other free, exhibiting the 'pendant' mode of bonding for the di-phosphine ligands, {Figure 2.1.1(d)}. Similarly, from $^{31}P-\{^1H\}$ n.m.r. studies they also proposed the structures of the hexanuclear cluster series $[Os_6(CO)_{22}(L)]$ [L= dppm, dppe, dppp, and dppb], with the organophosphine group linking the two Os_3 metal triangular metal fragments, {Figure 2.1.1(e)}.

The pendant mode of bonding for the di-phosphine ligand, dppe, was also observed in the solid state structure of the carbido penta-osmium cluster $[Os_5C(CO)_{15}\{Ph_2PCH_2CH_2PPh_2\}]$, {Figure 2.1.1(f)}.[35] The cluster geometry was described as 'wing-tip' bridged 'butterfly' resembling that adopted by the related cluster compounds $[Os_5C(CO)_{16}]$[36] and $[Os_5C(CO)_{15}I]^-$.[37] Interestingly, the dppe ligand was found to occupy a co-ordination site trans to an Os-Os bond, whereas in the related cluster, $[Os_5C(CO)_{15}I]^-$, the iodido ligand occupied a site trans to a carbonyl group. Raithby and co-workers suggested[35] that the site preference of the phosphine group could have been attributed to the relative donor/acceptor properties of the dppe ligand as compared to the nucleophile I^-.

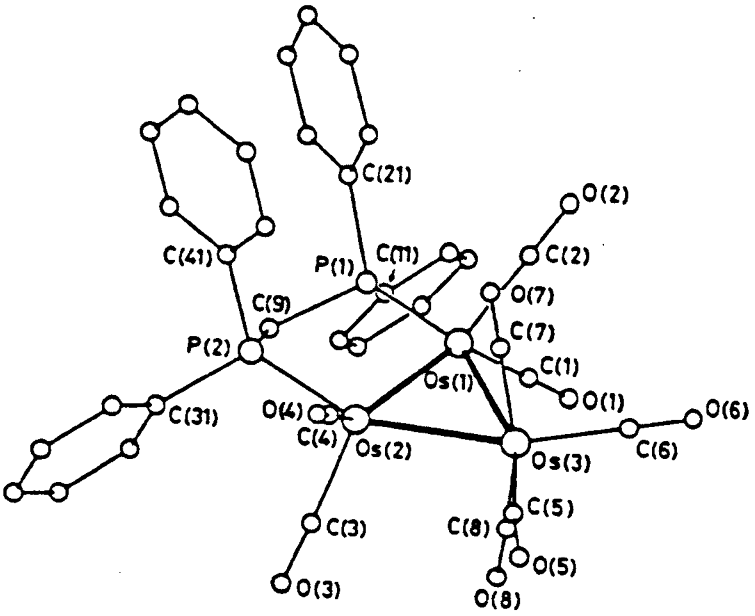

Figure 2.1.1(a). The molecular structure of $[Os_3(H)_2(CO)_8\{\mu\text{-dppm}\}]$.[31]

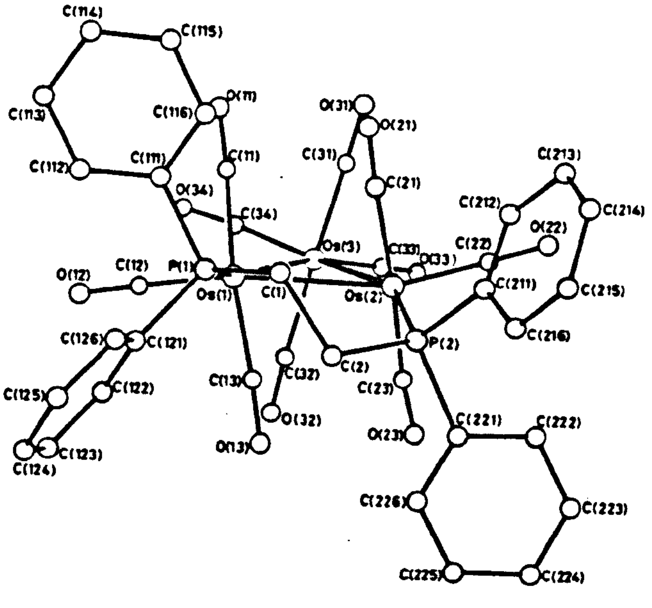

Figure 2.1.1(b). The molecular structure of $[Os_3(CO)_{10}\{\mu\text{-dppe}\}]$.[34]

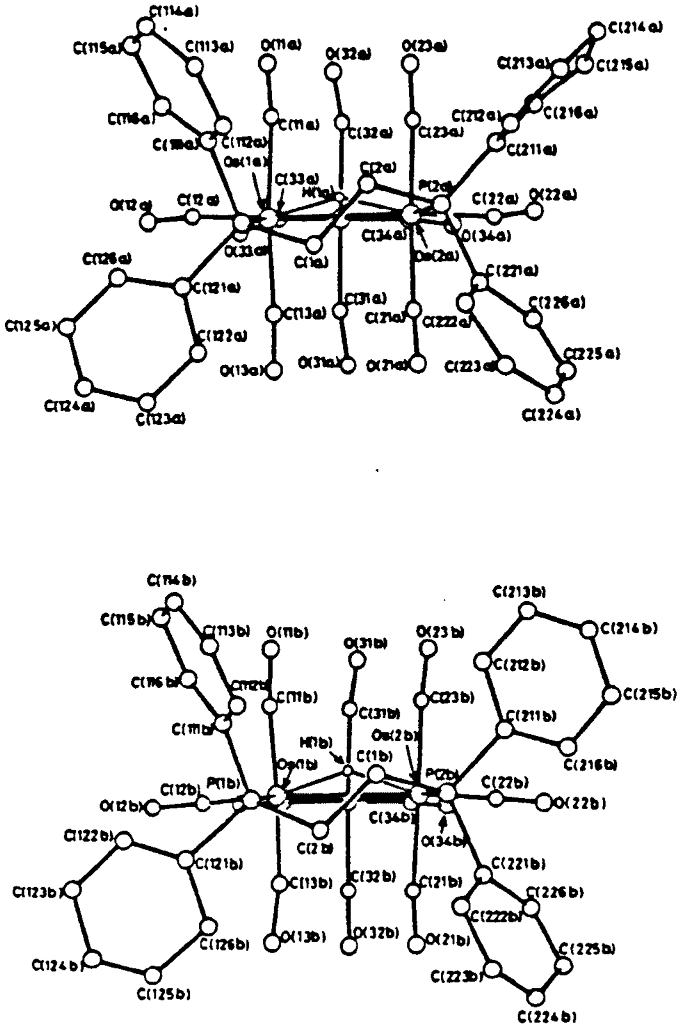

Figure 2.1.1(c). Molecular structures of two independent molecules of $[Os_3(\mu\text{-}H)(CO)_{10}\{\mu\text{-dppe}\}]$.[34]

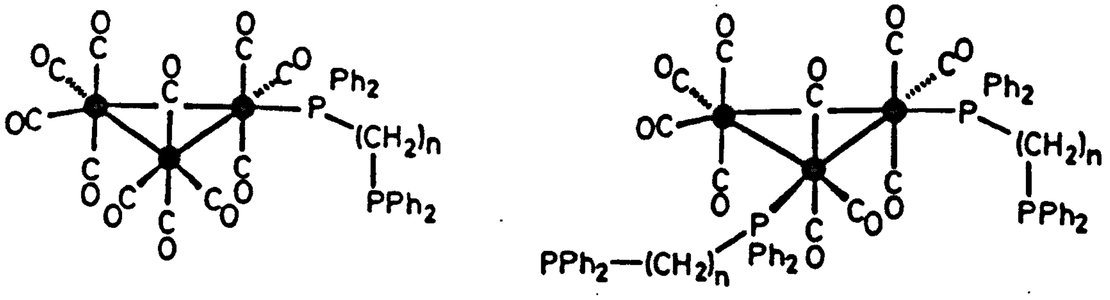

Figure 2.1.1(d).[33]

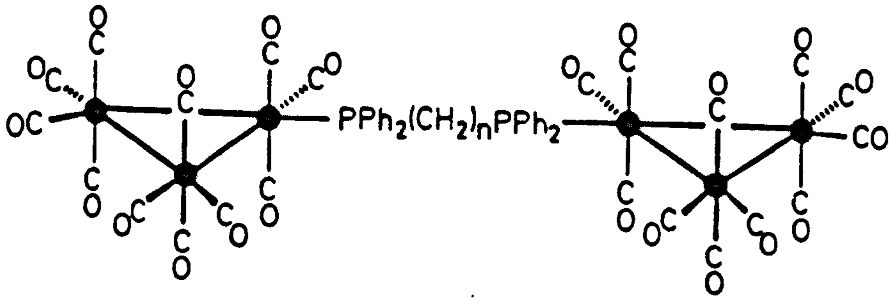

Figure 2.1.1(e).[33]

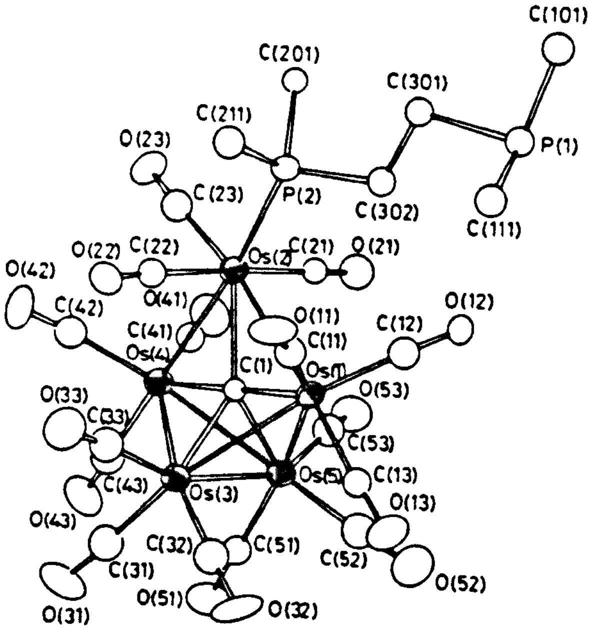

Figure 2.1.1(f). Molecular structure of $[Os_5C(CO)_{15}\{dppe\}]$.[35]

Section 2.1.2. Bonding modes characterised for bidentate phosphine ligands in heteronuclear cluster compounds of ruthenium and the observed fluxionality in solutions of related compounds containing Group IB metal phosphine fragments.

Heteronuclear ruthenium clusters containing bidentate organophosphine groups have not been studied extensively.[38,39] Their interest as potential heterogenous catalysts has initiated examination of their reactivity under conditions where they might display catalytic activity. The bonding modes adopted by the bridging phosphine ligands in these cluster compounds have been found to be similar to those already described. For example, the ruthenium-cobalt mixed-metal clusters $[Ru_3Co(H)_3(CO)_{10}\{Ph_2PCH_2CH_2PPh_2\}]$ and $[RuCo_3(H)(CO)_{10}\{\mu\text{-}Ph_2PCH_2CH_2PPh_2\}]$, reported by Pursiainen and Pakkanen, described two modes of bonding of the dppe ligand.[40] In the tri-ruthenium derivative, the phosphine group was found to chelate to one Ru atom, whereas in the tri-cobalt analogue, the bidentate ligand co-ordinated axially at two Co atoms, {Figures 2.1.2(a) and 2.1.2(b), respectively}.

Incorporation of Group IB hetero-metal atoms into triangular tri-ruthenium metal frameworks containing μ_1- and μ_2-diphosphines, was recently reported by Bruce and co-workers for the series of tetranuclear compounds $[MRu_3(CO)_9\{\mu_3\text{-}PPhCH_2PPh_2\}(PPh_3)]$ [M = Cu, Ag or Au].[41] All three complexes were found to be isostructural, with the $M(PPh_3)$ fragment bridging the same Ru-Ru bond as that bridged by the PPh group of the face-capping phosphido phosphine ligand, {Figure 2.1.2(c)}. Numerous studies of tetra-ruthenium hydrido clusters with $M(PR_3)$ groups [M = Cu, Ag or Au;R = monodentate or bidentate organophosphines] forming a part of the mixed-metal polyhedron have been reported in the last three years.[42-47] The interest in the chemistry of these novel cluster compounds has been initiated by their fluxional behaviour in solutions (section 1.1.9). In related clusters, where the two hetero-metal atoms are bridged by bidentate phosphine ligands, the structural data correlated from their respective X-ray studies has also revealed some interesting trends in the metal core geometries adopted in the solid state.

Salter and co-workers first reported the synthesis and dynamic behaviour in solution of the copper and silver ruthenium clusters, $[M_2Ru_4(\mu_3\text{-}H)_2(CO)_{12}\{\mu\text{-}Ph_2As(CH_2)_nPPh_2\}]$ [M = Cu or Ag;n = 1 or 2], containing an asymmetric bidentate ligand.[48] Comparison of the i.r. and n.m.r spectroscopic data to those previously reported for the related compounds with monodentate PPh_3 groups, $[M_2Ru_4(\mu_3\text{-}H)_2(CO)_{12}(PPh_3)_2]$ [M = Cu or Ag],[49,50] indicated that the species containing the asymmetric bidentate bridge adopted similar capped trigonal bi-pyramidal metal cores to those earlier established for the PPh_3 derivatives. At -90.0°C, the $^{31}P\text{-}\{^1H\}$ n.m.r spectra of the related clusters $[Cu_2Ru_4(\mu_3\text{-}H)_2(CO)_{12}\{\mu\text{-}Ph_2As(CH_2)_nPPh_2]$ [n = 1 or 2] showed two signals with different intensities, indicating that both of the two possible structural isomers were present in solution at low temperatures, {Figure 2.1.2(d)}.[48] Raising the temperature resulted in the peaks broadening and eventually coalescing into a singlet. To account for these observations, they suggested that some fluxional process interconverting the two distinct isomers was occuring in solutions of these related cluster compounds at ambient temperatures.

The ^{31}P n.m.r. spectra of the silver clusters $[Ag_2Ru_4(\mu_3\text{-}H)_2(CO)_{12}\{\mu\text{-}Ph_2As(CH_2)_nPPh_2\}]$ [n = 1 or 2] were more complex and difficult to interpret.[48] Importantly, the ^1H n.m.r. spectra at -90°C for the copper-ruthenium compound $[Cu_2Ru_4(\mu_3-H)_2(CO)_{12}\{\mu-Ph_2AsCH_2PPh_2\}]$ gave rise to hydrido signals with the presence of $^{31}P-^1H$ coupling. This was consistent with structural isomer (A), in which the phosphorus was attached to the copper atom bonded to the hydrido ligand, being predominant in solution, {Figure 2.1.2(d)}. However, for the related cluster $[Cu_2Ru_4(\mu_3-H)_2\{\mu-Ph_2As(CH_2)_2PPh_2\}]$, the ^1H n.m.r. spectrum at -80°C, exhibited hydrido signals with much smaller $^{31}P-^1H$ coupling. This was in agreement with structural isomer (B) being predominant in solution, with the phosphorus no longer attached to the copper atom bonded to the hydrogen atoms, {Figure 2.1.2(d)}. Therefore, by addition of one methylene group to the backbone of the asymmetric bridging ligand, $\mu-Ph_2AsCH_2PPh_2$, in the latter compound, a change in the relative proportions of isomers A and B was observed in solutions.

The retention of $^{31}P-^1H$ coupling in the ^1H n.m.r. spectra of $[Cu_2Ru_4(\mu_3-H)_2(CO)_{12}\{\mu-Ph_2AsCH_2PPh_2\}]$ indicated that the dissociation of the bridging phosphine ligand was not responsible for the observed fluxional behaviour in solution. An intramolecular metal core rearrangement process earlier proposed to account for similar observations in solution of the monodentate PPh_3 derivatives $[M_2Ru_4(H)_2(CO)_{12}(PPh_3)_2]$ [M = Cu, Ag or Au][49,50] was thought to occur here, even though the two hetero-metal atoms were held by the asymmetric bridging ligand. The Berry pseudo rotation mechanism[42] proposed for the intramolecular rearrangement of the metal core structures of the above monodentate PPh_3 clusters has been discussed in section 1.1.9.

To further investigate the fluxional behaviour observed in solutions of related tetra-ruthenium cluster compounds with Group IB metal atoms bridged by organophosphine ligands, Salter and co-workers subsequently reported both the spectroscopic and X-ray studies of the related clusters $[Ag_2Ru_4(\mu_3\text{-}H)_2(CO)_{12}\{\mu\text{-}Ph_2PCH_2PPh_2\}]$ and $[Au_2Ru_4(\mu\text{-}H)(\mu_3\text{-}H)(CO)_{12}\{\mu\text{-}Ph_2PCH_2PPh_2\}]$.[51] The i.r. and n.m.r. data for the silver derivative were found to be similar to those previously reported for the PPh_3 cluster, $[Ag_2Ru_4(\mu_3\text{-}H)_2(CO)_{12}(PPh_3)_2]$[49,50] supporting the presence of a similar capped trigonal bi-pyramidal metal core in the solid state to that already established for PPh_3 analogue. The X-ray analysis revealed the expected geometry with the dppm ligand bridging two Ag atoms, one co-ordinated to the axial and the other at an equatorial site, {Figure 2.1.2(e)}. In marked contrast, the corresponding spectroscopic data for the gold cluster was found to be different to that reported for the monodentate PPh_3 cluster $[Au_2Ru_4(\mu\text{-}H)(\mu_3\text{-}H)(CO)_{12}(PPh_3)_2]$[49,50] indicating the presence of different metal core geometry to the capped trigonal bi-pyramidal metal skeleton adopted by the PPh_3 cluster. This was confirmed with a single crystal X-ray analysis of the compound which described a capped square pyramidal metal framework, with the dppm ligand bridging the Au-Au bond of the square base, {Figure 2.1.2(f)}.[51] Interestingly, the series of reported copper cluster compounds $[Cu_2Ru_4(\mu_3\text{-}H)_2(CO)_{12}\{\mu\text{-}Ph_2P(CH_2)_nPPh_2\}]$ [n = 2,3,4,5][52] having variations in the lengths of the organic side chains of their respective bidentate ligand, were all found to adopt similar capped trigonal bi-pyramidal geometries to that previously characterised for the PPh_3 analogue, $[Cu_2Ru_4(\mu_3\text{-}H)_2(CO)_{12}(PPh_3)_2]$.[49,50]

All three compounds in the cluster series $[M_2Ru_4(H)_2(CO)_{12}\{\mu\text{-}Ph_2PCH_2PPh_2\}]$ [M = Cu, Ag or Au] were reported to exhibit fluxional behaviour in solutions, displaying a single resonance in their respective $^{31}P-\{^1H\}$ n.m.r spectrum at ambient temperatures for the two phosphorus atoms, which were clearly in non-equivalent sites in the solid state.[51] Similar fluxional behaviour in solutions of the sulphido clusters $[M_2Ru_3(\mu_3-S)(CO)_9\{\mu-dppm\}]$ [M = Cu or Au], was also reported, although there was a marked difference in their respective solid state metal core geometries.[53] The copper-ruthenium cluster was found to adopt a trigonal bi-pyramidal metal framework, with the dppm ligand co-ordinated to the two Cu atoms, one at the axial the other at an equatorial site. In contrast, the gold-ruthenium cluster adopted a distorted square pyramidal skeletal geometry, with the dppm ligand 'spanning' the Au-Au bond, again in marked difference to the trigonal bi-pyramidal framework established for the PPh_3 analogue $[Au_2Ru_3(\mu_3-S)(CO)_9(PPh_3)_2]$.[42]

These results were of further evidence to support that upon the replacement of monodentate by bidentate organophosphines in ruthenium clusters containing $CuPR_3$ and $AgPR_3$ groups [R = PPh_3 or $\mu-Ph_2PCH_2PPh_2$] there was no change in the solid state geometry, with respective structures adopting trigonal bi-pyramidal metal cores. However, in analogous clusters containing $AuPR_3$ units forming a part of a mixed-metal polyhedron, the replacement of monodenate phosphines in $[Au_2Ru_4(\mu-H)(\mu_3-H)(CO)_{12}(PPh_3)_2]$[49,50] to a bidentate group in $[Au_2Ru_4(\mu-H)(\mu_3-H)(CO)_{12}\{\mu-Ph_2PCH_2PPh_2\}]$[51] resulted in a change of the metal core structure from the capped trigonal bi-pyramid adopted by the PPh_3 derivative to the capped square pyramid described by the dppm analogue. Therefore, the variation in cluster geometry was not simply associated with the steric hinderance imposed by the bidentate ligand, but was more directed by the size of Group IB hetero-metal atoms bridged. Importantly, the Berry pseudo rotation mechanism first postulated to account for an intramolecular rearrangement of the metal core in the solutions of $[M_2Ru_3(\mu_3\text{-}S)(CO)_9(PPh_3)_2]$ [M = Cu or Au][42] and subsequently for many other related mixed-metal cluster compounds with Group IB metal phosphine fragments, was now supported with the reported X-ray structures of $[Au_2Ru_3(\mu_3\text{-}S)(CO)_9\{\mu\text{-}Ph_2PCH_2PPh_2\}]$[53] and $[Au_2Ru_4(\mu\text{-}H)(\mu_3\text{-}H)(CO)_{12}\{\mu\text{-}Ph_2PCH_2PPh_2\}]$.[51] The square pyramidal metal core geometries established for these two gold-ruthenium clusters were similar in structure, to the square pyramidal intermediate proposed within the Berry pseudo rotation mecahnism, {section 1.1.9;Figure 1.1.9(f)}, and therefore provided structural evidence to support the rearrangement pathway.

The X-ray studies of the novel clusters,
$[Au_2Ru_4(\mu\text{-}H)(\mu_3\text{-}H)(CO)_{12}\{\mu\text{-}Ph_2PCH{=}CHPPh_2\}]$
$[AuCuRu_4(\mu\text{-}H)(\mu_3\text{-}H)(CO)_{12}\{\mu\text{-}Ph_2PCH_2CH_2PPh_2\}]$
$[Au_3Ru_4(\mu\text{-}H)(CO)_{12}\{\mu\text{-}Ph_2PCH_2PPh_2\}(PPh_3)]$
presented in the subsequent sections have enabled the correlation of further structural features to account for the observed variation in solid state geometries of heteronuclear ruthenium clusters containing monodentate organophosphine groups attached to more than one gold atom, and those in which the hetero-metal atoms are bridged by bidentate phosphine ligands. Interesting trends in the M-M, M-Ru and M-P distances have also been established in comparison of the geometries of these novel mixed-metal compounds to those already characterised for related clusters.

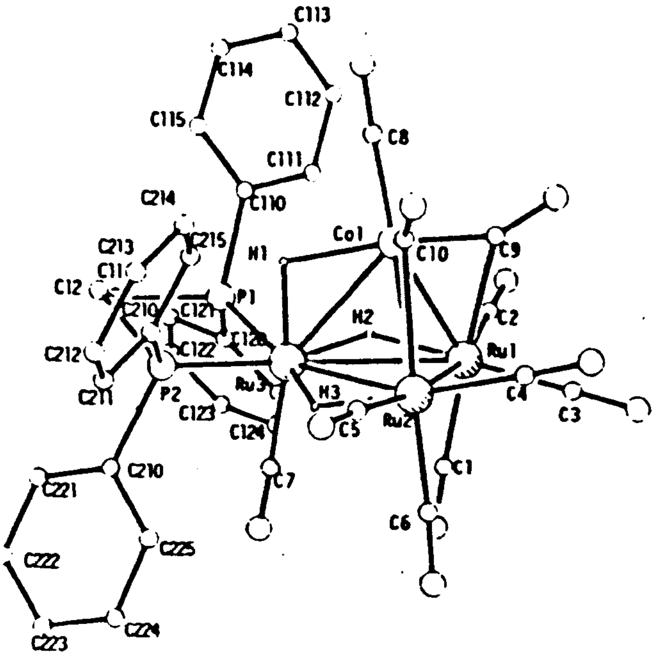

Figure 2.1.2(a). Molecular structure of [Ru$_3$Co(H)$_3$(CO)$_{10}${dppe}].[40]

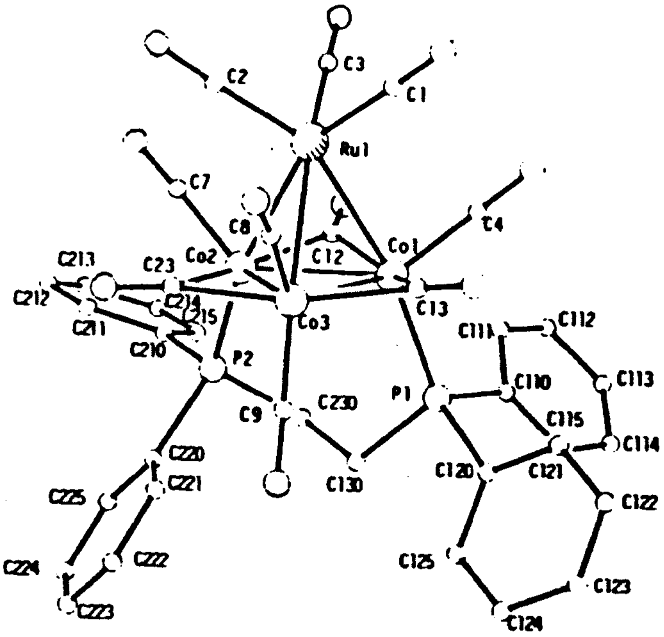

Figure 2.1.2(b). Molecular structure of [RuCo$_3$(H)(CO)$_{10}${μ-dppe}].[40]

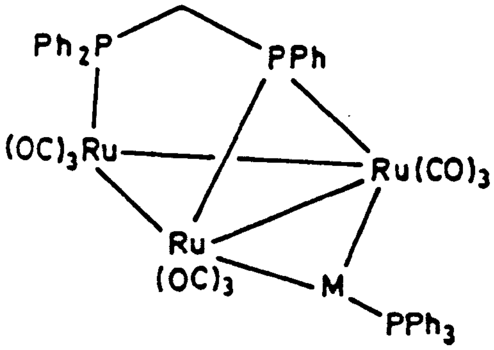

Figure 2.1.2(c). The molecular structure of the cluster series $[MRu_3(CO)_9\{\mu_3\text{-}PPhCH_2PPh_2\}(PPh_3)]$ [M = Cu, Ag, or Au].[41]

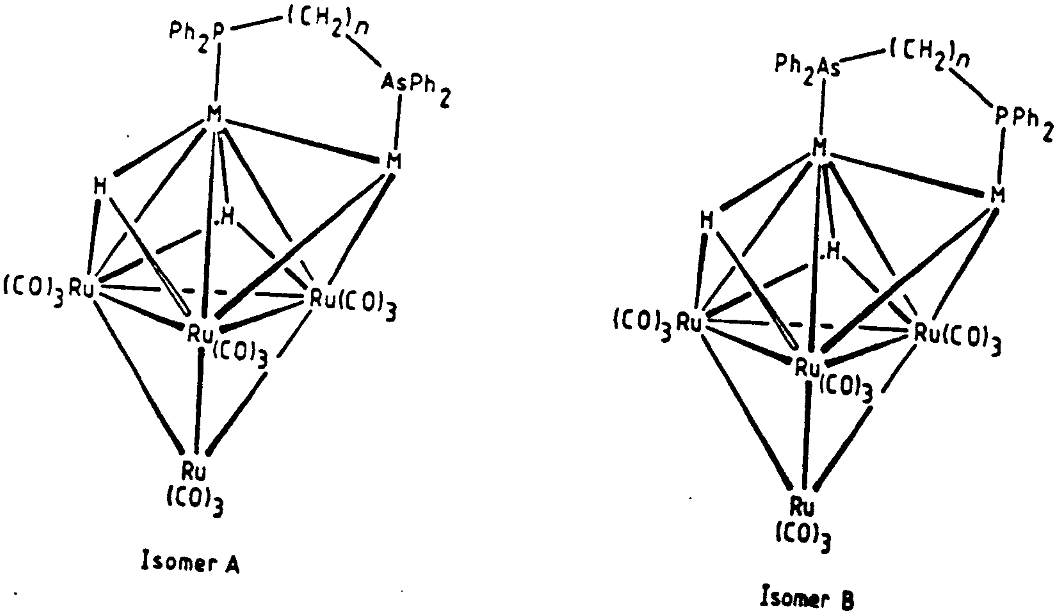

Figure 2.1.2(d). Structural isomers of $[M_2Ru_4(\mu_3\text{-}H)_2(CO)_{12}\{\mu\text{-}Ph_2As(CH_2)_nPPh_2\}]$ [M = Cu or Ag; n= 1 or 2].[48]

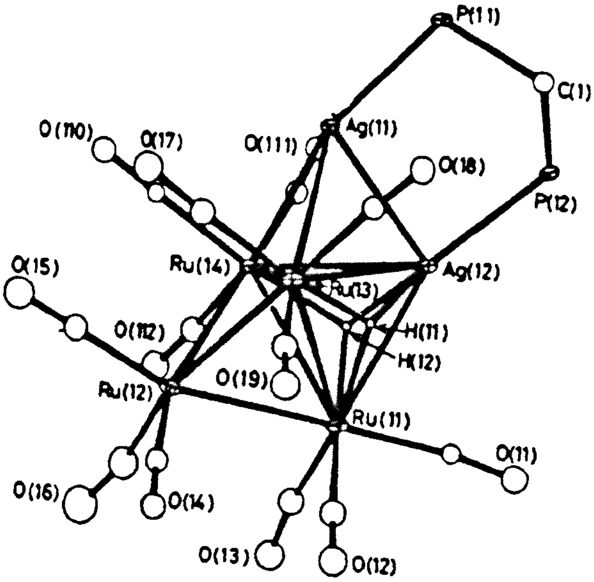

Figure 2.1.2(e). Molecular structure of the silver-ruthenium cluster $[Ag_2Ru_4(\mu_3\text{-}H)_2(CO)_{12}\{\mu\text{-dppm}\}]$.[51]

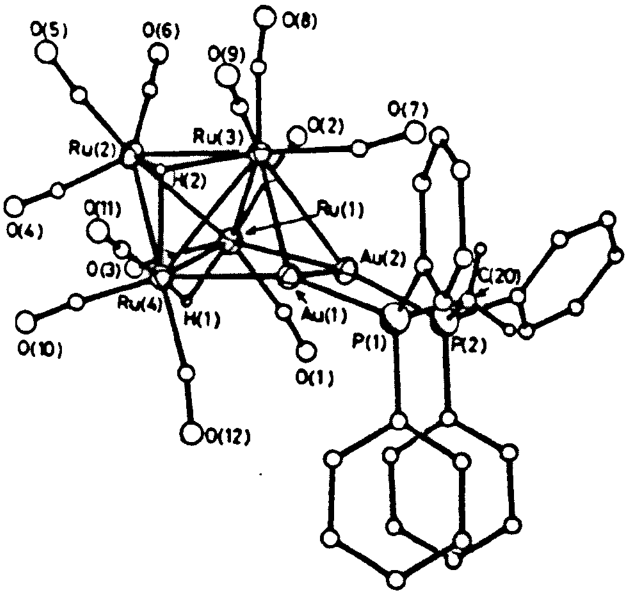

Figure 2.1.2(f). Molecular structure of the gold-ruthenium cluster $[Au_2Ru_4(\mu\text{-}H)(\mu_3\text{-}H)(CO)_{12}\{\mu\text{-dppm}\}]$.[51]

Section 2.2. X-ray analysis on the gold-ruthenium hexanuclear cluster $[Au_2Ru_4(\mu\text{-}H)(\mu_3\text{-}H)(CO)_{12}\{\mu\text{-}Ph_2PCH{=}CHPPh_2\}]$ (1).

Crystal data, methods of data collection, structure solution and refinement for (1) are presented in section 4.5.

Tables of Fractional co-ordinates, anisotropic temperature factors, bond lengths, bond angles, intermolecular, and intramolecular distances are given in the appendix, (Vol.2).

The X-ray diffraction study of the mixed-metal cluster compound $[Au_2Ru_4(\mu-H)(\mu_3-H)(CO)_{12}\{\mu-Ph_2PCH=CHPPh_2\}]$ (1) completed a series of di-gold tetra-ruthenium hydrido structures, having organophosphine ligands varied from the monodentate PPh_3 groups in $[Au_2Ru_4(\mu-H)(\mu_3-H)(CO)_{12}(PPh_3)_2]$ (2)[50] to the bidentate dppm bridge in $[Au_2Ru_4(\mu-H)(\mu_3-H)(CO)_{12}\{\mu-Ph_2PCH_2PPh_2\}]$ (3)[51] and lengthening of the organic side chain of the bridging phosphine ligand in $[Au_2Ru_4(\mu-H)(\mu_3-H)(CO)_{12}\{\mu-Ph_2PCH_2CH_2PPh_2\}]$ (4).[54] The results obtained from the X-ray analysis of (1) were of particular interest in establishing any structural differences within the metal framework resulting from the presence of an unsaturated ethene, {-CH=CH-}, organic 'link' bridging the two Au-P bonds.

2.2.1. Structural description of $[Au_2Ru_4(\mu-H)(\mu_3-H)(CO)_{12}\{\mu-Ph_2PCH=CHPPh_2\}]$ (1).

The X-ray study of the di-gold ruthenium cluster $[Au_2Ru_4(\mu-H)(\mu_3-H)(CO)_{12}\{\mu-Ph_2PCH=CHPPh_2\}]$ (1) established that the six metal atoms described a capped square pyramidal geometry, Figure 2.2.1. The square base was defined by the atoms, Au(1), Au(2), Ru(1) and Ru(4), with Ru(3) forming the apex of the pyramid. The triangular face defined by the atoms, Ru(1), Ru(3), and Ru(4) was further capped by Ru(2), and each ruthenium atom was found to carry three essentially linear carbonyl groups, {Ru-C-O 158-177(3)°}. The bis(diphenylphosphino) ethene ligand was found to bridge the Au-Au bond of the square base. Although it was not possible to locate the two H-ligands directly from the X-ray analysis, their positions were obtained from potential energy minimisation calculations.[55] The results gave reasonable minima in the potential energy for one hydride to bridge the bond Ru(1)-Ru(4) and the second to cap the triangular face Ru(1)-Ru(2)-Ru(3).

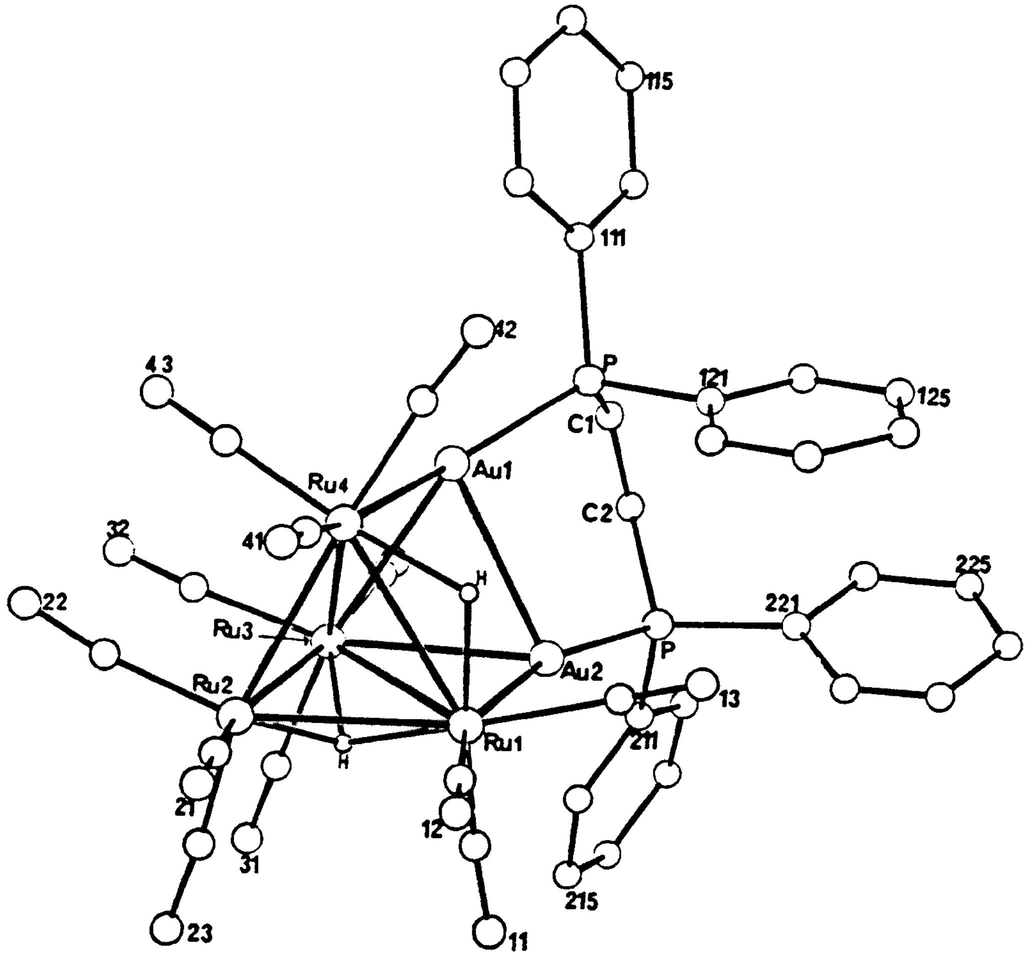

Figure 2.2.1. The molecular structure of the gold-ruthenium cluster $[Au_2Ru_4(\mu\text{-}H)(\mu_3\text{-}H)(CO)_{12}\{\mu\text{-}Ph_2PCH{=}CHPPh_2\}]$ (1). The carbonyl C atoms have the same numbering as the O atoms to which they are attached.

2.2.2. Results and Discussion.

The capped square pyramidal geometry established for the gold ruthenium mixed-metal cluster $[Au_2Ru_4(\mu\text{-}H)(\mu_3\text{-}H)(CO)_{12}\{\mu\text{-}Ph_2PCH{=}CHPPh_2\}]$ (1) closely resembled the metal frameworks characterised for the related compounds $[Au_2Ru_4(\mu\text{-}H)(\mu_3\text{-}H)(CO)_{12}\{\mu\text{-}Ph_2PCH_2PPh_2\}]$ (3),[51] {Figure 2.2.2(b)}, and $[Au_2Ru_4(\mu\text{-}H)(\mu_3\text{-}H)(CO)_{12}\{\mu\text{-}Ph_2PCH_2CH_2PPh_2\}]$ (4),[54] {Figure 2.2.2(c)}, but was markedly different to the capped trigonal bi-pyramidal geometry adopted by the PPh_3 derivative $[Au_2Ru_4(\mu\text{-}H)(\mu_3\text{-}H)(CO)_{12}(PPh_3)_2]$ (2),[50] {Figure 2.2.2(d)}. Table 2.2.2 lists the M-M bond lengths for (1) and those reported for the related cluster compounds, (2), (3) and (4).

The Au-Au distance of 2.861(2) Å in the structure of the hexanuclear cluster (1) was found to be longer than the Au-Au bonds reported for the analogous dppm cluster (3) {2.823(1) Å}[51] and the dppe derivative (4) {2.828(2) Å},[54] but all three bonds were markedly longer than the corresponding bond length in the monodentate PPh_3 structure (2) {2.791(1) Å}.[50] The range of Au-Ru distances in (1) {2.707-2.827(2) Å} was found to lie between the corresponding range of distances observed in (3) {2.682-2.947(2) Å} and (4) {2.777-2.965(2) Å}. However, the mean Au-Ru bond in (1) {2.770(2) Å} was 0.025 Å shorter than the mean bond in the structure of the dppm derivative (3) {mean Au-Ru 2.795(2) Å} and 0.074 Å shorter than the corresponding mean bond in the dppe analogue (4) {mean Au-Ru 2.844(2) Å}. Importantly, the mean Au-Ru bond lengths in (1), (3) and (4) were significantly shorter than the analogous mean distance in the monodentate PPh_3 cluster (2) {mean Au-Ru 2.917(2) Å}. The

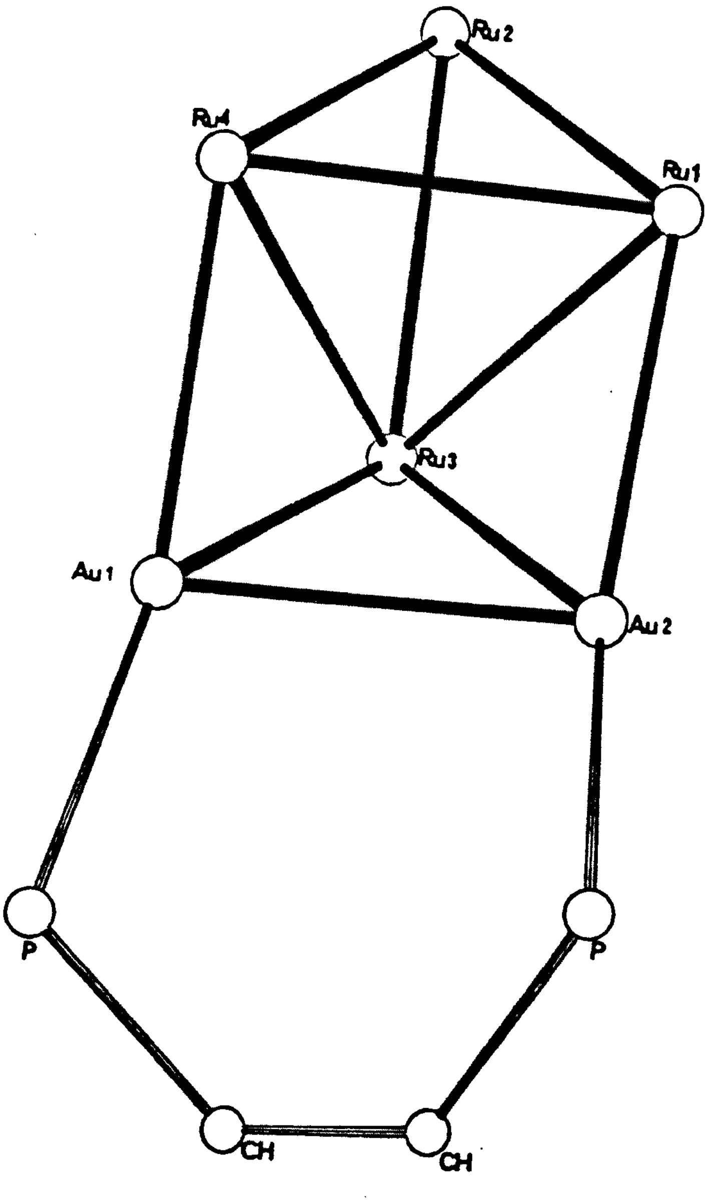

Figure 2.2.2(a). The metal core structure of the hexanuclear cluster $[Au_2Ru_4(\mu\text{-}H)(\mu_3\text{-}H)(CO)_{12}\{\mu\text{-}Ph_2PCH{=}CHPPh_2\}]$ (1). The hydrido and carbonyl ligands, together with the phenyl rings have been omitted for clarity.

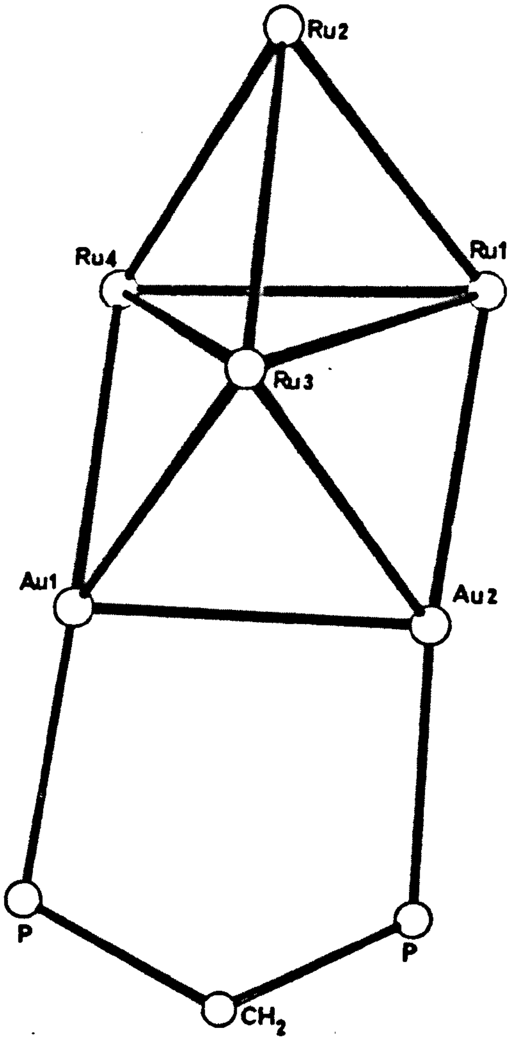

Figure 2.2.2(b). The metal core structure of $[Au_2Ru_4(\mu\text{-}H)(\mu_3\text{-}H)(CO)_{12}\{\mu\text{-}Ph_2PCH_2PPh_2\}]$ (3).[51] The hydrido and carbonyl ligands, together with the phenyl rings have been omitted for clarity.

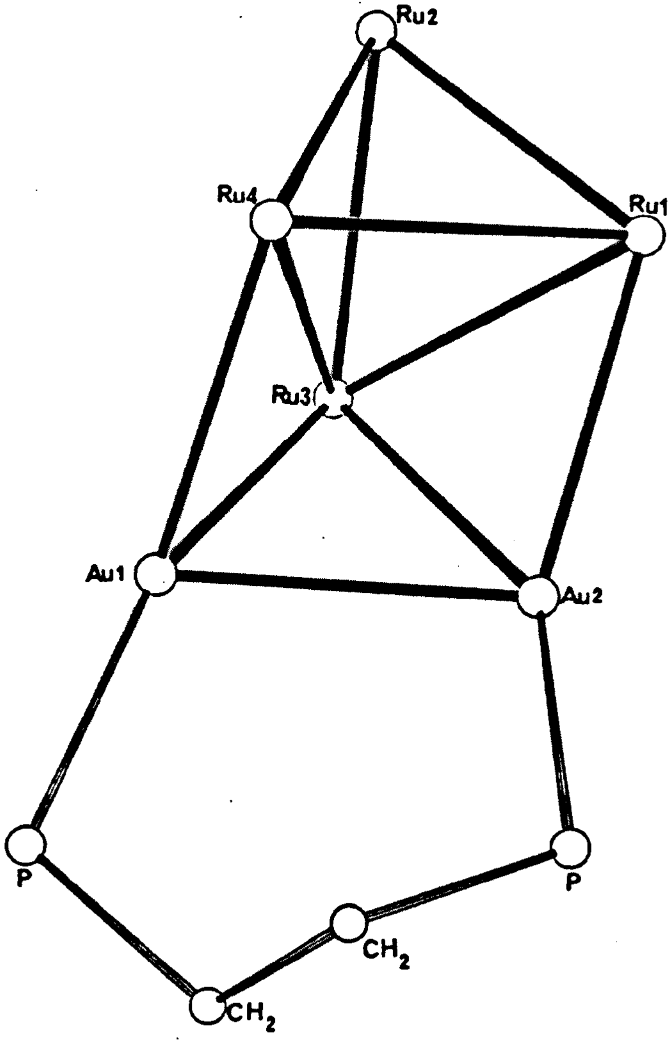

Figure 2.2.2(c). The metal-core structure of $[Au_2Ru_4(\mu\text{-}H)(\mu_3\text{-}H)(CO)_{12}\{\mu\text{-}Ph_2PCH_2CH_2PPh_2\}]$ (4).[54] The hydrido and carbonyl ligands, together with the phenyl rings have been omitted for clarity.

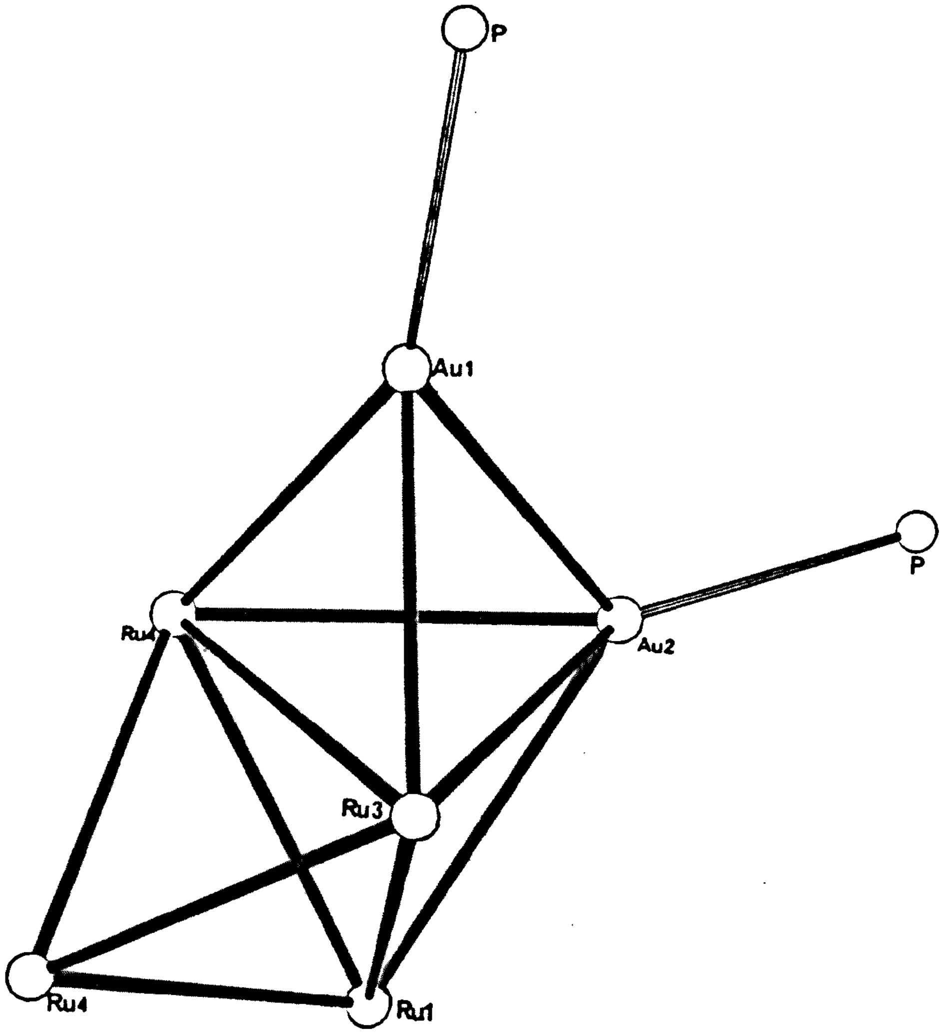

Figure 2.2.2(d). The metal-core structure of $[Au_2Ru_4(\mu\text{-}H)(\mu_3\text{-}H)(CO)_{12}\{(PPh_3)_2\}]$ (2).[50] The hydrido and carbonyl ligands, together with the phenyl rings have been omitted for clarity.

range of Ru-Ru distances in the hexanuclear cluster (1) {2.796-3.017(3) Å} was similar to that observed in the structures of (2) {2.788-3.011(2) Å}, (3) {2.791-3.006(2) Å} and (4) {2.782(3)-2.984(3) Å}, although the mean Ru-Ru distance in (1) {2.928(3) Å} was noteably longer than the corresponding mean bonds in (2) {2.892(2) Å}, (3) {2.917(2) Å} and (4) {2.879(3) Å}. Presence of μ_2- or μ_3-hydrido ligands is known to lengthen M-M bonds they bridge,[8,24,25] and as a result the mean of the four hydrido bridged Ru-Ru bonds in the three structurally related cluster compounds (1), (3), and (4), were longer than the mean of the two unbridged bonds, by 0.054 Å in (1), 0.083 Å in (3) and 0.031 Å in (4), {Table 2.2.2}.

In the related clusters $[Au_2Ru_4(\mu\text{-}H)(\mu_3\text{-}H)(CO)_{12}\{\mu\text{-}Ph_2PCH{=}CHPPh_2\}]$ (1) and $[Au_2Ru_4(\mu\text{-}H)(\mu_3\text{-}H)(CO)_{12}\{\mu\text{-}Ph_2PCH_2PPh_2\}]$ (3) the Ru-Ru bonds associated with the capping of a triangular Ru_3 face of the square pyramid by Ru(2), showed similar marked asymmetry, with one distance being considerably shorter than the other two:

	compound (1)	compound (3)[51]
bond	distance/ Å	
Ru(1)-Ru(2)	2.796(3)	2.791(2)
Ru(2)-Ru(3)	2.877(3)	2.873(2)
Ru(2)-Ru(4)	2.897(3)	2.899(2)

However in the dppe cluster $[Au_2Ru_4(\mu\text{-}H)(\mu_3\text{-}H)(CO)_{12}\{\mu\text{-}Ph_2PCH_2CH_2PPh_2\}]$ (4), the opposite asymmetry in the analogous bonds was observed with one Ru-Ru distance significantly longer than the other two.

compound (4)[54]

bond	distance/ Å
Ru(1)-Ru(2)	2.782(3)
Ru(2)-Ru(3)	2.844(3)
Ru(2)-Ru(4)	2.783(3)

The M-M distances around the pyramidal base in the related clusters (1), (3) and (4) are displayed in Figure 2.2.2(e). The two Au-Ru bonds of the square in (1) and (3) showed similar asymmetry, with the bond Au(1)-Ru(4) slightly longer than Au(2)-Ru(1), by 0.028 Å in (1) and 0.058 Å in (3).
However, the bond Au(2)-Ru(1) in the structure of the dppm complex (3), was markedly shorter than the corresponding bond in (1) and the dppe derivative (4). The important parameters of interest were the diagonal contacts between the metal atoms Au(1)...Ru(1) and Au(2)...Ru(4), {Figure 2.2.2(e)}. There was marked similarity between the two metal contacts in (1) and the dppm derivative (3), with the difference between the respective diagonals of 0.330 Å in (1) and 0.340 Å in (3), reflecting upon similar distortions of the square base. In contrast, the corresponding contacts in the dppe compound (4) showed a difference of 0.790 Å, displaying a far greater contraction of the base of the pyramid, with the contact distance Au(2)...Ru(4) {3.44(4) Å} being markedly shorter than any of the other M-M contacts within the square bases of all three structures. The observed distortions of the pyramidal cores in (1), (3) and (4) were thought to be attributed to the variation in the nature of the bidentate organophosphine groups bridging the two gold atoms. The degree of distortion imposed by the phosphine bridges in (1), (3) and (4) was also apparent upon the two Au-P bond lengths, with the distances in (1) and (3) being similar but significantly longer than those in (4):

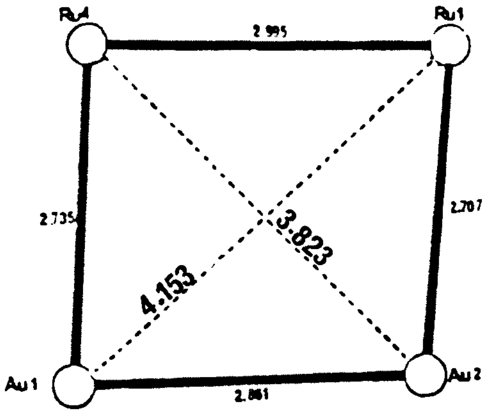

1

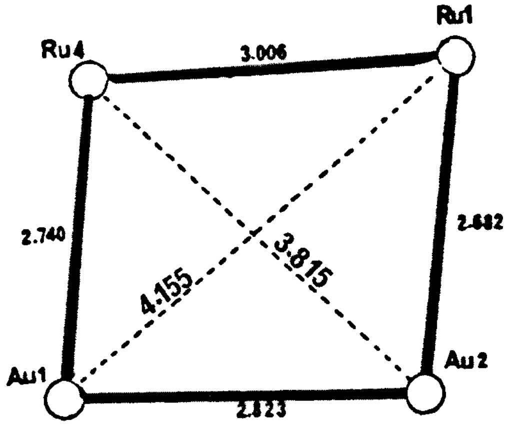

3

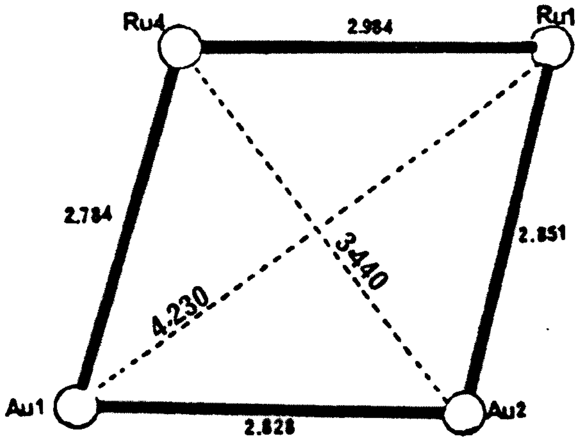

4

Figure 2.2.2(e). Metal geometry defining the pyramidal base in the structures of $[Au_2Ru_4(\mu\text{-}H)(\mu_3\text{-}H)(CO)_{12}\{\mu\text{-}Ph_2PCH{=}CHPPh_2\}]$ (1) $[Au_2Ru_4(\mu\text{-}H)(\mu_3\text{-}H)(CO)_{12}\{\mu\text{-}Ph_2PCH_2PPh_2\}\}]$ (3) $[Au_2Ru_4(\mu\text{-}H)(\mu_3\text{-}H)(CO)_{12}\{\mu\text{-}Ph_2P(CH_2)_2PPh_2\}]$ (4).

Compound	Distance/ Å	
	Au(1)-P(1)	Au(2)-P(2)
$[Au_2Ru_4(\mu\text{-}H)(\mu_3\text{-}H)(CO)_{12}\{\mu\text{-}Ph_2PCH{=}CHPPh_2\}]$ (1)	2.307(9)	2.311(8)
$[Au_2Ru_4(\mu\text{-}H)(\mu_3\text{-}H)(CO)_{12}\{\mu\text{-}Ph_2PCH_2PPh_2\}]$ (3)	2.308(4)	2.303(4)[51]
$[Au_2Ru_4(\mu\text{-}H)(\mu_3\text{-}H)(CO)_{12}\{\mu\text{-}Ph_2PCH_2CH_2PPh_2\}]$ (4)	2.286(4)	2.276(4)[54]

The more rigid constraint imposed on the Au-P bonds whilst 'linked' to the organic side chains in compounds (1) and (3) was further highlighted by similar Au-P-C 'bite' angles around the two phosphorus atoms, {Figure 2.2.2(f)}.

The X-ray analysis of the hexanuclear hydrido cluster $[Au_2Ru_4(\mu\text{-}H)(\mu_3\text{-}H)(CO)_{12}\{\mu\text{-}Ph_2PCH{=}CHPPh_2\}]$ (1) established that each ruthenium atom was bonded to three essentially linear -CO groups, {Ru-C-O 158-177(3)°}, with the greatest deviation from linearity found for CO(33). The same carbonyl ligand was found to make a short contact to Au(2) {Au(2)...C(33) 2.63(4) Å}, whereas an even shorter contact occurred with atom C(12) {Au(2)...C(12) 2.59(4) Å}. The shortest contact to Au(1) occurred with carbon atom, C(43) {Au(1)...C(43) 2.70(4) Å}. Similar short contacts were found to be a structural feature of several reported gold-heteronuclear clusters.[42-47] For example, in the tetranuclear cluster $[AuRu_3(CO)_9(C_2Bu^t)(PPh_3)]$ a short contact of 2.69(1) Å was observed to occur between the gold atom and one of the near linear carbonyl groups.[56] The Ru-CO range in (1) {1.79-1.92(5) Å} was similar to that observed in the related clusters (3) {Ru-CO 1.82-1.97(7) Å}[51] and (4) (1.82-1.91(6) Å}.[54] Correspondingly the range of C-O bond lengths in (1) {1.14-1.20(6) Å} was again comparable to that found in (3) {1.13-1.25(8) Å} and (4) {1.14-1.27(8) Å}. In (1) the C=C double

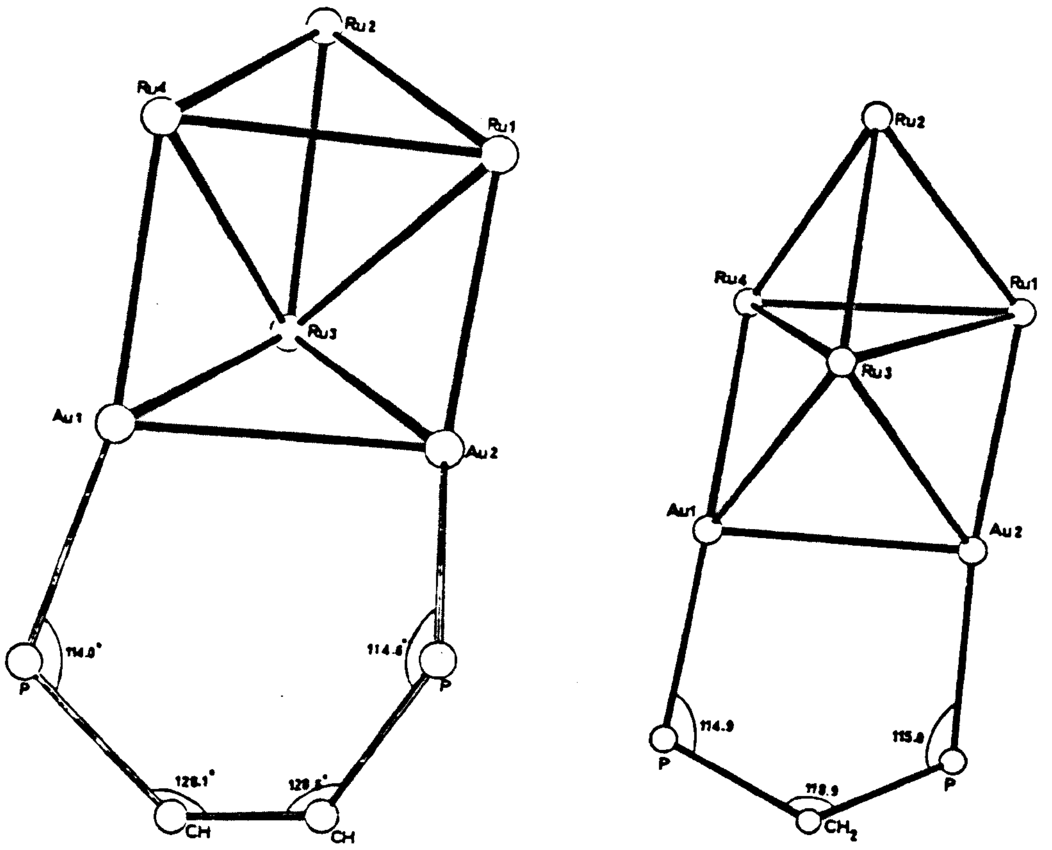

Figure 2.2.2(f). Geometry around the two P atoms in the structures of $[Au_2Ru_4(\mu\text{-}H)(\mu_3\text{-}H)(CO)_{12}\{\mu\text{-}Ph_2PCH{=}CHPPh_2\}]$ (1) and $[Au_2Ru_4(\mu\text{-}H)(\mu_3\text{-}H)(CO)_{12}\{\mu\text{-dppm}\}]$ (3).

bond distance of the organic backbone of the bidentate ligand {1.33(4) Å}, was observed to be significantly shorter than the C-C single bond distance of 1.55(1) Å in the analogous dppe cluster (4).[54] This was reflective of the extensive delocalisation of the π-electrons within the double bond, although the mean of the two P-C bond lengths of the bridging phosphine group in (1) {1.82(3) Å} was only slightly shorter than the corresponding mean bond in the dppe structure (4) {mean 1.85(1) Å}.

2.2.3 Conclusions.

Some preliminary conclusions were drawn from the structural data obtained from the X-ray study of the hexanuclear mixed-metal cluster $[Au_2Ru_4(\mu\text{-}H)(\mu_3\text{-}H)(CO)_{12}\{\mu\text{-}Ph_2PCH{=}CHPPh_2\}]$ (1) compared to the results previously reported for the related cluster compounds $[Au_2Ru_4(\mu\text{-}H)(\mu_3\text{-}H)(CO)_{12}\{\mu\text{-}Ph_2PCH_2PPh_2\}]$ (3)[51] and $[Au_2Ru_4(\mu\text{-}H)(\mu_3\text{-}H)(CO)_{12}\{\mu\text{-}Ph_2PCH_2CH_2PPh_2\}]$ (4).[54] The variation in the organophosphine ligands in these structures showed an interesting trend in the metal frameworks adopted by these species in the solid state. The change from monodentate PPh_3 phosphine groups in $[Au_2Ru_4(\mu\text{-}H)(\mu_3\text{-}H)(CO)_{12}(PPh_3)_2]$ (2)[50] to the bidentate organophosphine groups in (1), (3), and (4), established a change in metal core geometry, from the capped trigonal bi-pyramidal in (2) to similar capped square pyramidal metal core structures in (1), (3) and (4). Importantly, variations in the organic side chains of the bidentate bridge, involving the lengthening of the backbone as characterised in (1) and the dppe derivative (4), showed that distortions present within the square base of the pyramids were guided by the nature of the organic substituent 'linking' the two Au-P bonds. The greatest rigidity and constraint imposed upon the two Au-P vectors was observed in the solid state structures of (3), where the two Au-P bonds were held parallel by a single methylene $\{-CH_2-\}$ fragment and in the metal skeleton of (1), where the corresponding vectors were held by the unsaturated ethene $\{-CH{=}CH-\}$ bridge.

A more marked distortion of the pyramidal core was observed in the structure of the hexanuclear cluster (4), with a saturated ethyl $\{-CH_2-CH_2-\}$ bridge 'spanning' the two Au-P bonds. The respective Au-P distances and corresponding Au-P-C 'bite' angles in (4) reflected upon greater freedom and flexibility of the two Au-P vectors giving rise to a short contact between two metal atoms of the square base [Au(**2**)...Ru(**4**) 3.44(4) Å]. This signified a metal core intermediate in structure to the capped trigonal bi-pyramidal adopted by the PPh_3 cluster (2) and the capped square pyramidal displayed by the dppm analogue (3). Importantly, although the length of the organic side chain of the phosphine bridges in (1) and (4) were similar, the geometry around the two Au-P bonds held by the unsaturated ethene bridge in (1), reflected upon an environment of greater constraint. The rigidity of the six membered ring Au-P-C=C-P-Au was thought to arise from the π-electron delocalisation from the C=C double bond of the organic unit to the adjacent P-C bonds of the bridge, although the mean of the two P-C bond lengths in (1) {1.82(3) Å} was only slightly shorter than the corresponding mean distance in the dppe structure (4) {1.85(1) Å}. The correlation of the structural results obtained from the X-ray analysis of the hexanuclear cluster compound $[Au_2Ru_4(\mu\text{-}H)(\mu_3\text{-}H)(CO)_{12}\{\mu\text{-}Ph_2PCH{=}CHPPh_2\}]$ (1) compared to those reported for related structures $[Au_2Ru_4(\mu\text{-}H)(\mu_3\text{-}H)(CO)_{12}(PPh_3)_2]$ (2), $[Au_2Ru_4(\mu\text{-}H)(\mu_3\text{-}H)(CO)_{12}\{\mu\text{-}Ph_2PCH_2PPh_2\}]$ (3) and

$[Au_2Ru_4(\mu\text{-}H)(\mu_3\text{-}H)(CO)_{12}\{\mu\text{-}Ph_2PCH_2CH_2PPh_2\}]$ (4) established that when two Au-P bonds were bridged by organic side chains, the resulting steric strains imposed upon them were a major factor in controlling the overall metal core geometry adopted in the solid state.

Table 2.2.2

Compound vector	(1)	(2)[50]	(3)[51] distance/ Å	(4)[54]
Au(1)-Au(2)	2.861(2)	2.791(1)	2.823(1)	2.828(2)
Au(1)-Ru(3)	2.827(2)	2.844(1)	2.810(2)	2.777(2)
Au(1)-Ru(4)	2.735(2)	2.840(1)	2.740(2)	2.784(2)
Au(2)-Ru(1)	2.707(2)	3.091(1)	2.682(2)	2.851(2)
Au(2)-Ru(3)	2.811(2)	2.859(1)	2.947(2)	2.965(2)
Au(2)-Ru(4)	-	2.949(1)	-	-
Ru(1)-Ru(2)	2.796(3)	2.788(2)	2.791(2)	2.782(3)
Ru(1)-Ru(3)	2.988(3)	2.966(2)	2.932(2)	2.935(3)
Ru(1)-Ru(4)	2.995(3)	2.948(2)	3.006(2)	2.984(3)
Ru(2)-Ru(3)	2.877(3)	2.821(2)	2.873(2)	2.844(3)
Ru(2)-Ru(4)	2.897(3)	2.817(2)	2.899(2)	2.783(3)
Ru(3)-Ru(4)	3.017(3)	3.011(2)	3.003(2)	2.947(3)

Section 2.3. X-ray analysis on the gold-copper hexanuclear cluster $[AuCuRu_4(\mu\text{-}H)(\mu_3\text{-}H)(CO)_{12}\{Ph_2PCH_2CH_2PPh_2\}]$ (1).

Crystal data, methods of data collection, structure solution and refinement are presented in section 4.6.

Tables of fractional co-ordinates, anisotropic temperature factors bond lengths, bond angles, intermolecular and intramolecular distances are given in the appendix, (Vol.2).

The X-ray analysis of the hexanuclear cluster compound $[AuCuRu_4(\mu\text{-}H)(\mu_3\text{-}H)(CO)_{12}\{\mu\text{-}Ph_2PCH_2CH_2PPh_2\}]$ (1) was carried out to extend the series of tetra-ruthenium mixed-metal clusters having Group IB metal atoms bonded to bidentate organophosphine ligands. The study of (1) was of particular interest due to the presence of two different coinage metals, (Cu and Au), incorporated into the metal polyhedron. The only previous reported X-ray structure of two different Group IB metal phosphine fragments forming a part of a mixed-metal polyhedron was for the hexanuclear cluster $[AgCuRu_4(\mu_3\text{-}H)_2(CO)_{12}(PPh_3)_2]$.[57] The results obtained from the study of (1) were of importance,in comparing the effects of the bridging organophosphine ligand upon the overall solid state geometry to those previously observed in structures of related Group IB heteronuclear cluster compounds.

2.3.1 Structural description of the mixed-metal cluster $[AuCuRu_4(\mu\text{-}H)(\mu_3\text{-}H)(CO)_{12}\{\mu\text{-}Ph_2PCH_2CH_2PPh_2\}]$ (1).

The X-ray analysis of the gold-copper mixed-metal cluster (1) established that the six metal atoms formed a capped trigonal bi-pyramidal geometry, Figure 2.3.1. The bonding arrangement of the two hetero-metal atoms, Cu and Au, on the ruthenium tetrahedron was envisaged to involve, the copper atom capping the ruthenium atoms Ru(1), Ru(3), and Ru(4), followed by the gold atom capping the adjacent face Cu(1)-Ru(3)-Ru(4), resulting in the formation of the Cu-Au bond. Each ruthenium atom was found to carry three essentially linear carbonyl groups {Ru-C-O 166-174(3)$^{\circ}$}, and the bis(diphenylphosphino)ethane ligand was found to bridge the Au-Cu bond of the metal framework. Although the two hydrido ligands were not located from the X-ray analysis, their positions were deduced from the potential energy minimisation calculations,[55] which gave reasonable minima in the potential energy for one hydride to bridge the bond, Ru(1)-Ru(3) and the other to cap the triangular face Ru(1)-Ru(2)-Ru(4).

2.3.2 Results and discussion.

The X-ray study of the copper-gold cluster compound $[AuCuRu_4(\mu\text{-}H)(\mu_3\text{-}H)(CO)_{12}\{\mu\text{-}Ph_2PCH_2CH_2PPh_2\}]$ (1) established a capped trigonal bi-pyramidal metal core structure which was markedly different to the capped square pyramidal skeletons adopted by the di-gold tetra-ruthenium clusters, $[Au_2Ru_4(\mu\text{-}H)(\mu_3\text{-}H)(CO)_{12}\{\mu\text{-}Ph_2PCH_2PPh_2\}]$ (2)[51] and $[Au_2Ru_4(\mu\text{-}H)(\mu_3\text{-}H)(CO)_{12}\{\mu\text{-}Ph_2PCH_2CH_2PPh_2\}]$ (3).[54] However, the metal framework characterised for (1) closely resembled the capped trigonal bi-pyramidal geometries displayed by the monodentate PPh_3 clusters,
$[AgCuRu_4(\mu_3\text{-}H)_2(CO)_{12}(PPh_3)_2]$ (5),[57]
$[Au_2Ru_4(\mu\text{-}H)(\mu_3\text{-}H)(CO)_{12}(PPh_3)_2]$,[50]
$[Cu_2Ru_4(\mu_3\text{-}H)_2(CO)_{12}(PPh_3)_2]$,[50]
and the series of di-copper ruthenium hydrido clusters containing bidentate organophosphine bridges of varying lengths of organic side chains, $[Cu_2Ru_4(\mu_3\text{-}H)_2(CO)_{12}\{\mu\text{-}Ph_2P(CH_2)_nPPh_2\}]$ (n = 2 (7), 3, 4, 5).[52] Table 2.3.2 lists the M-M bond lengths for the gold-copper cluster compound (1) and those reported for the di-gold ruthenium cluster (3) and the two independent molecules of the di-copper structure (7).

The Au-Cu distance of 2.614(3) Å established in the structure of the copper-gold cluster $[AuCuRu_4(\mu\text{-}H)(u_3\text{-}H)(CO)_{12}\{\mu\text{-}Ph_2PCH_2CH_2PPh_2\}]$ (1) was found to be markedly longer than the Cu-Cu bond length observed in the two independent molecules of the di-copper cluster $[Cu_2Ru_4(\mu_3\text{-}H)_2(CO)_{12}(\mu\text{-}Ph_2PCH_2CH_2PPh_2\}]$ (7) {2.505(3) (7a) and

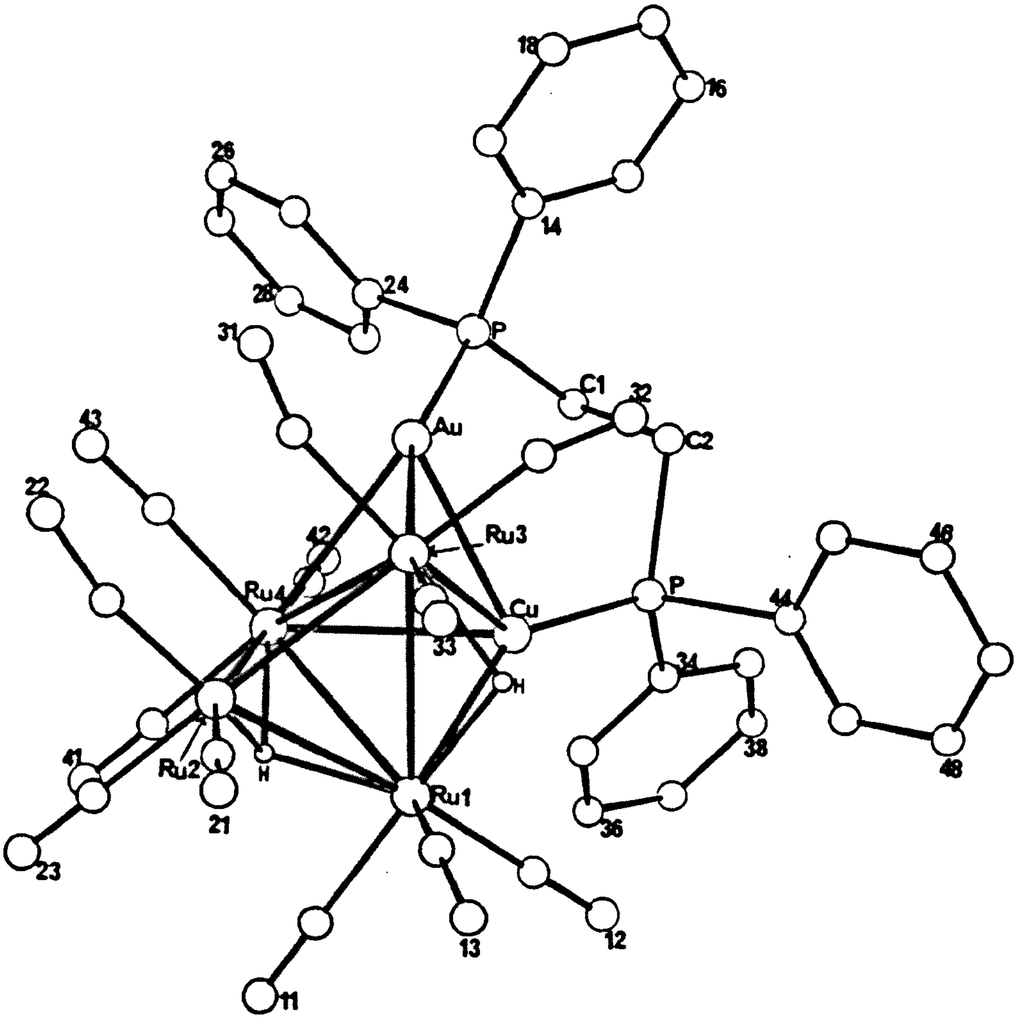

Figure 2.3.1. Molecular structure of the mixed-metal cluster, [AuCuRu$_4$(μ-H)(μ$_3$-H)(CO)$_{12}${μ-Ph$_2$PCH$_2$CH$_2$PPh$_2$}] (1). The carbonyl C atoms have the same numbering as the O atoms.

2.492(3) Å (7b)}, and significantly shorter than the Au-Au bond in the di-gold ruthenium compound (3), {2.828(2) Å}, (Table 2.3.2). Interestingly, the Au-Cu distance in (1) was shorter than the Ag-Cu distance reported for the monodentate PPh_3 hydrido cluster $[AgCuRu_4(\mu_3\text{-}H)_2(CO)_{12}(PPh_3)_2]$ (5) {Ag-Cu 2.764(1) Å).[57] The mean of the two Au-Ru bond lengths in the gold-copper ruthenium cluster (1) {2.823(3) Å} was found to be 0.028 Å longer than the mean of the four Au-Ru bonds in the structure of the di-gold ruthenium dppm derivative $[Au_2Ru_4(\mu\text{-}H)(\mu_3\text{-}H)(CO)_{12}\{\mu\text{-}Ph_2PCH_2PPh_2\}]$ (2) {mean 2.795(2) Å} and 0.021 Å shorter than the mean of the four Au-Ru distances in the di-gold ruthenium dppe analogue (3) {mean 2.844(2) Å}. Importantly, this mean bond in (1) was significantly shorter than the corresponding mean of the five Au-Ru bond lengths observed in the di-gold ruthenium PPh_3 compound $[Au_2Ru_4(\mu\text{-}H)(\mu_3\text{-}H)(CO)_{12}(PPh_3)_2]$ {mean 2.917(2) Å}.[50]

The mean of the three Cu-Ru distances in (1) {2.771(3) Å} was found to be 0.065 Å longer than the mean of the five Cu-Ru distances in the structure of the monodentate PPh_3 cluster, $[Cu_2Ru_4(\mu_3\text{-}H)_2(CO)_{12}(PPh_3)_2]$, (6) {mean 2.706(2) Å}.[50] This mean bond in (1) was also markedly longer than the mean of the five Cu-Ru bonds in both independent molecules of cluster compound (7) {mean 2.680(2) (7a) and 2.698(2) Å (7b)}. The triangular face, Ru(1)-Ru(3)-Ru(4), capped by the copper atom in (1) showed marked asymmetry, with one Cu-Ru distance significantly shorter than the other two, exhibiting the opposite asymmetry to that observed in the hexanuclear silver-copper ruthenium cluster (5), which also contained two different Group IB atoms forming a part of the mixed-metal polyhedron:

compound (1)		compound (5)[57]
bond	Distance/ Å	
Cu(1)-Ru(1)	2.674(3)	2.796(2)
Cu(1)-Ru(3)	2.817(3)	2.687(2)
Cu(1)-Ru(4)	2.822(3)	2.683(2)

The mean of the six Ru-Ru bonds defining the tetrahedron in the gold-copper ruthenium cluster (1) {2.885(3) Å} was observed to be slightly longer than the corresponding mean bond in the silver-copper ruthenium cluster (5) {mean 2.877(2) Å} Interestingly, in the structure of the gold-copper compound $[AuCuRu_4(\mu\text{-}H)(\mu_3\text{-}H)(CO)_{12}\{\mu\text{-}Ph_2PCH_2CH_2PPh_2\}]$ (1) the bonds, Ru(1)-Ru(2), Ru(3)-Ru(2) and Ru(2)-Ru(4) associated with the capping of the trigonal bi-pyramidal core by Ru(2), {Figure 2.3.1}, showed no obvious asymmetry, with the mean difference between the three bonds of 0.008 Å, (Table 2.3.2). This was observed to be similar to the mean difference of 0.006 Å between the related bonds in $[Cu_2Ru_4(\mu_3\text{-}H)_2(CO)_{12}(PPh_3)_2]$ and a difference of 0.001 Å in molecule (7a) and 0.003 Å in molecule (7b) of the cluster compound $[Cu_2Ru_4(\mu_3\text{-}H)_2(CO)_{12}\{\mu\text{-}Ph_2PCH_2CH_2PPh_2\}]$ (7) {Table 2.3.2}. In contrast, the related bond lengths in the analogous di-gold ruthenium dppe complex (3) revealed a mean difference of 0.041 Å, with the bond Ru(2)-Ru(3) bridged by a hydrido ligand being significantly longer than the bonds Ru(1)-Ru(2) and Ru(2)-Ru(4) in the structure, {Table 2.3.2}.

The Au-P bond length of 2.212(3) Å in (1) was found to be markedly shorter than the mean Au-P bond distances found in the structures of the following di-gold ruthenium clusters, $[Au_2Ru_4(\mu\text{-}H)(\mu_3\text{-}H)(CO)_{12}(PPh_3)_2]$ {mean 2.280(4) Å},[50]

$[Au_2Ru_4(\mu\text{-}H)(\mu_3\text{-}H)(CO)_{12}(\mu\text{-}Ph_2PCH_2PPh_2)]$ (2) {mean 2.305(4) Å}[51]
$[Au_2Ru_4(\mu\text{-}H)(\mu_3\text{-}H)(CO)_{12}(\mu\text{-}Ph_2PCH_2CH_2PPh_2)]$ (3) {mean 2.281(4) Å}.[54]
Correspondingly, the Cu-P distance of 2.149(4) in (1) was markedly shorter than the mean Cu-P distances observed in the related copper-ruthenium clusters,
$[AgCuRu_4(\mu_3\text{-}H)_2(CO)_{12}(PPh_3)_2]$ (5) {mean 2.203(3) Å},[57]
$[Cu_2Ru_4(\mu_3\text{-}H)_2(CO)_{12}(PPh_3)_2]$ {mean 2.233(2) Å}[50]
$[Cu_2Ru_4(\mu_3\text{-}H)_2(CO)_{12}(\mu\text{-}Ph_2PCH_2CH_2PPh_2)]$ (7) {mean 2.286(5) Å (7a) and 2.288 Å (7b)}[52]
The difference in the Au-P and Cu-P bond lengths of 0.063 Å in (1) was surprisingly not reflected upon the 'bite' angles around the two P atoms, {Au(1)-P(1)-C(1) 116.0(3);Cu(1)-P(2)-C(2) 115.0(3)°}.

The X-ray study of the hexanuclear cluster compound $[AuCuRu_4(\mu\text{-}H)(\mu_3\text{-}H)(CO)_{12}\{\mu\text{-}Ph_2PCH_2CH_2PPh_2\}]$ (1) established that each ruthenium atom was bonded to three essentially linear CO groups {Ru-C-O 166-174(3)°}, with the greatest deviation of a Ru-CO interbond angle of 162(3)° found for CO(11). An extremely short contact between the gold atom and one of the carbonyl ligands was observed, {Au...C(32) 2.60(3) Å}, whereas the shortest contact to the copper atom occurred at C(12), {Cu...C(12) 2.57(3) Å}. The Ru-CO range in (1) {1.82-1.95(6) Å} was found to be similar to that previously reported for the related clusters (2) {1.72-1.91(6) Å}[51] and (3) {1.82-1.97(7) Å}.[54] Similarly, the range of C-O bond lengths in (1) {1.02-1.26(9) Å} was comparable to that observed in (2) {1.13-1.25(8) Å} and (3) {1.14-1.27(8) Å}. The single C-C bond distance of the ethane fragment, $\{-CH_2-CH_2-\}$, linking the Cu-P and Au-P bonds in (1) {1.81(9) Å} was considerably longer than the analogous bond in the di-gold ruthenium cluster (3) {1.55(1) Å} and in the two independent molecules of the di-copper ruthenium compound (7) {1.54(3) Å in both (7a) and (7b)}.[52]

2.3.3 Conclusions.

The results obtained from the X-ray analysis of the hexanuclear cluster $[AuCuRu_4(\mu\text{-}H)(\mu_3\text{-}H)(CO)_{12}\{\mu\text{-}Ph_2PCH_2CH_2PPh_2\}]$ (1) put forward a very interesting relationship in the structures adopted by tetra-ruthenium clusters compounds having Group IB metal atoms bonded to organophosphine ligands. It was reported previously that tetra-ruthenium clusters containing two gold atoms adopt one of the two alternative geometries depending on the nature of the attached phosphine ligand.

ligand	$(PPh_3)_2$	$\mu\text{-}Ph_2P(CH_2)_{1,2}PPh_2$
geometry	capped trigonal bi-pyramid	capped square pyramid

From the reported single crystal X-ray structures of related di-gold ruthenium clusters, the capped trigonal bi-pyramidal geometry was characterised for the monodentate PPh_3 compound, $[Au_2Ru_4(\mu\text{-}H)(\mu_3\text{-}H)(CO)_{12}(PPh_3)_2]$,[50] whereas the analogous clusters with bidentate organophosphine bridges adopted similar capped square pyramidal metal frameworks as established for the the hexanuclear clusters,

$[Au_2Ru_4(\mu\text{-}H)(\mu_3\text{-}H)(CO)_{12}\{\mu\text{-}Ph_2PCH_2PPh_2\}]$ (2)[51] and

$[Au_2Ru_4(\mu\text{-}H)(\mu_3\text{-}H)(CO)_{12}\{\mu\text{-}Ph_2PCH_2CH_2PPh_2\}]$ (3).[54]

In contrast, the related di-copper ruthenium structures containing both monodentate and bidentate organophosphine groups of varying lengths of organic side chains, were all observed to adopt similar capped trigonal bi-pyramidal geometries in the solid state as reported for $[Cu_2Ru_4(\mu_3\text{-}H)_2(CO)_{12}(PPh_3)_2]$[50] and the cluster series $[Cu_2Ru_4(\mu_3\text{-}H)_2(CO)_{12}\{Ph_2P\{CH_2\}_nPPh_2\}]$ (n = 2 (7), 3, 4, and 5).[52] To account for the variations in the solid state structures of these gold-ruthenium and copper ruthenium cluster compounds, Salter and co-workers had proposed that when two Cu-P bonds were 'spanned' by organic side chains, the resulting steric constraints were minimal compared to those suffered by two Au-P vectors held by similar organic fragments, simply due to the smaller size of the Cu atom.[51,53] Therefore, it seemed probable that in related structures containing two gold atoms incorporated into the metal polyhedron, the observed rearrangement of the metal core in the solid state was a pathway through which the Au-P bonds were able to release some of the strains put upon them with the replacement of monodentate PPh_3 groups by bidentate phosphine ligands. Importantly, the gold-copper ruthenium cluster compound $[AuCuRu_4(\mu\text{-}H)(\mu_3\text{-}H)(CO)_{12}\{\mu\text{-}Ph_2PCH_2CH_2PPh_2\}]$ (1) retained the capped trigonal bi-pyramidal metal geometry. Thus, with the presence of a gold and a smaller copper atom forming a part of the mixed-metal polyhedron, the overall steric strains imposed by the bidentate organophosphine group in the metal framework of (1), were evidently less than those present in related clusters where two gold atoms were bridged by the bidentate phosphine ligands.

Table 2.3.2

M(1) = Cu in (1) and (7), Au in (3)

M(2) = Cu in (7), Au in (1) and (3)

	(1)	(3)[54*]	(7a)[*]	(7b)[52*]
M(1)-M(2)	2.614(3)	2.828(2)	2.505(3)	2.492(3)
M(1)-Ru(1)	2.674(3)	2.851(2)	2.652(3)	2.699(3)
M(1)-Ru(3)	2.817(3)	2.965(2)	2.708(3)	2.748(3)
M(1)-Ru(4)	2.822(3)	-	2.813(2)	2.788(2)
M(2)-Ru(3)	2.823(3)	2.777(2)	2.615(2)	2.603(2)
M(2)-Ru(4)	2.823(3)	2.784(2)	2.616(2)	2.654(2)
Ru(1)-Ru(2)	2.803(3)	2.782(3)	2.800(2)	2.792(2)
Ru(1)-Ru(3)	2.985(3)	2.935(3)	2.956(2)	2.977(2)
Ru(1)-Ru(4)	2.930(3)	2.984(3)	2.957(2)	2.963(2)
Ru(2)-Ru(3)	2.815(3)	2.844(3)	2.800(2)	2.795(2)
Ru(2)-Ru(4)	2.813(3)	2.783(3)	2.801(2)	2.790(2)
Ru(3)-Ru(4)	2.964(3)	2.947(3)	2.887(2)	2.895(2)

[*] re-numbered for comparison.

Section 2.4. X-ray analysis on the heptanuclear cluster $[Au_3Ru_4(\mu\text{-}H)(CO)_{12}\{\mu\text{-}Ph_2PCH_2PPh_2\}(PPh_3)]$ (1).

Crystal data, methods of data collection, structure solution and refinement for (1) are presented in section 4.7.

Tables of fractional co-ordinates, anisotropic temperature factors, bond lengths, bond angles, intermolecular and intramolecular distances are given in the appendix, (Vol.2).

The X-ray study of the heptanuclear cluster $[Au_3Ru_4(\mu\text{-}H)(CO)_{12}\{\mu\text{-}Ph_2PCH_2PPh_2\}(PPh_3)]$ (1) was carried out to extend the series of mixed-metal cluster compounds containing Group IB metal atoms bonded to either monodentate or bidentate organophosphine groups. The X-ray structure of the monodentate PPh_3 cluster $[Au_3Ru_4(\mu_3\text{-}H)(CO)_{12}(PPh_3)_3]$ (2) was previously reported by Howard and co-workers together with the synthesis and spectroscopic analysis of the Au_3Ru_4 dppm derivative (1).[45] The workers observed that from the close similarity between the i.r. spectra of (1) and (2) in the carbonyl stretching region, compound (1) was thought to adopt a similar bi-capped trigonal bi-pyramidal geometry as that established for (2). However, at ambient temperatures both ^1H and $^{31}P\text{-}\{^1H\}$ n.m.r. spectra of (1) were consistent with the two phosphorus atoms of the bidentate ligand being equivalent on the n.m.r. time scale, which was not in agreement with the metal core structure proposed from the i.r. spectroscopic data. Therefore, the characterisation of the solid state structure of (1) by X-ray analysis was of interest in establishing the metal core geometry and to account for the observed differences between the i.r. and n.m.r. spectroscopic data.

2.4.1 Structural description of the heptanuclear cluster (1).

The X-ray analysis of the mixed-metal cluster $[Au_3Ru_4(\mu\text{-}H)(CO)_{12}\{\mu\text{-}Ph_2PCH_2PPh_2\}(PPh_3)]$ (1) established that the seven metal atoms adopted a distorted bi-capped square pyramidal geometry, Figure 2.4.1. The square base was defined by the atoms Au(1), Au(2), Ru(2) and Ru(3), with Ru(1) forming the apex of the pyramid. The triangular face Au(1)-Ru(1)-Ru(2) was capped by the third gold atom, Au(3), with the metal atoms Ru(1), Ru(2), and Ru(3) further capped by the fourth ruthenium atom, Ru(4). Each ruthenium atom was found to carry three essentially linear carbonyl ligands, {Ru-C-O 165-177(3)^{o}}, and the bis(diphenylphosphino)methane ligand bridged the bond, Au(1)-Au(2) with the third gold atom, Au(3), bonded to a triphenyl phosphine group. Although the position of the hydride ligand was not located from the X-ray analysis, the longest Ru(3)-Ru(4) bond was thought to be bridged by a μ_2-H ligand, being consistent with the structural feature involving the lengthening of M-M bonds bridged by H-ligands.[8,24,25] The position of the H-ligand was deduced from potential energy minimisation calculations[55] which gave one suitable minima in P.E. for the ligand to bridge the bond, Ru(3)-Ru(4).

2.4.2 Results and Discussion.

The X-ray analysis of the heptanuclear cluster $[Au_3Ru_4(\mu-H)(CO)_{12}\{\mu-Ph_2PCH_2PPh_2\}(PPh_3)]$ (1) established a bi-capped square pyramidal metal core geometry which was in marked contrast to the bi-capped trigonal bi-pyramidal metal framework adopted by the monodentate PPh_3 cluster $[Au_3Ru_4(\mu_3-H)(CO)_{12}(PPh_3)_3]$ (2), {Figure 2.4.2}.[45] Table 2.4.2 lists the M-M bond lengths for the related Au_3Ru_4 hydrido cluster compounds (1) and (2).

Despite the fact that the Au(1)-Au(3) bond {2.749(2) Å} was unbridged whereas the Au(1)-Au(2) bond {2.758(2) Å} was spanned by the bidentate organophosphine ligand, the two Au-Au separations in (1) were similar, but significantly shorter than the mean Au-Au distance observed in (2), {2.830(2) Å}. Importantly, the Au-Au bond bridged by the dppm ligand {2.758(2) Å} was markedly shorter than the bond bridged by related organophosphine bidentate groups in the di-gold cluster compounds, $[Au_2Ru_4(\mu-H)(\mu_3-H)(CO)_{12}\{\mu-Ph_2PCH_2PPh_2\}]$

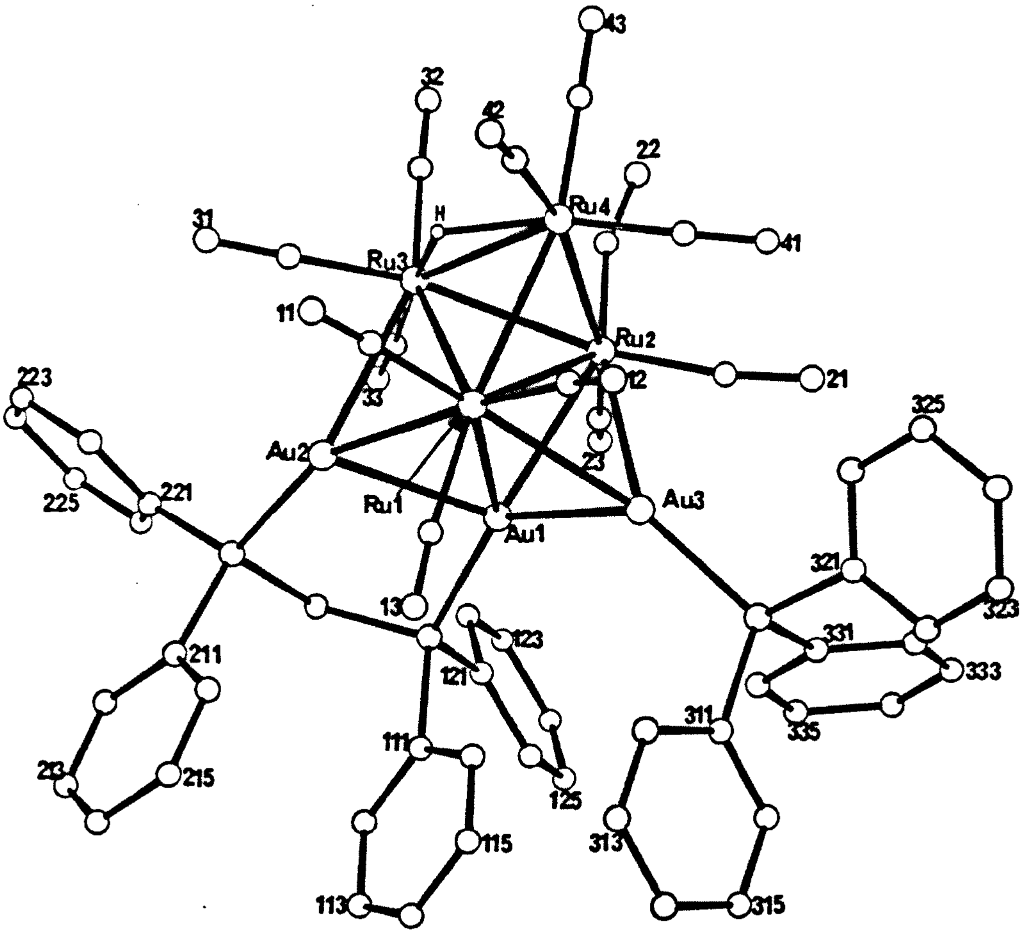

Figure 2.4.1. The molecular structure of the heptanuclear cluster $[Au_3Ru_4(\mu\text{-}H)(CO)_{12}\{\mu\text{-}Ph_2PCH_2PPh_2\}(PPh_3)]$ (1). The carbonyl C atoms have the same numbering as the O atoms to which they are attached.

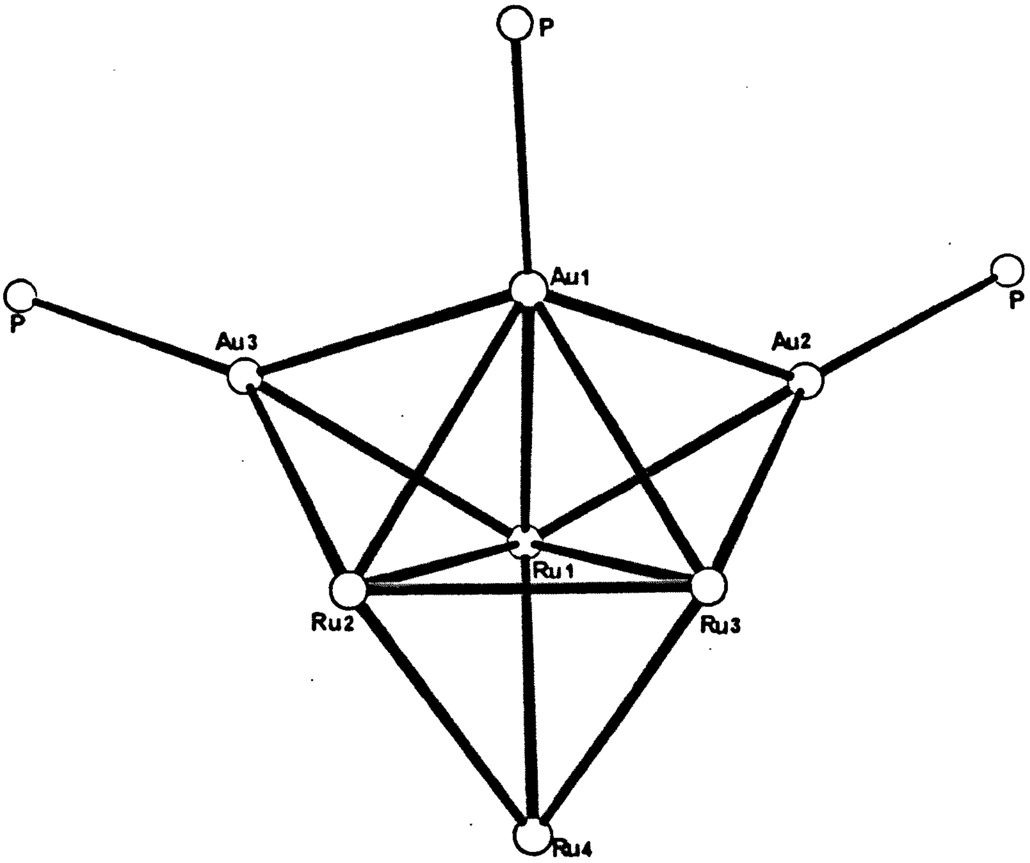

Figure 2.4.2(a) Molecular structure of $[Au_3Ru_4(\mu_3\text{-}H)(CO)_{12}(PPh_3)_3]$ (2).[45] The hydrido and carbonyl ligands, together with the phenyl rings have been omitted for clarity.

{Au-Au 2.823(1) Å}[51] and $[Au_2Ru_4(\mu\text{-}H)(\mu_3\text{-}H)(CO)_{12}\{\mu\text{-}Ph_2PCH_2CH_2PPh_2\}]$ {Au-Au 2.828(2) Å}.[54] The mean Au-Au bond length of 2.753(2) Å in (1) was also found to be markedly shorter than the mean Au-Au distances reported for related heptanuclear mixed-metal clusters,

compound	mean Au-Au/ Å
$[Au_3CoRu_3(CO)_{12}(PPh_3)_3]$	2.810(1)[58]
$[Au_3Ru_4(\mu\text{-}COMe)(CO)_9(PPh_3)_3]$	2.870(1)[43]

The overall range of Au-Ru bond lengths in (1) {2.762-2.920(2) Å} was similar to the range of distances observed in the monodentate PPh_3 cluster (2) {2.825-3.011(2) Å}, although the mean of the seven Au-Ru bond lengths in (2) {2.877(2) Å} was 0.037 Å longer than the mean of the six Au-Ru distances in (1) {mean 2.840(2) Å}. Interestingly, in (1), the two Au-Ru bonds associated with the third gold atom, Au(3), {Au(3)-Ru(1) 2.812(2);Au(3)-Ru(2) 2.898(2) Å} showed marked asymmetry, giving a difference between the two bonds of 0.086 Å, which was significantly larger than the corresponding difference of 0.013 Å observed in (2). Figure 2.4.2(b) displays the M-M bond lengths around the square base of the pyramidal core in $[Au_3Ru_4(\mu\text{-}H)(CO)_{12}\{\mu\text{-}Ph_2PCH_2PPh_2\}(PPh_3)]$ (1). The diagonal contacts between the metal atoms Au(1)...Ru(3) and Au(2)...Ru(2) defining the square, clearly signified a marked contraction of the base, with a difference between the two distances of 0.74(4) Å. This was similar to the distortion of the square base observed in the capped square-pyramidal structure of the di-gold tetra-ruthenium cluster compound $[Au_2Ru_4(\mu\text{-}H)(\mu_3\text{-}H)(CO)_{12}\{\mu\text{-}Ph_2PCH_2CH_2PPh_2\}]$[54] {Figure 2.2.2(e);section 2.2.2}.

The range of Ru-Ru distances observed in the Au_3Ru_4 dppm cluster compound (1) {2.773-3.044(3) Å} was similar to that reported for the related PPh_3 analogue (2) {2.801-3.001(3) Å}, but slightly shorter in

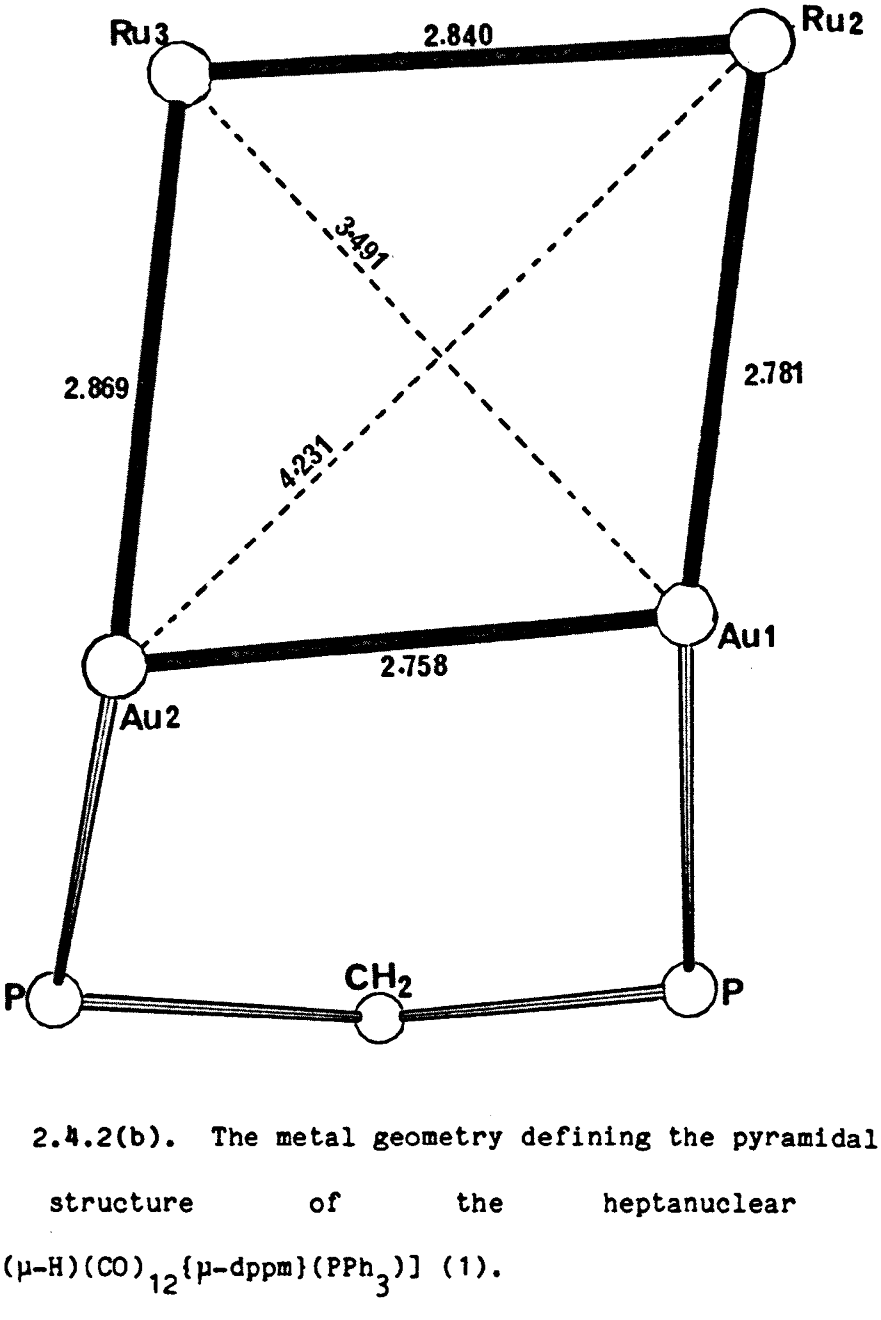

Figure 2.4.2(b). The metal geometry defining the pyramidal base in the structure of the heptanuclear cluster $[Au_3Ru_4(\mu\text{-}H)(CO)_{12}\{\mu\text{-}dppm\}(PPh_3)]$ (1).

range to those previously reported for the heptanuclear mixed-metal clusters, $[Au_3CoRu_3(CO)_{12}(PPh_3)_3]$ {2.802-3.001(5) Å}[58] and $[Au_3Ru_4(\mu\text{-}COMe)(CO)_9(PPh_3)_3]$ {2.895-2.913(3) Å}.[43] In (1) the three Ru-Ru distances associated with the capping of the square pyramidal core by Ru(4), showed slight asymmetry, with one bond being longer than the other two,

bond	distance/ Å
Ru(1)-Ru(4)	2.847(3)
Ru(2)-Ru(4)	2.733(3)
Ru(3)-Ru(4)	2.931(3).

In contrast, the corresponding bonds in (2) showed no obvious asymmetry with the mean difference in the three bonds of 0.014 Å, being markedly smaller than the mean difference of 0.118 Å observed in (1) {vide supra}. However, the mean of the six Ru-Ru bond lengths of the Ru_4 tetrahedron showed only a slight variation, with the mean bond in (1) {2.900(3) Å} being 0.006 Å longer than the mean bond in (2) {2.894(3) Å}.[45]

In the heptanuclear cluster $[Au_3Ru_4(\mu\text{-}H)(CO)_{12}\{\mu\text{-}Ph_2PCH_2PPh_2\}(PPh_3)]$ (1) the two Au-P distances bridged by the organic fragment, $-CH_2-$, were observed to be significantly different {Au(1)-P(1) 2.287(8);Au(2)-P(2) 2.306(8) Å}, but the mean difference of all three Au-P bonds {2.300(8) Å} was only slightly longer than the corresponding mean observed in the monodentate PPh_3 structure (2) {2.281(8) Å}. The mean Au-P bond length held by the methylene fragment in (1) {2.296(8) Å} was found to be similar to the mean of the two Au-P bonds 'linked' by a longer ethyl side chain of the bidentate ligand in the hexanuclear cluster $[Au_2Ru_4(\mu\text{-}H)(\mu_3\text{-}H)(CO)_{12}\{\mu\text{-}Ph_2PCH_2CH_2PPh_2\}]$ {2.291(4) Å}.[54] However, both these mean distances were significantly shorter than the mean

Au-P bonds bridged by the organic substituent, $-CH_2-$, in the related cluster compound, $[Au_2Ru_4(\mu\text{-}H)(\mu_3\text{-}H)(CO)_{12}\{\mu\text{-}Ph_2PCH_2PPh_2]$ {mean Au-P 2.305(4) Å}.[51]

The X-ray analysis of the heptanuclear cluster (1), established that each ruthenium atom was bonded to three essentially linear CO groups {Ru-C-O 165-177(3)°}, with the greatest deviation from linearity observed for CO(23), which was found to make a very short contact to Au(1), {Au(1)...C(23) 2.51(3) Å}. The range of Ru-CO bond lengths in (1) {1.83-1.92(3) Å} was similar to that reported for the related PPh_3 cluster (2) {1.86-1.90(8) Å}. Similarly the corresponding C-O range in (1) {1.13-1.24(5) Å} was also comparable to the range observed in (2), {1.14-1.21(8) Å}.

2.4.3 Conclusions.

The X-ray analysis on the heptanuclear mixed-metal cluster compound $[Au_3Ru_4(\mu\text{-}H)(CO)_{12}\{\mu\text{-}Ph_2PCH_2PPh_2\}(PPh_3)]$ (1) established that by replacing two of the three monodentate PPh_3 groups in $[Au_3Ru_4(\mu_3\text{-}H)(CO)_{12}(PPh_3)_3]$ (2)[45] with a bridging di-phosphine ligand in (1), the metal framework in the solid state was observed to rearrange from the bi-capped trigonal bi-pyramidal adopted by (2), to the bi-capped square pyramidal characterised for (1). The intramolecular contacts between the metal atoms forming the square base of the pyramid in (1) {Au(1)...Ru(3) 3.49 (3) and Au(2)...Ru(2) 4.23(3) Å} signified a marked distortion of the metal framework. In contrast, the pyramidal base in the di-gold ruthenium cluster $[Au_2Ru_4(\mu\text{-}H)(\mu_3\text{-}H)(CO)_{12}\{\mu\text{-}Ph_2PCH_2PPh_2\}]$ having the two Au-P bonds also 'linked' by the methylene unit reflected upon a less distorted square, {Au(1)...Ru(1) 4.15 (3) and Au(2)...Ru(4) 3.81(3) Å}.[51] Interestingly, the marked contraction of the pyramidal base in (1) was found to closely resemble that observed in the Au_2Ru_4 dppe cluster compound $[Au_2Ru_4(\mu\text{-}H)(\mu_3\text{-}H)(CO)_{12}\{\mu\text{-}Ph_2PCH_2CH_2PPh_2\}]$, in which the two Au-P bonds were bridged by a longer organic ethyl side chain, {Au(1)...Ru(1) **4.23**(3); Au(2)...Ru(4) **3.44**(3) Å}.

These results further supported that besides causing the observed change in metal core structures when two Au-P bonds were held by the bridging organic substituents, various degrees of distortion within the pyramidal frameworks were also present in the solid state structures of these gold-ruthenium mixed-metal cluster compounds. Importantly, the Au-Au bond bridged by the dppm ligand in the Au_3Ru_4 hydrido compound (1) was markedly shorter than the Au-Au bonds bridged by bidentate organophosphine groups in the related di-gold ruthenium clusters, {vide supra}. This reflected upon a greater steric congestion of the surface ligands in (1), especially with the incorporation of the third $Au(PPh_3)$ group into the metal polyhedron.

Table 2.4.2

Bond	Distance/ Å (1)	 (2)[45*]
Au(1)-Au(2)	2.758(2)	2.822(2)
Au(1)-Au(3)	2.749(2)	2.838(2)
Au(1)-Ru(1)	2.920(2)	2.832(2)
Au(1)-Ru(2)	2.781(2)	3.011(2)
Au(1)-Ru(3)	-	2.961(2)
Au(2)-Ru(1)	2.762(2)	2.834(2)
Au(2)-Ru(3)	2.869(2)	2.825(2)
Au(3)-Ru(1)	2.812(2)	2.831(2)
Au(3)-Ru(2)	2.898(2)	2.844(2)
Ru(1)-Ru(2)	3.044(3)	2.978(3)
Ru(1)-Ru(3)	2.967(3)	3.001(3)
Ru(1)-Ru(4)	2.847(3)	2.822(3)
Ru(2)-Ru(3)	2.840(3)	2.960(3)
Ru(2)-Ru(4)	2.773(3)	2.801(3)
Ru(3)-Ru(4)	2.931(3)	2.805(3)

* re-numbered for comparison.

Section 2.5. Comparison of the trends in metal frameworks, M-M, M-Ru and M-P bond lengths adopted in the solid state by related ruthenium mixed-metal cluster compounds containing Group IB metal atoms, Cu, Ag or Au bonded to either monodentate or bidentate organophosphine ligands.

2.5.1. The comparison of the solid state geometries adopted by ruthenium hydrido clusters containing Group IB metal phosphine groups forming a part of the mixed-metal polyhedron.

The X-ray analyses of the mixed-metal clusters, $[Au_2Ru_4(\mu\text{-}H)(\mu_3\text{-}H)(CO)_{12}\{\mu\text{-}Ph_2PCH{=}CHPPh_2\}]$, $[AuCuRu_4(\mu\text{-}H)(\mu_3\text{-}H)(CO)_{12}\{\mu\text{-}Ph_2PCH_2CH_2PPh_2\}]$ and $[Au_3Ru_4(\mu\text{-}H)(CO)_{12}\{\mu\text{-}Ph_2PCH_2PPh_2\}(PPh_3)]$ presented in sections 2.2, 2.3 and 2.4, respectively and comparison of their structural data to previously reported related structures of gold, copper and silver established an interesting trend in the metal frameworks these novel compounds adopted in the solid state, governed primarily by the type of organophosphine group bonded to the Group IB metal atoms. The reported X-ray structure of the di-gold tetra-ruthenium cluster $[Au_2Ru_4(\mu\text{-}H)(\mu_3\text{-}H)(CO)_{12}(PPh_3)_2]$ (1) described a capped trigonal bi-pyramidal metal geometry.[50] Interestingly, upon the replacement of two monodentate PPh_3 groups by a bidentate phosphine ligand, $\mu\text{-}Ph_2PCH_2PPh_2$, a change in the metal geometry to a capped square pyramidal metal core was observed, as characterised for the mixed-metal cluster $[Au_2Ru_4(\mu\text{-}H)(\mu_3\text{-}H)(CO)_{12}\{\mu\text{-}Ph_2PCH_2PPh_2\}]$ (2).[51]

Variations in the nature of the bidentate organophosphine ligands, involving the lengthening of the organic side chain was found to retain the capped square pyramidal metal frameworks in the hexanuclear clusters $[Au_2Ru_4(\mu\text{-}H)(\mu_3\text{-}H)(CO)_{12}\{\mu\text{-}Ph_2PCH_2CH_2PPh_2\}]$ (3)[54] and $[Au_2Ru_4(\mu\text{-}H)(\mu_3\text{-}H)(CO)_{12}\{\mu\text{-}Ph_2PCH{=}CHPPh_2\}]$ (4) (X-ray study presented in section 2.2). This series of di-gold ruthenium compounds was further extended to accommodate a third gold atom in the mixed-metal polyhedron, as structurally characterised for the heptanuclear clusters $[Au_3Ru_4(\mu_3\text{-}H)(CO)_{12}(PPh_3)_3]$ (5)[45] and

$[Au_3Ru_4(\mu\text{-}H)(CO)_{12}\{\mu\text{-}Ph_2PCH_2PPh_2\}(PPh_3)]$ (6) (X-ray study presented in section 2.4). Once again the replacement of two of the three PPh_3 groups in (5) to a bidentate phosphine bridge in (6) resulted in a rearrangement of the metal geometry from the bi-capped trigonal bi-pyramidal in (5)[45] to the bi-capped square pyramidal in (6).

Similar variations in metal core structures were also observed between the pentanuclear sulphido clusters $[Au_2Ru_3(\mu_3\text{-}S)(CO)_9(PPh_3)_2]$ (7)[42] and $[Au_2Ru_3(\mu_3\text{-}S)(CO)_9\{\mu\text{-}Ph_2PCH_2PPh_2\}]$ (8).[53] The PPh_3 derivative (7) adopted a trigonal bi-pyramidal metal core, whereas the related dppm analogue (8) displayed a distorted square pyramidal metal framework. Table 2.5.1(a) summarises the observed trends in the metal polyhedra of the gold-ruthenium mixed-metal cluster compounds (1)-(8).

From the observed trends in the metal frameworks of cluster compounds (1)-(8), an important conclusion was drawn. When two Au-P bonds were held parallel to the ruthenium tetrahedral metal core by organic side chains, the metal framework was found to rearrange from that adopted by related clusters in which the gold atoms were bonded to monodentate PPh_3 groups.

In total contrast, the series of heteronuclear clusters containing copper and silver atoms, $[M_2Ru_4(\mu_3\text{-}H)_2(CO)_{12}(L)]$ [M = Cu or Ag; L = $(PPh_3)_2$ or $\{\mu\text{-}Ph_2P(CH_2)_nPPh_2\}$ n = 1 or 2], all showed marked similarities in their respective solid state structures. The reported X-ray structures of the cluster compounds $[M_2Ru_4(\mu_3\text{-}H)_2(CO)_{12}(PPh_3)]$ [M = Cu (9) or Ag (10)][50] described capped trigonal bi-pyramidal geometries. Replacement of monodentate PPh_3 groups by bidentate phosphine ligand, dppm, resulted in no change in the metal core geometries with cluster compounds $[M_2Ru_4(\mu_3\text{-}H)_2(CO)_{12}\{\mu\text{-}Ph_2PCH_2PPh_2\}]$ [M = Cu (11)[52] or Ag (12)[51]] both adopting capped trigonal bi-pyramidal metal skeletons. Table 2.5.1(b) summarises the observed trends in the metal frameworks of the related copper and silver ruthenium cluster compounds (9)-(12) and di-copper ruthenium clusters with varying lengths of organic side chains of the bidentate ligand.

Interestingly, as discussed in sections 1.1.9 and 2.1.2 the reported $^{31}P-\{^1H\}$ n.m.r. studies of the cluster series $[M_2Ru_4(H)_2(CO)_{12}(PPh_3)_2]$ [M = Cu(9), Ag(10) an Au(1)] and $[M_2Ru_4(H)_2(CO)_{12}\{\mu-Ph_2PCH_2PPh_2\}]$ [M = Cu(11) ,Ag(12) and Au(2)] were consistent with the apparent fluxional behaviour of their structures in solutions.[50-54] The observed variations in their n.m.r. spectra were in agreement with an intramolecular rearrangement of their metal cores in solutions. A Berry pseudo rotation mechanism[42] involving the rearrangement of one trigonal bi-pyramidal metal framework to another equivalent metal core, via a square pyramidal intermediate, was proposed to account for these observations {section 1.1.9;Figure 1.1.9(f) and section 2.1.2}. Importantly, from band-shape analysis of their respective $^{31}P-\{^1H\}$ n.m.r spectra at various temperatures, Salter and co-workers reported that the Free energies of Activation (ΔG), associated with the proposed intramolecular metal core rearrangements in solutions of the above compounds, were controlled by the nature of the attached phosphine ligand:[51]

Table 2.5.1(c)

Compound		M = Cu	M = Ag	M = Au
$[M_2Ru_4(H)_2(CO)_{12}(PPh_3)]$	ΔG	40.9	40.0	42.0 KJ mol^{-1}
$[M_2Ru_4(H)_2(CO)_{12}\{dppm\}]$	ΔG	40.8	33.0	29.0 KJ mol^{-1}

These results clearly showed that the replacement of two monodentate PPh_3 groups by the bidentate $\mu-Ph_2PCH_2PPh_2$ ligand caused a noteable lowering of ΔG in both the silver and gold clusters. However, in the analogous copper cluster the corresponding ΔG values showed a negligable difference. The workers therefore suggested, that the observed variations in ΔG values were related to the degree of steric strains suffered by the respective M-P bonds, when freely co-ordinated to phenyl rings or held by bridging organic side chains.[51]

Importantly, although a significant drop in the ΔG value between the related silver clusters $[Ag_2Ru_4(\mu_3\text{-}H)_2(CO)_{12}(PPh_3)_2]$ (10) and $[Ag_2Ru_4(\mu_3\text{-}H)_2(CO)_{12}\{\mu\text{-}Ph_2PCH_2PPh_2\}]$ (12) was observed, indicating that the proposed rearrangement process in solutions was more favoured by the dppm derivative (12), the capped trigonal bi-pyramidal metal core characterised in the solid state established that the steric demands of the bridging organophosphine ligand were not sufficient to alter the metal polyhedral core adopted by the PPh_3 analogue (10). The very small difference in the ΔG values between the copper ruthenium clusters $[Cu_2Ru_4(\mu_3\text{-}H)_2(CO)_{12}(PPh_3)_2]$ (9) and $[Cu_2Ru_4(\mu_3\text{-}H)_2(CO)_{12}\{\mu\text{-}Ph_2PCH_2PPh_2\}]$ (11) reflected upon the steric strains imposed by the bidentate ligand in solutions of (11) being minimal, with both structures adopting similar capped trigonal bi-pyramidal geometries in the solid state. In contrast, the X-ray structure of the gold-ruthenium cluster $[Au_2Ru_4(\mu\text{-}H)(\mu_3\text{-}H)(CO)_{12}\{\mu\text{-}Ph_2PCH_2PPh_2\}]$ (2) established a capped square pyramidal metal core, in marked difference to the capped trigonal bi-pyramidal structure adopted by the parent monodentate PPh_3 cluster $[Au_2Ru_4(\mu\text{-}H)(\mu_3\text{-}H)(CO)_{12}(PPh_3)_2]$ (1).

This was consistent with the significant drop in the value of ΔG for the rearrangement process in solutions of cluster species (2), {Table 2.5.1(c)}. This indicated that the two Au-P vectors held by the organic side chain were subjected to greater steric constraint and the proposed rearrangement pathway in solutions enabled the release of some of these strains. Importantly, the capped square pyramidal geometry adopted in the solid state by (2) was similar in structure to the proposed metal skeleton for the intermediate in the Berry pseudo rotation rearrangement process, {Figure 1.1.9(f);section 1.1.9}. These observations therefore revealed, that the steric strains imposed by the bidentate organophosphine ligand were related to the size of the Group IB metal atom to which it was co-ordinated, with the larger gold atoms in (2) suffering the greatest strains, and exhibiting the observed change in metal core geometry.

Further evidence to support this conclusion resulted from the X-ray analysis of the hexanuclear cluster $[AuCuRu_4(\mu\text{-}H)(\mu_3\text{-}H)(CO)_{12}\{\mu\text{-}Ph_2PCH_2CH_2PPh_2\}]$ (13) (section 2.3), whose metal framework contained two different Group IB metal atoms bridged by a di-phosphine bidentate ligand. The six metal atoms adopted a capped trigonal bi-pyramidal geometry analogous to that characterised for the di-gold ruthenium cluster $[Au_2Ru_4(\mu\text{-}H)(\mu_3\text{-}H)(CO)_{12}(PPh_3)_2]$ (1)[50] and the di-copper ruthenium compound $[Cu_2Ru_4(\mu_3\text{-}H)_2(CO)_{12}(PPh_3)_2]$ (9). Although the dynamic behaviour of the cluster in solutions as yet has not been reported, the solid state structure illustrated that the steric demands placed upon the gold and copper atoms were not as severe as those present when the organic bridge held two Au-P bonds. Thus, the presence of the smaller copper atom minimised the constraint and rigidity within the metal framework of (13), with the expected rearrangement of the metal core to the capped square pyramidal geometry not observed in the solid state.

Table 2.5.1(a)

compound	phosphine ligand	geometry
$[Au_2Ru_4(\mu\text{-}H)(\mu_3\text{-}H)(CO)_{12}(PPh_3)_2]$ (1)[50]	PPh_3	capped tbp*
$[Au_2Ru_4(\mu\text{-}H)(\mu_3\text{-}H)(dppm)(CO)_{12}]$ (2)[51]	dppm	capped spy*
$[Au_2Ru_4(\mu\text{-}H)(\mu_3\text{-}H)(dppe)(CO)_{12}]$ (3)[54]	dppe	capped spy
$[Au_2Ru_4(\mu\text{-}H)(\mu_3\text{-}H)(dppol)(CO)_{12}]$(4)	dppol	capped spy
$[Au_3Ru_4(\mu_3\text{-}H)(CO)_{12}(PPh_3)_3]$ (5)[45]	PPh_3	bi-capped tbp
$[Au_3Ru_4(\mu\text{-}H)(CO)_{12}(dppm)(PPh_3)]$ (6)	dppm	bi-capped spy
$[Au_2Ru_3(\mu_3\text{-}S)(CO)_9(PPh_3)_2]$ (7)[42]	PPh_3	tbp
$[Au_2Ru_3(\mu_3\text{-}S)(CO)_9(dppm)]$ (8)[53]	dppm	spy

*tbp = trigonal bi-pyramidal and spy = square pyramidal

dppm = $\mu\text{-}Ph_2PCH_2PPh_2$, dppe = $\mu\text{-}Ph_2PCH_2CH_2PPh_2$, dppol = $\mu\text{-}Ph_2PCH{=}CHPPh_2$.

Table 2.5.1(b).

M = Cu or Ag

$[M_2Ru_4(\mu_3\text{-}H)_2(CO)_{12}(PPh_3)_2]^{50}$

monodentate PPh_3

capped tbp

$[M_2Ru_4(\mu_3\text{-}H)_2(CO)_{12}(dppm)]^{51}$

bidentate dppm

capped tbp

$[Cu_2Ru_4(\mu_3\text{-}H)_2(CO)_{12}(dppe)]^{52}$

bidentate dppe

capped tbp

$[Cu_2Ru_4(\mu_3\text{-}H)_2(CO)_{12}(dppp)]^{52}$

bidentate dppp

capped tbp

$[Cu_2Ru_4(\mu_3\text{-}H)_2(CO)_{12}(dpppe)]^{52}$

bidentate dpppe

capped tbp

*tbp = trigonal bi-pyramidal,

dppm = $\mu\text{-}Ph_2PCH_2PPh_2$, dppe = $\mu\text{-}Ph_2P(CH_2)_2PPh_2$, dppp = $\mu\text{-}Ph_2P(CH_2)_3PPh_2$ dpppe = $\mu\text{-}Ph_2P(CH_2)_5PPh_2$.

2.5.2. The observed distortions in the metal frameworks of related capped square pyramidal gold-ruthenium heteronuclear structures.

The X-ray analyses of the mixed-metal clusters,

$[Au_2Ru_4(\mu\text{-}H)(\mu_3\text{-}H)(CO)_{12}\{\mu\text{-}Ph_2PCH_2PPh_2\}]$ (2)[51]

$[Au_2Ru_4(\mu\text{-}H)(\mu_3\text{-}H)(CO)_{12}\{\mu\text{-}Ph_2PCH_2CH_2PPh_2\}]$ (3)[54]

$[Au_2Ru_4(\mu\text{-}H)(\mu_3\text{-}H)(CO)_{12}\{\mu\text{-}Ph_2PCH{=}CHPPh_2\}]$ (4)*

and $[Au_3Ru_4(\mu\text{-}H)(CO)_{12}\{\mu\text{-}Ph_2PCH_2PPh_2\}(PPh_3)]$ (8)*

*(X-ray structural studies presented in section 2.2 and 2.4, respectively), established that all four compounds adopted a basic square pyramidal metal core in the solid state. The interesting feature of comparison in the stuctures of these related clusters was the observed distortions present in the pyramidal metal frameworks, related to the variation of the side chain of the organophosphine bidentate bridge 'spanning' the two gold atoms. Figure 2.5.2 displays the M-M bond lengths of the square base in the structures of (2), (3), (4) and (8).

The Au-Au distance in (8) {2.758(2) Å} was significantly shorter than the corresponding bonds in the structures of (2), (3) and (4), {2.823(1), 2.828(2) and 2.861(2) Å, respectively}. The Au-Ru bonds defining the square base in all four structures exhibited asymmetry, with a difference between the two bonds of 0.088 Å in (8) 0.058 Å in (2) and 0.067 Å in (3). In contrast, the corresponding difference in (4) was considerably smaller {0.028 Å}. The degree of distortion within the base of the pyramidal cores in these related structures displayed an interesting variation. The difference between the diagonal contacts made by the four metal atoms of the square in (2) {0.340 Å} was found to be similar to the corresponding difference observed in (4) {0.330 Å}. However, the difference in both (3) and (8) were similar but noteably greater {0.790 and 0.740 Å, respectively}. The marked contraction of the square in (3) was anticipated due to a longer ethyl side chain, {$-CH_2-CH_2-$}, bridging the two Au-P bonds, resulting in a greater flexibility of the two vectors and giving the shortest contact between the metal atoms, Au(**2**) and Ru(**4**) in all four structures, {Figure 2.5.2}.

The presence of a similar distortion of the metal pyramidal core in the structure of the Au_3Ru_4 dppm cluster (8) was surprising, since a single methylene {$-CH_2-$} unit 'spanning' two of the three Au-P bonds would have been thought to enhance an environment of constraint and rigidity similar to that present in the Au_2Ru_4 dppm analogue (2). In the solid state structure of (4), with the two Au-P vectors held parallel by the unsaturated ethene bridge {-CH=CH-}, the lengthening of the organic chain of the bidentate ligand was observed to enhance less distortion of the square base. The observed differences between the diagonal contacts made by the four metal atoms of the square base in (4) were similar to those present in the analogous dppm cluster (2), where a single $-CH_2-$ fragment bridged the corresponding Au-P bonds, {Figure 2.5.2}. From these results it was concluded that, besides causing the change in metal core geometry in the solid state when monodentate phosphines were replaced by bidentate phosphine groups, the observed distortions within the metal frameworks of these related clusters were guided not only by the length of the organic backbone of the bidentate ligand, but also to the 'nature' of the organic substituent bridging the Au-P bonds.

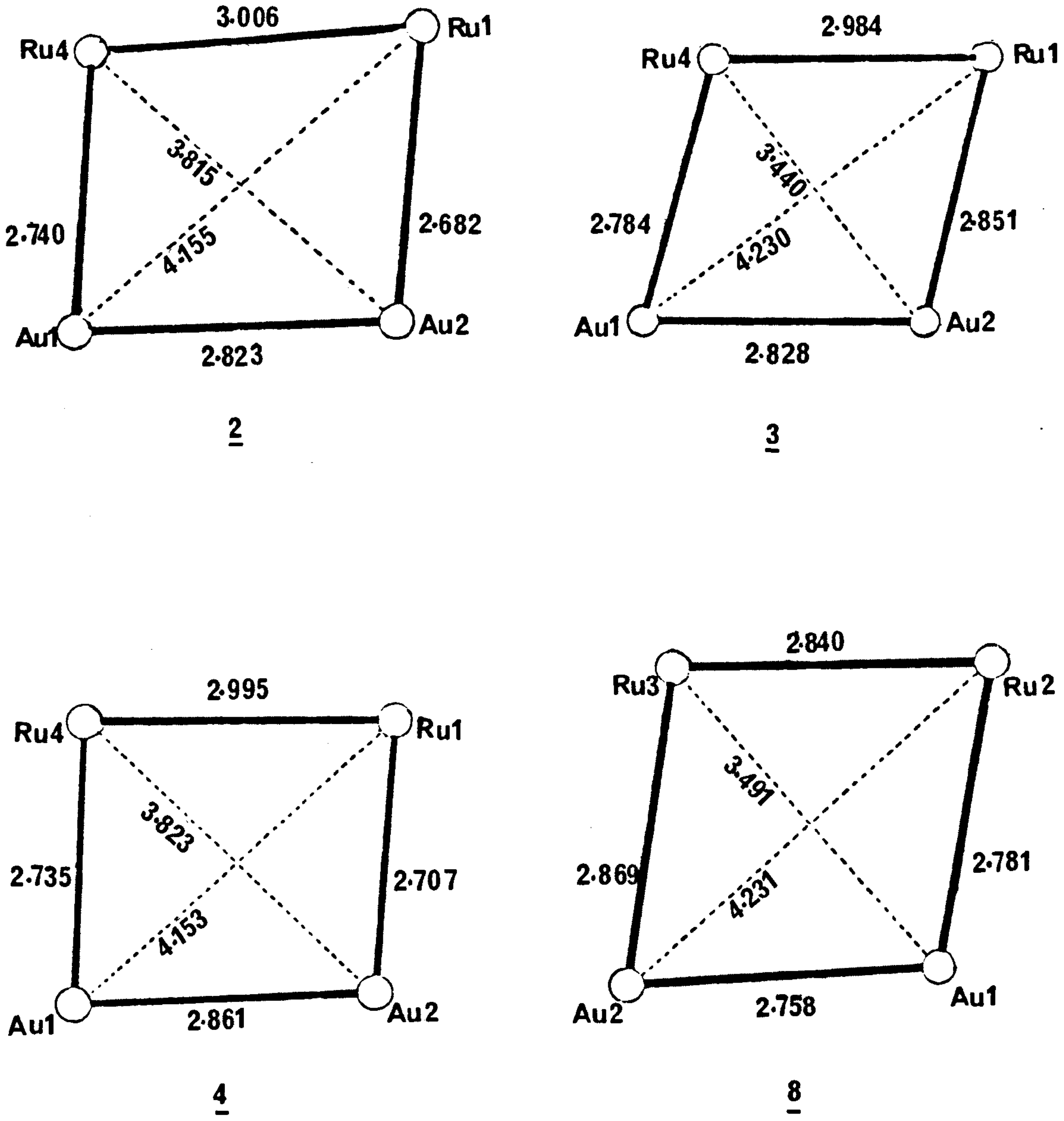

2 3

4 8

Figure 2.5.2

2.5.3 Trends in M-M, M-Ru and M-P bond lengths in related ruthenium clusters containing copper, silver and gold phosphine groups.

With the correlation of the structural data obtained from the X-ray studies of analogous tetra-ruthenium hydrido clusters with two ML fragments [M = Cu, Ag or Au; L = $(PPh_3)_2$ or bidentate dppm, dppe and dppol] forming a part of the mixed-metal polyhedron, interesting trends in the M-M, M-Ru and M-P bond lengths have been established. In the series of di-gold ruthenium hydrido clusters, the change from monodentate to bidentate organophosphines results in an overall change of metal core geometry in the solid state from the capped trigonal bi-pyramidal described by the PPh_3 cluster compound, to the capped square pyramidal adopted by the analogous structures with bidentate organophosphine bridges, {section 2.5.1}. The Au-Au bonds held by bridging phosphine groups in these related structures were observed to be markedly longer than the corresponding bond in the monodentate PPh_3 cluster compound:

Table 2.5.3(a)

compound	Au-Au distance/ Å
$[Au_2Ru_4(\mu\text{-}H)(\mu_3\text{-}H)(CO)_{12}(PPh_3)_2]$ (1)	2.791(1)[50]
$[Au_2Ru_4(\mu\text{-}H)(\mu_3\text{-}H)(CO)_{12}\{\mu\text{-}Ph_2PCH_2PPh_2\}]$ (2)	2.823(1)[51]
$[Au_2Ru_4(\mu\text{-}H)(\mu_3\text{-}H)(CO)_{12}\{\mu\text{-}Ph_2PCH_2CH_2PPh_2\}]$(3)	2.828(2)[54]
$[Au_2Ru_4(\mu\text{-}H)(\mu_3\text{-}H)(CO)_{12}\{\mu\text{-}Ph_2PCH{=}CHPPh_2\}]$ (4)	2.861(2)*

(* X-ray structure reported in section 2.2)

In contrast, the Au-Au bond bridged by the bidentate dppm group in the heptanuclear cluster $[Au_3Ru_4(\mu\text{-}H)(CO)_{12}\{\mu\text{-}Ph_2PCH_2PPh_2\}(PPh_3)]$ (5) {Au-Au 2.758(2) Å; X-ray structure reported in section 2.4} was significantly shorter than the corresponding bond in the analogous cluster with monodentate phosphine groups,

$[Au_3Ru_4(\mu_3\text{-H})(CO)_{12}(PPh_3)_3]$ (6) {2.822(2) Å}.[45] The same trend was observed between the reported pentanuclear sulphido clusters $[Au_2Ru_3(\mu_3\text{-S})(CO)_9(PPh_3)_2]$ (7)[42] and $[Au_2Ru_3(\mu_3\text{-S})(CO)_9\{\mu\text{-}Ph_2PCH_2PPh_2\}]$ (8),[53] with the Au-Au bond in (7) {2.957(2) Å} being markedly longer than in (8) {2.802(1) Å}.

In the series of reported copper and silver clusters, $[M_2Ru_4(\mu_3\text{-H})_2(CO)_{12}(L)]$ [M = Cu, Ag ; L = $(PPh_3)_2$ or $\{\mu\text{-}Ph_2PCH_2PPh_2\}$] the replacement of monodentate by bidentate phosphine ligands displayed no change in the metal core structures adopted in the solid state, with all cluster compounds exhibiting similar capped trigonal bi-pyramidal metal frameworks.[50,51] Importantly, there was an evident difference in the Group IB M-M bonds, with the Cu-Cu and Ag-Ag bonds co-ordinated to triphenyl phosphine groups being significantly longer than the corresponding bonds bridged by the bidentate dppm ligand:

Table 2.5.3(b)

compound	M-M distance/ Å
$[Cu_2Ru_4(\mu_3\text{-H})_2(CO)_{12}(PPh_3)_2]$ (9)	Cu-Cu 2.699(2)[50]
$[Ag_2Ru_4(\mu_3\text{-H})_2(CO)_{12}(PPh_3)_2]$ (10)	Ag-Ag 2.857(1)[50]
$[Cu_2Ru_4(\mu_3\text{-H})_2(CO)_{12}\{\mu\text{-}Ph_2PCH_2PPh_2\}]$ (11)	Cu-Cu 2.605(3)[52]
$[Ag_2Ru_4(\mu_3\text{-H})_2(CO)_{12}\{\mu\text{-}Ph_2PCH_2PPh_2\}]$ (12)	Ag-Ag 2.756(6)[51]

The M-Ru bonds (M = Cu, Ag or Au) also displayed a trend in these novel mixed-metal cluster compounds. The mean Au-Ru bonds in the di-gold ruthenium structures having bidentate phosphine groups, were found to be markedly shorter than the corresponding mean bond in the monodentate PPh_3 cluster compound:

Table 2.3.5(c)

compound	mean Au-Ru distance/ Å
$[Au_2Ru_4(\mu\text{-}H)(\mu_3\text{-}H)(CO)_{12}(PPh_3)_2]$ (1)	2.917(1)[50]
$[Au_2Ru_4(\mu\text{-}H)(\mu_3\text{-}H)(CO)_{12}\{\mu\text{-}Ph_2PCH_2PPh_2\}]$ (2)	2.795(2)[51]
$[Au_2Ru_4(\mu\text{-}H)(\mu_3\text{-}H)(CO)_{12}\{\mu\text{-}Ph_2PCH_2CH_2PPh_2\}]$(3)	2.844(2)[54]
$[Au_2Ru_4(\mu\text{-}H)(\mu_3\text{-}H)(CO)_{12}\{\mu\text{-}Ph_2PCH{=}CHPPh_2\}]$ (4)	2.770(2)[*]

([*] X-ray structure reported in section 3.2)

Similarly, the mean Au-Ru distance associated with the two gold atoms bridged by the bidentate phosphine ligand in the heptanuclear cluster $[Au_3Ru_4(\mu\text{-}H)(CO)_{12}\{\mu\text{-}Ph_2PCH_2PPh_2\}(PPh_3)]$ (5) {2.840(2) Å; X-ray structure reported in section 2.4} was again significantly shorter than the mean of the analogous bonds in the monodentate PPh_3 structure $[Au_3Ru_4(\mu_3\text{-}H)(CO)_{12}(PPh_3)_3]$ (6) {2.877(2) Å}.[45]

An opposite trend in the respective Cu-Ru and Ag-Ru bond lengths was observed in the related copper-ruthenium and silver-ruthenium compounds. The mean M-Ru distance in the structures containing the bidentate ligand was noteably longer than the corresponding mean bond observed in the monodentate PPh_3 analogues:

Table 2.3.5(d)

compound		mean M-Ru distance/ Å
$[Cu_2Ru_4(\mu_3\text{-}H)_2(CO)_{12}(PPh_3)_2]$ (9)	Cu-Ru	2.706(2)[50]
$[Ag_2Ru_4(\mu_3\text{-}H)_2(CO)_{12}(PPh_3)_2]$ (10)	Ag-Ru	2.894(1)[50]
$[Cu_2Ru_4(\mu_3\text{-}H)_2(CO)_{12}\{\mu\text{-}Ph_2PCH_2PPh_2\}]$ (11)	Cu-Ru	2.735(2)[52]
$[Ag_2Ru_4(\mu_3\text{-}H)_2(CO)_{12}\{\mu\text{-}Ph_2PCH_2PPh_2\}]$ (12)	Ag-Ru	2.931(6)[51]

Another interesting trend was further observed in comparison of the M-Ru and M-P bonds in the structures of these hexanuclear copper-ruthenium, silver-ruthenium and gold-ruthenium cluster compounds. In both series of clusters containing either the monodentate PPh_3 or bidentate dppm phosphine ligands, the mean Ag-P bond length was markedly longer than both the mean Cu-P and Au-P distances, which was not anticipated with respect to the increase in atomic number of the Group IB metal atom, Au > Ag > Cu. This trend was also observed in the respective mean M-Ru distances in the structures where the Group IB metal atoms were bridged by the dppm phosphine ligand. The mean Ag-Ru bond was significantly longer than both the mean Cu-Ru and Au-Ru lengths. However, in the related compounds with the hetero-metal atoms bonded to monodentate PPh_3 groups, the expected trend was observed, with the mean Au-Ru bond being markedly longer than both the mean Ag-Ru and Cu-Ru distances:

compound	mean M-Ru	mean M-P/ Å
$[Ag_2Ru_4(\mu_3\text{-}H)_2(CO)_{12}(PPh_3)_2]$	2.894(1)	2.401(4)[50]
$[Au_2Ru_4(\mu\text{-}H)(\mu_3\text{-}H)(CO)_{12}(PPh_3)_2]$	2.917(1)	2.284(3)[50]
$[Cu_2Ru_4(\mu_3\text{-}H)_2(CO)_{12}(PPh_3)_2]$	2.706(2)	2.234(3)[50]
$[Ag_2Ru_4(\mu_3\text{-}H)_2(CO)_{12}\{\mu\text{-}Ph_2PCH_2PPh_2\}]$	2.932(6)	2.422(5)[51]
$[Au_2Ru_4(\mu\text{-}H)(\mu_3\text{-}H)(CO)_{12}\{\mu\text{-}Ph_2PCH_2PPh_2\}]$	2.795(2)	2.305(4)[51]
$[Cu_2Ru_4(\mu_3\text{-}H)_2(CO)_{12}\{\mu\text{-}Ph_2PCH_2PPh_2\}]$	2.735(2)	2.229(4)[52]

Section 2.6. To account for the observed differences in metal core structures adopted by gold-ruthenium compounds, when two gold atoms are bonded to monodentate PPh_3 groups or bridged by bidentate phosphine ligands.

It has been discussed in section 1.1.1, that from molecular orbital calculations, Evans and Mingos have suggested that the bonding characteristics of an $Au(PR_3)$ group is primarily associated with the hybrid (s-z) orbital, donating one electron in the formation of 3c-2e ($-\mu_2$) and 4c-2e ($-\mu_3$) M-M bonds.[59,60] Therefore, the linear nature of this orbital results in its lobe pointing towards the midpoint of a M-M bond it bridges or to the centre of a 3 metal atom triangle it caps. This feature was thought to be a contributing factor in the observed change in the solid state metal core geometries when monodentate PPh_3 groups bonded to gold atoms were replaced by a bridging bidentate phosphine ligand, in the cluster series $[Au_2Ru_4(\mu\text{-}H)(\mu_3\text{-}H)(CO)_{12}L]$ [L = $(PPh_3)_2$ or dppm, dppe, dppol] and $[Au_3Ru_4(H)(CO)_{12}(PPh_3)L]$ [L = $(PPh_3)_2$ or dppm], {section 2.5}. Angles around the gold atoms in these novel gold ruthenium cluster compounds, relating the Au-P vectors and various centroids within the Ru_4 tetrahedron to which these bonds made linear contacts, were calculated to investigate whether the particular direction favoured by the Au-P bonds towards the ruthenium tetrahedron, governed the observed metal core rearrangements.

Figure 2.6(a)

[Au_2Ru_4(μ-H)(μ$_3$-H)$(CO)_{12}(PPh_3)_2$] (1)[50]

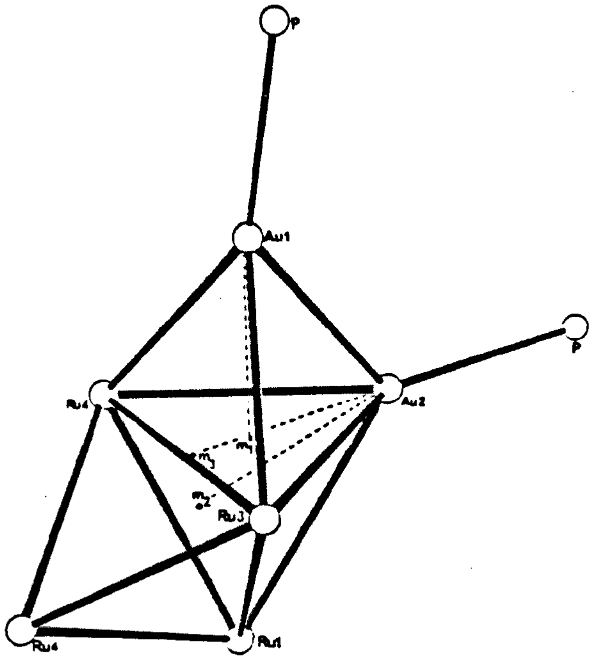

midpoint m(1) = centre of the triangle Au(2), Ru(3) Ru(4).

midpoint m(2) = centre of triangle Ru(1), Ru(3), Ru(4).

midpoint m(3) = centre of the bond Ru(3)-Ru(4).

The calculated angles showed that when two Au atoms were bonded to monodentate phosphine ligands as in (1), the bonding pattern involving the gold-phosphine group, Au(2)PPh_3, capping the metal atoms Ru(1), Ru(3), and Ru(4) resulted in a near linear angle being made to the centroid of this Ru_3 triangle, {P(2)-Au(2)-m(2) 176.0°}. The second gold-phosphine group, Au(1)PPh_3, was also observed to make a near linear contact to the centre of the face Au(2)-Ru(3)-Ru(4) it capped, {P(1)-Au(1)-m(1) 174.0°}.

Figure 2.6(b)

$[Au_2Ru_4(\mu\text{-}H)(\mu_3\text{-}H)(CO)_{12}\{\mu\text{-}Ph_2PCH_2PPh_2\}]$ (2)[51]

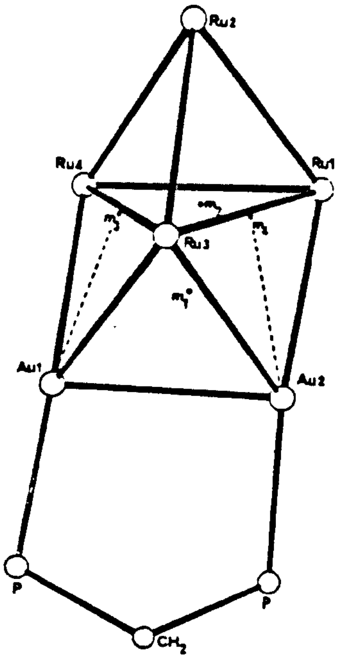

midpoint m(1) = centre of triangle Au(2), Ru(3) and Ru(4).

midpoint m(2) = centre of triangle Ru(1), Ru(3) Ru(4).

midpoint m(3) = centre of bond Ru(3)-Ru(4).

midpoint m(4) = centre of bond Ru(1)-Ru(3).

With the cleavage of the bond Au(2)-Ru(4) in the trigonal bi-pyramidal metal core structure of (1) {Figure 2.6(a)}, giving rise to the capped square pyramidal metal framework in (2), the gold atom, Au(2), which capped an Ru_3 face of the ruthenium tetrahedron in (1) was now envisaged to bridge the bond Ru(1)-Ru(3), giving an approximately linear angle to the midpoint of this vector, {P(2)-Au(2)-m(4) 168.0°}. The second gold atom, Au(1), was still adopting a μ_3-bonding mode by capping the face Au(2)-Ru(3)-Ru(4), although a markedly non-linear angle to the mid-point of this triangular face was observed, {P(1)-Au(1)-m(1) 137.0°}. The Au(1)-P(1) vector infact made a near linear angle to the midpoint of the bond Ru(3)-Ru(4), {Figure 2.6(b)}. These results indicated a predominance of μ_2-bonding character for both gold atoms, being constrained by the bridging phosphine group, preventing any linear contacts to be made to the centres of the faces capped by the related gold atoms in the monodentate PPh_3 structure (1).

Figure 2.6(c)

$[Au_2Ru_4(\mu\text{-}H)(\mu_3\text{-}H)(CO)_{12}\{\mu\text{-}Ph_2PCH_2CH_2PPh_2\}]$ (3)[54]

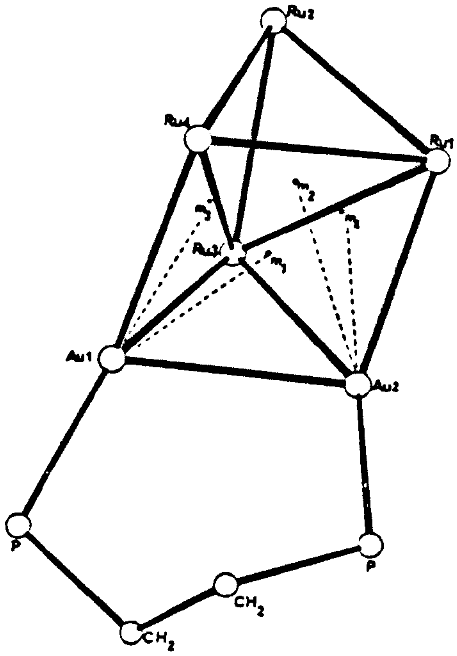

midpoint m(1) = centre of triangle Au(2), Ru(3) and Ru(4).

midpoint m(2) = centre of triangle Ru(1), Ru(3) Ru(4).

midpoint m(3) = centre of bond Ru(3)-Ru(4).

midpoint m(4) = centre of bond Ru(1)-Ru(3).

With the lengthening of the organic side chain in (3), the presence of an ethane fragment bridging the two Au-P bonds also displayed linear angles to the centres of the Ru-Ru bonds they essentially bridged {P(1)-Au(1)-m(3) 162.0°; P(2)-Au(2)-m4 163.0°} similar to that observed in the dppm analogue (2), {Figure 2.6(b)}. However, the greater flexibility of the two Au-P bonds in the structure of (3) was seen by the approximate linearity of the angles made towards the centroids of the faces capped by the related gold atoms in the monodentate PPh_3 cluster (1), {P(1)-Au(1)-m(1) 158.0 and P(2)-Au(2)-m(2) 155.0°}, reflecting upon a greater contraction of the square pyramidal framework.

Figure 2.6(d)

[$Au_2Ru_4(\mu\text{-}H)(\mu_3\text{-}H)(CO)_{12}\{\mu\text{-}Ph_2PCH{=}CHPPh_2\}$] (4)

(X-ray study presented in section 2.2}

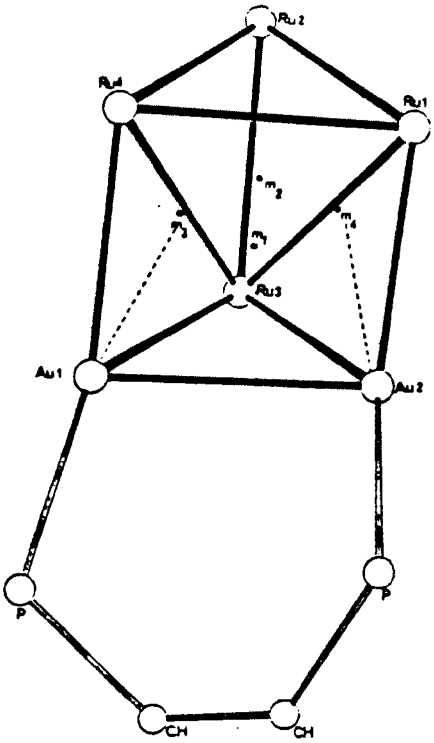

midpoint m(1) = centre of triangle Au(2), Ru(3) and Ru(4).
midpoint m(2) = centre of triangle Ru(1), Ru(3) Ru(4).
midpoint m(3) = centre of bond Ru(3)-Ru(4).
midpoint m(4) = centre of bond Ru(1)-Ru(3).

As observed in cluster compounds (2) and (3), {Figures 2.6(b) and 2.6(c), respectively}, the presence of an unsaturated ethene fragment 'linking' the Au-P bonds in (4), allowed near linear angles to be made to the centres of the Ru-Ru bonds they essentially edge-bridged, {P(1)-Au(1)-m3 165.0°; P(2)-Au(2)-m4 168.0°}. However, both vectors displayed markedly non-linear angles to the mid-points of the triangular faces {P(1)-Au(1)-m(1) 135.0° and P(2)-Au(2)-m(2) 141.0}, similar to that observed in the dppm derivative (2), but in contrast to that displayed by the two Au-P bonds in (3). These results indicated that unlike the situation in compound (3), where the two Au-P vectors were held by a saturated ethyl bridge, {$-CH_2-CH_2-$}, the presence of an unsaturated ethene unit, {-CH=CH-}, in (4) created an environment of greater constraint and rigidity.

Figure 2.6(e)

$[AuCuRu_4(\mu\text{-}H)(\mu_3\text{-}H)(CO)_{12}\{\mu\text{-}Ph_2PCH_2CH_2PPh_2\}]$ (5)

(X-ray study presented in section 2.3)

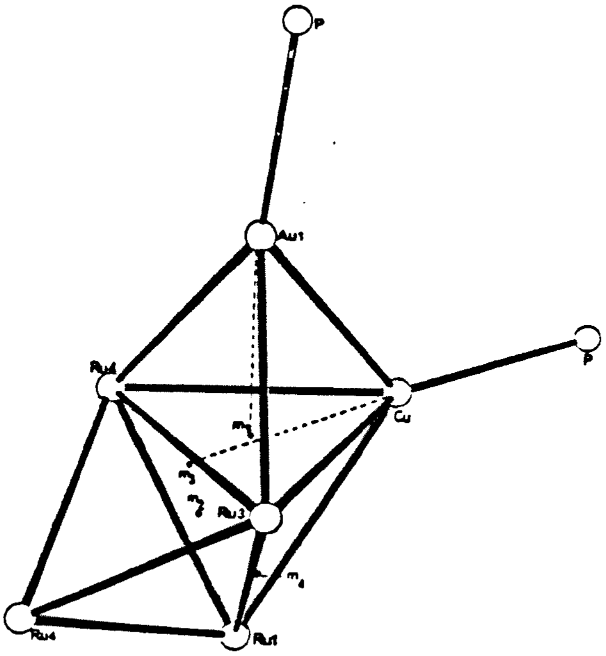

midpoint m(1) = centre of triangle Cu(1), Ru(3) and Ru(4).

midpoint m(2) = centre of triangle Ru(1), Ru(3) Ru(4).

midpoint m(3) = centre of bond Ru(3)-Ru(4).

midpoint m(4) = centre of bond Ru(1)-Ru(3).

The need to form linear contacts to the mid-point of the face capped by an $Au(PR_3)$ group was evident in the angles calculated in the copper-gold ruthenium cluster compound (5). The bonding of the hetero-metal atoms was envisaged to involve the Cu atom firstly capping the metal atoms Ru(1), Ru(3) and Ru(4), followed by the gold atom capping the face Cu-Ru(3)-Ru(4). The Au(1)-P(1) vector displayed a μ_3-bonding mode by making a near linear angle to the midpoint of the face it capped, {P(1)-Au(1)-m(1) 168.0°}. The greater distortion of the Cu-P vector was reflected upon a more μ_2-bonding character adopted towards the centre of the bond Ru(3)-Ru(4), {P(2)-Cu(1)-m(3) 171.0°}.

Figure 2.6(f)

$[Au_3Ru_4(\mu_3\text{-}H)(CO)_{12}(PPh_3)_3]$ (6)[45]

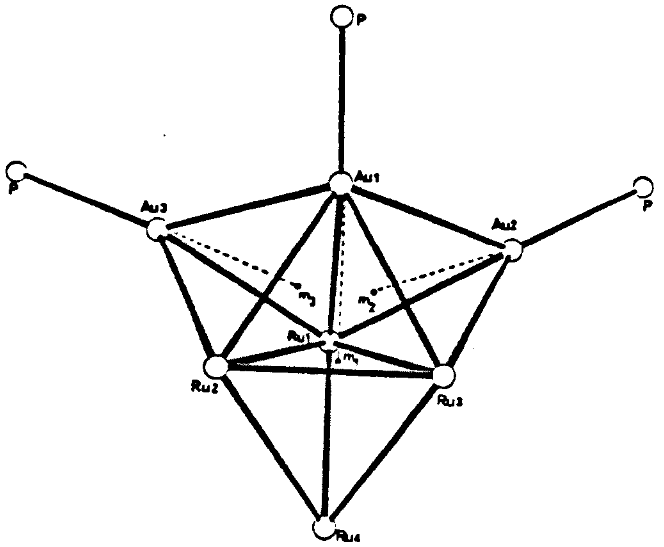

midpoint m(1) = centroid of triangle Ru(1), Ru(2), Ru(3)

midpoint m(2) = centroid of triangle Au(1), Ru(1), Ru(3)

midpoint m(3) = centroid of triangle Au(1), Ru(1), Ru(2)

In the heptanuclear cluster (6) all three Au-P bonds maintained the expected near linear angles to the centres of the faces they capped.

Figure 2.6(g)

$[Au_3Ru_4(\mu_2\text{-}H)(CO)_{12}\{\mu\text{-}Ph_2PCH_2PPh_2\}(PPh_3)]$

(X-ray study presented in section 2.4)

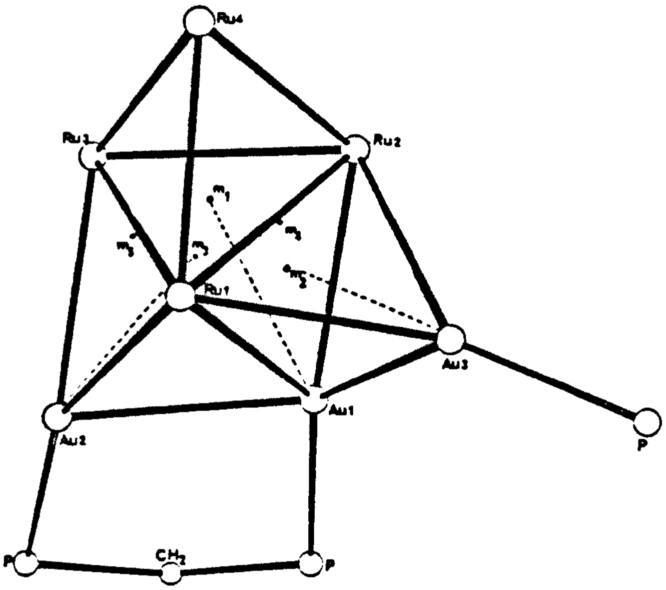

midpoint m(1) = centroid of triangle Ru(1), Ru(2), Ru(3)

midpoint m(2) = centroid of triangle Au(1), Ru(1), Ru(2)

midpoint m(3) = centroid of triangle Au(1), Ru(1), Ru(3)

midpoint m(4) = centre of bond Ru(1)-Ru(2)

midpoint m(5) = centre of bond Ru(1)-Ru(3)

In cluster compound (7), the various contacts made by the $Au(PR_3)$ groups to the centroids of the Ru_4 tetrahedron reflected upon a marked distortion of the bi-capped square pyramidal metal core geometry. This was seen by the two Au-P bonds 'spanned' by the dppm ligand making non-linear angles towards the mid-points of the Ru-Ru bonds they essentially edge-bridged, {P(1)-Au(1)-m(4) 150.0°

P(2)-Au(2)-m(5) 153.4°}. However, the two vectors were observed to make near-linear contacts to the respective centres of the faces capped by the two related gold atoms in the monodentate PPh_3 analogue (6), {Figure 2.6(f)} {P(1)-Au(1)-m(1) 159.0°;P(2)-Au(2)-m(3) 161.0°}. The third gold atom bonded to a PPh_3 group was observed to make a near-linear angle to the face it capped, {P(3)-Au(3)-m(2) 168.0°}. These results indicated that, although two of the three Au-P bonds were bridged by a single $-CH_2-$ fragment, the expected rigidity and constraint within the metal framework was not observed. The calculated angles reflected upon the bonding character of the two Au atoms bridged by the dppm ligand, being intermediate betwwen $-\mu_2$ and $-\mu_3$.

Correlation of the results obtained from these calculations revealed that the linear nature of the bonding adopted by the $Au(PR_3)$ groups was best maintained, when the gold atoms were bonded to monodentate PPh_3 groups, as observed in the structures of $[Au_2Ru_4(\mu-H)(\mu_3-H)(CO)_{12}(PPh_3)_2]$ (1) and $[Au_3Ru_4(\mu_3-H)(CO)_{12}(PPh_3)_3]$ (6), {Figures 2.6(a) and 2.6(f), respectively}. However, with the replacement of these phosphine groups by bidentate organophosphine ligands bridging two gold atoms, the resulting constraint made it impossible for the Au-P bonds to maintain their linear contacts to the centroids of the faces capped by the gold atoms,in the metal core structure of the analogous PPh_3 cluster. Therefore, the energetically favoured pathway through which the two Au-P bonds could maintain their linearity was the observed rearrangement of the metal framework, to square pyramidal skeletons as established for $[Au_2Ru_4(\mu-H)(\mu_3-H)(CO)_{12}\{\mu-Ph_2PCH_2PPh_2\}]$ (2),51 $[Au_2Ru_4(\mu-H)(\mu_3-H)(CO)_{12}\{\mu-Ph_2PCH_2CH_2PPh_2\}]$ (3)[54]

$[Au_2Ru_4(\mu\text{-}H)(\mu_3\text{-}H)(CO)_{12}\{\mu\text{-}Ph_2PCH{=}CHPPh_2\}]$ (4), and $[Au_3Ru_4(\mu\text{-}H)(CO)_{12}\{\mu\text{-}Ph_2PCH_2PPh_2\}(PPh_3)]$ (7). In the solid state structure of (2), where the two Au-P bonds were held by a single methylene unit, both vectors displayed a greater predominance of μ_2-bonding character, {Figure 2.6(b)}. A situation reflecting upon marked constraint, preventing the two Au-P bonds from pointing towards the centres of the faces capped by the related gold atoms in the PPh_3 compound (1).

Lengthening of the organic side chain of the bridging bidentate group in clusters (3) and (4), again established an interesting variation in the directions adopted by the two Au-P bonds towards the Ru_4 tetrahedron. In (3), the presence of the saturated ethyl bridge displayed greater flexibility of the Au-P vectors, with both bonds making near linear contacts not only to the mid-points of the Ru-Ru bonds they essentially edge-bridged, but also to the centres of the two faces capped by the gold atoms in the PPh_3 structure (1), {Figure 2.6(c)}. This indicated, that upon the lengthening of the organic backbone of the bidentate ligand in (3), the metal geometry was intermediate in structure to the capped trigonal bi-pyramidal adopted by $[Au_2Ru_4(\mu\text{-}H)(\mu_3\text{-}H)(CO)_{12}(PPh_3)_2]$ (1) and the capped square pyramidal described by $[Au_2Ru_4(\mu\text{-}H)(\mu_3\text{-}H)(CO)_{12}\{\mu\text{-}Ph_2PCH_2PPh_2\}]$ (2).

In the hexanuclear cluster $[Au_2Ru_4(\mu\text{-}H)(\mu_3\text{-}H)(CO)_{12}\{\mu\text{-}Ph_2PCH{=}CHPPh_2\}]$ (4), both Au-P vectors were observed to make near linear angles to the Ru-Ru bonds they bridged, but displayed marked non-linear contacts to the centroids of the faces capped by the two gold atoms in the PPh_3 cluster (1), {Figure 2.6(d)}. The only feasible explanation of the marked constraint of the two Au-P vectors in the structure of (4), was the probable delocalisation of the π-electrons from the ethene fragment to the adjacent P-C bonds of the bidentate bridge, creating rigidity within the six membered Au-P-CH=CH-P-Au ring. In the solid state structure of the copper-gold cluster compound $[AuCuRu_4(\mu-H)(\mu_3-H)(CO)_{12}\{\mu-Ph_2PCH_2CH_2PPh_2\}]$ (5), the six metal atoms defined a capped trigonal bi-pyramidal geometry. The Au-P bond was observed to make the expected near-linear angle to the centre of the face it capped, whereas the Cu-P vector was apparently distorted, exhibiting a near linear contact not to the Ru_3 face it capped, but to a Ru-Ru bond of that face. Therefore, having one gold and another smaller Group IB metal atom forming a part of the six metal polyhedron minimised the steric strains suffered by the Au-P vector, allowing it to point towards the centre of the face it capped, with the rearrangement of the metal core in the solid state not being observed.

In the heptanuclear mixed-metal cluster compound $[Au_3Ru_4(\mu_3-H)(CO)_{12}(PPh_3)_3]$ (6),[45] all three Au-P bonds displayed near linear angles to the mid-points of the faces they capped, {Figure 2.6(f)}. Interestingly, in the structure of the analogous dppm compound $[Au_3Ru_4(\mu-H)(CO)_{12}\{\mu-Ph_2PCH_2PPh_2\}(PPh_3)]$ (7), the two Au-P vectors 'linked' by a methylene fragment, also made approximately linear angles to the centres of the faces capped by the related gold atoms in the PPh_3 analogue (6), {Figure 2.6(g)}. This was rather surprising, as in the di-gold ruthenium structure (2), where the two Au-P bonds were also held by a methylene unit, an environment of rigid constraint within the five membered ring $-Au-P-CH_2-P-Au-$ was observed, preventing the two Au-P vectors from pointing towards the mid-points of the faces capped by the two gold atoms in the trigonal bi-pyramidal structure of the monodentate PPh_3 compound (1), {vide supra}. The metal framework in (7), was therefore intermediate in structure to the bi-capped trigonal bi-pyramidal metal skeleton adopted by cluster compound (6) and a non-distorted bi-capped square pyramidal metal core. This marked distortion in the geometry of (7) could have been attributed to the incorporation of a third Au(PPh_3) group into the metal polyhedron, increasing the overall surface ligand congestion and contracting the pyramidal core.

Setion 2.7. References.

1. K.K. Cheung, T.F. Lai, and K.S. Mok, J. Chem. Soc.(A), 1971, 1644.
2. A.R. Sanger, J. Chem. Soc., Chem. Commun., 1975,893.
3. H. Schmidbaur, Angew. Chem. Int.Ed.Engl., 1976, 15, 728.
4. C.A. Tolman, Chem. Rev., 1977, 77, 313.
5. M.A.F.D.R. Pinto, P.J. Sadler, S. Neilde, M.R. Sanderson, A. Subbiah, and R. Kuroda, J. Chem. Soc., Chem. Commun., 1980, 13.
6. M.P. Brown, J.R. Fisher, R.H. Hill, R.J. Puddephatt, and K.R. Seddon, Inorg. Chem., 1981, 20, 3516.
7. A.J. Deeming and M. Underhill, J. Chem. Soc., Dalton Trans., 1973, 2727.
8. M.R. Churchill, F.J. Hollander, and J.P Hutchinson, Inorg. Chem., 1977, 16, 2655.
9. J.J. De Boer, J.A. van Doorn, and C. Masters, J. Chem. Soc., Chem. Commun., 1978, 1005
10. G. Huttner, J. Schneider, G. Mohr, and J. von Seyerl, L. Wohlfahrt, Angew. Chem., Int.Ed.Engl., 1979, 18, 76.
11. A. Arduini, A.A. Bahsoun, J.A. Osborn, and C. Voelker, Angew. Chem., Int.Ed.Engl., 1980, 19, 1024

12. S.C. Brown, J. Evans, and M. Webster, J. Chem. Soc., Dalton Trans., 1981, 2263.

13. C.T. Hayward and R. Shapley, Inorg. Chem., 1982, 21, 3816.

14. A. Poe and V.C. Sekhar, J. Am. Chem. Soc., 1984, 106, 5034.

15. A.L. Balch, R.R. Guimerans, J. Linehan, Inorg. Chem., 1985, 24, 290.

16. A.L. Balch, J. Linehan, M.M. Olmstead, Inorg. Chem., 1985, 24, 3975.

17. A.L. Balch, L.A. Fossett, R.R. Guimerans, M.M. Olmstead, and P.E. Reedy, Inorg. Chem., 1986, 25, 1397.

18. F.A. Cotton and B.E. Hanson, Inorg. Chem., 1977, 16, 3369.

19. A.W. Coleman, D.F. Jones, P.H. Dixneuf, C. Brisson, J.J. Bonnet, and G. Lavigne, Inorg. Chem., 1984, 23, 952.

20. P.J. Roberts and J. Trotter, J. Chem. Soc.(A), 1971, 1479.

21. G. Lavigne, N. Lugan, and J.J. Bonnet, Acta Cryst., 1982, B38, 1911.

22. M.I. Bruce, T.W. Hambley, B.K. Nicholson, and M.R. Snow, J. Organomet. Chem., 1982, 235, 83.

23. M.I. Bruce, E. Horn, O. bin Shawkataly, M.R. Snow, E.R.T Tiekink and M.L. Williams, J. Organomet. Chem., 1986, 316, 187.

24. J.R. Shapley, S.I. Richter, M.R. Churchill and R.A. Lashewycz, J. Am. Chem. Soc., 1977, 99, 7384.

25. J.R. Shapley, S.I. Richter, M.R. Churchill and R.A. Lashewycz, Inorg. Chem., 1980, 19, 1277.

26. J. Evans, B.P. Gracey, L.R. Gray, and M. Webster, J. Organomet. Chem., 1982, 240, C61.

27. B.F.G. Johnson, J. Lewis, J.N. Nicholls, J. Puga, P.R. Raithby, M.J. Rosales, M. McPartlin, and W. Clegg, J. Chem. Soc., Dalton Trans., 1983, 277.

28. J. Evans, B.P. Gracey, A.G. Jones, and M. Webster, Acta.Cryst., 1987, C43, 2286.

29. A. Sirigu, M. Bianchi, and E. Benedetti, J. Chem. Soc., Chem. Commun., 1969, 596.

30. J.A. Clucas, D.F. Foster, M.M. Harding, and A.K. Smith, J. Chem. Soc., Chem. Commun., 1984, 949.

31. J.A. Clucas, M.M. Harding, and A.K. Smith, J. Chem. Soc., Chem. Commun., 1985, 1280.

32. S.R. Hodge, B.F.G. Johnson, J. Lewis, and P.R. Raithby, J. Chem. Soc., Dalton Trans., 1987, 931.

33. A.J. Deeming, S. Donovan-Mtunzi, S.E. Kabir, J. Organomet. Chem., 1987, 333, 253.

34. A.J. Deeming, S. Donovan-Mtunzi, S.E. Kabir, K.I. Hardcastle, K. Henrick, M. McPartlin, J. Chem. Soc., Dalton Trans., 1988, 579.

35. B.F.G. Johnson, J. Lewis, P.R. Raithby, M.J. Rosales, and D.A. Welch, J. Chem. Soc., Dalton Trans., 1986, 453.

36. B.F.G. Johnson, J. Lewis, W.J.H. Nelson, J.N. Nicholls, J. Puga, P.R. Raithby, M.J. Rosales, M. Schröder, and M.D. Vargas, J. Chem. Soc., Dalton Trans., 1983, 2447.

37. P.F. Jackson, B.F.G. Johnson, J. Lewis, W.J.H Nelson, J.N. Nicholls, and M. McPartlin, J. Chem. Soc., Chem. Commun., 1980, 564.

38. S.S.D. Brown, I.D. Salter, and B.M. Smith, J. Chem. Soc., Chem. Commun., 1985, 1439; and ref. cited therein.

39. S.S.D. Brown, I.J. Colquhoun, W. McFarlane, M. Murray, I.D. Salter, and V. Šik, J. Chem. Soc., Chem. Commun., 1986, 53.

40. J. Pursiainen and T.A. Pakkanen, J. Organomet. Chem., 1986, 309, 187.

41. M.I. Bruce, M.L. Williams, J.M. Patrick, B.W. Skelton, and A.H. White, J. Chem. Soc., Dalton Trans., 1986, 2557.

42. L.J. Farrugia, M.J. Freeman, M. Green, A.G. Orpen, F.G.A. Stone, and I.D. Salter, J. Organomet. Chem., 1983, 249, 273.

43. L. W. Bateman, M. Green, K.A. Mead, F.G.A. Stone, R.M. Mills, I.D. Salter, and P. Woodward, J. Chem. Soc., Dalton Trans., 1983, 2599.

44. G.B. Ansell, M.A. Modrick, and J.S. Bradley, Acta Cryst., 1984, C40, 365.

45. J.A.K. Howard, I.D. Salter, and F.G.A. Stone, Polyhedron, 1984, 3, 567.

46. M.I. Bruce O. bin Shawkataly, and B.K. Nicholson, J. Organomet. Chem., 1985, 286, 427.

47. R.A. Brice, S.C. Pearse, I.D. Salter, and K. Henrick, J. Chem. Soc., Dalton Trans., 1986, 2181.

48. S.S.D. Brown, P.J. McCarthy, and I.D. Salter, J. Organomet. Chem., 1986, 306,C27.

49. M.J. Freeman, M. Green, A.G. Orpen, I.D. Salter, and F.G.A. Stone, J. Chem. Soc., Chem. Commun., 1983, 1332.

50. M.J. Freeman, A.G. Orpen and I.D. Salter, J. Chem. Soc., Dalton Trans., 1987, 379.

51. P.A. Bates, S.S.D. Brown, A.J. Dent, M.B. Hursthouse, G.F.M. Kitchen, A.G. Orpen, I.D. Salter, and V. Šik, J. Chem. Soc. Chem. Commun., 1986, 600.

52. S.S.D. Brown, I.D. Salter, and L. Toupet J. Chem. Soc. Dalton Trans., 1988, 757.

53. S.S.D. Brown, S. Hudson, I.D. Salter, and M. McPartlin J. Chem. Soc., Dalton Trans., 1987, 1967.

54. S.S.D. Brown and I.D. Salter, unpublished work.

55. A.G. Orpen, J. Chem. Soc., Dalton Trans., 1980, 2509.

56. P. Braunstein, G. Predieri, A. Tiripicchio, and E.Sappa, Inorg. Chim. Acta. 1982, 63, 113

57. M.J. Freeman, A.G. Orpen, and I.D. Salter, J. Chem. Soc., Dalton Trans., 1987, 1001.

58. M.I. Bruce and B.K. Nicholson, Organometallics, 1984, 3, 101.

59. D.G. Evans and D.M.P. Mingos, J. Organomet. Chem., 1982, 232, 171.

60. K.P. Hall and D.M.P. Mingos, Prog. Inorg. Chem., 1984, 32, 237.

CHAPTER 3

Structural studies of homonuclear hydrido cluster compounds of ruthenium and osmium.

Section 3.1. Introduction.

Characterisation of hydrido ligands in transition metal clusters using X-ray diffraction methods has proved to be a difficult problem for crystallographers. This is attributed to the small X-ray scattering ability of H atoms being 'swamped' by transition metals of higher electron density to which they are bonded.[1] Since the scattering of X-rays is roughly proportional in amplitude to the number of electrons in an atom, this problem becomes more severe as surrounding transition metal atoms become heavier and as the number of metals bonded to the H-atom increases.[1] Various qualitative techniques have been used to predict hydride positions in cluster compounds, involving criteria such as M-M bond lengths,[2] electron counting,[3] ligand orientation[4,5] and analysis of ligand polyhedron.[6-8] From the vast number of transition metal hydrido compounds structurally characterised in the solid state, it has been recognised that hydrogen ligands occupy distinct co-ordination sites on the metal atoms, and have finite steric requirements.[9-11] The following sections are intended to describe some of the early work carried out by crystallographers in trying to deduce positions of hydrido ligands from X-ray data, using both indirect and direct methods and have paved the way for well established 'tools' which are now frequently used in locating the ligand in transition metal clusters.

Indirect location of H-atoms using X-ray data.

Difficulties in determining H atom positions in mononuclear compounds were first encountered with the X-ray diffraction studies of the hydrido complexes, trans-$[PtHBr(PEt_3)_2]$ and $[MnH(CO)_5]$.[12,13] Gaps or 'holes' in the co-ordination sphere around the metal atoms were interpreted to be a result of the steric influences of the missing H atom. For example, in the platinum hydride complex, $[PtHBr(PEt_3)_2]$, Owston and co-workers observed that the bromine and phosphorus atoms were found to be coplanar with the platinum atom, giving P-Pt-Br angles of 94.0°. This ruled out a possibility of a trigonal pyramidal co-ordination around the platinum atom. The bond lengths and angles dictated that the four atoms, one bromine, two phosphorus, and one hydrogen bound to the platinum atom formed a trans-square planar configuration, {Figure 3.1(a)}.[12]

Location of H atoms in cluster compounds using indirect methods was first reported by Churchill and co-workers, with the X-ray structure analysis of the trinuclear cluster monoanion $[Re_3(\mu\text{-}H)_2(CO)_{12}]^-$, {Figure 3.1(b)}.[14] They observed that two of the three Re-Re bonds {3.173(1) and 3.181(1) Å} were significantly longer than the third {3.035(1) Å}. The axial carbonyls at each Re atom were more or less regularly arranged, with the equatorial Re-Re-CO angles involving the short side of the triangle, {Re(2)-Re(3)-CO(5) and Re(3)-Re(2)-CO(4)} being 91.0 and 95.0° respectively. In contrast, the corresponding equatorial angles at the two longer bonds, Re(2)-Re(1)-CO(2) and Re(3)-Re(1)-CO(1), were found to be significantly larger, {106.0 and 107.0° respectively}, with the angles, Re(1)-Re(2)-CO(3) and Re(1)-Re(3)-CO(6) of 112.0 and 118.0°, respectively, being the largest of all the cis-angles. Thus, the equatorial carbonyl groups at the bonds Re(1)-Re(2) and Re(1)-Re(3) were observed to be "pushed" back away from Re(1), leading to the conclusion that the H-atoms were situated nearer the Re(1)-Re(2) and Re(1)-Re(3) edges of the three atom triangle.[14]

In 1971 Churchill and Wormald reported the crystal structure of the hexa-ruthenium di-hydrido cluster $[Ru_6(\mu_3\text{-}H)_2(CO)_{18}]$, {Figure

3.1.(c)}.[15] The X-ray structural data was used to establish the first crystallographic evidence for two triply bridging H-ligands. The molecule was found to crystallise in the space group $P2_1/c$ and the asymmetric unit was found to consist of two half molecules of $[Ru_6(\mu_3\text{-}H)_2(CO)_{18}]$, rather than one entire molecule. Therefore, there were two unrelated sets of the molecules within the unit cell, one set centred on a special position at $^1/_2,0,0;^1/_2,^1/_2,^1/_2$ and the other centred at a special position $0,0,^1/_2;0,^1/_2,0$. The workers observed that in both crystallographically independent clusters, two opposite triangular faces of the Ru_6 octahedron were markedly enlarged, with Ru-Ru distances of these faces ranging from 2.950-2.959(3) Å, averaging 2.954(3) Å, whilst the remaining M-M distances varied from 2.858-2.874(3) Å, averaging 2.867(3) Å, {Figure 3.1(d)}.

Dispositioning of carbonyl ligands around the Ru_6 cluster in both molecules also showed systematic irregularities, with ligands being distorted away from the enlarged equatorial faces. For example, the carbonyl ligands CO(1) and CO(3) attached to Ru(1) {molecule 1, Figure 3.1(c)}, were found not to be axial to the enlarged 'open' face Ru(1)-Ru(2)-Ru(3) {OC(1)-Ru(1-Ru(2) 132.0° and OC(3)-Ru(1)-Ru(3) 130.2°}. The carbonyl, CO(1) was in fact found to be nearly axial to the face Ru(1)-Ru(2')-Ru(3) giving the angles OC(1)-Ru(1)-Ru(3) = 88.6° and OC(1)-Ru(1)-Ru(2') = 104.6°, whereas CO(3) was found to be approximately axial to the face Ru(1)-Ru(2)-Ru(3') giving the angles, OC(3)-Ru(1)-Ru(2) = 88.2° and OC-Ru(1)-Ru(3') = 105.7°. Similarly the angles OC(2)-Ru(1)-Ru(2') and OC(2)-Ru(1)-Ru(3') {77.8 and 78.3° respectively} showed that CO(2) was 'leaning' over the face Ru(1)-Ru(2')-Ru(3'). Similar dispositioning of carbonyl ligands were also observed at Ru(2) and Ru(3).[15] The workers concluded that there were three carbonyl groups in an axial conformation relative to each of the six small triangular faces of the Ru_6 octahedron in both molecules, whilst no carbonyl ligands were in a truly axial position relative to the two enlarged faces, Ru(1)-Ru(2)-Ru(3) and Ru(1')-Ru(2')-Ru(3') in molecule 1; Ru(11)-Ru(12)-Ru(13) and Ru(11')-Ru(12')-Ru(13') in molecule 2. From these observations, the two hydrido-ligands were thought to triply bridge the two enlarged faces in both molecules of the asymmetric unit.

The effects of bridging hydrido ligands on metal cluster geometry was further assessed by Churchill and co-workers, with the X-ray structure of $[Os_3W(\mu\text{-}H)(CO)_{12}(\eta^5\text{-}C_5H_5)]$.[16] The molecule adopted a tetrahedral metal core, with the tungsten atom co-ordinated to the cyclo-pentadiene ring and two terminal -CO ligands, whereas each Os atom carried three terminal carbonyl groups, with a bridging carbonyl 'spanning' the Os-W vector {Figure 3.1(e)}. The workers observed that the three Os-Os distances showed marked asymmetry, with Os(2)-Os(3) {2.932(2) Å} being significantly longer than the remaining two bonds, {Os(1)-Os(2) 2.784(2) and Os(1)-Os(3) 2.799(2) Å}. The bond length considerations led to the conclusion, that the hydride occupied a μ_2-site about the Os(2)-Os(3) vector. They postulated three symmetrical orientations of the ligand about this vector:

(a) the hydride ligand was thought to lie in, or close to, the Os(1)-Os(2)-Os(3) plane,

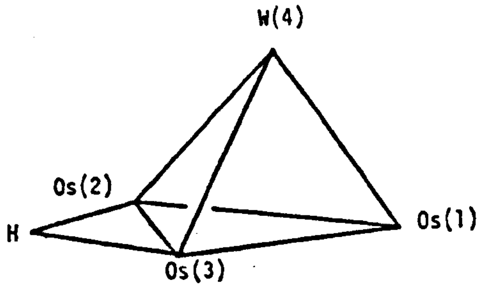

(b) the ligand was thought to lie in, or close to, the Os(2)-Os(3)-W(4) plane,

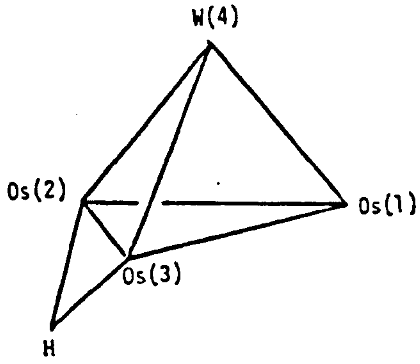

(c) the hydride was thought to occupy a site intermediate between (a) and (b), such that the Os(2)-H-Os(3) plane acted as an external bisector of the Os(1)-Os(2)-Os(3) and Os(2)-Os(3)-W(4) planes,

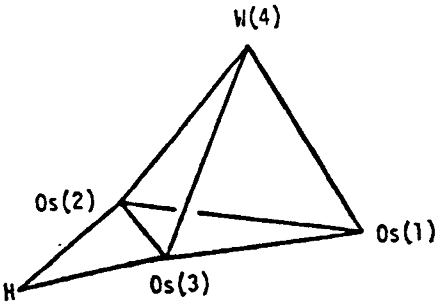

The workers distinguished between these three possibilities by using the established principle:[14,15]

Abnormally large M-M-L angles should be observed for ligand (L) adjacent to, and in the same plane as a simple unsupported (μ_2-H)-M system.

This was found to be consistent with the equatorial carbonyl groups adjacent to the bond Os(2)-Os(3) {Os(3)-Os(2)-C(21) 113.6(12), and Os(2)-Os(3)-C(31) 113.1°} 'splayed' out in relation to the other equatorial carbonyl groups at the two unbridged Os-Os bonds {mean equatorial OC-Os-Os 93.2(12)°}. These results supported that the H-ligand was lying in, or close to, the Os(1)-Os(2)-Os(3) plane.

The dispositioning of carbonyl groups adjacent to hydride bridged M-M bonds was found to be an important criterion in the indirect approach of locating H-atom sites, especially when a μ_2-hydrido ligand was accompained by another μ_2- bridging ligand about the same vector.

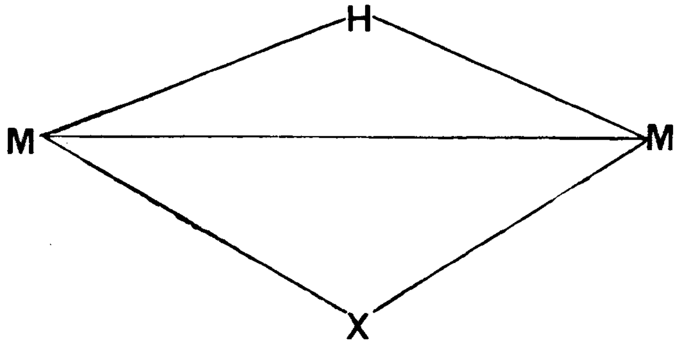

For example, in the tri-osmium cluster $[Os_3(\mu-H)(u-Cl)(CO)_{10}]$, {Figure 3.1(f)}, Churchill and Lashewycz observed that the characteristic lengthening of Os-Os bonds bridged by hydrido ligands was not apparent in the three Os-Os distances of the triangular metal framework.[17] The longest bond, Os(1)-Os(3) {2.846(1) Å} was found to be 0.014(1) Å longer than the mean of the two shorter bonds, {Os(1)-Os(2) 2.829(1) and Os(2)-Os(3) 2.836(1) Å}. The chlorine atom was found to bridge the slightly longer bond Os(1)-Os(3). The equatorial carbonyl ligands, CO(11) and CO(31), adjacent to this bond were markedly "pushed" back, {Os(3)-Os(1)-C(11) 118.6(4) and

Os(1)-Os(3)-C(31) 117.8(4)°}, in relation to the remaining equatorial -CO groups at the other two Os-Os bonds {mean equatorial Os-Os-CO 99.3(4)°}. Since the H-ligand was not located directly from the X-ray analysis, they concluded that the observed dispositioning of the respective carbonyl groups at Os(1)-Os(3), was supportive evidence of a μ_2-H site at this bond.

These early reports of the characteristic effects of hydrido ligands on metal geometries formed a basis from which potential sites of surface hydrido ligands were subsequently deduced indirectly in many transition metal clusters of varying nuclearities in the period 1975-1980.[18-21] The reliability of such qualitative indirect methods was well illustrated with the X-ray structural data of the $[PPN]^+$ salt of $[Ru_6H(CO)_{18}]^-$ characterised by McPartlin and co-workers.[22]

In contrast to the analogous osmium monohydride[23] $[Os_6H(CO)_{18}]^-$, {Figure 3.1(g)}, where the μ_3-H site was deduced by the 'pushing' back of neighbouring -CO ligands together with lengthening of respective Os-Os bonds, in $[Ru_6H(CO)_{18}]^-$, no bond lengthening or "pushing" back of -CO ligands was observed. It was also noted that the carbonyl distribution in the ruthenium monoanion was almost identical to that of the dianion[23] $[Os_6(CO)_{18}]^{2-}$ (Figures 3.1(h) and 3.1(i), respectively), with none of the dispositioning of carbonyl ligands that would be associated with the presence of surface H-ligands. From these observations the workers concluded that the hexanuclear monoanion $[Ru_6H(CO)_{18}]^-$ was the first example of an interstitial H atom in a metal carbonyl cluster.[22] Subsequent neutron diffraction study of the $[Ph_4As]^+$ salt established that the H-atom was indeed sited in the centre of the Ru_6 octahedral cage.[24] It has been recognised that as cluster size increases, the ratio of surface area to the number of metal atoms decreases, and as a result interstitial ligands become important in preventing surface ligand overcrowding. The distribution of carbonyl ligands on the metal polyhedra, was an invalueable tool again used by McPartlin and co-workers in establishing an interstitial tetrahedral site for the hydrido ligand in the deca-osmium carbido cluster $[HOs_{10}C(CO)_{24}]^-$, {Figure 3.1(j)}.[25] The carbonyl distribution was found to closely resemble that previously established for the dianion[26] $[Os_{10}C(CO)_{24}]^{2-}$, {Figure 3.1(k)}, with these surface ligands remaining almost perpendicular to the faces of the metal core. ^1H n.m.r. studies of the $[PPN]^+$ salt revealed that the H-ligand in $[HOs_{10}C(CO)_{24}]^-$ was directly bonded to the metal core, and since it could not be accommodated on the cluster surface, it was concluded that the ligand was interstitial. This was supported by a slight expansion of one of the four tetrahedral caps by 0.018 Å.

Similar strategies were used by these workers in deducing interstitial sites for all four hydrido ligands in the deca-osmium dianion[27] $[H_4Os_{10}(CO)_{24}]^{2-}$. The carbonyl distribution in the tetra-hydrido dianion was again found to be very similar to that established in the carbido dianion[26] $[Os_{10}C(CO)_{24}]^{2-}$, {Figures 3.1(l) and 3.1.(m), respectively}. Although the n.m.r. data for the H_4Os_{10} cluster was more consistent with the presence of surface H-ligands in solution, the solid state geometry showed that the individual means of six Os-Os bonds of three of the four tetrahedral caps {2.839, 2.839, 2.829 Å} were significantly longer than the mean of the fourth cap {2.809 Å}.[27] More importantly the mean values of the three enlarged Os_4 caps were found to be markedly longer than the mean of the two tetrahedral caps in the octanuclear dianion $[Os_8(CO)_{22}]^{2-}$ {2.793(1) Å},[28] the largest non-carbido cluster previously reported. It was also observed that the central Os_6 cavity in the tetra-hydrido dianion $[H_4Os_{10}(CO)_{24}]^{2-}$ had enlarged significantly, with a mean octahedral Os-Os distance of 2.857(1) Å, being longer than the corresponding value for the Os_6 cavity in the octanuclear cluster $[Os_8(CO)_{22}]^{2-}$ {2.831(1) Å}. From these results McPartlin and co-workers concluded that three of the four H ligands were sited in the three enlarged tetrahedral caps and the fourth in the expanded Os_6 octahedral cage.[27]

From the few examples described in this section, it is clear that qualitative methods which involve criteria such as M-M bond distances and surface ligand distribution in accommodating H-atoms, have generally proved to be useful techniques in locating potential hydrido ligand sites in transition metal clusters.

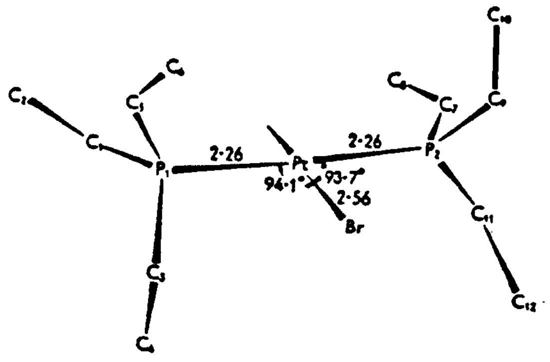

Figure 3.1(a).[12]

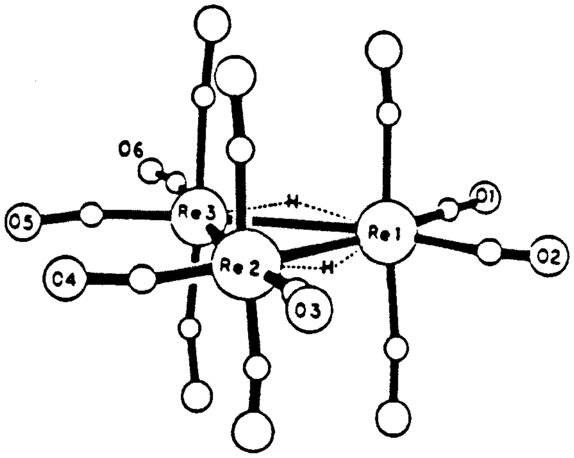

Figure 3.1(b).[14]

Molecular structures of

$[PtHBr(PEt_3)_2]$ $[Re_3(\mu\text{-}H)_2(CO)_{12}]^-$.

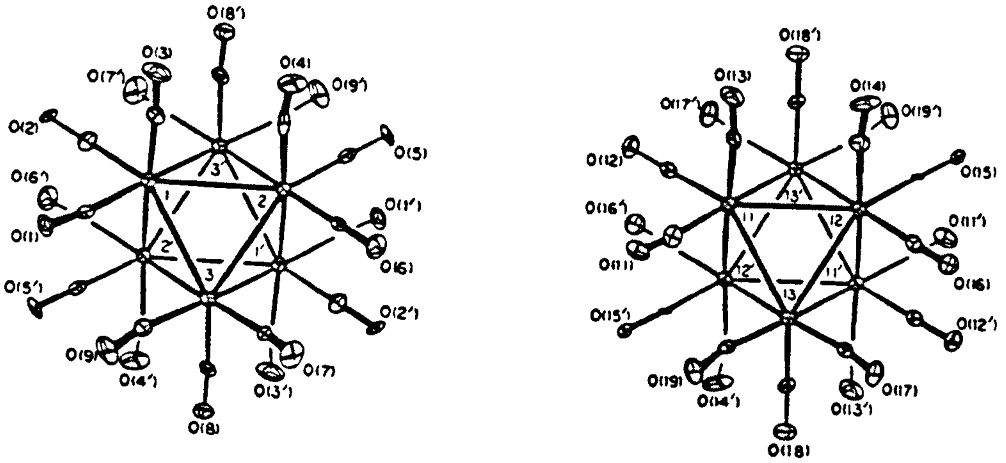

Figure 3.1(c). Two independent molecules of the hexa-ruthenium cluster $[Ru_6(\mu_3\text{-}H)_2(CO)_{18}]$.[15]

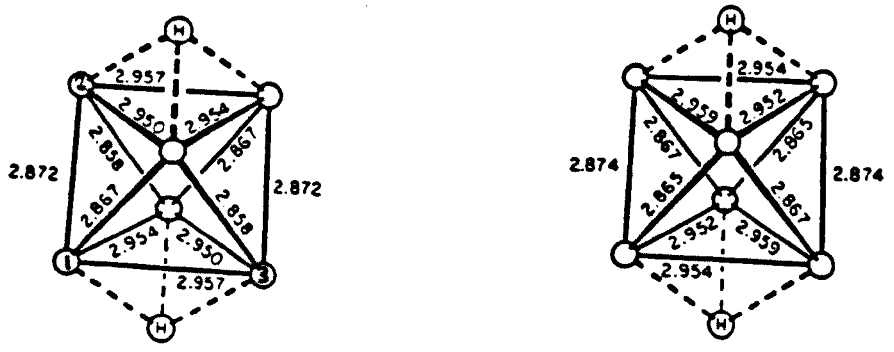

Figure 3.1(d). The geometry defining the octahedral metal core in the two independent molecules of $[Ru_6(\mu_3\text{-}H)_2(CO)_{18}]$.[15]

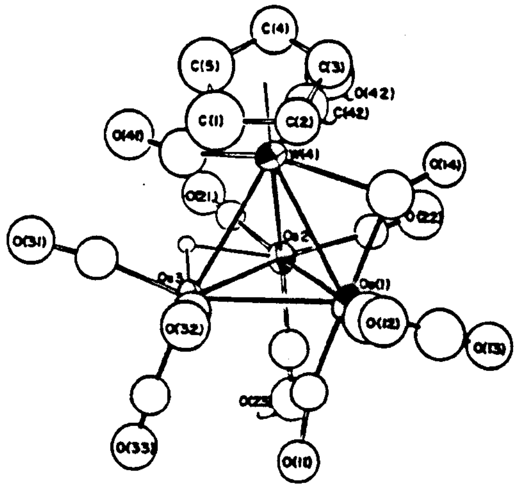

Figure 3.1(e). Molecular structure of $[\mathrm{OsW}(\mu\text{-H})(\mathrm{CO})_{12}(\eta^5\text{-C}_5\mathrm{H}_5)]$.[16]

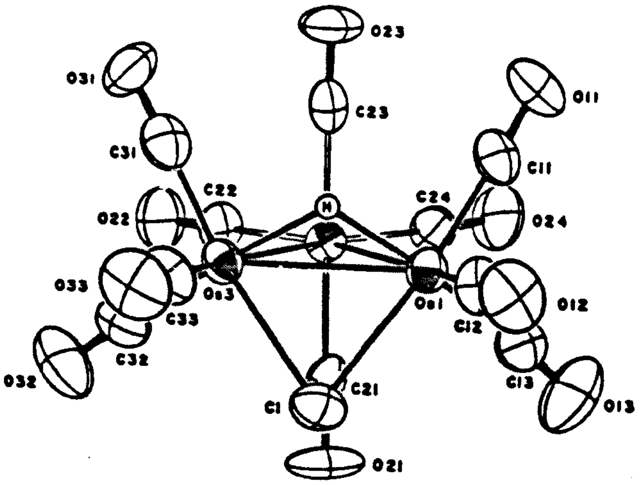

Figure 3.1(f). Molecular structure of $[\mathrm{Os}_3(\mu\text{-H})(\mu\text{-Cl})(\mathrm{CO})_{10}]$.[17]

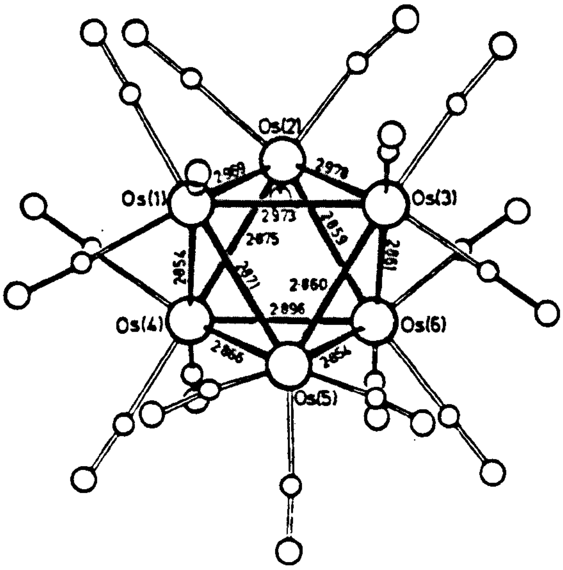

Figure 3.1(g). Molecular structure of the osmium monohydride $[Os_6H(CO)_{18}]^-$.[23]

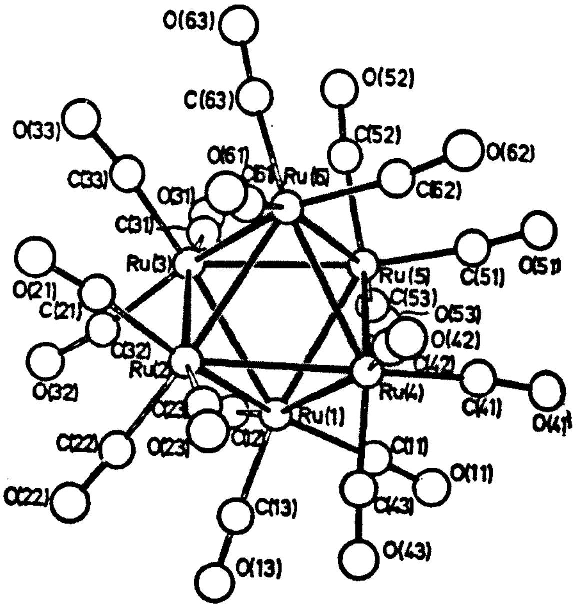

Figure 3.1(h). Molecular structure of the hexa-ruthenium monoanion $[Ru_6H(CO)_{18}]^-$.[22]

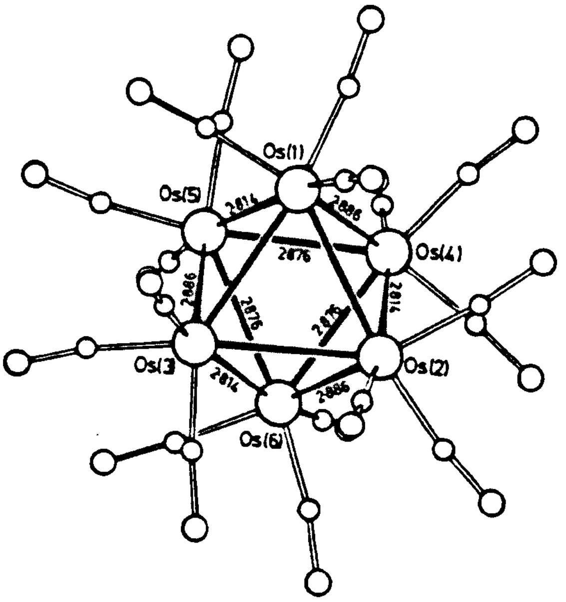

Figure 3.1(i). Molecular structure of the hexa-osmium dianion $[Os_6(CO)_{18}]^{2-}$.[23]

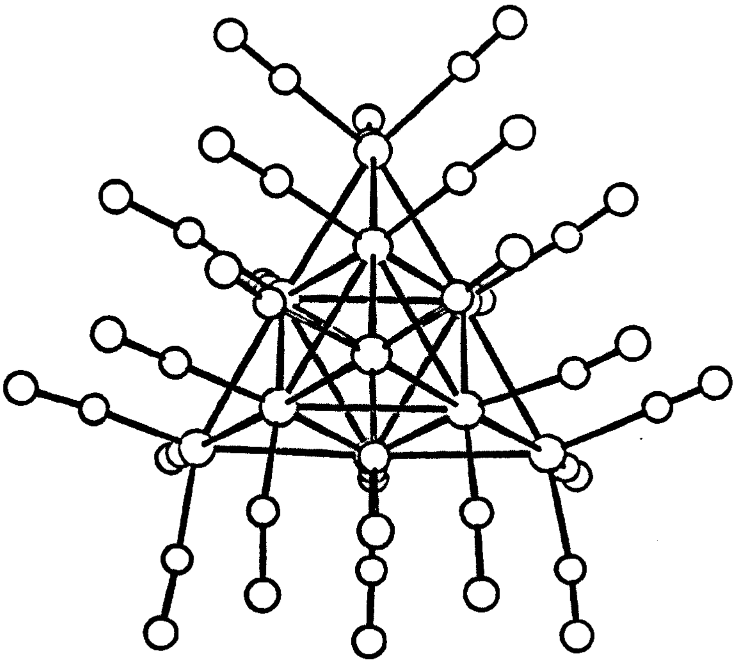

Figure 3.1(j). Molecular structure of the deca-osmium monohydride $[HOs_{10}C(CO)_{24}]^-$.[25]

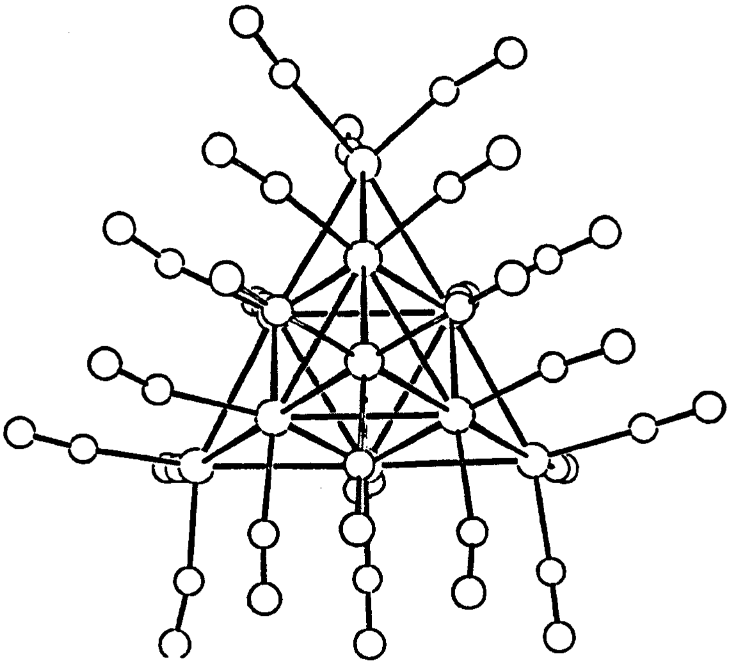

Figure 3.1(k). Molecular structure of the deca-osmium dianion $[Os_{10}C(CO)_{24}]^{2-}$.[26]

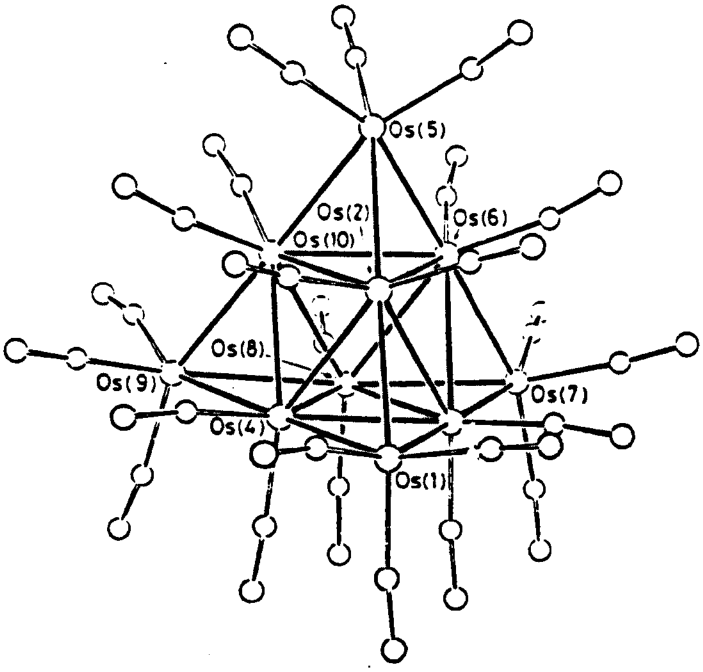

Figure 3.1(l). Carbonyl distribution in the structure of the tetra-hydrido dianion $[H_4Os_{10}(CO)_{24}]^{2-}$.[27]

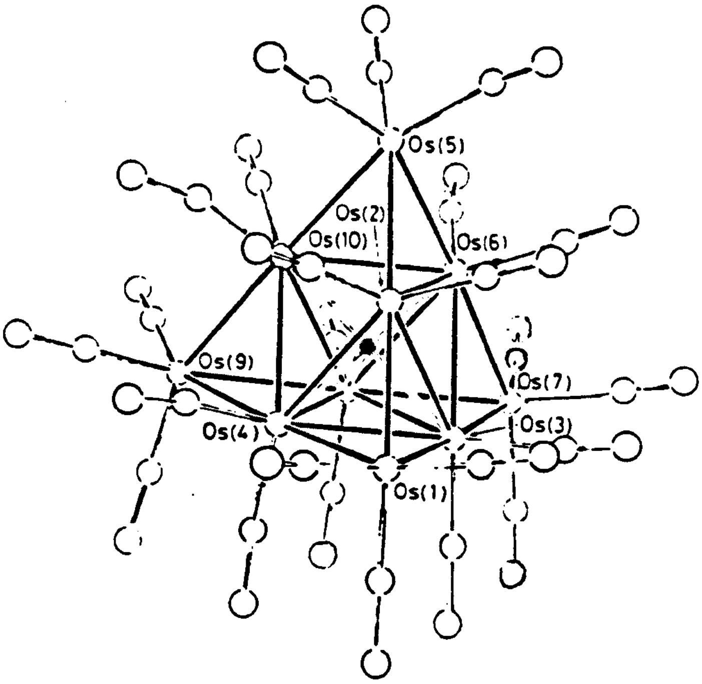

Figure 3.1(m). Carbonyl distribution in the structure of the non-hydrido deca-osmium dianion $[Os_{10}C(CO)_{24}]^{2-}$.[26]

Section 3.1.1. Direct methods of locating H atoms from X-ray data.

It is more common these days to find H atom positions directly from X-ray data, especially for hydride ligands bonded to first row transition metals as opposed to the heavier transition metals. The first location of a hydrido ligand from X-ray data was reported in 1963 by La Placa and Ibers.[29] In this classic study, they suggested that since the X-ray scattering ability from hydrogen is largely confined to low angle data, it was possible to enhance hydrogen peaks in difference-Fourier maps by removing the high angle reflections in the calculation of structure factors. Using this approach a Rh-H distance of 1.72(15) Å was determined in the complex $[RhH(CO)(PPh_3)_3]$.

In 1973 Bau and co-workers reported the first example of directly locating hydrido ligands in a metal cluster, with the X-ray analysis of $[Mn_3(\mu\text{-}H)_3(CO)_{12}]$.[6] In this compound, the H atoms were suspected to lie in bridging positions in the equatorial plane. A difference-Fourier map showed promising peaks at likely positions for the H-ligands, but were masked by a large number of background peaks. A second difference-Fourier map using low angle reflections in approximately two-thirds of the data (1102 reflections; $\sin\Theta/\lambda = 0.43$ $Å^{-1}$) gave an improved map with some background peaks still remaining. Finally, a difference-Fourier map was calculated using one-thrid of the data (553 reflections; $\sin\Theta/\lambda = 0.33$ $Å^{-1}$) which clearly revealed the hydrogen atom positions. Thus, it was confirmed that the hydrogen atoms were sited in the equatorial Mn_3 plane in positions that bridged pairs of atoms, with an average Mn-H bond length of 1.711(11) Å, {Figure 3.1.1(a)}.

The use of low angle data preferentially to enhance hydrogen positions in difference-Fourier maps was also used by Bau and co-workers for the location of a u_2-H site in the trinuclear cluster $[Fe_3(\mu-H)(CO)_9(SR)]$ [R = i-C_3H_7 and t-C_4H_9].[30] Low angle data was collected (708 reflections) and each reflection was scanned twice. The data was used to calculate a series of difference-Fourier maps with decreasing ($\sin\theta/\lambda$) limits {0.33, 0.25, 0.17 $\mathring{A}^{-1}$}. They were able to locate the presence of a bridging hydrogen below the basal plane of the three iron atoms, Figure {3.1.1(b)}.

In 1976 Bau and Wilson also reported that the method of "Fourier-averaging" was practical in locating face-bridging H atoms in $[Re_4(H)_4(CO)_{12}]$.[31] They found that Fourier maps with high angle data being omitted as desribed above, gave electron density maps with ambiguous sites for the hydrido ligands. The problem of detecting one electron (from the hydrogen) in the presence of 225 electrons (from three Re atoms) was much more unfavourable. However, they were able to rationalise that if a molecule has several hydrogens and is of high symmetry, it was possible to use information from several different sections of the electron density map and bring them together to form a usable composite. Accordingly they calculated difference-Fourier maps corresponding to the six non-crystallographic mirror planes of the Re_4 tetrahedron and superimposed them. The resulting composite gave well resolved peaks for face-bridging positions and with no electron density at alternative edge-bridging or terminal positions. Such an approach was found to be limited, since it was only applicable to molecules of high internal symmetry.

Although the direct location of H-atoms from X-ray data was often possible, results were unpredictable and were based on sufficient low angle data. From the early reports in the literature Bau concluded that R values did not necessarily guarantee successful location of H atom sites, and conversely structures with less satisfactory R values, sometimes produced acceptable H positions.[10] Further problems of certifying positions of hydrido ligands became apparent when the H co-ordinates were found not to converge during least squares refinement, and in cases where they did, there was no guarantee that the refined positional parameters were better than the peak position obtained from Fourier-maps.[32-37] Consequently, neutron diffraction, though requiring larger crystals and access to suitable neutron source, was the preferred method for accurate location of H-atom positions in cluster compounds.[38] Since neutrons unlike X-rays are diffracted by most elements with similar efficiencies, hydrido ligands are not masked by adjacent heavy metal atoms and can therefore be easily located. Thus, neutron diffraction was found to offer advantages over X-ray diffraction. Various reports of combined X-ray and neutron diffraction studies showed that since neutron diffraction locates true nuclear positions, whereas X-ray diffraction methods measure electron density, M-H bond lengths determined by the former technique were often significantly shorter than those measured by the latter.[39]

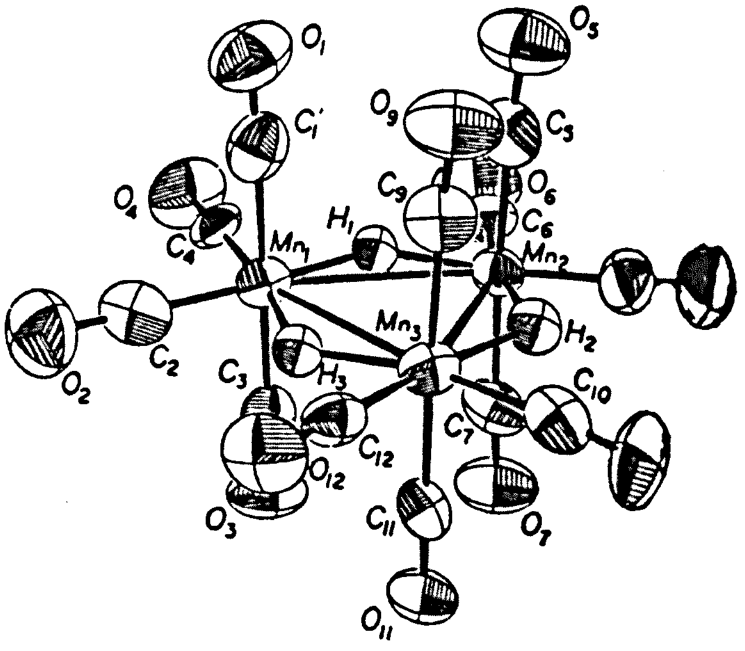

Figure 3.1.1(a). Molecular structure of $[Mn_3(\mu\text{-}H)_3(CO)_{12}]$.[6]

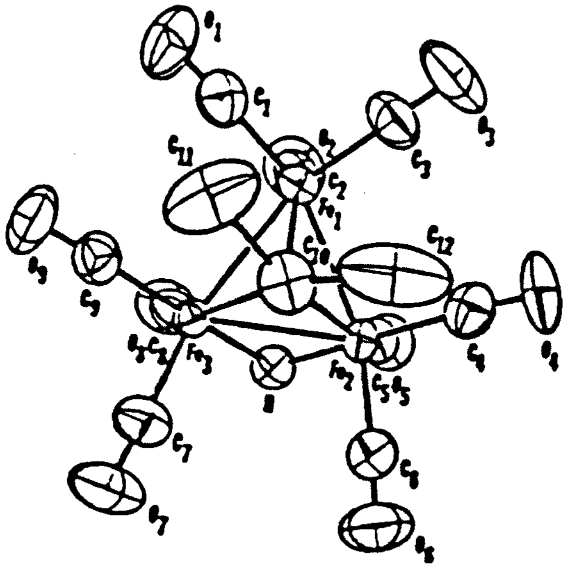

Figure 3.1.1(b). Molecular structure of $[Fe_3(\mu\text{-}H)(CO)_9(SR)]$ $[R = i\text{-}C_3H_7$ or $t\text{-}C_4H_9]$.[30]

Section 3.1.2. Other quantitative methods for estimating H-positions in cluster compounds.

There have been several reports of calculating potential hydrido positions based on consideration of intramolecular steric interactions between non-bonding atoms, with known geometry of a molecule.[40-43] In 1980 Orpen reported a quantitative procedure for indirectly locating hydride ligands bound to transition metals in cluster compounds, and compared the results to those established from neutron diffraction studies.[44] A computer program now widely used by crystallographers, was written which calculated a most likely site for a hydride ligand in a cluster. The technique was based on the following information:

(i) Atomic positions of all the non-hydrogen atoms within the molecule established from the X-ray study.

(ii) Parameters specifying the non-bonded interactions between hydride(s) and all other atoms within the cluster.

(iii) Hydride site to be examined (terminal, μ_2, μ_3) and the atoms to which the hydride was thought to be bonded to.

(iv) M-H bond lengths appropriate to these sites.

Using the above data, the program calculated the potential energy, V(r), over all the intramolecular non-bonded contacts involving the hydride(s) in question, using the expression:

$$V(r) = \frac{a \exp(-br)}{r^d} - \frac{-c}{r^6}$$

V(r) - in Kcal mol^{-1},

r - the interatomic separation involved (Å),

a,b,c,d - parameters dependant upon the atomic type of the second atom in the H...X contact. Using the following parameters for a metal atom,

a	b	c	d
43500	3.54	540	0.00

the program first estimated 26 initial hydride positions generated in a 3 x 3 x 3 grid around the atom or atoms to which the H-ligand was thought to be bonded. These positions were subsequently refined by a minimisation function M:

$$M = \sum_{i} V(ri) + \sum_{k} |(Rk-R)/S|^{2}$$

Rk - interatomic distances of the kth atom

Rs - specified M-H distance (usually 1.85 Å)

S- allowed error (usually 0.05 Å).

The first summation was directed over all the atoms within an approximate radius of 3.5 Å, which had to be specified not to be bonded to the H-ligand(s). The latter summation involved all the atoms to which the hydride was bonded.

The calculated minima in the P.E. was rejected if the M-H bond length was too far from that specified or if the calculations gave unrealistically short non-bonded contacts. The acceptable minima were grouped into sets and were further optimised, with the corresponding P.E. of each site determined. The following average site energies were reported by Orpen:[44]

site	energy/Kcal mol^{-1}
terminal	4.8
edge-bridging $(-\mu_2)$	2.76
face-capping $(-\mu_3)$	0.37

This method was found to be useful in cluster compounds where hydrogen atom positions inferred from the lengthening of M-M bonds and "pushing" back of adjacent carbonyl groups were disputeable. For example, in the capped square pyramidal hexanuclear cluster[23] $[Os_6(H)_2(CO)_{18}]$, several hydride sites including a variety of face bridging, edge bridging and terminal sites were tested. The results gave suitable minima in P.E. for the two hydrido ligands to bridge opposite edges of the square base, {Figure 3.1.2(a)}. There were found to be limitations of this indirect method, firstly the program failed to give reasonable minima in P.E. if the hydrides were bonded asymmetrically and secondly if the ligand was assumed to be interstitial.

Another technique used to investigate surface sites of H-ligands was based upon the characteristic 'pushing back' of adjacent equatorial carbonyl groups in accommodation of the H-ligand, (section 3.1).[14-21] The method involved computer graphics which generated a computer simulated 'space-filling' models of a cluster molecule using the program of Keller.[45] The computed model of the molecule was obtained directly from the atomic co-ordinates established from the X-ray analysis, and each atom was drawn as spheres of radii corresponding equally to their respective Van der Walls values {for example, Os 2.35, Ru 2.35, Fe 2.15, C 1.60, O 1.40, H 1.20 Å}. The relatively large size of the metal atom Van der Walls spheres, was found to obscure the surface ligands and cause difficulty in deducing the surface ligand contacts. Modifications of the model involving the assignment of covalent radii to the metal core atoms (1.45 Å), allowed a clear view of the ligand contacts. In cases of suspected $-\mu_2$ or $-\mu_3$ H sites occupied on the surface of a metal cluster, adjacent carbonyl groups were found to be pushed back to reveal a clear 'gap' in the carbonyl coverage, through which the respective metal atoms bonded were readily seen.

This application was found to successfully predict hydrido sites in cluster compounds where other indirect methods had failed. For example, in the neutral iodo-derivative[46] $[HOs_8(CO)_{22}I]$, a μ_2-H site was expected since indirect methods had previously assigned a μ_2-H site in the analogous monoanion[47] $[HOs_8(CO)_{22}]^-$. However no evidence supporting this site was obtained from either the bond lengths or potential energy calculations. A space-filling model[48] of the neutral cluster $[HOs_8(CO)_{22}I]$ showed one gap in the carbonyl surface distribution, through which the 'bonding' spheres of three Os atoms were visible. The areas of the three Os atoms were found to be unequal indicating that the hydrido ligand was unsymmetrically bridging the three osmium atoms. A recent review by Henrick, McPartlin and Morris discusses the use of this facility in more detail.[48]

The characteristic lengthening of M-M bonds, together with the presence of large M-M-C angles associated with carbonyl ligands cis to bridged M-M bonds, have been important structural features in deducing hydrido ligand positions indirectly from the X-ray data of homonuclear ruthenium and osmium hydrido clusters presented in the following sections. In particular, the carbonyl distribution on the surface of the high nuclearity clusters $[H_5Os_{10}(CO)_{24}]^-$ and $[HOs_{11}C(CO)_{27}]^-$, together with an observed pattern in the Os-Os bond lengths in their respective geometries, have been consistent with the hydrido ligands occupying interstitial sites. These results compared to those previously established for related clusters, have further supported the tendency for the hydrogen atom to become encapsulated within the metal frameworks of high nuclearity cluster compounds in the solid state.

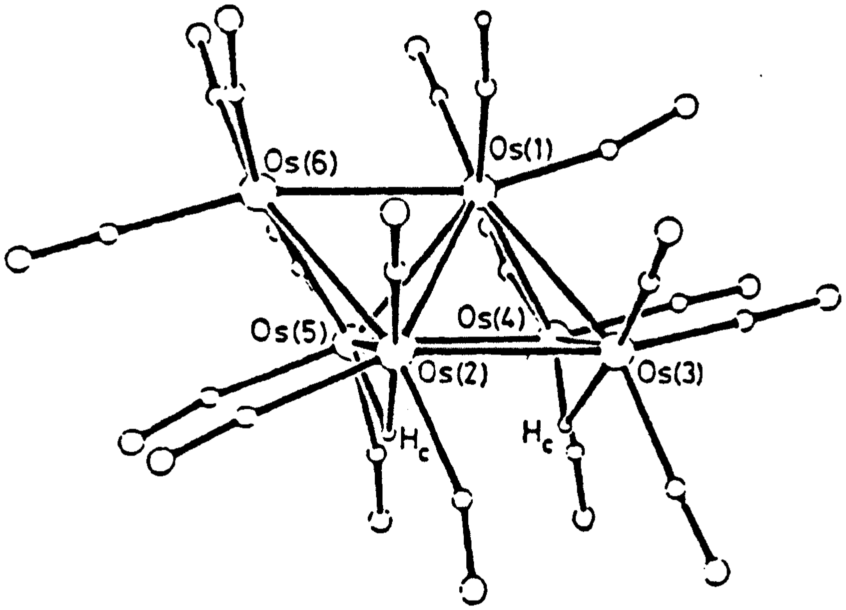

Figure 3.1.2. Molecular structure of the neutral di-hydrido osmium cluster $[Os_6H_2(CO)_{18}]$.[23]

Section 3.2. X-ray structural analyses of two tri-osmium isomers $[Os_3H_2(CCHOEt)(CO)_9]$ (1) and $[Os_3H_2(HCCOEt)(CO)_9]$ (2).

Crystal data, methods of data collection, structure solution and refinement, for both (1) and (2) are presented in section 4.8.

Tables of atomic co-ordinates, bond lengths, inter-bond angles, intermolecular and intramolecular distances are given in the appendix (Vol.2).

3.2.1 Introduction.

For related neutral trinuclear clusters of the iron triad, nucleophilic attack by suitable reagents has been reported to occur at different electrophilic centres in the molecule.[49-52] For example, (a) the reaction between the tri-osmium cluster $[Os_3(CO)_{13}]$ and a primary amine, RNH_2, established the addition of the anion, RNH^-, to occur at the carbon of the bridging carbonyl group to yield the complex $[Os_3H(CO)_{10}(RNCHO)]$.[53,54]

(b) Reactions of $[Os_3H_2(CO)_{10}]$ with anions, such as halides displayed direct nucleophilic attack at the metal atoms.[55-57]

(c) Addition of the nucleophile, PMe_2Ph, to the tri-osmium complex $[Os_3H(CO)_{10}(CH{=}CH_2)]$ was found to yield the adduct $[Os_3H(CO)_{10}(HCCH_2PMe_2Ph)]$, describing the common attack at the unsaturated electrophilic centre of the hydrocarbon.[58-60]

Doubly and triply bridging $C{\equiv}CR$ ligands are also known to be susceptible to nucleophilic attack at either the α or β-carbon sites.[61-64] For example, the μ_2-η^2-alkynyl ligand in the complex $[Fe_2(C{\equiv}CPh)(PPh_2)(CO)_6]$ was observed to react with nucleophiles such as phosphines, phosphites, isonitriles and carbenes forming adducts derived from the attack at the α-carbon of the acitylide ligand.[65,66] The same compound was also found to react with secondary amines with the nucleophilic attack at the β-carbon.[67] Addition of the nucleophile, PMe_2Ph, to the tri-osmium cluster $[Os_3H(\mu\text{-}C{\equiv}CR)(CO)_{10}]$ occured at the β-carbon to give the complex, $[Os_3H(\mu\text{-}C{=}CRPMe_2Ph)(CO)_{10}]$,[54] whereas the same phosphine was found to add to the α-carbon of the alkyne group in $[Os_3H(\mu_3\text{-}C{\equiv}CR)(CO)_9]$ to form the adduct $[Os_3H(\mu_3\text{-}RC{=}CPMe_2Ph)(CO)_9]$ [R = H or Me].[68] Another recent report of an intramolecular nucleophilic attack at the α-carbon of a transient μ_3-alkynyl group in the trinuclear osmium compound $[Os_3(HC_2CH_2CH_2OH)(CO)_{10}]$, involved thermal decarboxylation to yield $[Os_3H_2(\mu_3\text{-}C{=}CCH_2CH_2O)(CO)_9]$.[69] The few examples described above clearly illustrate the selectivity of nucleophilic reagents when adding to trinuclear clusters containing a μ_3-alkyne group.

The reaction involving the tri-osmium cluster $[Os_3H(C{\equiv}CH)(CO)_9]$ with ethanol at room temperature gave two isomeric compounds, {scheme 3.2.1}. The major product (73% yield) was formulated spectroscopically as $[Os_3H_2(CCHOEt)(CO)_9]$, which resulted from the nucleophilic attack of the OEt^- at the β-carbon. The minor product (9% yield) was formulated as $[Os_3H_2(HCCOEt)(CO)_9]$ resulting from the attack of the anion at the α-carbon.[70] In both proposed structures the proton from the ethanol was thought to add to the metal framework. X-ray studies of the two isomers were therefore carried out to establish the bonding mode of the organo ligand in their respective solid state structures.

3.2.2 Structural description of the minor isomer {yield 9%} (1) and the major isomer {yield 73%} (2).

The X-ray structural study of isomers (1) and (2) established that both molecules adopted similar triangular metal geometries, {Figures 3.2.2(a) and 3.2.2(b), respectively}. The nine carbonyl groups in both structures were found to be distributed in two equatorial and one axial site at each of the three Os atoms. The characteristic difference in the solid state structures of (1) and (2) was the attachment of the ethoxy vinyl hydrocarbon ligand. The ligand in isomer (1) was found to attach to all three Os atoms through the α-carbon, C(1), whilst the β-carbon, C(2), was with bonding distance to only one osmium atom, Os(3). Although the vinyl

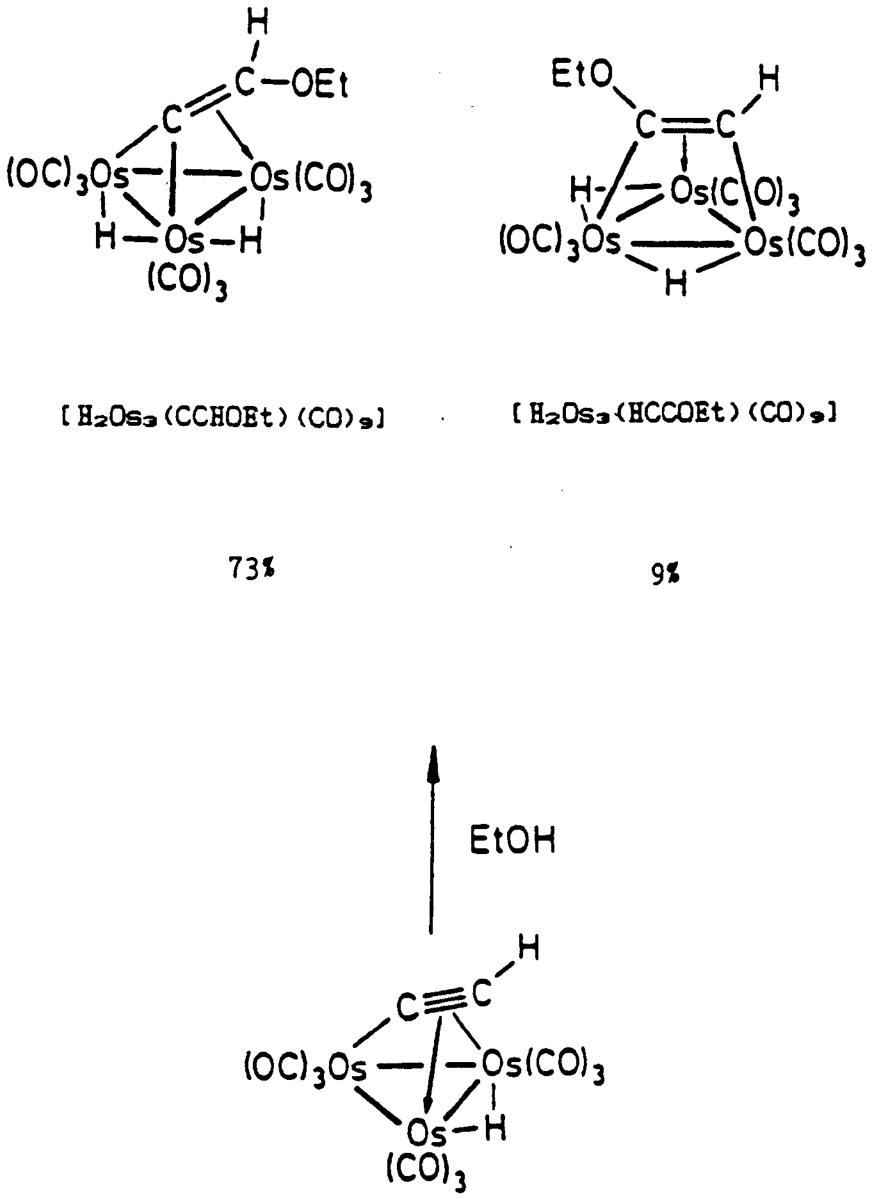

[$H_2Os_3(CCHOEt)(CO)_9$] [$H_2Os_3(HCCOEt)(CO)_9$]

73% 9%

[$Os_3H(C{\equiv}CH)(CO)_9$]

Scheme 3.2.1.

proton was not located from the X-ray analysis, its presence was inferred from the ^1H n.m.r. spectrum which exhibited a corresponding signal at δ 8.31 at -79°C. The most likely position of attachment of this proton was thought to be at the β -carbon, C(2), since the α -carbon, C(1), was already co-ordinated to the three osmium atoms, {Figure 3.2.2(a)}. Importantly, the X-ray structural formulation of the minor isomer (yield 9%), with the OEt^- group attached at the β-carbon, $[Os_3H_2(CCHOEt)(CO)_9]$ (1) was not consistent with the corresponding formulation proposed from the ^1H n.m.r. assignments (scheme 3.2.1).[70]

The X-ray structure of isomer (2) revealed that the organo group was attached to Os(1) and Os(3) through C(1), with C(2) bonded to both Os(2) Os(3), {Figure 3.2.2(b)}. Again, the vinyl proton was not located from the X-ray analysis, but the ^1H n.m.r. signal at δ 6.24 at -69°C indicated its presence, and was thought to be attched to the β -carbon, C(2), since the α -carbon, C(1), was already linked to Os(1), Os(3) and the ethoxy group (OEt). This structural formulation for the major isomer (yield 73%) with the OEt^- group attached at the α -carbon in $[Os_3H_2(HCCOEt)(CO)_9]$ (2) was again inconsistent with its earlier formulation from the ^1H n.m.r. data, {scheme 3.2.1}. Therefore, the X-ray structures of (1) and (2) clearly established that the structural formulations made on the basis of the ^1H n.m.r. data were incorrect. Discussion with the synthetic collaborators revealed that the n.m.r. assignments to the proposed structures of (1) and (2) were based in comparison with the ^1H n.m.r. spectrum of the non-ethoxy analogue $[Os_3H_2(CO)_9(C{=}CH_2)]$.[65] However, if the effect of the OEt^- group was considered in the interpretation of the ^1H n.m.r. spectra, the corresponding δ values were found to be consistent with the positions of the vinyl protons predicted from the

X-ray structures of (1) and (2). For instance, in $[Os_3H_2(CCHOEt)(CO)_9]$ (1) since the vinyl proton was assumed to be attached to the β-carbon C(2), it would therefore be less shielded from the negative charge of the neighbouring OEt^- group, and as result would give the observed downfield signal at δ 8.31 at -79.0°C. Since the corresponding proton in $[Os_3H_2(HCCOEt)(CO)_9]$ (2) was also thought to be attached to the β-carbon, C(2), but being at opposite end of the double bond to the ethoxy group, the vinyl proton would be more shielded from the negative charge of the OEt^- and therefore give rise to the less downfield signal at δ 6.24 observed at -69.0°C. From these results the reaction scheme was subsequently corrected as illustrated in scheme 3.2.2.

Although the two hydrido ligands in both isomers were not located directly from their respective X-ray analyses, the positions were deduced from potential energy minimisation calculations.[44] Suitable minima in P.E. were obtained for the two hydrido ligands to bridge the edges Os(1)-Os(2) and Os(2)-Os(3) in isomer (1); Os(1)-Os(2) and Os(2)-Os(3) in isomer (2). Further evidence supporting these sites came from 'space-filling' models of the molecule,[45] where the equatorial carbonyl ligands associated with the respective bridged Os bonds were clearly 'pushed' back, showing a gap through which the atomic spheres of the hydride bridged osmium atoms could readily be seen in both molecules, {Figures 3.2.2(c) and 3.2.2(d), respectively}.

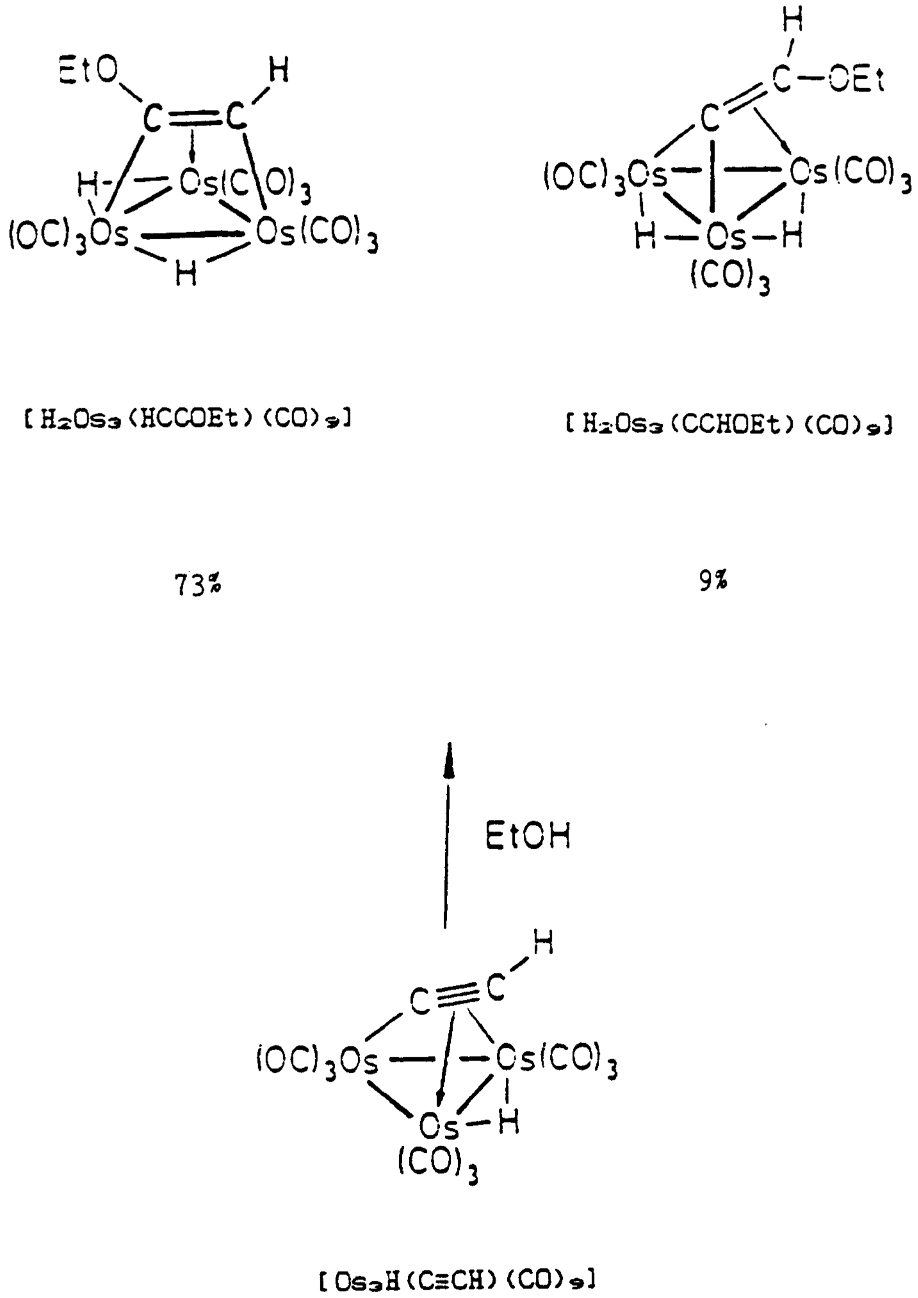

$[H_2Os_3(HCCOEt)(CO)_9]$

$[H_2Os_3(CCHOEt)(CO)_9]$

$[Os_3H(C\equiv CH)(CO)_9]$

Scheme 3.2.2.

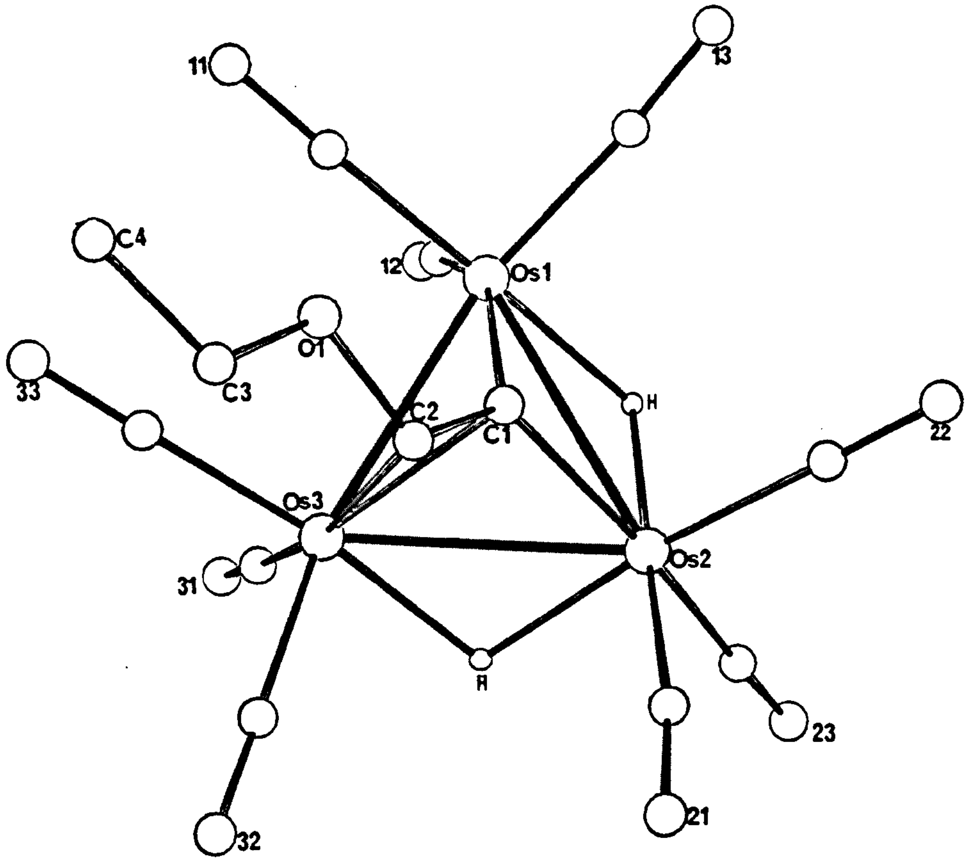

Figure 3.2.2(a). The molecular structure of the tri-osmium cluster $[Os_3H_2(CCHOEt)(CO)_9]$ (1). The carbonyl C atoms have the same numbering as the O atoms to which they are attached.

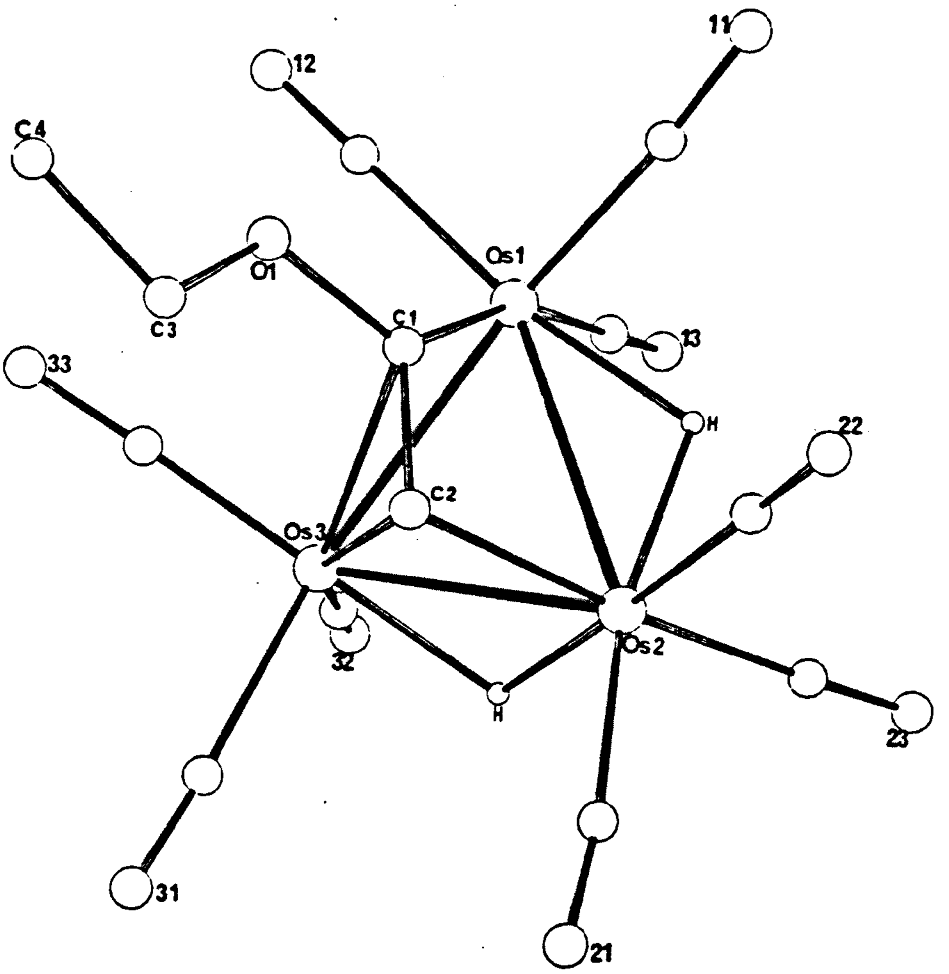

Figure 3.2.2(b). The molecular structure of $[Os_3H_2(HCCOEt)(CO)_9]$ (2). The carbonyl C atoms have the same numbering as the O atoms to which they are attached.

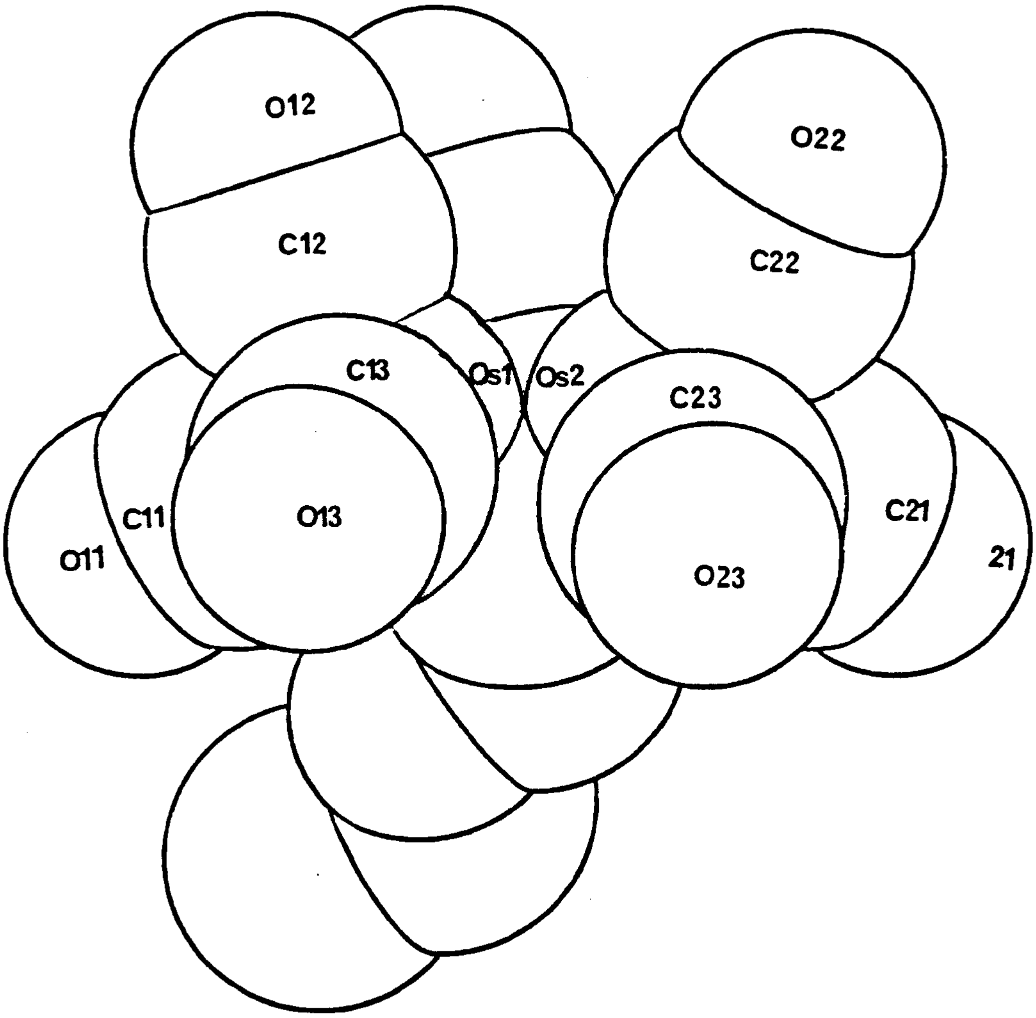

Figure 3.2.2(c). A computed 'space filling' model of the molecule $[Os_3H_2(CCHOEt)(CO)_9]$ (1). A view along the hydride bridged edge Os(1)-Os(2), showing a gap between the carbonyl groups CO(12) and CO(22) through which the atomic spheres of Os(1) and Os(2) can be seen.

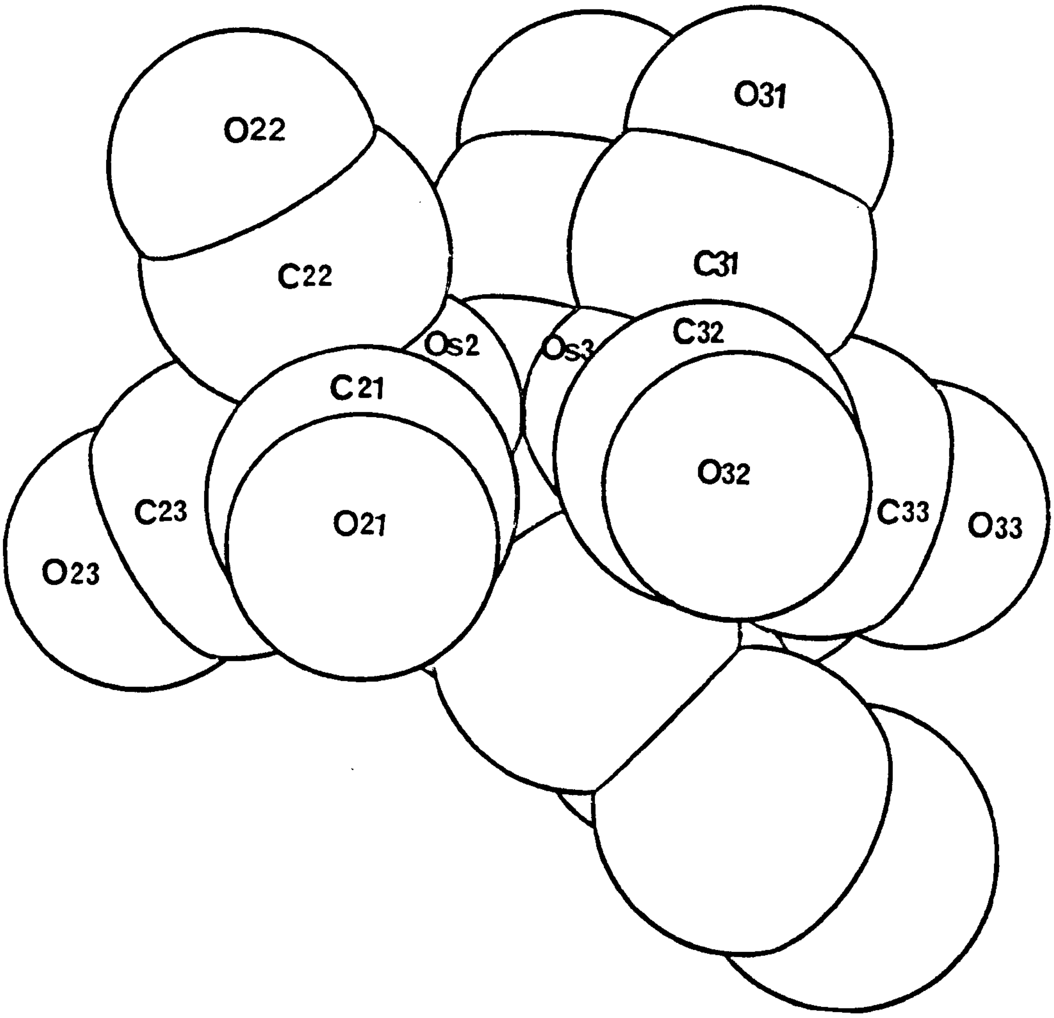

Figure 3.2.2(d). A computed 'space filling' model of the molecule $[Os_3H_2(CCOHEt)(CO)_9]$ (1). A view along the hydride bridged edge Os(2)-Os(3), showing a gap between the carbonyl groups CO(22) and CO(31) through which the atomic spheres of Os(2) and Os(3) can be seen.

3.2.3 Results and discussion.

The X-ray analysis of the two isomeric structures $[Os_3H_2(CCHOEt)(CO)_9]$ (1) and $[Os_3H_2(HCCOEt)(CO)_9]$ (2), {Figures 3.2.2(a) and 3.2.2(b), respectively}, described triangular metal frameworks similar to those previously observed for the Os_3 cluster compounds $[Os_3H_2(CO)_{11}]$ (3),[71] $[Os_3(CO)_{12}]$ (4),[71] and the zwitterionic adducts, $[Os_3H(CO)_9(HC{=}CPMe_2Ph)]$ (5)[68] and $[Os_3H(CO)_9(MeC{=}CCH_2PMe_2Ph)]$ (6).[68] Table 3.2.3 lists the selected bond lengths for (1) and (2).

The mean of the three Os-Os bonds in $[Os_3H_2(CCHOEt)(CO)_9]$ (1) {2.840(1) Å} was found to be significantly shorter than the mean bond in the related isomer $[Os_3H_2(HCCOEt)(CO)_9]$ (2) {2.867(2) Å}, however both mean bond lengths were noteably shorter than the corresponding values in the di-hydrido cluster $[Os_3H_2(CO)_{11}]$ (3) {2.918(2) Å} and the non-hydrido tri-osmium compound $[Os_3(CO)_{12}]$ (4) {2.867(2) Å}. In both (1) and (2) the marked asymmetry in the three Os-Os distances, with two bonds being longer was consistent with the characteristic lengthening of M-M bonds bridged by hydrogen ligands. Interestingly, the longest Os-Os bond in (2) was found to be 0.123 Å longer than the longest bond in (1), although both bonds were bridged by hydrido ligands. This lengthening of Os-Os bonds bridged by H-ligands was also apparent in the related clusters $[Os_3H(CO)_9(HC{=}CPMe_2Ph)]$ (5) and $[Os_3H(CO)_9(MeC{=}CCH_2PMe_2Ph)]$ (6),[68] where the bridged edge of the triangular framework was found to be 0.200 Å longer than the mean of the two unbridged bonds in (5) and 0.232 Å in (6). Another distinct feature of the presence of the two edge-bridging H-ligands in (1) and (2) was the expected displacement of equatorial carbonyl groups adjacent to the bridged Os-Os bond relative to those around the other Os-Os bond.

C-Os-Os angles cis to the bridged bonds Os(1)-Os(2) and Os(2)-Os(3) in isomer (1):

	angle/$^{\circ}$
C(12)-Os(1)-Os(2)	114.5(6)
C(22)-Os(2)-Os(1)	119.7(5)
C(22)-Os(2)-Os(3)	117.1(5)
C(31)-Os(3)-Os(2)	109.4(6)

C-Os-Os angles cis to the unbridged bond, Os(1)-Os(3):

C(11)-Os(1)-Os(3)	93.1(6)
C(12)-Os(1)-Os(3)	103.3(6)
C(31)-Os(3)-Os(1)	94.2(6)
C(33)-Os(3)-Os(1)	92.5(6)

C-Os-Os angles cis to the bridged bonds, Os(1)-Os(2) and Os(2)-Os(3) in isomer (2):

C(11)-Os(1)-Os(2)	103(1)
C(23)-Os(2)-Os(1)	108(1)
C(23)-Os(2)-Os(3)	125(1)
C(32)-Os(3)-Os(2)	112(1)

C-Os-Os angles cis to the unbridged bond, Os(1)-Os(3):

C(12)-Os(1)-Os(3)	101(1)
C(13)-Os(1)-Os(3)	106(1)
C(32)-Os(3)-Os(1)	95(1)
C(33)-Os(3)-Os(1)	90(2)

Similar structural observations were also reported for the di-hydrido cluster (3)[71] and the zwitterionic complexes (5) and (6).[68]

The nine carbonyl groups in both (1) and (2) were terminal, with a range of Os-CO bond lengths of 1.85-1.99(2) Å in (1) and 1.78-1.98(5) Å in (2). The corresponding C-O distances were found to range from 1.06-1.18(3) Å in (1) and 1.08-1.22(6) Å in (2). All nine carbonyl groups in both structures were found to be near linear {Os-C-O range 173-179(2) in (1); 164-177(6)° in (2)}.

The bonding of the ethoxy vinyl organo ligand in isomer (1), {Figure 3.2.2(a)}, was established to occur via the attack of the nucleophile, OEt^-, at the β-carbon of the acetyl acetylene group in the parent compound [$Os_3H(C\equiv CH)(CO)_9$], {scheme 3.2.2.}. All three osmium atoms were co-ordinated to the α-carbon, C(1), with Os(2) also linked to the β-carbon, C(2) which formed the η^2- linkage. The Os-C bonds associated with C(1) showed asymmetry with the bond C(1)-Os(3) {2.21(1) Å} being significantly longer than the bonds, C(1)-Os(1) and C(1)-Os(2) {2.01(1) and 2.06(1) Å, respectively}. The two longer Os-C bonds associated with the attachment of the vinyl ligand, C(1)-Os(3) and C(2)-Os(3) were both forming an η^2-linkage at Os(3), {Table 3.2.3}. Similar asymmetry was also present in isomer (2) with the two bonds involved in the η^2-linkage at Os(3) {C(1)-Os(3) 2.45(5) Å and C(2)-Os(3) 2.32(4) Å} being significantly longer than the two σ-Os-C bonds {C(1)-Os(1) 1.86(5) Å and C(2)-Os(2) 2.08(5) Å}. The marked lengthening of the two Os-C bonds associated with the attachment of a vinyl ligand to form an η^2-linkage at one osmium atom in a triangular metal framework, was also observed in other related cluster compounds:

compound	*a	b	c	d
[$Os_3H(CO)_9(HC{=}CPMe_2Ph$] (5)	2.12(1)	2.06(1)	2.22(1)	2.25(1)[68]
[$Os_3H(CO)_9(MeC{=}CCH_2PMe_2Ph$] (6)	2.13(1)	2.12(1)	2.24(2)	2.29(1)[68]
[$Os_3(CO)_{10}(Ph_2C_2)$] (7)	2.18(1)	2.07(1)	2.18(1)	2.29(1)[72]
[$Os_3(CO)_7(Ph_4C_4)(Ph_2C_2)$] (8)	2.16(2)	2.08(2)	2.22(2)	2.28(2)[73]

*(a and b are σ-Os-C bonds while c and d are the Os-C lengths in the η^2-linkage).

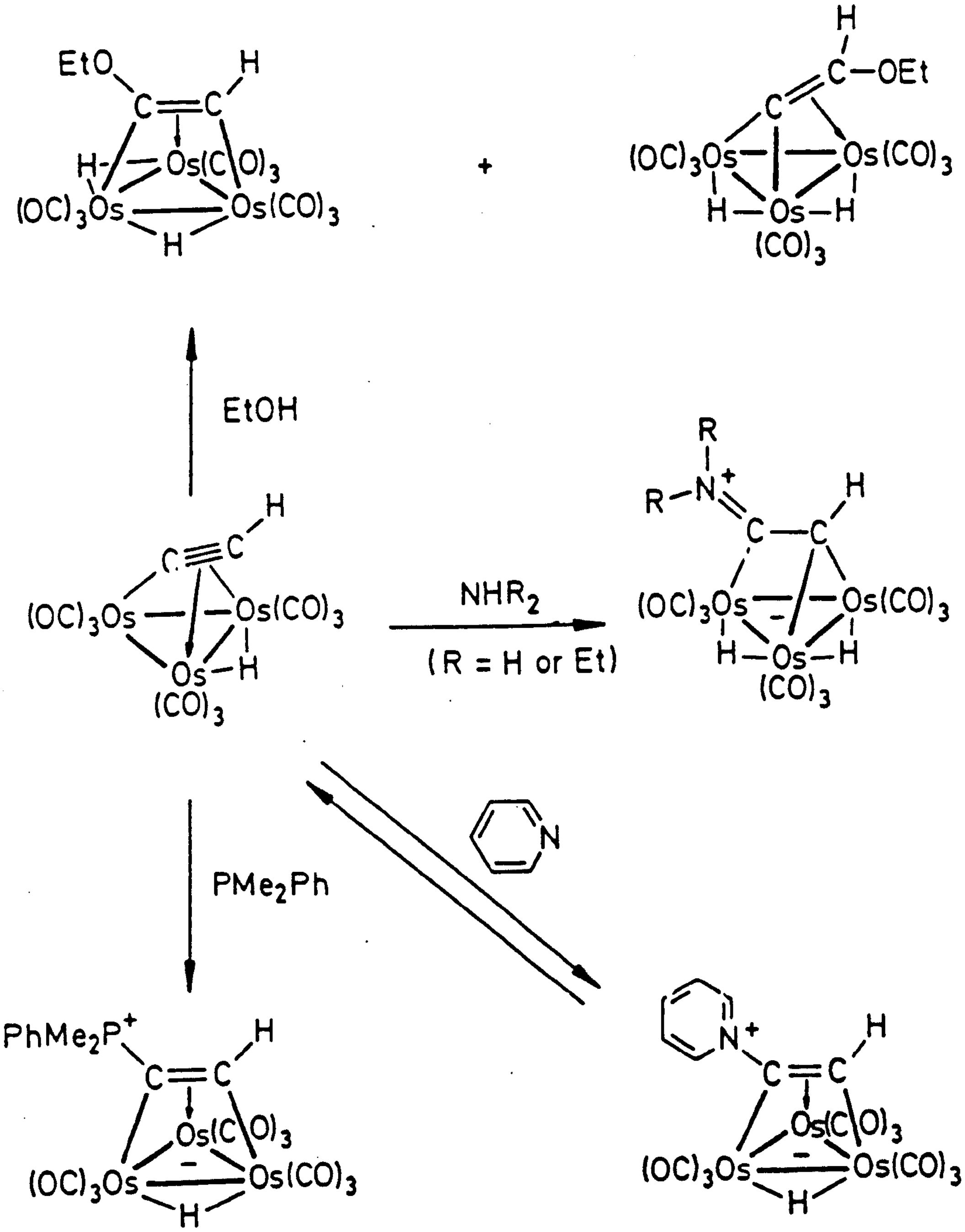

Scheme 3.2.4.

In the tri-osmium complexes (2), (7) and (8), the relative twist of the vinyl ligand out of a symmetrical arrangement was apparent, with one σ-Os-C bond being longer than the other {C(2)-Os(2) > C(1)-Os(1) in (2), Table 3.2.3; a > b in (7) and (8)}. This shorter bond was associated with the longer of the two Os-C bond of the η^2-linkage {C(1)-Os(3) > C(2)-Os(3) in (2), Table 3.2.3; d > c in (7) and (8)}. Surprisingly, even with the α-phosphonium centre in (5) and the β-phosphonium centre in (6), there was no apparent distortion in the bonding of the attached hydrocarbon, with the respective differences in the σ-Os-C and Os-C bonds associated with the η^2-linkage being barely significant (vide supra).

3.2.4 Conclusions.

The X-ray structural analysis of the two isomeric compounds $[Os_3H_2(CCHOEt)(CO)_9]$ (1) and $[Os_3H_2(HCCOEt)(CO)_9]$(2) further established that doubly and triply bridging C=CR ligands co-ordinated to triangular metal frameworks are susceptible to nucleophilic attack at the α-or β- carbon. Together with previously reported[74] nucleophiles, NH_3, Et_2NH, NC_5H_5 and PMe_2Ph, the reagent EtOH used in the formation of (1) and (2) supported that in the parent compound $[Os_3H(\mu_3\text{-}C\equiv CR)(CO)_9]$ [R = H or Me] nucleophilic addition to the triple bond of the organic substituent occurred predominantly at the α-carbon, {Scheme 3.2.4}.

Granozzi and co-workers had previously reported that from c.n.d.o. (complete neglect of diffrential overlap) calculations, the α-carbon of the alkynyl complex $[Os_3H(CO)_9(\mu_3\text{-}C\equiv CR)]$ appeared to be the most electrophilic, carrying more positive charge than the neighbouring β-carbon and therefore supported the preference of nucleophilic reagents in attacking at this site.[75]

Table 3.2.3

bond	distance/ Å	
	(1)	(2)
Os(1)-Os(2)	2.883(1)	3.006(2)
Os(1)-Os(3)	2.774(1)	2.770(2)
Os(2)-Os(3)	2.863(1)	2.824(2)
bonds associated with the organic ligand:		
Os(1)-C(1)	2.01(1)	1.86(5)
Os(2)-C(1)	2.06(1)	-
Os(3)-C(1)	2.21(1)	2.45(5)
Os(1)-C(2)	-	-
Os(2)-C(2)	-	2.08(3)
Os(3)-C(2)	2.43(1)	2.32(4)
C(1)-C(2)	1.38(2)	1.40(5)
C(2)-O(2)	1.40(2)	1.58(5)
C(3)-O(2)	1.43(2)	1.46(4)
C(3)-C(4)	1.46(4)	1.49(6)

Section 3.3. X-ray structural analysis of a crystalline modification of the salt $[Ru_4H_3(CO)_{12}][N(PPh_3)_2]$.

Crystal data, methods of data collection structure solution and refinement are presented in section 4.9.

Tables of atomic co-ordinates, bond lengths, inter-bond angles, intermolecular and intramolecular distances are given in the appendix (Vol.2).

3.3.1 Introduction.

Early studies of the neutral tetra-hydride clusters $[M_4H_4(CO)_{12}]$ [M = Ru or Os] indicated the presence of more than one isomer in solution.[76,77] Subsequent X-ray analysis established only one isomeric form in the solid state, with a D_{2d} symmetry of the M_4H_4 core.[78,79] The ^{1}H n.m.r. studies of the related monoanion clusters $[M_4H_3(CO)_{12}]^-$ [M = Ru or Os] showed the existence of both the C_2 and C_{3v} isomers in solution.[80,81] The presence of both structural forms in the solid state for the salt $[N(PPh_3)_2][Ru_4H_3(CO)_{12}]$ were subsequently established by X-ray structural studies, although three crystalline modifications for analogous osmium salt, $[N(PPh_3)_2][Os_4H_3(CO)_{12}]$, all exhibited virtual C_2 symmetry of the molecule.[82] The ^{1}H n.m.r. studies of hydrido ligands in solutions of several other ruthenium cluster compounds such as, $[Ru_4H_4(CO)_{10}L]$,[83] $[Ru_4H_4(CO)_{10}(\mu\text{-}L)]$[20] [L = $Ph_2PCH_2CH_2PPh_2$] and $[Ru_4H_4(CO)_{12-n}\{P(OMe)_3\}_n]$ [n = 1-4][84] were consistent with the H-ligands being scrambled over the metal frameworks, giving rise to low energy barriers to rearrangement.

In the solid state the reported tetra-hydrides $[Ru_4H_4(CO)_{10}(PPh_3)_2]$[80,85] $[Ru_4H_4(CO)_{12}]$[78] and $[Ru_4H_4(CO)_{11}\{P(OMe)_3\}]$[31] all adopted metal-hydrogen skeletons approximating D_{2d} symmetry, whereas the related clusters $[Ru_4H_4(CO)_{10}L]$[83] and $[Ru_4H_4(CO)_{10}(\mu\text{-}L)]$[20] adopted a Ru_4H_4 metal frameworks possessing only C_s symmetry. These results together with theoretical calculations carried out by Hoffmann and co-workers on the staggered and eclipsed conformations of $[M_4H_n(CO)_{12}]$ cluster compounds, supported that alternative M-hydrogen arrangements can differ little in energy.[86]

During the early stages of data collection the unit cell parameters of the tetra-ruthenium tri-hydrido salt [PPN][$Ru_4H_3(CO)_{12}$] (1), {section 4.9} indicated the presence of a different crystalline modification to the C_2 and C_{3v} tautomers of the anion previously reported by McPartlin and Nelson.[82] Therefore, the X-ray analysis of (1) was of interest in establishing a possible novel isomeric form for the Ru_4H_3 metal-hydrogen core and provide further evidence to support that, as cluster size increases, (and hence the number of possible metal polyhedra), the likelihood of isolating different structural forms of a molecule in the solid state becomes more probable.

3.3.2 Structural description of $[Ru_4H_3(CO)_{12}]^-$ (1).

The X-ray analysis of the tetra-ruthenium tri-hydrido monoanion (1) established a ruthenium tetrahedral core, with each metal atom carrying three essentially linear carbonyl groups {Ru-C-O 173-177(3)°}, Figure 3.3.2. The $Ru(CO)_3$ units of the metal core were found to adopt a staggered conformation relative to the three adjacent Ru-Ru bonds. Although the three hydrido ligands were not located directly from the X-ray analysis, their positions were deduced from the potential energy minimisation calculations.[44] Suitable minima in P.E. were obtained for the three H-ligands to bridge the edges Ru(1)-Ru(4), Ru(2)-Ru(3) and Ru(2)-Ru(4). The positioning of the H-ligands established the virtual C_2 symmetry of the molecule.

3.3.3 Discussion and results.

X-ray analysis of the ruthenium tri-hydrido monoanion (1), {Figure 3.3.2} confirmed a C_2 symmetry of the molecule which was identical to that earlier reported for a different crystalline

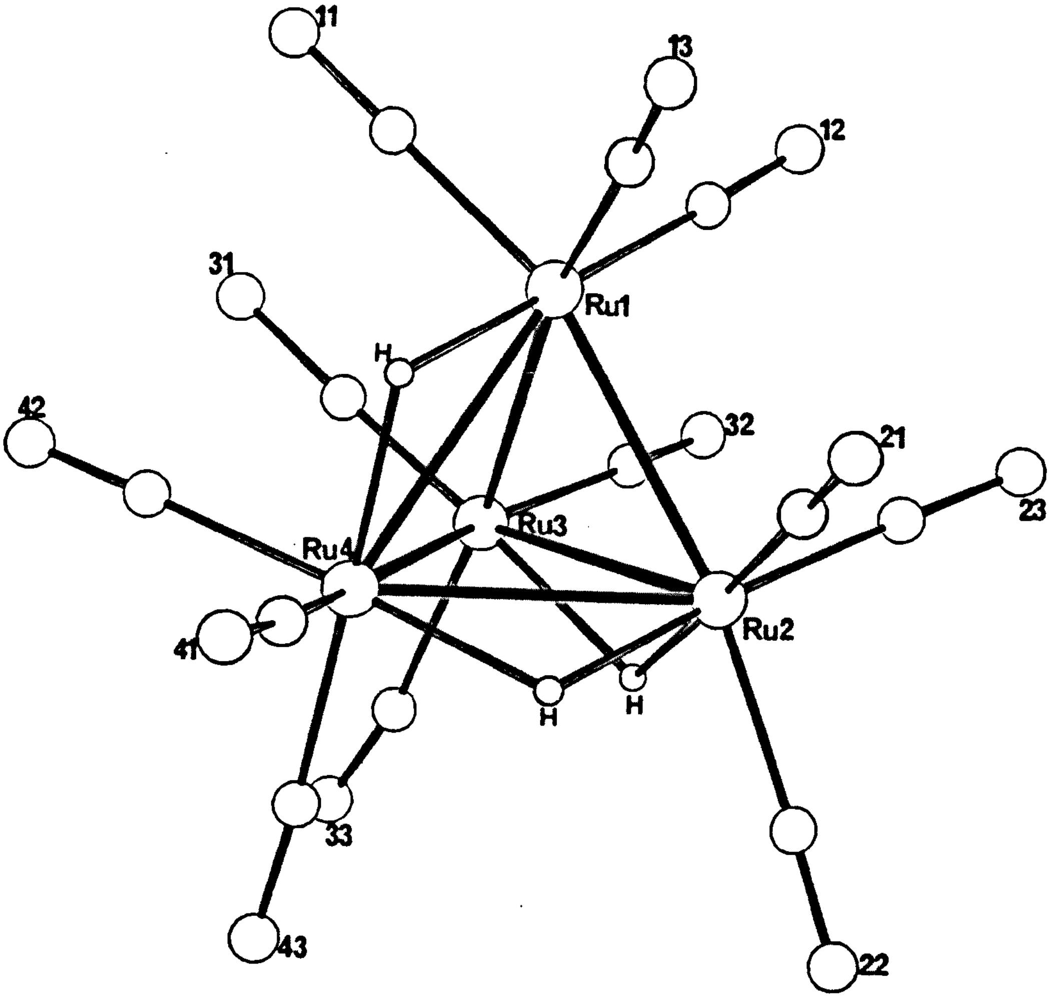

Figure 3.3.2. The molecular structure of the tri-hydrido ruthenium monoanion $[Ru_4H_3(CO)_{12}]^-$ (1). The carbonyl C atoms have the same numbering as the O atoms to which they are attached.

modification of the salt $[N(PPh_3)_2][Ru_4H_3(CO)_{12}]$ and that adopted by the related osmium monoanion $[Os_4H_3(CO)_{12}]^-$.[82] The overall structure of (1) was found to be distinctly different to the analogous C_{3v} isomer of the monoanion $[Ru_4H_3(CO)_{12}]^-$ (2),[82] {Figure 3.3.3}, and the neutral tetra-hydrido cluster $[Ru_4H_4(CO)_{12}]$ (3).[78] Table 3.3.3 lists the Ru-Ru bond lengths for the structurally related cluster compounds (1), (2) and (3).

The mean of the six Ru-Ru distances defining the tetrahedral core in the structure of the tetra-ruthenium monoanion in (1) {2.858(3) Å} was found to be slightly shorter than the mean of the six bonds in the structure of the C_{3v} isomer (2) {2.862(1) Å}, but both bond lengths were significantly shorter than the corresponding mean bond in the tetra-hydrido cluster (3) {2.895(9) Å}. In (1) the marked asymmetry in the Ru-Ru bonds, with three lengths being significantly shorter than the other three, (Table 3.3.3), was consistent with the three longer edges being bridged by hydrido ligands, {Figure 3.3.2}. This characteristic lengthening of Ru-Ru bonds was also observed in the structure of the C_{3v} isomer (2), where the three outer edges of the Ru_4 tetrahedron were found to be markedly longer than the remaining Ru-Ru bonds, (Table 3.3.3). In the tetra-hydrido cluster (3) the bond Ru(1)-Ru(3) bridged by the fourth H-ligand was found to be 0.181 Å longer to the analogous non-bridged bond in (1) and 0.173 Å in (2). Addition of u_2D-H ligands bridging M-M bonds has also shown to have the distinct effect of 'pushing' back adjacent equatorial carbonyl groups in a wide variety of hydrido clusters.[20,31,78-80,83,85] This feature was evident in the structure of the monoanion $[Ru_4H_3(CO)_{12}]^-$ (1), with the carbonyl ligands cis to the three hydride bridged Os-Os bonds having very much larger Ru-Ru-C angles {mean 114(1)°} than those to the other unbridged Ru-Ru bonds

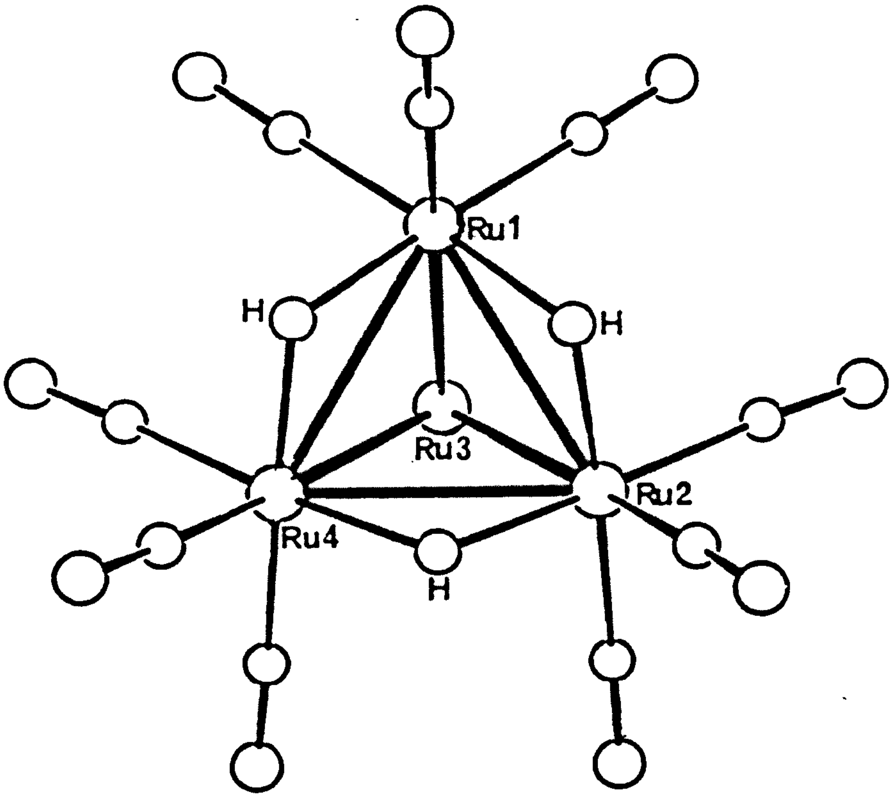

Figure 3.3.3. The isomer of the monoanion $[Ru_4H_3(CO)_{12}]^-$ (2) of virtual C_{3v} symmetry. The carbonyl groups attached to Ru(3) have been omitted for clarity.[82]

{mean 95(1)$^\circ$}. Similar splaying out of -CO groups was also reported for the related structures (2)[82] and (3).[78] The 12 terminal carbonyl ligands in (1) all exhibited near linear angles {Ru-C-O 173-177(3)$^\circ$}. The mean Ru-CO distance in (1) (1.89(3) Å} was found to be smaller than the corresponding values in (2) {1.91(4) Å} and in (3) {1.92(1) Å}. In contrast the mean C-O distance in (1) (1.14(5) Å} was larger than the mean values in the structures of both (2) {1.13(5) Å} and (3) {1.12(1) Å}.

3.3.4 Conclusions.

X-ray analysis of the tri-hydrido ruthenium monoanion $[Ru_4H_3(CO)_{12}]^-$ (1) established that the PPN salt was isomorphous to the osmium analogue $[Os_4H_3(CO)_{12}]^-$.[82] The geometry described a virtual C_2 symmetry of the Ru_4H_3 metal-hydrogen core which was previously reported for another crystalline modification of the parent salt $[PPN][Ru_4H_3(CO)_{12}]$, but was different in structure to the C_{3v} tautomer of the anion.[82] These results further supported that alternative M-H frameworks can differ little in energy, enabling the existence of such discrete structural forms in the solid state. Interestingly, characterisation of several different modifications of the analogous osmium hydrido salt $[PPN][Os_4H_3(CO)_{12}]$ showed that the molecule crystallised in one form, exhibiting C_2 symmetry for the Os_4H_3 skeleton, although ^1H n.m.r. studies of the of the monoanion were consistent with the presence of both C_2 and C_{3v} isomers in solutions. Importantly, the existence of structural isomers reflects upon the methods used for cluster preparation, isolation and crystallisation. For example, it was reported that the protonation of the dianion $[Os_6(CO)_{18}]^{2-}$ in CH_2Cl_2 using HCl(g) gave the isomer $[Os_6H_2(CO)_{18}]$ whose X-ray structure established an octahedral metal core.[87] However on standing in solution the isomer rearranged to the previously characterised capped square pyramidal Os_6 skeleton,[23] which was initially prepared through a different method by acidifying the dianion in MeCN using concentrated sulphuric acid.

Table 3.3.3.

bond	distance/ Å		
	(1)	(2)[82*]	(3)[78]
Ru(1)-Ru(2)	2.799(3)	2.936(1)	2.784(8)
Ru(1)-Ru(3)	2.769(3)	2.777(1)	2.950(9)
Ru(1)-Ru(4)	2.911(3)	2.935(1)	2.945(8)
Ru(2)-Ru(3)	2.941(3)	2.786(1)	2.948(8)
Ru(2)-Ru(4)	2.943(3)	2.941(1)	2.956(7)
Ru(3)-Ru(4)	2.788(3)	2.799(1)	2.788(8)

*re-numbered for comparison

Section 3.4. X-ray structural analysis of the hexanuclear cluster $[Os_6H_2(CO)_{17}P(OMe)_3]$ (1).

Crystal data, methods of data collection, structure solution and refinement are presented in section 4.10.

Final Tables of atomic co-ordinates, bond lengths, inter-bond angles, intermolecular and intramolecular distances are given in the appendix (Vol.2)

3.4.1 Introduction.

It has been well established that when hydrogen ligands are incorporated into high nuclearity osmium clusters, their solid state geometries are often unpredictable.[23,88-91] Wades theory applied to transition metal M_6 cluster compounds with 86 valence electrons predicts an octahedral structure, with seven skeletal bonding electrons.[92] The reported structures of the hexanuclear osmium dianion $[Os_6(CO)_{18}]^{2-}$ and the hydrido monoanion $[Os_6H(CO)_{18}]^-$ described the expected octahedral metal geometry.[23] Interestingly, the neutral di-hydrido analogue $[Os_6H_2(CO)_{18}]$ was observed to adopt a capped square pyramidal geometry.[23] The alternative metal core displayed by the hydrido cluster was rationalised in terms of Wade theory:[92-94]

All transition metal carbonyls with 86 valence electrons have seven pairs of skeletal bonding electrons. For hexanuclear clusters these may be accommodated in a closo-octahedral metal core, whereas in M_7 clusters, the seven skeletal electron pairs are utilised in a mono-capped octahedral geometry.

This illustrated that closo- and nido- versions of the same polyhedra require the same number of skeletal electron pairs. Therefore, the mono-capped nido-octahedral (capped square pyramid) structure adopted by the hydrido cluster $[Os_6H_2(CO)_{18}]$ was an alternative framework for the accommodation of seven skeletal electron pairs in an M_6 cluster compound. McPartlin and co-workers previously suggested[23] that the mono-capped square-pyramidal arrangement rather than the octahedral adopted by this di-hydrido cluster may have resulted from the preference of bridging hydrides for sites of lowest co-ordination as observed in borohydride chemistry.[95] The X-ray study of the cluster compound

$[Os_6H_2(CO)_{17}P(OMe)_3]$ (1) was therefore of interest in comparing relative structural features to those earlier established for the di-hydrido osmium cluster $[Os_6H_2(CO)_{18}]$ and to observe whether the presence of the phosphite group resulted in any distinct changes in the solid state structure.

3.4.2 Structural description of $[Os_6H_2(CO)_{17}P(OMe)_3]$ (1).

The X-ray analysis of the hexanuclear di-hydrido cluster (1) established that the six osmium atoms formed a capped square pyramidal geometry, {Figure 3.4.2(a)}. The basal atoms, Os(2), Os(3), Os(4), and Os(5) defined the square, with Os(1) forming the apex of the pyramid. Os(6) further capped the face defined by the atoms Os(1), Os(2) and Os(5). Of the six osmium atoms, Os(4) was bonded to two terminal carbonyl groups, and the organophosphine ligand, $P(OMe)_3$, whereas the remaining five metal atoms were all found to be bonded to three terminal -CO groups, one at an axial and two at equatorial sites. Although the two hydrido ligands were not located directly from the X-ray analysis, their presence was inferred by the longer osmium bonds: Os(2)-Os(5) 2.907(3) and Os(3)-Os(4) 2.996(3) Å. The potential energy minimisation routine[44] used to determine hydride positions on metal cluster surfaces, gave one suitable minima in P.E. for a hydride to bridge the basal bond Os(2)-Os(5). No suitable minima was obtained at the opposite edge, of the base Os(3)-Os(4), or at the face Os(1)-Os(3)-Os(4). This was attributed to the presence of the phosphite ligand bonded to Os(4), giving unreliable results in potential energy.

Computer simulated 'space-filling' model of the molecule[45] viewed on the face Os(1)-Os(3)-Os(4), showed a clear gap in the carbonyl contacts, whose 'hole' size was comparable to the

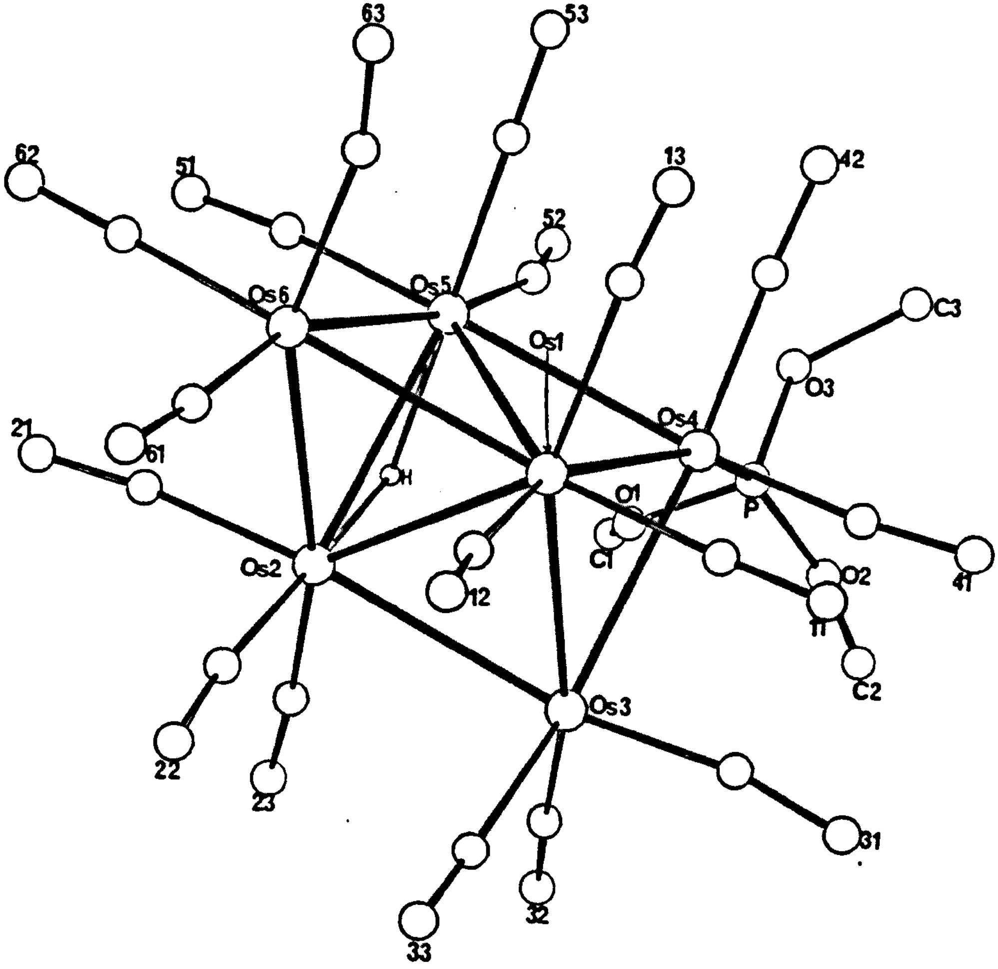

Figure 3.4.2(a). The molecular structure of the hexa-ruthenium osmium cluster $[Os_6H_2(CO)_{17}P(OMe)_3]$ (1). The carbonyl C atoms have the same numbering as the O atoms to which they are attached.

μ_2-H site established by McPartlin and co-workers in the structure of the octanuclear cluster $[HOs_8(CO)_{22}]^-$.[88]
Therefore, the second hydrogen atom was assumed to adopt a μ_2-bonding mode at the edge Os(3)-Os(4).

3.4.3 Discussion and results.

The capped square pyramidal geometry characterised for the hexanuclear osmium cluster $[Os_6H_2(CO)_{17}P(OMe)_3]$ (1) {Figure 3.4.2(a)}, was found to be similar to the metal-framework adopted by the related di-hydrido cluster $[Os_6H_2(CO)_{18}]$ (2),[23] {Figure 3.4.3(a)}, but with one -CO group at Os(4) replaced by the 2e donor phosphine ligand, $P(OMe)_3$. The metal core structure of (1) was found to be distinctly different to the octahedral skeletal geometries adopted by the hexanuclear anionic clusters, $[Os_6(CO)_{18}]^{2-}$ and $[Os_6H(CO)_{18}]^-$, {section 3.1;Figures 3.1(g) and 3.1(i), respectively}.[23] Table 3.4.3 lists the Os-Os bond lengths for the structurally related cluster compounds (1) and (2).

The range of Os-Os bond lengths in the structure of the hexanuclear cluster (1) {2.784(3)-2.996(3) Å} was found to be similar to the range observed in the solid state structure of the related di-hydrido cluster (2) {2.805-2.965(4) Å}, and the 'spiked' trigonal bi-pyramidal structure $[Os_6H_2(CO)_{19}]$ {2.748-2.997(2) Å}.[89] The mean Os-Os bond distance in the structure of (1) {2.856(3) Å} was observed to be 0.002 Å longer than the corresponding mean bond in (2), {2.854(4) Å}. However, both these mean bond lengths were noteably shorter than the mean Os-Os bond distance observed in the structure of the monohydride $[Os_6H(CO)_{18}]^-$, {mean 2.931(3) Å}. The Os-Os bond lengths of the square base in both (1)

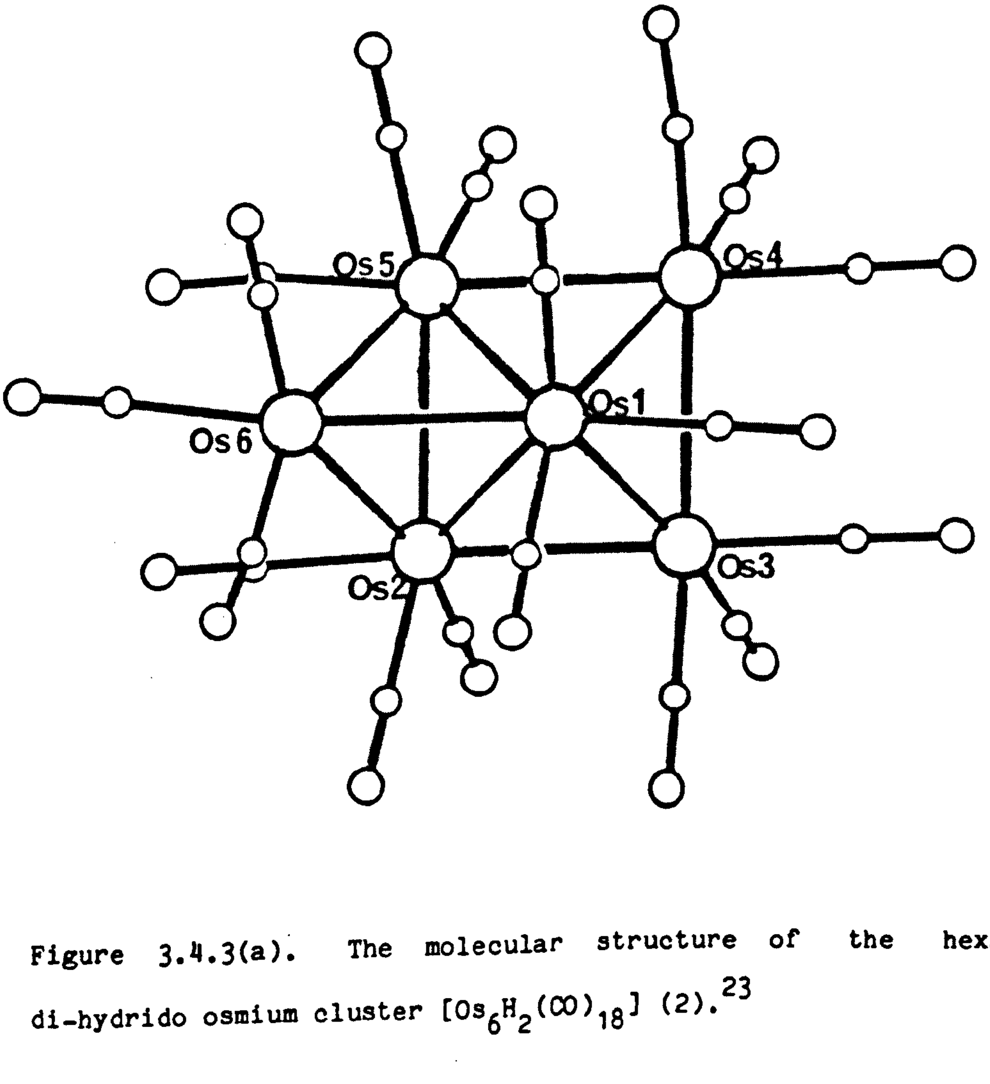

Figure 3.4.3(a). The molecular structure of the hexanuclear di-hydrido osmium cluster $[Os_6H_2(CO)_{18}]$ (2).[23]

and (2) showed marked asymmetry, with two bonds being significantly longer than the other two. In (1) the difference between the two longer Os-Os bonds, Os(2)-Os(5) and Os(3)-Os(4) {0.089 Å} was larger than the corresponding difference in (2) {0.073 Å}. The bonds, Os(3)-Os(4) and Os(4)-Os(5) were observed to be very similar in length in both (1) and (2), despite the fact that one carbonyl group at Os(4) in the structure of (2) was replaced by the phosphine ligand in (1) {Figures 3.4.2(a) and 3.4.3(a) respectively;Table 3.4.3}.

From potential energy minimisation calculations[44] one of the two hydrido ligands in (1) was thought to bridge the basal bond Os(2)-Os(5) and the second hydride was assumed to bridge the opposite edge of the square, Os(3)-Os(4) or cap the triangular face Os(1)-Os(3)-Os(4). The mean bond of this face {2.914(3) Å} was found to be longer not only to the mean bonds of the other two uncapped faces of the pyramid, {Os(1)-Os(2)-Os(3) 2.843(3) Å; Os(1)-Os(4)-Os(5) 2.862(3) Å}, but also to the mean distance of the face Os(2)-Os(5)-Os(6) {2.829(3) Å} whose basal edge Os(2)-Os(5) was already confirmed to be bridged by a hydrido ligand, {Figure 3.4.2(a)}. Interestingly, in the related di-hydrido cluster (2), the analogous face of the square pyramid, Os(1)-Os(3)-Os(4) {mean 2.888(4) Å} was also observed to be enlarged in comparison to the other two uncapped faces Os(1)-Os(2)-Os(3) {mean 2.848(4) Å}, Os(1)-Os(4)-Os(5) {mean 2.847(4) Å} and to the face Os(2)-Os(5)-Os(6) {mean 2.834(4) Å} whose basal edge, Os(2)-Os(5) was already thought to be bridged by a hydrido ligand, {Figure 3.4.3(a)}.

In the hexanuclear cluster $[Os_6H_2(CO)_{17}P(OMe)_3]$ (1), the bond Os(1)-Os(4) trans to the phosphite ligand was found to be 0.066 Å longer to the bond Os(1)-Os(5) which was trans to a carbonyl group, {Table 3.4.3}. This lengthening reflected upon the weaker

π-acceptor properties of the phosphite ligand compared to the carbonyl group. Correspondingly, the non-bonded contacts between the three oxygen atoms of the phosphite ligand and carbonyl ligands on the adjacent osmium atoms, Os(3) and Os(5) were in the order of 3.0 Å, and it was therefore envisaged that a shorter trans Os-Os bond to the phosphine group, $P(OMe)_3$, would have resulted in greater steric congestion between the surface ligands. The weaker π-acceptor ability of the phosphite ligand was also reported by Raithby and co-workers for the planar cluster $[Os_6(CO)_{17}\{POMe)_3\}_4]$, where the Os-Os bonds trans to the four phosphite groups were ca. 0.05 Å longer than the other Os-Os bonds in the structure.[96] In (1) the three Os-Os bonds associated with the capping of the square pyramidal metal core by Os(6), showed marked asymmetry with one bond being significantly longer than the other two:

compound $[Os_6H_2(CO)_{17}P(OMe)_3]$ (1)

bond	distance/ Å
Os(1)-Os(6)	2.854(3)
Os(2)-Os(6)	2.798(3)
Os(5)-Os(6)	2.784(3)

Similar asymmetry was also observed in the reported di-hydrido cluster (2):

compound $[Os_6H_2(CO)_{18}]$ (2)[23]

bond	distance/ Å
Os(1)-Os(6)	2.850(4)
Os(2)-Os(6)	2.805(4)
Os(5)-Os(6)	2.805(4)

However, the mean of the six bonds involved in the tetrahedral cap from Os(6), was very similar in both (1) {2.831(3) Å} and (2)

{2.834(3) Å}, signifying no apparent expansion of the cap in either structure.

X-ray analysis of (1) established that 5 of the 6 osmium atoms were bonded to three terminal -CO groups with Os(4) only carrying two -CO groups, but all 17 carbonyl ligands exhibited expected linearity, {Os-C-O 163-178(5)°}. The range of Os-CO distances in (1) {1.74-1.97(6) Å} was found to lie in the range previously observed in related clusters,[23,88-91] with the corresponding range of C-O distances, 1.12-1.25(8) Å. In (1) the phosphine ligand, $P(OMe)_3$, was found to co-ordinate at an equatorial site at Os(4). The Os(4)-P(4) bond length of 2.28(1) Å was similar to the mean of the four Os-P bonds in the 'raft' structure $[Os_6(CO)_{17}\{POMe)_3\}_4]$ {2.24(2) Å}.[96] The angles around the 4 co-ordinate P atom, were slightly larger than the expected tetrahedral angle of 108.0°:

Os(4)-P(4)-O(1) = 110(2)°
Os(4)-P(4)-O(2) = 121(4)°
Os(4)-P(4)-O(3) = 123(3)°

This was probably attributed to the maximum displacement of the oxygen atoms of the organophosphine ligand in minimising the repulsive interaction of the lone pair electron clouds of the three oxygen atoms. The two carbonyl groups in near proximity to the phosphorus ligand at Os(4), showed no distortion with marked linearity of the angles, Os(4)-(C41)-O(41) 176(5)° and Os(4)-C(42)-O(42) 173(5)°. However the Os(4)-C(42) distance of 1.93(6) Å was significantly longer than the Os(4)-C(41) bond length of 1.79(5) Å.

3.4.4 Conclusions.

X-ray analysis of the di-hydrido cluster $[Os_6H_2(CO)_{17}P(OMe)_3]$ (1) described a capped square pyramidal geometry similar to the metal framework adopted by the neutral di-hydrido analogue $[Os_6H_2(CO)_{18}]$ (2).[23] The overall electron count for the hexanuclear cluster (1) was rationalised as follows:

firstly using the E.A.N. rule

atom/groups	number of electrons donated
6 x Os	48
17 x CO	34
2 x H	2
$P(OMe)_3$	2
total	----
	86e

and secondly using the procedure which takes into account polyhedral structures fused at edges, triangular and square faces:[97]

fused polyhedra in parent cluster	number of electrons characteristic of polyhedron
square pyramid	74
tetrahedron	60
sub-total	-----
	134e

Since a triangular face of the osmium square pyramidal core was being shared by Os(6), {Figure 3.4.2}, 48e had to be subtracted from the above sub-total to give the expected electron count of 86e characteristic of an M_6 cluster.[92-94] The replacement of one carbonyl group in the di-hydrido cluster $[Os_6H_2(CO)_{18}]$ (2) by the 2e donor organophosphine ligand, $P(OMe)_3$ in $[Os_6H_2(CO)_{17}P(OMe)_3]$ (1) was observed to retain the capped square pyramidal metal core structure in which the organophosphine ligand imposed the least steric strain upon the metal polyhedron. In contrast to both (1) and (2), the ruthenium di-hydrido cluster $[Ru_6H_2(CO)_{18}]$ was reported to adopt the expected octahedral geometry,[15] indicating that metal atoms must play a critical role in determining the stereiochemistry in the soild state, rather than solely the surface ligands.

Table 3.4.3.

bond	distance/ Å	
	(1)	(2)[23]
Os(1)-Os(2)	2.815(3)	2.828(4)
Os(1)-Os(3)	2.850(3)	2.849(4)
Os(1)-Os(4)	2.895(3)	2.851(4)
Os(1)-Os(5)	2.829(3)	2.829(4)
Os(1)-Os(6)	2.854(3)	2.850(4)
Os(2)-Os(3)	2.865(3)	2.868(4)
Os(2)-Os(5)	2.907(3)	2.892(4)
Os(2)-Os(6)	2.798(3)	2.805(4)
Os(3)-Os(4)	2.996(3)	2.965(4)
Os(4)-Os(5)	2.862(3)	2.860(4)
Os(5)-Os(6)	2.784(3)	2.805(4)

Section 3.5. X-ray analysis of the di-hydrido heptanuclear osmium cluster $[Os_7H_2(CO)_{22}]$ (1).

Crystal data, methods of data collection, structure solution and refinement for (1) are presented in section 4.11.

Final Tables of atomic co-ordinates, bond lengths, inter-bond angles, intermolecular and intramolecular distances are given in the appendix (Vol.2).

During data collection, the unit cell dimensions and the volume of the heptanuclear cluster $[Os_7H_2(CO)_{22}]$ (1) were found to be different to the reported parameters of the analogous di-hydrido cluster $[Os_7H_2(CO)_{22}].[CH_2Cl_2]$ (2).[91] The X-ray analysis of (1) was therefore carried out to establish a different metal core geometry to the novel triangular fused trigonal bi-pyramidal adopted by (2). The X-ray structures of the related clusters, $[Os_7H_2(CO)_{21}]$ (3)[91] and $[Os_7H_2(CO)_{20}]$ (4),[90] were previously reported, and Figure 3.5 displays the unusual geometeries adopted by these heptanuclear clusters during the loss and gain of CO.

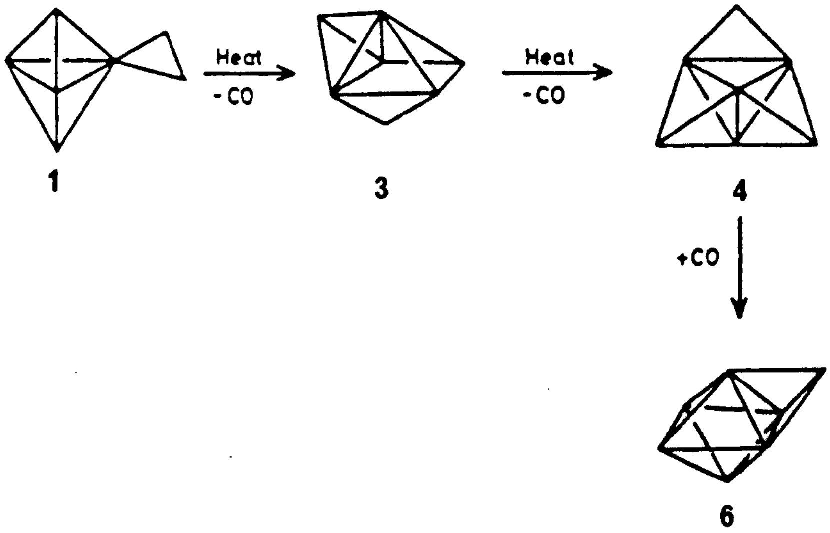

Figure 3.5

3.5.1 Structural description of $[Os_7H_2(CO)_{22}]$ (1).

The X-ray analysis of (1) established an identical triangular fused trigonal bi-pyramidal metal framework previously observed for the reported compound $[Os_7H_2(CO)_{22}].[CH_2Cl_2]$, {Figure 3.5.1}. The five osmium atoms, Os(1), Os(2), Os(3), Os(4) and Os(5) formed the basic trigonal bi-pyramidal metal core with Os(6) and Os(7) forming a triangular fusion with Os(1). Four of the seven osmium atoms were found to be bonded to three terminal carbonyl groups, with Os(1), whose vertex was shared by Os(6) and Os(7), carrying only two terminal -CO groups. The remaining eight carbonyl ligands were distributed four at both Os(6) and Os(7). All 22 carbonyl ligands displayed expected linearity {Os-C-O range 166-179(4)^{o}}. Although the two hydrido ligands were not located directly from the X-ray analysis, they were thought to bridge the longer Os(1)-Os(5) and Os(1)-Os(6) edges, analogous to that reported for the solvated molecule $[Os_7H_2(CO)_{22}].[CH_2Cl_2]$ (2).[91] These sites were deduced from potential energy minimisation calculations,[44] which gave suitable minima in P.E. for the two H-ligands to bridge these two long Os-Os bonds.

3.5.2 Discussion and results.

The metal core of the heptanuclear cluster $[Os_7H_2(CO)_{22}]$ (1) was a type not previously observed, nor anticipated in accommodating the observed electron count of a 102 valence electrons. The overall structure of (1) was found to closely resemble the 'spiked' trigonal bi-pyramidal metal core adopted by the hexanuclear molecule $[Os_6H_2(CO)_{19}]$ (5),[89] {Figure 3.5.2(a)}. The metal framework in (1) was formally thought to be derived from the metal skeleton of (5) by the replacement of a -CO group by an $Os(CO)_4$ unit, bridging the 'spike' Os(1)-Os(6) bond in (5), followed by a swing of the terminal H-ligand in (5) to a μ_2-bridging mode in (1). The solid state

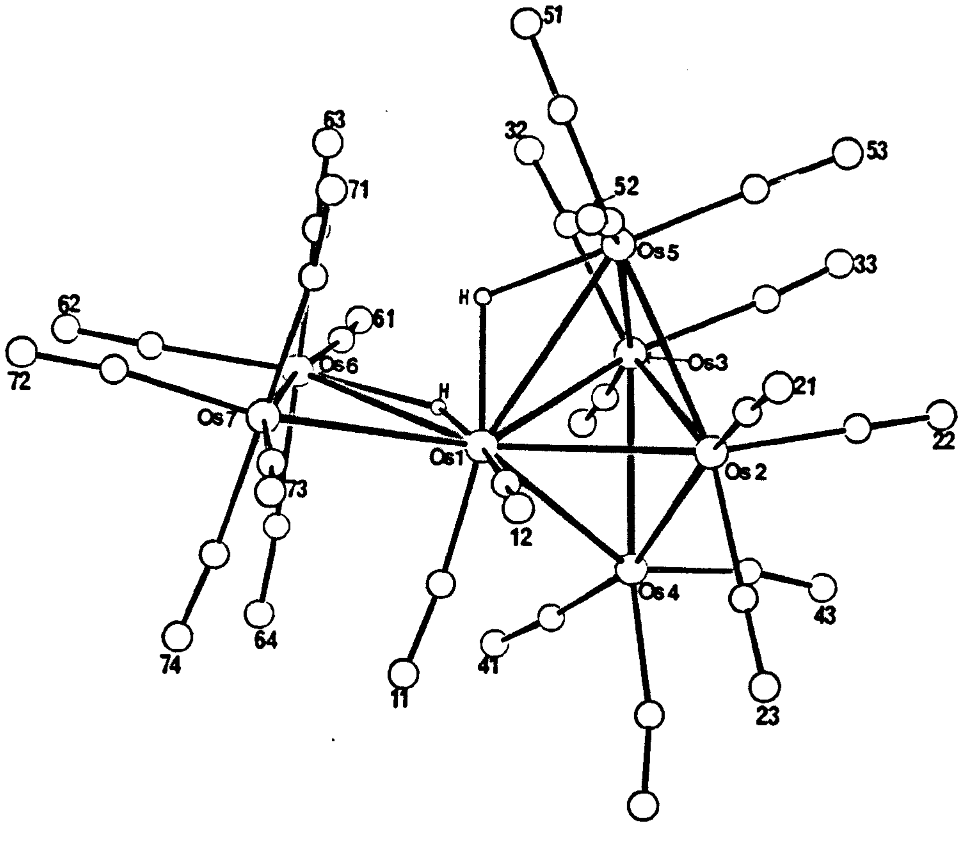

Figure 3.5.1. Molecular structure of the heptanuclear osmium cluster $[Os_7H_2(CO)_{22}]$ (1). The carbonyl C atoms have the same numbering as the O atoms to which they are attached.

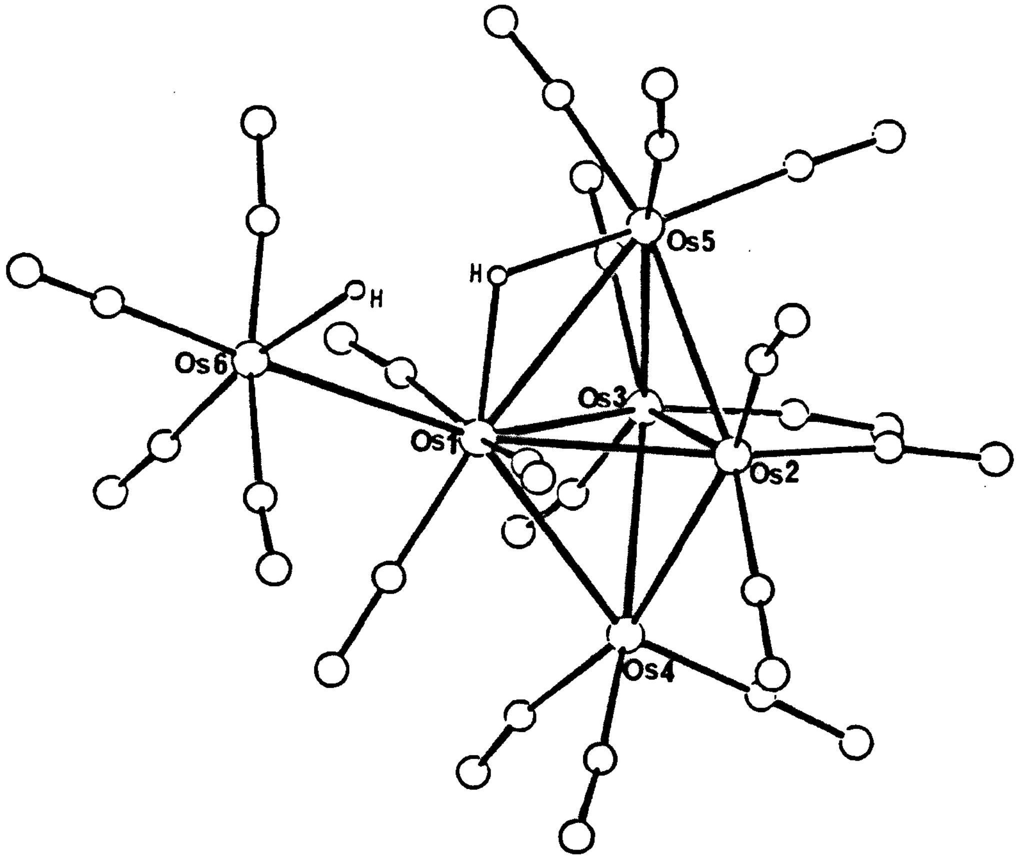

Figure 3.5.2(a). Molecular structure of $[Os_6H_2(CO)_{19}]$ (5).[89]

geometry of (1) was also observed to be different to the edge-bridged capped square pyramidal core adopted by the related heptanuclear cluster $[Os_7H_2(CO)_{21}]$ (3),[91] and the bi-capped tetrahedral metal geometry adopted by $[Os_7H_2(CO)_{20}]$,[90] {Figures 3.5.2(b) and 3.5.2(c), respectively}. Table 3.5.2 lists the M-M bond lengths for the heptanuclear cluster (1) and the structurally related hexanuclear compound $[Os_6H_2(CO)_{19}]$ (5).

The range of Os-Os bond lengths in the structure of the heptanuclear di-hydrido cluster $[Os_7H_2(CO)_{22}]$ (1) {2.732-3.078(1) Å} was found to be similar to that observed in the hexanuclear osmium cluster $[Os_6H_2(CO)_{19}]$ (5) {2.748-2.997(2) Å}, but longer than the corresponding ranges reported for related heptanuclear compounds, $[Os_7H_2(CO)_{21}]$ (3) {2.726-3.033(3) Å}[91] and $[Os_7H_2(CO)_{20}]$ (4) {2.697-2.993(4) Å}.[90] The mean of the 12 Os-Os bond lengths in the structure of (1) {2.869(1) Å} was observed to be 0.027 Å longer than the mean of the 10 Os-Os bond distances in (5), {mean 2.842(2) Å}. In both (1) and (5), the hydride bridged edge of the trigonal bi-pyramid, Os(1)-Os(5), was found to be the longest, {Table 3.5.2}. Lengthening of M-M bonds is characteristic of bridging or capping H-ligands,[98] which was also reflected in the longer Os(1)-Os(6) bond bridged by the second hydrido ligand in (1), {Figure 3.5.1}. In the heptanuclear cluster $[Os_7H_2(CO)_{22}]$ (1) the second characteristic feature involving the 'pushing' back of cis carbonyl groups adjacent to the H-bridged bonds was evident, for example, with the angles C(52)-Os(5)-Os(1) 118.4(3) and C(61)-Os(6)-Os(1) 119.1(3)$^\circ$ being bigger than the mean of the corresponding equatorial angles at unbridged Os-Os bonds {mean 93.2(3)$^\circ$}. The marked similarity in the solid state structures of (1) and (5)[89] was further reflected in similar asymmetry in the Os-Os bonds of the trigonal bi-pyramidal

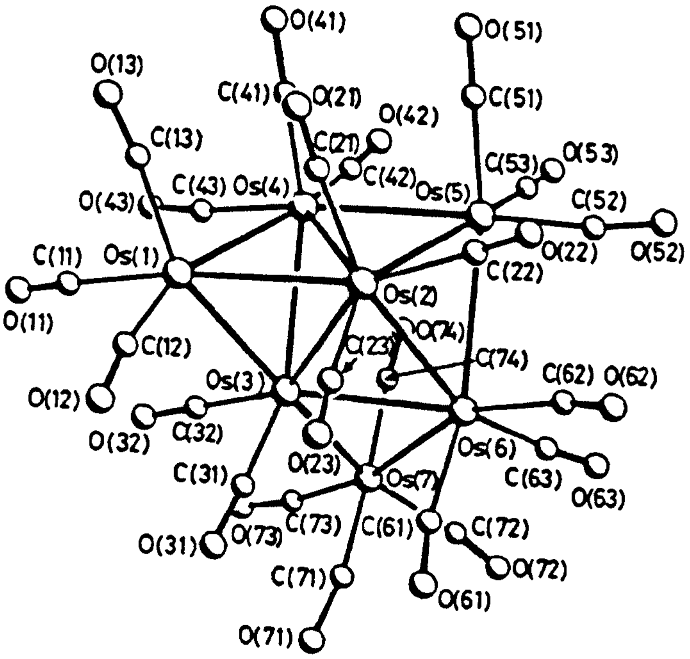

Figure 3.5.2(b). Molecular structure of [$Os_7H_2(CO)_{21}$] (3).[91]

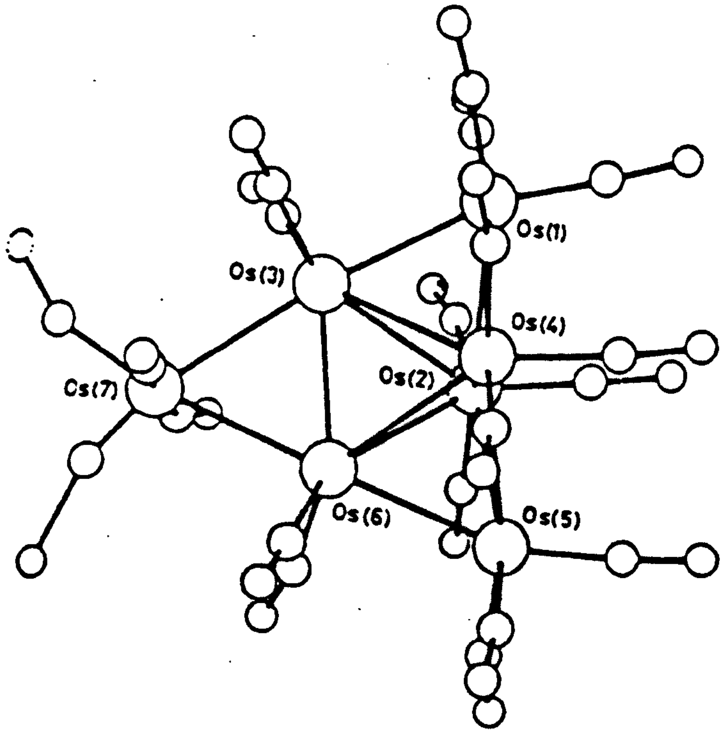

Figure 3.5.2(c). Molecular structure of [$Os_7H_2(CO)_{20}$] (4).[90]

metal core. In both clusters the four respective bonds associated with Os(1) were markedly longer than the other five bonds, with the bond Os(1)-Os(5) being the longest M-M bond in both structures, {Table 3.5.2}.

The X-ray analysis of $[Os_7H_2(CO)_{22}]$ (1) established that four osmium atoms Os(2), Os(3), Os(4) and Os(5) were bonded to three terminal carbonyl groups, whereas Os(1), at which the fusion of atoms Os(6) and Os(7) occurred carried only two -CO groups. Both Os(6) and Os(7) were found to be bonded to four terminal carbonyl ligands, and all 22 carbonyl groups displayed expected linearity, {Os-C-O 168-179(4)°}. The range of of Os-CO distances in (1), {1.83-1.94(3) Å} was similar to the range observed in (5), {1.82-1.94(5) Å} together with the corresponding range of C-O bond lengths, {C-O range in (1) 1.14-1.21(3); in (5) 1.20-1.17(6) Å}.

3.5.3 Conclusions.

The unusual solid state geometries adopted by the osmium hydrido clusters,

compound	geometry
$[Os_7H_2(CO)_{22}]$ (1)	triangular fused trigonal bi-pyramidal
$[Os_7H_2(CO)_{21}]$ (3)[91]	edge-bridged capped square pyramid
$[Os_7H_2(CO)_{20}]$ (4)[90]	edge-bridged bi-capped tetrahedron
$[Os_6H_2(CO)_{19}]$ (5)[89]	'spiked' trigonal bi-pyramid

supported previous conclusions reported by McPartlin and co-workers, that when hydrogen ligands were present, osmium cluster geometries were often unpredictable.[23] Interestingly, in this series of heptanuclear osmium clusters the 98e capped octahedral geometry adopted by the non-hydrido cluster $[Os_7(CO)_{21}]$[99] was the only metal polyhedron easily predictable by simple skeletal electron counting procedures. The electron counts in the related clusters (1) {102e}, (3) {100e} and (4) {98e} were all rationalised by the electron counting method which takes into account polyhedral structures fused at edges, triangular and square faces:[97]

$[Os_7H_2(CO)_{22}]$ (1)	fused polyhedra	nos. of electrons characteristic of polyhederon
	trigonal bi-pyramid	72e
	triangle	48e
		-----
	sub-total	120e

since a vertex of the osmium trigonal bi-pyramidal core was being shared by Os(6) and Os(7) in the structure of (1), {Figure 3.5.1}, 18e had to be subtracted from the sub-total, to give the expected electron count of 102.

$[Os_7H_2(CO)_{21}]$ (3)	fused polyhedra	nos. of electrons characteristic of polyhederon
	square pyramid	74e
	tetrahedron	60e
	triangle	48e
		-----
	sub-total	182e

since both an edge and a face of the osmium square pyramidal metal framework were being shared in the solid state structure of (3), {Figure 3.5.2(b)}, a total of 82e {34 from the share of an edge and 48 from a share of a face} had to be subtracted from the sub-total, to give the expected electron count of 100e.

$[Os_7H_2(CO)_{20}]$ (4)	fused polyhedra	nos. of electrons characteristic of polyhederon
	3 x tetrahedron	180e
	triangle	48e
		-----
	sub-total	228e

Since two faces and an edge were being shared in the metal core structure of (4), (Figure 3.5.2(c)), 130e {34e from the share of an edge and 96e from the share of two faces} electrons had to be subtracted from the sub-total, to give 98e predicted by the E.A.N. rule.

Table 3.5.2.

Bond	Distance/ Å	
	(1)	(5)[89*]
Os(1)-Os(2)	2.876(1)	2.862(2)
Os(1)-Os(3)	2.868(1)	2.842(2)
Os(1)-Os(4)	2.964(1)	2.936(2)
Os(1)-Os(5)	3.078(1)	2.997(2)
Os(1)-Os(6)	3.052(1)	2.925(2)
Os(1)-Os(7)	2.887(1)	-
Os(2)-Os(3)	2.776(1)	2.775(2)
Os(2)-Os(4)	2.752(1)	2.748(2)
Os(2)-Os(5)	2.795(1)	2.787(2)
Os(3)-Os(4)	2.732(1)	2.757(2)
Os(3)-Os(5)	2.787(1)	2.794(2)
Os(6)-Os(7)	2.861(1)	-

[*] re-numbered for comparison.

Section 3.6. X-ray structural analysis of the heptanuclear cluster $[Os_7H_2(CO)_{19}\{MeC{=}CMe\}]$ (1).

Crystal data, methods of data collection, structure solution and refinement for (1) are presented in section 4.12

Final Tables of atomic co-ordinates, bond lengths, inter-bond angles, intermolecular and intramolecular distances are given in the appendix (Vol.2).

The X-ray analysis of the di-hydrido hepta-osmium cluster $[Os_7H_2(CO)_{19}\{MeC{=}CMe\}]$ (1) was carried out to extend the series of hydrido heptanuclear osmium clusters whose solid state geometries had previously establised unusual metal core structures.[90,91] The X-ray structure of (1) was of further interest in assigning the bonding mode of the hydrocarbon and to observe whether the co-ordination of this organic ligand to the metal polyhedron would effect the overall surface ligand congestion, resulting in a novel metal core geometry in the accommodation of the observed electron count of a 100 valence electrons.

3.6.1 Structural description of $[Os_7H_2(CO)_{19}\{MeC{=}CMe\}]$ (1).

X-ray analysis established that the di-hydrido heptanuclear cluster (1) adopted an edge-bridged capped square pyramid, Figure 3.6.1(a). The four osmium atoms, Os(1), Os(3), Os(4) and Os(5) defined the square with Os(2) forming the apex of the pyramid. The triangular face, Os(1)-Os(2)-Os(3) of the pyramid was capped by Os(7), with Os(6) bridging the opposite basal atoms Os(4) and Os(5) of the square. Of the four basal atoms, Os(1) and Os(5), were bonded to three terminal -CO groups, whereas Os(3) and Os(4) carried two terminal carbonyl groups. The apical atom, Os(2) together with Os(6) and Os(7) were all bonded to three terminal carbonyl groups. The 4e donor substituted alkyne fragment, {MeC=CMe}, was envisaged to σ bond to Os(4) and Os(5) and form an η^2-linkage at Os(6), {Figure 3.6.1(a)}. Although the two hydrido ligands were not located directly from the X-ray analysis, their positions were deduced from potential energy minimisation calculations.[44] Reasonable minima in P.E. were obtained for one of the hydrides to bridge the bond Os(1)-Os(3) of the square base and the second to symmetrically cap the triangular face Os(4)-Os(5)-Os(6). However, examination of the geometry around the μ_3-H ligand revealed a close contact distance to the carbon atom of the carbonyl ligand CO(63), {C(63)...H 1.987 Å}. The calculations failed to give a suitable value in P.E. for the corresponding μ_2-site at the edge, Os(4)-Os(5), for this second H-atom and therefore the ligand was thought to adopt an asymmetric μ_3 bonding mode. However, the μ_2-site was more favoured by examination of a computer simulated space filling model of the molecule,[45] {Figure 3.6.1(b)}, where a view onto the triangular face Os(4)-Os(5)-Os(6), clearly showed the carbonyl ligands at these metal atoms 'pushed back' to exhibit a 'hole' size characteristic of a μ_2-H site, analogous to that established for the H-atom in the octanuclear osmium cluster $[HOs_8(CO)_{22}]^-$.[88]

3.6.2 Discussion and results.

The edge-bridged capped square pyramidal metal geometry established for the heptanuclear osmium cluster $[Os_7H_2(CO)_{19}\{MeC{=}CMe\}]$ (1), {Figure 3.6.1(a)} was structurally different to the edge-bridged capped square pyramidal metal framework adopted by the related cluster $[Os_7H_2(CO)_{21}]$ (2),[91] {Figure 3.6.2}. The seven metal atom core in (1) was envisaged to consist of five osmium metal atoms forming a square pyramid with the sixth Os atom bridging one edge of the square base, with the opposite face capped by the seventh Os atom. The metal skeleton of (2) was based on a similar 5 osmium atom square pyramid with one basal edge bridged by the sixth Os atom, but in contrast to (1), the seventh Os atom capped the adjacent face to the bridged Os-Os bond of the square, {Figure 3.6.2}. However, both the solid state structures of (1) and (2) were

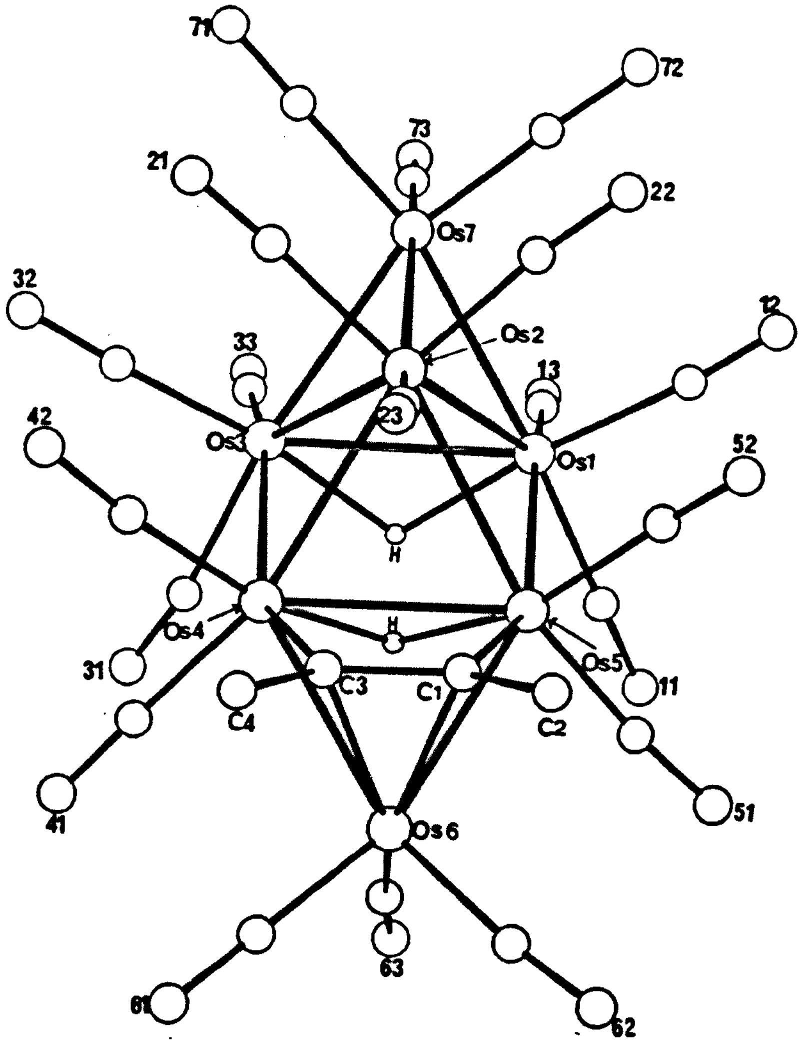

Figure 3.6.1(a). Molecular structure of the heptanuclear osmium cluster $[Os_7H_2(CO)_{19}\{MeC{=}CMe\}]$ (1). The carbonyl C atoms have the same numbering as the O atoms to which they are attached.

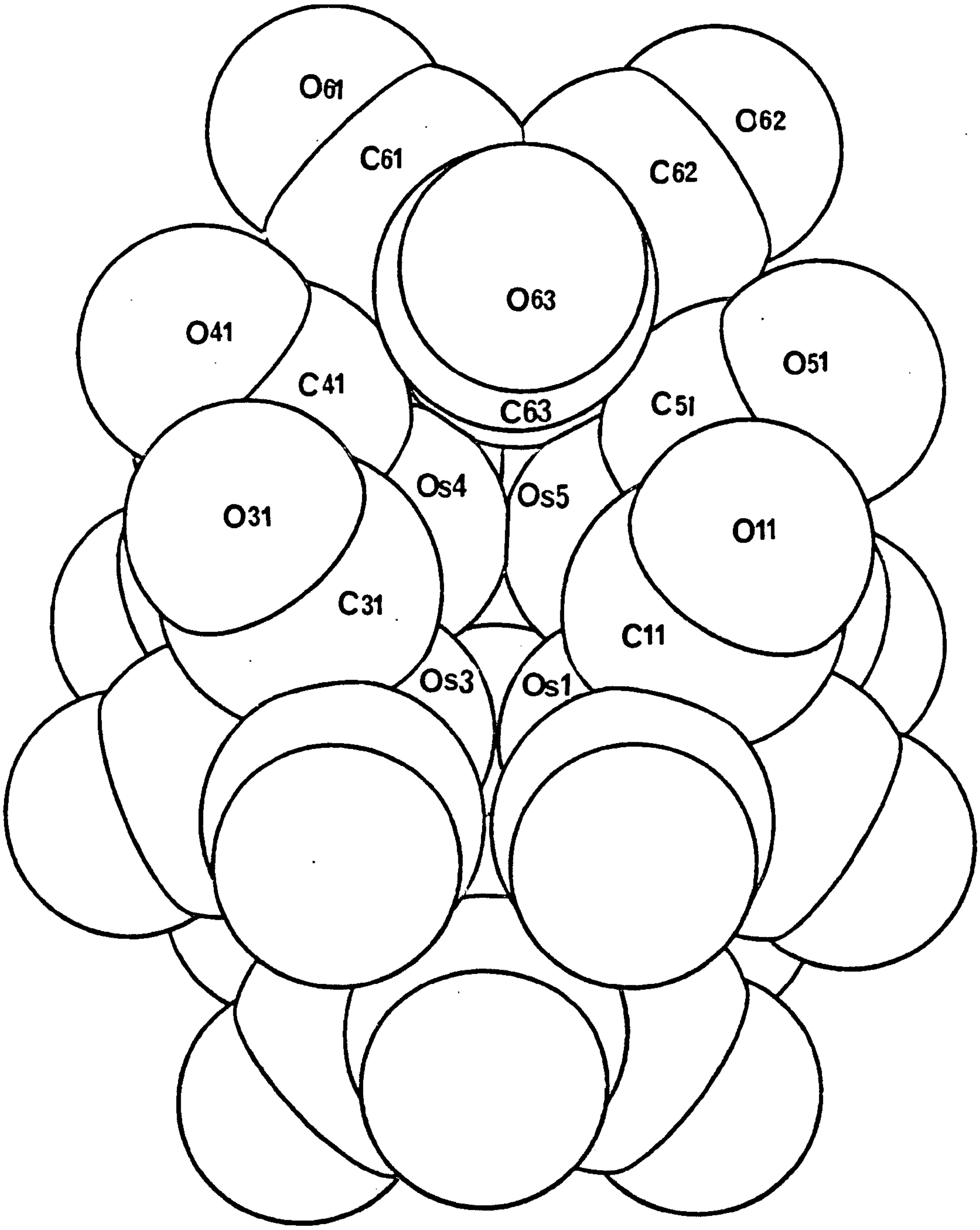

Figure 3.6.1(b). Computed 'space-filling' model of the molecule $[Os_7H_2(CO)_{19}\{MeC{=}CMe\}]$. A view onto the edge Os(4)-Os(5) shows a gap between the carbonyl groups CO(41) and CO(51) through which the atomic spheres of Os(4) and Os(5) can be seen.

different to the edge bridged bi-capped tetrahedral geometry adopted by the related analogue $[Os_7H_2(CO)_{20}]$ (3).[90] Table 3.6.2 lists the Os-Os bond lengths for the structurally related cluster compounds (1) and (2).

The range of Os-Os bond lengths in the solid state structure of the heptanuclear cluster (1) {2.770-2.919(1) Å} was found to be similar to that observed in the di-hydrido analogue (2) {2.726-3.033(2) Å}, although the mean Os-Os bond length in (1), {2.840(1) Å}, was found to be 0.025 Å shorter than the corresponding mean bond in (2), {2.865(2) Å}. The hydride bridged edge of the square base Os(1)-Os(3) showed marked lengthening in both (1) {2.919(1) Å} and (2) {2.942(2) Å}, whereas the opposite edge, Os(4)-Os(5), bridged by the second H-ligand in (1) {2.783(1) Å} was found to be significantly shorter than the analogous bond bridged by the H-ligand in (2) {3.033(2) Å}. The mean Os-Os bond length of the four bonds defining the square base in (1) {2.856(1) Å} was found to be 0.053 Å smaller than the corresponding mean in (2) {2.909(2) Å}. In (1) the mean bond of the triangular face, Os(4)-Os(5)-Os(6), associated with the bridging osmium atom Os(6), {2.789(1) Å}, was found to be 0.063 Å smaller than the mean of the face Os(3)-Os(4)-Os(6) {2.852(2) Å} associated with the bridging atom, Os(6) in the structure of the related di-hydride (2). In both (1) and (2) the three Os-Os bonds involved with the capping of the square pyramidal core by Os(7), showed marked asymmetry, with one bond being significantly longer than the other two:

$[Os_7H_2(CO)_{19}\{MeC{=}CMe\}]$ (1)		$[Os_7H_2(CO)_{21}]$ (2)[91]	
bond	distance/ Å		
Os(1)-Os(7)	2.770(1);	Os(1)-Os(7)	2.785(2)
Os(2)-Os(7)	2.911(1);	Os(2)-Os(7)	2.922(2)
Os(3)-Os(7)	2.802(1);	Os(3)-Os(7)	2.726(2)

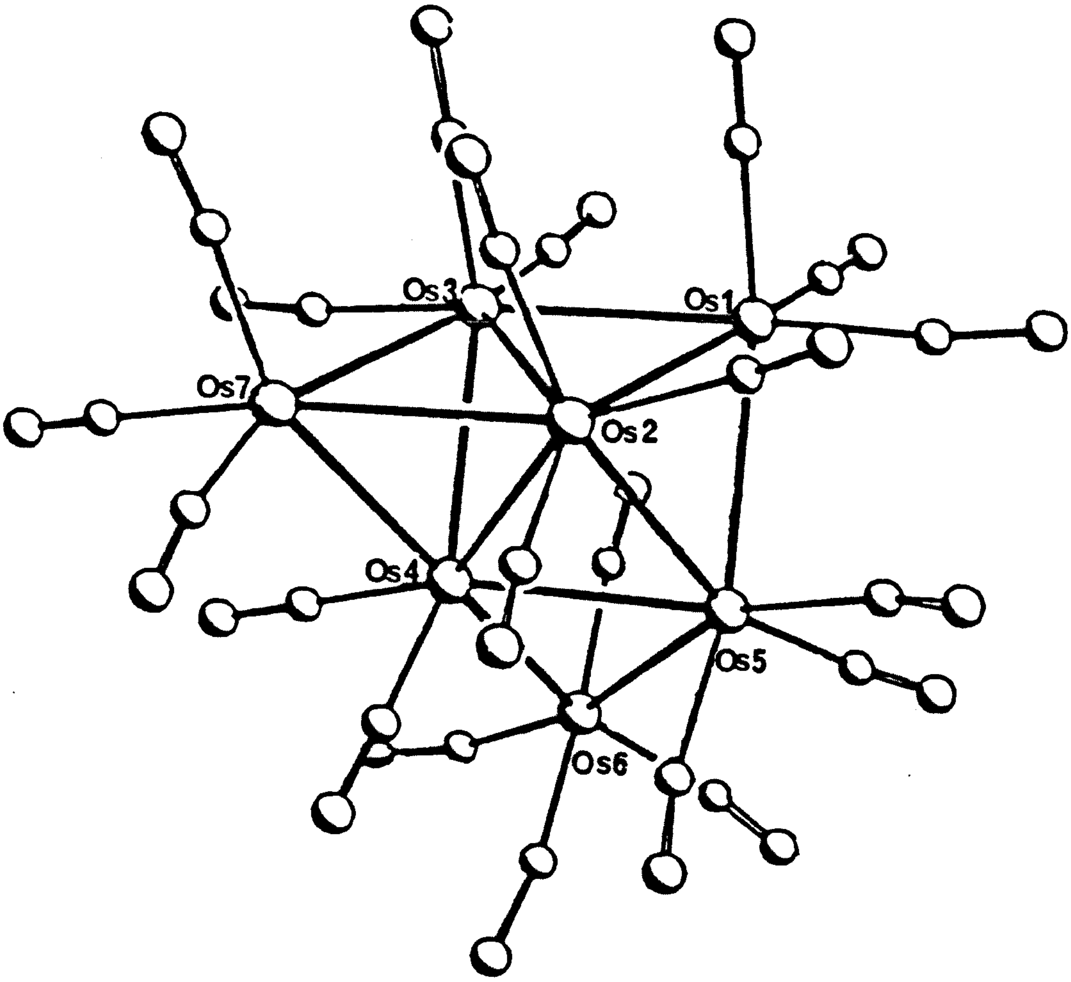

Figure 3.6.2. Molecular structure of $[Os_7H_2(CO)_{21}]$ (2).[91]

However, the tetrahedral cap from Os(7) in (1) was found to be slightly enlarged to the analogous cap in (2) {mean of the six tetrahedral Os-Os bonds in (1) 2.847(1) Å and 2.834(2) Å in (2)}. Besides the characteristic lengthening of the Os-Os bonds bridged by the two H-ligands, equatorial carbonyl groups adjacent to the bridged Os-Os bonds were found to be 'pushed' back. For example, the carbonyl ligands cis to the hydride bridged bond, Os(1)-Os(3), were observed to have much larger Os-Os-C angles {C(11)-Os(1)-Os(3) 116(1);C(31)-Os(3)-Os(1) 114(1)°}, than those cis to the unbridged Os-Os bonds, {mean C-Os-Os 94(1)°}.

The organic fragment, MeC=CMe, was found to co-ordinate at the triangular face Os(4)-Os(5)-Os(6), attaching to Os(4) and Os(5) via two σ-bonds {C(1)-Os(5) 2.07(4) Å and C(3)-Os(4) 2.15(4) Å} and forming an η^2-linkage at Os(6) {C(1)-Os(6) 2.22(4)) and C(3)-Os(6) 2.26(4) Å}. The longer σ-Os(4)-C(3) bond was associated with the longer Os(6)-C(3) of the η^2-linkage, indicating a somewhat symmetrical arrangement of the ligand at this face. This was found to be opposite to that reported for some related tri-osmium clusters having a vinyl ligand bonded to the three metal atoms:

compound	*a	b	c	d/ Å
$[Os_3(CO)_{10}(Ph_2C_2)]$	2.18(1)	2.07(1)	2.18(1)	2.29(1)[72]
$[Os_3(CO)_7(Ph_4C_4)(Ph_2C_2)]$	2.16(2)	2.08(2)	2.22(2)	2.28(2)[73]

*(a and b are σ-Os-C bonds while c and d are Os-C lengths in the η^2-linkage).

In the above tri-osmium clusters the shorter σ-Os-C bond, (b), was found to be associated with the longer Os-C bond of the η^2-linkage, (d), reflecting upon the relative twist of the vinyl ligand out of a symmetrical arrangement.

3.6.3 Conclusions.

The X-ray analysis of the heptanuclear osmium cluster $[Os_7H_2(CO)_{19}\{MeC{\equiv}CMe\}]$(1) established an overall edge-bridged capped square pyramidal geometry similar in structure to that adopted by the hydrido cluster $[Os_7H_2(CO)_{21}]$ (2).[91] These results further supported that the energy differences between alternative M-H frameworks can be very small and isolation of novel geometries in the solid state becomes more probable. The observed electron count of 100 valence electrons in both (1) and (2) was rationalised readily by the electron counting method which takes into account structures which are fused at edges, triangular or square faces:[97]

fused polyhedra	number of electrons characteristic of polyhedron
square pyramid	74
tetrahedron	60
triangle	48
sub-total	----
	182

since both a triangular face and an edge of the square pyramidal metal core structure were shared in both (1) and (2), {Figures 3.6.1(a) and 3.6.2(a)}, a total of 82e (34 from the share of an edge and 48 from the share of a face) had to be subtracted from the sub-total to give an overall electron count of 100e.

Table 3.6.2.

bond	distance/ Å	
	(1)	(2)[91*]
Os(1)-Os(2)	2.845(1)	2.850(2)
Os(1)-Os(3)	2.919(1)	2.942(2)
Os(1)-Os(5)	2.856(1)	2.857(2)
Os(1)-Os(6)	-	-
Os(1)-Os(7)	2.770(1)	2.785(2)
Os(2)-Os(3)	2.839(1)	2.776(2)
Os(2)-Os(4)	2.882(1)	2.941(2)
Os(2)-Os(5)	2.854(1)	2.852(2)
Os(2)-Os(7)	2.911(1)	2.922(2)
Os(3)-Os(4)	2.868(1)	2.807(2)
Os(3)-Os(6)	-	2.783(2)
Os(3)-Os(7)	2.802(1)	2.726(2)
Os(4)-Os(5)	2.783(1)	3.033(2)
Os(4)-Os(6)	2.801(1)	2.967(2)
Os(4)-Os(7)	-	-
Os(5)-Os(6)	2.786(1)	-

[*] re-numbered for comparison.

Section 3.7. X-ray analysis of the deca-osmium penta-hydrido monoanion $[H_5Os_{10}(CO)_{24}][N(PPh_3)_2].(CH_2Cl_2)$.

Crystal data, methods of data collection, structure solution and refinement are presented in section 4.13.

Final Tables of atomic co-ordinates, bond lengths, inter-bond angles, intermolecular and intramolecular distances are given in the appendix (Vol.2).

3.7.1 Introduction.

The X-ray analysis of the deca-osmium penta-hydrido monoanion $[H_5Os_{10}(CO)_{24}]^-$ (1), was carried out to complete a series of related high nuclearity Os_{10} hydrido clusters. The synthesis and X-ray structure of the tetra-hydrido analogoue $[H_4Os_{10}(CO)_{24}]^{2-}$ (2) was reported previously and whose ^1H n.m.r. spectrum in CH_2Cl_2 at ambient temperatures revealed a singlet, with no $^{187}Os-^1H$ satellites detected, due to the broadness of the signal.[27] These results were consistent with the four hydrogen atoms being fluxional in solutions at room temperature. However, on slowly cooling a solution of (2) to 193 K in $CDCl_2$, the broad singlet was observed to disappear, giving rise to two new broad signals in a ratio of 1:1. The signals were still too broad to observe $^{187}Os-^1H$ satellites, and therefore at low temperatures there appeared two types of hydride environments, with one of the four protons migrating into the central octahedron.[100]

The dianion (2) was found to react reversibly with I_2 to yield the monoanion $[H_4Os_{10}(CO)_{24}I]^-$, (scheme 3.7.1), whose ^1H n.m.r spectrum in $CDCl_2$ at ambient temperatures showed two broad peaks in a ratio of 3:1.[100] The tetra-hydrido dianion (2) was also found to react with an equivalent of $[Cu(NCMe)_4]$ $[PF_6]$ to yield the mixed-metal cluster anion $[H_4Os_{10}(CO)_{24}Cu(NCMe)]^-$ (scheme 3.7.1). The ^1H n.m.r. spectrum in $CDCl_2$ at ambient temperatures revealed two broad overlapping resonances in a ratio of 3:1.[100] These results were found to be consistent with the solutions of the dianion (2) and its derivatives, having three interstitial hydrogen atoms in three of the four tetrahedral caps and one in the octahedral cage. The X-ray structural data of the deca-osmium dianion $[H_4Os_{10}(CO)_{24}]^{2-}$ (2) was also found to support the presence of these interstitial hydrido ligand sites in the solid state (sections 3.1 and 3.7.3).[27]

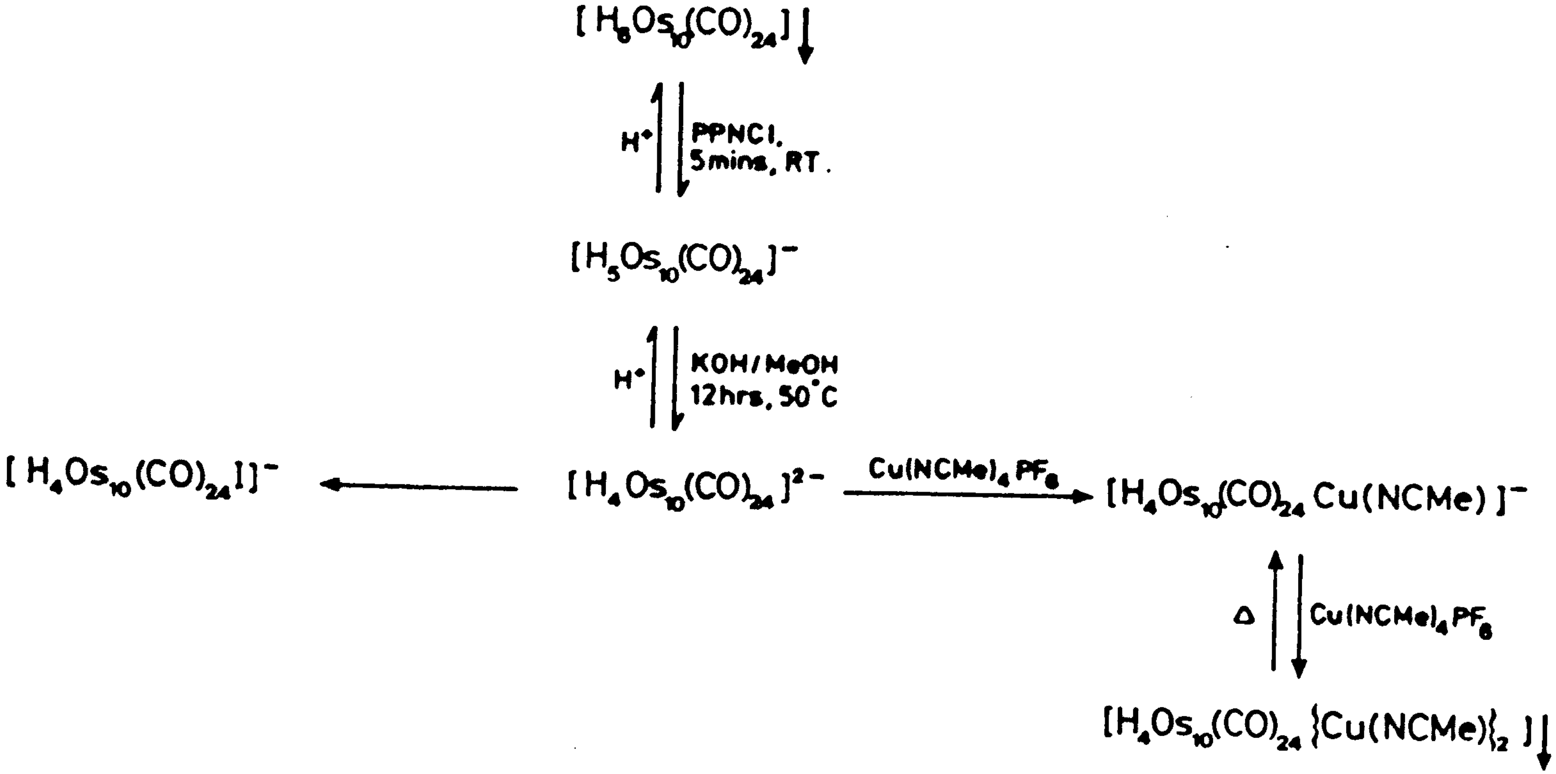
[H8Os10(CO)24]↓
H+
PPNCl,
5mins, RT.
[H5Os10(CO)24]−
H+
KOH/MeOH
12hrs, 50°C
[H4Os10(CO)24I]−
[H4Os10(CO)24]2−
Cu(NCMe)4PF6
[H4Os10(CO)24Cu(NCMe)]−
Δ
Cu(NCMe)4PF6
[H4Os10(CO)24{Cu(NCMe)}2]↓

Scheme 3.7.1.

Protonation of the dianion (2) in CH_2Cl_2 was found to yield the penta-hydrido monoanion $[H_5Os_{10}(CO)_{24}]^-$ (1), characterised previously only by i.r. spectroscopy.[27] The ^1H n.m.r. spectrum of (1) at ambient temperatures showed two broad signals in the intensity ratio of 4:1. The spectrum was found to remain unaltered on cooling to 193 K, and due to the broadness of the two signals, no $^{187}Os-^1H$ satellites could be detected, (Figure 3.7.1).[100] Therefore, in solutions it was possible that all five hydrogen atoms occupied the five interstitial sites in the metal core skeleton of the deca-osmium penta-hydrido monoanion (1). The X-ray structure of (1) was therefore of interest in establishing a pattern in the solid state geometry of the Os_{10} metal framework analogous to that observed by McPartlin and co-workers for the tetra-hydrido dianion (2) and perhaps support the n.m.r. evidence in proposing interstitial bonding modes of the five hydrogen atoms in the monoanion cluster compound $[H_5Os_{10}(CO)_{24}]^-$ (1).

3.7.2 Structural description of $[H_5Os_{10}(CO)_{24}]^-$ (1).

X-ray analysis of the penta-hydrido monoanion (1) established a tetra-capped octahedral metal core geometry, Figure 3.7.2(a). The six osmium atoms, Os(2), Os(3), Os(4), Os(6), Os(8) and Os(10) defined the octahedron, with four triangular faces further capped by the remaining atoms; faces, Os(2)-Os(3)-Os(4) capped by Os(1); Os(2)-Os(6)-Os(10) capped by Os(5); Os(3)-Os(6)-Os(8) capped by Os(7); and Os(4)-Os(8)-Os(10) capped by Os(9). The four capping osmium atoms were found to carry three terminal carbonyl groups, whereas the six metal atoms defining the octahedron were bonded to two terminal -CO groups. All 24 carbonyl ligands displayed expected

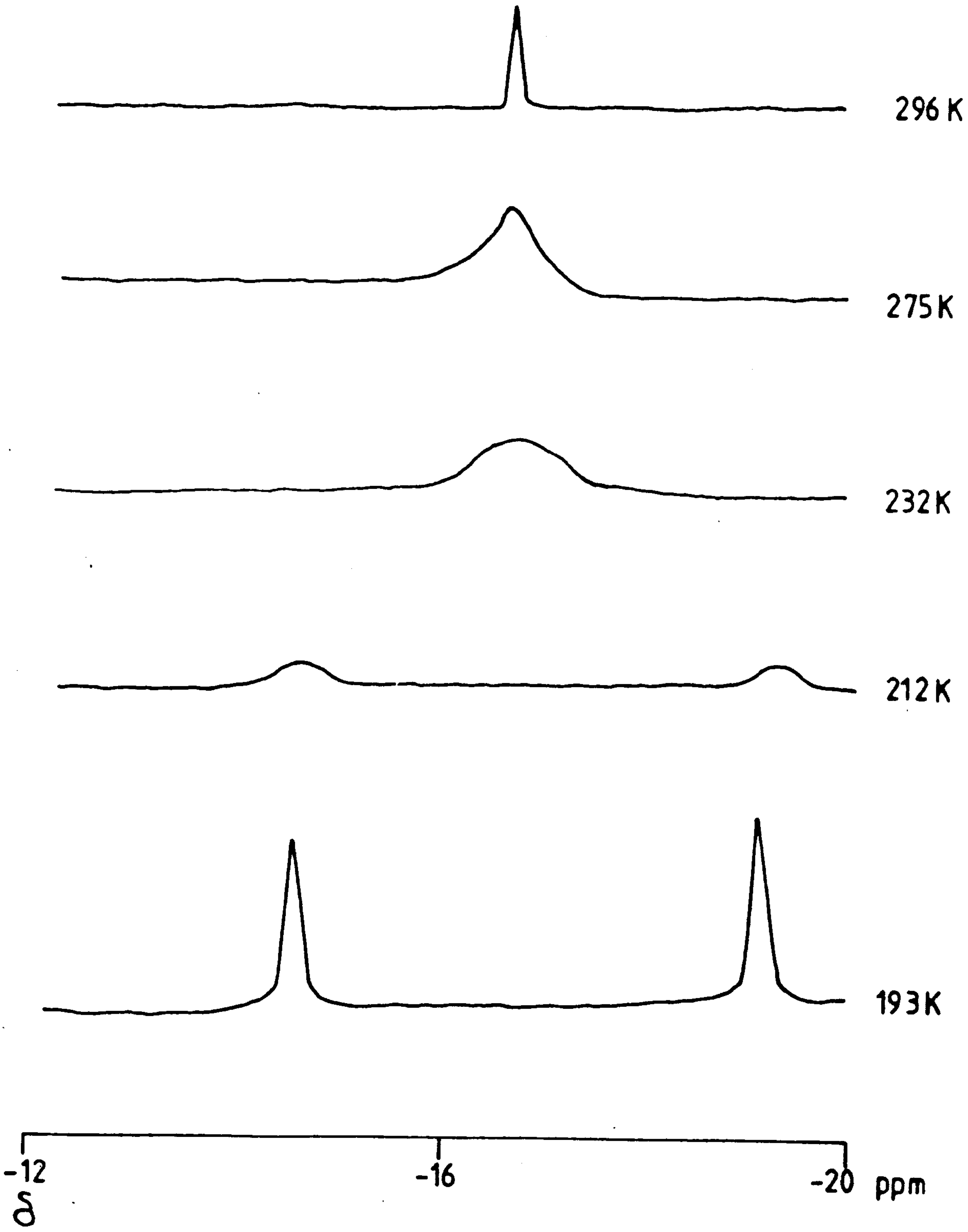

Figure 3.7.1. The ^1H n.m.r. spectrum of $[H_5Os_{10}(CO)_{24}][PPN]$ (2).[100]

linearity {Os-C-O range 162-178(4)^{o}}. Interestingly, the carbonyl distribution in (1) was found to be very similar to the carbido dianion[26] $[Os_{10}C(CO)_{24}]^{2-}$, {Figure 3.7.2(b)}. Although it was impossible to locate the hydrido ligands from the X-ray analysis , the presence of five H-atoms (contributing a total of 5 electrons) was deduced from the observed Os_{10} geometry, for which skeletal electron counting methods[92,94] require the same number of electrons as accommodated in the carbido cluster $[Os_{10}C(CO)_{24}]^{2-}$, (which possess 134e). The presence of the H-ligands was also inferred from the ^{1}H n.m.r. data, which showed two broad singlets in a ratio of 4:1. Examination of the carbonyl distribution in the monoanion $[H_5Os_{10}(CO)_{24}]^-$ showed no displacement, with the ligands remaining almost perpendicular to the faces of the metal core, a feature not normally observed when hydrogen atoms are attached to the surface of a cluster.[10,15]

3.7.3 Discussion and results.

The tetra-capped octahedral metal core structure established for the penta-hydrido monoanion $[H_5Os_{10}(CO)_{24}]^-$ (1), {Figure 3.7.3(a)}, was found to be similar in geometry to that adopted by the tetra-hydrido analogue $[H_4Os_{10}(CO)_{24}]^{2-}$ (2),[27] {Figure 3.7.3(b)}. Both metal frameworks were similar to those characterised for the mono-hydrido carbido cluster $[HOs_{10}C(CO)_{24}]^-$ (3)[25] and the non-hydrido dianion $[Os_{10}C(CO)_{24}]^{2-}$ (4),[26] {Figures 3.7.3(c) and 3.7.3(d), respectively}. The important difference in the overall structures of (1) and (2) was the absence of the carbido atom in the octahedral cavity. Table 3.7.3 lists the Os-Os bond lengths for penta-hydrido monoanion (1) and the closely related tetra-hydrido dianion (2).

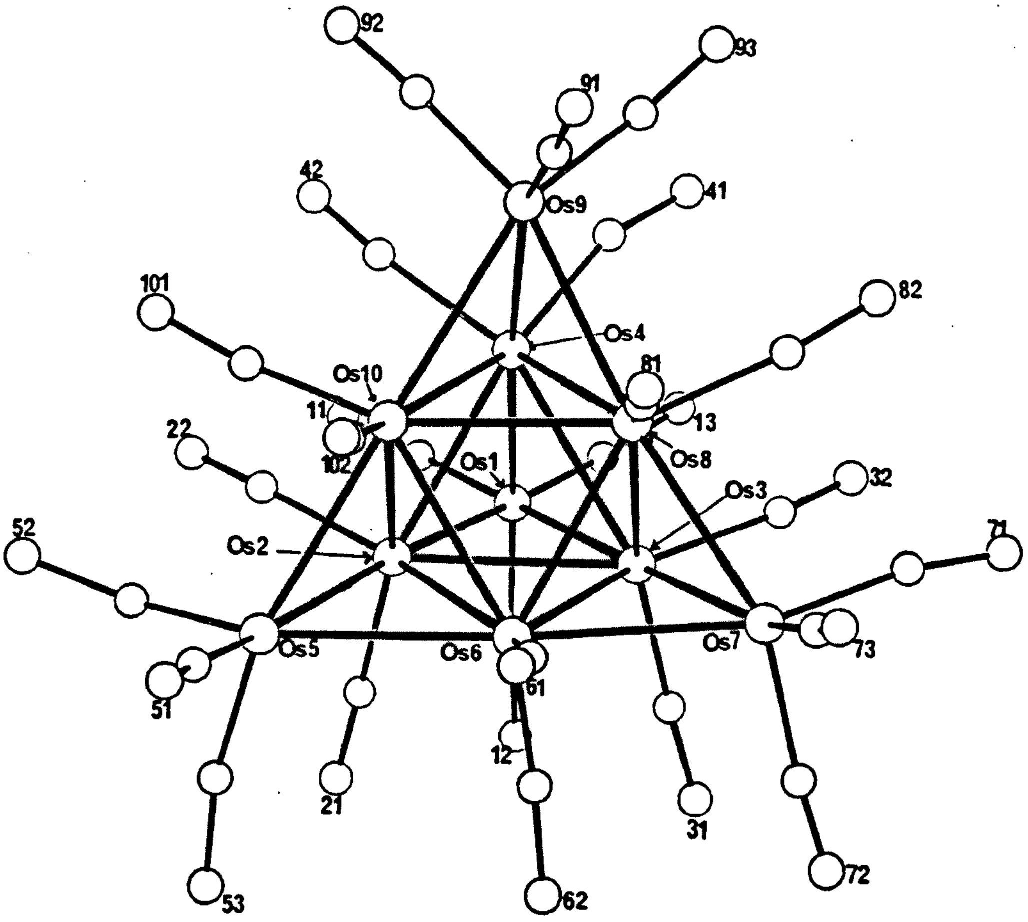

Figure 3.7.2(a). The molecular structure of the penta-hydrido monoanion $[H_5Os_{10}(CO)_{24}]^-$. The carbonyl C atoms have the same numbering as the O atoms to which they are attached.

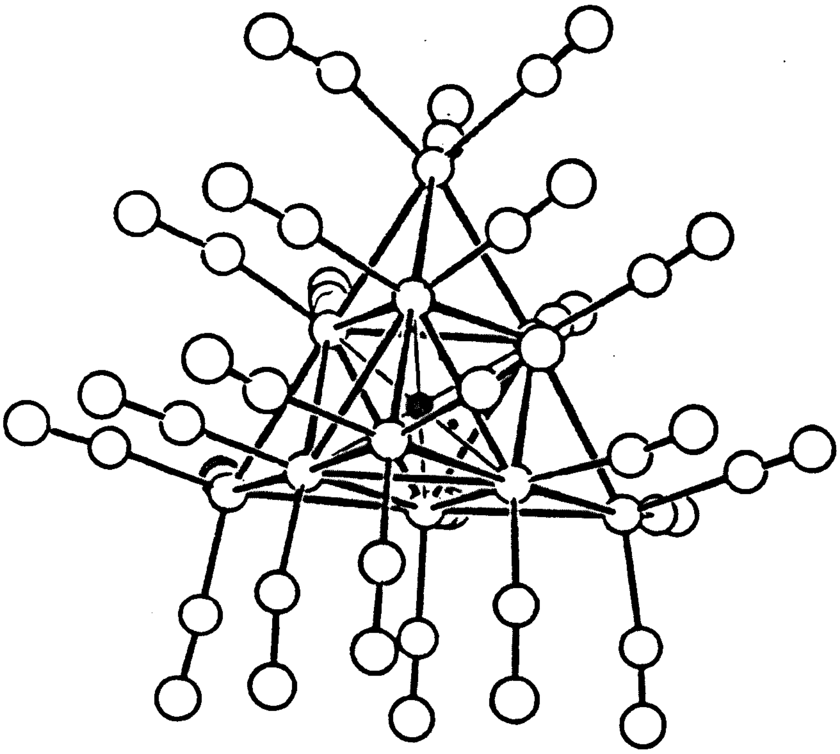

Figure 3.7.2(b). The carbonyl distribution in the decaosmium carbido dianion $[Os_{10}C(CO)_{24}]^{2-}$.[26]

The range of Os-Os bond lengths in the structure of the penta-hydrido monoanion $[H_5Os_{10}(CO)_{24}]^-$ (1) {2.748-2.923(3) Å} was found to be similar to that observed in the tetra-hydrido dianion $[H_4Os_{10}(CO)_{24}]^{2-}$ (2) {2.750-2.924(2) Å}. The mean of the 24 Os-Os bond lengths in (1) {2.834(3) Å} was observed to be 0.005 Å longer than the corresponding mean bond distance in (2) {2.829(2) Å}. The mean Os-Os bond distance of the octahedral cavity in (1) {2.845(3) Å} was found to be slightly shorter than the corresponding mean in (2) {2.857(1) Å}. However, both distances were found to be significantly shorter than the mean bond of the osmium octahedron encapsulating a carbido atom in $[HOs_{10}C(CO)_{24}]^-$ (3) {2.883(1) Å},[25] as expected from the known tendency of interstitial C atoms to produce polyhedral expansion.[101] The three Os-Os bonds associated with Os(1), Os(5), Os(7) and Os(9) tetra-capping the octahedral metal core, {Figure 3.7.2(a)} showed similar asymmetry, with one Os-Os bond significantly longer than the other two, {Table 3.7.3}. Importantly, it was the three bonds from Os(9), capping the triangular face Os(4)-Os(8)-Os(10), which exhibited the more marked asymmetry in the bond lengths, with the bond Os(9)-Os(10) {2.923(3) Å} being longer not only to the mean of the two remaining bonds of the μ_3-cap, {mean of the bonds Os(4)-Os(9) and Os(8)-Os(9) = 2.809(3) Å}, but also being the longest Os-Os bond in the structure, {Table 3.7.3}.

There was no sign of the characteristic displacement of the carbonyl ligands in (1), normally observed when hydrogen atoms are attached at the polyhedral surface of a cluster,[10,15] with the equatorial carbonyl groups at each of the four osmium atoms associated with each Os_4 cap remaining almost perpendicular to the faces of the metal core:

cap from Os(1)

mean cis Os-Os-C angles at bonds,

Os(1)-Os(2) = $95.0(3)^{\circ}$

Os(1)-Os(3) = $96.0(3)^{\circ}$

Os(1)-Os(4) = $99.0(3)^{\circ}$

cap from Os(5)

Os(5)-Os(2) = $94.0(3)^{\circ}$

Os(5)-Os(6) = $98.0(3)^{\circ}$

Os(5)-Os(10) = $97(3)^{\circ}$

cap from Os(7)

Os(7)-Os(3) = $95.0(3)^{\circ}$

Os(7)-Os(6) = $93.0(3)^{\circ}$

Os(7)-Os(8) = $93.0(3)^{\circ}$

cap from Os(9)

Os(9)-Os(4) = $91.0(3)^{\circ}$

Os(9)-Os(8) = $95.0(3)^{\circ}$

Os(9)-Os(10) = $100.0(3)^{\circ}$

Importantly, the carbonyl distribution in the penta-hydrido monoanion (1), {Figure 3.7.2(a)}, was found to be similar to that established for the non-hydrido carbido cluster $[Os_{10}C(CO)_{24}]^{2-}$ (4),[26] {Figure 3.7.2(b)}. From similar observations between the carbonyl distribution in the hexa-ruthenium hydrido cluster,[22] $[Ru_6H(CO)_{18}]^-$, and in the non-hydrido osmium dianion,[23] $[Os_6(CO)_{18}]^{2-}$, McPartlin and co-workers proposed the presence of the first interstitial H-atom in a carbonyl cluster which was subsequently confirmed by a neutron diffraction study.[24] The workers also reported that from the very close similarity of the carbonyl distribution in the mono-hydrido cluster $[HOs_{10}C(CO)_{24}]^-$ (3), {Figure

3.7.3(c)}, to that established for the carbido dianion (4), {Figure 3.7.3(d)}, the H-ligand was presumed to be interstitial.[25] The X-ray structural data of (3) supported the hydride being encapsulated in one of the capping tetrahedral sites. A small expansion of this cap was observed, with a mean Os-Os bond of 2.856(1) Å being longer than the mean distance of 2.837(1) Å of the other three capping tetrahedra. Importantly, this mean bond of the larger tetrahedral cap was significantly bigger than the mean of the four capping groups in the parent non-hydrido deca-osmium dianion (4) {2.835(2) Å}.

The workers also used the same analogy to deduce the interstitial nature of the four hydrido ligands in the tetra-hydrido osmium dianion $[H_4Os_{10}(CO)_{24}]^{2-}$ (2). The mean Os-Os bond length of one of the four capping tetrahedra {2.809(2) Å} was found to be significantly shorter than the mean bond of the three remaining caps, {2.839(2), 2.839(2), and 2.829(2) Å}.[27] They also observed that the mean bonds of the three larger Os_4 capping units were markedly longer than the corresponding mean bond of the two capping tetrahedra in the octanuclear osmium dianion $[Os_8(CO)_{22}]^{2-}$ {2.793(1) Å}.[28] From these results they proposed that three of the four H-atoms were located in the three enlarged Os_4 caps. The fourth hydride in the tetra-hydrido dianion (2) was thought to be interstitial in the Os_6 octahedral cavity, since the mean of the 12 Os-Os bonds defining the octahedron {2.857(1) Å} was markedly longer than the corresponding mean of the octahedral cavity in $[Os_8(CO)_{22}]^{2-}$ {2.831(1) Å}, the largest non-carbido osmium cluster previously reported.[28]

Using the above structural patterns in deducing potential interstitial sites for the H-ligands in (2) and (3), the geometry of the penta-hydrido deca-osmium cluster $[H_5Os_{10}(CO)_{24}]^-$ (1) was

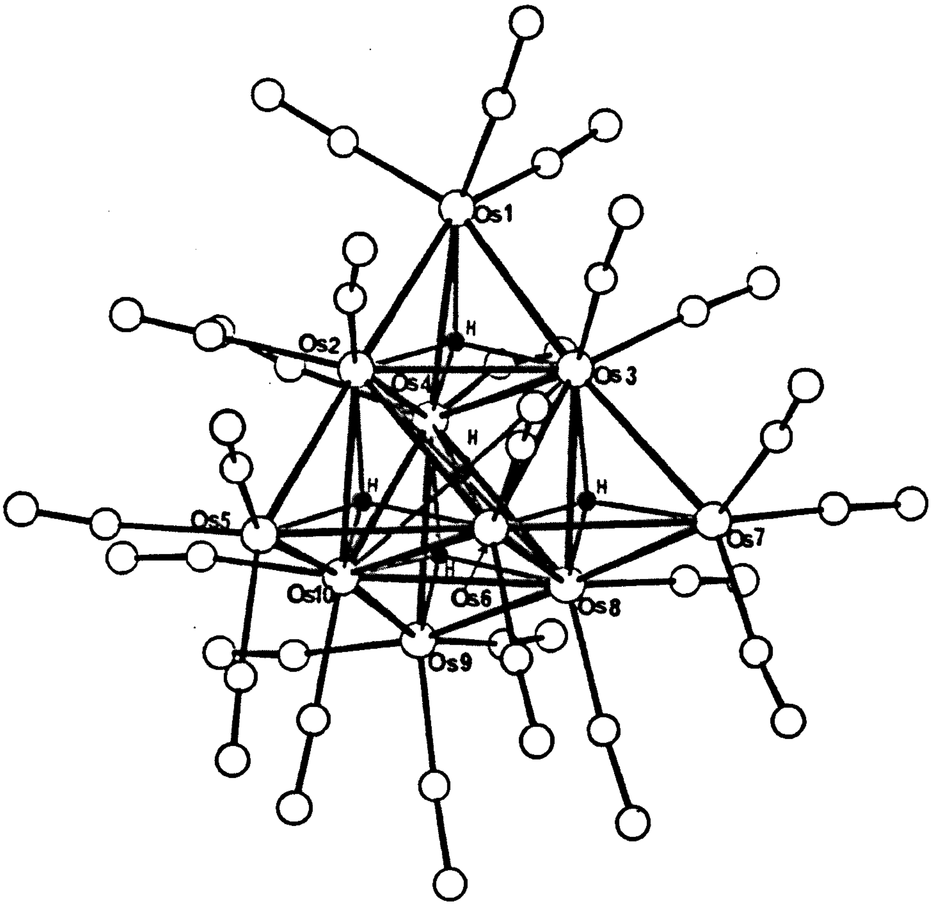

Figure 3.7.3(a). The solid state structure of the decaosmium pentahydrido monoanion $[H_5Os_{10}(CO)_{24}]^-$ (1), showing all five H atoms occupying interstitial sites.

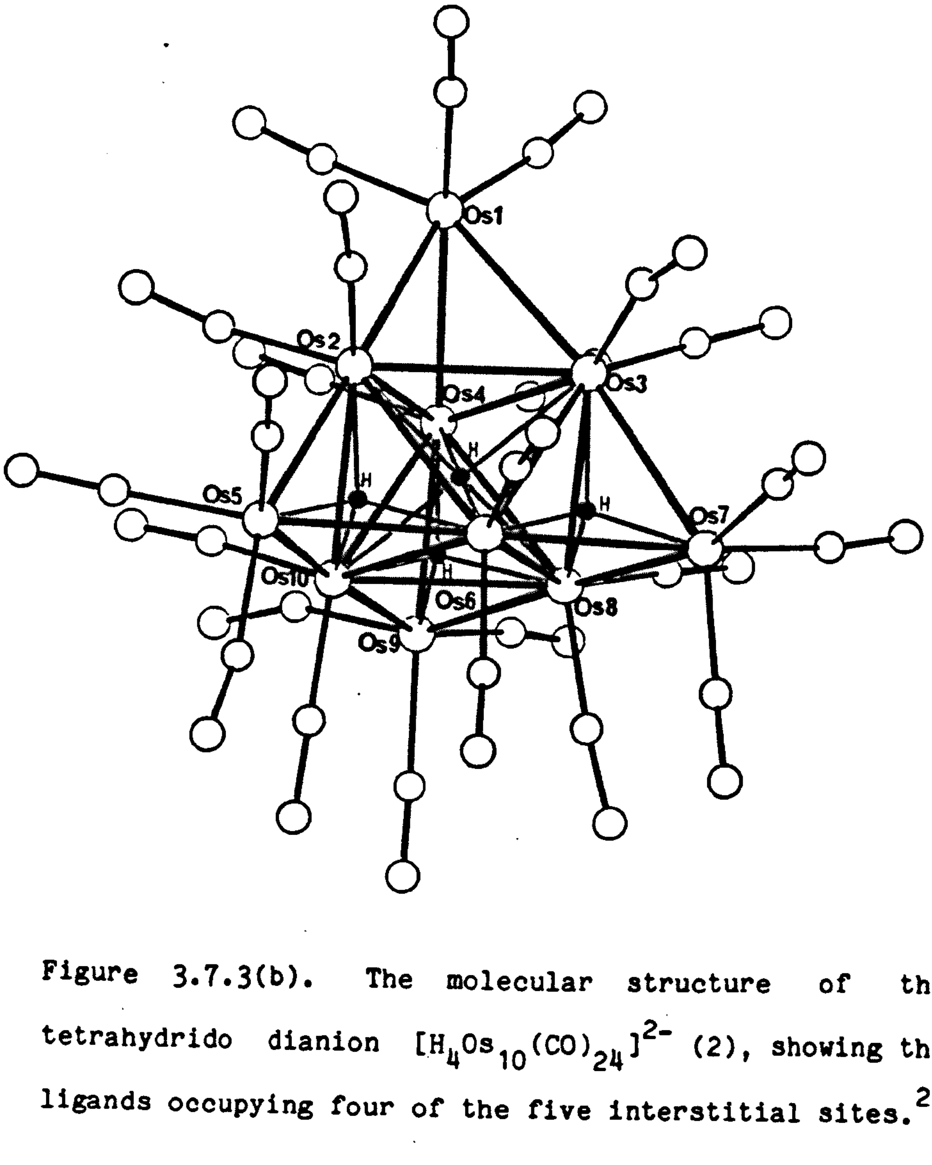

Figure 3.7.3(b). The molecular structure of the decaosmium tetrahydrido dianion $[H_4Os_{10}(CO)_{24}]^{2-}$ (2), showing the four hydrido ligands occupying four of the five interstitial sites.[27]

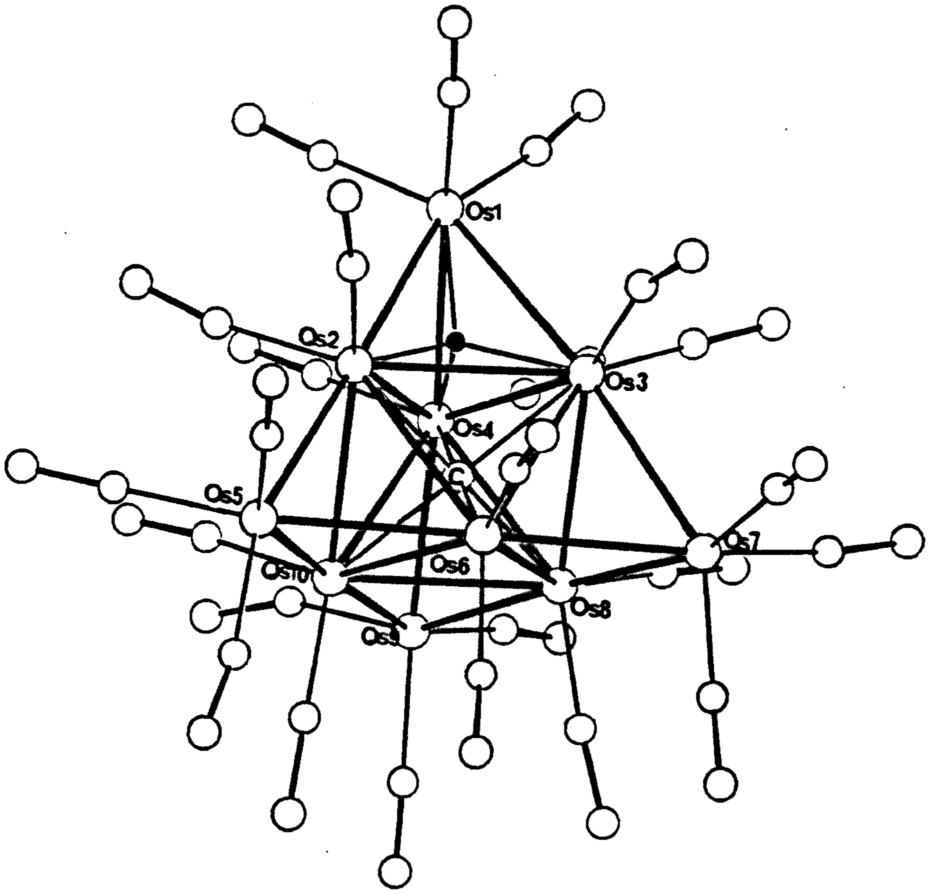

Figure 3.7.3(c). The molecular structure of the decaosmium carbido monoanion $[HOs_{10}C(CO)_{24}]^-$, showing the hydrido ligand occupying an interstitial site in one of the four tetrahedral caps (3).[25]

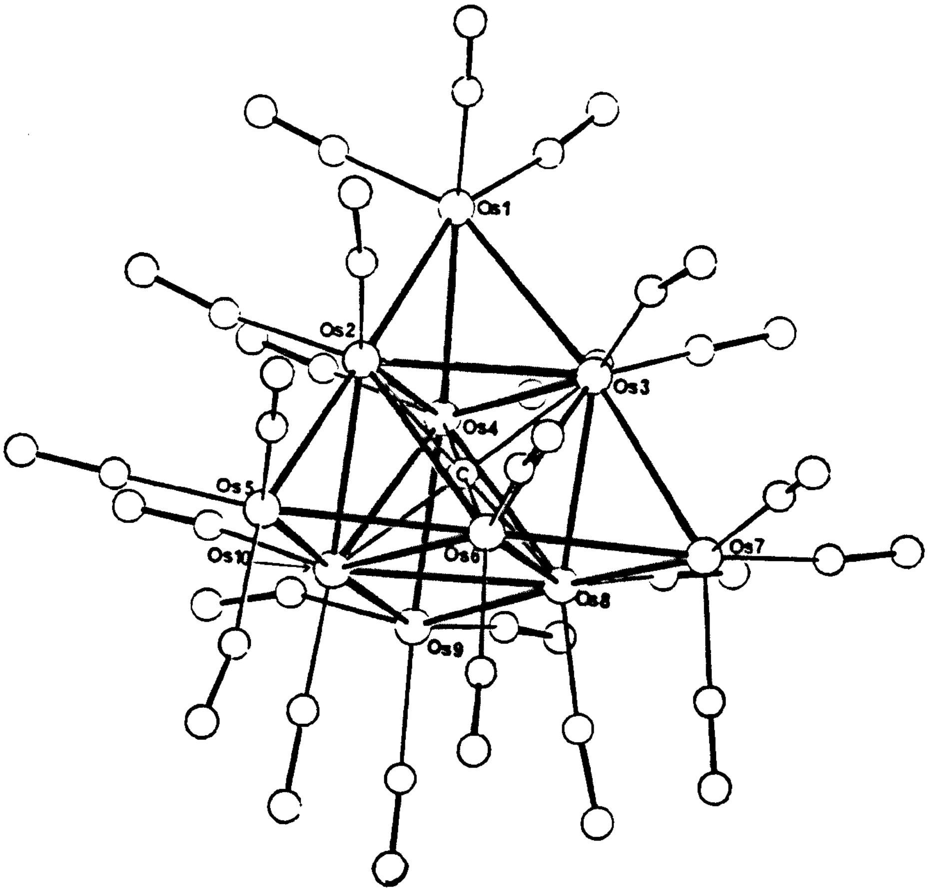

Figure 3.7.3(d). Molecular structure of the carbido dianion $[Os_{10}C(CO)_{24}]^{2-}$ (4).[26]

examined for similar trends in Os-Os bond lengths. The mean of the 12 Os-Os bond lengths defining the Os_6 octahedral metal core in (1) was observed to be 2.845(3) Å, (Table 3.7.3). This mean bond distance was found to be smaller than the corresponding mean bond in (2) {2.857(2) Å}, but was markedly longer in comparison to that observed in the octanuclear dianion $[Os_8(CO)_{22}]^{2-}$ {2.831(1) Å}.[28] This evident expansion of the octahedral cavity in (1), supported one of the five H-ligands occupying this interstitial site. Using the same analogy, the six Os-Os bonds of the four tetrahedral caps in the structures of the deca-osmium penta-hydrido monoanion (1) and the closely related tetra-hydrido dianion (2) were examined:

<u>Table</u> <u>3.7.3(b)</u>

cap from Os(1)

bond	(1)	(2)[27]
Os(1)-Os(2)	2.759(3)	2.804(2)
Os(1)-Os(3)	2.799(3)	2.776(2)
Os(1)-Os(4)	2.894(3)	2.795(2)
Os(2)-Os(3)	2.865(3)	2.881(2)
Os(2)-Os(4)	2.794(3)	2.831(2)
Os(3)-Os(4)	2.910(3)	2.768(2)
	--------	--------
mean	2.837(3)	2.809(2)

cap from Os(5)

bond	(1)	(2)
Os(2)-Os(5)	2.764(3)	2.853(2)
Os(2)-Os(6)	2.900(3)	2.903(2)
Os(2)-Os(10)	2.799(3)	2.823(2)
Os(5)-Os(6)	2.903(3)	2.796(2)
Os(5)-Os(10)	2.842(3)	2.776(2)
Os(6)-Os(10)	2.833(3)	2.881(2)
	--------	--------
mean	2.840(3)	2.839(2)

cap from Os(7)

bond	(1)	(2)
Os(3)-Os(6)	2.885(3)	2.903(2)
Os(3)-Os(7)	2.809(3)	2.750(2)
Os(3)-Os(8)	2.885(3)	2.817(2)
Os(6)-Os(7)	2.862(3)	2.780(2)
Os(6)-Os(8)	2.783(3)	2.924(2)
Os(7)-Os(8)	2.748(3)	2.863(2)
mean	2.829(3)	2.839(2)

cap from Os(9)

bond	(1)	(2)
Os(4)-Os(8)	2.873(3)	2.810(2)
Os(4)-Os(9)	2.813(3)	2.775(2)
Os(4)-Os(10)	2.834(3)	2.826(2)
Os(8)-Os(9)	2.769(3)	2.888(2)
Os(8)-Os(10)	2.785(3)	2.917(2)
Os(9)-Os(10)	2.923(3)	2.754(2)
mean	2.833(3)	2.828(2)

The above results showed that in the structure of the penta-hydrido monoanion $[H_5Os_{10}(CO)_{24}]^-$, the mean Os-Os bond distance from cap 1 {2.837(3) Å} was noteably larger than the corresponding mean bond in the tetra-hydrido dianion $[H_4Os_{10}(CO)_{24}]^{2-}$ (2), {2.809(2) Å}. This was significant, since McPartlin and co-workers had previously observed[27] that this mean bond in the tetra-hydrido cluster (2) was very close to the mean of the two capping tetrahedra in the octanuclear dianion $[Os_8(CO)_{22}]^{2-}$ {2.793(1) Å}.[28] From this comparison, it was evident that the tetrahedral cap from Os(1) in the dianion (2) had not enlarged significantly to encapsulate an H-atom. In contrast, the analogous cap in the penta-hydrido cluster $[H_5Os_{10}(CO)_{24}]^-$ (1) had enlarged by 0.028 Å to that in (2) and 0.044 Å to the mean of the two caps in the octanuclear dianion $[Os_8(CO)_{22}]^{2-}$. This indicated that perhaps the second H-ligand was occupying this interstitial tetrahedral site. Comparison of the remaining three caps in (1) and (2) {Table 3.7.3(b)}, exhibited very similar mean Os-Os bond distances. Importantly, the mean bonds of these three caps in both the penta-hydride (1) and the tetra-hydride (2) signified marked expansion of the Os_4 caps when compared to the mean of the two Os_4 capping units in the octanuclear dianion $[Os_8(CO)_{22}]^{2-}$ {mean 2.793(1) Å}; The tetrahedral cap from Os(5) had enlarged by 0.047 Å in (1) and 0.046 Å in (2); cap from Os(7) had enlarged by 0.036 Å in (1) and 0.046 Å in (2); cap from Os(9) had enlarged by 0.040 Å in (1) and 0.035 Å in (2). The observed enlargement of all four tetrahedral caps in the deca-osmium penta-hydrido cluster compound (1) provided structural evidence to support that four of the five H-ligands were sited at these interstitial holes.

3.7.4 Conculsions.

The X-ray analysis of the deca-osmium non-carbido cluster $[H_5Os_{10}(CO)_{24}]^-$ (1) established a pattern in the tetra-capped octahedral metal geometry, supporting that all five interstitial sites of the metal core could be occupied by the H-atoms. These results further reflected upon the tendency of hydrido ligands to become encapsulated within the metal frameworks of high nuclearity osmium clusters:

cluster	H-site
$[HOs_{10}C(CO)_{24}]^-$ (3)	tetrahedral
$[H_4Os_{10}(CO)_{24}]^{2-}$ (2)	3 tetrahedral and one octahedral
$[H_5Os_{10}(CO)_{24}]^-$ (1)	4 tetrahedral and one octahedral

All three deca-osmium clusters were found to adopt similar tetra-capped octahedral metal core geometries, and the characteristic feature relating all three clusters was the close similarity in the carbonyl distribution to that previously established in the solid state structure of the non-hydrido cluster compound $[Os_{10}C(CO)_{24}]^{2-}$ (4).[26] Using earlier strategies adopted in deducing the interstitial sites for the cluster species (2) and (3), comparative study of the geometry of the penta-hydrido cluster (1) indicated that, assuming the interstitial location of the hydrido-ligands in solutions deduced from ^1H n.m.r data was maintained in the solid state, it appeared that all five hydrogen atoms were encapsulated within the 10 metal atom polyhedron. Examination of respective Os-Os bond lengths in (1), indicated that four of the five H-atoms were sited within the four tetrahedral caps and the fifth in the Os_6 octahedral cavity.

Table 3.7.3.

bond	(1)	(2)[27]
Os(1)-Os(2)	2.759(3)	2.804(2)
Os(1)-Cs(3)	2.799(3)	2.776(2)
Os(1)-Os(4)	2.894(3)	2.795(2)
Os(2)-Os(3)	2.865(3)	2.881(2)
Os(2)-Os(4)	2.794(3)	2.831(2)
Os(2)-Os(5)	2.764(3)	2.853(2)
Os(2)-Os(6)	2.900(3)	2.903(2)
Os(2)-Os(10)	2.799(3)	2.823(2)
Os(3)-Os(4)	2.910(3)	2.768(2)
Os(3)-Os(6)	2.885(3)	2.903(2)
Os(3)-Os(7)	2.809(3)	2.750(2)
Os(3)-Os(8)	2.885(3)	2.817(2)
Os(4)-Os(8)	2.873(3)	2.810(2)
Os(4)-Os(9)	2.813(3)	2.775(2)
Os(4)-Os(10)	2.834(3)	2.826(2)
Os(5)-Os(6)	2.903(3)	2.796(2)
Os(5)-Os(10)	2.842(3)	2.776(2)
Os(6)-Os(7)	2.862(3)	2.780(2)
Os(6)-Os(8)	2.783(3)	2.924(2)
Os(6)-Os(10)	2.833(3)	2.881(2)
Os(7)-Os(8)	2.748(3)	2.863(2)
Os(8)-Os(9)	2.769(3)	2.888(2)
Os(8)-Os(10)	2.785(3)	2.917(2)
Os(9)-Os(10)	2.923(3)	2.754(2)

Section 3.8. X-ray analysis of the undeca-osmium hydrido cluster $[HOs_{11}C(CO)_{27}][PPh_3Me]$ (1).

Crystal data, methods of data collection, structure solution and refinement for (1) are presented in section 4.14.

Final tables of atomic co-ordinates, bond lengths, inter-bond angles, intermolecular and intramolecular distances are given in the appendix (Vol.2).

3.8.1 Introduction.

A great number of high nuclearity metal carbonyl clusters have been prepared by pyrolysis of mononuclear or trinuclear starting materials. The reaction of $Os_3(CO)_{12}$ was proved to be sensitive to temperature, time and moisture, yielding a range of nuclearities,[102-108] the highest being the deca-osmium dianion $[Os_{10}C(CO)_{24}]^{2-}$.[26] The X-ray studies of the hydrido deca-osmium clusters $[HOs_{10}C(CO)_{24}]^-$, and $[H_4Os_{10}(CO)_{24}]^{2-}$ showed characteristic features in their respective metal core geometries which supported the presence of interstitial H-ligands (sections 3.1 and 3.7.3).[25,27] The first undeca-osmium cluster $[Os_{11}C(CO)_{27}]^{2-}$, being one of the products resulting from the pyrolysis of $Os_3(CO)_{12}$, was structurally characterised by X-ray diffraction of the $[PPh_3Me]^+$ salt.[109] Protonation of the dianion was found to yield the monoanion hydrido cluster $[HOs_{11}C(CO)_{27}]^-$ (1). It has been recognised that as cluster size increases, the ratio of surface area to the number of metal atom decreases, and as a result interstitial ligands become important in preventing surface ligand congestion around the metal polyhedron. Therefore the X-ray analysis of the first undeca-osmium hydrido cluster (1) was of interest in establishing the bonding mode of the H-atom and perhaps further support the preference of the ligand to occupy interstitial sites in these high nuclearity osmium clusters.

3.8.2 Structural description of $[HOs_{11}C(CO)_{27}]^-$ (1).

Due to the poor crystallographic data, the metal framework of (1) was well established, but the positions of all the light atoms were not found with certainty. The Os_{11} metal core structure adopted by (1) in the solid state could be described as a bi-capped square pyramid sharing its square face with a trigonal prism, which was also bi-capped on its triangular faces, {Figure 3.8.2(a)}. The square pyramid was defined by the basal atoms Os(2), Os(4), Os(6), Os(8) with Os(3) forming the apex of the pyramid. The faces, Os(2)-Os(4)-Os(3) and Os(3)-Os(6)-Os(8) were capped by Os(1) and Os(7), respectively. The fused trigonal prism was defined by the atoms, Os(2), Os(4), Os(6), Os(8), Os(10) and Os(11), whose faces Os(2)-Os(6)-Os(11) and Os(4)-Os(8)-Os(10), were capped by the Os(5) and Os(9), respectively. The carbido atom was found to be interstitial in the prismatic cavity. Although satisfactory refinement of the carbonyl atom parameters was not achieved in the structure of the monohydride (1), reasonable maxima corresponding to 26 of the 27 carbonyl atoms were located in a series of difference-Fourier syntheses and showed approximately the same distribution to those established in the copper derivative $[Os_{11}C(CO)_{27}Cu(NCMe)]^-$, {Figure 3.8.2(b)}.[109] The capping osmium atoms, Os(1), Os(5), Os(7) and Os(9) were found to carry three terminal carbonyl ligands, whereas the remaining seven osmium atoms carried two terminal -CO groups, {Figure 3.8.2(a)}. All attempts to locate suitable positions for the atoms of a phenyl ring of the $[PPh_3Me]^+$ cation and a μ_2-carbonyl group thought to bridge the edge, Os(10)-Os(11), by comparison with the structure of the $Os_{11}Cu$ derivative and also inferred from the i.r. data, had failed.

3.8.3 Discussion and Results.

The X-ray analysis of the monohydrido deca-osmium cluster $[HOs_{11}C(CO)_{27}]^-$ (1), (Figure 3.8.2(a)), established a metal core geometry almost identical to that previously observed in the solid state structures of the related dianion $[Os_{11}C(CO)_{27}]^{2-}$ (2),[109]

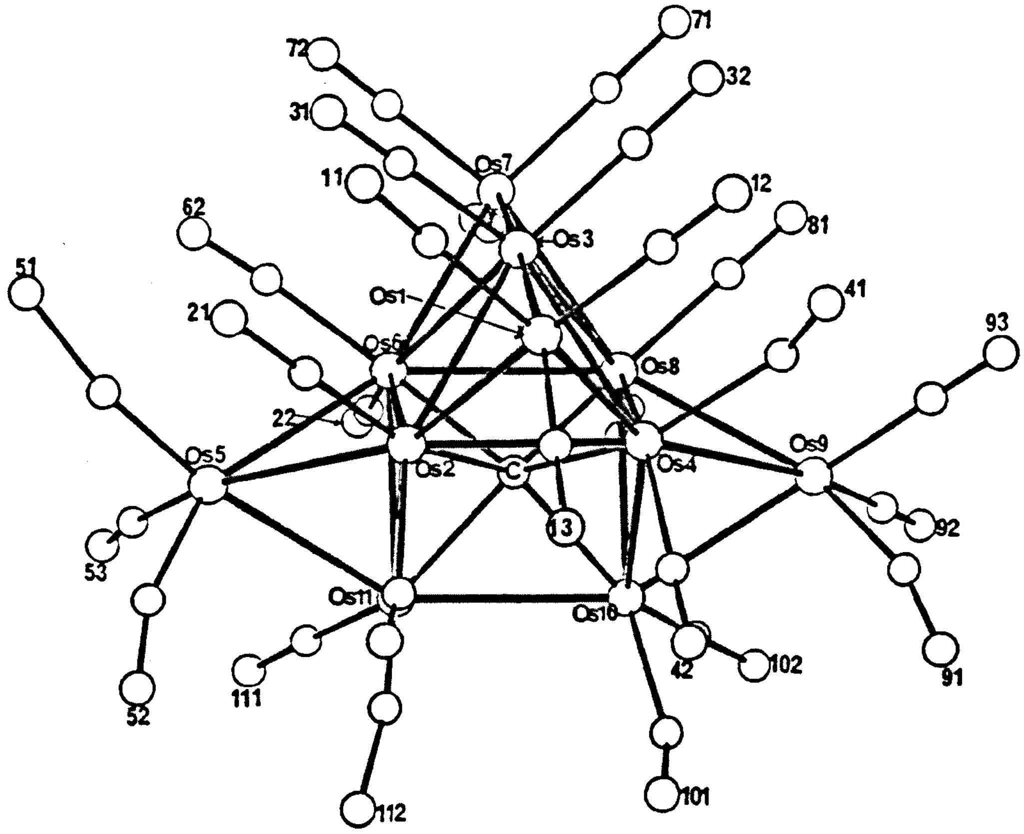

Figure 3.8.2(a). The molecular structure of the undecaosmium cluster monoanion $[HOs_{11}C(CO)_{27}]^-$. The carbonyl C atoms have the same numbering as the O atoms to which they are attached.

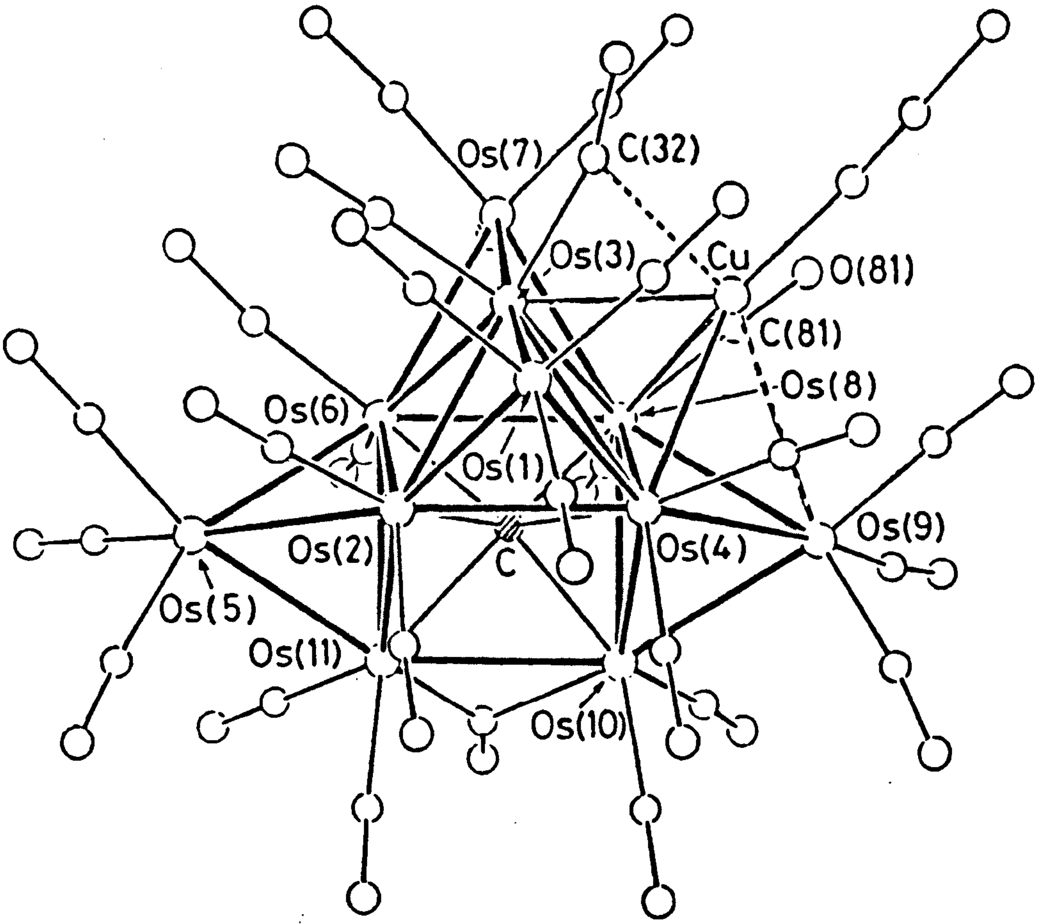

Figure 3.8.2(b). Molecular structure of the copper-osmium cluster $[Os_{11}C(CO)_{27}Cu(NCMe)]^{-}$.[109]

{Figure 3.8.3(a)}, and the $Cu(NCMe)^+$ derivative $[Os_{11}C(CO)_{27}Cu(NCMe)]^-$ (3),[109] {Figure 3.8.3(b)}. The Os_{11} unit in all three structures was found to be composed of a basic trigonal prism with tetrahedral caps on both end triangular faces, and a square pyramidal cap on one square face, this in turn being bi-capped by two tetrahedra. Table 3.8.3 lists the Os-Os bonds for the related cluster compounds, (1), (2) and (3)

The overall range of Os-Os bond lengths in the structure of the HOs_{11} monoanion cluster (1), {2.703-2.883(8) Å} was found to be slightly smaller than the corresponding range in the Os_{11} dianion (2), {2.710-2.896(10) Å} and the $Os_{11}Cu$ derivative (3) {2.733-2.904(2) Å}. However, the mean Os-Os bond length in (1) {2.773 Å} was found to be significantly shorter than the corresponding mean distances in both (2) {2.794 Å} and (3) {2.804 Å}. In the analysis of the monohydride (1), the carbido atom was located within the trigonal prismatic cavity, with a mean Os-C bond of 2.13(9) Å. The three related structures (1), (2), and (3) were found to be the first examples of a carbido atom occupying a trigonal prismatic site in clusters of the iron triad, although clusters of the cobalt triad have been known to favour prismatic sites for interstitial carbido atoms.[110-112]

The nine Os-Os bonds defining the trigonal prism showed marked variations, with the mean of the nine bonds in (1) {2.783 Å} being significantly shorter than the corresponding mean values in (2) {2.835 Å} and (3) {2.838 Å;Table 3.8.3}. These mean Os-Os bonds in (2) and (3) were longer in comparison to normal Os-Os bond lengths, and were consistent with the known tendency of encapsulated carbido atoms to markedly lengthen surrounding M-M bonds.[25,26] Interestingly, in the monohydride (1), the trigonal prismatic cavity had not enlarged significantly, although a carbido atom was located at this

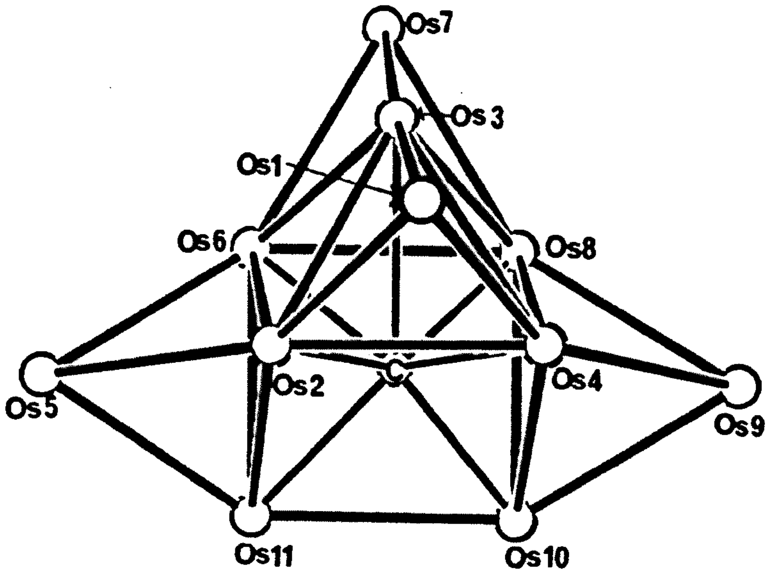

Figure 3.8.3(a). Metal core structure of the undecaosmium cluster dianion $[Os_{11}C(CO)_{27}]^{2-}$.[109]

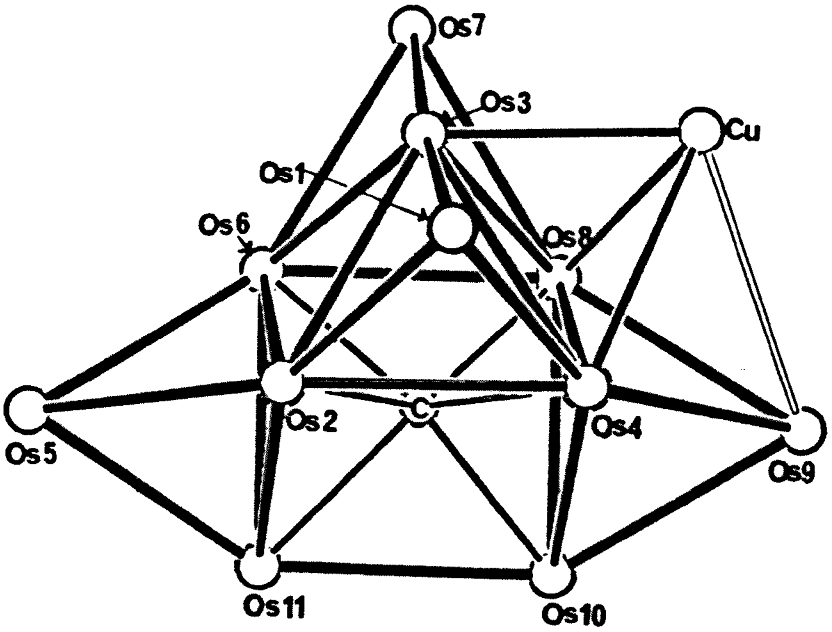

Figure 3.8.3(b). Metal core structure of the copper-osmium cluster $[Os_{11}C(CO)_{27}Cu(NCMe)]^-$ (3).

site. The longest Os-Os bond in the structure of (1), Os(1)-Os(3), was found to be 0.137 Å longer than the analogous bond in (2) and 0.150 Å longer in (3), {Table 3.8.3}. The mean of the three Os-Os bonds {Os(3)-Os(4); Os(3)-Os(8); Os(4)-Os(8); mean 2.825 Å} associated with the μ_3-Cu atom capping the face Os(3)-Os(4)-Os(8) in the structure of the copper derivative $[Os_{11}C(CO)_{27}Cu(NCMe)]^-$ (3) was found to be markedly longer than the mean bonds of the corresponding triangular faces in the hydrido analogue $[HOs_{11}C(CO)_{27}]^-$ (1) {2.744 Å} and the dianion $[Os_{11}C(CO)_{27}]^{2-}$ (3) {2.764(7) Å}. The ^1H n.m.r. spectrum of the hydrido monoanion $[HOs_{11}C(CO)_{27}]^-$ showed a hydride resonance at δ -19.1, which was found not to change over a range of temperatures down to -80 K, similar to that observed for the solutions of the deca-osmium hydrido cluster $[HOs_{10}C(CO)_{24}]^-$ (4) whose hydride signal was downfield by 4 p.p.m.[25] The ^1H n.m.r. spectrum of (1) also showed the presence of ^{187}Os-^1H satellites in the ratio of 2:1:1, {Figure 3.8.3(c)}. The X-ray analysis of the deca-osmium hydrido cluster (4) had previously revealed that the carbonyl distribution closely resembled that established in the non-hydrido analogue $[Os_{10}C(CO)_{24}]^{2-}$ (5).[26] One tetrahedral cap in the overall structure of (4) was found to be significantly enlarged in comparison to the mean of the Os-Os bonds of the four capping tetrahedra in (5), and the hydride in (4) was therefore presumed to occupy an interstitial site in this enlarged Os_4 cavity, {sections 3.1 and 3.7.3}. In view of the close similarity of the ^1H n.m.r. spectra if (1) and (4), it seemed probable that the H-ligand in the undeca-osmium cluster (1) was also sited in one of the four tetrahedral caps of the Os_{11} metal core. Table 3.8.3(b) lists the mean Os-Os bond lengths associated with the four tetrahedral caps in the structures of $[HOs_{11}C(CO)_{27}]^-$ (1) and the related Os_{11} cluster compounds $[Os_{11}C(CO)_{27}]^{2-}$ (2) and $[Os_{11}C(CO)_{27}Cu(NCMe)]^-$ (3).[109]

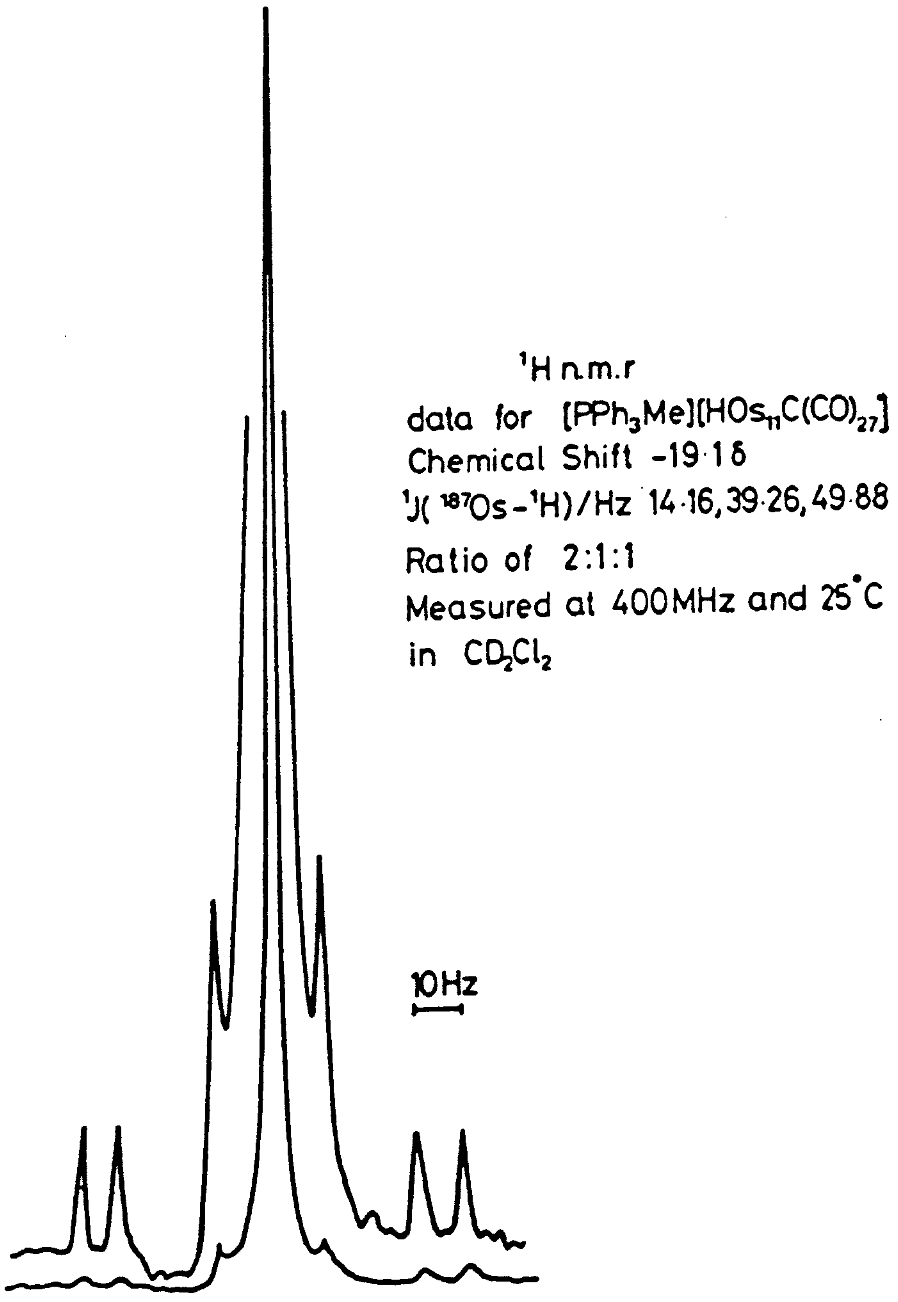
^{1}H n.m.r
data for $[PPh_3Me][HOs_{11}C(CO)_{27}]$
Chemical Shift −19·1δ
$^1J(^{187}Os-^1H)$/Hz 14·16, 39·26, 49·88
Ratio of 2:1:1
Measured at 400MHz and 25°C
in CD_2Cl_2
10Hz

Figure 3.8.3(c).

Table 3.8.3(b).

square pyramidal caps

Cap from Os(1)

	(1)	(2)	(3)
Os(1)-Os(2)	2.773(7)	2.768(8)	2.798(2)
Os(1)-Os(3)	2.883(8)	2.746(6)	2.733(2)
Os(1)-Os(4)	2.764(7)	2.760(10)	2.824(2)
mean of three bonds			
	2.807	2.758	2.785
Os(2)-Os(3)	2.759(6)	2.750(8)	2.755(2)
Os(2)-Os(4)	2.796(6)	2.840(8)	2.848(2)
Os(3)-Os(4)	2.767(7)	2.734(10)	2.822(2)
mean of six bonds			
	2.791	2.766	2.797

Cap from Os(7)

	(1)	(2)	(3)
Os(7)-Os(3)	2.814(8)	2.710(7)	2.738(2)
Os(7)-Os(6)	2.706(6)	2.788(9)	2.794(2)
Os(7)-Os(8)	2.745(6)	2.812(9)	2.790(2)
mean of three bonds			
	2.755	2.770	2.774
Os(3)-Os(6)	2.754(7)	2.753(8)	2.735(2)
Os(3)-Os(8)	2.764(7)	2.780(7)	2.827(2)
Os(6)-Os(8)	2.800(6)	2.831(9)	2.847(2)
mean of six bonds			
	2.764	2.779	2.788

Trigonal Prism caps.

Cap from Os(5)

	(1)	(2)	(3)
Os(5)-Os(2)	2.773(7)	2.782(6)	2.813(2)
Os(5)-Os(6)	2.777(6)	2.803(7)	2.801(2)
Os(5)-Os(11)	2.728(7)	2.739(7)	2.739(2)
mean of three bonds			
	2.759	2.774	2.784
Os(2)-Os(6)	2.703(8)	2.796(8)	2.810(2)
Os(2)-Os(11)	2.848(7)	2.836(9)	2.868(2)
Os(6)-Os(11)	2.790(6)	2.896(7)	2.809(2)
mean of six bonds			
	2.770	2.809	2.807

Cap from Os(9)

	(1)	(2)	(3)
Os(9)-Os(4)	2.771(7)	2.785(8)	2.815(2)
Os(9)-Os(8)	2.788(7)	2.802(10)	2.820(2)
Os(9)-Os(10)	2.703(6)	2.817(7)	2.754(2)
mean of three bonds			
	2.754	2.801	2.796
Os(4)-Os(8)	2.703(8)	2.778(8)	2.826(2)
Os(4)-Os(10)	2.827(7)	2.865(8)	2.904(2)
Os(8)-Os(10)	2.796(6)	2.859(10)	2.824(2)
mean of six bonds			
	2.765	2.818	2.840

The above results showed that by considering the mean of the six Os-Os bonds at each of the four tetrahedral caps, there was no significant expansion in any of the caps in the structure of the monohydride $[HOs_{11}C(CO)_{27}]^-$ (1), with mean bonds of the two caps of the trigonal prism being significantly smaller in comparison to those in the dianion $[Os_{11}C(CO)_{27}]^{2-}$ (2) and the copper analogue $[Os_{11}C(CO)_{27}Cu(NCMe)]^-$ (3). In the deca-osmium cluster $[HOs_{10}C(CO)_{24}]^-$ (4) the enlarged Os_4 capping group thought to contain the interstitial H-ligand was observed to have a mean Os-Os bond length of 2.856(1) Å which was found to be 0.018 Å longer than the mean Os-Os bonds of the other three symmetry related Os_4 caps.[25]

However, if the mean values of the three Os-Os bond lengths from the four capping $Os(CO)_3$ groups in the related structures (1), (2) and (3) were considered {thus excluding three Os-Os bonds in (3) known to be elongated by the presence of the μ_3-Cu(NCMe) ligand}, with one exception, the mean for each capping group in both the Os_{11} dianion (2) and the $Os_{11}Cu$ derivative (3) were found to be greater than the corresponding mean values in the monohydride (1), {Table 3.8.3(b)}. Significantly it was the mean of the three bonds from Os(1) capping the square pyramid in (1) that was found to break this pattern, being longer than any mean bond in the structure. This appeared to favour that the H-ligand in $[HOs_{11}C(CO)_{27}]^-$ (1) was inside this capping Os_4 tetrahedron. Unfortunately, the poor quality of the only X-ray data obtained for the undeca-osmium hydride (1), resulted in the carbonyl ligands not being found with certainty and without essential evidence of the carbonyl distribution it was impossible, on structural grounds, to completely rule out the possibility that the apparent slight swelling of the cap from Os(1) was perhaps due to a μ_2-H bridging the bond Os(1)-Os(3) causing this to be the longest Os-Os bond in the structure (2.883(8) Å). However, two factors supported the interstitial site for the H-ligand,

(a) a μ_2-H site was not consistent with the ^1H n.m.r. spectrum, which showed the presence of $^{187}Os-^1H$ satelites in a 2:1:1 ratio.

(b) The close similarity between the ^1H n.m.r. spectrum of the monohydride (1) and the interstitial hydrido cluster $[HOs_{10}C(CO)_{24}]^-$ (4), structurally well characterised.[25]

3.8.4. Conclusions.

Although the quality of the X-ray data was poor, the metal core adopted by the undeca-osmium cluster $[HOs_{11}C(CO)_{27}]^-$ established a structure which consisted of a trigonal prism with tertrahedral caps on both faces and a square pyramidal cap on one square face which in turn was bi-capped by two tetrahedra. A similar metal core was also adopted by the related clusters $[Os_{11}C(CO)_{27}]^{2-}$ (2) and $[Os_{11}C(CO)_{27}Cu(NCMe)]^-$ (3).[109] By correlating the structural data for all three related cluster compounds (1), (2) and (3), the capping tetrahedral cavity 'sizes' were assessed {Table 3.8.3(b)}. It was observed that by considering the mean of three Os-Os bond lengths from each capping osmium atom {thus excluding three Os-Os bonds in (3) known to be elongated by the presence of the μ_3-Cu(NCMe) ligand}, three caps were found to be markedly larger in the dianion (2) and the copper derivative (3) than in the hydrido monoanion (1). The cap from Os(1) in the structure of the monoanion (1) was found to be larger {mean Os-Os 2.807 Å} than any other tetrahedral cap in the three structures. Assuming that the tetrahedral location deduced for the hydride ligand in solutions of $[HOs_{11}C(CO)_{27}]^-$ (1) from $^{187}Os-^1H$ n.m.r. data, was maintained in the solid state, it appeared that the hydrido ligand was located in the tetrahedron formed by the capping of a face of the square pyramid by Os(1). The accommodation of the observed electron count of 148 valence electron in the solid state structure of (1) was best rationalised using the procedure which takes into account polyhedral structures fused at edges, triangular and square faces:[97]

fused polyhedron	electron count characteristic of polyhedron
trigonal prism	90e
square pyramid	74e
4 x tetrahedrons	240e
sub-total	-----
	404e

A total of 256e had to be subtracted from the sub-total, since the four capping tetrahedra, {Figure 3.8.2(a)}, shared four triangular faces {48e per face shared} and the square pyramid shared a square face of the trigonal prism {64e}, therefore 404-256 = 148e.

Table 3.8.3.

Bond	(1)	(2)[109]	(3)[109]
Os(1)-Os(2)	2.773(7)	2.768(8)	2.798(2)
Os(1)-Os(3)	2.883(8)	2.746(6)	2.733(2)
Os(1)-Os(4)	2.764(7)	2.760(10)	2.824(2)
Os(2)-Os(3)	2.759(6)	2.750(8)	2.755(2)
Os(2)-Os(4)	2.796(6)	2.840(8)	2.848(2)
Os(2)-Os(5)	2.773(7)	2.782(6)	2.813(2)
Os(2)-Os(6)	2.703(8)	2.796(8)	2.810(2)
Os(2)-Os(11)	2.848(7)	2.836(8)	2.868(2)
Os(3)-Os(4)	2.767(7)	2.734(10)	2.822(2)
Os(3)-Os(6)	2.754(7)	2.753(8)	2.735(2)
Os(3)-Os(7)	2.814(8)	2.710(7)	2.738(2)
Os(3)-Os(8)	2.764(7)	2.780(7)	2.827(2)
Os(4)-Os(8)	2.703(8)	2.778(8)	2.826(2)
Os(4)-Os(9)	2.771(7)	2.785(8)	2.815(2)
Os(4)-Os(10)	2.827(7)	2.865(8)	2.904(2)
Os(5)-Os(6)	2.777(6)	2.803(7)	2.801(2)
Os(5)-Os(11)	2.728(6)	2.739(7)	2.739(2)
Os(6)-Os(7)	2.706(6)	2.788(9)	2.794(2)
Os(6)-Os(8)	2.800(6)	2.831(9)	2.847(2)
Os(6)-Os(11)	2.790(6)	2.896(7)	2.809(2)
Os(7)-Os(8)	2.745(7)	2.812(9)	2.790(2)
Os(8)-Os(9)	2.788(7)	2.802(10)	2.820(2)
Os(8)-Os(10)	2.796(6)	2.859(10)	2.824(2)
Os(9)-Os(10)	2.703(6)	2.817(7)	2.754(2)
Os(10)-Os(11)	2.784(6)	2.817(7)	2.809(2)
Os(3)-Cu			2.598(4)
Os(4)-Cu			2.709(4)
Os(8)-Cu			2.627(4)
Os(9)...Cu			3.156(4)

Section 3.9. References.

1. P. Luger, Modern X-ray Analysis on Single Crystals, Walter de Gruyter, Berlin, 1980.
2. M.R. Churchill, B.G. De Boer, and F.J. Rotella, Inorg. Chem., 1976, 15, 1843.
3. M.J. Mays and R.N.F. Simpson, J. Chem. Soc.(A), 1968, 444.
4. M.R. Churchill and F.J. Hollander, Inorg. Chem., 1979, 18, 161.
5. P. Chini, J. Organomet. Chem., 1980, 37, 200.
6. S.W. Kirtley, J.P. Olsen, and R. Bau, J. Am. Chem. Soc., 1973, 95, 4532.
7. R.K. Brown, J.M. Williams, A.J. Sirak, and E.L. Muetterties, Inorg. Chem., 1980, 19, 370.
8. G. Ciani, G. D'Alfouse, M. Freni, P. Romiti, and A. Sironi, J. Organomet. Chem., 1979, 170, C15.
9. R. Bau, R.G. Teller, S.W. Kirtley, and T.F. Koetzle, Accounts of Chem. Res., 1979, 12, 176.
10. R.G. Teller and R. Bau, Struct. Bonding (Berlin), 1981, 44, 1.
11. D.S. Moore and D. Robinson Chem.Soc. Rev., 1983, 12, 415.
12. P.G. Owston, J.M. Partridge, J.M. Rowe, Acta Cryst., 1960, 13, 246.

13. S.J. La Placa, W.C. Hamilton, J.A. Ibers, Inorg. Chem., 1964, 3, 1491.

14. M.R. Churchill, P.H. Bird, H.D. Kaesz, R. Bau, B. Fontal, J. Am. Chem. Soc., 1968, 90, 7135.

15. M.R. Churchill, and J. Wormald, J. Am. Chem. Soc., 1971, 93, 5670.

16. M.R. Churchill and F.J. Hollander, Inorg. Chem., 1979, 18, 843.

17. M.R. Churchill, R.A. Lashewycz, Inorg. Chem., 1979, 18, 1926.

18. M. Catti, G. Gervasio, and S.A. Mason, J. Chem. Soc., Dalton Trans., 1977, 2260.

19. A.G. Orpen, A.V. Rivera, E.G. Bryan, D. Pippard, G.M. Sheldrick and K.D. Rouse, J. Chem. Soc., Chem. Commun., 1978, 723.

20. M.R. Churchill, R.A. Lashewycz, J.R. Shapley, and S.I. Richter, Inorg. Chem., 1980, 19, 1277.

21. C.J. Gilmore, and P. Woodward, J. Chem. Soc.(A), 1971, 3453.

22. C.R. Eady, B.F.G. Johnson, J. Lewis, M.C. Malatesta, P. Machin, M. McPartlin, J. Chem. Soc., Chem. Commun., 1976, 945.

23. M. McPartlin, C.R. Eady, B.F.G. Johnson, J. Lewis, J. Chem. Soc., Chem. Commun., 1976, 883.

24. P.F. Jackson, B.F.G. Johnson, J. Lewis, P.R. Raithby, M. McPartlin, W.J.H. Nelson, K.D. Rouse, J. Allibon, and S.A. Mason, J. Chem. Soc., Chem. Commun., 1980, 295.

25. P.F. Jackson, B.F.G. Johnson, J. Lewis, M. McPartlin, W.J.H. Nelson, J. Chem. Soc., Chem. Commun., 1982, 49.

26. P.F. Jackson, B.F.G. Johnson, J. Lewis, M. McPartlin, W.J.H. Nelson, J. Chem. Soc., Chem. Commun., 1980, 224.

27. D. Braga, J. Lewis, B.F.G. Johnson, M. McPartlin, W.J.H. Nelson, M.D. Vargas, J. Chem. Soc., Chem. Commun., 1983, 241.

28. P.F. Jackson, B.F.G. Johnson, J. Lewis, and P.R. Raithby, J. Chem. Soc., Chem. Commun., 1980, 60.

29. S.J. La Placa and J.A. Ibers, J. Am. Chem. Soc., 1963, 85, 3501.

30. R.Bau, B. Don, R. Greatrex, R.J. Haines, R.A. Love, R.D. Wilson, Inorg. Chem., 1975, 14, 3021.

31. R. Bau and R.D. Wilson, ibid, 1976, 98, 4687.

32. G.M. Sheldrick, and J.P. Yesinowski, J. Chem. Soc., Dalton Trans., 1975, 873.

33. M.R. Churchill and R.A. Lashewycz, Inorg. Chem., 1979, 18, 3261.

34. M.A. Beno, J. Am. Chem. Soc., 1980, 102, 4542.

35. R.W. Broach and J.M. Williams, Inorg. Chem., 1979, 18, 314.

36. A.G. Orpen, D. Pippard, G.M. Sheldrick, and K.D. Rouse, Acta Cryst., 1978, B34, 2466.

37. P.L. Johnson, S.A. Cohen, T.J. Marks, and J.M Williams, J. Am. Chem. Soc., 1978, 100, 2709.

38. G.E. Bacon, Neutron Diffraction, 3rd Ed., Clarendon Press, Oxford, 1975.

39. J.L. Petersen, and J.M. Williams, Inorg. Chem., 1978, 17, 1308.

40. G. Ciani, D. Gusto, M. Manassero, and A. Albinati, J.Chem.Soc ., Dalton Trans., 1976, 1943.

41. A. Bertolucci, G. Ciani, M. Freni, P.Romiti, V.G. Albano, and A. Albinati, J. Organomet. Chem., 1976, 117, C37.

42. V.G. Albano P.L. Bellon, J. Organomet. Chem., 1972, 37, 151.

43. G. Longoni, M. Manassero, M. Sansoni, J. Organomet. Chem., 1979, 174, C41.

44. A.G. Orpen, J. Chem. Soc., Dalton Trans., 1980, 2509.

45. Schakal-Program Von E. Keller, Universität Freiburg 1980. Modified by the author of the program in 1982 for application to high-resolution color graphic terminal.

46. D. Braga, K. Henrick, B.F.G. Johnson, J. Lewis, M. McPartlin, W.J.H. Nelson, J. Organomet. Chem., 1983, 249, C21.

47. D. Braga, K. Henrick, B.F.G. Johnson, J. Lewis, M. McPartlin, W.J.H. Nelson, M.D. Vargas, J. Chem. Soc., Chem. Commun., 1984, 2151.

48. K. Henrick, M. McPartlin, J. Morris, Angew. Chem., Int.Ed.Engl., 1986, 25, 853.

49. A.J. Deeming, S. Hasso, and M. Underhill, J. Chem. Soc., Dalton Trans., 1975, 1614.

50. E.G. Bryan, B.F.G. Johnson, and J. Lewis, J. Chem. Soc., Dalton Trans., 1977, 1328.

51. A.D. Clauss , J.R. Shapley, and S.R. Wilson, J. Am. Chem. Soc., 1981, 103, 7387.

52. E. Sappa, A. Tiripicchio, and A.M. Manotti Lanfredi, J. Organomet. Chem., 1983, 249, 391.

53. K.A. Azam, C. Yin Choo, and A.J. Deeming, J. Chem. Soc., Dalton Trans., 1978, 1201.

54. A.J. Arce, and A.J. Deeming, J. Chem. Soc., Chem. Commun., 1980, 1102.

55. J.R. Shapley, J.B. Keister, M.R. Churchill, B.G. De Boer, J. Am. Chem. Soc., 1975, 97, 4145.

56. A.J. Deeming and S. Hasso, J. Organomet. Chem., 1976, 114, 313.

57. S. Kennedy, J.J. Alexander, and S.G. Shore, 1981, J. Organomet. Chem., 1981, 219, 385.

58. O. Eisenstein and R. Hoffmann, J. Am. Chem. Soc., 1981, 103, 4308.

59. A.J. Deeming and S. Hasso, J. Organomet. Chem., 1976, <u>113</u>, C39.

60. M.R. Churchill, B.G. De Boer, J.R. Shapley, and J. • Keister, J. Am. Chem. Soc., 1976, <u>98</u>, 2357.

61. A.J. Carty, N.J. Taylor, H.N. Paik, W. Smith, and J.G. Yule, J. Chem. Soc., Chem. Commun., 1976, 41.

62. A.J. Deeming and S. Hasso, J. Organomet. Chem., 1976, <u>112</u>, C36.

63. S. Aime, and A.J. Deeming, J. Chem. Soc., Dalton Trans., 1983, 1807.

64. R. Nast, Coord. Chem. Rev., 1982, <u>47</u>, 89.

65. A.J. Deeming, and M. Underhill, J. Chem. Soc., Dalton Trans., 1974, 1415.

66. R.T. Edlin, J.R. Norton, and K. Mislow, Organometallics, 1982, <u>1</u>, 561.

67. A.J. Carty, N.J. Taylor, H.N. Paik, W. Smith, and J.G. Yule, J. Chem. Soc., Chem. Commun., 1975, 309.

68. K. Henrick, M. McPartlin, A.J. Deeming, S. Hasso, and P. Manning, J. Chem. Soc., Dalton Trans., 1982, 899.

69. F. Dahan and R. Mathieu, J. Chem. Soc., Chem. Commun., 1984, 432.

70. T. Adatia, R. Bhusate, A.J. Deeming, S. Kabir, and M.McPartlin, J. Chem. Soc., Dalton Trans., in press.

71. M.R. Churchill and B.G. De Boer, Inorg. Chem., 1977, 16, 878.

72. M. Tachikawa, J.R. Shapley, and C.G. Pierpont, J. Am. Chem. Soc., 1975, 97, 7172.

73. G. Ferraris and G. Gervasio, J. Chem. Soc., Dalton Trans., 1973, 1933.

74. E. Boyar, A.J. Deeming, and S.E. Kabir, J. Chem. Soc., Dalton Trans., 1987, 551

75. G. Granozzi, E. Tondello, R. Bertoncello, S. Aime, and D. Osella, Inorg. Chem., 1983, 22, 744.

76. J.R. Moss and W.A.G. Graham, J. Organomet. Chem., 1970, 23, C47.

77. B.F.G. Johnson, R.D. Johnston, J. Lewis, B.H. Robinson and G. Wilkinson, J. Chem. Soc.(A), 1968, 2856.

78. R.D. Wilson, S.M. Wu, R.A. Love, and R. Bau, Inorg. Chem., 1978, 17, 1271.

79. B.F.G. Johnson, J. Lewis, P.R. Raithby, and C. Zuccaro, Acta. Cryst., 1981, B37, 1728.

80. J.W. Koepke, J.R. Johnson, S.A.R. Knox, and H.D. Kaesz, J. Am. Chem. Soc., 1975, 97, 3947.

81. B.F.G. Johnson, J. Lewis, P.R. Raithby, G.M. Sheldrick, K. Wong and M. McPartlin, J. Chem. Soc., Dalton Trans., 1978, 673.

82. M. McPartlin and W.J.H. Nelson, J. Chem. Soc., Dalton Trans., 1986, 1557.

83. M.R. Churchill, and F.J. Hollander, Inorg. Chem., 1978, 17, 1950.

84. S.A.R. Knox, and H.D. Kaesz, J. Am. Chem. Soc., 1971, 93, 4594.

85. K. Sasvari, P. Main, F.H. Cano, M. Martinez-Ripoll and P. Frediani, Acta. Cryst., 1979, B35, 87.

86. R. Hoffmann, B.E.R. Schilling, R. Bau, H.D. Kaesz, and D.M.P. Mingos, J. Am. Chem. Soc., 1978, 100, 6088.

87. J. Lewis, and B.F.G. Johnson, Pure Appl.Chem., 1982, 54, 97.

88. D. Braga, K. Henrick, B.F.G Johnson, J. Lewis, M. McPartlin, W.J.H. Nelson, and M.D. Vargas, J. Chem. Soc., Chem. Commun., 1982, 419.

89. B.F.G. Johnson, R. Khattar, J. Lewis, M. McPartlin, J. Morris, and G.L. Powell J. Chem. Soc., Chem. Commun., 1986, 507.

90. E.J. Ditzel, H.D. Holden, B.F.G. Johnson, J. Lewis, A.J. Sanders, and M.J. Taylor, J. Chem. Soc., Chem. Commun, 1982, 1373.

91. B.F.G Johnson, J. Lewis, M. McPartlin, J. Morris, G.L. Powell, P.R. Raithby, and M.D. Vargas, J. Chem. Soc., Chem. Commun., 1986, 429.

92. K. Wade, Adv. Inorg. Chem. Radiochem., 1976, 18, 1.

93. M. McPartlin, and D.M.P. Mingos, Polyhedron, 1984, 3, 1321.

94. M. McPartlin, Polyhedron, 1984, 3, 1279.

95. R.E. Williams, Adv. Inorg. Chem. Radiochem., 1976, 18, 91.

96. R.J. Goudsmit, B.F.G. Johnson, J. Lewis, P.R. Raithby, and K.H. Whitmire, J. Chem. Soc., Chem. Commun., 1982, 640.

97. D.M.P. Mingos J. Chem. Soc., Chem. Commun., 1983, 706

98. J.R. Shapley, G.A. Pearson, M. Tachikawa, G.E. Schmidt, M.R. Churchill, and F.J. Hollander, J. Am.Chem.Soc., 1981, 103.

99. C.R. Eady, B.F.G. Johnson, J. Lewis, R. Mason, P.B. Hitchcock, and K.M. Thomas, J. Chem. Soc., Chem. Commun., 1977, 385.

100. T. Adatia, D. Braga, M. McPartlin, A. Sironi, S.R. Drake, B.F.G. Johnson, J. Lewis, W.J.H. Nelson, M.D. Vargas, J. Chem. Soc., Dalton Trans., submitted for publication; S.R. Drake, B.F.G. Johnson, and J. Lewis, J. Chem. Soc., Dalton Trans., 1988, 1517.

101. B.F.G. Johnson, J. Lewis, S.W. Sankey, K. Wong, M. McPartlin, and W.J.H. Nelson, J. Organomet.Chem., 1980, 91, C3.

102. C.R. Eady, B.F.G. Johnson, and J. Lewis, J. Chem. Soc., Dalton Trans., 1975, 2606.

103. C.R. Eady, B.F.G. Johnson, B.E. Reihert, and G.M. Sheldrick, J. Chem. Soc., Chem. Commun., 1976, 271.

104. P.F. Jackson, B.F.G. Johnson, J. Lewis, W.J.H. Nelson, and M. McPartlin, J. Chem. Soc., Dalton Trans., 1982, 2009.

105. J.M. Fernandez, B.F.G. Johnson, J. Lewis, P.R. Raithby, and G.M. Sheldrick, Acta Crystallogr., 1984, B34, 7978.

106. M.J. Mays and P.D. Gavens, J. Organomet.Chem., 1977, 124, C37.

107. B.F.G. Johnson, J. Lewis, W.J.H. Nelson, J.N. Nicholls, and M.D. Vargas, J. Organomet. Chem., 1983, 249, 255.

108. J.P. Attard, B.F.G. Johnson, J. Lewis, J. Mace, M. McPartlin, and A. Sironi, J. Chem. Soc., Chem. Commun., 1984, 48.

109. D. Braga, K. Henrick, B.F.G. Johnson, J. Lewis, M. McPartlin, W.J.H. Nelson, A. Sironi, and M.D. Vargas, J. Chem. Soc. Chem. Commun., 1983, 1131.

110. V.G. Albano, M. Sansoni, P.Chini, S. Martinengo, and D. Strumolo, J. Chem. Soc., Dalton Trans., 1975, 305.

111. V.G. Albano, M. Sansoni, P. Chini, S. Martinengo, J. Chem. Soc., Dalton Trans., 1973, 651.

112. V.G. Albano, M. Sansoni, P. Chini, S. Martinengo, J. Chem. Soc., Dalton Trans., 1974, 299.

Chapter 4. The X-ray structure determination method.

4.1. Introduction: Selection and mounting of a crystal.

To obtain the best possible solution for any crystal structure, data collected from the diffractometer has to be as accurate as possible, which in turn means that the crystal chosen for analysis has to be of good quality. Certain features are of importance in choosing a single crystal. Firstly, the crystal is selected to be as small as possible within the experimental constraints, collimators usually have a diameter between 0.5 and 1.0 mm, thus crystals have to be smaller than 0·5 mm. Secondly, the crystal shape should be as spherical as possible with visible natural faces. In each case the single crystal to be analysed was mounted on the end of a thin quartz fibre, held onto a brass pin by adhesives (1:1 mix of expoxy resin and expoxy hardener), and was then mounted on to the goniometer head of the Philips PW1100 diffractometer.

4.1.1 Centering of the crystal.

The Philips PW1100 diffractometer consists of four circles, which allow the mounted crystal to be brought into various orientations. Two circles, namely ϕ and χ are used to adjust the crystal orientation relative to the diffractometer co-ordinate system. The ω circle permits the centering of the crystal lattice planes at a given angle of ω to the direction of the primary beam and finally on the fourth angle 2θ the detector can be moved to an angle 2θ to the primary beam. Thus, the crystal orientation is defined by the three angular settings, ϕ, χ, ω , and the detector position is determined by the fourth angle, 2θ.

4.1.2. Data collection.*

Before data collection was carried out, the unit cell dimensions and the orientation of the crystal had to be determined. This was achieved by using a computerised peak hunting routine. Initially this involves variation in the setting of the four diffractometer circles; 4 to 15 in ω, -80 to 80 in χ, and 0 to 360° in ϕ. When radiation was found above background, the maximum diffraction was measured and the angles, ω, χ, ϕ associated with the reflection together with the intensity of the peak were centered upon and stored. This procedure continued until 25 peaks were found and from this data the computer was able to determine a Dirichlet reduced unit cell together with an orientation matrix (UB), and a matrix M, which contained information about the reciprocal unit cell parameters. A standard unit cell was then found by examination of this matrix and applying the necessary information to the computer to change the UB matrix. Having obtained a standard cell, the results were refined and the direct lattice constants determined.

Least squares analysis was then carried out on the setting angles of 25 high angle reflections with θ ca. 10° and counts $(I/s^{-1}) > 1000$, which produced more accurate unit cell dimensions. The intensity relationships were checked at this stage by driving to a range of reflections, to confirm the crystal system. Having obtained satisfactory unit cell dimensions, data collection was initiated. Several strong reflections were scanned to examine their peak profile and to decide on the optimum scan width. All structures presented in this thesis had data collected at a constant scan speed of 0.05 s^{-1}. All intensity data were collected in the unique volume corresponding to the crystal Laue symmetry at ambient temperatures. A scan mode was chosen in which weak reflections which gave:

$$I_t - 2/I_t < I_b$$

on the first scan were not re-examined.

I_t - count rate at the top of reflection profile.

I_b - average count rate of two background measurements on either side of peak profile.

Reflections with $I_t < 500\ s^{-1}$ were rescanned to improve their accuracy. The maximum values for the machine indices (HKL) were chosen as appropriate, being set to the maximum value of h, k, l, that had to be measured. This was found to depend amongst other things, the size of the crystal under analysis. Boundary and sequence matrices were selected, allowing the operator to maximise the use of the diffractometer time, as the segment of the diffraction circle to be scanned could be altered, preventing the measurement of equivalent reflections. Finally, three reference reflections were chosen and re-measured every five hours, any drop in their intensities signified a problem, the two most common faults being either the crystal had moved or decomposed.

* X-rays from a Mo-K α (λ =0.71069 Å) source, monochromated by a single graphite crystal were used throughout data collection.

After data collection, the raw intensity data $(I_{hkl})raw$ and the estimated standard deviation for each reflection were obtained. These were corrected for Lorentz (L) and polarisation (p) factors using the expression:

$$(I_{hkl})_{corr.} = (I_{hkl})raw(Lp)^{-1}.$$

These corrections for the loss in the intensity of the X-ray beam as a result of polarisation and geometric factors are:

$$p = (1 + \cos^2 2\theta)/2 \text{ and } L = 1/\sin 2\theta$$

The estimated standard errors, $\sigma(I)$, of the intensities (I_{hkl}) were obtained from the expression:

$$\sigma(I)_{corr.} = [\sigma^2(I) + (0.04I)^2]^{1/2}$$

where K is an "instability" constant and a value of 0.04 was assigned to it. Equivalent reflections were merged and the raw data was converted to a form suitable for use with the SHELX suite of programs.[1]

4.1.3. The Phase problem.

Diffraction of X-rays occurs after initial scattering by the electrons associated with the atoms within the unit cell. The electron density (ρ_{xyz}) at any point x, y, z throughout the unit cell may be expressed as a three dimensional Fourier series:-

$$\rho_{xyz} = V^{-1}\sum_h \sum_k \sum_l F_{hkl}e^{-2\pi i(hx + ky + lz)} \qquad [4.1.3(a)]$$

where V is the unit cell volume.

To be able to find the positions of the atoms, electron density maps must be calculated over the unique part of the unit cell. The problem is that the phase of the structure factor F_{hkl} cannot be experimentally measured. If the positions and type of the N atoms in the unit cell were known, the structure factors could be calculated:-

$$F_{hkl} = \sum_{n=1}^{n=N} (f_n)_{hkl} \qquad e^{2\pi i(hx_n + ky_n + lz_n)} \qquad [4.1.3(b)]$$

where f_n is the scattering factor of the n^{th} atom, whose value is a function of $\sin\theta$ and the number of electrons in the atom. F_{hkl} is a complex number and so written as the sum of a real and imaginary portion.

$$F_{hkl} = A_{hkl} + iB_{hkl}$$
$$F_{hkl} = F_{hkl}\cos\phi_{hkl} + i(F_{hkl}\sin\phi_{hkl}) \qquad [4.1.3(c)]$$

To be able to solve the structure under analysis, some way of obtaining preliminary values of the structure factors F_{hkl} must be found. The value of F_{hkl} cannot be calculated directly since it is the squared modulus $|F_{hkl}|^2$ that equals the intensity I_{hkl}. The unknown angle, ϕ_{hkl}, associated with F_{hkl} must be estimated before any electron density map can be calculated, and this is known as the phase problem. Solving the phase problem is determining the phase of F_{hkl}, and this is the first stage of any structural analysis.

For centrosymmetric structures, for every atom at x, y, z, there is an equivalent atom at -x, -y, -z. Only N/2 independent atoms are then present in the unit cell, and the remaining N/2 atoms being related to these by the inversion centre. It can be shown that the phase angles for centrosymmetric crystals are restricted to having one of two values, 0 or 180°. Substituting these values into expression 4.1.3(c) gives:-

$$F_{hkl} = |F_{hkl}|\cos 0$$
$$\text{or } F_{hkl} = |F_{hkl}|\cos 180.$$

As cos0 is +1 and cos180 is -1, the phase problem is reduced to a matter of finding the signs of the F_{hkl} values. For non-centrosymmetric structures this is not the case and the value of the phase angle, which can be between 0 and 360°, must be determined.

4.1.4. Methods used to solve the phase problem.

Two main methods are usually used to solve the phase problem, either via the Patterson or by direct methods. A Patterson synthesis has been used during the analysis of each structure presented in this thesis and will be the only technique discussed. A Patterson vector map can be obtained directly from the observed intensity data using the equation:-

$$P_{uvw} = V^{-1}\sum_h \sum_k \sum_l (F_{hkl})^2 \, e^{-2\pi i(hu + kv + lw)}.$$

This is a three dimensional map which has a peak for every pair of atoms within the real unit cell. These peaks are situated in a particular direction and distance from the origin, which corresponds to the vector between the pair of atoms in the real unit cell. Each peak is at a position (u, v, w) related to the atomic co-ordinates,

x_1, y_1, z_1 and x_2, y_2, z_2 of the two atoms by:-

(a) $u = x_1 - x_2$

(b) $v = y_1 - y_2$

(c) $w = z_1 - z_2$.

The height of each peak in a Patterson map is proportional to the product of the atomic numbers of the atoms involved. The highest peaks in the Patterson map always occur at the origin and all atoms contribute to it. Subsequent peaks usually correspond to the vectors of the heaviest atoms in the unit cell. Taking the u, v, w values, positions of the 'heavy' atoms in the real unit cell can be found algebraically. These positions can be used to calculate preliminary structure factors and hence an electron density map from which more atoms can be obtained.

4.1.5. Fourier synthesis.

Once the position of some of the atoms are found, either from a Patterson map or from direct methods, they are then used to calculate an electron density map. First the co-ordinates of the found atoms are used to calculate F_{hkl} values (F_c), and so, assign phases to F_o values for all hkl. If the atoms of the partial solution contribute significantly to the diffracting power of the structure being studied, the phase determination will be almost correct. An electron density map is then calculated from the three dimensional Fourier series:-

$$\rho_{xyz} = V^{-1}\sum_h \sum_k \sum_l F_{hkl} e^{-2\pi i(hx + ky + lz)}.$$

Positions of the unfound atoms within the asymmetric unit cell are obtained by employing two alternative methods of calculating Fourier maps. The first involves applying the phases of all F_c values to the experimentally obtained structure amplitudes F_o in the above equation. This method is particularly useful if the partial solution contributes in a non-random way to the total diffraction, (i.e. if atoms are in special positions or one of pseudo symmetry). For centrosymmetric space groups the Fourier maps are produced by a simplified equation:-

$$\rho_{xyz} = V^{-1}\sum_h \sum_k \sum_l S_c F_o \; e^{-2\pi i(hx + ky + lz)}$$

where (S_c) is the calculated sign of each F_{hkl}. From the observed-Fourier map the fractional co-ordinates of other atoms may be obtained. These are used to calculate a new set of F_c values and the new phases used to calculate a better Fourier map. Once the position of most of the non-hydrogen atoms are found a difference-Fourier map can be obtained. In this Fourier calculation, the calculated phases are applied to the difference between the observed structure amplitude Fo and the calculated structure factor, F_c, and for centrosymmetric space groups the expression used is:-

$$\rho_{xyz} = V^{-1}\sum_h \sum_k \sum_l S_c(F_o - F_c) \; e^{-2\pi i(hx + ky + lz)}.$$

These are iterative procedures and successive use slowly builds up the structure contained in the asymmetric part of the unit cell, from which the whole crystal structure may be generated.

4.1.6. Refinement.

For each crystal structure, the structural model can be expressed mathematically by a number of parameters. These are the positional co-ordinates and temperature factors of each atom, and one or more scale factors. Since structure solution occurs in stages, the initial parameters for each atom in the structure can only be regarded as preliminary, and therefore a method needs to be derived which allows an improvement of the model. A three dimensional least squares procedure is normally used in which, the function $\sum w(||F_o|-|F_c||)^2$ is minimised during refinement. The weighting factor, w, is assigned to each reflection to take into account the different precision of the observed structure amplitudes, F_o.

The reliability of the results obtained from the refinement of a given structural model is conveniently expressed in terms of the R-factor. The R-factor is the average difference between the calculated structure amplitudes, (F_c), and the observed structure amplitudes, (F_o):

$$R = \Sigma k||F_o|-|F_c|| / \Sigma k|F_o|$$

$$R_w = \sum w^{1/2}||F_o|-|F_c|| / \sum w^{1/2}|F_o|$$

Since the observed structural amplitudes are derived from the experiment, and the calculated structure amplitudes from the structural model, the R-value can be regarded as an indication to how well the model fits the real structure.

Section 4.2. Analysis and experimental data for the tetranuclear cluster compound $[AgRu_3(CO)_9(C_2Bu^t)(PPh_3)]$ (1) {X-ray study presented in section 1.2}.

4.2.1 Crystal data for (1).

$C_{33}H_{24}AgO_9PRu_3$, M = 1006.38, Monoclinic, space group $P2_1/n$, a = 16.117(3), b = 16.791(3), c = 14.488(3) Å, β = 110.98(2)°, U = 3660.9 $Å^3$, F(000) = 1952, μ(Mo-K_α) = 16.64 cm^{-1}, Z = 4, D_c = 1.83g cm^{-3}.

4.2.2. Data collection for $[AgRu_3(CO)_9(C_2Bu^t)(PPh_3)]$ (1).

Data for a single crystal of (1) was collected using the methods outlined in sections 4.1-4.1.2. Table 4.2.2 lists the parameters associated with data collection.

Table 4.2.2

Crystal size = 0.44 x 0.48 x 0.21 mm

θ-range $3 < 0 < 25$

h,k,l range

$-19 < h < 19$

$0 < k < 20$

$0 < l < 17$

Scan width 0.7°

Number of unique reflections (N) with $I/\sigma(I) > 3.0$ = 3161.

4.2.3 Structure solution for $[AgRu_3(CO)_9(C_2Bu^t)(PPh_3)]$ (1).

Systematic abscences in the data showed the following conditions limiting diffraction,

0k0; k= 2n

indicating the presence of a 2_1 screw axis running parallel in direction to the b axis and

$h0l; h+l = 2n$

characterising an n-glide plane having its translational component running parallel in direction to the diagonal of the a-c plane in the monoclinic unit cell. The equivalent positions of the non-standard space group $P2_1/n$ were systematically generated from the equivalent positions of the standard space group $P2_1/c$, by considering the change in the relative positions and direction, of the two translational symmetry elements within the non-standard cell. The equivalent positions for $P2_1/c$ are:[2]

(a) x,y,z (b) $-x,-y,-z$ (c) $x,1/2-y,1/2+z$ (d) $-x,1/2+y,1/2-z$

Equivalent positions (a) and (b) relate atoms through the inversion centre at the origin of the unit cell,

(c) represents the operation of the c-glide plane, perpendicular to the b axis,

(d) represents the symmetry operation of the 2_1 screw axis.

Note, in order that the positions generated by (c) and (d) are related by the centre of symmetry at the origin of the unit cell, the c-glide is positioned at, , $y = 0.25$, and correspondingly the 2_1 screw axis is at $x = 0$, , $z = 0.25$.

Figure 4.2.3(a) illustrates a 2-dimensional representation of a standard monoclinic unit cell in the space group Pc, looking down on the b axis onto the a-c plane. The translation of the c-glide runs in direction parallel to the c axis.

By changing the direction of the c-axis and re-defining the origin, an alternative monoclinic unit cell can be obtained, Figure 4.2.3(b). In this 'new' cell the translational component of the glide plane now runs parallel to the diagonal of the a-c plane and is referred to as the n-glide. The symmetry operation of this glide plane involves the reflection of a point x,y,z through the plane of symmetry to an intermediate point {x,1/2-y,z}, followed by a translation of the point 1/2 a unit cell along both the a and the c axis, to a point 1/2+x, 1/2-y, 1/2+z.

The symmetry operation of the n-glide may be represented algebraically by,

1/2+x,1/2-y,1/2+z

and is an equivalent position in the non-standard space group. It has already been mentioned that the 2_1 screw axis in the standard cell is positioned at x = 0, z = 0.25, Figure 4.2.3(c).

In the non-standard cell {Figure 4.2.3(d)}, the 2_1 screw axis is now the line perpendicular to the a-c plane at x = 0.25 and z = 0.25.

The symmetry operation of a 2_1 screw axis in this non-standard cell involves rotation through a 180° of a point x,y,z to an intermediate point {1/2-x, y, 1/2-z} followed by translation of 1/2 a unit cell along the b-axis to the point 1/2-x, 1/2+y, 1/2-z, the equivalent position resulting from the 2_1 screw axis in the space group $P2_1/n$. The four equivalent positions for the non-standard space group $P2_1/n$ are therefore:

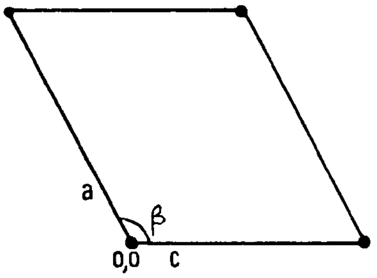

Figure 4.2.3(a).

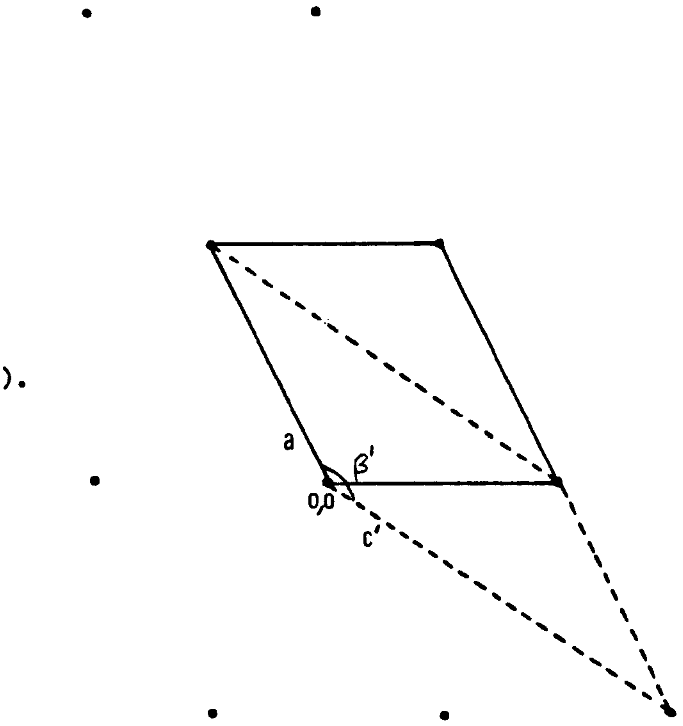

Figure 4.2.3(b).

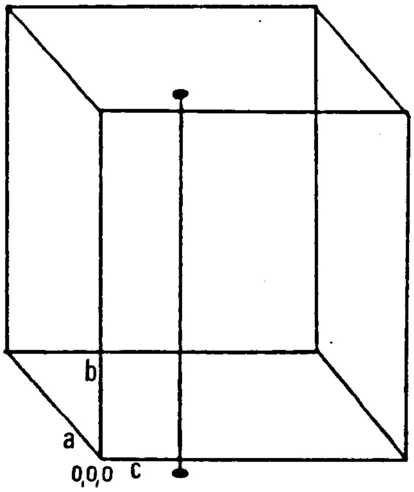

Figure 4.2.3(c).

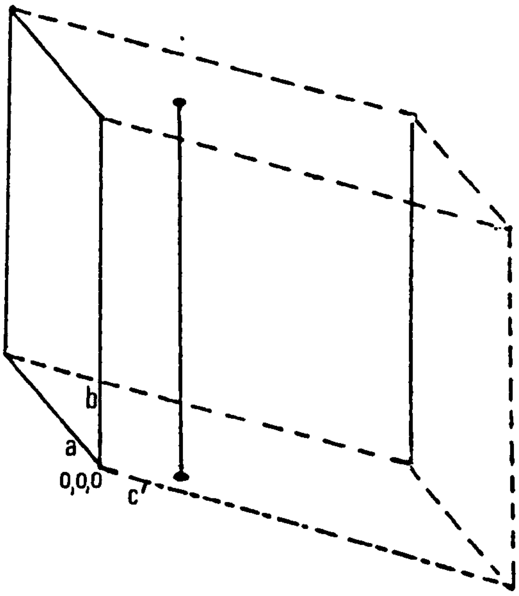

Figure 4.2.3(d).

(a) x,y,z (b) $-x,-y,-z$ (c) $1/2+x,1/2-y,1/2+z$ (d) $1/2-x,1/2+y,1/2-z$

Strategy of Patterson solution.

Stage 1.

Using the equivalent positions for this space group, the following unique algebraic vector sets between atoms related by the symmetry translations of the 2_1 screw axis and the n-glide plane {Table 4.2.3(a)} together with vectors between non-symmetry related atoms positioned at x_1,y_1,z_1 and x_2,y_2,z_2 {Table 4.2.3(b)} were generated.

Table 4.2.3(a)

$2x,2y,2z$	(a)
$1/2,1/2+y,1/2$	(b)
$1/2+x,1/2,1/2+z$	(c)

Table 4.2.3(b)

x_1-x_2,y_1-y_2,z_1-z_2	(a)
x_1+x_2,y_1+y_2,z_1+z_2	(b)
$1/2-(x_1-x_2),1/2-(y_1+y_2),1/2-(z_1-z_2)$	(c)
$1/2-(x_1+x_2),1/2-(y_1-y_2),1/2-(z_1+z_2)$	(d)

Stage 2.

Reported metal-metal bond distances lie in the region 2.60-3.10 Å, and will be referred to as 'short' vectors. Since the height of each peak in a Patterson map is proportional to the product of the atomic numbers of the atoms involved, peaks corresponding to vectors between metal atoms are usually prominent, and exhibit high maxima in the map. Examination of the Patterson map, {Table 4.2.3(c)}, revealed five 'short' vectors of this type.

Height (arbitary units)	u	v	w
208	-0.077	0.000	0.144
149	0.068	0.082	0.181
108	0.001	0.000	0.212
102	0.162	0.078	0.034
92	0.035	0.164	0.000

The analytical formulation of the silver-ruthenium cluster under analysis was $C_{33}H_{24}AgO_9Ru_3$. Using the directional properties of vectors the above short vectors were used to construct a 'butterfly' arrangement relating the four metal atoms as a starting point in structure solution.

Note. The intensity symmetry of a monoclinic crystal system, $I_{hkl} = I_{h-kl} = I_{-hk-l} = I_{-h-k-l}$, belongs to the Laue group 2/m. Since the X-ray diffraction from a single crystal gives intensity symmetry and not the crystal symmetry, Patterson functions also exhibit the symmetry of the data. Therefore a Patterson map of a monoclinic crystal system displays the relationship:

$u,v,w = u,-v,w = -u,v,-w = -u,-v,-w$

Height				
149	x_1-x_2	y_1-y_2	z_1-z_2	
	0.050	0.081	0.181	1-2
149	x_1-x_3	y_1-y_3	z_1-z_3	
	0.084	-0.081	0.178	1-3
92	x_2-x_3	y_2-y_3	z_2-z_3	
	0.034	-0.162	-0.003	2-3
102	x_1-x_4	y_1-y_4	z_1-z_4	1-4
	0.162	-0.078	0.035	
208	x_3-x_4	y_3-y_4	z_3-z_4	3-4
	0.078	0.003	-0.143	

Stage 3.

Taking the vector 1-2, the next stage was to locate the remaining vectors between atom 1 and 2 listed in Table 4.2.3(b). The main aim of this exercise was to obtain the vector,

$$x_1+x_2, y_1+y_2, z_1+z_2$$

since its combination with vector,

$$x_1-x_2, y_1-y_2, z_1-z_2$$

would give the vector sets,

$$2x_1, 2y_1, 2z_1 \text{ and } 2x_2, 2y_2, 2z_2$$

from which possible fractional atomic co-ordinates for the two atoms could be deduced. The best approach at this stage was to start with vector (c),

$$1/2-(x_1-x_2), 1/2-(y_1+y_2), 1/2-(z_1-z_2) \qquad \text{(c)}$$

0.450 ? 0.319

since the only unknown value in this expression was $1/2-(y_1+y_2)$. A corresponding vector was found at height (101):

0.449 0.175 0.320

This gave a potential numerical value for the unknown, y_1+y_2, to be 0.325.

Stage 4

Using the above value for y_1+y_2, the Patterson map was next examined for the vector,

x_1+x_2, y_1+y_2, z_1+z_2 (b)

? 0.325 ?

corresponding vector was found in the Patterson map at, Height (119)

-0.465 0.324 0.370

Stage 5

The validity of this newly found vector was checked with the presence of vector (d) in the map,

$1/2-(x_1+x_2), 1/2-(y_1-y_2), 1/2-(z_1+z_2)$ (d)

calculated values

-0.035 0.419 0.130

observed values

(177) -0.035 0.419 0.127

Stage 6

It was now possible to use the numerical values for the vector sets,

$x_1-x_2, y_1-y_2, z_1-z_2$ (a)

$x_1+x_2, y_1+y_2, z_1+z_2$ (b)

to obtain the potential values for the vector sets,

$2x_1, 2y_1, 2z_1$ and $2x_2, 2y_2, 2z_2$

x_1-x_2	y_1-y_2	z_1-z_2	(a)
0.050	0.081	0.181	
x_1+x_2	y_1+y_2	z_1+z_2	(b)
-0.465	0.324	0.370	
-----	-----	------	
$2x_1$	$2y_1$	$2z_1$	[addition of (a) and (b)]
-0.415	0.405	0.551	
$2x_2$	$2y_2$	$2z_2$	[subtraction of (a) from (b)]
-0.515	0.243	0.189	

Stage 7

To confirm the validity of the vector sets calculated above, the Patterson map was examined for the difference vectors between atoms 1 and 2 and corresponding atoms related by the symmetry of the translational element 2_1 giving vectors in the Harker plane 1/2+2x, 1/2, 1/2+2z (u, 1/2, w). Intermolecular difference vectors in the Harker line, 1/2, 1/2+2y, 1/2 (1/2, v, 1/2), relating atoms 1 and 2 to corresponding atoms by the translation of the n-glide plane, together with those vectors arising from the presence of the inversion centre at the origin of the unit cell, were also examined:

	atom 1				atom 2		
	$2x_1$	$2y_1$	$2z_1$;		$2x_2$	$2y_2$	$2z_2$ (a)
calculated values							
	-0.415	0.405	0.551;		-0.515	0.243	0.189
observed values							
(61)	0.413	0.405	0.443;	(68)	0.486	0.244	0.193

$1/2 \quad 1/2-2y_1 \quad 1/2; \qquad 1/2 \quad 1/2-2y_2 \quad 1/2$ (b)

calculated values

0.5 0.095 0.5; 0.5 0.256 0.5

observed values

(393) 0.5 0.079 0.5; (113) 0.5 0.256 0.5

$1/2-2x_1 \quad 1/2 \quad 1/2-2z_1; \qquad 1/2+2x_2 \quad 1/2 \quad 1/2+z_2$ (c)

calculated values

-0.085 0.5 -0.051; -0.015 0.5 -0.311

observed values

(106) 0.083 0.5 0.052; (76) 0.015 0.5 0.308

Stage 8

The positions of two metal atoms were now confirmed from the Patterson map,

$2x_1 \quad 2y_1 \quad 2z_1 \longrightarrow x_1 \quad y_1 \quad z_1$

-0.415 0.405 0.551 -0.2075 0.2025 0.2755

$2x_2 \quad 2y_2 \quad 2z_2 \longrightarrow x_2 \quad y_2 \quad z_2$

-0.515 0.243 0.189 -0.2575 0.1215 0.0945

Stage 9

Using the above values the 'butterfly' arrangement relating the four metal atoms (stage 2) could now be solved. The difference vectors between atoms 1-3, 2-3, 1-4, and 3-4, {Table 4.2.3(b)}, together with the corresponding vectors between these and their symmetry related atoms in the unit cell, {Table 4.2.3(a)}, were calculated and found in the Patterson map:

vector	height	u	v	w
x_1-x_3, y_1-y_3, z_1-z_3	(149)	0.084	-0.081	0.178
x_1+x_3, y_1+y_3, z_1+z_3	(194)	-0.499	0.500	0.375
$2x_3$, $2y_3$, $2z_3$	(114)	-0.562	-0.586	0.195
$1/2-(x_1-x_3)$, $1/2-(y_1+y_3)$, $1/2-(z_1-z_3)$	(188)	0.416	0.000	0.322
$1/2-(x_1+x_3)$, $1/2-(y_1-y_3)$, $1/2-(z_1+z_3)$	(175)	-0.005	0.420	0.128
$1/2$, $1/2+2y_3$, $1/2$	(393)	0.500	0.079	0.500
$1/2+2x_3$, $1/2$, $1/2+2z_3$	(112)	0.082	0.500	0.302
x_2-x_3, y_2-y_3, z_2-z_3	(92)	0.034	-0.162	-0.003
x_2+x_3, y_2+y_3, z_2+z_3	(114)	0.438	0.414	0.195
$1/2-(x_2-x_3)$, $1/2-(y_2+y_3)$, $1/2-(z_2-z_3)$	(100)	-0.466	0.095	0.497
$1/2-(x_2+x_3)$, $1/2-(y_2-y_3)$, $1/2-(z_2+z_3)$	(113)	0.052	0.339	0.308
x_1-x_4, y_1-y_4, z_1-z_4	(102)	0.162	-0.078	0.035
x_1+x_4, y_1+y_4, z_1+z_4	(166)	-0.423	0.500	0.482
$1/2-(x_1-x_4)$, $1/2-(y_1+y_4)$, $1/2-(z_1-z_4)$	(196)	0.340	0.000	0.466
$1/2-(x_1+x_4)$, $1/2-(y_1-y_4)$, $1/2-(z_1+z_4)$	(97)	-0.075	0.424	0.019
$2x_4$, $2y_4$, $2z_4$	(56)	0.263	0.444	0.490
$1/2$, $1/2+2x_4$, $1/2$	(393)	0.500	0.079	0.500
$1/2+2x_4$, $1/2$, $1/2+2z_4$	(110)	0.241	0.500	0.015
x_3-x_4, y_3-y_4, z_3-z_4	(208)	0.078	0.003	-0.143
x_3+x_4, y_3+y_4, z_3+z_4	(125)	0.354	0.423	0.338
$1/2-(x_3-x_4)$, $1/2-(y_3+y_4)$, $1/2-(z_3-z_4)$	(143)	-0.409	0.080	0.353
$1/2-(x_3+x_4)$, $1/2-(y_3-y_4)$, $1/2-(z_3+z_4)$	(215)	0.161	0.500	0.160

The Patterson map had now been solved for one silver and three ruthenium atoms, {based upon the relative heights at which the vectors 2x,2y,2z, appeared in the map} and the following fractional co-ordinates were used as a starting set in the next stage of structure solution.

Ru(1)	-0.2075	0.2025	0.2755
Ru(2)	-0.2575	0.1215	0.0945
Ru(3)	-0.2915	0.2905	0.0985
Ag	-0.3690	0.2810	0.2410

Table 4.2.3(c).

HEIGHT	U	V	W	DISTANCE/Å
393.0	0.500	0.079	0.500	8.797
215.0	0.161	0.500	0.160	8.848
208.0	-0.077	0.000	0.144	2.783
196.0	0.340	0.000	0.466	7.009
194.0	-0.499	0.500	0.375	13.998
188.0	0.416	0.000	0.322	6.658
177.0	-0.035	0.419	0.127	7.298
176.0	-0.083	0.419	0.217	7.161
175.0	-0.005	0.420	0.128	7.292
166.0	-0.423	0.500	0.482	14.135
149.0	0.068	0.082	0.181	2.814
143.0	-0.409	0.080	0.353	9.775
125.0	0.354	0.423	0.338	9.326
119.0	-0.465	0.324	0.370	11.969
116.0	0.125	0.339	0.159	6.200
114.0	0.438	0.414	0.195	9.585
113.0	0.500	0.256	0.500	9.701
113.0	0.052	0.339	0.308	7.095
112.0	0.082	0.500	0.302	9.340
110.0	0.241	0.500	0.015	9.220
109.0	-0.113	0.159	0.149	4.233
108.0	0.001	0.000	0.212	3.066
108.0	0.001	0.000	0.212	3.066
106.0	0.083	0.500	0.052	8.492
102.0	0.162	0.078	0.034	2.803
101.0	0.449	0.175	0.320	7.647
100.0	-0.466	0.095	0.497	10.526
97.0	-0.075	0.424	0.019	7.243
94.0	0.001	0.000	0.456	6.601
94.0	0.001	0.000	0.456	6.601
92.0	0.035	0.164	0.000	2.811
92.0	-0.035	0.164	0.000	2.811
76.0	0.015	0.500	0.308	9.470
68.0	0.486	0.244	0.193	8.383
67.0	-0.297	0.500	0.434	12.429
61.0	0.413	0.405	0.443	10.058
56.0	0.263	0.444	0.490	10.120
53.0	-0.208	0.000	0.187	5.008
50.0	-0.211	0.000	0.487	8.861
46.0	0.287	0.500	0.113	9.441
45.0	-0.369	0.500	0.029	10.384
45.0	-0.276	0.077	0.309	7.467
41.0	-0.335	0.000	0.009	5.447
40.0	0.500	0.083	0.000	8.178
36.0	-0.498	0.086	0.286	10.367
33.0	0.227	0.416	0.389	8.898
33.0	-0.174	0.295	0.374	8.523
33.0	-0.487	0.254	0.007	8.965
33.0	-0.420	0.408	0.018	9.700
32.0	-0.411	0.088	0.117	7.548
32.0	0.251	0.295	0.338	7.121
32.0	-0.240	0.174	0.187	6.192

4.2.4. Structure refinement for $[AgRu_3(CO)_9(C_2Bu^t)(PPh_3)]$ (1).

In the next stage of structure solution, the overall scale factors were allowed to refine in 1 cycle, whereas 2 full-matrix cycles were used to refine the fractional co-ordinates and isotropic temperature factors of the four metal atoms, ($R = 0.1760; R_w = 0.1763$). The resulting difference-Fourier map revealed suitable positions for the phosphorus and atoms of six of the nine carbonyl groups. The fractional co-ordinates of these 'newly' found atoms were incorporated into the calculation of structure factors but were not refined, whereas two full-matrix least squares cycles used to improve the refined isotropic parameters of the phosphorus and the four metal atoms, reduced the R-factor to 14.20%. The second difference-Fourier synthesis showed suitable maxima in the electron density map for the carbon atoms of the three phenyl rings, the atom positions of the remaining three carbonyl groups and the t-butylacetylide ligand. The six carbon atoms of each phenyl ring were grouped and incorporated into subsequent stages of structure refinement as rigid hexagons [d(C-C) 1.395 Å;C-C-C = 120°]. The sp^2 C-H phenyl H atoms were geometrically calculated to ride at respective carbon atoms, with C-H distances of 1.08 Å and fixed temperature factors of 0.08 $Å^2$. Further refinement on the parameters of all the non-hydrogen atoms in 2 full-matrix least squares cycles, with the Ag, P and three Ru atoms treated as anisotropically vibrating atoms lowered the R-factor to 7.80%. The difference-Fourier map calculated at this stage disclosed few residual maxima in the region of the metal atoms, with maximum height of 0.9 e $Å^{-3}$.

Finally, 4 full-matrix least squares cycles of refinement on the parameters of all the non-hydrogen atoms converged at $R = 0.0689$ and

$R_w = 0.0613$, with weights of $1/\sigma^2(F_0)$ assigned to individual reflections.

Note. In this and subsequent structure analyses, the SHELX 76 suite of programs were used for calculations,[1] with complex neutral-atom scattering factors assigned to respective atoms.[2]

<u>Section</u> <u>4.3.</u> Analysis and experimental data for the copper-ruthenium cluster compounds $[Cu_2Ru_4(\mu_3\text{-}H)_2(CO)_{12}\{P(C_6H_{11})_3\}_2]$ (1) and $[Cu_2Ru_4(\mu_3\text{-}H)_2(CO)_{12}\{P(CHMe_2)_3\}_2]$ (2) {X-ray studies presented in section 1.3}.

4.3.1. Crystal data for (1) : $C_{48}H_{68}O_{12}Cu_2P_2Ru_4$, M = 1430.08, Monoclinic, space group $P2_1/n$, a = 23.450(3), b = 22.475(3), c = 10.816(2) Å, β = 101.45(2)°, U = 5587.00 $Å^3$, F(000) = 2744, μ(Mo-Kα) = 20.24 cm^{-1}, Z = 4, D_c = 1.70 g cm^{-3}.

4.3.2. Crystal data for (2) : $C_{30}H_{44}O_{12}Cu_2P_2Ru_4$, M = 1189.69, Monoclinic, space group $P2_1$, a = 12.666(2), b = 15.115(3), c = 12.317(2) Å, β = 104.01(2)°, U = 2287.90 $Å^3$, F(000) = 1168, μ(Mo-Kα) = 21.60 cm^{-1}, Z = 2, D_c = 1.71 g cm^{-3}

4.3.3. Data collection for $[Cu_2Ru_4(\mu_3\text{-}H)_2(CO)_{12}\{P(C_6H_{11})_3\}_2]$ (1) and $[Cu_2Ru_4(\mu_3\text{-}H)_2(CO)_{12}\{P(CHMe_2)_3\}_2]$ (2).

Data sets for a single crystal for both (1) and (2) were collected using the methods outlined in sections 4.1-4.1.2. Table 4.3.3 summarises the parameters associated with data collection.

Table 4.3.3

Crystal size = 0.24 x 0.22 x 0.18 mm (1)

Crystal size = 0.22 x 0.26 x 0.15 mm (2)

θ-range $3 < 0 < 25$ for both (1) and (2)

h,k,l range

$-28 < h < 27$ (1) $-16 < h < 16$ (2)

$0 < k < 27$ $0 < k < 19$

$0 < l < 13$ $0 < l < 15$

Scan width 0.7° for both (1) and (2)

Number of unique reflections (N) with $I/\sigma(I) > 3.0$ = 2544 (1) and 2031 (2).

4.3.4 Structure solution and refinement for $[Cu_2Ru_4(\mu_3\text{-}H)_2(CO)_{12}\{P(C_6H_{11})_3\}_2]$ (1).

The positions of three ruthenium atoms were deduced from a Patterson syhthesis. The remaining non-hydrogen atoms were subsequently located from a series of difference-Fourier maps. During the final stages of structure solution, refinement of the overall scale factors together with 2 separate full-matrix least squares cycles used to refine the isotropic parameters of all the non-hydrogen atoms, converged at $R = 0.1410$ and $R_w = 0.1420$. At this stage an empirical absorption correction was applied to the data using DIFABS.[3] Subsequently, using 1 cycle to refine the overall scale factors and two separate full-matrix least squares cycles for the fractional co-ordinates and isotropic temperature factors of the non-hydrogen atoms, the R-factor reduced to 11.21%. The two hydrogen atoms bonded to each carbon atom of the cyclohexyl rings were geometrically calculated [d(C-H) 1.08 Å] and included in the atom list with fixed temperature factors of 0.08 $Å^2$. The two hydrido ligands were not located directly from the X-ray data, although potential energy calculations,[4] gave suitable positions for both atoms to occupy μ_3-sites on Ru_2Cu faces, {section 1.3.1}. Anisotropic temperature factors were next assigned to the four Ru, two Cu and two P atoms, whose parameters together with the isotropic parameters of the remaining non-hydrogen atoms were allowed to refine in 2 full-matrix least squares cycles, ($R = 0.0859$;$R_w = 0.0861$). The difference-Fourier map calculated at this stage revealed few residual maxima in the region of the metal atoms, with maximum height of 1.0 e $Å^{-3}$.

Finally, 4 full-matrix cycles of refinement on the parameters of all the non-hydrogen atoms converged at $R = 0.0735$ and $R_w = 0.0745$, with weights of $1/\sigma^2(F_o)$ assigned to individual reflections.

4.3.5 Structure solution and refinement for $[Cu_2Ru_4(\mu_3\text{-}H)_2(CO)_{12}\{P(CHMe_2)_3\}_2]$ (2).

The only condition limiting diffraction in the data set was,

0k0; k = 2n

which indicated that the monoclinic space group was either the non-centrosymmetric $P2_1$ or the centrosymmetric $P2_1/m$. As there were two molecules in the unit cell, the non-centrosymmetric space group was initially assumed and the positions of the four ruthenium atoms were deduced from a Patterson synthesis in this space group. Taking the fractional co-ordinates of these metal atoms and allowing the overall scale factors to refine independently in 1 least squares cycle, an observed-Fourier map was calculated, ($R = 0.3621; R_w = 0.3625$). The electron density map showed suitable maxima for the two copper and two phosphorus atoms. Subsequently, 1 cycle was used to refine the overall scale factors, whereas two separate full-matrix least squares cycles were used to refine the fractional co-ordinates and isotropic temperature factors of the six metal and two phosphorus atoms, ($R = 0.1721; R_w = 0.1734$). The difference-Fourier map showed atom positions for 7 of the 12 carbonyl groups. The parameters of these 'newly' found atoms were incorporated into the calculation of structure factors, but were not refined, whereas 2 full-matrix cycles were used to improve the refined isotropic parameters of the six metal and two phosphorus atoms, ($R = 0.1520; R_w = 0.1490$). The second difference-Fourier map revealed suitable positions for the atoms of the remaining carbonyl groups and 9 carbon atoms of the organophosphine groups, ($-CHMe_2$) bonded to P(1) and 8 of the corresponding carbon atoms at P(2). All the non-hydrogen atoms except one methyl carbon atom of the fragment, $CHMe_2$, at P(2) were now located. All attempts to find a suitable position for this missing carbon atom failed. This aroused some suspicion, and as a result the geometry around P(2) was examined carefully. The angles, Cu(2)-P(2)-{$CHMe_2$} were found to be in the order of 135.0° markedly enlarged from the expected tetrahedral angles of 108.0°. Similar angles were observed at P(1), and subsequent difference-Fourier maps with these atoms left out of the structure factor calculations failed to give improved positions for the carbon atoms of the organic substituents at either phosphorus atom.

At this stage it appeared possible that there was probably marked disorder of the organophosphine ligands. However, it was noticed that there were significant correlations between the parameters of metal atoms, Ru(3) and Ru(4) and their carbonyl ligands together with some of the carbon atoms of the $CHMe_2$ groups in the least squares refinement, a characteristic sign of structure solution in the wrong space group, or the presence of pseudo-symmetry. As a result of this, the possibility that the correct space group was $P2_1/m$ was re-considered. The presence of a mirror plane is usually characterised by numerous vector peaks of the type 0,v,0 (due to pairs of atoms related by the mirror symmetry). In the Patterson map of this structure only one vector of this type was present.

height	u	v	w	distance/ Å
196	0	0.195	0	2.947

This 'short' vector had been initially used in deducing the positions of two independent ruthenium atoms in the non-centrosymmetric space group $P2_1$.

Ru(3)	0.230	0.193	0.220
Ru(4)	0.228	0.000	0.220

This meant that if the space group were $P2_1/m$, Ru(3) and Ru(4) must be related by a mirror plane perpendicular to the b axis at y = 0.096 in the monoclinic unit cell. Interestingly, the following atom positions established in the non-centrosymmetric space group were now also observed to lie in the mirror plane:

atom	x	y	z
Ru(1)	0.270	0.096	0.048
Ru(2)	0.043	0.094	0.032
Cu(1)	0.320	0.094	0.420
Cu(2)	0.087	0.089	0.287
P(1)	0.463	0.098	0.611
P(2)	-0.043	0.094	0.367
C(21)	-0.107	0.089	0.026
O(21)	-0.204	0.097	0.005
C(11)	0.428	0.083	0.098
O(11)	0.527	0.086	0.123

The scarcity of the maxima in the Patterson map of 0,v,0 could now be explained by the observation that the 'heavy' atoms had y values close to 0.096. Thus, they appeared to lie in the mirror plane of the space group $P2_1/m$.

Therefore, structure determination was repeated in the centrosymmetric space group $P2_1/m$, using the co-ordinates of the four ruthenium two copper and two phosphorus atoms as a starting set. By convention, the mirror plane in this space group is positioned to be perpendicular to the b axis at y = 0.25 in order to fix the centre of symmetry at the origin of the unit cell. Therefore, the positions of Ru(3), Ru(4), Cu(1), Cu(2), P(1), and P(2) found to lie in the mirror plane were 'fixed' at y = 0.25 along the b axis and were assigned occupancy factors of 0.5. Since Ru(2) was generated from Ru(1) via the mirror symmetry, its position did not have to be included in the atom list.

An observed-Fourier map was next calculated, revealing three carbonyl groups for Ru(1), since this atom was independent of the mirror plane. For each of the remaining two ruthenium atoms {in the mirror plane}, the atoms of one carbonyl group were found to be in the mirror plane (with co-ordinates in the y direction of 0.25), whereas the atoms of the second carbonyl group were well out of the mirror. The atoms of the third carbonyl group bonded to these two Ru atoms were generated by mirror symmetry from the atoms of the second -CO ligand, and as a result did not have to be included in the atom list. Two least squares cycles were next used to refine the isotropic parameters of the five metal and two phosphorus atoms, whereas the fractional co-ordinates of the 'newly' found atoms were incorporated into the calculation of structure factors, but were not refined, ($R = 0.2210; R_w = 0.2214$).

The refinement now had no significant correlations between any of the atom parameters, and the calculated difference-Fourier map gave suitable positions for all the carbon atoms of the organic fragments, $-CHMe_2$, bonded to atoms, P(1) and P(2). However, the two methyl carbons of each $-CHMe_2$ unit were observed to occur as double images (related by the mirror). The positions of both related atoms were taken and given occupancy factors of 0.5. The parameters of these newly found atoms were incorporated into the atom list, and the resulting geometry around the two P atoms was again examined. As observed in the structure solved in the non-centrosymmetric space group, the P-C bond lengths were relatively long {mean 2.110 A}, with the corresponding $Cu-P-CHMe_2$ angles being markedly distorted from the expected tetrahedral angles. Although the geometry of the organophosphine ligands was not satisfactory, structure solution looked more promising, since all the carbon atom positions of the organic substituent at both phosphorus atoms were now located.

However, subsequent refinement on the metal and P atom parameters with anisotropic temperature factors was not encouraging (R = 0.1710 R_w = 0.1713). Therefore it appeared that the true space group was infact the non-centrosymmetric $P2_1$, with apparent mirror symmetry being due to a high proportion of the atoms being co-planar and lying perpendicular to the b-axis. To proceed with structure refinement in this space group the origin in the y-direction was set invariant by fixing a co-ordinate of y = 0.25, to metal atom Ru(2). All atoms thought to be related closely by the pseudo mirror symmetry were calculated using the equivalent position, x, 1/2-y, z and were included in the atom list. Previously, structure solution in the space group $P2_1/m$, had revealed that the atom positions of the two methyl carbon atoms of each $-CHMe_2$ fragment bonded to the P atoms occurred in pairs related by the pseudo mirror plane {vide supra}. Therefore, for structure refinement in the non-centrosymmetric space group $P2_1$, one atom position of each pair was selected with difficulty to break the pseudo mirror symmetry, allowing refinement to converge in this space group. In all subsequent stages of refinement, atoms related by the pseudo mirror symmetry were refined in the same blocked full-matrix least square cycles, separately from the remaining atoms. Subsequently, during refinement of all the non-hydrogen atom parameters in 2 full-matrix least squares cycles, the overall geometry of the two $Cu-P-\{CHMe_2\}_3$ units was constrained to refine at specified distances, {Cu-P 1.90(5) Å;P-C 1.85(5) Å;C-C 1.50(5) Å}. At this stage an empirical absorption correction was applied to the data using DIFABS.[3] Thereafter, using 1 cycle to refine the overall scale factors and two separate blocked full-matrix cycles for the parameters of all the non-hydrogen atoms, the R-factor reduced to 15.92%. Anisotropic temperature factors were next assigned to the four Ru, two Cu, and two P atoms, whilst only their parameters refined in 3 blocked full-matrix least squares cycles, ($R = 0.1310; R_w = 0.1315$). The calculated difference-Fourier map at this stage disclosed few residual maxima in the region of the metal atoms, with maximum height of 0.8 e $\mathring{A}^{-3}$.

Finally, 4 blocked full-matrix cycles of refinement on the parameters of all the non-hydrogen atoms, with the Cu-P, P-C and C-C bond lengths of the Group IB metal organophosphines, $CuP(CHMe_2)_3$, constrained to refine at specified distances, {vide supra}, converged at $R = 0.0795$ and $R_w = 0.0830$, with weights of $1/\sigma^2(F_o)$ assigned to individual reflections.

Section 4.4. Analyses and experimental data for the copper-ruthenium and silver-ruthenium cluster compounds $[M_2Ru_4(\mu\text{-}CO)_3(CO)_{10}(PPh_3)_2]$ [M = Cu (1) and Ag (2); X-ray studies presented in section 1.4].

4.4.1 Crystal data for (1) :- $C_{49}H_{30}Cu_2O_{13}P_2Ru_4$, M = 1419.79, Monoclinic, space group $P2_1/n$, a = 22.110(2), b = 17.247(3), c = 14.407(3) Å, β = 93.44(2)°, U = 5483.94 $Å^3$, F(000) = 2768, μ(Mo-Kα) = 18.12 cm^{-1}, Z = 4, D_c = 1.72 g cm^{-3}.

4.4.2 Crystal data for (2) :- $C_{49}H_{30}Ag_2O_{13}P_2Ru_4$, M = 1508.44, Triclinic, space group $P\bar{1}$, (no. 2) a = 24.685(3), b = 10.710(2), c = 10.137(3) Å, α = 102.03(2), β = 96.20(2), γ = 86.47(2)°, U = 2603.69 $Å^3$, F(000) = 1456, μ(Mo-Kα) = 18.07 cm^{-1}, Z = 2, D_c = 1.93 g cm^{-3}.

4.4.3 Data collection for $[Cu_2Ru_4(\mu\text{-}CO)_3(CO)_{10}(PPh_3)_2]$ (1) and $[Ag_2Ru_4(\mu\text{-}CO)_3(CO)_{10}(PPh_3)_2]$ (2).

Data sets for a single crystal of both (1) and (2) were collected using the methods outlined in sections 4.1-4.1.2. Table 4.4.3 summarises the parameters associated with data collection.

Table 4.4.3

Crystal size = 0.25 x 0.22 x 0.13 mm (1)

Crystal size = 0.29 x 0.22 x 0.10 mm (2)

θ-range $3 < 0 < 25$ for both (1) and (2)

h,k,l range

$-28 < h < 28$ (1)	$-40 < h < 40$ (2)
$0 < k < 22$	$-18 < k < 18$
$0 < l < 18$	$0 < l < 17$

Scan width 0.8° for both (1) and (2)

Number of unique reflections (N) with $I/\sigma(I) > 3.0$ = 4467 (1) and 5065 (2).

4.4.4 Structure solution and refinement for $[Cu_2Ru_4(\mu\text{-}CO)_3(CO)_{10}(PPh_3)_2]$ (1).

The positions of three ruthenium atoms were deduced from a Patterson synthesis. Taking the fractional co-ordinates of these metal atoms and allowing the scale factors to refine in one least squares cycle, an observed-Fourier map was calculated, ($R = 0.3820; R_w = 0.3900$). The resulting electron density map revealed five distinct peaks of varying electron density. The fractional co-ordinate of the highest peak was assigned to the fourth ruthenium atom and the fractional co-ordinates of the following four peaks to the two copper and two phosphorus atoms, respectively. In the next stage of structure solution, the overall scale factors refined in 1 cycle, whereas 2 separate full-matrix least squares cycles were used to refine the isotropic parameters of the six metal and two P atoms, ($R = 0.1610; R_w = 0.1615$). The difference-Fourier map revealed suitable atom positions for 10 of the 13 carbonyl groups and 3 of the six phenyl rings. The parameters of these 'newly' found atoms were incorporated into the calculation of structure factors, but were not refined, whereas, the refined isotropic parameters of the six metal and two P atoms were further improved using 2 full-matrix cycles, ($R = 0.1120,; R_w = 0.1118$). The second difference-Fourier synthesis exhibited maxima in the electron density map for the atoms of the remaining three carbonyl groups, and the three phenyl rings. The six carbon atoms of each phenyl ring were grouped and included in subsequent stages of structure refinement as rigid hexagons, [d(C-C) 1.395 Å;C-C-C = 120°]. The sp^2 C-H phenyl atoms at each ring were geometrically calculated to ride at the respective carbon atoms at distances of 1.08 Å, with fixed temperature factors of 0.08 $\mathring{A}^2$. In the final stages of structure refinement, 2 full-matrix cycles on the parameters of all the non-hydrogen atoms, with the six metal and two phosphorus atoms treated as anisotropically vibrating atoms, reduced the R-factor to 7.08%. The difference-Fourier map calculated at this stage showed few residual maxima in the region of the metal atoms, with maximum height of 0.8 e $\mathring{A}^{-3}$.

Finally, 5 cycles of full-matrix least squares refinement on the parameters of all the non-hydrogen atoms converged at $R = 0.0659$ and $R_w = 0.0660$ with weights of $w = 1/\sigma^2 F_o$ assigned to individual reflections.

4.4.5 Structure solution and refinement for $[Ag_2Ru_4(\mu\text{-}CO)_3(CO)_{10}(PPh_3)_2]$ (2).

The positions of three ruthenium atoms were obtained from a Patterson map. Taking the fractional co-ordinates of these atoms, and allowing the overall scale factors to refine in 1 least squares cycle, ($R = 0.3921; R_w = 0.4001$), an observed-Fourier map was calculated. The electron density map gave suitable maxima for the remaining ruthenium, two silver, and two phosphorus atoms. Subsequently, the overall scale factors were refined in 1 cycle, whereas 2 separate full-matrix cycles were used to refine the fractional co-ordinates and isotropic temperature factors of the six metal and two phosphorus atoms, ($R = 0.1730; R_w = 0.1735$). The difference-map revealed atom positions for 8 of the 13 carbonyl groups, and 4 of the 6 phenyl rings. The parameters of these 'newly' found atoms were incorporated into the calculation of structure factors, but were not refined, whereas the isotropic parameters of the six metal and two P atoms were allowed to further refine in two full-matrix least squares cycles, ($R = 0.1220; R_w = 0.1225$). The second difference-Fourier map showed suitable atom positions for the remaining 5 carbonyl groups and the 2 phenyl rings. The six carbon atoms at each phenyl ring were grouped to form rigid hexagons [d(C-C) 1.395 Å; C-C-C = 120°], and hydrogen atoms at each ring were calculated to ride at the respective carbon atoms at distances of 1.08 Å, with fixed temperature factors of 0.08 $Å^2$. In the next stage of structure refinement, the parameters of the four Ru, two Ag and two P atoms were assigned anisotropic temperature factors, and together with the fractional co-ordinates and isotropic temperature factors of the remaining non-hydrogen atoms, 2 full-matrix cycles used to refine all their parameters converged at $R = 0.0638$ and

$R_w = 0.0635$. The resulting difference-Fourier map revealed few residual peaks in close proximity to the metal atoms, with maximum height of 0.8 e $Å^{-3}$.

Finally, 5 full-matrix cycles of refinement on the atomic and thermal parameters of all the non-hydrogen atoms converged at $R = 0.0503$ and $R_w = 0.0513$ with weights of $w = 1/\sigma^2 F_o$ assigned to individual reflections.

Section 4.5. Analysis and experimental data for the hexanuclear cluster compound $[Au_2Ru_4(\mu\text{-}H)(\mu_3\text{-}H)(CO)_{12}\{\mu\text{-}Ph_2PCH{=}CHPPh_2\}]$ (1), {X-ray study presented in section 2.2}.

4.5.1 Crystal data for (1) :- $C_{38}H_{24}Au_2O_{12}P_2Ru_4$, M = 1532.48, Monoclinic, space group I2/c, (non-standard C2/c), a = 33.673(4), b = 12.275(2), c = 23.057(3) Å, β = 97.828(2)°, U = 9441.484 $Å^3$, F(000) = 5636, μ(Mo-K_α) = 72.04 cm^{-1}, Z = 8, D_c = 1.82 g cm^{-3}. (For C2/c a = 38.098, b = 12.274, c = 23.134 Å, β = 119.0°).

4.5.2 Data collection.

Data for a single crystal of $[Au_2Ru_4(\mu\text{-}H)(\mu_3\text{-}H)(CO)_{12}\{\mu\text{-}Ph_2PCH{=}CHPPh_2\}]$ (1) was collected using the methods outlined in sections 4.1-4.1.2. Table 4.5.2 summarises the parameters associated with data collection.

Table 4.5.2

Crystal size = 0.25 x 0.22 x 0.15 mm

θ-range 3 < 0 < 25

h,k,l range

$-41 < h < 41$

$0 < k < 15$

$0 < l < 28$

Scan width 0.8°

Number of unique reflections (N) with $I/\sigma(I) > 3.0$ = 3377.

4.5.3 Structure solution for $[Au_2Ru_4(\mu\text{-}H)(\mu_3\text{-}H)(CO)_{12}\{\mu\text{-}Ph_2PCH{=}CHPPh_2\}]$.

Inspection of the processed data showed the following conditions limiting diffraction:

hkl; h+k+l=2n and h0l; l=2n

indicating the presence of a Body-centered unit cell with a c-glide plane running parallel in direction to the c axis and perpendicular to the b axis at y = 0. The possible monoclinic space groups could therefore be Ic (non-standard Cc) or I2/c (non-standard C2/c), and at this stage it was impossible to distinguish between the two. By definition, a C-face centered unit cell has an extra lattice point in the middle of the a-b plane, {Figure 4.5.3(a)}, and as a result a point x,y,z is symmetry related to a point translated by a vector, t = 1/2(a+b).

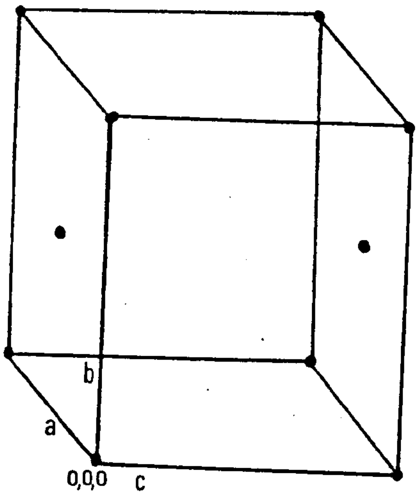

Figure 4.5.3(a)

Figure 4.5.3(b) illustrates a monoclinic Body-centered cell with the extra lattice point in the middle of the unit cell, and in this case a point x,y,z is further symmetry related to a point translated by a vector, t = 1/2(a+b+c)

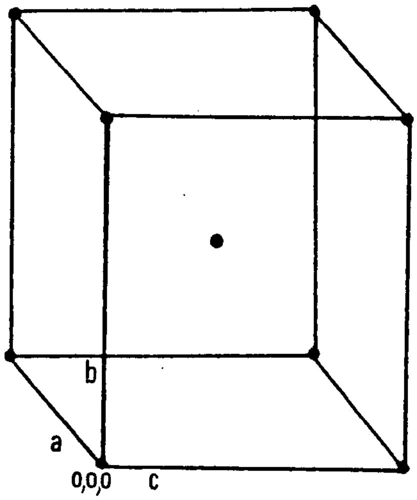

Figure 4.5.3(b)

In the space group Cc, the symmetry operation of the c-glide plane perpendicular to the b axis at y = 0, on a point x, y, z involves a reflection of the point through the plane of symmetry to an intermediate point {x,-y,z}, followed by translation of 1/2 the unit cell to give the equivalent position x, -y, 1/2+z. This point is further related to the position 1/2-x,1/2+y, 1/2+z. Similarly in the non-standard space group Ic, the equivalent position generated by the operation of the c-glide plane, x, -y, 1/2+z is further related by symmetry to the position, 1/2-x, 1/2+y, -z, arising from Body-centering of the unit cell. The four unique equivalent positions for the space groups Cc and Ic are listed in Table 4.5.3(a).

Table 4.5.3(a).

Cc	Ic
(0,0,0;1/2,1/2,0) +	(0,0,0;1/2,1/2,1/2) +
x,y,z	x,y,z
x,-y,1/2+z	x,-y,1/2+z

For the centrosymmetric space group C2/c, the c-glide plane still lies perpendicular to the b axis at y = 0, whereas the 2 fold axis runs parallel in direction to the b-axis but is now perpendicular to the c axis at z = 0.25 in order to fix the centre of symmetry at the origin of the unit cell. The symmetry operation of a 2-fold axis in this space group therefore involves a rotation through a 180^0 of a point x, y, z about the b axis to an equivalent point -x, y, 1/2-z. This point is further related to the position 1/2+x, 1/2-y, 1/2-z, by the translation vector, t = 1/2(a+b) arising from the C-face centering of the unit cell. In the non-standard space group I2/C the equivalent position arising from the operation of the 2-fold rotation, $-x,y,1/2-z$ is also related by symmetry to the point, $1/2+x,1/2-y,z$, by the translation vector, $t = 1/2(a+b+c)$ due to the I-face centering of the unit cell. The eight unique equivalent positions for the space groups C2/c and I2/c are listed in Table 4.5.3(b).

Table 4.5.3(b)

C2/c	I2/c
(0,0,0;1/2,1/2,0) +	(0,0,0;1/2,1/2,1/2) +
x,y,z	x,y,z
$-x,-y,-z$	$-x,-y,-z$
$x,-y,1/2+z$	$x,-y,1/2+z$
$-x,y,1/2-z$	$-x,y,1/2-z$

Stage 1. The use of the Patterson map to distinguish between the space groups Ic and I2/c.

The vector sets relating atoms by symmetry operations of a c-glide translation or a 2-fold rotation in the space groups Ic and I2/c are listed in Table 4.5.3(c)

Table 4.5.3(c)

Ic	I2/c
(0,0,0;1/2,1/2,0) +	(0,0,0;1/2,1/2,1/2) +
$0,2y,1/2$ (a)	$2x,2y,2z$ (a)
	$0,2y,1/2$ (b)
	$2x,0,1/2+2z$ (c)

The presence of an excess of 38 peaks in the Patterson map, {Table 4.5.3(e)}, of the type,

$u,0,w$

in the Harker plane,

$2x,0,1/2+2z$

unambiguously indicated the presence of a 2-fold rotational axis within the unit cell. The centrosymmetric space group I2/c was also inferred by the calculation of the density with 8 molecules in the unit cell. The vector sets relating two non-symmetry atoms in one molecule, positioned at x_1,y_1,z_1 and x_2,y_2,z_2 in the space group I2/c are listed in Table 4.5.3(d).

Table 4.5.3(d)

$(0,0,0;1/2,1/2,1/2)$ +

x_1-x_2,y_1-y_2,z_1-z_2 (a)

x_1+x_2,y_1+y_2,z_1+z_2 (b)

$x_1-x_2,y_1+y_2,1/2-(z_1-z_2)$ (c)

$x_1+x_2,y_1-y_2,1/2-(z_1+z_2)$ (d)

Stage 2. Strategy of Patterson solution.

In section 4.2.3, it has already been mentioned that the height of each peak in the Patterson map is proportional to the product of the atomic numbers of the atoms involved, and therefore peaks corresponding to M-M vectors are normally prominent and are referred to as 'short vectors'. The Patterson map, {Table 4.5.3(e)}, revealed 6 'short vectors' in the region 2.762-4.179 Å, corresponding to potential M-M bonds and contacts.

Height (arbitary units)	u	v	w
356	0.074	0.000	0.078
215	0.000	0.224	0.000
111	0.071	0.095	-0.033
111	0.004	0.080	0.118
80	0.080	0.200	0.105
73	0.071	0.228	0.067

A triangle relating 3 of the six metal atoms was constructed using the above 'short vectors.

Height				
	x_1-x_2	y_1-y_2	z_1-z_2	(1-2)
356	0.074	0.000	0.076	
	x_1-x_3	y_1-y_3	z_1-z_3	(1-3)
215	0.005	-0.221	0.011	
	x_2-x_3	y_2-y_3	z_2-z_3	(2-3)
73	-0.069	-0.221	-0.065	

Stage 3

Taking the vector 1-2, the next stage was to locate the symmetry related vectors listed in Table 4.5.3(d). The main aim of this exercise was to obtain the vector,

$$x_1+x_2, y_1+y_2, z_1+z_2$$

since its combination with,

$$x_1-x_2, y_1-y_2, z_1-z_2$$

would give the vector sets,

$$2x_1, 2y_1, 2z_1, \; 2x_2, 2y_2, 2z_2$$

from which the potential positions for atoms 1 and 2 could be obtained.

The best approach at this stage was to start with the symmetry vector,

$x_1-x_2, y_1+y_2, 1/2+(z_1-z_2)$ (c)

since the only unknown value in the expression was, y_1+y_2. The Patterson map was therefore examined for the vector type,

x_1-x_2, y_1+y_2, $1/2+(z_1-z_2)$

calculated values,

0.074 ? 0.424

observed values,

(301) 0.074 0.500 -0.424

This now gave a preliminary numerical value for the unknown, y_1+y_2 to be 0.5.

Stage 4.

Using the above value for y_1+y_2, the Patterson map was next examined for the vector,

x_1+x_2, y_1+y_2, z_1+z_2 (b)

the corresponding vector was found in the map at,

(310) 0.245 0.500 0.217

Stage 5

The validity of this newly found vector was checked by looking for,

x_1+x_2, y_1-y_2, $1/2+(z_1+z_2)$ (d)

calculated values,

0.245 0.000 -0.283

observed values,

(308) 0.244 0.000 -0.286

Stage 6

It was now possible to use the numerical values for the vector sets,

$$x_1-x_2, y_1-y_2, z_1-z_2 \quad (a)$$

$$x_1+x_2, y_1+y_2, z_1+z_2 \quad (b)$$

to obtain the vector sets,

$$2x_1, 2y_1, 2z_1, \ 2x_2, 2y_2, 2z_2$$

x_1-x_2	y_1-y_2	z_1-z_2	(a)
0.074	0.000	0.076	
x_1+x_2	y_1+y_2	z_1+z_2	(b)
0.245	0.500	0.217	

$2x_1$	$2y_1$	$2z_1$	
0.319	0.500	0.293	[addition of a and b]
$2x_2$	$2y_2$	$2z_2$	
0.171	0.500	0.141	[subtraction of a from b].

Stage 7

The Patterson map was next examined for vectors relating atoms 1 and 2 to corresponding atoms by symmetry of the 2-fold rotation, giving vectors in the Harker plane 2x,0,1/2+2z (u,0,w), and translation of the c-glide, exhibiting vectors in the Harker line 0,2y,1/2 (0,v,1/2), {Table 4.5.3(c)}. Vectors relating atoms 1 and 2 to corresponding atoms through the centre of symmetry were also checked:

	atom 1				atom 2			
	$2x_1$	$2y_1$	$2z_1$;		$2x_2$	$2y_2$	$2z_2$	(a)
calculated values								
	0.319	0.500	0.293;		0.171	0.500	0.141	
observed values								
(165)	0.319	0.500	0.293;	(148)	0.170	0.500	0.139	
	0	$2y_1$	1/2;		0	$2y_2$	1/2	(b)
calculated values								
	0	0.500	0.5;		0	0.500	0.5	
observed values								
(641)	0	0.500	0.5;	(641)	0	0.500	0.5	
	$2x_1$	0	$1/2+2z_1$;		$2x_2$	0	$1/2+2z_2$	(c)
calculated values								
	0.319	0	-0.207;		0.171	0	-0.359	
observed values								
(173)	0.318	0	-0.209;	(178)	0.171	0	-0.362	

Stage 8

The positions of the two atoms were now confirmed from the Patterson map,

$2x_1$	$2y_1$	$2z_1 \longrightarrow$	x_1	y_1	z_1
0.319	0.500	0.293	0.1595	0.250	0.1465
$2x_2$	$2y_2$	$2z_2 \longrightarrow$	x_2	y_2	z_2
0.171	0.500	0.141	0.0855	0.250	0.0705

Stage 9

Using the positions of atoms 1 and 2, the triangle constructed initially, (stage 2), could now be solved. For the vectors 1-3 and 2-3 both the intramolecular {Table 4.5.3(d)} and intermolecular {Table 4.5.3(c)} difference vectors were calculated and checked as follows:

vector	height	u	v	w
$x_1-x_3,\ y_1-y_3,\ z_1-z_3$	(215)	0.005	-0.221	0.011
$x_1+x_3,\ y_1+y_3,\ z_1+z_3$	(77)	0.312	-0.280	0.280
$x_1+x_3,\ y_1-y_3,\ 1/2+(z_1+z_3)$	(79)	0.312	0.222	-0.220
$x_1-x_3,\ y_1+y_3,\ 1/2+(z_1-z_3)$	(144)	-0.002	-0.292	0.491
$2x_3,\ 2y_3,\ 2z_3$	(19)	0.307	-0.059	0.269
$0,\ 2y_3,\ 1/2$	(152)	0.000	0.105	0.500
$2x_3,\ 0,\ 1/2+2z_3$	(173)	0.318	0.000	-0.209
$x_2-x_3,\ y_2-y_3,\ z_2-z_3$	(73)	-0.069	-0.221	-0.065
$x_2+x_3,\ y_2+y_3,\ z_2+z_3$	(128)	0.240	-0.292	0.196
$x_2+x_3,\ y_2-y_3,\ 1/2+(z_2+z_3)$	(125)	0.240	-0.221	-0.303
$x_2-x_3,\ y_2+y_3,\ 1/2+(z_2-z_3)$	(71)	0.070	-0.291	-0.432

The Patterson map was now solved for one gold and two ruthenium atoms (based on the relative heights at which the 2x,2y,2z vector sets were located), and the following fractional co-ordinates were used as a starting set in the next stage of structure solution.

Au(1)	0.1595	0.250	0.1465
Ru(1)	0.0855	0.250	0.0705
Ru(2)	0.1535	-0.0295	0.1345

Table 4.5.3(e).

HEIGHT	U	V	W	DISTANCE
641.0	0.500	0.000	0.000	16.836
641.0	0.000	0.500	0.500	13.060
641.0	0.500	0.000	0.000	16.836
356.0	0.074	0.000	0.078	2.868
356.0	0.426	0.500	0.422	17.323
310.0	0.255	0.000	0.283	10.052
310.0	0.245	0.500	0.217	10.932
308.0	0.244	0.000	-0.286	11.214
308.0	0.256	0.500	-0.214	12.162
301.0	0.074	0.500	-0.424	12.087
301.0	0.426	0.000	-0.076	14.686
215.0	0.000	0.224	0.000	2.750
215.0	0.500	0.276	0.500	19.364
215.0	0.000	0.224	0.000	2.750
178.0	0.171	0.000	-0.362	10.766
178.0	0.329	0.500	-0.138	13.421
173.0	0.182	0.500	-0.291	11.465
173.0	0.318	0.000	-0.209	12.326
165.0	0.181	0.000	0.207	7.211
165.0	0.319	0.500	0.293	13.376
152.0	0.500	0.395	0.000	17.521
152.0	0.000	0.105	0.500	11.600
152.0	0.500	0.395	0.000	17.521
148.0	0.330	0.000	0.361	12.945
148.0	0.170	0.500	0.139	8.701
144.0	0.002	0.292	-0.491	11.884
144.0	-0.498	0.208	0.009	16.992
144.0	-0.002	0.292	0.491	11.884
144.0	0.498	0.208	-0.009	16.992
128.0	0.240	0.292	0.196	9.414
128.0	0.260	0.208	0.304	10.751
125.0	0.260	0.280	-0.197	10.951
125.0	0.240	0.220	-0.303	11.696
111.0	-0.496	0.420	-0.382	18.521
111.0	0.004	0.080	0.118	2.878
111.0	0.496	0.420	0.382	18.521
111.0	-0.004	0.080	-0.118	2.878
111.0	0.071	0.095	-0.033	2.855
111.0	0.429	0.405	-0.467	19.792
109.0	0.309	0.199	0.162	10.844
109.0	0.191	0.301	0.338	10.104
101.0	0.264	0.288	0.419	12.707
101.0	0.236	0.212	0.081	8.329
96.0	0.312	0.081	-0.330	13.821
96.0	0.188	0.419	-0.170	9.415
90.0	0.240	0.085	-0.404	13.179
90.0	0.260	0.415	-0.096	10.620
89.0	0.240	0.438	0.098	9.713
89.0	0.260	0.062	0.402	11.876
86.0	0.079	0.301	-0.395	10.501
86.0	0.421	0.199	-0.105	14.905
85.0	0.493	0.305	-0.127	17.647
85.0	0.007	0.195	-0.373	8.961
82.0	0.334	0.193	0.388	13.591
82.0	0.166	0.307	0.112	6.941

80.0	0.080	0.200	0.105	4.168
80.0	0.420	0.300	0.395	16.169
80.0	0.070	0.435	0.460	11.822
80.0	0.430	0.065	0.040	14.405
79.0	0.313	0.427	0.175	11.969
79.0	0.187	0.073	0.325	9.152
79.0	0.312	0.222	-0.220	12.572
79.0	0.188	0.278	-0.280	10.224
77.0	0.333	0.285	-0.112	12.350
77.0	0.167	0.215	-0.388	11.503
77.0	0.312	0.280	0.280	12.058
77.0	0.188	0.220	0.220	8.022
76.0	0.264	0.182	-0.086	9.631
76.0	0.236	0.318	-0.414	13.790
76.0	0.492	0.193	0.368	17.714
76.0	0.008	0.307	0.132	4.828
76.0	0.495	0.073	-0.120	17.287
76.0	0.005	0.427	-0.380	10.231
73.0	0.432	0.298	0.050	14.891
73.0	0.068	0.202	0.450	10.610
73.0	0.068	0.317	-0.051	4.743
73.0	0.432	0.183	-0.449	19.101
73.0	0.310	0.307	-0.338	14.355
73.0	0.190	0.193	-0.162	8.186
73.0	0.429	0.272	0.433	16.740
73.0	0.071	0.228	0.067	3.864
71.0	0.232	0.000	0.059	7.745
71.0	0.268	0.500	0.441	14.054
71.0	0.430	0.209	-0.068	14.996
71.0	0.070	0.291	-0.432	11.132
69.0	0.070	0.000	0.473	10.839
69.0	0.430	0.500	0.027	15.661
63.0	0.303	0.122	0.041	10.228
63.0	0.197	0.378	0.459	12.586
63.0	0.194	0.500	-0.051	9.155
63.0	0.306	0.000	-0.449	15.569
51.0	0.497	0.500	-0.119	18.379
51.0	-0.003	0.000	0.381	8.799
51.0	-0.497	0.500	0.119	18.379
51.0	0.003	0.000	-0.381	8.799
48.0	0.303	0.000	0.150	10.317
48.0	0.197	0.500	0.350	11.498
45.0	0.195	0.264	-0.049	7.544
45.0	0.305	0.236	-0.451	15.846
37.0	0.074	0.076	-0.408	10.098
37.0	0.426	0.424	-0.092	15.673
36.0	0.337	0.500	-0.088	13.298
36.0	0.163	0.000	-0.412	11.600
36.0	0.192	0.138	0.442	11.427
36.0	0.308	0.362	0.058	11.195
28.0	0.163	0.098	0.082	5.685
28.0	0.337	0.402	0.418	14.704
27.0	0.094	0.342	-0.481	12.657
27.0	0.406	0.158	-0.019	13.874
27.0	0.351	0.356	-0.193	13.890
27.0	0.149	0.144	-0.307	9.385
25.0	0.233	0.078	0.177	8.391
25.0	0.267	0.422	0.323	12.037
25.0	0.007	0.500	-0.001	6.142
25.0	0.007	0.500	-0.001	6.142

4.5.4 Structure refinement for $[Au_2Ru_4(\mu\text{-}H)(\mu_3\text{-}H)(CO)_{12}\{\mu\text{-}Ph_2PCH{=}CHPPh_2\}]$ (1).

Taking the fractional co-ordinates of the gold and two ruthenium atoms obtained from the Patterson synthesis, and using 1 least squares cycle to refine the overall scale factors, an observed-Fourier map was calculated, ($R = 0.4220; R_w = 0.4231$). The fractional co-ordinates of five prominent maxima in the electron density map were assigned to the remaining gold, two ruthenium and two phosphorus atoms, respectively. In the next stage of structure solution, the overall scale factor was allowed to refine in 1 cycle, separately from the 2 full-matrix least squares cycles used to refine the fractional co-ordinates and isotropic temperature factors of the six metal and two phosphorous atoms, ($R = 0.1720; R_w = 0.1725$). The difference-Fourier map revealed suitable atom positions for the 12 carbonyl groups and two of the four phenyl rings. The parameters of these newly found 'light' atoms were not refined, whereas 2 full-matrix cycles were used to improve the refined parameters of the six metal and two phosphorus atoms, ($R = 0.1360; R_w = 0.1365$). The second difference-Fourier map showed atom positions for the remaining two phenyl rings and the two carbon atoms of the ethene fragment, {-CH=CH-}, bridging the two Au-P bonds. The six carbon atoms of each ring were grouped as rigid hexagons [d(C-C) = 1.395 Å;C-C-C = 120°], with the sp^2 C-H, phenyl hydrogen atoms geometrically calculated to ride at respective carbon atoms at distances of d(C-H) = 1.08 Å, with fixed temperature factors of 0.08 $Å^2$. Although the two hydrido ligands were not located directly from the X-ray analysis, suitable positions were deduced from potential energy calculations[4] for one hydride to cap an Ru_3 face and the second to bridge an Ru-Ru edge of the tetrahedron, {section 2.2}.

The parameters of the two hydrido ligands were incorporated into the calculation of structure factors, but were not refined. In the final stages, the two Au, four Ru and two P atoms were assigned anisotropic temperature factors, and refinement of their parameters together with the isotropic parameters of the remaining non-hydrogen atoms in 2 full-matrix cycles, reduced the R-factor 7.10%.

Finally, 4 full-matrix least squares cycles of refinement on the atomic positions and thermal parameters of all the non-hydrogen atoms converged at $R = 0.0603$ and $R_w = 0.0605$, with weights of $1/\sigma^2F_o$ assigned to individual reflections.

Section 4.6. Analysis and experimental data for the gold-copper ruthenium mixed-metal compound $[CuAuRu_4(\mu\text{-}H)(\mu_3\text{-}H)(CO)_{12}\{\mu\text{-}Ph_2PCH_2CH_2PPh_2\}]$ (1), {X-ray study presented in section 2.3}.

4.6.1 Crystal data for (1) :- $C_{38}H_{26}CuAuO_{12}P_2Ru_4$, M = 1401.06, Monoclinic, space group $P2_1/c$, a = 12.688(2), b = 27.383(4), c = 13.828(2) Å, β= 104.122(2)°, U = 4659.14 $Å^3$, F(000) = 2650, μ(Mo-Kα) = 47.12 cm^{-1}, Z = 4, D_c = 2.10 g cm^{-3}.

4.6.2 Data collection for $[CuAuRu_4(\mu-H)(\mu_3-H)(CO)_{12}\{\mu-Ph_2PCH_2CH_2PPh_2\}]$ (1).

Data for a single crystal of (1) was collected using the methods outlined in sections 4.1-4.1.2. Table 4.6.2 summarises the parameters associated with data collection.

Table 4.6.2

Crystal size = 0.22 x 0.22 x 0.19 mm

θ-range 3 < 0 < 25

h,k,l range

-15 < h < 15

0 < k < 33

0 < l < 16

Scan width 0.8°

Number of unique reflections (N) with I/σ(I) > 3.0 = 2577.

4.6.3 Structure Solution and Refinement.

Inspection of the processed data showed the following conditions limiting diffraction:

hol; l = 2n

OkO; k = 2n

characterising the space group $P2_1/c$. The position of the gold and three ruthenium atoms were deduced from a Patterson synthesis. Taking the fractional co-ordinates of these metal atoms and allowing the overall scale factors to refine in 1 least squares cycle, an observed-Fourier map was calculated, ($R = 0.4200; R_w = 0.4212$). The electron density map revealed four distinct peaks of varying electron density. The fractional co-ordinate of the highest peak was assigned to the fourth ruthenium atom, and the fractional co-ordinates of the next three peaks to the copper and two phosphorus atoms, respectively. Subsequently, the overall scale factor was refined in 1 cycle, separately from the two full-matrix least square cycles used to refine the isotropic parameters of the six metal and two phosphorus atoms, ($R = 0.1610; R_w = 0.1613$). The difference-Fourier map showed suitable atom positions for 8 of the 12 carbonyl groups and 3 of the 4 phenyl rings. The parameters of these newly found 'light' atoms were not refined, whereas 2 full-matrix cycles were used to improve the refined parameters of the six metal and two phosphorus atoms, ($R = 0.1420; R_w = 0.1427$). The second difference-Fourier map revealed suitable maxima for the atoms of the remaining four carbonyl groups, 1 phenyl ring and the two carbon atoms of the ethyl fragment, {$-CH_2CH_2-$}, bridging the Cu-P and Au-P bonds. The six carbon atoms of each phenyl ring were grouped to form rigid hexagons, [d(C-C) 1.395 Å;C-C-C = 120°]. The corresponding H atoms at each ring were calculated [d(C-H) 1.08 Å], with fixed temperature factors of 0.08 $Å^2$. Although the two hydrido ligands were not located directly from the X-ray analysis, suitable positions were obtained from potential energy calculations,[4] for one hydride to cap an Ru_3 face and other to bridge an Ru-Ru edge of the ruthenium tetrahedron, {section 2.3.1}. In the next stage, anisotropic temperature factors were assigned to the Au, Cu, four Ru and two P atoms, whose parameters together with the isotropic parameters of the remaining non-hydrogen atoms were allowed to refine in 2 full-matrix least square cycles, ($R = 0.0722; R_w = 0.0720$). The resulting difference-Fourier map at this stage disclosed few residual peaks in the region of the metal atoms, with maximum height of 0.9 e $\mathring{A}^{-3}$. Finally, 4 full-matrix cycles of refinement on the parameters of all the non-hydrogen atoms converged at $R = 0.0605$ and $R_w = 0.0603$ with weights of $1/\sigma^2F_o$ assigned to individual reflections.

Section 4.7 Analysis and experimental data for the heptanuclear cluster $[Au_3Ru_4(\mu\text{-}H)(CO)_{12}\{\mu\text{-}Ph_2PCH_2PPh_2\}(PPh_3)]$ (1), {X-ray study presented in section 2.4}.

4.7.1 Crystal data for (1):- $C_{55}H_{38}Au_3O_{12}P_3Ru_4$, M = 1978.65, Monoclinic, space group $P2_1/n$, (non-standard for $P2_1/c$) a = 15.412(2) b = 24.835(3), c = 15.613(2) Å, β = 102.87(2)°, U = 5832.57 Å^3, F(000) = 3688, μ(Mo-Kα) = 82.76 cm^{-1}, Z = 4, D_c = 2.25 g cm^{-3}.

4.7.2 Data collection.

Data for a single crystal of $[Au_3Ru_4(\mu\text{-}H)(CO)_{12}\{\mu\text{-}Ph_2PCH_2PPh_2\}(PPh_3)]$ was collected using the methods described in sections 4.1-4.1.2. Table 4.7.2 summarises the parameters associated with data collection.

Table 4.7.2.

Crystal size = 0.25 x 0.25 x 0.15 mm

θ-range $3 < 0 < 25$

h,k,l range

$-25 < h < 25$

$0 < k < 35$

$0 < l < 20$

Scan width 0.7°

Number of unique reflections (N) with $I/\sigma(I) > 3.0$ = 2985.

4.7.3 Structure solution and refinement.

The Patterson map was solved for two gold and two ruthenium atoms which defined a tetrahedron. Using the fractional co-ordinates of these atoms and allowing the overall scale factors to refine in 1 least squares cycle, an observed-Fourier map was calculated, ($R = 0.3620; R_w = 0.3628$). The electron density map revealed suitable maxima for the remaining gold, two ruthenium and three phosphorus atoms. Subsequently, the overall scale factor was refined in 1 cycle, separately from the 2 full-matrix cycles used to refine the fractional co-ordinates and isotropic temperature factors of the seven metal and three phosphorus atoms, ($R = 0.1520$; $R_w = 0.1526$). The difference-Fourier map showed suitable atom positions for the 9 of the 12 carbonyl groups and 4 of 7 phenyl rings. The parameters of these newly found atoms were incorporated into the calculation of structure factors, but were not refined, whereas 3 full-matrix cycles were used to improve the refined isotropic parameters of the seven metal and three phosphorus atoms, ($R = 0.1320$; $R_w = 0.1328$). The second difference-Fourier map showed suitable atom positions for the remaining non-hydrogen atoms. The six carbon atoms of each phenyl ring were grouped to form rigid hexagons, [d(C-C) 1.395 Å; C-C-C = 120°] and corresponding hydrogen atoms at each ring were geometrically calculated [d(C-H) 1.08 Å] and were included into the structure refinement with fixed temperature factors of 0.08 $Å^2$. Although the hydrido ligand was not located directly from the X-ray analysis, a suitable position for the ligand to bridge an Ru-Ru edge of the Ru_4 tetrahedron was obtained from potential energy calculations.[4] The parameters of this atom were incorporated into the calculation of structure factors, but were not refined. In the final stages of structure solution, 3 full-matrix least squares cycles of refinement on the parameters of all the non-hydrogen atoms, with the three Au, four Ru and three P atoms treated as anisotropically vibrating atoms, reduced the R-factor to 7.22%. The difference-Fourier map at this stage showed few residual peaks in close proximity to the metal atoms, with maximum height of 1.4 e $Å^{-3}$.

Finally 4 full-matrix least squares cycles of refinement on the atomic and thermal parameters of all the non-hydrogen atoms converged at, R = 0.0636 and R_w = 0.0601, with weights of $w = 1/\sigma^2 F_o$ assigned to individual reflections.

Section 4.8 Analyses and experimental data for the trinuclear isomers $[Os_3H_2(CCHOEt)(CO)_9]$ (1) and $[Os_3H_2(HCCOEt)(CO)_9]$ (2), {X-ray studies presented in section 3.2}.

4.8.1 Crystal data for $[Os_3H_2(CCHOEt)(CO)_9]$ (1): $C_{13}H_8O_{10}Os_3$, M = 894.80, Monoclinic, space group $P2_1/n$, a = 19.416(3), b = 11.512(2), c = 8.622(2) Å, β = 103.38(2)°, U = 1874.85 Å^3 F(000) = 1576, μ(Mo-K_α) = 195.33 cm^{-1}, Z = 4, D_c = 3.17 g cm^{-3}.

4.8.2 Crystal data for $[Os_3H_2(HCCOEt)(CO)_9]$ (2): $C_{13}H_8O_{10}Os_3$, M = 894.80, Monoclinic, space group Cc, a = 15.054(3), b = 10.114(2), c = 12.902(2) Å, β = 107.75(2)°, U = 1870.89 Å^3 F(000) = 1576, μ(Mo-K_α) = 195.75 cm^{-1}, Z = 4, D_c = 3.17 g cm^{-3}.

4.8.3 Data collection for $[Os_3H_2(CCHOEt)(CO)_9]$ (1) and $[Os_3H_2(HCCOEt)(CO)_9]$ (2).

Data sets for a single crystal of both (1) and (2) were collected using the methods described in section 4.1-4.1.2 and Table 4.8.3 summarises the parameters associated with data collection.

Table 4.8.3

Crystal size = 0.25 x 0.22 x 0.13 mm (1) 0.20 x 0.22 x 0.10 mm (2)

θ-range 3 < 0 < 25 for both (1) and (2)

h,k,l range

-28 < h < 28 (1)	-24 < h < 24 (2)
0 < k < 17	0 < k < 16
0 < l < 13	0< < l < 20

Scan width 0.9° for (1) and 0.80° for (2)

Number of unique reflections (N) with $I/\sigma(I) > 3.0$ = 2985 (1) and 2894 (2).

4.8.4 Structure solution and refinement for $[Os_3H_2(CCHOEt)(CO)_9]$ (1).

The processed data showed the following conditions limiting diffraction,

0k0; k = 2n

h0l; h+l = 2n

which were characteristic for the space group $P2_1/n$ (non standard setting for $P2_1/c$). The Patterson map was solved for the three osmium atoms. In the next stage of structure solution, the overall scale factors were refined in one cycle, separately from the 2 full-matrix least squares cycles used to refine the fractional co-ordinates and isotropic temperature factors of the three osmium atoms (R = 1610; R_w = 0.1618). The difference-Fourier map revealed suitable atom positions for all 9 carbonyl groups, the oxygen and four carbon atoms of the ethoxy vinyl ligand. The fractional co-ordinates and isotropic temperature factors of these newly found atoms together with the refined isotropic parameters of the metal atoms were allowed to refine in 2 full-matrix least squares cycles (R = 0.0810; R_w = 0.0800). At this stage an empirical absorption correction was made to the data set using DIFABS.[3] Subsequent refinement of the overall scale factors together with two separate blocked full-matrix cycles on the isotropic parameters of all the non-hydrogen atoms, converged at R = 0.0610 and R_w = 0.0589. The three osmium atoms together with the atoms of the 9 carbonyl groups and ethoxy ligand were next assigned anisotropic temperature factors whilst their parameters refined in 2 full-matrix least squares cycles, (R = 0.0580 R_w = 0.0577). The resulting difference-Fourier map showed few residual peaks in close proximity to the metal atoms, with maximum height of 0.8 e Å^{-3}. The positions of the two hydrido ligands were obtained from potential energy minimisation calculations,[4] for each ligand to bridge an Os-Os bond of the triangular metal framework, (section 3.2.2). The parameters of these ligands were included into the calculation of structure factors but were not refined.

Finally, 3 full-matrix least squares cycles of refinement on the parameters of all the non-hydrogen atoms converged at R = 0.0435 and R_w = 0.0439, with weights of $1/\sigma^2(F_o)$ assigned to individual reflections.

4.8.5 Structure solution for $[Os_3H_2(HCCOEt)(CO)_9]$ (2)

The following conditions limiting diffraction were observed in the data,

hkl; h+k = 2n

h0l; l = 2n

Indicating the presence of a c-glide plane running parallel in direction to the c axis and perpendicular to the b axis at y = 0 in the monoclinic C-face centered unit cell. The space groups could therefore be Cc or C2/c and at this stage it was impossible to distinguish between the two. The equivalent positions for the space groups Cc and C2/c were obtained by addition of the overall translational vector, t = (1/2,1/2,0) to the symmetry elements of c and 2/c. Ultimately eight equivalent positions were generated for the space group C2/c and four equivalent positions for Cc:

C2/c (0,0,0; 1/2,1/2,0) +

(a) x,y,z; (b) -x,-y,-z; (c) x,-y,1/2+z; (d) -x,y,1/2-z.

Cc (0,0,0; 1/2,1/2,0) +

(a) x,y,z; (b)x,-y,1/2+z.

The vectors in the Harker planes and lines, relating pairs of atoms by symmetry operations of the 2-fold rotation and the c-glide translation in both space groups were next generated:

C2/c (0,0,0; 1/2,1/2,0) +

(a) 0,2y,1/2; (b) 2x,0,1/2+z.

Cc (0,0,0; 1/2,1/2,0) +

(a) 0,2y,1/2.

Stage 1 in structure solution.

To distinguish between the centrosymmetric space group C2/c and the non centrosymmetric space group Cc, the Patterson map, {Table 4.8.5(a)} was examined for peaks of the type u, 0, w. These peaks characterise the presence of the point group symmetry element, 2, relating pairs of atoms by the symmetry operation involving a rotation through a 180° about the symmetry axis. The Patterson map showed an excess of twenty peaks of this type, {Table 4.8.5(a)}. However, calculation of the density gave a reasonable value with four molecules in the unit cell and structure solution was therefore proceeded in the non-centrosymmetric space group Cc. Table 4.8.5(b) lists the vectors between non-symmetry related atoms, positioned at x_1, y_1, z_1 and x_2, y_2, z_2, generated from the equivalent positions of the space group Cc.[2]

Table 4.8.5(b)

(0,0,0;1/2,1/2,0) +

x_1-x_2, y_1-y_2, z_1-z_2 (a)

x_1-x_2, y_1+y_2, $1/2+(z_1-z_2)$ (b)

Stage 2.

The Patterson map showed three 'short' vectors in the range 2.805-3.017 Å corresponding to the three expected Os-Os vectors.

These vectors were used to formulate a triangle relating the three metal atoms:

Height (arbitary units)	u	v	w
	x_1-x_2	y_1-y_2	z_1-z_2
1-2 (155)	0.074	-0.277	0.042
	x_1-x_3	y_1-y_3	z_1-z_3
1-3 (152)	0.124	-0.102	-0.104
	x_2-x_3	y_2-y_3	z_2-z_3
2-3 (144)	0.050	0.175	-0.146

Stage 3.

Taking the vector 1-2,

x_1-x_2	y_1-y_2	z_1-z_2
0.074	-0.277	0.042

vector (b) {Table 4.8.5(b)} was looked for in the Patterson map,

x_1-x_2	y_1+y_2	$1/2+(z_1-z_2)$ (b)
0.074	?	-0.458

a corresponding vector was found at height (316)

-0.077	0.500	0.454

This gave a potential numerical value for y_1+y_2 to be 0.5 and therefore the presence of the vector type, 0, v, 1/2, in the Harker line, 0, 2y, 1/2 could now be checked for since,

y_1-y_2 = -0.278 (i)

y_1+y_2 = 0.500 (ii)

$2y_1$ 0.222 [addition of i + ii]

$2y_2$ 0.778 (-0.222) [subtraction of ii from i]

The Patterson map showed a corresponding vector at height (318) 0, 0.224, 0.5, which was equivalent for both $2y_1$ and $2y_2$.

Stage 4.

Taking the vector 1-3

x_1-x_3	y_1-y_3	z_1-z_3
0.124	-0.102	-0.104

the vector, x_1-x_3, y_1+y_3, $1/2+(z_1-z_3)$, was found at height (150),

0.124	0.331	0.396

therefore, $y_1-y_3 = -0.104$

$y_1+y_3 = 0.331$

$2y_1$ 0.227

$2y_3$ 0.435

The symmetry related vector 0, $2y_3$, 1/2 in the Harker line 0, v, 1/2 was located; (167) 0, 0.433, 0.5.

Stage 5.

Taking the vector 2-3,

x_2-x_3	y_2-y_3	z_2-z_3
0.050	0.175	-0.146

the vector, x_2-x_3, y_2+y_3, $1/2+(z_2-z_3)$ was found at height (140)

0.048	0.609	0.351

therefore, $y_2-y_3 = 0.175$

$y_2+y_3 = 0.609$

$2y_2$ 0.784

$2y_3$ 0.434

Stage 6.

Two independent sets of values of $2y_1$, $2y_2$, $2y_3$ were now obtained from the above stages,

$2y_1$	0.222 and 0.227	y_1	= 0.113
$2y_2$	0.778 and 0.784	y_2	= 0.391
$2y_3$	0.435 and 0.434	y_3	= 0.217

the results were in good agreement and the average value of y_1, y_2 and y_3 were taken in further stages of structure solution.

Stage 7.

In the non-centrosymmetric space group Cc, the translational component of c-glide runs parallel in direction to the c axis and is perpendicular to the b axis at $y = 0$. The origin can be chosen arbitarily in the x and z directions in this space group. Therefore the co-ordinate of osmium atom (1) was set invariant at $x = 0$ and $z = 0$:

Os(1)	0.000	0.113	0.000

Stage 8.

To assign the fractional co-ordinates to the remaining two osmium atoms, the position of Os(1) was used in algebraically manipulating the vectors used in the formation of the triangle relating the three metal atoms, (stage 2), to give the following fractional co-ordinates for Os(2) and Os(3):

Os(2)	-0.075	0.391	0.042
Os(3)	-0.049	0.217	0.103

Table 4.8.5(a).

HEIGHT	U	V	W	DISTANCE
318.0	0.500	0.276	0.500	8.744
318.0	0.000	0.224	0.500	6.837
318.0	0.000	0.224	0.500	6.837
316.0	-0.077	0.500	0.454	8.085
316.0	0.423	0.000	0.454	7.219
167.0	0.500	0.067	0.500	8.314
167.0	0.000	0.433	0.500	7.797
167.0	0.000	0.433	0.500	7.797
155.0	-0.426	0.223	0.042	6.973
155.0	0.074	0.277	0.042	3.003
152.0	-0.124	0.102	0.104	2.807
152.0	0.376	0.398	0.104	6.739
150.0	0.124	0.331	0.396	5.914
150.0	-0.376	0.169	0.396	8.871
144.0	0.453	0.325	0.145	7.282
144.0	-0.046	0.175	0.145	2.811
140.0	-0.454	0.106	0.355	9.377
140.0	0.046	0.394	0.355	5.950
85.0	-0.001	0.000	0.099	1.282
85.0	0.499	0.500	0.099	8.820
85.0	-0.001	0.000	0.099	1.282
67.0	0.002	0.000	0.157	2.017
67.0	-0.498	0.500	0.157	9.754
67.0	0.002	0.000	0.157	2.017
64.0	0.002	0.000	0.244	3.139
64.0	-0.498	0.500	0.244	10.299
64.0	0.002	0.000	0.244	3.139
62.0	0.000	0.000	0.500	6.451
62.0	0.500	0.500	0.500	9.708
62.0	0.000	0.000	0.500	6.451
60.0	0.000	0.000	0.365	4.709
60.0	0.500	0.500	0.365	9.099
60.0	0.000	0.000	0.365	4.709
27.0	-0.074	0.500	0.353	7.117
27.0	0.426	0.000	0.353	6.638
27.0	-0.081	0.500	0.295	6.662
27.0	0.419	0.000	0.295	6.296
26.0	-0.002	0.218	0.397	5.585
26.0	0.498	0.282	0.397	8.195
26.0	-0.002	0.218	0.397	5.585
24.0	0.494	0.286	0.249	7.709
24.0	-0.006	0.214	0.249	3.897
23.0	0.000	0.213	0.000	2.154
23.0	0.500	0.287	0.000	8.067
23.0	0.000	0.213	0.000	2.154
23.0	0.482	0.375	0.000	8.187
23.0	-0.482	0.375	0.000	8.187
23.0	0.018	0.125	0.000	1.293
23.0	-0.018	0.125	0.000	1.293
23.0	-0.004	0.214	0.332	4.816
23.0	0.496	0.286	0.332	7.935
23.0	-0.004	0.214	0.332	4.816
22.0	-0.420	0.000	0.030	6.451
22.0	0.080	0.500	0.030	5.185
20.0				

4.8.6 Structure refinement for [Os_3H_2(HCCOEt)$(CO)_9$] (2).

Using the positions of the three osmium atoms deduced from the Patterson synthesis as a starting set, a series of difference-Fourier maps subsequently revealed suitable maxima in the electron density maps for all the remaining non-hydrogen atoms. There were no significant correlations during refinement between the parameters of any of the atoms which might have been expected, if in fact the space group were the centrosymmetric C2/c. Two cycles of refinement on the isotropic atom parameters of all the non -hydrogen atoms converged at $R = 0.0590$ and $R_w = 0.0571$. At this stage an empirical absorption correction was made to the data set using DIFABS.[3] Subsequently the overall scale factor was refined in 1 cycle, separately from the two full-matrix least squares cycles used to improve the refined parameters of all the non-hydrogen atoms ($R = 0.0412$ and $R_w = 0.0419$). Anisotropic temperature factors were next assigned to the three Os, and the oxygen atoms of the 9 carbonyl groups during further refinement of their parameters in 2 full-matrix cycles, ($R = 0.0391$:$R_w = 0.0395$). The positions of the two hydrido ligands were obtained from potential energy minimisation calculations[4] (section 3.2.2) and were included in the calculation of structure factors but were not refined.

Finally, 4 full-matrix least squares cycles of refinement on the parameters of all the non-hydrogen atoms converged at $R = 0.0317$ and $R_w = 0.0315$ with weights of $1/\sigma^2(F_o)$ assigned to individual reflections.

Section 4.9 Analysis and experimental data for the tetra-ruthenium hydrido cluster $[Ru_4H_3(CO)_{12}][PPN]$ (1), {X-ray study presented in section 3.3}.

4.9.1 Crystal data for (1): $C_{48}H_{33}NO_{12}P_2Ru_4$, M = 1281.73, Monoclinic, space group $P2_1/c$, a = 11.721(2), b = 28.978(4), c = 14.822(3) Å, β = 100.28(2)°, U = 4953.46 $Å^3$, F(000) = 2560, $\mu(Mo-K_\alpha)$ = 16.98 cm^{-1}, Z = 4, D_c = 1.72 g cm^{-3}.

4.9.2 Data collection for $[Ru_4H_3(CO)_{12}][PPN]$ (1).

Data for a single crystal of (1) was collected using the methods described in sections 4.1-4.1.2. Table 4.9.2 lists the parameters associated with data collection.

Table 4.9.2

Crystal size = 0.22 x 0.18 x 0.20 mm

θ-range 3 < 0 < 25

h,k,l range

$-18 < h < 18$

$0 < k < 36$

$0 < l < 15$

Scan width 0.8°

Number of unique reflections (N) with $I/\sigma(I) > 3.0$ = 2566.

4.9.3 Structure solution and refinement for $[Ru_4H_3(CO)_{12}][PPN]$ (1).

The positions of the four ruthenium atoms were deduced from a Patterson synthesis. In the next stage of structure solution, 1 least squares cycle was used to refine the overall scale factors, whereas the fractional co-ordinates and isotropic temperature factors of the four metal atoms were allowed to refine in 2 separate blocked full-matrix cycles (R = 0.1410 and R_w = 0.1415). The difference-Fourier map revealed suitable positions for the P and the

N atoms of the counter ion and all the 12 carbonyl groups. Subsequently, 2 full-matrix least squares cycles were used to refine the isotropic parameters of these newly found atoms and the refined parameters of the four ruthenium atoms ,($R = 0.0820$, $R_w = 0.0817$). The second difference-Fourier map revealed atom positions for all the carbon atoms of the three phenyl groups of the counter ion. The six carbon atoms of each phenyl ring were grouped to form rigid hexagons [d(C-C) = 1.395 Å;C-C-C = 120°], with the sp^2 C-H phenyl hydrogen atoms geometrically calculated to ride at respective carbon atoms at distances of 1.08 Å, with fixed temperature factors of 0.08 $Å^2$. Anisotropic temperature factors were next assigned to the phosphorus, nitrogen and the four ruthenium atoms, whilst only their parameters refined in 3 blocked full-matrix cycles, ($R = 0.0602$, $R_w = 0.0608$). Suitable positions for the three hydrido ligands were obtained from potential energy minimisation calculations,[4] for each ligand to bridge a Ru-Ru edge of the ruthenium tetrahedron (section 3.3.2). The parameters of these atoms were included in the calculation of stucture factors, but were not refined.

Finally, 3 full-matrix least squares cycles of refinement on the parameters of all the non-hydrogen atoms converged at $R = 0.0523$ and $R_w = 0.0519$, with weights of $1/\sigma^2(F_o)$ assigned to individual reflections.

Section 4.10 Analysis and experimental data for the hexanuclear osmium cluster compound $[Os_6H_2(CO)_{17}P(OMe)_3]$ (1), {X-ray study presented in section 3.4}.

4.10.1 Crystal data for $[Os_6H_2(CO)_{17}P(OMe)_3]$ (1):

$C_{20}H_{11}O_{20}POs_6$, M = 1743.46, Orthorhombic, space group $Pna2_1$, a = 21.960(3), b = 9.487(2), c = 15.270(3) Å, $\alpha = \beta = \gamma = 90^\circ$, U = 3181.27 $Å^3$, F(000) = 3048, $\mu(Mo\text{-}K_\alpha) = 115.29\ cm^{-1}$, Z = 4, $D_c = 3.64\ g\ cm^{-3}$.

4.10.2 Data collection for $[Os_6H_2(CO)_{17}P(OMe)_3]$ (1).

Data for a single crystal of (1) was collected using the methods outlined in sections 4.1-4.1.2 and Table 4.10.2 summarises the parameters associated with data collection.

Table 4.10.2

Crystal size = 0.20 x 0.24 x 0.20 mm

θ-range $3 < 0 < 25$

h,k,l range

$0 < h < 30$

$0 < k < 13$

$0 < l < 21$

Scan width 0.6°

Number of unique reflections (N) with $I/\sigma(I) > 3.0$ = 2288.

4.10.3 Structure solution and refinement for $[Os_6H_2(CO)_{17}P(OMe)_3]$ (1).

The following conditions limiting diffraction in the data were consistent with the non-centrosymmetric space group $Pna2_1$,

0kl; k+l = 2n h0l; h = 2n 00l; l = 2n

and the positions of three osmium atoms were deduced in this space group from a Patterson synthesis. Taking the fractional co-ordinates of these three metal atoms and allowing the overall scale factors to refine independently in 1 least squares cycle, an observed-Fourier map was calculated, ($R = 0.2921$, $R_w = 0.3220$). The electron density map showed suitable maxima for the remaining three osmium atoms and the phosphorus atom of the phosphite ligand. Subsequently, the overall scale factors were refined in 1 cycle, separately from the 2 full-matrix least squares cycles used to refine the fractional co-ordinates and isotropic temperature factors of the P and six metal atoms, ($R = 0.1420$ and $R_w = 0.1425$). The difference-Fourier map revealed suitable atom positions for the three oxygen atoms of the organophosphine ligand and of 10 of the 17 carbonyl groups. The positions of these newly found atoms were included into the structure factor calculations but were not refined, whereas a further 2 full-matrix cycles were used to improve the refined isotropic parameters of the P and six osmium atoms, ($R = 0.1010$;$R_w = 0.1015$). The second difference-Fourier map revealed atom positions for the remaining carbonyl groups. Subsequently, 2 full-matrix cycles used to refine the isotropic parameters of all the non-hydrogen atoms reduced the R-factor to 8.20%. At this stage an empirical absorption correction was made to the data using DIFABS.[3] After this procedure the overall scale factors were again refined separately from the 2 blocked full-matrix cycles used to improve the refined isotropic parameters of all the non-hydrogen atoms, ($R = 0.0612$;$R_w = 0.0610$). Anisotropic temperature factors were next assigned to the P and six Os atoms during refinement of only their parameters in 2 full-matrix least squares cycles, ($R = 0.0552$;$R_w = 0.0525$). The resulting difference-Fourier map revealed few residual peaks in close proximity to the metal atoms, with maximum height of 0.9 e $\mathring{A}^{-3}$. The position of one of the two hydrido ligands was successfully located from potential energy calculations[4] (section 3.4), and whose parameters were included in the calculation of structure factors, but were not refined.

Finally, 4 full-matrix least squares cycles of refinement on the parameters of all the non-hydrogen atoms coverged at $R = 0.0410$, and $R_w = 0.0417$ with weights of $1/\sigma^2(F_o)$ assigned to individual reflections.

Section 4.11 Analysis and experimental data for the heptanuclear hydrido cluster [$Os_7H_2(CO)_{22}$] (1), {X-ray study presented in section 3.5}.

4.11.1 Crystal data for [$Os_7H_2(CO)_{22}$] (1): $C_{22}H_2O_{22}Os_7$, M = 1949.63, Monoclinic, space group $P2_1/c$, a = 18.707(3), b = 9.408(2), c = 19.011(3) Å, β = 100.23, U = 3292.66 $Å^3$, F(000) = 3368 μ(Mo-K_α) = 221.02 cm^{-1}, Z = 4, D_c = 3·64g cm^{-3}.

4.11.2 Data collection for [$Os_7H_2(CO)_{22}$] (1).

Data for a single crystal of (1) was collected using the methods outlined in sections 4.1-4.1.2 and Table 4.11.2 summarises the parameters associated with data collection.

Table 4.11.2.

Crystal size = 0.18 x 0.18 x 0.15 mm

θ-range $3 < 0 < 25$

h,k,l range

$-24 < h < 24$

$0 < k < 12$

$0 < l < 24$

Scan width 0.8°

Number of unique reflections (N) with $I/\sigma(I) > 3.0$ = 3715.

4.11.3 Structure solution and refinement for [$Os_7H_2(CO)_{22}$] (1).

The following conditions limiting diffraction were observed to be present in the data and were characteristic for the space group $P2_1/c$:

0k0; k = 2n

h0l; l = 2n

The positions of four of the seven osmium atoms were deduced from a Patterson synthesis. Using the fractional co-ordinates of these atoms and allowing the overall scale factors to refine in 1 least squares cycle, an observed-Fourier map was calculated, ($R = 0.2520$; $R_w = 0.2527$). The electron density map revealed suitable maxima for the remaining three osmium atoms. In the next stage of structure solution, the overall scale factor was refined in 1 cycle, separately from the 2 full-matrix least squares cycles used to refine the fractional co-ordinates and isotropic thermal parameters of the seven metal atoms, ($R = 0.1416$ and $R_w = 0.1415$). The difference-Fourier map revealed atom positions for all the 22 carbonyl groups. The parameters of these 'newly' found atoms together with the refined isotropic parameters of the metal atoms were allowed to refine in 2 full-matrix cycles, ($R = 0.0811$ and $R_w = 0.0798$). At this stage an empirical absorption correction was made to the data using the DIFABS.[3] Subsequently, using 1 cycle to refine the overall scale factors and 2 separate blocked full-matrix least squares cycles to improve the refined isotropic parameters of the non-hydrogen atoms, the R-factor reduced to 5.67%. Anisotropic temperature factors were next assigned to the seven osmium atoms during refinement of only their parameters in 2 full-matrix cycles, ($R = 0.0501$;$R_w = 0.0497$). The difference-Fourier map revealed a few residual peaks in close proximity to the metal atoms, with maximium height of 0.9 e Å^{-3}. The positions of the two hydrido ligands were obtained from potential energy calculations[4] (section 3.5.1) and whose parameters were included in the calculation of structure factors, but were not refined.

Finally, 4 full-matrix least squares cycles of refinement on the parameters of all the non-hydrogen atoms converged at $R = 0.0421$, and $R_w = 0.0418$ with weights of $1/\sigma^2(F_o)$ assigned to individual reflections.

Section 4.12 Analysis and experimental data for $[Os_7H_2(CO)_{19}\{MeC{=}CMe\}]$ (1), {X-ray study presented in section 3.6}.

4.12.1 Crystal data for $[Os_7H_2(CO)_{19}\{MeC{=}CMe\}]$ (1): $C_{23}H_8O_{19}Os_7$, M = 1919.69, Monoclinic, space group $P2_1/n$, a = 37.741(4), b = 9.082(2), c = 22.563(3) Å, β = 112.75(2)°, U = 7132.10 $Å^3$, F(000) = 2752, μ(Mo-Kα) = 119.58 cm^{-1}, Z = 4, D_c = 2.70 g cm^{-3}.

4.12.2 Data collection for $[Os_7H_2(CO)_{19}\{MeC{=}CMe\}]$ (1).

Data for a single crystal of (1) was collected using the methods outlined in sections 4.1-4.1.2. Table 4.12.2 lists the parameters associated with data collection.

Table 4.12.2.

Crystal size = 0.18 x 0.20 x 0.21 mm

θ-range 3 < θ < 25

h,k,l range

$-55 < h < 55$

$0 < k < 12$

$0 < l < 27$

Scan width 0.8°

Number of unique reflections (N) with $I/\sigma(I) > 3.0$ = 2788.

4.12.3 Structure solution and refinement for $[Os_7H_2(CO)_{19}\{MeC{=}CMe\}]$ (1).

The following conditions limiting diffraction were observed in the data and were characteristic for the non-standard monoclinic space group $P2_1/n$:

0k0; k = 2n

h0l; h+l = 2n

The positions of four of the seven osmium atoms were deduced from a

Patterson synthesis. Taking the fractional co-ordinates of these atoms and allowing the overall scale factors to refine in 1 least squares cycle, an observed-Fourier map was calculated, ($R = 0.3621; R_w = 0.3630$). The electron density map showed three prominent peaks of similar electron density which were assigned to the remaining Os atoms. In the next stage of structure solution, 1 cycle was used to refine the overall scale factors, whereas two separate full-matrix least squares cycles were used to refine the fractional co-ordinates and isotropic temperature factors of the seven osmium metal atoms, ($R = 0.1516$ and $R_w = 0.1525$). The difference-Fourier map revealed suitable atom positions for the 19 carbonyl groups and the carbon atoms of the substituted alkyne ligand, {MeC=CMe}. The parameters of the newly found atoms together with the refined isotropic parameters of the metal atoms were subjected to a further 2 full-matrix cycles of refinement, ($R = 0.0911$ and $R_w = 0.0898$). At this stage an empirical absorption correction was made to the data using DIFABS.[3] Subsequently, the overall scale factor was refined in 1 cycle, separately from the 2 blocked full-matrix least squares cycles used to improve the refined isotropic parameters of the non-hydrogen atoms, ($R = 0.0667$, $R_w = 0.0661$). Anisotropic temperature factors were next assigned to the seven osmium atoms, whilst only their parameters refined in 2 full-matrix cycles, ($R = 0.0552; R_w = 0.0553$). The positions of one of the two hydrido ligands was unambiguously obtained from potential energy calculations[4] (section 3.6.1). The hydrogen atoms at the two methyl carbon atoms of the substituted alkyne ligand, MeC=CMe, were included in the final stages of structure refinement at calculated positions [d(C-H) 1.08 Å], with fixed thermal parameters of 0.08 Å^2.

Finally, 4 full-matrix cycles of refinement on the parameters of all the non-hydrogen atoms converged at $R = 0.0481$, and $R_w = 0.0488$ with weights of $1/\sigma^2(F_0)$ assigned to individual reflections.

Section 4.13 Analysis and experimental data for the deca-osmium cluster $[H_5Os_{10}(CO)_{24}][N(PPh_3)_2].(CH_2Cl_2)$, {X-ray study presented in section 3.7}.

4.13.1 Crystal data for $[H_5Os_{10}(CO)_{24}][PPN].(CH_2Cl_2)$ (1):

$C_{61}H_{37}O_{24}P_2NCl_2Os_{10}$, M = 3202.80, Monoclinic, space group $P2_1/c$, a = 11.749(2), b = 17.682(3), c = 35.061(4) Å, β = 92.57(2)°, U = 7276.45 $Å^3$, F(000) = 5704, μ(Mo-Kα) = 168.82 cm^{-1}, Z = 4, D_c = 2.18 g cm^{-3}.

4.13.2 Data collection for $[H_5Os_{10}(CO)_{24}][PPN].(CH_2Cl_2)$ (1).

Data for a single crystal of (1) was collected using the methods described in sections 4.1-4.1.2 and Table 4.13.2 lists the parameters associated with data collection.

Table 4.13.2.

Crystal size = 0.19 x 0.21 x 0.21 mm

θ-range $3 < 0 < 25$

h,k,l range

$-15 < h < 15$

$0 < k < 22$

$0 < l < 44$

Scan width 0.7°

Number of unique reflections (N) with $I/\sigma(I) > 3.0$ = 2758.

4.13.3 Structure solution and refinement for $[H_5Os_{10}(CO)_{24}][PPN].(CH_2Cl_2)$ (1).

The positions of six osmium atoms defining an octahedron were deduced from a Patterson synthesis. Subsequent difference-Fourier maps revealed suitable maxima in the electron density maps for all the remaining non-hydrogen atoms. The six carbon atoms of each phenyl ring of the counter ion $[N(PPh_3)_2]^+$ were grouped and included in subsequent stages of structure refinement as rigid hexagons [d(C-C) = 1.395 Å;C-C-C = 120°]. In the next stage of structure solution the overall scale factors were refined in 1 cycle, separately from the 2 blocked full-matrix least squares cycles used to refine the isotropic parameters of all the non-hydrogen atoms, (R = 0.0910 and R_w = 0.0915). At this stage an empirical absorption correction was made to the data using DIFABS.[3] Subsequently, the overall scale factors were refined separately from the 2 blocked full-matrix cycles used to improve the isotropic parameters of the non-hydrogen atoms (R = 0.0767, R_w = 0.0761). Anisotropic temperature factors were next assigned to the 10 osmium, two P, and two Cl atoms (of the solvent molecule), whilst only their parameters refined in 2 full-matrix cycles, (R = 0.0630;R_w = 0.0635). The resulting difference-Fourier map showed few maxima in the region of the metal atoms, with maximum height of 1.3 e $Å^{-3}$.

Finally, 4 full-matrix least squares cycles of refinement on the parameters of all the non-hydrogen atoms converged at R = 0.0521, and R_w = 0.0528 with weights of $1/\sigma^2(F_o)$ assigned to individual reflections.

Section 4.14 Analysis and experimental data for $[HOs_{11}C(CO)_{27}][PPh_3Me]$ (1), {X-ray study presented in section 3.8}.

4.14.1 Crystal data for $[HOs_{11}C(CO)_{27}][PPh_3Me]$ (10):

$C_{47}H_{19}O_{27}POs_{11}$, M = 3138.81, Triclinic, space group $P\bar{1}$ (No.2), a = 16.788(3), b = 17.019(3), c = 11.019(2)) Å, α = 103.34(2), β = 93.77(2), γ = 101.54(2)°, U = 2980.67 $Å^3$, F(000) = 2736, μ(Mo-Kα) = 225.35 cm^{-1}, Z = 2, D_c = 2.68 g cm^{-3}.

4.14.2 Data collection for $[HOs_{11}C(CO)_{27}][PPh_3Me]$ (1).

Data for a single crystal of (1) was collected using the methods outlined in sections 4.1-4.1.2 and Table 4.14.2 summarises the parameters associated with data collection.

Table 4.14.2.

Crystal size = 0.50 x 0.48 x 0.15 mm

θ-range   3 < 0 < 25

h,k,l range

$-20 < h < 20$

$-20 < k < 20$

$0 < l < 13$

Scan width 0.9°

Number of unique reflections (N) with $I/\sigma(I) > 3.0$ = 3266.

Crystals of (1) diffracted very weakly so that a relatively large crystal was necessary; azimuthal scan data could not be collected due to the onset of decomposition in the last stages of data collection.

4.14.3 Structure solution and refinement for $[HOs_{11}C(CO)_{27}][PPh_3Me]$ (1).

The structure of (1) was solved from a Patterson synthesis from which 4 osmium atoms forming one capping tetrahedron were located.

The remaining seven osmium atoms were located from an observed-Fourier map. The positions of most of the non-hydrogen atoms were located with some difficulty from subsequent difference-Fourier syntheses. No suitable maxima could be located for the atoms of one phenyl ring of the $[PPh_3Me]^+$ cation, nor for one carbonyl group thought to bridge the bond, Os(10)-Os(11), as inferred from the i.r. data. Several strategies were employed in attempting to deduce the positions of these atoms, but they could not be located with certainty. An empirical absorption correction[3] was applied to the data, which allowed relatively satisfactory refinement of the parameters of the atoms that had been located, but did not help with the location of the missing atoms. Anisotropic temperature factors were assigned to the Os and P atoms, and full-matrix refinement of the parameters of the located non-hydrogen atoms gave $R = 0.1089$ and $R_w = 0.1086$ with weights of $1/\sigma^2(F_0)$ assigned to individual reflections.

Section 4.15. References.

1. G.M. Sheldrick, SHELX 76 program system, University of Cambridge, 1976.

2. 'International Tables of X-ray Crystallography' Kynoch press, Birmingham, 1965.

3. N. Walker and D. Stuart, Acta Cryst., 1983, A39, 158.

4. A.G. Orpen, J. Chem. Soc., Dalton Trans., 1980, 2509.

Section 5. Publications.

Synthesis of Group 1B Sandwich Cluster Compounds with $[Pt_3(\mu\text{-}CO)_3(PPh_3)_3]$ and the Structural Characterisation of $[M\{Pt_3(\mu\text{-}CO)_3(PPh_3)_3\}_2]PF_6$ (M = Au or Cu) by Single-crystal *X*-Ray Techniques†

Malcolm F. Hallam and D. Michael P. Mingos*
Inorganic Chemistry Laboratory, University of Oxford, South Parks Road, Oxford OX1 3QR
Trushar Adatia and Mary McPartlin*
School of Chemistry, The Polytechnic of North London, Holloway, London N7 8DB

Sandwich cluster compounds of the type $[M\{Pt_3(\mu\text{-}CO)_3(PPh_3)_3\}_2]PF_6$ [M = Cu (**1a**) or Au (**1b**)], where the Group 1B metal is co-ordinated simultaneously to two planar $[Pt_3(\mu\text{-}CO)_3(PPh_3)_3]$ *triangulo* rings, have been synthesised from $[Pt_3(\mu\text{-}CO)_3(PPh_3)_4]$ and either $[Cu(MeCN)_4]PF_6$ or $[Au(L)Cl]$ (L = CO or Me_2S) in the presence of an excess of $TlPF_6$. Complexes (**1a**) and (**1b**) are both dark red crystalline solids and are isomorphous. They have been characterised using $^{31}P\text{-}\{^1H\}$ n.m.r. and single-crystal *X*-ray techniques.

Sandwich cluster compounds $[M\{Pt_3(\mu\text{-}CO)_3(PPh_3)_3\}_2]PF_6$ [M = Cu (**1a**) or Au (**1b**)] have been obtained from reaction of $[Pt_3(\mu\text{-}CO)_3(PPh_3)_4]$ with either $[Cu(MeCN)_4]PF_6$ or $[Au(L)Cl]$ (L = CO or Me_2S) in the presence of excess $TlPF_6$. A number of related cluster compounds have been synthesised previously in which two platinum triangular units are co-ordinated to a heterometal atom in a 'sandwich' fashion. Yamamoto *et al.*[1] have characterised the compound $[Hg\{Pt_3(\mu\text{-}CNC_6H_3Me_2\text{-}2,6)_3(CNC_6H_3Me_2\text{-}2,6)_3\}_2]$ (**2**), a neutral complex formed during the Na–Hg reduction of $[Pt(CNC_6H_3Me_2\text{-}2,6)_2Cl_2]$ in the presence of excess 2,6-xylyl isocyanide, together with the homometallic cluster $[Pt_7(CNC_6H_3Me_2\text{-}2,6)_{12}]$.[2] Both compounds are unusual in containing isocyanides as the only ligand. Venanzi and co-workers[3] have synthesised the compound $[Hg_2\{Pt_3(\mu\text{-}CO)_3(PPhPr^i_2)_3\}_2]$ (**3**) which is also a neutral complex, formed from the triangular platinum cluster $[Pt_3(\mu\text{-}CO)_3(PPhPr^i_2)_3]$ by reaction with metallic mercury. This compound contains a Hg_2 unit sandwiched between two platinum triangles which may also be considered as derived from two $[Pt_3Hg(\mu\text{-}CO)_3(PPhPr^i_2)_3]$ clusters linked by a long Hg–Hg bond. Most recently, Venanzi and co-workers[4] have reported the cationic complex $[Ag\{Pt_3(\mu\text{-}CO)_3(PPr^i_3)_3\}_2]^+$ (**4**) which they prepared by adding excess AgO_3SCF_3 to a solution of the triangular cluster $[Pt_3(\mu\text{-}CO)_3(PPr^i_3)_3]$, but they were unable to synthesise the corresponding gold compound by this route.

We report here the syntheses and *X*-ray structure analyses of the first sandwich compounds of this type linked by Cu^I and Au^I atoms.

Results and Discussion

Our initial attempts to synthesise sandwich cluster compounds from $[Pt_3(\mu\text{-}CO)_3\{P(C_6H_{11})_3\}_3]$ and gold(I) complexes failed because the gold complexes abstracted phosphine from the cluster.[5] Venanzi and co-workers[4] had encountered similar difficulties with $[Pt_3(\mu\text{-}CO)_3(PPr^i_3)_3]$, although they had successfully synthesised the corresponding silver sandwich compound. Our use of $[Pt_3(\mu\text{-}CO)_3(PPh_3)_4]$,[6] which has an additional and labile phosphine ligand co-ordinated to the *triangulo* cluster, as a starting material for the synthesis of this type of sandwich compound, proved successful, leading to the formation of Au^I and Cu^I compounds of this type.

When equimolar amounts of $[Pt_3(\mu\text{-}CO)_3(PPh_3)_4]$ and either $[Au(CO)Cl]$ or $[Au(Me_2S)Cl]$ were stirred together in

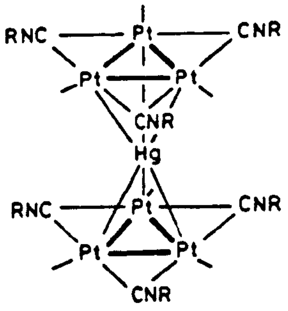

(**2**); R = $C_6H_3Me_2\text{-}2,6$

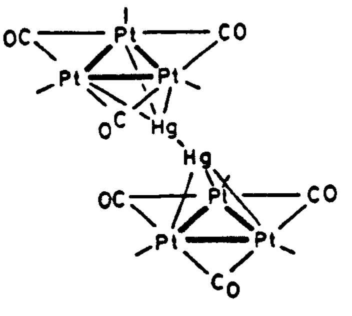

(**3**)

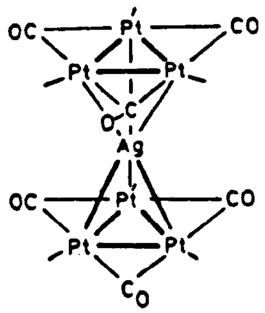

(**4**)

---

† Bis[1,2; 2,3; 1,3-tri-μ-carbonyl-1,2,3-tris(triphenylphosphine)triplatinio]-gold(I) (6 *Pt–Pt*) (6 *Au–Pt*) hexafluorophosphate and -copper(I) (6 *Pt–Pt*) (6 *Cu–Pt*) hexafluorophosphate respectively.

Supplementary data available: see Instructions for Authors, *J. Chem. Soc., Dalton Trans.*, 1988, Issue 1, pp. xvii—xx.

Table 1. Selected bond lengths (Å) for $[M\{Pt_3(\mu\text{-}CO)_3(PPh_3)_3\}_2]PF_6$ [M = Cu (**1a**) or Au (**1b**)]

	(**1a**)	(**1b**)
Pt(1)–Pt(2)	2.650(2)	2.683(1)
Pt(1)–Pt(3)	2.648(2)	2.683(1)
Pt(2)–Pt(3)	2.651(2)	2.683(1)
Pt(1)–M	2.605(4)	2.729(1)
Pt(2)–M	2.598(2)	2.731(1)
Pt(3)–M	2.598(3)	2.725(1)
Pt(1)–P(1)	2.241(8)	2.242(4)
Pt(2)–P(2)	2.235(10)	2.249(5)
Pt(3)–P(3)	2.242(8)	2.250(4)
Pt(1)–C(1)	2.08(3)	2.053(18)
Pt(1)–C(2)	2.03(3)	2.051(15)
Pt(2)–C(2)	2.05(3)	2.086(15)
Pt(2)–C(3)	2.19(4)	2.054(17)
Pt(3)–C(1)	2.15(3)	2.041(16)
Pt(3)–C(3)	2.15(4)	2.126(17)
P(1)–C(111)	1.81(3)	1.828(13)
P(1)–C(121)	1.773(12)	1.789(11)
P(1)–C(131)	1.793(10)	1.808(11)
P(2)–C(211)	1.813(10)	1.802(10)
P(2)–C(221)	1.813(11)	1.824(10)
P(2)–C(231)	1.753(10)	1.807(12)
P(3)–C(311)	1.833(12)	1.822(12)
P(3)–C(321)	1.797(10)	1.807(10)
P(3)–C(331)	1.785(12)	1.809(12)
C(1)–O(1)	1.12(4)	1.189(24)
C(2)–O(2)	1.20(4)	1.174(19)
C(3)–O(3)	1.08(5)	1.123(21)
P(4)–F(1)	1.728(1)	1.530(23)
P(4)–F(2)	1.541(1)	1.542(15)
P(4)–F(3)	1.523(1)	1.523(21)

In this and subsequent Tables the e.s.d.s are in parentheses.

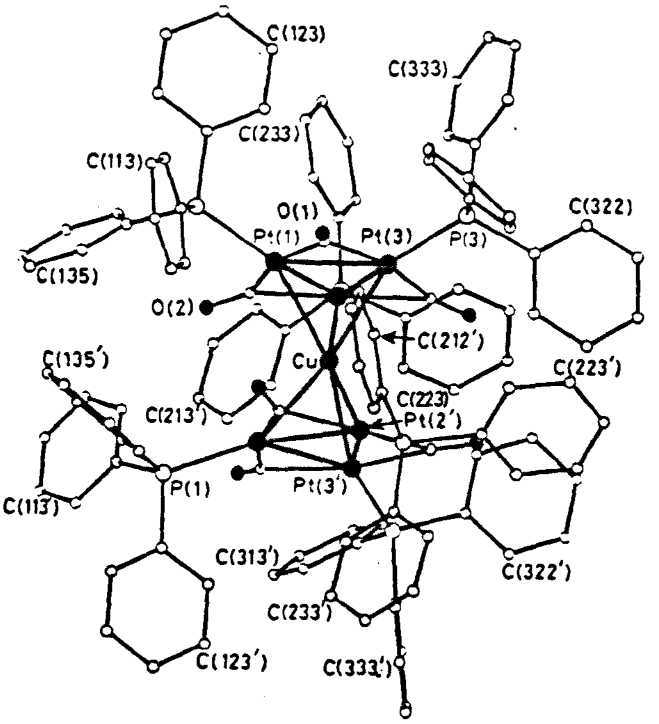

Figure 1. The structure of the cationic sandwich complex $[Cu\{Pt_3(\mu\text{-}CO)_3(PPh_3)_3\}_2]^+$ (**1a**) showing the atomic numbering scheme; the numbers for the C atoms of the phenyl rings run consecutively from the atom bonded to phosphorus

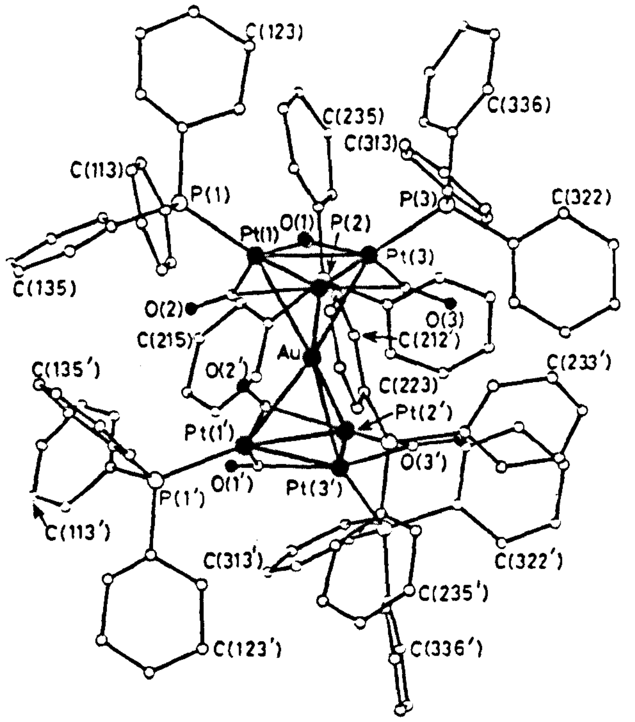

Figure 2. The structure of the cationic sandwich complex $[Au\{Pt_3(\mu\text{-}CO)_3(PPh_3)_3\}_2]^+$ (**1b**) showing the atomic numbering scheme; the numbers for the C atoms of the phenyl rings run consecutively from the atom bonded to phosphorus

benzene together with an excess of $TlPF_6$, a dark red precipitate was formed. Recrystallisation of this solid from CH_2Cl_2–hexane gave deep red crystals of $[Au\{Pt_3(\mu\text{-}CO)_3(PPh_3)_3\}_2]PF_6$ (**1b**) in *ca.* 86% yield. The i.r. spectrum of (**1b**) (Nujol mull) showed a single carbonyl stretching mode at 1 833 cm^{-1}, which is consistent with the presence of a C_3 axis in the molecule.[7] The corresponding copper complex $[Cu\{Pt_3(\mu\text{-}CO)_3(PPh_3)_3\}_2]PF_6$ (**1a**) was synthesised from $[Pt_3(\mu\text{-}CO)_3(PPh_3)_4]$ and $[Cu(MeCN)_4]PF_6$ in benzene, in *ca.* 80% yield. This compound also shows a single carbonyl stretching mode at 1 837 cm^{-1}.

The $^{31}P\text{-}\{^1H\}$ n.m.r. spectrum of (**1b**) in CD_2Cl_2 shows the characteristic features of a symmetrical $[Pt_3X_3(PR_3)_3]$ triangular unit, but the lines are quite broad and at room temperature long-range couplings between the two Pt_3 triangles could not be distinguished.[7,8]

Single-crystal *X*-ray diffraction studies of (**1a**) and (**1b**) established the structures shown in Figures 1 and 2 respectively. Selected intramolecular bond lengths and angles are summarised in Table 1 and 2. Each of the $[M\{Pt_3(\mu\text{-}CO)_3(PPh_3)\}_2]^+$ cations has a crystallographically imposed two-fold rotation axis, which passes through the Group 1B metal atom and relates the two Pt_3 triangles. The two structures are very similar with the six platinum atoms in each defining a structure intermediate between a trigonal prism and an octahedron. The Pt–Pt distances in (**1a**) are equal within experimental error [2.648(2)—2.650(2) Å] and in (**1b**) all three Pt–Pt lengths have the same value, 2.683(1) Å, being significantly longer than those in (**1a**). These distances lie in the range observed for 42e triangular cluster compounds, 2.65—2.75 Å, but are shorter than those usually observed in 44e triangular clusters, 2.86—2.90 Å.[9] The theoretical reason for this geometric observation has been discussed in some detail previously.[8] The equivalence of the Pt–Pt bonds within each of the compounds (**1a**) and (**1b**)

Table 2. Selected bond angles (°) for $[M\{Pt_3(\mu\text{-}CO)_3(PPh_3)_3\}_2]PF_6$ [M = Cu (**1a**) or Au (**1b**)]

	(**1a**)	(**1b**)
Pt(3)–Pt(1)–Pt(2)	60.0(1)	60.0(1)
M–Pt(1)–Pt(2)	59.2(1)	60.6(1)
M–Pt(1)–Pt(3)	59.3(1)	60.5(1)
P(1)–Pt(1)–Pt(2)	145.8(3)	145.3(1)
P(1)–Pt(1)–Pt(3)	140.1(2)	140.4(1)
P(1)–Pt(1)–M	148.7(3)	147.5(1)
C(1)–Pt(1)–Pt(2)	112.3(9)	108.8(4)
C(1)–Pt(1)–Pt(3)	52.4(9)	48.9(5)
C(1)–Pt(1)–M	82.3(8)	80.7(4)
C(1)–Pt(1)–P(1)	95.2(9)	98.7(4)
C(2)–Pt(1)–Pt(2)	49.8(8)	50.1(4)
C(2)–Pt(1)–Pt(3)	109.8(8)	110.1(4)
C(2)–Pt(1)–M	82.4(8)	82.4(4)
C(2)–Pt(1)–P(1)	103.5(8)	103.1(4)
C(2)–Pt(1)–C(1)	161(1)	158.1(6)
Pt(1)–M–Pt(1)	109.2(2)	112.3(1)
Pt(3)–Pt(2)–Pt(1)	59.9(1)	60.0(1)
M–Pt(2)–Pt(1)	59.5(1)	60.5(1)
M–Pt(2)–Pt(3)	59.3(1)	60.4(1)
P(2)–Pt(2)–Pt(1)	139.9(2)	140.2(1)
P(2)–Pt(2)–Pt(3)	145.4(2)	145.7(1)
P(2)–Pt(2)–M	149.2(2)	147.4(1)
C(3)–Pt(2)–Pt(1)	111(1)	111.1(5)
C(3)–Pt(2)–Pt(3)	52(1)	51.3(5)
C(3)–Pt(2)–M	83(1)	82.2(6)
C(3)–Pt(2)–P(2)	102(1)	102.7(6)
C(2)–Pt(2)–Pt(1)	49.1(8)	49.0(4)
C(2)–Pt(1)–Pt(3)	109.0(8)	108.9(4)
C(2)–Pt(2)–M	82.2(9)	81.8(5)
C(2)–Pt(2)–P(2)	97.5(9)	97.8(5)
C(2)–Pt(2)–C(3)	160(1)	159.3(7)
Pt(2)–Pt(3)–Pt(1)	60.0(1)	60.0(1)
M–Pt(3)–Pt(1)	59.5(1)	60.6(1)
M–Pt(3)–Pt(2)	59.3(1)	60.7(1)
P(3)–Pt(3)–Pt(1)	145.6(2)	145.5(1)
P(3)–Pt(3)–Pt(2)	140.0(3)	140.1(1)
P(3)–Pt(3)–M	148.8(3)	147.3(1)
C(1)–Pt(3)–Pt(1)	50.1(9)	49.3(5)
C(1)–Pt(3)–Pt(2)	109.9(9)	109.1(5)
C(1)–Pt(3)–M	81.2(7)	81.0(4)
C(1)–Pt(3)–P(3)	104.1(8)	104.5(4)
C(3)–Pt(3)–Pt(1)	113(1)	108.8(5)
C(3)–Pt(3)–Pt(2)	53(1)	48.9(5)
C(3)–Pt(3)–M	84.0(9)	81.1(4)
C(3)–Pt(3)–P(3)	94(1)	98.3(4)
C(3)–Pt(3)–C(1)	162(1)	157.0(6)
Pt(3)–M–Pt(3)	135.2(3)	136.1(1)
Pt(2)–M–Pt(1)	61.2(1)	58.9(1)
Pt(3)–M–Pt(1)	61.2(1)	58.9(1)
Pt(3)–M–Pt(2)	61.4(1)	58.9(1)
C(111)–P(1)–Pt(1)	113.4(9)	112.7(4)
C(121)–P(1)–Pt(1)	112(1)	113.4(5)
C(121)–P(1)–C(111)	106(1)	106.6(6)
C(131)–P(1)–Pt(1)	116.8(7)	115.8(4)
C(131)–P(1)–C(111)	104(1)	103.6(6)
C(131)–P(1)–C(121)	103(1)	103.6(7)
C(211)–P(2)–Pt(2)	114.4(8)	113.5(4)
C(221)–P(2)–Pt(2)	115(1)	115.5(4)
C(221)–P(2)–C(211)	102(1)	103.6(5)
C(231)–P(2)–Pt(2)	113(1)	113.3(5)
C(231)–P(2)–C(211)	106(1)	106.7(6)
C(231)–P(2)–C(221)	104(1)	103.1(6)
C(311)–P(3)–Pt(3)	116.5(8)	116.0(4)
C(321)–P(3)–Pt(3)	113.4(8)	112.9(4)
C(321)–P(3)–C(311)	104(1)	103.5(6)
C(331)–P(3)–Pt(3)	112(1)	112.7(5)
C(331)–P(3)–C(311)	103(1)	103.7(6)
C(331)–P(3)–C(321)	106(1)	107.1(6)
Pt(3)–C(1)–Pt(1)	77(1)	81.9(7)
O(1)–C(1)–Pt(1)	146(3)	139(1)
O(1)–C(1)–Pt(3)	136(3)	139(1)
Pt(3)–C(3)–Pt(2)	75(2)	79.8(6)
O(3)–C(3)–Pt(2)	136(3)	143(1)
O(3)–C(3)–Pt(3)	146(4)	137(2)
Pt(2)–C(2)–Pt(1)	81(1)	80.9(5)
O(2)–C(2)–Pt(1)	139(2)	139(1)
O(2)–C(2)–Pt(2)	139(2)	139(1)
C(112)–C(111)–P(1)	123(2)	121.9(9)
C(116)–C(111)–P(1)	117(2)	118.0(7)
C(122)–C(121)–P(1)	118(1)	118(1)
C(126)–C(121)–P(1)	122(2)	122(1)
C(132)–C(131)–P(1)	118(1)	119.0(9)
C(136)–C(131)–P(1)	122(2)	121(1)
C(212)–C(211)–P(2)	117(2)	117.6(9)
C(216)–C(211)–P(2)	123(1)	122.4(8)
C(222)–C(221)–P(2)	121(2)	120.3(7)
C(226)–C(221)–P(2)	119(2)	119.7(7)
C(232)–C(231)–P(2)	116(2)	118(1)
C(236)–C(231)–P(2)	124(2)	121.9(9)
C(312)–C(311)–P(3)	119(2)	118.1(9)
C(316)–C(311)–P(3)	120(2)	121.8(8)
C(322)–C(321)–P(3)	123(2)	122.4(8)
C(326)–C(321)–P(3)	117(1)	117.5(7)
C(332)–C(331)–P(3)	119(2)	119.5(8)
C(336)–C(331)–P(3)	121(2)	120(1)
F(2)–P(4)–F(1)	94.6(1)	91(1)
F(3)–P(4)–F(1)	83.4(1)	89(1)
F(3)–P(4)–F(2)	88.4(1)	89(1)
F(1)–P(4)–F(1)	180.0	180.0
F(2)–P(4)–F(2)	180.0	180.0
F(3)–P(4)–F(3)	180.0	180.0

contrasts with the observed structures of (**3**) and (**4**) where in both cases one Pt–Pt length is shorter than the other two.[3,4]

The mean Pt–Cu distance in (**1a**) is 2.600(3) Å and the mean Pt–Au distance in (**1b**) is 2.728(1) Å. The latter is slightly shorter than the Pt–Au distances found in the following tetrahedral Pt_3Au cluster compounds: $[Pt_3Au(CO)_3\{P(C_6H_{11})\}_4]^+$ [2.758(5) Å],[10] $[Pt_3Au(CO)_2(SO_2)\{P(C_6H_{11})_3\}_4]^+$ [2.758(5) Å],[11] $[Pt_3Au(\mu\text{-}Cl)(SO_2)_2\{P(C_6H_{11})_3\}_3\{P(C_6H_4F\text{-}p)_3\}]$ [2.769(1) Å],[11] and the trigonal bipyrimidal Pt_3Au_2 cluster compound $[Pt_3Au_2(\mu\text{-}Cl)(SO_2)_2\{P(C_6H_{11})_3\}_3\{P(C_6H_4F\text{-}p)_3\}_2]$ [2.785(2) Å].[12]

In (**1a**) and (**1b**) the opposite triangular metal planes are parallel to within 0.12 and 0.06° respectively. The distances between the centroids of the Pt_3 planes in the copper and gold sandwich clusters are 4.270 [(**1a**)] and 4.492 Å [(**1b**)] which reflects the difference of 0.127 Å in the mean Pt–M separations. The two triangles in each structure are twisted from an eclipsed D_{3h} conformation by similar angles of 21.5 [(**1a**)] and 22.3° [(**1b**)], Figure 3. In the analogous Hg complex $[Hg\{Pt_3(\mu\text{-}CNC_6H_3Me_2\text{-}2,6)_3(CNC_6H_3Me_2\text{-}2,6)_3\}_2]$ (**2**) the two Pt_3 triangles are twisted by 11.0° from the eclipsed conformation.[2] This relatively small twist angle may be related to the greater length of the Pt–Hg bonds which results in the greater Pt_3 triangle separation in (**2**) of 4.95 Å. However, this simple steric argument is not consistent with the observation that in the cationic Ag^I sandwich $[Ag\{Pt_3(\mu\text{-}CO)_3(PPr^i{}_3)_3\}_2]^+$ (**4**) an exactly staggered conformation (twist angle of 60°) is adopted,[4] although the separation of the Pt_3 triangles (judged by the Pt–Ag lengths) is greater than in either (**1a**) or (**1b**) potentially allowing a more eclipsed conformation. Theoretical studies have indicated that in clusters with layers of platinum triangles the rotational barriers are very small and the observed solid-

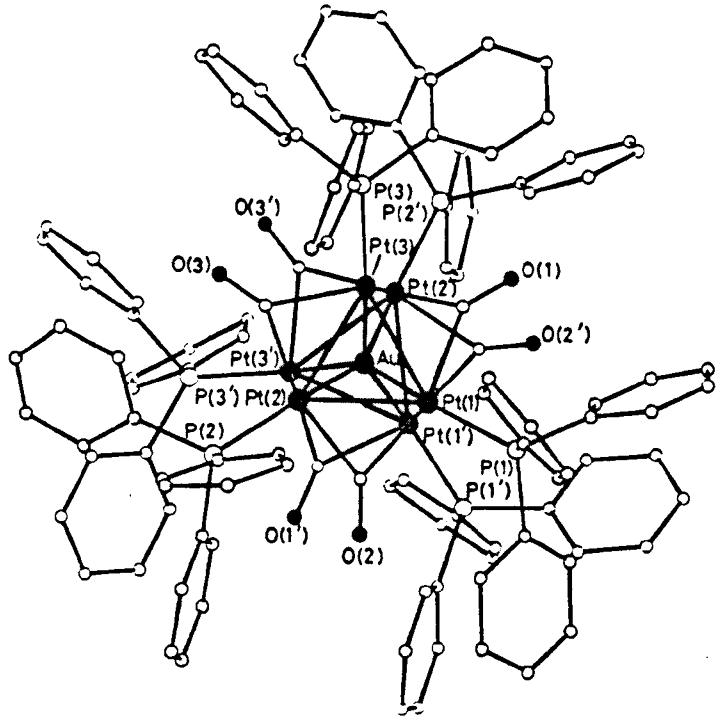

Figure 3. A view of the cation (**1b**) showing the virtual C_3 symmetry present in the clusters $[M\{Pt_3(\mu\text{-}CO)_3(PPh_3)_3\}_2]^+$

state conformation could be influenced by crystal-packing effects.[9]

The bridging CO ligands are symmetrically co-ordinated around the platinum triangles with Pt–C distances in the ranges 2.03(3)—2.19(4) Å for (**1a**) and 2.041(16)—2.126(17) Å for (**1b**). The Pt–P distances are in the ranges 2.235(10)—2.242(8) Å for (**1a**) and 2.242(4)—2.250(4) Å for (**1b**). The carbonyls are displaced from the planes of the three metal atoms and towards the central Group 1B metal atom with mean deviations of the O atoms from the Pt_3 planes being 0.28 [(**1a**)] and 0.33 Å [(**1b**)]. The phosphine ligands are also displaced from the plane of the Pt_3 plane, but in this instance away from the central atom, with mean P atom deviations from the plane of −0.88 for (**1a**) and −0.86 Å for (**1b**). The mean angle between the Pt–P vectors and the Pt_3 planes [−14.91 in (**1a**) and −14.83° in (**1b**)] is markedly greater than that of the Pt–C vectors [2.35 in (**1a**) and 2.37° in (**1b**)] in both compounds. Displacement of the carbonyl and organophosphine ligands from the Pt_3 plane in similar directions were also observed in the related silver compound (**4**).[4]

The bonding in the sandwich compounds of the type described in this paper and in (**2**), (**3**), and (**4**) has been discussed previously.[9,13] The primary bonding interactions result from the overlap of the Pt_3 ring orbitals of a_1 symmetry and the $(n + 1)s$ valence orbital of the Group 1B metal atom. A three-centre orbital interaction results and in $[M\{Pt_3(\mu\text{-}CO)_3(PR_3)_3\}_2]^+$ (M = Cu, Ag, or Au), which have a total of 94 valence electrons only the most stable in-phase combination is occupied. In $[Hg\{Pt_3(\mu\text{-}CNR)_3(CNR)_3\}_2]$, (**2**), which has a total of 96 valence electrons an additional orbital of a_2'' symmetry is occupied, which is localised predominantly on the Pt_3 triangles.

Experimental

The reactions were routinely carried out using Schlenk-line techniques under an atmosphere of pure dry N_2 and using dry oxygen-free solvents. Microanalyses (C, H, and N) were carried out by Mr. M. Gascoyne and his staff of this laboratory. Infrared spectra were recorded on a Perkin-Elmer 1710 Fourier-transform i.r. spectrometer as Nujol mulls between KBr discs and calibrated using polystyrene film. Unless otherwise stated, proton decoupled ^{31}P and ^{195}Pt n.m.r. spectra were recorded in deuteriated solvents on a Bruker AM250 spectrometer operating at 101.26 and 53.77 MHz respectively. Chemical shifts were referenced externally to aqueous solutions of trimethyl phosphate and $Na_2[PtCl_6]$ respectively. Chemical shifts were taken as positive to high frequency of the reference. Computer simulations of the n.m.r. spectra were carried out using a program developed by Professor R. K. Harris, then of the University of East Anglia, and adopted for use on the Oxford University VAX system by Dr. A. E. Derome.

Synthesis of $[Au\{Pt_3(\mu\text{-}CO)_3(PPh_3)_3\}_2]PF_6$, (**1b**).—(*a*) *Using* $[Au(Me_2S)Cl]$. $[Pt_3(\mu\text{-}CO)_3(PPh_3)_4]\cdot C_6H_6$ (0.24 g, 0.13 mmol) was dissolved in benzene (30 cm^3) and $TlPF_6$ (0.15 g, 0.43 mmol) added with stirring followed by $[Au(Me_2S)Cl]$ (0.04 g, 0.14 mmol). After 15 min, a dark red solid gradually precipitated as the solution became colourless. The solid was filtered off and extracted with CH_2Cl_2. Addition of hexane gave, on standing, deep red crystals of $[Au\{Pt_3(\mu\text{-}CO)_3(PPh_3)_3\}_2]PF_6$. Yield: 0.20 g (88%).

(*b*) *Using* $[Au(CO)Cl]$. The same product was obtained on reacting $[Pt_3(\mu\text{-}CO)_3(PPh_3)_4]$ (0.23 g, 0.13 mmol) with $[Au(CO)Cl]$ (0.04 g, 0.13 mmol) in the presence of $TlPF_6$ (0.14 g, 0.40 mmol) according to the same procedure as above. Yield: 0.18 g (82%) (Found: C, 41.6; H, 2.9; Au, 6.3; Pt, 34.0. $C_{114}H_{90}AuF_6O_6P_7Pt_6$ requires C, 42.1; H, 2.8; Au, 6.1; Pt, 36.0%). I.r. (cm^{-1}): ν(CO) 1 833vs, ν(PF_6) 838s. $^{31}P\text{-}\{^1H\}$ n.m.r. in CD_2Cl_2 solution: $\delta(^{31}P)$ 31.9 p.p.m. Single crystals were grown for *X*-ray diffraction by slow diffusion of diethyl ether into an acetone solution.

Table 3. Fractional atomic co-ordinates for $[M\{Pt_3(\mu\text{-}CO)_3(PPh_3)_3\}_2]PF_6$ [M = Cu (**1a**) or Au (**1b**)]

	(**1a**)			(**1b**)		
Atom	*x*	*y*	*z*	*x*	*y*	*z*
Pt(1)	−0.037 82(2)	0.152 04(2)	0.168 73(2)	−0.039 66(2)	0.151 08(4)	0.164 73(3)
Pt(2)	0.027 32(2)	0.282 98(2)	0.168 84(2)	0.026 63(2)	0.282 54(4)	0.164 74(3)
Pt(3)	−0.070 69(2)	0.315 07(2)	0.168 80(2)	−0.072 17(2)	0.316 25(4)	0.164 79(3)
M	0.000 00	0.250 46(7)	0.250 00	0.000 00	0.249 98(6)	0.250 00
P(1)	−0.068 3(3)	0.021 5(3)	0.135 3(2)	−0.070 0(2)	0.021 1(3)	0.131 4(2)
P(2)	0.090 3(3)	0.319 0(3)	0.134 7(3)	0.090 6(2)	0.318 0(3)	0.131 7(2)
P(3)	−0.137 4(3)	0.409 3(3)	0.135 0(4)	−0.138 7(2)	0.411 0(3)	0.131 6(2)
C(1)	−0.110 1(7)	0.194 7(6)	0.174 2(7)	−0.109 2(6)	0.201 8(10)	0.169 4(7)
O(1)	−0.148 9(5)	0.175 1(9)	0.178 7(9)	−0.148 5(5)	0.177 6(8)	0.176 8(5)
C(2)	0.039 3(5)	0.150 7(9)	0.171 5(5)	0.038 4(5)	0.148 2(9)	0.168 1(6)
O(2)	0.075 3(5)	0.099 9(9)	0.178 3(9)	0.073 8(5)	0.098 7(8)	0.178 0(5)
C(3)	−0.010 0(7)	0.409 6(7)	0.172 0(7)	−0.007 6(6)	0.400 7(11)	0.169 2(7)
O(3)	0.003 4(5)	0.476 4(7)	0.180 8(7)	0.001 7(5)	0.417 6(8)	0.177 0(5)
C(111)	−0.118 5(8)	−0.022 8(15)	0.159 7(8)	−0.119 4(4)	−0.024 2(7)	0.157 3(4)
C(112)	−0.162 3(8)	−0.069 3(15)	0.128 7(8)	−0.162 5(4)	−0.072 5(7)	0.127 5(4)
C(113)	−0.197 1(8)	−0.108 9(15)	0.150 7(8)	−0.197 2(4)	−0.111 1(7)	0.149 6(4)
C(114)	−0.188 0(8)	−0.102 1(15)	0.203 7(8)	−0.188 8(4)	−0.101 4(7)	0.201 4(4)
C(115)	−0.144 2(8)	−0.055 6(15)	0.234 7(8)	−0.145 7(4)	−0.053 1(7)	0.231 2(4)
C(116)	−0.109 4(8)	−0.016 0(15)	0.212 7(8)	−0.111 0(4)	−0.014 5(7)	0.209 2(4)
C(121)	−0.097 9(9)	0.024 9(17)	0.067 2(7)	−0.100 0(5)	0.023 3(9)	0.064 0(4)
C(122)	−0.116 2(9)	0.105 2(17)	0.044 4(7)	−0.117 0(5)	0.103 2(9)	0.040 7(4)
C(123)	−0.140 9(9)	0.110 7(17)	−0.008 9(7)	−0.141 2(5)	0.107 6(9)	−0.011 8(4)
C(124)	−0.147 5(9)	0.035 9(17)	−0.039 3(7)	−0.148 4(5)	0.032 0(9)	−0.041 0(4)
C(125)	−0.129 2(9)	−0.044 4(17)	−0.016 5(7)	−0.131 4(5)	−0.047 9(9)	−0.017 7(4)
C(126)	−0.104 4(9)	−0.049 9(17)	0.036 8(7)	−0.107 2(5)	−0.052 3(9)	0.034 8(4)
C(131)	−0.020 2(7)	−0.064 2(12)	0.144 5(7)	−0.021 1(4)	−0.064 3(7)	0.141 7(5)
C(132)	0.017 9(7)	−0.057 3(12)	0.119 6(7)	0.018 1(4)	−0.057 9(7)	0.118 6(5)
C(133)	0.057 1(7)	−0.121 0(12)	0.127 3(7)	0.057 8(4)	−0.120 9(7)	0.127 8(5)
C(134)	0.058 3(7)	−0.191 6(12)	0.159 8(7)	0.058 2(4)	−0.190 5(7)	0.160 1(5)
C(135)	0.020 2(7)	−0.198 5(12)	0.184 6(7)	0.019 0(4)	−0.196 9(7)	0.183 3(5)
C(136)	−0.019 1(7)	−0.134 8(12)	0.177 0(7)	−0.020 6(4)	−0.133 8(7)	0.174 1(5)
C(211)	0.151 4(7)	0.257 3(15)	0.159 8(8)	0.150 5(3)	0.255 5(7)	0.157 5(4)
C(212)	0.169 6(7)	0.241 0(15)	0.212 8(8)	0.167 2(3)	0.237 7(7)	0.209 4(4)
C(213)	0.217 2(7)	0.196 2(15)	0.235 0(8)	0.214 5(3)	0.192 8(7)	0.231 7(4)
C(214)	0.246 7(7)	0.167 7(15)	0.204 1(8)	0.245 1(3)	0.165 7(7)	0.202 2(4)
C(215)	0.228 6(7)	0.184 0(15)	0.151 1(8)	0.228 4(3)	0.183 5(7)	0.150 3(4)
C(216)	0.180 9(7)	0.228 8(15)	0.129 0(8)	0.181 2(3)	0.228 4(7)	0.127 9(4)
C(221)	0.113 6(10)	0.430 8(13)	0.145 4(10)	0.113 5(4)	0.430 5(6)	0.141 4(4)
C(222)	0.164 5(10)	0.450 6(13)	0.178 3(10)	0.164 5(4)	0.449 5(6)	0.173 5(4)
C(223)	0.181 2(10)	0.537 3(13)	0.186 0(10)	0.180 8(4)	0.535 9(6)	0.182 9(4)
C(224)	0.147 0(10)	0.604 1(13)	0.160 7(10)	0.146 1(4)	0.603 2(6)	0.160 3(4)
C(225)	0.096 1(10)	0.584 2(13)	0.127 8(10)	0.095 2(4)	0.584 1(6)	0.128 2(4)
C(226)	0.079 4(10)	0.497 6(13)	0.120 2(10)	0.078 9(4)	0.497 8(6)	0.118 7(4)
C(231)	0.070 1(10)	0.307 7(17)	0.067 4(8)	0.070 6(5)	0.305 8(9)	0.063 5(4)
C(232)	0.028 7(10)	0.249 2(17)	0.046 0(8)	0.027 9(5)	0.251 0(9)	0.040 4(4)
C(233)	0.012 4(10)	0.231 1(17)	−0.006 7(8)	0.011 4(5)	0.238 8(9)	−0.012 1(4)
C(234)	0.037 5(10)	0.271 6(17)	−0.038 2(8)	0.037 7(5)	0.281 3(9)	−0.041 4(4)
C(235)	0.079 0(10)	0.330 1(17)	−0.016 9(8)	0.080 4(5)	0.336 1(9)	−0.018 2(4)
C(236)	0.095 3(10)	0.348 2(17)	0.035 9(8)	0.096 8(5)	0.348 3(9)	0.034 3(4)
C(311)	−0.201 2(8)	0.383 2(15)	0.144 0(8)	−0.201 4(4)	0.385 8(7)	0.141 6(5)
C(312)	−0.228 6(8)	0.308 3(15)	0.121 2(8)	−0.228 3(4)	0.310 9(7)	0.119 0(5)
C(313)	−0.275 1(8)	0.284 2(15)	0.130 7(8)	−0.274 6(4)	0.285 8(7)	0.128 5(5)
C(314)	−0.294 3(8)	0.335 1(15)	0.163 0(8)	−0.293 9(4)	0.335 6(7)	0.160 6(5)
C(315)	−0.267 0(8)	0.410 0(15)	0.185 9(8)	−0.267 0(4)	0.410 5(7)	0.183 2(5)
C(316)	−0.220 4(8)	0.434 1(15)	0.176 4(8)	−0.220 7(4)	0.435 6(7)	0.173 7(5)
C(321)	−0.122 9(9)	0.518 1(12)	0.159 9(8)	−0.123 6(4)	0.519 4(6)	0.157 3(4)
C(322)	−0.139 8(9)	0.592 1(12)	0.129 3(8)	−0.140 5(4)	0.593 9(6)	0.127 9(4)
C(323)	−0.130 7(9)	0.674 8(12)	0.151 6(8)	−0.130 9(4)	0.675 9(6)	0.150 5(4)
C(324)	−0.104 7(9)	0.683 7(12)	0.204 5(8)	−0.104 3(4)	0.683 4(6)	0.202 5(4)
C(325)	−0.087 8(9)	0.609 7(12)	0.235 1(8)	−0.087 4(4)	0.609 0(6)	0.231 8(4)
C(326)	−0.096 9(9)	0.527 0(12)	0.212 8(8)	−0.097 0(4)	0.526 9(6)	0.209 3(4)
C(331)	−0.154 6(10)	0.418 2(18)	0.066 5(8)	−0.156 3(5)	0.420 2(8)	0.063 3(4)
C(332)	−0.116 0(10)	0.398 1(18)	0.043 7(8)	−0.120 0(5)	0.394 6(8)	0.039 4(4)
C(333)	−0.127 7(10)	0.406 4(18)	−0.009 6(8)	−0.132 7(5)	0.402 9(8)	−0.013 1(4)
C(334)	−0.177 9(10)	0.434 9(18)	−0.040 0(8)	−0.181 8(5)	0.436 9(8)	−0.041 7(4)
C(335)	−0.216 4(10)	0.455 0(18)	−0.017 2(8)	−0.218 1(5)	0.462 5(8)	−0.017 7(4)
C(336)	−0.204 7(10)	0.446 6(18)	0.036 0(8)	−0.205 3(5)	0.454 2(8)	0.034 7(4)
P(4)	0.750 00	0.250 00	0.500 00	0.750 00	0.250 00	0.500 00
F(1)	0.619 6(8)	0.276 0(13)	0.466 8(8)	0.770 9(8)	0.309 8(13)	0.466 8(8)
F(2)	0.074 9(6)	0.162 4(14)	0.466 5(8)	0.806 7(6)	0.229 7(14)	0.534 7(8)
F(3)	0.077 48(8)	0.169 8(12)	0.463 0(8)	0.753 4(8)	0.173 4(12)	0.466 4(8)

Synthesis of $[Cu\{Pt_3(\mu\text{-}CO)_3(PPh_3)_3\}_2]PF_6$. (**1a**). Contact between the product and metal implements (*e.g.* spatula) was avoided in this synthesis since decomposition had been a problem in early attempts. $[Pt_3(\mu\text{-}CO)_3(PPh_3)_4]\cdot C_6H_6$ (0.40 g, 0.22 mmol) was dissolved in benzene (30 cm^3) and $[Cu(MeCN)_4]PF_6$ (0.08 g, 0.21 mmol) added with stirring. During the course of an hour a deep red precipitate was formed as the solution became almost colourless. The solid was filtered off and extracted into CH_2Cl_2. Slow addition of diethyl ether gave deep red crystals of $[Cu\{Pt_3(\mu\text{-}CO)_3(PPh_3)_3\}_2]PF_6$. Yield; 0.28 g (81%) (Found: C, 43.6; H, 3.0; Cu, 2.1. $C_{114}H_{90}CuF_6O_6P_7Pt_6$ requires C, 43.9; H, 2.8; Cu, 2.0%). *X*-Ray microanalysis confirmed that the Pt:Cu atom ratio was 6:1. I.r. (cm^{-1}): ν(CO) 1 837vs, ν(PF_6) 839s. Single crystals were grown for *X*-ray diffraction by slow diffusion of diethyl ether into a CH_2Cl_2 solution.

Reaction of $[Pt_3(\mu\text{-}CO)_3\{P(C_6H_{11})_3\}_3]$ *with* $[Au(CO)Cl]$.—$[Pt_3(\mu\text{-}CO)_3\{P(C_6H_{11})_3\}_3]\cdot C_6H_6$ (0.30 g, 0.19 mmol) was dissolved in benzene (25 cm^3). $TlPF_6$ (0.10 g, 0.29 mmol) and $[Au(CO)Cl]$ (25 mg, 0.10 mmol) were added and the solution stirred for 12 h during which time it darkened considerably. The solvent was removed *in vacuo* and the residue extracted into CH_2Cl_2. Addition of ethanol gave, on standing at −20 °C, bright red crystals of $[Pt_3Au(\mu\text{-}CO)_3\{P(C_6H_{11})_3\}_4]PF_6$. Yield: 0.14 g (35% based on Pt) (Found: C, 42.6; H, 5.9. $C_{75}H_{132}AuF_6O_3P_5Pt_3$ requires C, 42.2; H, 6.2%). $^{31}P\text{-}\{^1H\}$ N.m.r. in CD_3Cl_2 solution: $\delta(^{31}P)$ 51.8 (3 P), 82.4 (1 P) p.p.m. (lit.[11] 51.9, 82.7 p.p.m.).

X-*Ray Structure Analyses*.—*Crystal data for* (**1a**). $C_{114}H_{90}CuF_6O_6P_7Pt_6$, M = 3 118.54, monoclinic, space group $C2/c$, a = 26.583(3), b = 15.331(2), c = 27.366(3) Å, β = 108.56(2)°, U = 10 554 Å^3, $F(000)$ = 5 852, μ(Mo-K_α) = 79.42 cm^{-1}, Z = 4, D_c = 1.96 g cm^{-3}.

Crystal data for (**1b**). $C_{114}H_{90}AuF_6O_6P_7Pt_6$, M = 3 252.22, monoclinic, space group $C2/c$, a = 26.637(3), b = 15.371(2), c = 27.821(3) Å, β = 108.73(2)°, U = 10 788 Å^3, $F(000)$ = 7 452, μ(Mo-K_α) = 155.05 cm^{-1}, Z = 4, D_c = 2.00 g cm^{-3}.

The methods of data collection, data processing, and absorption correction used for compounds (**1a**) and (**1b**) are similar to those described previously.[14] The crystals selected for data collection had dimensions 0.44 × 0.48 × 0.21 mm [(**1a**)] and 0.24 × 0.24 × 0.16 mm [(**1b**)]. A scan width of 0.8° was used to collect data in the θ range 3—25° for both crystals. 360 Azimuthal scan data for (**1a**) and 432 for (**1b**) were used in absorption correction and relative transmission factors varied from 1.000 to 0.810 for (**1a**) and 1.000 to 0.903 for (**1b**). Equivalent reflections were merged to give 5 998 data for (**1a**) and 5 050 data for (**1b**) with $I/\sigma(I) \geq 3.0$.

Structure solution and refinement.[15] For (**1b**) the three independent platinum atoms and the gold atom were found from a Patterson synthesis. The structure of (**1a**) was assumed to be isomorphous with (**1b**) from the close relationships in the unit-cell dimensions and systematic absences. The metal positions from (**1b**) were therefore used as a starting set in the solution of (**1a**). The remaining non-hydrogen atoms were found from subsequent difference Fourier syntheses, after several cycles of refinement of metal atom parameters. Blocked full-matrix least-squares refinement of the atomic positional and thermal parameters converged at final R and R' values of 0.0443 and 0.0442 respectively for (**1a**) and 0.0484 and 0.0464 respectively for (**1b**). The phenyl rings were treated as rigid hexagons (C–C = 1.395 Å) and the hydrogen atoms were included in the structure factor calculations at calculated positions (C–H = 1.08 Å) with fixed thermal parameters of 0.08 Å^2. Anisotropic thermal parameters were assigned to the metals, phosphorus, and fluorine atoms during the final cycles of least-squares refinement for both (**1a**) and (**1b**). Fractional atomic co-ordinates are given in Table 3.

Acknowledgements

The S.E.R.C. is thanked for financial support and Johnson Matthey Ltd. for the generous loan of gold and platinum metals.

References

1 Y. Yamamoto, H. Yamazaki, and T. Sakurai, *J. Am. Chem. Soc.*, 1982, **104**, 2329.

2 Y. Yamamoto, K. Aoki, and H. Yamazaki, *Chem. Lett.*, 1979, 391.

3 A. Albinati, A. Moor, P. S. Pregosin, and L. M. Venanzi, *J. Am. Chem. Soc.*, 1982, **104**, 7672.

4 A. Albinati, K-H. Dahmen, A. Togni, and L. M. Venanzi, *Angew. Chem., Int. Ed. Engl.*, 1985, **24**, 766.

5 R. W. M. Wardle and D. M. P. Mingos, unpublished work.

6 J. Chatt and P. Chini, *J. Chem. Soc. A*, 1970, 1538.

7 A. Moor, P. S. Pregosin, and L. M. Venanzi, *Inorg. Chim. Acta*, 1981, **48**, 153.

8 D. M. P. Mingos and R. W. M. Wardle, *Transition Met. Chem. (Weinheim, Ger.)*, 1985, **10**, 441.

9 D. J. Underwood, R. Hoffmann, K. Tatsumi, A. Nakamura, and Y. Yamamoto, *J. Am. Chem. Soc.*, 1985, **107**, 5968.

10 C. E. Briant, R. W. M. Wardle, and D. M. P. Mingos, *J. Organomet. Chem.*, 1984, **267**, C49.

11 D. M. P. Mingos and R. W. M. Wardle, *J. Chem. Soc., Dalton Trans.*, 1986, 73.

12 D. M. P. Mingos, P. Oster, and D. J. Sherman, *J. Organomet. Chem.*, 1987, **320**, 257.

13 D. I. Gilmour and D. M. P. Mingos, *J. Organomet. Chem.*, 1986, **302**, 127.

14 P. F. Jackson, B. F. G. Johnson, J. Lewis, W. J. H. Nelson, and M. McPartlin, *J. Chem. Soc., Dalton Trans.*, 1982, 2099.

15 G. M. Sheldrick, SHELX 76, Crystal Solving Package, University of Cambridge, 1976.

Received 9th February 1987; *Paper* 7/234

The Heteronuclear Cluster Chemistry of the Group 1B Metals. Part 5.[1] *X*-Ray Crystal Structure and Dynamic Behaviour of the Heptanuclear Mixed-metal Cluster $[Au_3Ru_4(\mu\text{-}H)(CO)_{12}(\mu\text{-}Ph_2PCH_2PPh_2)(PPh_3)]$†

Trushar Adatia and Mary McPartlin *
School of Chemistry, The Polytechnic of North London, London N7 8DB
Ian D. Salter *
Department of Chemistry, University of Exeter, Exeter EX4 4QD

A single-crystal *X*-ray diffraction study of the mixed-metal gold cluster $[Au_3Ru_4(\mu\text{-}H)(CO)_{12}(\mu\text{-}Ph_2PCH_2PPh_2)(PPh_3)]$ (**1**) reveals a different core geometry to the bicapped trigonal-bipyramidal structure adopted by the closely related species $[Au_3Ru_4(\mu_3\text{-}H)(CO)_{12}(PPh_3)_3]$ (**2**). The metal skeleton of (**1**) may be described as a distorted Au_2Ru_3 square pyramid with two adjacent triangular faces capped by the metal atoms of a $Ru(CO)_3$ and a $Au(PPh_3)$ unit. The $Ph_2PCH_2PPh_2$ group bridges the Au–Au edge of the square base of the pyramid, the hydrido ligand bridges a Ru–Ru edge of the capping $Ru(CO)_3$ unit, and each ruthenium atom is bonded to three terminal carbonyl groups. Knowledge of the structure of (**1**) allows further insight into the nature of the dynamic behaviour that (**1**) and (**2**) exhibit in solution at ambient temperature.

Although mixed-metal cluster compounds containing one or more $Au(PR_3)$ (R = alkyl or aryl) groups are currently attracting a great deal of attention,[1–3] detailed investigations of similar species with bidentate diphosphines remain rare.[1,4,5] The structure of $[Au_3Ru_4(\mu\text{-}H)(CO)_{12}(\mu\text{-}Ph_2PCH_2PPh_2)(PPh_3)]$ (**1**) has been determined to investigate the relationship between its skeletal geometry and that of its tris(monodentate phosphine) analogue $[Au_3Ru_4(\mu_3\text{-}H)(CO)_{12}(PPh_3)_3]$ (**2**).[3] The work was prompted by the recent observation that when two PPh_3 groups in the hexanuclear species $[Au_2Ru_4(\mu_3\text{-}H)(\mu\text{-}H)(CO)_{12}(PPh_3)_2]$ (**3**) are replaced by one $Ph_2PCH_2PPh_2$ ligand in $[Au_2Ru_4(\mu_3\text{-}H)(\mu\text{-}H)(CO)_{12}(\mu\text{-}Ph_2PCH_2PPh_2)]$ (**4**), the metal core structure of the cluster is altered from a capped trigonal bipyramid to a capped square pyramid.[5,6] Previously, because of the close similarity between the i.r. and ^1H n.m.r. spectroscopic data of the heptanuclear clusters (**1**) and (**2**), it had been thought that (**1**) adopted the same bicapped trigonal-bipyramidal metal core geometry as that earlier established for its tris(monodentate phosphine) analogue (**2**) by *X*-ray diffraction study.[3]

Results and Discussion

The *X*-ray structure analysis shows that the Au_3Ru_4 skeleton of (**1**) is not based on a trigonal-bipyramidal geometry as originally thought,[3] but may be described as a distorted Au_2Ru_3 square pyramid, capped on two adjacent triangular faces by a $Ru(CO)_3$ and a $Au(PPh_3)$ unit. The molecular configuration of (**1**) is illustrated in the Figure, and selected interatomic distances and bond angles are summarised in Table 1.

The basal atoms Au(1), Au(2), Ru(2), and Ru(3) and the apical atom Ru(1) define the square pyramid and the Au(1)Ru(1)Ru(2) and Ru(1)Ru(2)Ru(3) faces of this Au_2Ru_3 unit are capped by Au(3) and Ru(4), respectively. The $Ph_2PCH_2PPh_2$ ligand bridges the two gold atoms Au(1) and Au(2), which form one edge of the square base, the hydrido ligand bridges one edge, Ru(3)–Ru(4), of the Ru_4 tetrahedral cap, and each ruthenium atom is bonded to three essentially linear carbonyl groups [M–C–O 165(2)—177(3)°]. There are several short Au···C(carbonyl) intramolecular contacts [2.51(3)—2.84(4) Å]; similar short distances have been observed previously between carbonyl ligands and gold atoms in other heteronuclear cluster compounds.[1,7–9]

Although the Au(1)–Au(3) edge of the Au_2Ru_2 tetrahedral cap is unbridged, whereas the Au(1)–Au(2) edge of the square pyramid is bridged by the bidentate diphosphine ligand, there is only a slight difference between the two Au–Au separations [2.749(2) and 2.758(2) Å respectively]. Both of these Au–Au distances are markedly shorter than those found in the tris(monodentate phosphine) analogue (**2**) [2.822(2) and 2.838(2) Å][3] and it is interesting that in the gold–ruthenium diphosphine clusters $[Au_2Ru_4(\mu_3\text{-}H)(\mu\text{-}H)(CO)_{12}(\mu\text{-}Ph_2PCH_2PPh_2)]$ and $[Au_2Ru_3(\mu_3\text{-}S)(CO)_9(\mu\text{-}Ph_2PCH_2PPh_2)]$ the Au–Au edges bridged by the $Ph_2PCH_2PPh_2$ ligand are also considerably longer [2.823(1)[5] and 2.802(1)[1] Å respectively] than the Au–Au distances in (**1**). The Au–Ru distances observed in (**1**) [2.762(3)—2.920(2) Å] cover a similar range to those found in (**2**) [2.825(2)—3.011(3) Å],[3] but the individual bond lengths are slightly shorter in the former cluster. As observed in (**2**),[3] the unbridged Ru–Ru edges of the Ru_4 tetrahedron in (**1**) [Ru(1)–Ru(4), Ru(2)–Ru(3), Ru(2)–Ru(4), and Ru(3)–Ru(4)] are shorter [2.774(3)—2.931(3) Å] than the Ru–Ru distances bridged by the gold atoms [Ru(1)–Ru(2) 3.044(3) and Ru(1)–Ru(3) 2.967(4) Å].

The molecular configuration of (**1**) clearly exhibits a difference in the mode of bonding of the two basal gold atoms spanned by the bidentate diphosphine group. Both Au atoms are bonded to the apical atom Ru(1) but, in addition, Au(1) is also bonded to the capping atom Au(3). This difference is reflected in different Au–P bond lengths [Au(1)–P(1) 2.287(8) and Au(2)–P(2) 2.307(8) Å]. Although the differences in these Au–P distances are of low significance, the larger value, that to the uncapped gold atom [Au(2)], is very close to the Au–P bond lengths found in the structurally related hexanuclear cluster (**4**) [2.304(3) and 2.309(3) Å],[10] where both gold atoms exhibit similar uncapped basal environments to that adopted by Au(2).

The metal core geometry of (**1**) is very closely related to the capped square-pyramidal structure adopted by the hexanuclear cluster (**4**),[5] with one $AuRu_2$ face of the latter being capped by a $Au(PPh_3)$ group in the heptanuclear species. Interestingly, the

---

† 1,2-μ-[Bis(diphenylphosphino)methane]-4,4,4,5,5,5,6,6,6,7,7,7-dodecacarbonyl-6,7-μ-hydrido-3-triphenylphosphine-*cyclo*-1,2,3-trigold-4,5,6,7-tetraruthenium (2 *Au–Au*) (6 *Au–Ru*) (6 *Ru–Ru*).

Supplementary data available: see Instructions for Authors, *J. Chem. Soc., Dalton Trans.*, 1988, Issue 1, pp. xvii—xx.

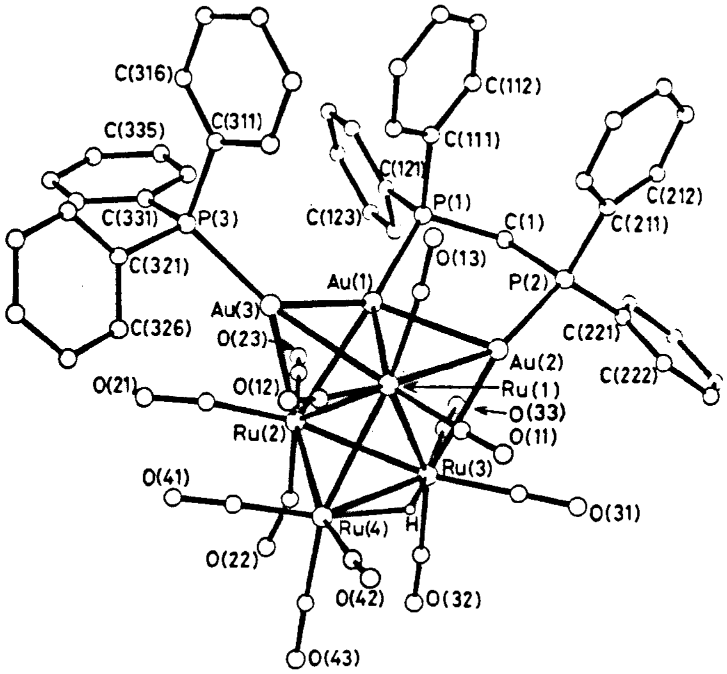

Figure. The molecular structure of $[Au_3Ru_4(\mu\text{-}H)(CO)_{12}(\mu\text{-}Ph_2PCH_2PPh_2)(PPh_3)]$ (**1**) showing the bicapped square-pyramidal metal framework. The carbonyl C-atoms have the same numbers as the oxygens to which they are bonded

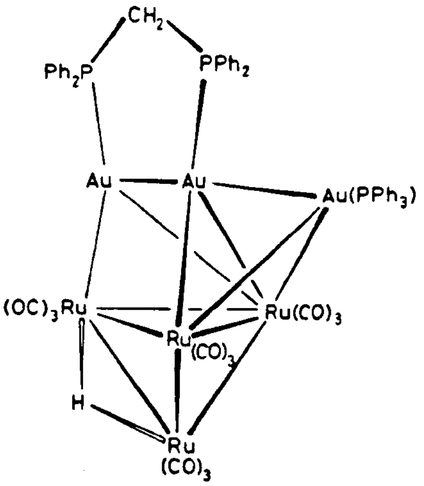

(**1**)

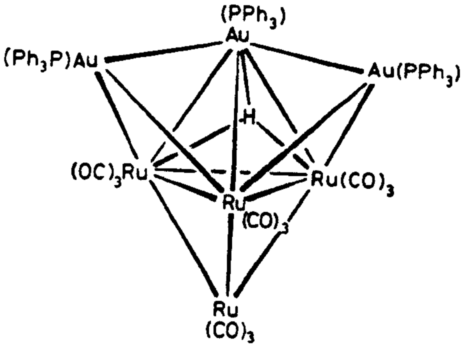

(**2**)

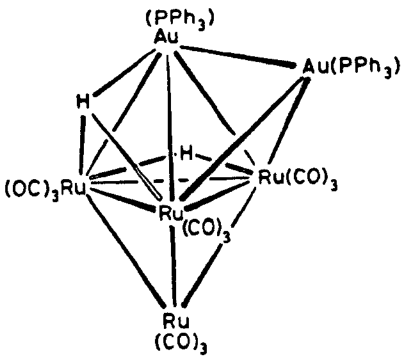

(**3**)

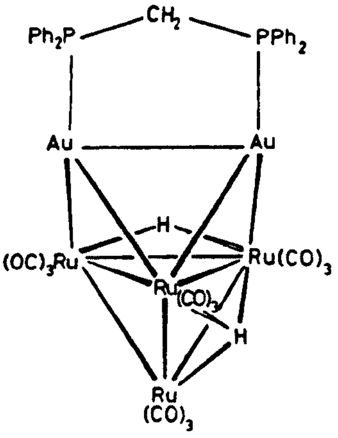

(**4**)

Table 1. Selected bond lengths (Å), and angles (°), with estimated standard deviations in parentheses, for $[Au_3Ru_4(\mu\text{-}H)(CO)_{12}(\mu\text{-}Ph_2PCH_2PPh_2)(PPh_3)]$ (**1**)

Au(1)–Au(2)	2.758(2)	Au(1)–Au(3)	2.749(2)	Ru(3)–Ru(4)	2.931(4)	Ru(3)–C(31)	1.83(4)
Au(1)–Ru(1)	2.920(2)	Au(1)–Ru(2)	2.781(2)	Ru(3)–C(32)	1.86(3)	Ru(3)–C(33)	1.88(3)
Au(1)–P(1)	2.287(8)	Au(2)–Ru(1)	2.762(3)	Ru(3)–H	1.857	Ru(4)–C(41)	1.94(4)
Au(2)–Ru(3)	2.869(2)	Au(2)–P(2)	2.307(8)	Ru(4)–C(42)	1.91(3)	Ru(4)–C(43)	1.84(3)
Au(3)–Ru(1)	2.812(3)	Au(3)–Ru(2)	2.898(3)	Ru(4)–H	1.845	P(1)–C(1)	1.87(3)
Au(3)–P(3)	2.305(9)	Ru(1)–Ru(2)	3.044(3)	P(1)–C(111)	1.798(23)	P(1)–C(121)	1.82(3)
Ru(1)–Ru(3)	2.967(4)	Ru(1)–Ru(4)	2.847(3)	P(2)–C(1)	1.80(3)	P(2)–C(211)	1.779(21)
Ru(1)–C(11)	1.85(3)	Ru(1)–C(12)	1.92(3)	P(2)–C(221)	1.82(3)	P(3)–C(311)	1.801(18)
Ru(1)–C(13)	1.90(3)	Ru(2)–Ru(3)	2.840(4)	P(3)–C(321)	1.795(23)	P(3)–C(331)	1.800(24)
Ru(2)–Ru(4)	2.774(3)	Ru(2)–C(21)	1.92(4)	Ru–CO	1.82(3)—1.94(4)	Mean Ru–CO	1.86(3)
Ru(2)–C(22)	1.82(3)	Ru(2)–C(23)	1.89(3)				
Au(3)–Au(1)–Au(2)	115.6(1)	Ru(1)–Au(1)–Au(2)	58.1(1)	Au(3)–Ru(2)–Au(1)	57.9(1)	Ru(1)–Ru(2)–Au(1)	60.0(1)
Ru(1)–Au(1)–Au(3)	59.4(1)	Ru(2)–Au(1)–Au(2)	101.6(1)	Ru(1)–Ru(2)–Au(3)	56.4(1)	Ru(3)–Ru(2)–Au(1)	78.3(1)
Ru(2)–Au(1)–Au(3)	63.2(1)	Ru(2)–Au(1)–Ru(1)	64.5(1)	Ru(3)–Ru(2)–Au(3)	114.8(1)	Ru(3)–Ru(2)–Ru(1)	60.4(1)
P(1)–Au(1)–Au(2)	90.0(2)	P(1)–Au(1)–Au(3)	132.6(2)	Ru(4)–Ru(2)–Au(1)	117.3(1)	Ru(4)–Ru(2)–Au(3)	95.4(1)
P(1)–Au(1)–Ru(1)	140.0(2)	P(1)–Au(1)–Ru(2)	153.2(2)	Ru(4)–Ru(2)–Ru(1)	58.4(1)	Ru(4)–Ru(2)–Ru(3)	62.9(1)
Ru(1)–Au(2)–Au(1)	63.9(1)	Ru(3)–Au(2)–Au(1)	78.2(1)	Ru(2)–Ru(3)–Ru(1)	63.2(1)	Ru(4)–Ru(3)–Au(2)	113.8(1)
Ru(3)–Au(2)–Ru(1)	63.6(1)	P(2)–Au(2)–Au(1)	98.8(2)	Ru(4)–Ru(3)–Ru(1)	57.7(1)	Ru(4)–Ru(3)–Ru(2)	57.4(1)
P(2)–Au(2)–Ru(1)	156.3(3)	P(2)–Au(2)–Ru(3)	131.6(2)	Ru(2)–Ru(4)–Ru(1)	65.6(1)	Ru(3)–Ru(4)–Ru(1)	61.8(1)
Ru(1)–Au(3)–Au(1)	63.3(1)	Ru(2)–Au(3)–Au(1)	58.9(1)	Ru(3)–Ru(4)–Ru(2)	59.6(1)	C(41)–Ru(4)–Ru(1)	105.0(9)
Ru(2)–Au(3)–Ru(1)	64.4(1)	P(3)–Au(3)–Au(1)	131.1(2)	C(111)–P(1)–Au(1)	114.9(7)	C(111)–P(1)–C(1)	108(1)
P(3)–Au(3)–Ru(1)	152.9(2)	P(3)–Au(3)–Ru(2)	141.3(2)	C(121)–P(1)–Au(1)	118.9(7)	C(121)–P(1)–C(1)	101(1)
Au(2)–Ru(1)–Au(1)	58.0(1)	Au(3)–Ru(1)–Au(1)	57.3(1)	C(211)–P(2)–Au(2)	119.0(8)	C(211)–P(2)–C(1)	105(1)
Au(3)–Ru(1)–Au(2)	113.4(1)	Ru(2)–Ru(1)–Au(1)	55.5(1)	C(221)–P(2)–Au(2)	117.2(8)	C(221)–P(2)–C(1)	101(1)
Ru(2)–Ru(1)–Au(2)	95.2(1)	Ru(2)–Ru(1)–Au(3)	59.2(1)	C(321)–P(3)–Au(3)	113.4(7)	C(321)–P(3)–C(311)	104.6(9)
Ru(3)–Ru(1)–Au(1)	74.2(1)	Ru(3)–Ru(1)–Au(2)	60.0(1)	C(331)–P(3)–Au(3)	110.4(9)	C(331)–P(3)–C(311)	106(1)
Ru(3)–Ru(1)–Au(3)	113.5(1)	Ru(3)–Ru(1)–Ru(2)	56.4(1)	C(311)–P(3)–Au(3)	115.7(8)	Mean Ru–C–O	174(3)
Ru(4)–Ru(1)–Au(1)	110.7(1)	Ru(4)–Ru(1)–Au(2)	120.1(1)	Ru–C–O	165(2)—177(3)		
Ru(4)–Ru(1)–Au(3)	95.7(1)	Ru(4)–Ru(1)–Ru(2)	56.1(1)				
Ru(4)–Ru(1)–Ru(3)	60.5(1)	C(11)–Ru(1)–Au(1)	140(1)				

same structural relationship is also observed between the metal frameworks of (**2**) and (**3**), with one $AuRu_2$ face of the capped trigonal-bipyramidal core[6] of the hexanuclear species (**3**) being capped by an extra $Au(PPh_3)$ fragment in the heptanuclear cluster (**2**).[3] Thus, replacing two PPh_3 groups attached to gold atoms in (**2**) and (**3**) by a $Ph_2PCH_2PPh_2$ ligand causes a very similar distortion of the metal core geometry in both cases.

The tris(monodentate phosphine) heptanuclear cluster (**2**) is known to exhibit interesting dynamic behaviour in solution at ambient temperatures. Previous variable-temperature ^1H and $^{31}P\text{-}\{^1H\}$ n.m.r. studies indicate that the metal framework is undergoing an intramolecular rearrangement which exchanges the three gold atoms between the two distinct coinage metal sites in the ground-state structure.[3] Similar studies on the analogous heptanuclear cluster (**1**) show that the two phosphorus nuclei of the $Ph_2PCH_2PPh_2$ group are equivalent on the n.m.r. time-scale.[3] As this observation is inconsistent with the ground-state structure of $[Au_3Ru_4(\mu\text{-}H)(CO)_{12}(\mu\text{-}Ph_2PCH_2PPh_2)(PPh_3)]$ (**1**) and no low-energy pathways for direct scrambling of phosphorus ligands have been reported, it would seem that the metal skeleton of (**1**) is also undergoing an intramolecular rearrangement in solution and that the fluxional process exchanges the environments of the two gold atoms attached to the bidentate diphosphine group between the two distinct types observed at Au(1) and Au(2).

A restricted Berry pseudo-rotation mechanism has previously been proposed,[1,5,6,8] for the intramolecular metal core rearrangements exhibited by a variety of heteronuclear Group 1B metal clusters which have a trigonal-bipyramidal M_2Ru_3 (M = Cu, Ag, or Au) unit incorporated into their metal skeletons. In the present work it has been shown that $[Au_3Ru_4(\mu\text{-}H)(CO)_{12}(\mu\text{-}Ph_2PCH_2PPh_2)(PPh_3)]$ (**1**) has a solid-state structure with a metal core markedly distorted from the bicapped trigonal-bipyramidal geometry, observed in its analogue $[Au_3Ru_4(\mu_3\text{-}H)(CO)_{12}(PPh_3)_3]$ (**2**), towards a bicapped square-pyramidal arrangement of the type required as an intermediate in the above mechanism. This observation provides further evidence for the theory that metal core rearrangements are also implicated in the dynamic behaviour of these clusters. In the case of the tris(monodentate phosphine) cluster (**2**), which has two distinct phosphorus environments in the solid state, a series of site interchanges between the central and each of the outer positions must be invoked to explain the equivalence of the phosphorus atoms. It is reasonable to propose that this Au_3Ru_4 core rearrangement, like that of the M_2Ru_3 clusters, proceeds by a series of metal core site exchanges involving a Berry pseudo-rotation exchange of two gold atoms, but here further accompanied by a concomitant movement of the third gold atom to an equivalent site bridging a different face. In the case of (**1**) it is the two phosphorus atoms of a bidentate ligand that are equivalent and this restricts the mobility of the two gold atoms they bridge. In the original report of the n.m.r. data insufficient evidence was available to conclude whether the $Au(PPh_3)$ group in (**1**) was involved in the rearrangement.[3] The structure established in the *X*-ray analysis makes most probable a series of polyhedral rearrangements which interchange the third gold atom, Au(3) in the Figure, between the site capping the $Au(1)Ru_2$ face to one capping a $Au(2)Ru_2$ face, thus making the environments of Au(1) and Au(2) equivalent on the n.m.r. time-scale. This could proceed by a successive change in bonding of the Au(3) atom between face-capping and edge-bridging sites, known to be relatively similar in energy,[11–13] accompanied by an overall rearrangement of the framework by a Berry pseudo-rotation mechanism.

Table 2. Fractional atomic co-ordinates, with estimated standard deviations in parentheses, for $[Au_3Ru_4(\mu\text{-}H)(CO)_{12}(\mu\text{-}Ph_2PCH_2PPh_2)(PPh_3)]$ (1)

Atom	x	y	z
Au(1)	0.095 44(8)	0.160 80(4)	0.215 92(9)
Au(2)	−0.041 71(8)	0.097 67(5)	0.246 57(8)
Au(3)	0.244 23(8)	0.106 03(5)	0.194 73(8)
Ru(1)	0.122 32(16)	0.048 20(9)	0.268 96(16)
Ru(2)	0.226 91(16)	0.142 12(9)	0.366 43(16)
Ru(3)	0.072 42(16)	0.104 50(10)	0.418 40(15)
Ru(4)	0.235 03(17)	0.039 97(9)	0.439 50(16)
P(1)	−0.005 1(6)	0.214 1(3)	0.123 9(5)
P(2)	−0.160 0(6)	0.150 1(3)	0.176 8(6)
P(3)	0.332 8(5)	0.117 0(3)	0.095 0(5)
C(11)	0.058 2(21)	−0.009 9(13)	0.296 9(20)
O(11)	0.017 0(16)	−0.046 0(10)	0.309 7(16)
C(12)	0.221 3(23)	0.002 0(13)	0.264 8(21)
O(12)	0.274 2(15)	−0.026 9(9)	0.252 3(14)
C(13)	0.064 6(22)	0.042 4(13)	0.148 6(22)
O(13)	0.040 7(16)	0.034 2(10)	0.072 0(16)
C(21)	0.344 0(25)	0.153 4(13)	0.346 3(22)
O(21)	0.416 5(16)	0.161 7(9)	0.343 2(15)
C(22)	0.257 6(23)	0.159 4(13)	0.482 7(23)
O(22)	0.287 5(18)	0.172 5(10)	0.556 1(18)
C(23)	0,190 5(20)	0.214 0(12)	0.338 0(19)
O(23)	0.181 3(17)	0.260 8(10)	0.337 1(16)
C(31)	−0.025 7(25)	0.063 5(14)	0.421 4(24)
O(31)	−0.094 6(19)	0.040 5(11)	0.429 3(17)
C(32)	0.094 2(21)	0.122 3(12)	0.536 6(21)
O(32)	0.111 2(16)	0.132 3(9)	0.610 6(17)
C(33)	0.019 5(20)	0.172 6(12)	0.391 4(19)
O(33)	−0.012 9(14)	0.215 1(8)	0.380 5(13)
C(41)	0.355 1(22)	0.039 8(12)	0.420 3(20)
O(41)	0.425 2(16)	0.037 2(9)	0.410 0(14)
C(42)	0.222 8(21)	−0.035 7(13)	0.453 4(20)
O(42)	0.217 1(18)	−0.082 3(11)	0.451 5(17)
C(43)	0.277 0(23)	0.046 3(13)	0.558 8(23)
O(43)	0.299 7(18)	0.051 5(10)	0.634 8(18)
C(1)	−0.114 0(19)	0.214 4(10)	0.157 5(19)
C(112)	−0.098 2(12)	0.214 7(7)	−0.053 3(14)
C(113)	−0.111 0(12)	0.197 2(7)	−0.140 0(14)
C(114)	−0.052 0(12)	0.160 4(7)	−0.163 4(14)
C(115)	0.019 8(12)	0.141 0(7)	−0.100 1(14)
C(116)	0.032 6(12)	0.158 6(7)	−0.013 4(14)
C(111)	−0.026 4(12)	0.195 4(7)	0.010 0(14)
C(122)	0.007 3(15)	0.316 8(10)	0.192 0(14)
C(123)	0.023 0(15)	0.372 2(10)	0.192 7(14)
C(124)	0.048 3(15)	0.396 6(10)	0.121 7(14)
C(125)	0.057 8(15)	0.365 7(10)	0.049 8(14)
C(126)	0.042 1(15)	0.310 4(10)	0.049 0(14)
C(121)	0.016 8(15)	0.285 9(10)	0.120 1(14)
C(212)	−0.306 0(14)	0.152 3(8)	0.036 0(14)
C(213)	−0.350 1(14)	0.138 8(8)	−0.049 3(14)
C(214)	−0.311 6(14)	0.102 4(8)	−0.097 8(14)
C(215)	−0.229 1(14)	0.079 4(8)	−0.061 1(14)
C(216)	−0.185 1(14)	0.092 9(8)	0.024 1(14)
C(211)	−0.223 5(14)	0.129 3(8)	0.072 7(14)
C(221)	−0.240 4(14)	0.170 0(10)	0.240 5(14)
C(222)	−0.274 5(14)	0.128 2(10)	0.282 7(14)
C(223)	−0.338 3(14)	0.139 0(10)	0.331 2(14)
C(224)	−0.367 9(14)	0.191 6(10)	0.337 6(14)
C(225)	−0.333 8(14)	0.233 4(10)	0.295 3(14)
C(226)	−0.270 0(14)	0.222 7(10)	0.246 8(14)
C(311)	0.282 2(12)	0.099 4(7)	−0.016 8(9)
C(312)	0.224 9(12)	0.055 3(7)	−0.034 1(9)
C(313)	0.187 0(12)	0.040 8(7)	−0.120 6(9)
C(314)	0.206 4(12)	0.070 5(7)	−0.189 8(9)
C(315)	0.263 6(12)	0.114 6(7)	−0.172 6(9)
C(316)	0.301 5(12)	0.129 1(7)	−0.086 1(9)
C(321)	0.433 5(11)	0.078 2(7)	0.120 7(14)
C(322)	0.489 0(11)	0.072 3(7)	0.061 9(14)
C(323)	0.564 8(11)	0.040 0(7)	0.083 9(14)
C(324)	0.585 1(11)	0.013 6(7)	0.164 7(14)
C(325)	0.529 6(11)	0.019 5(7)	0.223 5(14)
C(326)	0.453 9(11)	0.051 8(7)	0.201 5(14)
C(331)	0.367 2(17)	0.186 1(7)	0.092 6(14)
C(332)	0.455 4(17)	0.203 7(7)	0.109 8(14)
C(333)	0.474 3(17)	0.258 5(7)	0.107 3(14)
C(334)	0.405 0(17)	0.295 8(7)	0.087 5(14)
C(335)	0.316 9(17)	0.278 3(7)	0.070 3(14)
C(336)	0.298 0(17)	0.224 4(7)	0.072 9(14)
H	0.121 25	0.038 41	0.458 80

Experimental

The cluster $[Au_3Ru_4(\mu\text{-}H)(CO)_{12}(\mu\text{-}Ph_2PCH_2PPh_2)(PPh_3)]$ (1) was prepared as previously described[3] and crystals suitable for *X*-ray diffraction studies were grown slowly, by layer diffusion, from a dichloromethane–light petroleum (b.p. 40—60 °C) solution at −20 °C.

Crystal Data.—$C_{55}H_{38}Au_3O_{12}P_3Ru_4$, $M = 1\,978$, monoclinic, space group $P2_1/n$, $a = 15.412(2)$, $b = 24.835(3)$, $c = 15.613(2)$ Å, $\beta = 102.87(2)°$, $U = 5\,832.57$ Å^3, $F(000) = 3\,688$, $\mu(\text{Mo-}K_\alpha) = 82.76$ cm^{-1}, $Z = 4$, and $D_c = 2.25$ g cm^{-3}.

The methods of data collection, data processing, and absorption correction used for (1) were similar to those described previously.[14] The crystal selected for data collection had dimensions 0.44 × 0.48 × 0.21 mm. A scan width of 0.8° was used to collect data in the θ range 3—25°. 360 Azimuthal scan data were used in absorption correction and relative transmission factors varied from 1.000 to 0.810. Equivalent reflections were merged to give 5 998 data with $I/\sigma(I) > 3.0$.

Structure Solution and Refinement.[15]—The structure of (1) was solved from a Patterson synthesis in which two gold atoms were located. The remaining metal and non-hydrogen atoms were found from subsequent difference Fourier syntheses. The hydrido ligand site was deduced from potential energy minimisation calculations,[16] and was included in the structure factor calculations with a thermal parameter U of 0.08 Å^2, but not refined. Blocked full-matrix refinement of the atomic positional and thermal parameters converged to final R and R' values of 0.0443 and 0.0442 respectively. The phenyl groups were treated as rigid hexagons [d(C–C) = 1.395 Å] and the hydrogen atoms were included in the structure factor calculations at calculated positions [d(C–H) = 1.08 Å] with fixed thermal parameters of 0.08 Å^2. Anisotropic thermal parameters were assigned to the metal, and P atoms during the final cycles of refinement.

Fractional atomic co-ordinates are listed in Table 2. Additional material available from the Cambridge Crystallographic Data Centre comprises thermal parameters, H-atom co-ordinates, and intermolecular distances.

Acknowledgements

We thank the S.E.R.C. for a Studentship (T. A.) and the Nuffield Foundation for support, Johnson Matthey Ltd. for a generous loan of gold and ruthenium salts, and Mrs. L. J. Salter for drawing the diagrams.

References

1 Part 4, S. S. D. Brown, S. Hudson, I. D. Salter, and M. McPartlin, *J. Chem. Soc., Dalton Trans.*, 1987, 1967.

2 For example, K. P. Hall and D. M. P. Mingos, *Prog. Inorg. Chem.*, 1984, **32**, 237; P. Braunstein and J. Rose, *Gold Bull.*, 1985, **18**, 17 and refs. therein.

3 J. A. K. Howard, I. D. Salter, and F. G. A. Stone, *Polyhedron*, 1984, **3**, 567.

4 For example, S. S. D. Brown, P. J. McCarthy, and I. D. Salter, *J. Organomet. Chem.*, 1986, **306**, C27 and refs. therein.

5 P. A. Bates, S. S. D. Brown, A. J. Dent, M. B. Hursthouse, G. F. M. Kitchen, A. G. Orpen, I. D. Salter, and V. Šik, *J. Chem. Soc., Chem. Commun.*, 1986, 600.

6 M. J. Freeman, A. G. Orpen, and I. D. Salter, *J. Chem. Soc., Dalton Trans.*, 1987, 379.

7 L. W. Bateman, M. Green, K. A. Mead, R. M. Mills, I. D. Salter, F. G. A. Stone, and P. Woodward, *J. Chem. Soc., Dalton Trans.*, 1983, 2599.

8 L. J. Farrugia, M. J. Freeman, M. Green, A. G. Orpen, F. G. A. Stone, and I. D. Salter, *J. Organomet. Chem.*, 1983, **249**, 273.

9 B. F. G. Johnson, D. A. Kaner, J. Lewis, P. R. Raithby, and M. J. Taylor, *J. Chem. Soc., Chem. Commun.*, 1982, 314; B. F. G. Johnson, J. Lewis, W. J. H. Nelson, M. D. Vargas, D. Braga, K. Henrick, and M. McPartlin, *J. Chem. Soc., Dalton Trans.*, 1986, 975; J. A. Iggo, M. J. Mays, P. R. Raithby, and K. Henrick, *ibid.*, 1984, 633.

10 S. S. D. Brown, A. J. Dent, G. F. M. Kitchen, A. G. Orpen, and I. D. Salter, unpublished work.

11 D. M. P. Mingos, *Polyhedron*, 1984, **3**, 1289.

12 S. R. Bunkhall, H. D. Holden, B. F. G. Johnson, J. Lewis, G. N. Pain, P. R. Raithby, and M. J. Taylor, *J. Chem. Soc., Chem. Commun.*, 1984, 25.

13 K. Henrick, B. F. G. Johnson, J. Lewis, J. Mace, M. McPartlin, and J. Morris, *J. Chem. Soc., Chem. Commun.*, 1985, 1617.

14 P. F. Jackson, B. F. G. Johnson, J. Lewis, W. J. H. Nelson, and M. McPartlin, *J. Chem. Soc., Dalton Trans.*, 1982, 2099.

15 G. M. Sheldrick, SHELX 76, Crystal Structure Solving Package, University of Cambridge, 1976.

16 A. G. Orpen, *J. Chem. Soc., Dalton Trans.*, 1980, 2509.

Received 19*th May* 1987; *Paper* 7/893

Deprotonation of a Heterodinuclear Transition-metal Hydride Complex and Reactions of the Anion with Electrophiles: *X*-Ray Crystal Structures of $[(\eta^5-C_5H_5)(OC)_2Mo\{\mu-Ag(PPh_3)\}(\mu-PPh_2)Mn(CO)_4]$ and $[(\eta-C_5H_5)(OC)_2-Mo(\mu-I)(\mu-PPh_2)Mn(CO)_4]$†

Andrew D. Horton and Martin J. Mays*
University Chemical Laboratory, Lensfield Road, Cambridge CB2 1EW
Trushar Adatia, Kim Henrick, and Mary McPartlin
School of Chemistry, The Polytechnic of North London, Holloway Road, London N7 8DB

Deprotonation of $[(\eta^5-C_5H_5)(OC)_2Mo(\mu-H)(\mu-PPh_2)Mn(CO)_4]$ with base gives the heterodinuclear anion $[(\eta^5-C_5H_5)(OC)_2Mo(\mu-PPh_2)Mn(CO)_4]^-$ which has been isolated as its $[NEt_4]^+$ salt. This anion reacts with complexes of Group 1B metals to give heterotrinuclear complexes of the type $[(\eta^5-C_5H_5)(OC)_2Mo(\mu-ML)(\mu-PPh_2)Mn(CO)_4]$ [ML = Au(PPh$_3$), Au(PMe$_2$Ph), or Ag(PPh$_3$)]. A single-crystal *X*-ray diffraction study established the structure of the silver-containing complex. The metal atom triangle [Mo–Mn 3.190(2), Ag–Mn 2.664(2), and Ag–Mo 2.874(2) Å] is bridged by a PPh$_2$ group along the Mo–Mn edge [Mo–P 2.387(4) and Mn–P 2.272(4) Å]. The bridging phosphorus atom lies 0.3 Å out of the plane of the three metal atoms resulting in an angle between this plane and the Mo–Mn–(μ-P) plane of 7.59°. The phosphorus atom in the PPh$_3$ group lies 0.11 Å out of the Mo–Mn–Ag plane on the same side of the plane as the phosphido ligand. The heterodinuclear anion reacts with iodine to give, as the major product, the iodo-bridged compound $[(\eta^5-C_5H_5)(OC)_2Mo(\mu-I)(\mu-PPh_2)Mn(CO)_4]$ which has been characterised by a single-crystal *X*-ray diffraction study. The two metal atoms in this complex are 3.978(2) Å apart indicating the absence of a metal-metal bond and the angle between the planes defined by Mo–Mn–(μ-I) and Mo–Mn–(μ-P) is 145.0°. Loss of one molecule of CO during the reaction of the heterodinuclear anion with I$_2$ accounts for the formation of $[(\eta^5-C_5H_5)(OC)_2Mo(\mu-I)(\mu-PPh_2)Mn(CO)_3]$ which is obtained as a minor product. The major product is converted in near quantitative yield into the minor product on photolysis and the minor product is similarly converted into the major product on treatment with CO.

The deprotonation of hydrogen-bridged metal–metal bonds is a common route to anionic homodinuclear metal carbonyl complexes[1–3] and has been extended in a limited number of cases to the formation of anionic heteronuclear derivatives.[4] The reactions of anions formed in this way have not been widely studied, although treatment with complexes of other metals and, in particular, those of Groups 1B,[1,2,5–8] 2B,[9] and 8[2] has been used to obtain a variety of mixed-metal complexes.

The reaction of $[Mn(CO)_5]^-$ with $[Mo(CO)_6]$ gives a molybdenum–manganese anionic complex, $[MoMn(CO)_{10}]^-$, which was isolated as its tetramethylammonium salt.[9] This complex undergoes metal–metal bond fission under mild conditions and a neutral protonated analogue could not be obtained. We have previously reported the preparation of the phosphido-bridged molybdenum–manganese complex, $[(\eta^5-C_5H_5)(OC)_2Mo(\mu-H)(\mu-PPh_2)Mn(CO)_4]$,[10] and, in this paper, we describe its deprotonation to give the corresponding anion. The reactions of this anion with complexes of Group 1B metals and with I$_2$ are also reported. The preparation of the closely related anion $[(\eta^5-C_5H_5)(OC)_2Mo\{\mu-P(C_6H_4Me-p)_2\}-Mn(CO)_4]^-$ has recently been described by Casey and Bullock[11] but its protonation was the only reaction of this anion which was investigated.

Results and Discussion

Preparation and Properties of $[NEt_4][(\eta^5-C_5H_5)(OC)_2Mo-(\mu-PPh_2)Mn(CO)_4]$.—Reaction of $[(\eta^5-C_5H_5)(OC)_2Mo(\mu-H)-(\mu-PPh_2)Mn(CO)_4]$ (**1**) with KOH in absolute ethanol leads to the formation of a dark red solution of $K[(\eta^5-C_5H_5)(OC)_2-Mo(\mu-PPh_2)Mn(CO)_4]$ from which $[NEt_4][(\eta^5-C_5H_5)(OC)_2-Mo(\mu-PPh_2)Mn(CO)_4]$ (**2**) was obtained as an orange solid after metathesis with [NEt$_4$]Br and precipitation from Et$_2$O–CH$_2$Cl$_2$ (1:1). Complex (**2**) was identified by comparison of its i.r. and ^{1}H n.m.r. spectra with those of the analogous complex prepared by Casey and Bullock.[11] The temperature dependence of the ^{1}H n.m.r. resonances due to the phenyl group over the range 213—321 K is again attributed to a fluxional process which interconverts the environments of the two phenyl groups in a similar manner to that postulated for the $\mu-P(C_6H_4-p)_2$ complex[11] and to that which interconverts the methyl groups in $[(\eta^5-C_5H_5)(OC)_2Mo(\mu-AsMe_2)Fe(CO)_4]$.[12]

Reactions of the Anion (**2**) *with Group* 1B *Metal Complexes*.—Reaction of complex (**2**) at room temperature in CH$_2$Cl$_2$ solution with a small excess of [AuI(PPh$_3$)], [AuCl(PMe$_2$Ph)], or [{AgCl(PPh$_3$)}$_4$] gives the heterotrinuclear complexes $[(\eta^5-C_5H_5)(OC)_2Mo(\mu-ML)(\mu-PPh_2)Mn(CO)_4]$ [M = Au, L = PPh$_3$ (**3a**) or PMe$_2$Ph (**3b**); M = Ag, L = PPh$_3$ (**3c**)] in high yield. The complexes have been characterised on the basis of i.r. and ^{1}H n.m.r. spectroscopy and, in the case of (**3c**), by an *X*-ray diffraction study.

The i.r. [ν(CO)] spectra of (**3a**)—(**3c**) show, in each case, six absorption bands in an overall pattern similar to that observed for (**1**). However, the absolute frequencies of the carbonyl

---

† 1,1,1,1,2,2-Hexacarbonyl-2-η-cyclopentadienyl-μ-diphenylphosphido-μ-triphenylphosphineargentio-manganesemolybdenum(*Mn–Mo*) and 1,1,1,1,2,2-hexacarbonyl-2-η-cyclopentadienyl-μ-diphenylphosphido-μ-iodo-manganesemolybdenum.

Supplementary data available: see Instructions for Authors, *J. Chem. Soc., Dalton Trans.*, 1988, Issue 1, pp. xvii—xx.

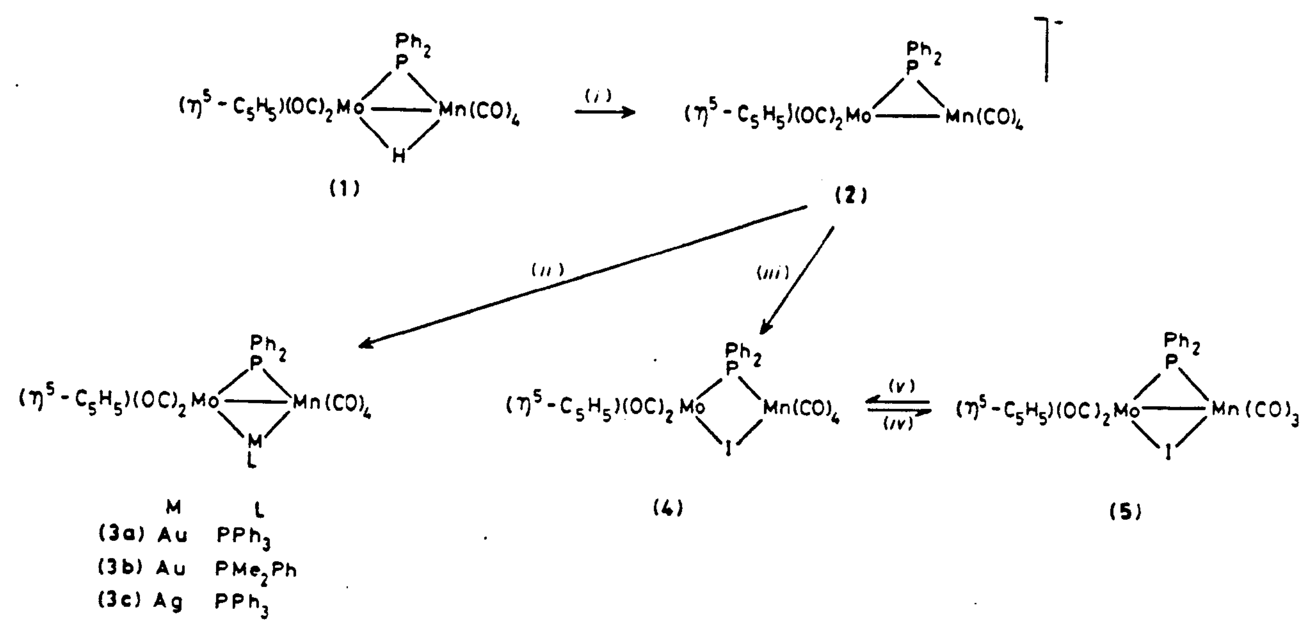

Scheme. Synthesis and proposed structures of the new complexes. Reagents: (*i*) KOH, ethanol, [NEt$_4$]Br; (*ii*) [AuI(PPh$_3$)], [AuCl(PMe$_2$Ph)], or [{AgCl(PPh$_3$)}$_4$], CH$_2$Cl$_2$; (*iii*) I$_2$, CH$_2$Cl$_2$; (*iv*) *h*ν, hexane–benzene (5:1); (*v*) CO, hexane–benzene (5:1)

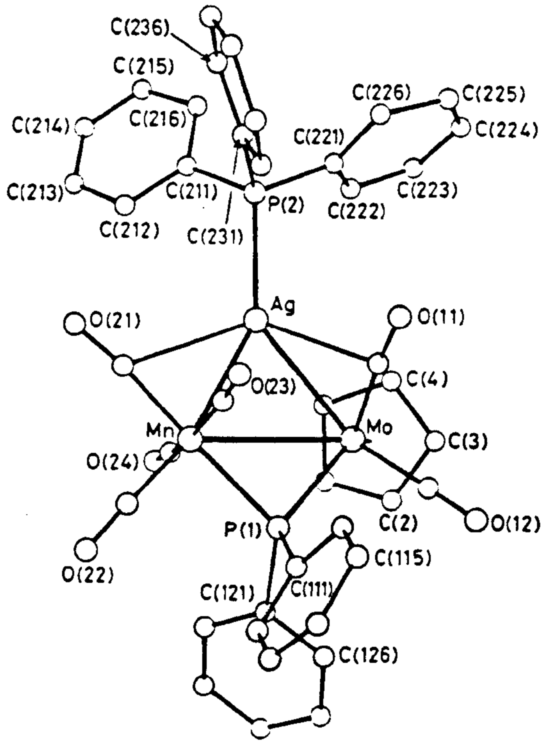

Figure 1. Molecular structure of [(η^5-C$_5$H$_5$)(OC)$_2$Mo{μ-Ag(PPh$_3$)}(μ-PPh$_2$)Mn(CO)$_4$] (**3c**) showing the crystallographic numbering

absorptions are intermediate between those of complexes (**1**) and (**2**) suggesting that the M′–Au(Ag) bonds are polarised with significant negative charge on the molybdenum and manganese centres (M′).[13] The ^{1}H n.m.r. spectra of the complexes are consistent with the presence in solution of a single isomer, containing a μ-AuL or μ-AgL group. Few complexes containing a μ-bridging silver atom have been structurally characterised[14,15] and, to examine the effect of replacement of a μ-H by a μ-AgL group, an *X*-ray diffraction study has been carried out on (**3c**). Suitable crystals of complex (**3c**) were grown by slow evaporation of a hexane–CH$_2$Cl$_2$ (1:1) solution at 0 °C.

The molecular structure of (**3c**) is shown in Figure 1. Table 1 lists selected bond lengths and bond angles. The silver atom lies 0.30 Å above the Mo–Mn–P(1) plane, resulting in an angle between this plane and the Mo–Mn–Ag plane of 7.59°. The deviation from coplanarity in (**3c**) is somewhat greater than in the related complex, [Mn$_2${μ-Au(PMe$_2$Ph)}(μ-PPh$_2$)(CO)$_8$],[1] in which the gold atom is situated only 0.06 Å above the Mn–Mn–P(1) plane. The difference may be related to steric interaction between the bulky cyclopentadienyl and μ-Ag(PPh$_3$) groups in (**3c**). The phosphorus atom in the PPh$_3$ group lies 0.11 Å above the Mo–Mn–Ag plane, on the same side of the plane as the phosphido ligand.

The reduced covalent radius of Mn compared to Mo may only partially explain the asymmetric bridging of the μ-Ag(PPh$_3$) group [Ag–Mn 2.664(2), Ag–Mo 2.874(2) Å]. Thus the difference in the two metal–metal distances of *ca.* 0.21 Å compares with a difference of only *ca.* 0.12 Å in the two metal-bridging phosphorus distances. The Ag–Mn bond distance is only slightly shorter than the average Au–Mn bond distance (2.688 Å) in [Mn$_2${μ-Au(PMe$_2$Ph)}(μ-PPh$_2$)(CO)$_8$].[1] The manganese centre is approximately octahedrally co-ordinated by the silver atom, phosphido ligand, and four carbonyl ligands. The ligands around the molybdenum centre adopt the familiar approximate square-pyramidal geometry (if the Mo–Mn bond is ignored). The greater steric requirement of the μ-AgL group, compared to the μ-H group, results in the movement of the equatorial carbonyl ligands on Mn away from the former group, with an increase in the Mo–Mn–CO (*trans* to PPh$_2$) angle from 116.1(2)° in (**1**)[10] to 129.3(5)° in (**3c**) and a decrease in the Mo–Mn–CO (*trans* to Ag) angle from 148.6(2) to 135.6(5)°. This increase of 13.2° in the displacement from the μ-ML group of the carbonyl (*trans* to PPh$_2$) may be compared to the increase of 8.4° for the related Mn$_2$Au system.[1] Steric crowding involving the bulky μ-Ag(PPh$_3$) group may also partly explain the increase in the Mo–Mn bond distance from 3.088(1) Å in (**1**) to 3.190(2) Å in (**3c**). The average Mn–CO and Mo–CO bond distances are the same within error limits in (**1**) and (**3c**). Further, all the carbonyl ligands in (**3c**) are near-linear; the greatest deviation, an Mn–CO interbond angle of 172(1)°, is

Table 1. Selected bond lengths (Å) and angles (°) for complexes (3c) and (4)

	(3c)	(4)		(3c)	(4)
Mo–Mn	3.190(2)	3.978(2)	Mo–C(11)	1.954(16)	1.951(12)
Mo–Ag	2.874(2)		Mo–C(12)	1.950(17)	2.009(13)
Mo–I		2.865(1)	Mn–C(21)	1.830(16)	1.815(12)
Mn–Ag	2.664(2)		Mn–C(22)	1.755(18)	1.810(13)
Mn–I		2.710(2)	Mn–C(23)	1.883(18)	1.873(12)
Mo–P(1)	2.387(4)	2.545(3)	Mn–C(24)	1.829(17)	1.849(12)
Mn–P(1)	2.272(4)	2.388(3)			
Ag–P(2)	2.414(4)		Range of C–O	1.113—1.165(17)	1.127—1.151(12)

(3c)

Mn–Ag–Mo	70.2(1)	P(2)–Ag–Mo	139.4(1)	C(22)–Mn–Mo	135.6(5)	C(23)–Mn–Ag	80.9(5)
P(2)–Ag–Mn	150.2(1)	C(11)–Ag–Mo	41.0(3)	C(22)–Mn–C(21)	95.1(7)	C(23)–Mn–P(1)	90.5(5)
C(11)–Ag–Mn	88.6(4)	C(11)–Ag–P(2)	112.7(4)	C(23)–Mn–Mo	88.4(5)	C(23)–Mn–C(22)	97.3(7)
C(21)–Ag–Mo	109.9(3)	C(21)–Ag–Mn	39.8(3)	C(23)–Mn–C(21)	87.8(7)	C(24)–Mn–Mo	84.0(5)
C(21)–Ag–P(2)	110.7(3)	C(21)–Ag–C(11)	121.2(5)	C(24)–Mn–Ag	83.1(5)	C(24)–Mn–C(21)	86.1(7)
Mn–Mo–Ag	51.8(1)	P(1)–Mo–Ag	96.8(1)	C(24)–Mn–P(1)	94.9(5)	C(24)–Mn–C(23)	164.0(7)
C(11)–Mo–Ag	64.4(4)	C(11)–Mo–Mn	89.8(5)	C(24)–Mn–C(22)	98.0(8)	C(111)–P(1)–Mo	123.5(5)
P(1)–Mo–Mn	45.3(1)	C(11)–Mo–P(1)	107.8(5)	Mn–P(1)–Mo	86.4(1)	C(121)–P(1)–Mo	113.5(5)
C(12)–Mo–Ag	142.0(4)	C(12)–Mo–Mn	119.2(5)	C(111)–P(1)–Mn	113.7(5)	C(121)–P(1)–C(111)	101.1(6)
C(12)–Mo–P(1)	81.4(5)	Mo–Mn–Ag	58.0(1)	C(121)–P(1)–Mn	120.0(5)	C(221)–P(2)–Ag	112.9(5)
C(12)–Mo–C(11)	79.9(6)	P(1)–Mn–Mo	48.3(1)	C(211)–P(2)–Ag	115.6(5)	C(231)–P(2)–Ag	111.7(5)
P(1)–Mn–Ag	106.0(1)	C(21)–Mn–Mo	129.3(5)	C(221)–P(2)–C(211)	104.0(7)	C(231)–P(2)–C(221)	105.2(7)
C(21)–Mn–Ag	71.5(5)	C(22)–Mn–Ag	166.4(5)	C(231)–P(2)–C(211)	106.7(7)		
C(21)–Mn–P(1)	177.1(5)	C(22)–Mn–P(1)	87.5(5)				
				Range of M–C–O	175—179(2)		

(4)

P–Mo–I	73.7(1)	C(11)–Mo–P	118.0(4)	C(24)–Mn–I	88.7(4)	C(23)–Mn–C(22)	90.6(5)
C(12)–Mo–I	129.4(3)	C(12)–Mo–C(11)	77.1(4)	C(24)–Mn–C(21)	88.8(5)	C(24)–Mn–P	90.4(3)
P–Mn–I	79.1(1)	C(12)–Mo–P	78.9(3)	C(24)–Mn–C(23)	177.3(5)	C(24)–Mn–C(22)	92.1(5)
C(21)–Mn–P	172.4(4)	C(21)–Mn–I	93.4(4)	Mn–P–Mo	107.5(1)	Mn–I–Mo	91.0(1)
C(22)–Mn–P	94.2(3)	C(22)–Mn–I	173.2(3)	C(111)–P–Mn	107.3(3)	C(111)–P–Mo	114.8(3)
C(23)–Mn–I	88.7(4)	C(22)–Mn–C(21)	93.3(5)	C(121)–P–Mn	115.5(3)	C(121)–P–Mo	110.0(3)
C(23)–Mn–C(21)	90.7(5)	C(23)–Mn–P	89.8(3)			C(121)–P–C(111)	101.9(4)
				Range of M–C–O	175—179(1)		

seen for CO(21) (*trans* to PPh_2), and is ascribed to the bending back of the oxygen from the PPh_3 ligand on Ag for steric reasons. Although the separation of the silver atom and the two adjacent carbonyl ligands, CO(21), 2.711(16) Å, and CO(11), 2.688(14) Å, approaches that required for incipient bridging of the Ag–Mn and Ag–Mo bonds, there is no evidence for such an interaction in the i.r. [ν(CO)] spectrum of (3c).

The Mn–P(1) bond distance, 2.272(4) Å, and the Mo–P(1) distance, 2.387(4) Å, are reduced from the corresponding distances in (1) of 2.294(2) and 2.435(1) Å respectively. The greater reduction in the Mo–P(1) distance may reflect a greater increase in the electron density, available for π bonding to phosphorus, at the molybdenum centre, as a result of the asymmetric bridging of the μ-Ag(PPh_3) group. In contrast, the similar Mn_2Au complex shows no significant change in Mn–P bond distances on replacement of the μ-H by the μ-AuL group.[1] The modification of the metal–phosphorus bond distances in the Mo–Mn–P triangle results in a large increase in the phosphido group bite angle (Mn–P–Mo) from 81.5(0)° in (1) to 86.4(1)° in (3c).

Reaction of Complex (**2**) *with Iodine*.—The reaction of complexes containing metal–metal bonds with electrophiles may lead to cleavage of the metal–metal bonds in some cases. This is particularly true of electrophiles such as X^+ (X = halogen) which may bridge metal–metal bonds as three-electron donor ligands. Thus the reaction of I_2 with $[Fe_2(CO)_4(\eta^5\text{-}C_5H_5)_2]$ proceeds *via* electrophilic attack to give an iodo-bridged cationic intermediate which then reacts with I^- to give $[Fe(CO)_2(\eta^5\text{-}C_5H_5)I]$.[16] The reaction of I_2 with heterodinuclear metal–metal bonded complexes, *e.g.* with $[(OC)_5MnAu(PPh_3)]$ to give $[Mn(CO)_5I]$ and $[AuI(PPh_3)]$,[17] may proceed similarly and, in an attempt to isolate an iodo-bridged heterodinuclear intermediate in the Mo–Mn system, the reaction of (2) with I_2 has been studied.

On stirring complex (**2**) in CH_2Cl_2 with an equimolar quantity of I_2 a dark red crystalline solid is obtained in 76% yield. This yield is halved if the amount of I_2 used is halved, indicating that 1 mol of I_2 is needed per mol of (**2**) as expected if electrophilic attack of I^+ is involved.

The molecular structure of the dark red crystalline solid has been determined by an *X*-ray diffraction study, which reveals that it is the iodo-bridged complex $[(\eta^5\text{-}C_5H_5)(OC)_2Mo(\mu\text{-}I)(\mu\text{-}PPh_2)Mn(CO)_4]$ (**4**). Crystals of (**4**) suitable for the *X*-ray study were grown by slow evaporation of a solution in hexane–CH_2Cl_2 (1 : 1) at 0 °C. The molecular structure of (**4**) is shown in Figure 2 and Table 1 lists selected bond lengths and bond angles.

The phosphido and iodo ligands bridge the two metal atoms, which are separated by a distance of 3.978(2) Å, compared to 3.088(1) Å in the μ-H complex, (1).[10] This large separation is consistent with the absence of a Mo–Mn bond in (4), as expected on the basis of the 18-electron rule, and may be compared to a Mo–Mo separation of 4.441(1) Å in the bis(iodo)-bridged complex, $[Mo_2(\mu\text{-}I)_2(CO)_4(\eta^5\text{-}C_5H_5)_2]$.[18] Even allowing for differences in the covalent radius between Mo and Mn the intermetal separation in (4) is significantly reduced compared to the bis(iodo) complex, indicating lower geometrical flexibility of the μ-PR_2 ligand compared to the μ-I

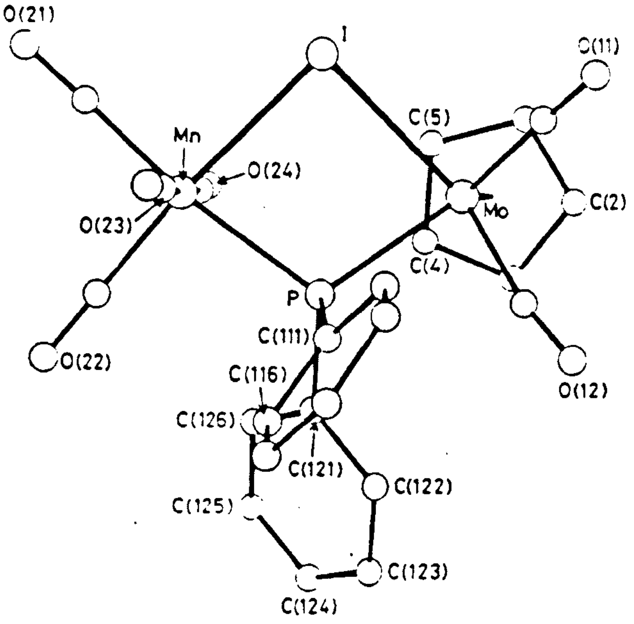

Figure 2. Molecular structure of $[(\eta^5\text{-}C_5H_5(OC)_2Mo(\mu\text{-}I)(\mu\text{-}PPh_2)\text{-}Mn(CO)_4]$ (4) showing the crystallographic numbering

ligand. The Mn–I bond distance of 2.710(2) Å compares to 2.689(2) A in the only previous *X*-ray structural determination on an iodo-bridged heterodimetallic complex, $[(OC)_4Mn(\mu\text{-}I)(\mu\text{-}COCH_2CH_2CH_2)Pt(PBu^t{}_2Me)_2]$.[19] The Mo–I bond distance of 2.865(1) Å compares closely to that of 2.853(1) Å in $[Mo_2(\mu\text{-}I)_2(CO)_4(\eta^5\text{-}C_5H_5)_2]$.[18] The Mo–I–Mn angle of 91.0(1)° is at the lower end of the range of values for iodo ligands bridging two non-bonded metals; the corresponding angle in $[Mo_2(\mu\text{-}I)_2(CO)_4(\eta^5\text{-}C_5H_5)_2]$ is 102.24(2)° and in $[Os_4H_3(\mu\text{-}I)(CO)_{12}]$[20] is 87.9(2)°. The bridging angle of the phosphido group, Mo–P–Mn, of 107.5(1)° compares with 81.5(0)° for (1), which contains a Mo–Mn bond. The M–P bond distances in (4) are *ca.* 0.1 Å greater than in (1). The iodo and phosphido groups adopt a relative orientation (with respect to the Mo–Mn vector) intermediate between transoid and cisoid: the angle between the planes containing Mo–Mn–I and Mo–Mn–P is 145.0°. The relative geometry of the bridging groups may be determined by the requirement to minimise steric interaction between the ligands on the two metals.

The distribution of the six ligands on Mn, comprising four carbonyl groups and the phosphido and iodo groups, is close to octahedral, the largest deviation from ideal being the P–Mn–I interbond angle of 79.1(1)°. The mean Mn–CO bond distance of 1.832(10) Å is equal, within error limits, to the corresponding distance in (1), with the longest Mn–CO distance being observed for the axial carbonyl ligands as expected on the basis of the relative π-acid character of the *trans* ligands on Mn. The ligands on Mo adopt a square-pyramidal geometry with mean Mo–CO and mean Mo–C(cyclopentadienyl) bond distances identical within error limits to the corresponding distances in (1).

The infrared [ν(CO)] and ^{13}C n.m.r. spectra of complex (4) show the same pattern of resonances as observed for (1),[10] indicating that (1) and (4) have similar structures in solution. The absence of a metal–metal bond in (4), however, is revealed by its ^{31}P n.m.r. spectrum, which shows a resonance at δ −135.4 p.p.m. attributable to the $\mu\text{-}PPh_2$ group as compared to the resonance at δ 17.5 p.p.m. for this group in (1). These values are consistent with data on a wide range of $\mu\text{-}PR_2$ complexes which suggest that, in most cases, resonances in the range δ −100 to −350 p.p.m. may be expected if a metal–metal bond is absent and in the range δ 150 to −100 p.p.m. if such a bond is present.[21]

In the reaction of complex (2) with I_2 small quantities of an orange solid are isolated in addition to the major product (4). The yield of this minor product increases if the reaction mixture is stirred in daylight after the initial reaction with I_2 is complete, and (4) is converted into it in near-quantitative yield on irradiation with u.v. light. On the basis of spectroscopic evidence the minor product is formulated as $[(\eta^5\text{-}C_5H_5)(OC)_2Mo(\mu\text{-}I)(\mu\text{-}PPh_2)Mn(CO)_3]$ (5) which is derived from (4) by loss of a CO ligand and concomitant metal–metal bond formation. Thus the ^{13}CO n.m.r. spectrum of (5) shows three resonances of relative intensity 1 and a 'triplet' resonance of relative intensity 2. This latter resonance may be ascribed to two superimposed doublets. The $^{31}P\text{-}\{^1H\}$ n.m.r. spectrum shows a singlet resonance at δ −49.3 p.p.m., this shift [as compared to the corresponding resonance in (4)] being consistent with metal–metal bond formation.[21]

There are two possible structures for (5), one with four CO ligands on Mn and one on Mo, the other with three CO ligands on Mn and two on Mo. The latter structure, shown in the Scheme, is preferred on the basis of the close similarity of the i.r. [ν(CO)] spectrum of (5) to that of a related μ-acyl complex, $[(\eta^5\text{-}C_5H_5)(OC)_2Mo\{\mu\text{-}C(O)C_6H_{11}\}(\mu\text{-}PPh_2)Mn(CO)_3]$, the structure of which has been determined by *X*-ray analysis.[22]

Stirring a solution of (5) under CO at room temperature leads, after 1 h, to near-quantitative regeneration of (4). Such reversible metal–metal bond cleavage in bridged heterodinuclear complexes on reaction with two-electron donor ligands has been observed in related systems.[23]

Experimental

All reactions were carried out under a nitrogen atmosphere in nitrogen-saturated solvents distilled from an appropriate drying agent and stored over 4A molecular sieves. The instrumentation used to obtain spectroscopic data has been previously described.[1] Phosphorus-31 n.m.r. chemical shifts are given relative to $P(OMe)_3$ with upfield shifts negative. All n.m.r. spectra were recorded at 298 K unless otherwise specified. Preparative thin-layer chromatography (t.l.c.) was carried out on commercial Merck plates coated with a 0.25 mm layer of silica. Complex (1) was prepared as previously described by us.[10]

Synthesis of $[NEt_4][(\eta^5\text{-}C_5H_5)(OC)_2Mo(\mu\text{-}PPh_2)Mn(CO)_4]$ (2).—A mixture of complex (1) (0.23 g, 0.4 mmol) and powdered KOH (0.023 g, 0.41 mmol) were stirred in absolute ethanol (10 cm³) for 24 h at room temperature to give a dark red solution. A solution of $[NEt_4]Br$ (0.084 g, 0.4 mmol) in absolute ethanol (10 cm³) was added by syringe and the solvent removed *in vacuo*. The residue was extracted with acetone and the acetone then removed *in vacuo*. Precipitation from Et_2O–CH_2Cl_2 (1:1) solution gave (2) (0.18 g, 64%) as an orange solid (Found: C, 51.9; H, 5.1; N, 1.9. $C_{31}H_{35}MnMoNO_6P$ requires C, 53.2; H, 5.0; N, 2.0%); $\nu_{max.}$(CO) at 2 003m 1 911s, 1 873s, and 1 785m cm⁻¹ (CH_2Cl_2). N.m.r.: ¹H (CD_3COCD_3) at 215 K, δ 7.8—7.0 (m, 10 H, Ph), 4.82 (s, 5 H, C_5H_5), 3.46 (m, 8 H, CH_2CH_3), and 1.33 (m, 12 H, CH_2CH_3).

Reactions of Complex (2) *with Group* 1B *Metal Complexes*.—(*a*) *With* $[AuI(PPh_3)]$. A solution of complex (2) (0.024 g, 0.034 mmol) and $[AuI(PPh_3)]$ (0.023 g, 0.039 mmol) in CH_2Cl_2 (5 cm³) changed colour instantly (10 s) from orange to bright red on being stirred at room temperature. I.r. monitoring indicated that the reaction had gone *ca.* 90% to completion and the addition of further small quantities of $[AuI(PPh_3)]$ or longer reaction times did not increase the product yield. The solvent was removed *in vacuo* and the residue applied to t.l.c. plates. Elution with light petroleum (b.p. 40—60 °C) in ethyl acetate (9:1) gave a trace of an unidentified yellow product,

Table 2. Fractional atomic co-ordinates for [(η^5-C$_5$H$_5$)(OC)$_2$Mo{μ-Ag(PPh$_3$)}(μ-PPh$_2$)Mn(CO)$_4$] (3c)

Atom	*x*	*y*	*z*
Ag	0.270 17(7)	0.019 06(7)	0.192 96(8)
Mo	0.198 84(8)	0.127 92(8)	0.300 76(8)
Mn	0.143 49(13)	0.118 93(13)	0.101 54(13)
P(1)	0.103 6(2)	0.210 8(2)	0.193 0(2)
P(2)	0.386 0(2)	−0.086 1(2)	0.202 2(3)
C(1)	0.087 8(10)	0.036 8(11)	0.320 6(11)
C(2)	0.110 9(12)	0.091 8(10)	0.387 3(10)
C(3)	0.196 7(13)	0.075 8(11)	0.432 1(10)
C(4)	0.228 1(12)	0.005 4(12)	0.391 2(12)
C(5)	0.161 7(12)	−0.021 1(10)	0.322 1(11)
C(11)	0.319 6(11)	0.153 7(10)	0.298 0(10)
O(11)	0.391 8(7)	0.173 2(9)	0.300 9(8)
C(12)	0.214 0(10)	0.241 1(11)	0.355 6(10)
O(12)	0.221 5(9)	0.305 6(8)	0.390 8(8)
C(21)	0.181 1(10)	0.044 4(10)	0.031 5(10)
O(21)	0.198 3(9)	0.003 3(8)	−0.018 9(8)
C(22)	0.067 0(11)	0.172 8(12)	0.021 5(10)
O(22)	0.016 7(9)	0.209 0(9)	−0.030 6(8)
C(23)	0.240 9(12)	0.189 6(10)	0.100 8(10)
O(23)	0.297 5(8)	0.230 8(8)	0.095 8(9)
C(24)	0.072 8(11)	0.029 8(10)	0.118 0(10)
O(24)	0.027 9(8)	−0.027 2(8)	0.125 0(8)
C(111)	0.121 7(9)	0.327 5(9)	0.173 0(9)
C(112)	0.054 2(11)	0.374 8(11)	0.122 9(10)
C(113)	0.072 6(12)	0.463 7(13)	0.103 8(12)
C(114)	0.149 5(14)	0.496 3(14)	0.136 1(13)
C(115)	0.218 5(13)	0.450 9(14)	0.184 9(12)
C(116)	0.204 6(11)	0.363 2(11)	0.202 0(10)
C(121)	0.011 0(9)	0.212 9(9)	0.200 8(9)
C(122)	−0.076 6(10)	0.165 1(11)	0.150 2(10)
C(123)	−0.159 6(11)	0.161 4(12)	0.167 7(11)
C(124)	−0.177 4(11)	0.207 6(11)	0.231 8(11)
C(125)	−0.111 7(10)	0.257 3(11)	0.282 2(10)
C(126)	−0.028 0(9)	0.260 9(9)	0.266 7(9)
C(211)	0.351 6(9)	−0.191 5(9)	0.154 2(9)
C(212)	0.277 4(10)	−0.195 2(11)	0.089 2(10)
C(213)	0.250 9(13)	−0.275 9(13)	0.051 2(13)
C(214)	0.297 6(12)	−0.348 5(13)	0.077 4(12)
C(215)	0.369 9(12)	−0.346 5(12)	0.140 6(11)
C(216)	0.400 6(11)	−0.267 3(11)	0.180 6(10)
C(221)	0.441 1(9)	−0.112 0(9)	0.306 5(9)
C(222)	0.395 2(11)	−0.158 6(11)	0.356 4(11)
C(223)	0.436 2(14)	−0.175 0(14)	0.438 8(15)
C(224)	0.517 8(15)	−0.147 3(15)	0.475 0(16)
C(225)	0.564 2(18)	−0.106 8(16)	0.429 8(16)
C(226)	0.527 4(14)	−0.088 2(14)	0.342 6(14)
C(231)	0.470 2(9)	−0.046 1(10)	0.155 6(9)
C(232)	0.477 0(12)	0.044 7(12)	0.148 1(12)
C(233)	0.542 8(13)	0.080 2(14)	0.114 4(12)
C(234)	0.600 7(13)	0.027 0(14)	0.089 0(12)
C(235)	0.593 9(13)	−0.062 6(14)	0.095 0(12)
C(236)	0.528 8(11)	−0.099 3(12)	0.127 4(11)

Table 3. Fractional atomic co-ordinates for [(η^5-C$_5$H$_5$)(OC)$_2$Mo(μ-I)(μ-PPh$_2$)Mn(CO)$_4$] (4)

Atom	*x*	*y*	*z*
I	−0.015 39(3)	−0.227 59(7)	−0.034 18(7)
Mo	−0.135 89(3)	−0.272 43(8)	−0.056 40(8)
Mn	−0.021 90(6)	−0.260 83(13)	−0.307 97(16)
P	−0.119 4(1)	−0.213 3(2)	−0.295 7(2)
C(1)	−0.136 2(5)	−0.433 6(10)	0.099 4(12)
C(2)	−0.192 0(5)	−0.397 3(10)	0.048 8(12)
C(3)	−0.203 4(5)	−0.426 1(10)	−0.091 9(13)
C(4)	−0.154 5(5)	−0.483 8(9)	−0.126 8(12)
C(5)	−0.112 6(5)	−0.488 1(9)	−0.009 7(12)
C(11)	−0.124 8(5)	−0.142 7(11)	0.085 1(12)
O(11)	−0.121 4(4)	−0.070 3(9)	0.171 5(10)
C(12)	−0.202 0(5)	−0.155 4(12)	−0.116 7(11)
O(12)	−0.240 4(4)	−0.089 2(9)	−0.149 2(9)
C(21)	0.053 9(5)	−0.296 4(11)	−0.292 7(13)
O(21)	0.101 0(4)	−0.321 7(10)	−0.287 0(12)
C(22)	−0.035 0(5)	−0.277 1(10)	−0.492 9(13)
O(22)	−0.043 4(4)	−0.285 9(9)	−0.608 7(9)
C(23)	−0.006 9(4)	−0.089 1(12)	−0.323 7(13)
O(23)	0.004 1(3)	0.012 9(8)	−0.335 5(10)
C(24)	−0.035 5(4)	−0.429 7(11)	−0.283 5(11)
O(24)	−0.040 8(3)	−0.534 9(7)	−0.267 8(9)
C(111)	−0.130 8(4)	−0.046 8(8)	−0.339 6(9)
C(112)	−0.124 8(4)	0.044 6(9)	−0.238 6(11)
C(113)	−0.129 9(5)	0.173 0(11)	−0.273 6(12)
C(114)	−0.141 8(5)	0.208 7(12)	−0.409 7(13)
C(115)	−0.146 4(5)	0.120 7(11)	−0.511 7(13)
C(116)	−0.141 3(4)	−0.008 7(10)	−0.477 1(11)
C(121)	−0.173 3(4)	−0.290 1(8)	−0.426 0(9)
C(122)	−0.228 5(4)	−0.239 6(9)	−0.453 6(11)
C(123)	−0.270 0(5)	−0.298 6(11)	−0.555 3(12)
C(124)	−0.255 9(5)	−0.402 9(11)	−0.619 1(12)
C(125)	−0.203 8(4)	−0.454 8(10)	−0.592 9(11)
C(126)	−0.161 5(4)	−0.396 1(9)	−0.495 3(10)

followed by a bright red band which, on evaporation of the solvent, gave bright red crystals of [(η^5-C$_5$H$_5$)(OC)$_2$Mo{μ-Au(PPh$_3$)}(μ-PPh$_2$)Mn(CO)$_4$] (**3a**) (0.03 g, 86%); $\nu_{max.}$(CO) at 2 028m, 1 959s, 1 942s, 1 936s, 1 925m, and 1 857m cm^{-1} (n-hexane). N.m.r.: ^{1}H (CDCl$_3$), δ 7.9—7.2 (m, 25 H, Ph) and 4.65 (s, 5 H, C$_5$H$_5$).

(*b*) *With* [AuCl(PMe$_2$Ph)]. A solution of complex (**2**) (0.024 g, 0.034 mmol) and [AuCl(PMe$_2$Ph)] (0.014 g, 0.038 mmol) in CH$_2$Cl$_2$ (5 cm^3) were allowed to react as in (*a*) to give an unidentified purple product (0.002 g) and bright red crystalline [(η^5-C$_5$H$_5$)(OC)$_2$Mo{μ-Au(PMe$_2$Ph)}(μ-PPh$_2$)Mn(CO)$_4$] (**3b**) (0.025 g, 81%) (Found: C, 40.7; H, 3.0. C$_{46}$H$_{38}$MnMoO$_6$P$_2$ requires C, 41.2; H, 2.9%); $\nu_{max.}$(CO) at 2 030m, 1 961s, 1 944s, 1 937s, 1 921m, and 1 853m cm^{-1} (n-hexane). N.m.r.: ^{1}H (CDCl$_3$), δ 7.9—7.2 (m, 15 H, Ph), 4.80 (s, 5 H, C$_5$H$_5$), and 1.99 [d, 6 H, ^2J(PH) 8.9 Hz, P*Me*$_2$Ph].

(*c*) *With* [{AgCl(PPh$_3$)}$_4$]. A solution of complex (**2**) (0.024 g, 0.034 mmol) and [{AgCl(PPh$_3$)}$_4$] (0.016 g, 0.01 mmol) in CH$_2$Cl$_2$ (5 cm^3) were allowed to react as in (*a*) to give an unidentified yellow complex (0.002 g) and bright red crystalline [(η^5-C$_5$H$_5$)(OC)$_2$Mo{μ-Ag(PPh$_3$)}(μ-PPh$_2$)Mn(CO)$_4$] (**3c**) (0.023 g, 72%); $\nu_{max.}$(CO) at 2 033m, 1 955m, 1 942s, 1 935s, 1 911m, and 1 843m cm^{-1} (n-hexane). N.m.r.: ^{1}H (CDCl$_3$), δ 7.8—7.2 (m, 25 H, Ph) and 4.67 (s, 5 H, C$_5$H$_5$).

Reaction of Complex (**2**) *with Iodine.*—Complex (**2**) (0.024 g, 0.034 mmol) was dissolved in CH$_2$Cl$_2$ (10 cm^3) and I$_2$ (0.0045 g, 0.018 mmol) added to give an instant colour change from orange to bright red. I.r. monitoring showed *ca.* 50% conversion of (**2**) into a new product. Addition of a further quantity of I$_2$ (0.045 g, 0.018 mmol) resulted in essentially complete conversion of (**2**). The solvent was removed *in vacuo* and the residue applied to the base of a t.l.c. plate. Elution with hexane–CH$_2$Cl$_2$ (9:1) gave a red band followed by an orange band. The red band. after evaporation of the solvent. gave dark red crystals of $[(\eta^5\text{-}C_5H_5)(OC)_2Mo(\mu\text{-}I)(\mu\text{-}PPh_2)Mn(CO)_4]$ (4) (0.018 g, 76%) (Found: C, 39.5; H, 2.2; P, 4.7. $C_{23}H_{15}IMnMoO_6P$ requires C, 39.7; H, 2.2; P, 4.5%); mass spectrum, *m/e* 696 (M^+), $M^+ - n$CO (n = 1—6); $\nu_{max.}$(CO) at 2 077m, 2 010s, 1 981s, 1 967s, 1 960s, and 1 894s cm^{-1} (n-hexane). N.m.r.: ^{1}H ($CDCl_3$), δ 8.0—7.3 (m, 10 H, Ph) and 5.20 (s, 5 H, C_5H_5); ^{13}C ($CDCl_3$, 233 K, ^{1}H gated decoupled), δ 250.7 [d, ^2J(PC) 22.9, 1 MoCO(*cis*)], 247.2 [s, 1 MoCO(*trans*)], 219.7 [d, ^2J(PC) 13.8, 1 MnCO], 214.6 [d, ^2J(PC) 17.6, 1 MnCO], 211.2 [d, ^2J(PC) 13.8, 1 MnCO], 208.5 [d, ^2J(PC) 3.9 Hz, 1 MnCO], 143.7—128.2 (m, Ph), and 94.9 (s, C_5H_5); ^{31}P ($CDCl_3$, ^{1}H gated decoupled), δ −135.4 p.p.m. (s, μ-PPh_2). The orange band, after evaporation of the solvent, gave as an orange solid the complex $[(\eta^5\text{-}C_5H_5)(OC)_2Mo(\mu\text{-}I)(\mu\text{-}PPh_2)Mn(CO)_3]$ (5) (Found: C, 39.2; H, 2.3; P, 4.6. $C_{22}H_{15}IMnMoO_5P$ requires C, 39.6; H, 2.3; P, 4.6%); $\nu_{max.}$(CO) at 2 028s, 1 991m, 1 952m, 1 931m, and 1 920 (sh) cm^{-1} (n-hexane). N.m.r.: ^{1}H ($CDCl_3$), δ 7.6—7.2 (m, 10 H, Ph), 5.56 (s, 5 H, C_5H_5); ^{13}C ($CDCl_3$, 233 K, ^{1}H gated decoupled), δ 229.4 [d, ^2J(PC) 14.8, 1 CO)], 229.2 [d, ^2J(PC) 14.1, 1 CO], 226.4 (s, 1 CO), 224.8 [d, ^2J(PC) 18.9, 1 CO], 220.9 [d, ^2J(PC) 19.9 Hz, 1 CO], 141.3—127.2 (m, Ph), and 90.8 (s, C_5H_5); ^{31}P ($CDCl_3$, ^{1}H gated decoupled), δ −49.3 p.p.m. (s, μ-PPh_2).

Photolysis of Complex (4).—A solution of complex (4) (0.01 g, 0.014 mmol) in a mixture of hexane (25 cm^3) and benzene (5 cm^3) was irradiated with u.v. light (Hanovia, medium-pressure lamp) at room temperature for 1 h. The solvent was removed *in vacuo* and the residue applied to t.l.c. plates. Elution with hexane–CH_2Cl_2 (9:1) gave a trace of unreacted (4) and (5) (0.0085 g, 90%).

Reaction of Complex (5) *with Carbon Monoxide*.—Carbon monoxide was bubbled through a solution of complex (5) (0.01 g, 0.015 mmol) in hexane (25 cm^3)–benzene (5 cm^3) for 2 h at room temperature. T.l.c. separation of the products in the dark gave (4) (0.095 g, 91%) and a trace of (5).

Crystal Structure Determinations.—Crystal data. (3c), $C_{41}H_{30}AgMnMoO_6P_2$, M = 939.35, monoclinic, a = 15.745(3), b = 15.382(3), c = 16.536(3) Å, β = 104.69(2)°, U = 3 873.9 Å^3, space group $P2_1/c$, Z = 4, D_c = 1.610 g cm^{-3}, $F(000)$ = 1 872.

(4), $C_{23}H_{15}IMnMoO_6P$, M = 696.08, monoclinic, a = 23.689(5), b = 10.639(2), c = 9.894(2) Å, β = 99.95(2)°, U = 2 456.0 Å^3, space group $P2_1/n$, Z = 4, D_c = 1.882 g cm^{-3}, $F(000)$ = 1 344.

Data collection. Data were collected on a Philips PW1100 diffractometer in the θ range 3—25°, with a scan width of 0.80°, using Mo-K_α radiation [μ(Mo-K_α) 11.59 (3c) and 22.11 cm^{-1} (4)] by the technique described previously.[24] Lorentz polarisation corrections were applied, and equivalent reflections were merged to give 3 445 (3c) and 2 618 (4) data with $I/\sigma(I) > 3.0$.

Structure solution and refinement.[25] The co-ordinates of the metal atoms were deduced from Patterson syntheses, and the remaining non-hydrogen atoms were located from subsequent Fourier-difference syntheses. The hydrogen atoms were included in geometrically idealised positions and were constrained to 'ride' on the relevant carbon atoms with common isotropic thermal parameters which were refined [final values 0.12 (3c), and 0.068 (phenyl) and 0.10 (cyclopentadienyl) (4)]. All non-hydrogen atoms were assigned anisotropic thermal parameters in the final cycles of full-matrix refinement which converged at R 0.0712 (R' 0.0701) (3c) and 0.0449 (0.0445) (4) with weights of $w = 1/\sigma^2F_o$ assigned to the individual reflections.

The final atomic co-ordinates are given in Tables 2 and 3 respectively for (3c) and (4). Additional material available from the Cambridge Crystallographic Data Centre comprises H-atom co-ordinates, thermal parameters, and remaining bond lengths and angles.

Acknowledgements

We thank the S.E.R.C. and BP Chemicals Limited for financial support and Dr. A. G. Kent for valuable discussion.

References

1 J. A. Iggo, M. J. Mays, P. R. Raithby, and K. Henrick, *J. Chem. Soc., Dalton Trans.*, 1984, 633.
2 M. J. Mays, P. R. Raithby, P. L. Taylor, and K. Henrick, *J. Chem. Soc., Dalton Trans.*, 1984, 959.
3 J. L. Petersen and R. P. Stewart, *Inorg. Chem.*, 1980, **19**, 186.
4 H. W. Walker, C. T. Kresge, P. C. Ford, and R. G. Pearson, *J. Am. Chem. Soc.*, 1979, **101**, 7428.
5 B. F. G. Johnson, D. A. Kaner, J. Lewis, P. R. Raithby, and M. J. Taylor, *J. Chem. Soc., Chem. Commun.*, 1982, 314.
6 G. A. Carriedo, J. A. K. Howard, F. G. A. Stone, and M. J. Went, *J. Chem. Soc., Dalton Trans.*, 1984, 2545.
7 J. W. Lauher and K. Wald, *J. Am. Chem. Soc.*, 1981, **103**, 7648.
8 M. I. Bruce and B. K. Nicholson, *Organometallics*, 1984, **3**, 101.
9 J. A. Iggo and M. J. Mays, *J. Chem. Soc., Dalton Trans.*, 1984, 643; U. Anders and W. A. G. Graham, *J. Am. Chem. Soc.*, 1967, **89**, 539.
10 A. D. Horton, M. J. Mays, and P. R. Raithby, *J. Chem. Soc., Chem. Commun.*, 1985, 247; A. D. Horton, M. J. Mays, and P. R. Raithby, *J. Chem. Soc., Dalton Trans.*, 1987, 1557.
11 C. P. Casey and R. M. Bullock, *Organometallics*, 1984, **3**, 1100.
12 C. P. Casey and R. M. Bullock, *J. Organomet. Chem.*, 1981, **218**, C47.
13 D. G. Evans and D. M. P. Mingos, *J. Organomet. Chem.*, 1982, **232**, 171.
14 R. Uson, J. Fornies, M. Tomas, J. M. Casas, F. A. Cotton, and L. R. Falvello, *J. Am. Chem. Soc.*, 1985, **107**, 2556.
15 G. N. Mott, N. J. Taylor, and A. J. Carty, *Organometallics*, 1983, **2**, 447.
16 R. J. Haines and A. L. du Preez, *J. Chem. Soc. A*, 1970, 2341.
17 C. E. Coffey, J. Lewis, and R. S. Nyholm, *J. Chem. Soc.*, 1964, 1741.
18 M. D. Curtis, N. A. Fotinos, K. R. Han, and W. M. Butler, *J. Am. Chem. Soc.*, 1983, **105**, 2686.
19 M. Berry, J. Martin-Gil, J. A. K. Howard, and F. G. A. Stone, *J. Chem. Soc., Dalton Trans.*, 1980, 1625.
20 B. F. G Johnson, J. Lewis, P. R. Raithby, G. M. Sheldrick, K. Wong, and M. McPartlin, *J. Chem. Soc., Dalton Trans.*, 1978, 673.
21 H. C. Foley, W. C. Finch, C. G. Pierpont, and G. L. Geoffroy, *Organometallics*, 1982, **1**, 1379.
22 T. Adatia, A. D. Horton, K. Henrick, M. J. Mays, and M. McPartlin, *J. Chem. Soc., Chem. Commun.*, 1986, 1206.
23 S. Rosenberg, R. R. Whittle, and G. L. Geoffroy, *J. Am. Chem. Soc.*, 1984, **106**, 5934.
24 M. K. Cooper, P. J. Guerney, and M. McPartlin, *J. Chem. Soc., Dalton Trans.*, 1982, 757.
25 G. M. Sheldrick, SHELX 76 program for crystal structure determination, University of Cambridge, 1976.

Received 17th August 1987; Paper 7/1517

Acyl Group Flipping in Heterodimetallic Complexes; *X*-Ray Crystal Structures of $[(\eta^5\text{-}C_5H_5)MoMn\{\mu\text{-}C(O)C_6H_{11}\}(\mu\text{-}PPh_2)(CO)_5]$ and $[(\eta^5\text{-}C_5H_5)MoMn\{\mu\text{-}C(O)\text{-}CH_2CH_2CH_3\}(\mu\text{-}PPh_2)(CO)_6]$

Trushar Adatia,[a] Kim Henrick,[a] Andrew D. Horton,[b] Martin J. Mays,[b] and Mary McPartlin[a]

[a] *School of Chemistry, The Polytechnic of North London, Holloway Road, London, N7 8DB, U.K.*
[b] *University Chemical Laboratory, Lensfield Road, Cambridge, CB2 1EW, U.K.*

Photolytic reaction of the heterodimetallic complex $[(\eta^5\text{-}C_5H_5)MoMn(\mu\text{-}H)(\mu\text{-}PPh_2)(CO)_6]$ with alkenes gives μ-acyl complexes shown by an *X*-ray analysis of $[(\eta^5\text{-}C_5H_5)MoMn\{\mu\text{-}C(O)C_6H_{11}\}(\mu\text{-}PPh_2)(CO)_5]$ to contain the Mo–C–O–Mn grouping; reaction with CO results in reversible metal–metal bond cleavage and flipping of the μ-acyl co-ordination to Mo–O–C–Mn, as shown by an *X*-ray analysis on $[(\eta^5\text{-}C_5H_5)MoMn\{\mu\text{-}C(O)CH_2CH_2CH_3\}(\mu\text{-}PPh_2)(CO)_6]$.

The η^2-co-ordination of μ-acyl ligands through carbon and oxygen to one or more metal centres is a feature of various mechanisms which have been proposed for the Fischer–Tropsch reaction.[1] In this communication we describe a heterodimetallic system in which μ-acyl ligands can be induced to flip reversibly (Scheme 1) by addition or removal of CO under mild conditions and report *X*-ray structure analyses of the two products. This flipping reaction, which is the first observed for an acyl ligand bridging two different metals, could provide a model for the migration of a μ-acyl ligand on a metal surface. A related flipping reaction in a triosmium complex has been reported but this is not influenced by CO nor were the structures of the two μ-acyl isomers investigated by *X*-ray analysis.[2]

Photolytic reaction of a hexane : benzene solution of the heterodimetallic complex, $[(\eta^5\text{-}C_5H_5)MoMn(\mu\text{-}H)(\mu\text{-}PPh_2)(CO)_6]$ (**1**),[3] with a variety of alkenes (ethene, propene, but-1-ene, *cis*-but-2-ene, *trans*-but-2-ene, cyclohexene) at

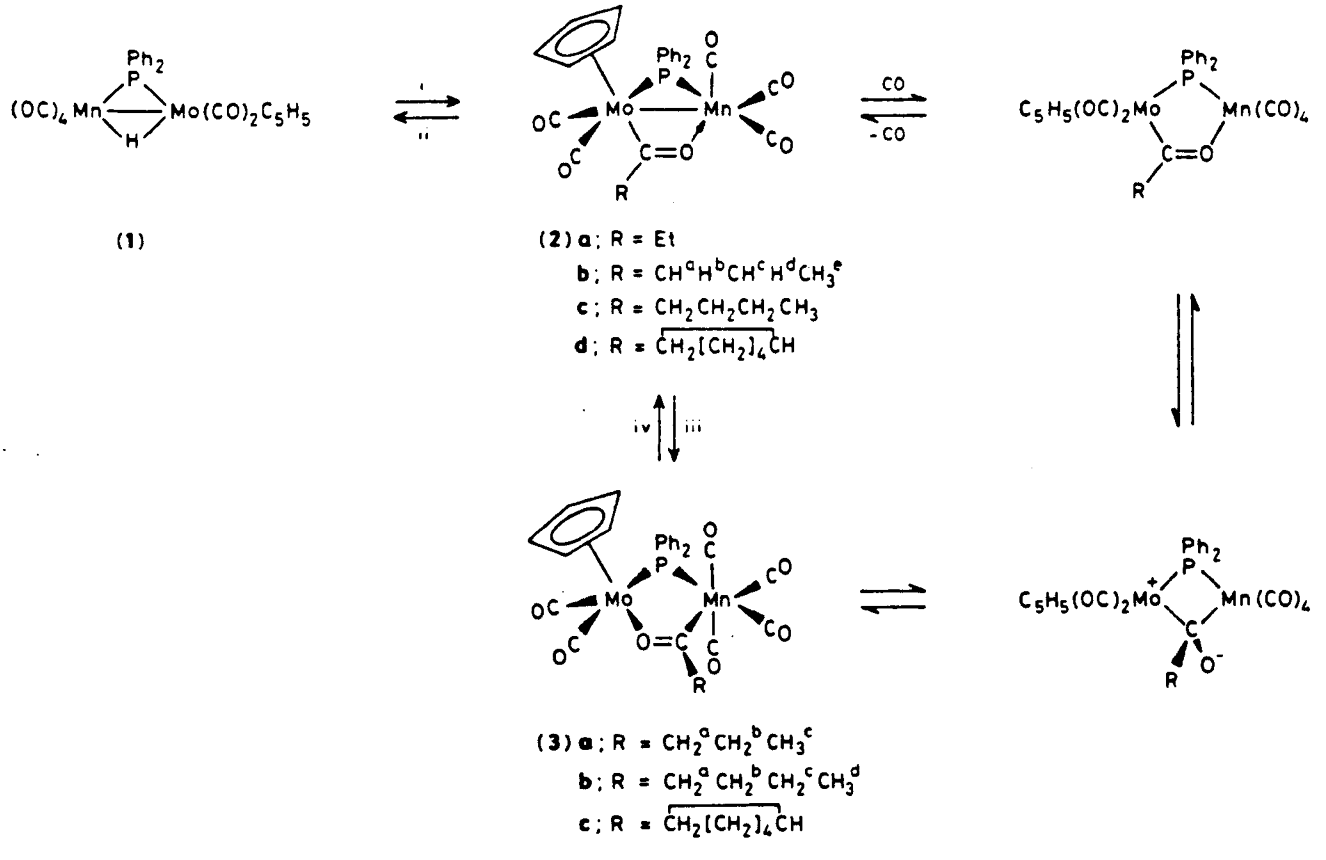

Scheme 1. i, *hν* in hexane : benzene (3 : 1), 18 °C, with ethene, propene, but-1-ene, *cis*-but-2-ene, *trans*-but-2-ene, or cyclohexene: ii, benzene, N_2, 45 °C; iii, benzene, CO (1 atm), 18 °C; iv, hexane : CH_2Cl_2 (10 : 1), N_2, 18 °C

room temperature gives the complexes (**2a**—**d**)† (Scheme 1) in yields ranging from 17% [(**2c**), but-1-ene] to 83% [(**2b**), propene].

X-Ray structure analysis, Figure 1, shows that the acyl ligand in complex (**2d**) spans the Mn–Mo vector, bonding through C(1) to Mo(1) and through O(1) to Mn(1) with a geometry similar to that found in analogous acyl complexes[4—7] and a Mn–Mo distance of 2.963(2) Å, typical for a single Mn–Mo bond.[3]‡ The characteristic acyl CO stretching frequency of 1494 cm^{-1} observed in the i.r. spectrum of (**2d**) provides confirmatory evidence that the bonding of the ligand approximates more closely to the μ-acyl rather than the alternative μ-oxycarbene representation.[8]

Spectroscopic studies on complexes (**2a**—**d**)† indicate that their structures in solution are similar to that found for (**2d**) in the solid state. Most significant is the acyl carbon resonance for (**2b**) at δ 298.5 in the ^{13}C n.m.r. spectrum, showing characteristic *cis* coupling[9] to the phosphido bridge [*J*(PC) 13.7 Hz].

On stirring a solution of (**2b**) in benzene for 1 h under 1 atm CO at room temperature the red complex [(η^5-C_5H_5)MoMn{μ-C(O)$CH_2CH_2CH_3$}(μ-PPh_2)$(CO)_6$] (**3a**)† was formed in *ca.* 95% conversion, as shown by i.r. spectroscopy. *X*-Ray structure analysis, Figure 2, shows that the acyl ligand again bridges the Mn–Mo vector with an intermetal separation of 3.99 Å which is *ca.* 1 Å longer than in (**2d**).‡ Addition of a molecule of CO thus results in breaking of the Mn–Mo bond but, in addition, the carbon atom of the μ-acyl ligand is now bonded to Mn(1) and the oxygen atom to

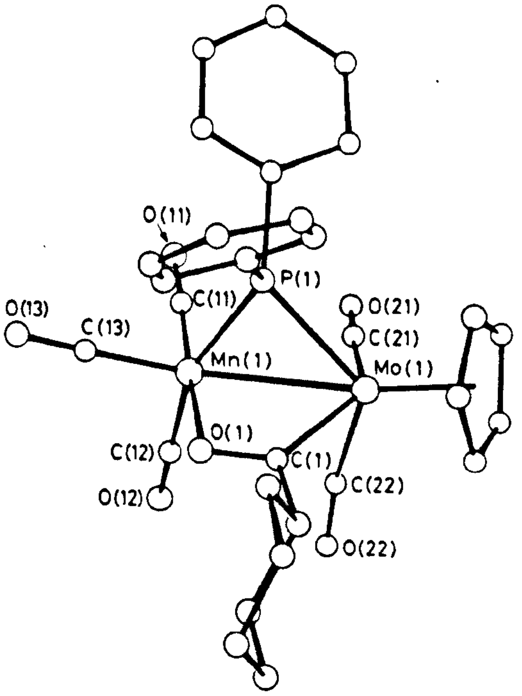

Figure 1. The molecular structure of [(η^5-C_5H_5)MoMn{μ-C(O)-C_6H_{11}}(μ-PPh_2)$(CO)_5$] (**2d**). Mn(1)–Mo(1) 2.963(2); Mn(1)–P(1) 2.265(3); Mo(1)–P(1) 2.488(3); Mn(1)–C(11) 1.759(11); Mn(1)–C(12) 1.824(12); Mn(1)–C(13) 1.770(12); Mo(1)–C(21) 2.012(11); Mo(1)–C(22) 1.999(12); Mo(1)–C(of C_5H_5 ring, aver.) 2.339(10); Mo(1)–C(1) 2.200(10); Mn(1)–O(1) 2.027(6); C(1)–O(1) 1.256(10) Å. Mn(1)–P(1)–Mo(1) 76.9(1); Mo(1)–C(1)–O(1) 118.1(6); Mn(1)–O(1)–C(1) 109.3(6)°.

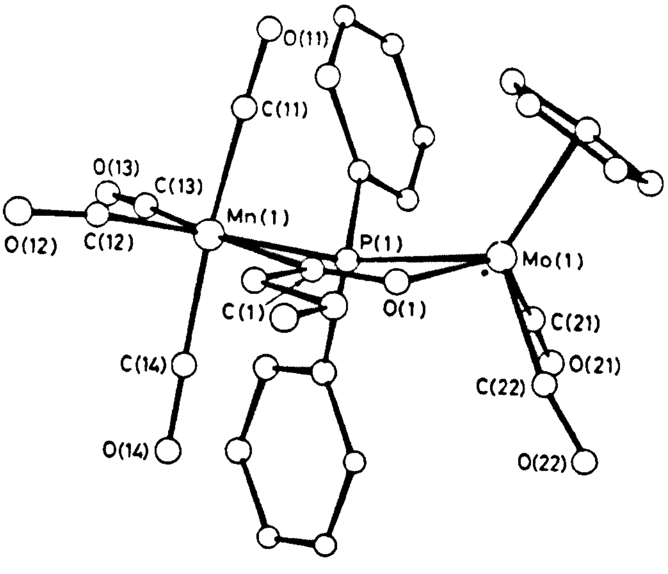

Figure 2. The molecular structure of [(η^5-C_5H_5)MoMn-{μ-C(O)$CH_2CH_2CH_3$}(μ-PPh_2)$(CO)_6$] (**3a**). Mn(1) ··· Mo(1) 3.99; Mn(1)–P(1) 2.388(6); Mo(1)–P(1) 2.510(5); Mn(1)–C(11) 1.76(3); Mn(1)–C(12) 1.762(21); Mn(1)–C(13) 1.81(3); Mn(1)–C(14) 1.792(21); Mo(1)–C(21) 1.897(21); Mo(1)–C(22) 1.907(23); Mo(1)–C (of C_5H_5 ring, aver.) 2.318(17); Mn(1)–C(1) 2.043(19); Mo(1)–O(1) 2.162(12); C(1)–O(1) 1.252(19) Å. Mn(1)–P(1)–Mo(1) 108.9(2); Mn(1)–C(1)–O(1) 123(1); Mo(1)–O(1)–C(1) 138(1)°.

---

† *Selected spectroscopic data*: [i.r. (ν_{CO} cm^{-1}) measured in hexane solution; ^{1}H, ^{13}C, and ^{31}P n.m.r. in $CDCl_3$ solution, ^{31}P shifts relative to $P(OMe)_3$ at 0 p.p.m. with upfield shifts negative; *J* in Hz]. (**2b**), ν_{CO} 2023s, 1968m, 1946m, 1922m, 1913sh [1510w, $\nu_{C(O)R}$]; ^{1}H n.m.r. δ 2.19 [ddd, $J(H^aH^b)$ 16.3, $J(H^aH^d)$ 8.3, $J(H^aH^c)$ 6.8, 1H, H^a], 1.57 [ddd, $J(H^bH^c)$ 8.7, $J(H^bH^d)$ 5.6, 1H, H^b], 1.13 [ddqd, $J(H^cH^d)$ 14.1, $J(H^cH^e)$ 7.3, 1H, H^c], 0.85 [ddqd, $J(H^dH^e)$ 7.3, 1H, H^d], 0.55 [t, 3H, $CH_3{}^e$]; ^{13}C n.m.r. δ 298.5 [d, ^2J(PC) 13.7, C(O)R], 63.6, 17.6, 13.5 [s, $CH_2CH_2CH_3$].

(**2d**), ν_{CO} 2021s, 1965m, 1946m, 1919m, 1910sh [1494w, $\nu_{C(O)R}$]; ^{1}H n.m.r. δ 2.1—0.3 [m, 11H, C_6H_{11}]; ^{13}C n.m.r. δ 300.8 [d, ^2J(PC) 14.0, C(O)R], 69.4 [s, C(O)*C*HC_5H_{10}], 29.1, 26.2, 25.8, 25.4, 25.1 [s, C(O)CHC_5H_{10}]; ^{31}P n.m.r. δ 3.54 p.p.m. [s, μ-PPh_2].

(**3a**), ν_{CO} 2057m, 1993m, 1965m, 1961sh, 1953s, 1891m, [1505w, $\nu_{C(O)R}$]; ^{1}H n.m.r. δ 3.08 [t, *J* (H^aH^b) 6.9, 2H, $CH_2{}^a$], 1.40 [m, *J* (H^bH^c) 7.2, 2H, $CH_2{}^b$], 0.81 [t, 3H, $CH_3{}^c$], ^{13}C n.m.r. δ 330.3 [s, C(O)R], 67.4, 18.4, 13.6 [s, $CH_2CH_2CH_3$].

(**3b**), ν_{CO} 2058m, 1993m, 1966s, 1961sh, 1953s, 1892m; ^{1}H n.m.r. δ 3.10 [t, $J(H^aH^b)$ 7.1, 2H, $CH_2{}^a$], 1.35 [m, *J* (H^bH^c) 7.1, 2H, $CH_2{}^b$], 1.18 [m, $J(H^cH^d)$ 7.1, 2H, $CH_2{}^c$], 0.87 [t, 3H, $CH_3{}^d$].

(**3c**), ν_{CO} 2055m, 1992m, 1964s, 1961sh, 1951m, 1891m, [1488w, $\nu_{C(O)R}$]; ^{1}H n.m.r. δ 3.43 [m, 1H, C(O)C*H*C_5H_{10}], 1.9—0.8 [m, 10H, C(O)CHC_5H_{10}]; ^{13}C n.m.r. δ 334.7 [s, *C*(O)R], 71.9 [s, C(O)*C*HC_5H_{10}], 28.1—25.2 [m, 5C, C(O)CHC_5H_{10}]; ^{31}P n.m.r. δ −70.2 p.p.m. [s, μ-PPh_2].

‡ *Crystal data*: (**2d**) $C_{29}H_{26}MnMoO_6P$, *M* = 652.37, monoclinic, space group $P2_1/c$, a = 9.118(3), b = 14.632(4), c = 20.687(3) Å, β = 101.25(4)°, U = 2706.9 Å^3, D_c = 1.600 g cm^{-3}, Z = 4, $F(000)$ = 1320, μ(Mo-K_α) = 9.41 cm^{-1}, $I/\sigma(I) \geq 3.0$, θ range 3—25°, R = 0.0501, R_w = 0.0476 for 2133 absorption-corrected diffractometer data.

(**3a**) $C_{27}H_{22}MnMoO_7P$, *M* = 640.32, monoclinic, space group $P2_1/n$, a = 28.669(6), b = 9.807(2), c = 9.588(2) Å, β = 93.23(2)°, U = 2691.45 Å^3, D_c = 1.57 g cm^{-1}, Z = 4, $F(000)$ = 1288, μ(Mo-K_α) = 9.48 cm^{-1}, $I/\sigma(I) \geq 3.0$, θ range 3—25°, R = 0.0607, R_w = 0.0586 for 1284 absorption-corrected diffractometer data. The crystals of (**2d**) and (**3a**) were obtained by recrystallisation from hexane : CH_2Cl_2 (1 : 1) under, respectively, N_2 and CO atmospheres.

Atomic co-ordinates, bond lengths and angles, and thermal parameters have been deposited at the Cambridge Crystallographic Data Centre. See Notice to Authors, Issue No. 1, 1986.

Mo(1), which is the opposite of the co-ordination in (**2d**). The geometry of the Mo–O–C–Mn group is similar to that found in analogous dimetallic complexes:[5,10—12] the Mo–O–C–Mn–P ring is approximately planar rather than folded as in (**2d**).

On the basis of spectroscopic studies it was determined that the solution structures of (**3a—c**) [(**3b**) and (**3c**) are formed on treatment of (**2c**) and (**2d**) respectively with CO] are similar to the solid state structure found for (**3a**). Particularly significant is the acyl CO stretching band in the i.r. spectrum [1505 cm^{-1} for (**3a**)] and the zero ^{31}P–^{13}C coupling for the acyl ^{13}C n.m.r. resonance [δ 330.3 for (**3a**)] as expected for *cis*-oriented acyl carbon and phosphido groups at Mn. Further, the observation that the methylene protons in (**3a**) are equivalent in the ^{1}H n.m.r. spectrum, unlike the diastereotopic methylene protons in (**2b**), reflects the increased symmetry in the environment of the n-propyl group at Mn in (**3a**) compared to that at Mo in (**2b**).

The reactions of (**1**) with alkenes to give (**2**) and of (**2**) with CO to give (**3**) are readily reversible under thermal conditions. Thus on stirring complex (**3a**) in 10:1 hexane : dichloromethane under N_2 at 18 °C for 24 h a product mixture of (**2b**) : (**3a**) of *ca.* 30 : 70 is obtained. Furthermore, whilst a solution of (**2b**) in benzene under N_2 at 18 °C is indefinitely stable, heating the solution to 45 °C gives a product mixture of (**1**) : (**2b**) of *ca.* 90 : 10 after 3 h. Such facile ejection of an alkene molecule from a μ-acyl ligand has not been previously observed. Indeed, the complexes [(η^5-C_5H_5)FeMn{μ-C(O)Me}(μ-PPh_2)$(CO)_5$] and [(η^5-C_5H_5)$_2$FeMo{μ-C(O)Me}(μ-PPh_2)$(CO)_3$], which are closely related to (**3**) (and in which in each case the acyl carbon is bonded to Fe) are not reported to undergo the first step of CO loss and the formation of metal–metal bonded derivatives.[10,11]

The first step in the formation of (**3**) from (**2**) may be the displacement of the Mn–Mo bond by CO as shown in Scheme 1. The ease with which the metal–metal bond in the structurally related complex [(η^5-C_5H_5)MoMn(μ-I)(μ-PPh_2)$(CO)_5$] is broken on stirring under CO, a reaction which is reversed on photolysis, provides precedent for such a step.[13] This could then be followed by formation of a metal–metal bonded oxycarbene complex from which (**3**) would be readily obtained.

The ready interconversion of (**2**) and (**3**) indicates that the thermodynamic stability of the two acyl bonding modes is comparable. This suggests that the oxophilicity of Mo and Mn in these complexes is similar and sensitive to a small change in the ligand environment.

We thank Dr. A. G. Kent for valuable discussion and the S.E.R.C. and B.P. Chemicals Limited for financial support.

Received, 1st May 1986; Com. 579

References

1 C. Masters, *Adv. Organomet. Chem.*, 1979, **17**, 61; C. K. Rofer-DePoorter, *Chem. Rev.*, 1981, **81**, 447.

2 C. M. Jensen, Y. J. Chen, and H. D. Kaesz, *J. Am. Chem. Soc.*, 1984, **106**, 4046.

3 A. D. Horton, M. J. Mays, and P. R. Raithby, *J. Chem. Soc., Chem. Commun.*, 1985, 247.

4 J. G. Jeffrey, A. G. Orpen, W. T. Robinson, F. G. A. Stone, and M. J. Went, *J. Chem. Soc., Chem. Commun.*, 1984, 396.

5 K. Henrick, J. A. Iggo, M. J. Mays, and P. R. Raithby, *J. Chem. Soc., Chem. Commun.*, 1984, 209.

6 C. E. Kampe, N. M. Boag, and H. D. Kaesz, *J. Am. Chem. Soc.*, 1983, **105**, 2896; R. Szostak, C. E. Strouse, and H. D. Kaesz, *J. Organomet. Chem.*, 1980, **191**, 243.

7 G. N. Mott, R. Granby, S. A. MacLaughlin, N. J. Taylor, and A. J. Carty, *Organometallics*, 1983, **2**, 189; A. Basu, S. Bhaduri, H. Khwaja, P. G. Jones, T. Schroeder, and G. M. Sheldrick, *J. Organomet. Chem.*, 1985, **290**, C19.

8 J. A. Marsella, J. C. Huffman, K. G. Caulton, B. Longato, and J. R. Norton, *J. Am. Chem. Soc.*, 1982, **104**, 6360.

9 L. J. Todd, J. R. Wilkinson, J. P. Hickley, D. L. Beach, and K. W. Barnett, *J. Organomet. Chem.*, 1978, **154**, 151.

10 R. P. Josen, J. B. Hoke, R. R. Whittle, G. L. Geoffroy, J. P. Hutchinson, and J. A. Zubieta, *Organometallics*, 1984, **3**, 846.

11 T. S. Targos, G. L. Geoffroy, and A. L. Rheingold, *J. Organomet. Chem.*, 1986, **299**, 223.

12 J. R. Blickensdorfer, C. B. Knobler, and H. D. Kaesz, *J. Am. Chem. Soc.*, 1975, **97**, 2686.

13 A. D. Horton, Ph.D. Thesis, Cambridge, 1986.

Journal of Organometallic Chemistry, 332 (1987) C6–C10
Elsevier Sequoia S.A., Lausanne – Printed in The Netherlands

Preliminary communication

The synthesis and structural characterization of the mixed-metal cluster compounds $[M_2Ru_4(\mu\text{-}CO)_3(CO)_{10}(PPh_3)_2]$ (M = Cu, Ag, Au): X-ray crystal structures of $[M_2Ru_4(\mu\text{-}CO)_3(CO)_{10}(PPh_3)_2]$ (M = Cu, Ag)

Scott S.D. Brown, Ian D. Salter*,
Department of Chemistry, University of Exeter, Exeter EX4 4QD (Great Britain)

Trushar Adatia and Mary McPartlin*
School of Chemistry, The Polytechnic of North London, London N7 8DB (Great Britain)

(Received June 23rd, 1987)

Abstract

The novel mixed-metal cluster compounds $[M_2Ru_4(\mu\text{-}CO)_3(CO)_{10}(PPh_3)_2]$ (M = Cu, Ag or Au) have been synthesized from $[N(PPh_3)_2]_2[Ru_4(CO)_{13}]\cdot THF$. Single-crystal X-ray diffraction studies on the copper- and silver-ruthenium clusters reveal that they adopt metal core structures consisting of a Ru_4 tetrahedron with $M(PPh_3)$ (M = Cu or Ag) groups capping two Ru_3 faces, in marked contrast to the capped trigonal bipyramidal skeletal geometries exhibited by the very closely related species $[M_2Ru_4H_2(CO)_{12}(PPh_3)_2]$ (M = Cu, Ag or Au), in which the two coinage metals are in close contact.

A very interesting feature of the chemistry of mixed-metal cluster compounds containing $M(PR_3)$ (M = Cu, Ag or Au; R = alkyl or aryl) fragments is the great variety of bonding modes displayed by the Group IB metal-phosphine groups and the large range of skeletal geometries exhibited by these species [1–5]. Herein we report the synthesis and structural characterization of the novel mixed-metal clusters $[M_2Ru_4(\mu\text{-}CO)_3(CO)_{10}(PPh_3)_2]$ (I, M = Cu; II, M = Ag; III, M = Au) and show that the formal replacement of two hydrido ligands in the closely related species $[M_2Ru_4H_2(CO)_{12}(PPh_3)_2]$ (IV, M = Cu; V, M = Ag; VI, M = Au) [5] by a carbonyl group in I–III has a remarkable effect on the metal framework structures adopted by these clusters.

Treatment of a dichloromethane solution of the salt $[N(PPh_3)_2]_2[Ru_4(CO)_{13}]\cdot$ THF [6] with two equivalents of the complex $[M(NCMe)_4]PF_6$ (M = Cu or Ag) at −30 °C, followed by the addition of two equivalents of PPh_3 affords the mixed-metal

0022-328X/87/$03.50

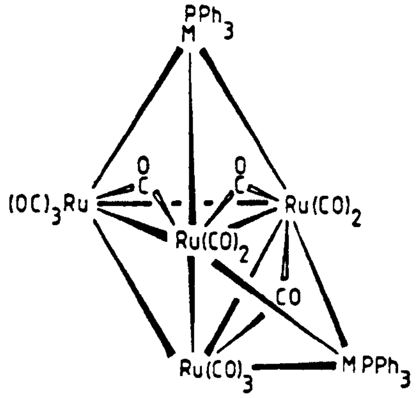

(I , M = Cu ;
II , M = Ag ;
III , M = Au)

cluster compounds I and II in ca. 35–40% yield. The analogous gold species, III, can

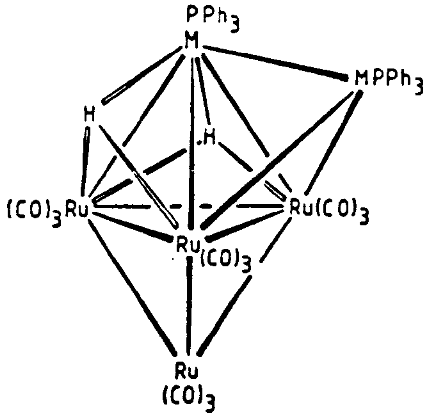

(IV , M = Cu ;
V , M = Ag)

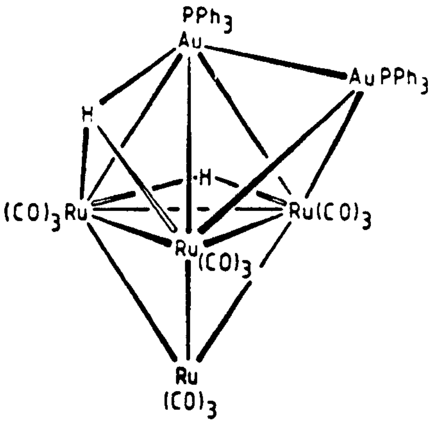

(VI)

be obtained in ca. 70% yield by treating a dichloromethane solution of the salt $[N(PPh_3)_2]_2[Ru_4(CO)_{13}]\cdot THF$ with a dichloromethane solution containing two equivalents of the complex $[AuCl(PPh_3)]$ at −30 °C, in the presence of $TlPF_6$. The IR spectra [7 *] of I–III are closely similar, suggesting that these clusters all adopt the same metal core geometry and the band between 1800 and 1785 cm^{-1} observed for each cluster is diagnostic of bridging carbonyl groups in all three. At −90 °C, the $^{31}P\text{-}\{^1H\}$ NMR spectra of I–III [7 *] show marked differences to those of the analogous dihydrido clusters IV–VI [5], suggesting that I–III adopt different metal

---

* Reference numbers with asterisks indicate notes in the list of references.

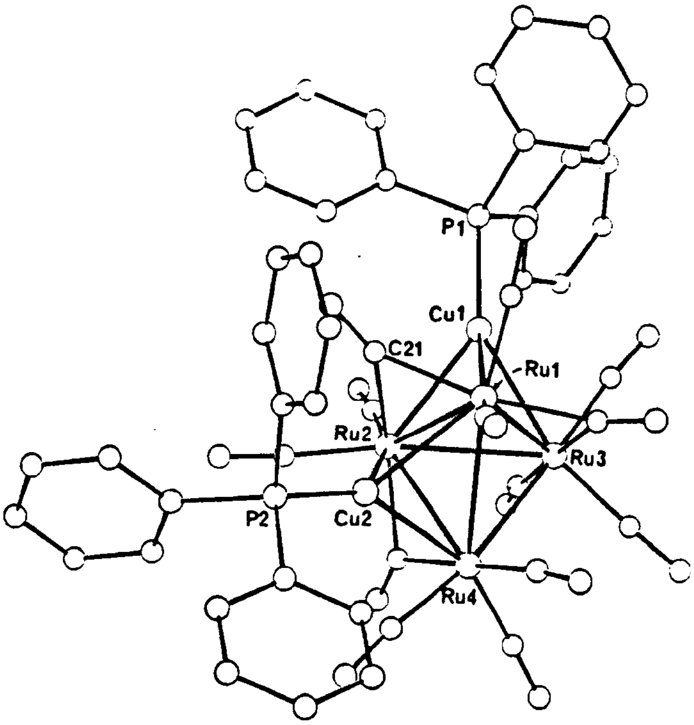

Fig. 1. Molecular structure of $[Cu_2Ru_4(\mu\text{-}CO)_3(CO)_{10}(PPh_3)_2]$ (I), which has virtual C_2 symmetry. Important dimensions: Ru(1)–Ru(2) 2.771(2); Ru(1)–Ru(3) 2.797(2); Ru(1)–Ru(4) 2.981(2); Ru(1)–Cu(1) 2.806(2); Ru(1)–Cu(2) 2.662(2); Ru(2)–Ru(3) 2.958(2); Ru(2)–Ru(4) 2.793(2); Ru(2)–Cu(1) 2.656(2); Ru(2)–Cu(2) 2.848(2); Ru(3)–Ru(4) 2.842; Ru(3)–Cu(1) 2.633(2); Ru(4)–Cu(2) 2.608(2); mean Cu–P 2.234(6); Ru–CO(terminal) 1.798(5)–1.891(3); Ru–CO(bridging) 2.031(4)–2.230(3) Å.

framework structures to those of IV–VI. Significantly, the complex second order splitting patterns reported in the $^{31}P\text{-}\{^1H\}$ NMR spectra of $[Ag_2Ru_4(\mu_3\text{-}H)_2\{\mu\text{-}Ph_2P(CH_2)_nPPh_2\}(CO)_{12}]$ (n = 1, 2 or 4) [8] and $[Ag_2Ru_3(\mu_3\text{-}S)(CO)_9(PPh_3)_2]$ [9], due to $^{107,109}Ag\text{-}^{107,109}Ag$ couplings and $^{107,109}Ag\text{-}^{31}P$ couplings through two bonds, are not observed for II, implying that the two silver atoms are not in close contact in the latter cluster.

X-ray structural analyses [*] of I and II show that both cluster compounds adopt a capped trigonal bipyramidal skeletal geometry (Figs. 1 and 2, respectively) consisting of a tetrahedron of ruthenium atoms with two Ru_3 faces capped by $M(PPh_3)$ (M = Cu or Ag) groups. The metal framework structures adopted by I–III are in marked contrast to those exhibited by the analogous dihydrido clusters IV–VI, in

---

[*] Crystal data for I: $C_{49}H_{30}O_{13}P_2Ru_4Cu_2$, $M = 1419.08$, monoclinic, space group $P2_1/n$, a 22.110(4), b 17.247(3), c 14.407(3) Å, β 93.44(2)°, U 5483.94 Å^3, $F(000) = 2768$, $\mu(Mo\text{-}K_\alpha)$ 18.12 cm^{-1}, $Z = 4$, D_c 1.72 g cm^{-3}. Data were collected on a Philips PW1100 diffractometer in the θ-range 3–25°, $I/\sigma(I) > 3.0$; present R-factor 0.0659 for 4467 reflections. Crystal data for II: $C_{49}H_{30}O_{13}P_2Ru_4Ag_2$, $M = 1507.72$, triclinic, space group $P\bar{1}$, a 24.685(5), b 10.710(2), c 10.137(2) Å, α 102.03(2), β 96.20(2), γ 86.47(2)° U 2603.69 Å^3, $F(000) = 1456$, $\mu(Mo\text{-}K_\alpha) = 18.07$ cm^{-1}, $Z = 2$, D_c 1.93 g cm^{-3}. Data were collected on a Philips PW1100 diffractometer in the θ-range 3–25°, $I/\sigma(I) > 3.0$; present R-factor 0.0503 for 5065 reflections.

Cu

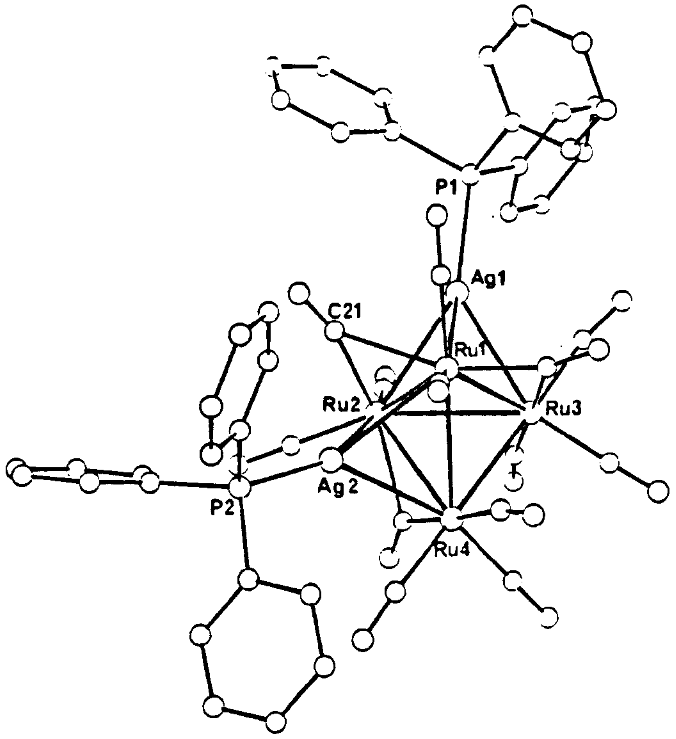

Fig. 2. Molecular structure of $[Ag_2Ru_4(\mu\text{-}CO)_3(CO)_{10}(PPh_3)_2]$ (II). The distances for CO(21) are very asymmetric: Ru(1)–C(21) 2.589(3) and Ru(2)–C(21) 1.967(4) Å. Other important dimensions: Ru(1)–Ru(2) 2.797(1); Ru(1)–Ru(3) 2.853(2); Ru(1)–Ru(4) 2.997(1); Ru(1)–Ag(1) 2.977(1); Ru(1)–Ag(2) 2.838(1); Ru(2)–Ru(3) 3.074(1); Ru(2)–Ru(4) 2.866(1); Ru(2)–Ag(1) 2.861(1); Ru(2)–Ag(2) 2.905(1); Ru(3)–Ru(4) 2.849(1); Ru(3)–Ag(1) 2.806(1); Ru(4)–Ag(2) 2.872(2); mean Ag–P 2.418(3); Ru–CO(terminal) 1.799(3)–1.922(4); Ru–CO(bridging) 1.953(3)–2.589(3) Å.

which one face of a Ru_4 tetrahedron is capped by a $M(PPh_3)$ (M = Cu, Ag or Au) group and a MRu_2 face of the MRu_3 tetrahedron so formed is further capped by the second $M(PPh_3)$ unit, so that the two coinage metals are in close contact [5]. Thus, the formal replacement of a carbonyl group in I–III by two hydrido ligands in IV–VI causes a fundamental change in the positions that the Group IB metals adopt on the ruthenium tetrahedra of these clusters. This alteration in metal framework geometry adds to previous evidence, both experimental [1,2] and theoretical [10], that the energy differences between the various structural types are small in many cases for heteronuclear clusters containing $M(PR_3)$ groups. A similar change in coinage metal arrangement has been previously observed for two Cu_2Ru_6 clusters when two carbonyl groups are formally replaced by a carbido ligand. Whereas in $[Cu_2Ru_6(CO)_{18}(C_6H_5Me)_2]$, the $Cu(C_6H_5Me)$ units cap opposite faces of a Ru_6 octahedron [11], the two copper atoms are in close contact in $[Cu_2Ru_6C(CO)_{16}(NCMe)_2]$ [12].

Acknowledgements. We thank the S.E.R.C. for studentships (T.A. and S.S.D.B.), the Nuffield Foundation for support, Johnson Matthey Ltd. for a generous loan of gold, silver, and ruthenium salts, and Mrs. L.J. Salter for drawing some of the display formulae.

References and notes

1 For example, R.A. Brice, S.C. Pearse, I.D. Salter, and K. Henrick, J. Chem. Soc., Dalton Trans., (1986) 2181; and ref. cited therein.

2 For example, I.D. Salter, Adv. Dynamic Stereochem., 2 (1987) in press; K. Henrick, B.F.G. Johnson, J. Lewis, J. Mace, M. McPartlin, and J. Morris, J. Chem. Soc., Chem. Commun., (1985) 1617; S.R. Bunkhall, H.D. Holden, B.F.G. Johnson, J. Lewis, G.N. Pain, P.R. Raithby, and M.J. Taylor, ibid., (1984) 25.

3 For example, M.I. Bruce, M.L. Williams, J.M. Patrick, B.W. Skelton, and A.H. White, J. Chem. Soc., Dalton Trans., (1986) 2557; and ref. cited therein.

4 For example, P. Braunstein, J. Rose, A. Dedieu, Y. Dusausoy, J.-P. Mangeot, A. Tiripicchio, and M. Tiripicchio-Camellini, J. Chem. Soc., Dalton Trans., (1986) 225; and ref. cited therein.

5 M.J. Freeman, A.G. Orpen, and I.D. Salter, J. Chem. Soc., Dalton Trans., (1987) 379.

6 A.A. Bhattacharyya, C.C. Nagel, and S.G. Shore, Organometallics, 2 (1983) 1187.

7 Selected spectroscopic data. For compound I, ν_{max}(CO) at 2062m, 2016vs, 2002s, 1949m(br), and 1799w(br) cm^{-1} (CH_2Cl_2). NMR: ^1H (CD_2Cl_2), δ 7.27–7.58 (m, Ph); ^{31}P-{^1H} (CD_2Cl_2/CH_2Cl_2) at −90 °C, δ 3.6 ppm (s). For compound II, ν_{max}(CO) at 2060m, 2014vs, 1997s, 1951m(br), and 1787w(br) cm^{-1}. NMR: ^1H (CD_2Cl_2), δ 7.28–7.54 (m, Ph); ^{31}P-{^1H} (CD_2Cl_2/CH_2Cl_2) at −90 °C, δ 16.4 ppm (2 × d, $^1J(^{109}AgP)$ 514, $^1J(^{107}AgP)$ 446 Hz). For compound III, ν_{max}(CO) at 2066m, 2023vs, 2006s, 1967m(br), and 1789w(br) cm^{-1}. NMR: ^1H (CD_2Cl_2) at −20 °C, δ 7.15–7.55 (m, Ph); ^{31}P-{^1H} (CD_2Cl_2/CH_2Cl_2) at −90 °C, δ 62.9 ppm (s).

8 S.S.D. Brown, I.J. Colquhoun, W. McFarlane, M. Murray, I.D. Salter, and V. Šik, J. Chem. Soc., Chem. Commun., (1986) 53.

9 S.S.D. Brown, S. Hudson, I.D. Salter, and M. McPartlin, J. Chem. Soc., Dalton Trans., (1987) in press.

10 D.M.P. Mingos, Polyhedron, 3 (1984) 1289.

11 G.B. Ansell, M.A. Modrick, and J.S. Bradley, Acta Cryst. C, 40 (1984) 365.

12 J.S. Bradley, R.L. Pruett, E. Hill, G.B. Ansell, M.E. Leonowicz, and M.A. Modrick, Organometallics, 1 (1982) 748.

PW-62563-C3-14:24-15/ 6/1988

COMIN1612G

Chemical Communications——Batch 50

INDEX TERMS
PHOSPHINE
CLUSTER
COPPER
CRYSTAL STRUCTURE
RUTHENIUM

Chemical Communications/1988/No.0/000–000/C

Effect of the Phosphine Ligand Cone Angle on the Metal Frameworks of Heteronuclear Cluster Compounds Containing Cu(PR$_3$) (R = alkyl or aryl) Groups: *X*-Ray Structure Analyses of [Cu$_2$Ru$_4$(μ_3-H)$_2$(CO)$_{12}$(PR$_3$)$_2$] (R = cyclo-C$_6$H$_{11}$ or CHMe$_2$)

Trushar Adatia,[a] Paul J. McCarthy,[b] Mary McPartlin,*[a] Mine Rizza,[a] and Ian D. Salter*[b]

[a] *School of Chemistry, The Polytechnic of North London, London N7 8DB, U.K.*
[b] *Department of Chemistry, University of Exeter, Exeter EX4 4QD, U.K.*

The cone angle of the phosphine ligands in the heteronuclear cluster compounds [Cu$_2$Ru$_4$(μ_3-H)$_2$(CO)$_{12}$(PR$_3$)$_2$] (R = alkyl or aryl) has a marked effect on the metal framework structure adopted; when R = CHMe$_2$, two skeletal isomers, which interconvert at ambient temperature, are present in solution, and when R = cyclo-C$_6$H$_{11}$, the cluster exhibits a previously unobserved type of Cu$_2$Ru$_4$ metal core structure.

Comparison of the structures of a series of analogous heteronuclear cluster compounds [Cu$_2$Ru$_4$(μ_3H)$_2$(CO)$_{12}$(PR$_3$)$_2$], which formally differ only in the nature of R [R = cyclo-C$_6$H$_{11}$(Cy), CHMe$_2$, or Ph], demonstrates that the metal framework is significantly altered by variations in the cone angles[1] of the monodentate phosphine ligands attached to the Cu atoms.

Treatment of a CH_2Cl_2 solution of [N(PPh$_3$)$_2$]$_2$[Ru$_4$(μ-H)$_2$(CO)$_{12}$][2] with 2 equiv. of the complex [Cu(NCMe)$_4$]PF$_6$ at −30 °C, followed by the addition of 2 equiv. of PR$_3$, affords the dark red cluster compounds [Cu$_2$Ru$_4$(μ_3-H)$_2$(CO)$_{12}$(PR$_3$)$_2$][R = Cy (1) or P(CHMe$_2$)$_3$ (2)]in *ca.* 60% yield. Although the i.r. and n.m.r. spectroscopic data† for (1) and (2) are consistent with the proposed formulations, the spectra of (1) are significantly different from those reported for the analogous PPh$_3$-containing species [Cu$_2$Ru$_4$(μ_3-H)$_2$(CO$_{12}$(PPh$_3$)$_2$] (3), implying that (1) adopts a different metal core structure from the capped trigonal bipyramidal skeletal geometry previously established for (3).[3] An *X*-ray diffraction study‡ of (1) reveals a novel metal framework structure consisting of a Ru$_4$ tetrahedron with one edge bridged by a Cu(PCy$_3$) unit and a non-adjacent face capped by the second Cu(PCy$_3$) group (Figure 1). At ambient temperature, the ^{31}P-{^{1}H} n.m.r. spectrum of (1) is a singlet, broadened by quadrupolar effects,[3] so the two Cu(PCy$_3$) units must be interchanging between edge-bridging and face-capping bonding modes in solution at this temperature. However, at −100 °C, two broadened singlets are observed in the ^{31}P-{^{1}H} n.m.r. spectrum, consistent with the ground state structure. Compound (1) is an unusual example of a mixed-metal cluster containing both edge-bridging and face-capping M(PR$_3$) (M = Cu, Ag, or Au) groups[4] and its skeletal geometry is in marked contrast to that of (3), in which both Cu(PPh$_3$) fragments are face-capping and the Cu atoms are in close contact [Cu–Cu 2.699(2) Å].[3]

In contrast to those of (1) and (3),[3] the ^{31}P-{^{1}H} and ^{1}H n.m.r. spectra of (2)† are consistent with the presence of two distinct skeletal isomers in solution at low temperatures. Three singlets (relative intensities 1 : 0.6 : 1) are visible in the ^{31}P-{^{1}H} n.m.r. spectrum at −90 °C and the ^{1}H n.m.r. high-field hydrido ligand signal consists of a sharp doublet [*J*(PH) 10 Hz] and a broadened singlet at −100 °C.

The two equal-intensity ^{31}P-{^{1}H} n.m.r. singlets and the ^{1}H n.m.r. high-field doublet closely resemble the low temperature n.m.r. data reported for (3), so they can be assigned to an isomer [(2A); 77% abundance] with a metal core of the type observed for (3).[3] An *X*-ray structure analysis‡ of (2) (Figure 2) shows a metal framework of the type predicted for the isomer (2A), which consists of a capped trigonal bipyramidal Cu$_2$Ru$_4$ unit, similar to that reported for (3),[3] with a direct Cu–Cu linkage.

The presence in solution of a second isomer [(**2B**); 23% abundance] is deduced from the remaining n.m.r. signals, the broadened ^{1}H n.m.r. singlet and the ^{31}P-{^{1}H} n.m.r. peak at δ 26.0. The ^{31}P-{^{1}H} n.m.r. spectrum of (**2B**) is a sharp singlet at −100 °C, in contrast to that of (1), which consists of two broadened signals at the same temperature. Thus the n.m.r. evidence is consistent with isomer (**2B**) having a Cu$_2$Ru$_4$ metal framework which is different not only from that in isomer (2A) but also from the edge-bridged trigonal bipyramid in (1). It seems probable that (**2B**) adopts a structure in which the Cu atoms cap different faces of the Ru$_4$ tetrahedron, giving the phosphine ligands identical environments, an arrangement which has been previously observed in [Cu$_2$Ru$_4$(μ-CO)$_3$(CO)$_{10}$(PPh$_3$)$_2$].[5] The possibility that (**2B**) has a metal core structure of the novel type observed for (1) and that the cluster framework undergoes dynamic behaviour similar to that of (1), with a lower free energy of activation, cannot be completely discounted on the evidence available. Only one type of crystal has so far been obtained from solutions of (2); thus the isomer (**2B**) has not yet been observed in the solid state. Very few examples of transition metal cluster compounds exhibiting skeletal isomerism have been reported previously.[6–8]

As the temperature is raised, the three ^{31}P-{^{1}H} n.m.r. peaks attributed to the two isomers of [Cu$_2$Ru$_4$(μ_3-H)$_2$(CO)$_{12}${P(CHMe$_2$)$_3$}$_2$], (**2A**) and (**2B**), all coalesce, as do the ^{1}H n.m.r. hydrido ligand signals. Eventually, at room temperature, a singlet, broadened by quadrupolar effects,[3] and a high-field triplet [*J*(PH) 5 Hz] are observed in the ^{31}P-{^{1}H} and ^{1}H n.m.r. spectra, respectively. Clearly, the isomers (**2A**) and (**2B**) are interconverting in solution at ambient temperature and the isomer (**2A**) additionally undergoes the fluxional process involving coinage metal site-exchange that has been previously observed for (3).[3] Dynamic behaviour involving rapid intramolecular rearrangements of the metal skeletons of Group 1B metal heteronuclear clusters is well established,[3,4] but reports of an equilibrium between two skeletal isomers in solution are rare.[7,8]

The variation in the metal framework structures of the series of clusters (1)—(3) can be related to the steric requirements of the phosphine ligands present. The capped trigonal bipyramidal metal core, with the Cu atoms in close contact, appears to be the preferred geometry for relatively small phosphines.[9] Thus, it is the only structure observed for the PPh_3- (cone angle 145°)[1] containing species (3).[3] However, with the slightly larger phosphine $P(CHMe_2)_3$ (cone angle 160°)[1], a second isomer (2B), which probably has two face-capping Cu atoms with no bonding interaction between them, is also present in solution at low temperatures. The most bulky phosphine PCy_3 (cone angle 170°)[1] seems to be too large to allow two $Cu(PCy_3)$ units to be adjacent in the metal framework of (1); instead, a novel type of structure, in which only one Cu atoms adopts a face-capping position and the other occupies a sterically less demanding edge-bridging site, is observed.

We thank the S.E.R.C. for studentships (to T. A. and P. J. M.), Johnson Matthey Ltd. for a loan of ruthenium trichloride, the Nuffield Foundation for support, and Mrs. L. J. Salter for drawing the display formulae.

Received, 25th April 1988; Com 8/01612G

References

1 C. A. Tolman, *Chem. Rev.*, 1977, **77**, 313.

2 S. S. D. Brown and I. D. Salter, *Organomet. Synth.*, vol. 4, in the press.

3 M. J. Freeman, A. G. Orpen, and I. D. Salter, *J. Chem. Soc., Dalton Trans.*, 1987, 379.

4 I. D. Salter, *Adv. Organomet. Chem.*, in the press.

5 S. S. D. Brown, I. D. Salter, T. Adatia, and M. McPartlin, *J. Organomet. Chem.*, 1987, **332**, C6.

6 B. R. Sutherland, D. M. Ho, J. C. Huffman, and K. G. Caulton, *Angew. Chem., Int. Ed. Engl.*, 1987, **26**, 135; G. A. Moehring, P. E. Fanwick, and R. A. Walton, *Inorg. Chem.*, 1987, **26**, 1861; K. Henrick, B. F. G. Johnson, J. Lewis, J. Mace, M. McPartlin, and J. Morris, *J. Chem. Soc., Chem. Commun.*, 1985, 1617; C. E. Briant, K. P. Hall, and D. M. P. Mingos, *ibid.*, 1984, 290; B. F. G. Johnson, D. A. Kaner, J. Lewis, P. R. Raithby, and M. J. Taylor, *Polyhedron*, 1982, **1**, 105.

7 S. R. Drake, B. F. G. Johnson, and J. Lewis, *J. Organomet. Chem.*, 1988, **340**, C31; B. R. Sutherland, K. Folting, W. E. Streib, D. M. Ho, J. C. Huffman, and K. G. Caulton, *J. Am. Chem. Soc.*, 1987, **109**, 3489; S. R. Bunkhall, H. D. Holden, B. F. G. Johnson, J. Lewis, G. N. Pain, P. R. Raithby, and M. J. Taylor, *J. Chem. Soc., Chem. Commun.*, 1984, 25.

8 C. P. Horwitz, E. M. Holt, C. P. Brock, and D. F. Shriver, *J. Am. Chem. Soc.*, 1985, **107**, 8136; C. P Horwitz and D. F. Shriver, *ibid.*, p. 8147.

9 P. J. McCarthy, I. D. Salter, and V. Šik, *J. Organomet. Chem.*, 1988, 000, 000.

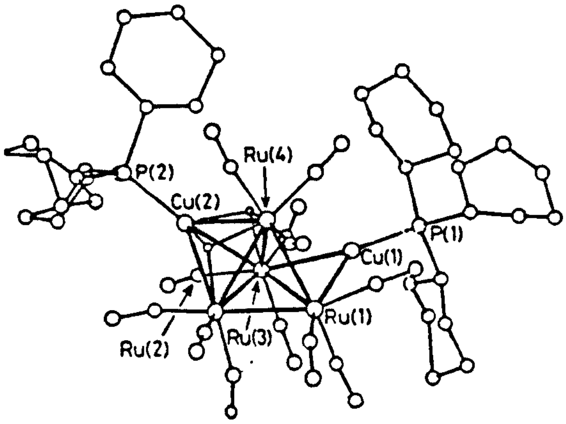

Figure 1. Molecular structure of $[Cu_2Ru_4(\mu_3\text{-}H)_2(CO)_{12}\{P(cyclo\text{-}C_6H_{11})_3\}_2]$ (1). Principal bond lengths: Ru(1)–Ru(2) 2.792(2), Ru(1)–Ru(3) 2.885(2), Ru(1)–Ru(4) 2.807(2), Ru(1)–Cu(1) 2.619(3), Ru(2)–Ru(3) 2.822(2), Ru(2)–Ru(4) 2.946(2), Ru(2)–Cu(2) 2.711(3), Ru(3)–Ru(4) 2.960(2), Ru(3)–Cu(1) 2.625(3), Ru(3)–Cu(2) 2.634(3), Ru(4)–Cu(2) 2.565(3), mean Cu–P 2.298(9), Ru–CO range 1.79—1.93(7) Å.

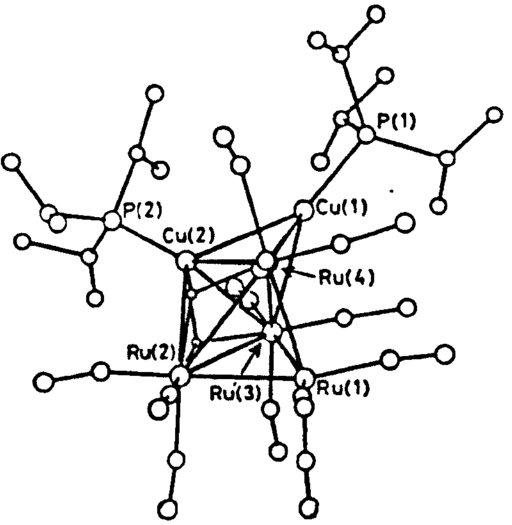

Figure 2. Molecular structure of $[Cu_2Ru_4(\mu_3\text{-}H)_2(CO)_{12}\{P(CHMe_2)_3\}_2]$ (2A). Principal bond lengths: Ru(1)–Ru(2) 2.835(4), Ru(1)–Ru(3) 2.699(7), Ru(1)–Ru(4) 2.743(8), Ru(2)–Ru(3) 3.253(4), Ru(2)–Ru(4) 3.204(4), Ru(2)–Cu(2) 3.049(5), Ru(3)–Ru(4) 2.906(5), Ru(3)–Cu(1) 2.780(8), Ru(3)–Cu(2) 2.616(10), Ru(4)–Cu(1) 2.911(9), Ru(4)–Cu(2) 2.585(10), Cu(1)–Cu(2) 3.010(6), mean Cu–P 2.318(11), Ru–CO range 1.78–2.06(4) Å.

---

† *Selected spectroscopic data* (i.r. in CH_2Cl_2; n.m.r. in CD_2Cl_2, coupling constants in Hz). Compound (1); i.r. ν_{CO} 2063m, 2030s, 2000vs, br., 1975sh, 1943m, br., 1928sh, and 1915sh cm^{-1}; ^1H n.m.r.: δ −16.44 [t, 2 H, μ_3-H, *J*(PH) 5] and 1.25—2.15 (m, 66 H, cyclo-C_6H_{11}); μ_3-H at −100 °C δ −17.12 (br. s, 1 H) and −16.18 (br. s, 1 H); ^{31}P-{^1H} δ 19.4 (br. s); at −100 °C δ 17.6 (br. s) and 17.2 (br. s). Compound (2); i.r. ν_{CO} 2063m, 2027s, 2000vs, br., 1980sh, and 1940m; v. br. cm^{-1}; ^1H n.m.r. δ −16.64 [t, 2 H, μ_3-H, *J*(PH) 5], 1.25 [d of d, 36 H, Me, *J*(PH) 14 and *J*(HH) 7], and 2.26 [overlapping d of sept, 6 H, C*H*Me_2, *J*(PH) and *J*(HH) 7]; μ_3-H at −100 °C δ −17.09 [d, isomer A, *J*(PH) 10] and −16.15 (s, v. br., isomer B); ^{31}P-{^1H}, δ 28.3 (br. s); at −90 °C δ 32.0 (s, isomer A, 1 P), 26.0 (s, isomer B, 0.6 P), and 18.7 (s, isomer A, 1 P).

‡ The positions of the two hydrido ligands are not known.

‡ *Crystal data* for (1): $C_{48}H_{68}O_{12}Cu_2P_2Ru_4$, *M* = 1429.37, monoclinic, space group $P2_1/n$, *a* = 23.450(3), *b* = 22.475(3), *c* = 10.816(2) Å, β = 101.45(2)°, *U* = 5587.00 Å^3, *F*(000) = 2744, $\mu(Mo\text{-}K_\alpha)$ = 20.24 cm^{-1}, *Z* = 4, D_c = 1.70 g cm^{-3}; *R* = 0.0735 for 2544 unique absorption-corrected data with $I/\sigma(I) > 3.($

Crystal data for (2): $C_{30}H_{44}O_{12}Cu_2P_2Ru_4$, *M* = 1189.37, monoclinic, space group $P2_1$, *a* = 12.666(2), *b* = 15.115(3), *c* = 12.317(2) Å, β = 104.01(2)°, *I* = 2287.90 Å^3, *F*(000) = 1168, $\mu(Mo\text{-}K_\alpha)$ = 21.60 cm^{-1}, *Z* = 2, D_c = 1.71 g cm^{-3}; *R* = 0.0795 for 2031 unique absorption-corrected data with $I/\sigma(I) > 3.0$.

Atomic co-ordinates, bond lengths and angles, and thermal parameters have been deposited at the Cambridge Crystallographic Data Centre. See Notice to Authors, Issue No. 1.

Note

Structural Comparison of Cluster Compounds containing an Edge-bridging $M(PPh_3)$ (M = Cu, Ag, or Au) Fragment. X-Ray Crystal Structure of $[AgRu_3(CO)_9(C_2Bu^t)(PPh_3)]$ †

Trushar Adatia and Mary McPartlin *
School of Chemistry, The Polytechnic of North London, London N7 8DB
Ian D. Salter *
Department of Chemistry, University of Exeter, Exeter, EX4 4QD

An *X*-ray diffraction study of $[AgRu_3(CO)_9(C_2Bu^t)(PPh_3)]$ shows that the cluster adopts a 'butterfly' metal-core structure, with the silver atom occupying a 'wing-tip' site. The t-butylacetylide ligand lies on the convex side of the 'butterfly' metal core, interacting with all three ruthenium atoms *via* one σ bond to the 'wing-tip' ruthenium site and two π bonds to the ruthenium atoms which form the 'hinge' of the 'butterfly'. Comparison of the structure with those reported for the analogous copper and gold containing species reveals that the M–P and M–Ru bond lengths are markedly longer for M = Ag than for M = Cu or Au.

The chemistry of mixed-metal cluster compounds is attracting considerable current interest, but detailed structural investigations of those containing one or more $Ag(PR_3)$ units are relatively rare.[1–3] The first comparative study of the effect of the nature of all three Group 1B metals on the structure of a series of related cluster compounds containing edge-bridging $M(PR_3)$ (M = Cu, Ag, or Au; R = alkyl or aryl) fragments has recently been reported by Bruce *et al.*[1] Their *X*-ray diffraction studies of the Group 1B metal clusters $[MRu_3(\mu_3\text{-}PhPCH_2PPh_2)(CO)_9(PPh_3)]$ (M = Cu, Ag, or Au) show 'butterfly' metal-core geometries with the coinage metal occupying a 'wing-tip' site. Interestingly, the Ag–P distance [2.422(3) Å] was found to be very long compared not only to Cu–P [2.228(2) Å] but also to Au–P [2.297(2) Å] and furthermore, the mean M–Ru distances are significantly longer for M = Ag than for M = Cu or Au [2.787(1), 2.603(1), and 2.760(1) Å, respectively]. Similar 'butterfly' skeletal geometries have previously been reported for the two mixed-metal clusters $[MRu_3(CO)_9(C_2Bu^t)(PPh_3)]$ [M = Cu (1)[4] or Au (3)[5]]. The present *X*-ray diffraction study of $[AgRu_3(CO)_9(C_2Bu^t)(PPh_3)]$ (2) completes the structural data for this series of analogous clusters, and allows detailed comparison of the structures for all three metals. It shows that the interesting trends observed in the earlier series[1] are also present here, as once again all bonds from the silver atom are markedly longer than the equivalent distances from copper or gold.

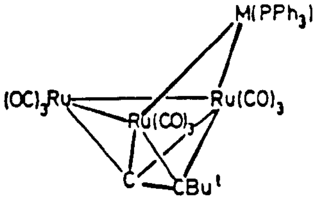

	M
(1)	Cu
(2)	Ag
(3)	Au

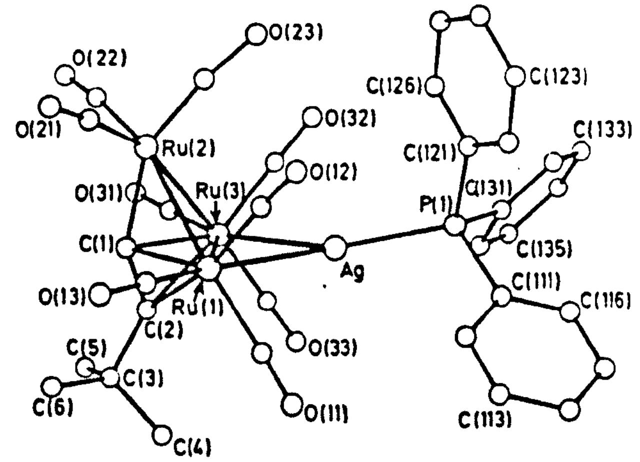

Figure. Molecular structure of $[AgRu_3(CO)_9(C_2Bu^t)(PPh_3)]$ (2), showing the crystallographic numbering. The carbon atom of each carbonyl group has the same number as the oxygen atom

Results and Discussion

X-Ray structure analysis shows that $[AgRu_3(CO)_9(C_2Bu^t)(PPh_3)]$ (2) adopts a similar 'butterfly' metal-core structure to those previously established for the analogous copper (1)[4] and gold (3)[5] species, with the heterometal atom in a 'wing-tip' site (Figure). The dihedral angle between the 'wings' of the 'butterfly' [Ru(1)–Ru(2)–Ru(3) and Ru(1)–Ru(3)–Ag] is 120.6°, which is intermediate in value between that of 115.7 in (1) and 129.3° in (3). The heteronuclear clusters (1)—(3) may all formally be envisaged as derived from $[Ru_3(\mu\text{-}H)(CO)_9(C_2Bu^t)]$ (4)[6] by replacement of the μ-H ligand by a bridging $M(PPh_3)$ fragment. Table 1 summarises the principal bond lengths for (2), and those reported for the related structures (1), (3), (4), and the

---

† μ_3-[t-butylethynyl-$C^1(Ru^{1-3})$, $C^2(Ru^{1,2})$]-1,1,1,2,2,2,3,3,3-nonacarbonyl-1,2-μ-[(triphenylphosphine)argentio]-*triangulo*-triruthenium.

Supplementary data available: see Instructions for Authors, *J. Chem. Soc., Dalton Trans.*, 1988, Issue 1, pp. xvii—xx.

Table 1. Selected bond lengths (Å) for $[AgRu_3(CO)_9(C_2(Bu^t)(PPh_3)]$ (2) compared with those of the related compounds $[MRu_3(CO)_9(C_2Bu^t)(PPh_3)]$ [M = Cu (1) or Au (3)], $[Ru_3(\mu\text{-}H)(CO)_9(C_2Bu^t)]$ (4), and $[Ru_3(CO)_9(C_2Bu^t)]^-$ (5) (renumbered where necessary)

Bond distances	(1)[4]	(2)	(3)[5]	(4)[6]	(5)[7]
Ru(1)–Ru(2)	2.819	2.814(3)	2.800	2.799	2.800
Ru(1)–Ru(3)	2.762	2.805(2)	2.820	2.792	2.655
Ru(2)–Ru(3)	2.808	2.799(3)	2.786	2.795	2.790
Ru(1)–M	2.603	2.788(3)	2.763	—	—
Ru(3)–M	2.603	2.785(3)	2.757	—	—
M–P(1)	2.217	2.405(9)	2.276	—	—
Ru(1)–C(1)	2.203	2.20(3)	2.22	2.214	2.18
Ru(2)–C(1)	1.945	2.02(3)	1.95	1.947	1.95
Ru(3)–C(1)	2.211	2.23(3)	2.19	2.207	2.16
Ru(1)–C(2)	2.260	2.27(3)	2.21	2.271	2.24
Ru(3)–C(2)	2.259	2.25(2)	2.27	2.268	2.24
C(1)–C(2)	1.313	1.28(4)	1.29	1.315	1.27

Table 2. Selected bond angles (°) for $[AgRu_3(CO)_9(C_2Bu^t)(PPh_3)]$ (2)

Ag–Ru(1)–Ru(2)	97.2(1)	Ag–Ru(1)–Ru(3)	59.7(1)
Ag–Ru(3)–Ru(1)	59.8(1)	Ag–Ru(3)–Ru(2)	97.7(1)
Ru(3)–Ag–Ru(1)	60.4(1)	Ru(3)–Ru(1)–Ru(2)	59.8(1)
Ru(3)–Ru(2)–Ru(1)	60.0(1)	Ru(2)–Ru(3)–Ru(1)	60.3(1)
P(1)–Ag–Ru(1)	145.5(2)	P(1)–Ag–Ru(3)	151.3(2)
C(1)–Ru(1)–Ru(2)	45.5(7)	C(1)–Ru(1)–Ru(3)	51.1(7)
C(1)–Ru(1)–Ag	110.7(7)	C(1)–Ru(1)–C(11)	128.0(1)
C(1)–Ru(1)–C(12)	131.0(1)	C(1)–Ru(1)–C(13)	92.0(1)
C(2)–Ru(1)–Ru(2)	77.5(6)	C(2)–Ru(1)–Ru(3)	51.3(5)
C(2)–Ru(1)–Ag	102.0(7)	C(2)–Ru(1)–C(11)	95.0(1)
C(2)–Ru(1)–C(12)	160.6(8)	C(2)–Ru(1)–C(13)	99.0(1)
C(2)–Ru(1)–C(1)	33.0(1)	C(1)–Ru(2)–Ru(1)	51.0(7)
C(1)–Ru(2)–Ru(3)	52.0(8)	C(1)–Ru(2)–Ru(3)	52.0(8)
C(1)–Ru(3)–Ru(1)	50.3(6)	C(1)–Ru(3)–Ru(2)	45.7(8)
C(1)–Ru(3)–Ag	110.0(7)	C(2)–Ru(3)–Ru(1)	51.8(7)
C(2)–Ru(3)–Ru(2)	78.1(7)	C(2)–Ru(3)–Ag	102.6(6)
C(2)–Ru(3)–C(1)	33.0(1)	Ru–C–O range	173(3)—179(3)

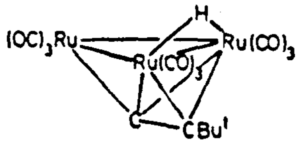

(4)

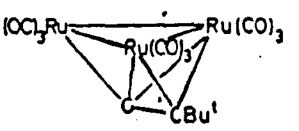

(5)

parent monoanion $[Ru_3(CO)_9(C_2Bu^t)]^-$ (5)[7] are also included for comparison. Table 2 lists selected bond angles for (2).

The present study shows that in the silver complex (2), as in all the complexes included in Table 1, the t-butylacetylide ligand lies on the convex side of the 'butterfly' metal core, interacting with all three ruthenium atoms *via* one σ bond to the 'wing-tip' atom [Ru(2)–C(1) 2.02(3) Å] and two π bonds, one to each of the atoms forming the 'hinge' of the 'butterfly' [Ru(1)–C(1) 2.20(3), Ru(1)–C(2) 2.27(3), Ru(3)–C(1) 2.23(3), and Ru(3)–C(2) 2.25(2) Å]. These bond lengths for (2) do not differ significantly from those reported for the related compounds (1), and (3)—(5) (Table 1). Each ruthenium atom in (2) has three essentially linear carbonyl ligands [Ru–C–O 173(3)—179(3)°]. An extremely short contact occurs between one of these ligands and the silver atom [Ag ··· C(32) 2.69(2) Å], which is very similar to a contact present in a disilver hexanuclear cluster $[Ag_2Ru_4(CO)_{12}(PPh_3)_2]$ [Ag(1) ··· C(32) 2.694(3) Å].[2] This type of Group 1B metal to carbonyl interaction is also a feature of a number of copper[4,8] and gold[9] mixed-metal clusters, and in the gold and copper analogues of (2), the same carbonyl ligand makes a short contact with the heterometal atom [Cu ··· C 2.469(7)[4] in (1) and Au ··· C 2.69(1)[5] Å in (3)].

In the silver compound (2), the lengths of the chemically equivalent bonds Ru(1)–Ru(2) and Ru(2)–Ru(3) [2.814(3) and 2.799(3) Å respectively are significantly different. There is no obvious reason for this, but, interestingly a slight asymmetry also occurs in the reported structures of not only the copper (1) and gold (3) compounds, but also in the related monoanion (5), where the Ru(1)–Ru(2) bonds are longer than the Ru(2)–Ru(3) bonds by 0.011, 0.014, and 0.010 Å respectively (Table 1).

The chemically unique Ru(1)–Ru(3) bond of length 2.655(3) Å reported for the 'parent' monoanion (5)[7] is very much shorter than the mean of the other two Ru–Ru bonds [2.795(2) Å]. In complex (2), the silver-bridged Ru(1)–Ru(3) bond [2.805(2) Å] is markedly elongated compared to the equivalent distance in (5), and is very close to the mean lengths of the other two unbridged Ru–Ru bonds [2.807(3) Å]. This observation is very similar to that reported for the analogous monohydrido species (4), where the hydrido-bridged Ru(1)–Ru(3) bond length [2.792(2) Å] is also longer than the equivalent distance in the monoanion (5), and is similar to the remaining Ru–Ru lengths [mean 2.797(2) Å].[6] In contrast to the silver complex (2), the bridged bond Ru(1)–Ru(3) in the copper complex (1) is markedly shorter (0.052 Å)[4] and that in the gold complex (3) is longer (0.027 Å)[5] than the mean of the other two Ru–Ru bonds. Thus, the length of the 'hinge' bond, bridged by $M(PPh_3)$, increases with increasing atomic number of the Group 1B metal in the order Cu < Ag < Au.

The most interesting feature of the present study is that the mean Ag–Ru length of 2.787(3) Å in (2) is not only very much longer than the mean Cu–Ru distance of 2.603(2) Å reported in (1),[4] but also considerably longer than the mean Au–Ru distance of 2.760(1) Å in (3).[5] This structural trend is also reflected in the M–P bond lengths, with the Ag–P bond [2.409(9) Å in (2)] being considerably longer than both the Cu–P and Au–P distances [2.217(2) in (1) and 2.276(3) Å in (3) respectively].

These results closely parallel those observed by Bruce *et al.*[1] for the series $[MRu_3(\mu_3\text{-}PhPCH_2PPh_2)(CO)_9(PPh_3)]$ (see above), in which all the bonds from the silver are markedly longer than the equivalent distances from both copper and gold, and they indicate that these structural features may be a general characteristic of mixed-metal clusters containing an edge-bridging $M(PR_3)$ (R = alkyl or aryl) unit.

Experimental

The cluster $[AgRu_3(CO)_9(C_2Bu^t)(PPh_3)]$ (2) was prepared as previously described[4] and crystals suitable for *X*-ray diffraction studies were grown from a light petroleum (b.p. 40 - 60 °C) solution by slow evaporation and subsequent cooling to −20 °C.

Crystal Data for (2).—$C_{33}H_{24}AgO_9PRu_3$, *M* = 1 006.17, monoclinic, *a* = 16.117(3), *b* = 16.791(13), *c* = 14.488(3) Å, β = 110.98(2)°, *U* = 3 660.9 Å³, space group $P2_1/n$, *Z* = 4, D_C = 1.80 g cm⁻³, *F*(000) = 1 984, μ(Mo-K_α) = 16.64 cm⁻¹.

The methods of data collection and data processing were similar to those described previously.[10] The crystal selected for data collection had dimensions 0.44 × 0.48 × 0.21 mm. A scan width of 0.80° in θ was used to collect data in the θ range 3—25° by the ω/2θ technique. Equivalent reflections were merged to give 3 161 data with $I/\sigma(I) > 3.0$. No absorption corrections were applied.

The positions of the metal atoms were deduced from a Patterson synthesis. The remaining non-hydrogen atoms were found from subsequent difference-Fourier syntheses. Aniso-

Table 3. Fractional atomic co-ordinates for $[AgRu_3(C_2Bu^t)(CO)_9(PPh_3)]$ (2)

Atom	*x*	*y*	*z*
Ru(1)	0.207 98(4)	0.203 14(15)	0.276 52(11)
Ru(2)	-0.257 5(2)	0.121 6(1)	0.095 1(1)
Ru(3)	-0.291 54(14)	0.284 81(14)	0.098 36(12)
Ag	-0.369 10(14)	0.281 03(14)	0.241 98(12)
P(1)	0.496 0(5)	0.293 5(5)	0.291 3(4)
C(11)	0.191 9(19)	0.280 6(19)	0.378 1(17)
O(11)	-0.178 4(15)	0.322 5(14)	0.444 7(14)
C(12)	-0.285 8(18)	0.133 9(18)	0.305 6(16)
O(12)	0.329 9(17)	0.095 8(16)	0.330 5(14)
C(13)	-0.114 4(24)	0.140 3(23)	0.341 7(21)
O(13)	0.049 4(18)	0.095 1(16)	0.384 9(15)
C(21)	0.197 0(26)	0.025 8(26)	0.135 1(22)
O(21)	-0.150 9(18)	-0.031 2(18)	0.162 8(15)
C(22)	-0.269 1(20)	0.109 4(20)	-0.037 6(19)
O(22)	-0.270 6(14)	0.108 4(14)	-0.119 0(13)
C(23)	-0.371 1(26)	0.080 8(22)	0.079 4(21)
O(23)	-0.440 5(18)	0.056 0(16)	0.075 2(14)
C(31)	-0.286 0(19)	0.303 5(21)	-0.024 4(19)
O(31)	-0.284 4(15)	0.314 1(14)	-0.104 7(14)
C(32)	-0.410 7(19)	0.256 3(16)	0.046 9(16)
O(32)	-0.487 6(16)	0.243 1(13)	0.010 2(13)
C(33)	-0.302 9(23)	0.390 8(24)	0.127 3(20)
O(33)	-0.311 8(18)	0.457 6(19)	0.144 6(15)
C(111)	-0.469 7(14)	0.328 2(12)	0.417 4(10)
C(112)	-0.385 2(14)	0.312 1(12)	0.486 0(10)
C(113)	-0.360 5(14)	0.341 4(12)	0.582 2(10)
C(114)	-0.420 3(14)	0.387 0(12)	0.609 8(10)
C(115)	-0.504 7(14)	0.403 1(12)	0.541 1(10)
C(116)	0.529 4(14)	0.373 8(12)	0.445 0(10)
C(121)	-0.546 7(14)	0.197 0(10)	0.285 8(12)
C(122)	-0.561 5(14)	0.162 3(10)	0.366 0(12)
C(123)	-0.599 5(14)	0.086 7(10)	0.356 7(12)
C(124)	-0.622 8(14)	0.045 8(10)	0.267 2(12)
C(125)	-0.608 0(14)	0.080 5(10)	0.187 0(12)
C(126)	0.570 0(14)	0.156 1(10)	0.196 3(12)
C(131)	-0.585 2(15)	0.355 5(13)	0.212 9(13)
C(132)	-0.673 9(15)	0.336 5(13)	0.194 6(13)
C(133)	-0.741 5(15)	0.383 6(13)	0.130 7(13)
C(134)	-0.720 3(15)	0.449 6(13)	0.085 0(13)
C(135)	-0.631 6(15)	0.468 7(13)	0.103 3(13)
C(136)	-0.564 0(15)	0.421 6(13)	0.167 3(13)
C(12)	-0.168 7(17)	0.210 9(19)	0.146 1(15)
C(2)	-0.145 8(16)	0.278 6(16)	0.189 0(14)
C(3)	-0.064 8(20)	0.331 8(19)	0.214 9(17)
C(4)	-0.070 1(24)	0.397 5(24)	0.286 8(21)
C(5)	-0.068 4(24)	0.374 0(24)	0.113 0(21)
C(6)	0.020 0(29)	0.275 0(28)	0.258 1(26)

tropic thermal parameters were assigned to the metal and phosphorus atoms during the final cycles of refinement.[11] Full-matrix refinement of the atomic positional and thermal parameters converged to final R and R' values of 0.0689 and 0.0613 respectively, with weights of $w = 1/\sigma^2 F_0$ assigned to the individual reflections. The phenyl groups were treated as rigid hexagons [d(C–C) = 1.395 Å, d(C–H) = 1.08 Å] with fixed thermal parameters of 0.08 Å for the H atoms.

The final atomic co-ordinates are listed in Table 3. Additional material available from the Cambridge Crystallographic Data Centre comprises thermal parameters, H-atom co-ordinates, and remaining bond distances and angles and intermolecular distances.

Acknowledgements

We thank the S.E.R.C. for a studentship (to T. A.), Johnson Matthey Ltd for a generous loan of silver and ruthenium salts, and Mrs L. J. Salter for drawing the diagrams.

References

1 M. I. Bruce, M. L. Williams, J. M. Patrick, B. W. Skelton, and A. H. White, *J. Chem. Soc., Dalton Trans.*, 1986, 2557.

2 S. S. D. Brown, I. D. Salter, T. Adatia, and M. McPartlin, *J. Organomet. Chem.*, 1987, 332, C6.

3 M. J. Freeman, A. G. Orpen, and I. D. Salter, *J. Chem. Soc., Dalton Trans.*, 1987, 379, 1001; S. S. D. Brown, I. D. Salter, V. Šik, I. J. Colquhoun, W. McFarlane, P. A. Bates, M. B. Hursthouse, and M. Murray, *ibid.*, 1988, ????; S. Bhaduri, K. Sharma, P. G. Jones, and C. Freire Erdbrügger, *J. Organomet. Chem.*, 1987, 326, C46; O. M. Abu-Salah and C. B. Knobler, *ibid.*, 1986, 302, C10; B. K. Teo and K. Keating, *J. Am. Chem. Soc.*, 1984, 106, 2224; B. K. Teo, M. C. Hong, H. Zhang, and D. B. Huang, *Angew. Chem., Int. Ed. Engl.*, 1987, 26, 897; C. E. Briant, R. G. Smith, and D. M. P. Mingos, *J. Chem. Soc., Chem. Commun.*, 1984, 586.

4 R. A. Brice, S. C. Pearse, I. D. Salter, and K. Henrick, *J. Chem. Soc., Dalton Trans.*, 1986, 2181.

5 P. Braunstein, G. Predieri, A. Tiripicchio, and E. Sappa, *Inorg. Chim. Acta*, 1982, 63, 113.

6 M. Catti, G. Gervasio, and S. A. Mason, *J. Chem. Soc., Dalton Trans.*, 1977, 2260.

7 C. Barner-Thorsen, K. I. Hardcastle, E. Rosenberg, J. Siegel, A. M. Manotti Lanfredi, A. Tiripicchio, and M. Tiripicchio-Camellini, *Inorg. Chem.*, 1981, 20, 4306.

8 For example, S. S. D. Brown, I. D. Salter, and L. Toupet, *J. Chem. Soc., Dalton Trans.*, 1988, ???? and refs. therein.

9 For example, S. S. D. Brown, I. D. Salter, D. B. Dyson, R. V. Parish, P. A. Bates, and M. B. Hursthouse, *J. Chem. Soc., Dalton Trans.*, 1988, ???? and refs. therein.

10 P. F. Jackson, B. F. G. Johnson, J. Lewis, W. J. H. Nelson, and M. McPartlin, *J. Chem. Soc., Dalton Trans.*, 1982, 2099.

11 G. M. Sheldrick, SHELX 76, Crystal Structure Solving Package, University of Cambridge, 1976.

Received 26th January 1988; *Paper* 8/00371H